POWER SYSTEM DYNAMICS
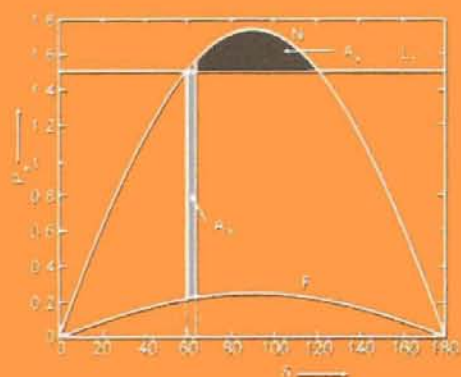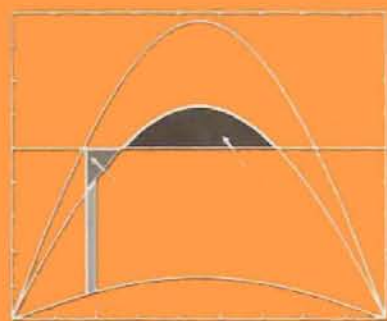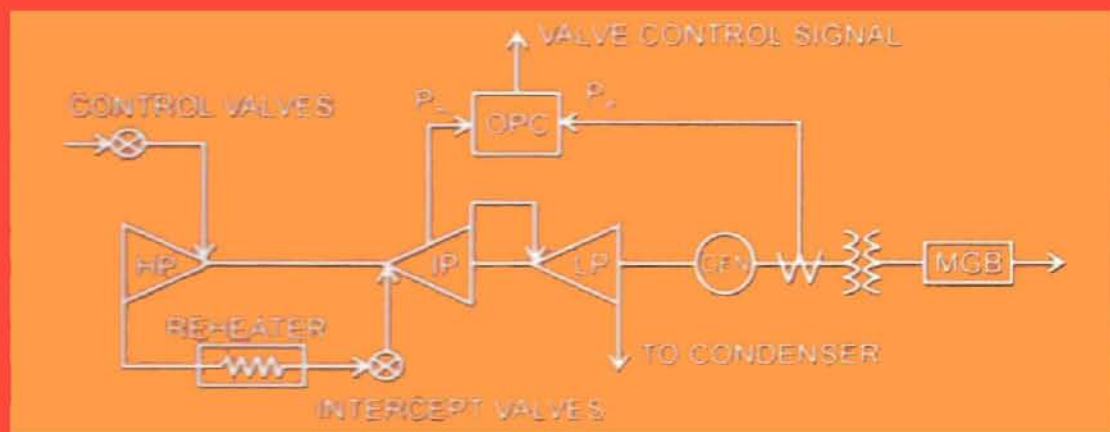
Stability and Control

K R PADIYAR

POWER SYSTEM DYNAMICS
Stability and control
Second Edition

"This page is Intentionally Left Blank"

POWER SYSTEM DYNAMICS

Stability and Control

Second Edition

K. R. Padiyar
Indian Institute of Science, Bangalore

TO

PROF. H N. RAMACHANDRA RAO

"This page is Intentionally Left Blank"

Contents

--

APPENDIX

"This page is Intentionally Left Blank"

Chapter 1

Basic Concepts

1.1 General

Modern power systems are characterized by extensive system interconnections and increasing dependence on control for optimum utilization of existing resources. The supply of reliable and economic electric energy is a major determinant of industrial progress and consequent rise in the standard of living. The increasing demand for electric power coupled with resource and environmental constraints pose several challenges to system planners. The generation may have to be sited at locations far away from load centres (to exploit the advantages of remote hydro power and pit head generation using fossil fuels). However, constraints on right of way lead to overloading of existing transmission lines and an impetus to seek technological solutions for exploiting the high thermal loading limits of EHV lines [1]. With deregulation of power supply utilities, there is a tendency to view the power networks as highways for transmitting electric power from wherever it is available to places where required, depending on the pricing that varies with time of the day.

Power system dynamics has an important bearing on the satisfactory system operation. It is influenced by the dynamics of the system components such as generators, transmission lines, loads and other control equipment (HVDC and SVC controllers). The dynamic behaviour of power systems can be quite complex and a good understanding is essential for proper system planning and secure operation.

1.2 Power System Stability

Stability of power systems has been and continues to be of major concern in system operation [2-7]. This arises from the fact that in steady state (under normal conditions) the average electrical speed of all the generators must remain the same anywhere in the system. This is termed as the *synchronous operation* of a system. Any disturbance small or large can affect the synchronous operation.

For example, there can be a sudden increase in the load or loss of generation. Another type of disturbance is the switching out of a transmission line, which may occur due to overloading or a fault. The stability of a system determines whether the system can settle down to a new or original steady state after the transients disappear.

The disturbance can be divided into two categories (a) small and (b) large. A small disturbance is one for which the system dynamics can be analysed from linearized equations (small signal analysis). The small (random) changes in the load or generation can be termed as small disturbances. The tripping of a line may be considered as a small disturbance if the initial (pre-disturbance) power flow on that line is not significant. However, faults which result in a sudden dip in the bus voltages are large disturbances and require remedial action in the form of clearing of the fault. The duration of the fault has a critical influence on system stability.

Although stability of a system is an integral property of the system, for purposes of the system analysis, it is divided into two broad classes [8].

1. Steady-State or Small Signal Stability
   A power system is steady state stable for a particular steady state operating condition if, following any small disturbance, it reaches a steady state operating condition which is identical or close to the pre-disturbance operating condition.

2. Transient Stability
   A power system is transiently stable for a particular steady-state operating condition and for a particular (large) disturbance or sequence of disturbances if, following that (or sequence of) disturbance(s) it reaches an acceptable steady-state operating condition.

It is important to note that, while steady-state stability is a function only of the operating condition, transient stability is a function of both the operating condition and the disturbance(s). This complicates the analysis of transient stability considerably. Not only system linearization cannot be used, repeated analysis is required for different disturbances that are to be considered.

Another important point to be noted is that while the system can be operated even if it is transiently unstable, small signal stability is necessary at all times. In general, the stability depends upon the system loading. An increase in the load can bring about onset of instability. This shows the importance of maintaining system stability even under high loading conditions.
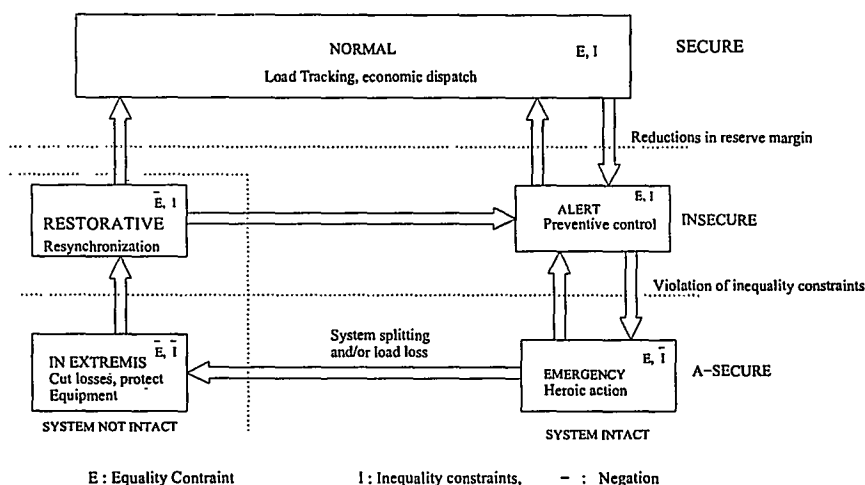
Figure 1.1: System Operating States

1.3 States of Operation and System Security - A Review

Dy Liacco [9], and Fink and Carlson [10] classified the system operation into 5 states as shown in Fig. 1.1. The system operation is governed by three sets of generic equations- one differential and two algebraic (generally non-linear). Of .the two algebraic sets, one set comprise equality constraints (E) which express balance between the generation and load demand. The other set consists of inequality constraints (I) which express limitations of the physical equipment (such as currents and voltages must not exceed maximum limits). The classification of the system states is based on the fulfillment or violation of one or both sets of these constraints.

1. **Normal Secure State:** Here all equality (E) and inequality (I) constraints are satisfied. In this state, generation is adequate to supply the existing load demand and no equipment is overloaded. Also in this state, reserve margins (for transmission as well as generation) are sufficient to provide an adequate level of security with respect to the stresses to which the system may be subjected. The latter may be treated as the satisfaction of security constraints.

2. **Alert State:** The difference between this and the previous state is that in this state, the security level is below some threshold of adequacy. This implies that there is a danger of violating some of the inequality (I) constraints when subjected to disturbances (stresses). It can also be said that

security constraints are not met. Preventive control enables the transition from an alert state to a secure state.

3. **Emergency State:** Due to a severe disturbance the system can enter emergency state. Here I constraints are violated. The system, however, would still be intact, and emergency control action (heroic measures) could be initiated to restore the system to alert state. If these measures are not taken in time or are ineffective, and if the initiating disturbance or a subsequent one is severe enough to overstress the system, the system will break down and reach 'In Extremis' state.

4. **In Extremis State:** Here both E and I constraints are violated. The violation of equality constraints implies that parts of system load are lost. Emergency control action should be directed at avoiding total collapse.

5. **Restorative State:** This is a transitional state in which I constraints are met from the emergency control actions taken but the E constraints are yet to be satisfied. From this state, the system can transit to either the alert or the normal state depending on the circumstances.

In further developments in defining the system states [11], the power system emergency is defined as due to either a

(i) *viability crisis* resulting from an imbalance between generation, loads and transmission whether local or system-wide or

(ii) *stability crisis* resulting from energy accumulated at sufficient level in swings of the system to disrupt its integrity.

'In Extremis' state corresponds to a system failure characterized by the loss of system integrity involving uncontrolled islandings (fragmentation) of the system and/or uncontrolled loss of large blocks of load.

It is obvious that the objective of emergency control action should be to avoid transition from emergency state to a failure state (In Extremis). The knowledge of system dynamics is important in designing appropriate controllers. This involves both the detection of the problem using dynamic security assessment and initiation of the control action.

1.4   System Dynamic Problems - Current Status and Recent Trends

In the early stages of power system development, (over 50 years ago) both steady state and transient stability problems challenged system planners. The development of fast acting static exciters and electronic voltage regulators overcame to

a large extent the transient stability and steady state stability problems (caused by slow drift in the generator rotor motion as the loading was increased). A parallel development in high speed operation of circuit breakers and reduction of the fault clearing time and reclosing, also improved system stability.

The regulation of frequency has led to the development of turbine speed governors which enable rapid control of frequency and power output of the generator with minimum dead band. The various prime-mover controls are classified as a) primary (speed governor) b) secondary (tie line power and frequency) and c) tertiary (economic load dispatch). However, in well developed and highly interconnected power systems, frequency deviations have become smaller. Thus tie-line power frequency control (also termed as automatic generation control) (AGC) has assumed major importance. A well designed prime-mover control system can help in improving the system dynamic performance, particularly the frequency stability.

Over last 25 years, the problems of low frequency power oscillations have assumed importance. The frequency of oscillations is in the range of 0.2 to 2.0 Hz. The lower the frequency, the more widespread are the oscillations (also called inter-area oscillations). The presence of these oscillations is traced to fast voltage regulation in generators and can be overcome through supplementary control employing power system stabilizers (PSS). The design and development of effective PSS is an active area of research.

Another major problem faced by modern power systems is the problem of voltage collapse or voltage instability which is a manifestation of steady-state instability. Historically steady-state instability has been associated with angle instability and slow loss of synchronism among generators. The slow collapse of voltage at load buses under high loading conditions and reactive power limitations, is a recent phenomenon.

Power transmission bottlenecks are faced even in countries with large generation reserves. The economic and environmental factors necessitate generation sites at remote locations and wheeling of power through existing networks. The operational problems faced in such cases require detailed analysis of dynamic behaviour of power systems and development of suitable controllers to overcome the problems. The system has not only controllers located at generating stations - such as excitation and speed governor controls but also controllers at HVDC converter stations, Static VAR Compensators (SVC). New control devices such as Thyristor Controlled Series Compensator (TCSC) and other FACTS controllers are also available. The multiplicity of controllers also present challenges in their design and coordinated operation. Adaptive control strategies may be required.

The tools used for the study of system dynamic problems in the past were simplistic. Analog simulation using AC network analysers were inadequate for considering detailed generator models. The advent of digital computers has not only resulted in the introduction of complex equipment models but also the simulation of large scale systems. The realistic models enable the simulation of systems over a longer period than previously feasible. However, the 'curse of dimensionality' has imposed constraints on on-line simulation of large systems even with super computers. This implies that on-line dynamic security assessment using simulation is not yet feasible. Future developments on massively parallel computers and algorithms for simplifying the solution may enable real time dynamic simulation.

The satisfactory design of system wide controllers have to be based on adequate dynamic models. This implies the modelling should be based on 'parsimony' principle- include only those details which are essential.

References and Bibliography

1. N.G. Hingorani, 'FACTS - Flexible AC Transmission System', Conference Publication No. 345, Fifth Int. Conf. on 'AC and DC Power Transmission', London Sept. 1991, pp. 1-7

2. S.B. Crary, **Power System Stability, Vol. I: Steady-State Stability,** New York, Wiley, 1945

3. S.B. Crary, **Power System Stability, Vol. II : Transient Stability,** New York, Wiley, 1947

4. E.W. Kimbark, **Power System Stability, Vol. I : Elements of Stability Calculations,** New York, Wiley, 1948

5. E.W. Kimbark, **Power System Stability, Vol. III : Synchronous Machines,** New York, Wiley, 1956

6. V.A. Venikov, **Transient Phenomenon in Electric Power Systems,** New York, Pergamon, 1964

7. R.T. Byerly and E.W. Kimbark (Ed.), **Stability of Large Electric Power Systems,** New York, IEEE Press, 1974

8. IEEE Task Force on Terms and Definitions, 'Proposed Terms and Definitions for Power System Stability', IEEE Trans. vol. PAS-101, No.7, July 1982, pp. 1894-1898

9. T.E. DyLiacco, 'Real-time Computer Control of Power Systems', Proc. IEEE, vol. 62, 1974, pp. 884-891

10. L.H. Fink and K. Carlsen, 'Operating under stress and strain', IEEE Spectrum, March 1978, pp. 48-53

11. L.H. Fink, 'Emergency control practices', (report prepared by Task Force on Emergency Control) IEEE Trans., vol. PAS-104, No.9, Sept. 1985, pp. 2336-2341

"This page is Intentionally Left Blank"

Chapter 2

Review of Classical Methods

In this chapter, we will review the classical methods of analysis of system stability, incorporated in the treatises of Kimbark and Crary. Although the assumptions behind the classical analysis are no longer valid with the introduction of fast acting controllers and increasing complexity of the system, the simplified approach forms a beginning in the study of system dynamics. Thus, for the sake of maintaining the continuity, it is instructive to outline this approach.

As the objective is mainly to illustrate the basic concepts, the examples considered here will be that of a single machine connected to an infinite bus (SMIB).

2.1 System Model

Consider the system (represented by a single line diagram) shown in Fig. 2.1. Here the single generator represents a single machine equivalent of a power plant (consisting of several generators). The generator G is connected to a double circuit line through transformer T. The line is connected to an infinite bus through an equivalent impedance Z_T. The infinite bus, by definition, represents a bus with fixed voltage source. The magnitude, frequency and phase of the voltage are unaltered by changes in the load (output of the generator). It is to be noted that the system shown in Fig. 2.1 is a simplified representation of a remote generator connected to a load centre through transmission line.
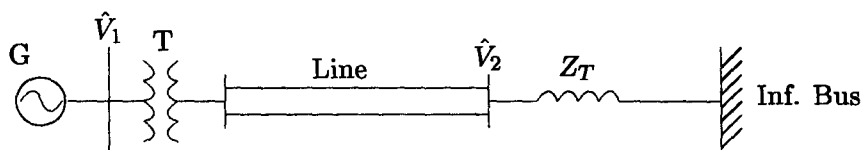
Figure 2.1: Single line diagram of a single machine system

The major feature in the classical methods of analysis is the simplified (classical) model of the generator. Here, the machine is modelled by an equiv-

alent voltage source behind an impedance. The major assumptions behind the model are as follows

1. Voltage regulators are not present and manual excitation control is used. This implies that in steady- state, the magnitude of the voltage source is determined by the field current which is constant.

2. Damper circuits are neglected.

3. Transient stability is judged by the first swing, which is normally reached within one or two seconds.

4. Flux decay in the field circuit is neglected (This is valid for short period, say a second, following a disturbance, as the field time constant is of the order of several seconds).

5. The mechanical power input to the generator is constant.

6. Saliency has little effect and can be neglected particularly in transient stability studies.

Based on the classical model of the generator, the equivalent circuit of the system of Fig. 2.1 is shown in Fig. 2.2. Here the losses are neglected for simplicity. x_e is the total external reactance viewed from the generator terminals. The generator reactance, x_g, is equal to synchronous reactance x_d for steady-state analysis. For transient analysis, x_g is equal to the direct axis transient reactance x'_d. In this case, the magnitude of the generator voltage E_g is proportional to the field flux linkages which are assumed to remain constant (from assumption 4).
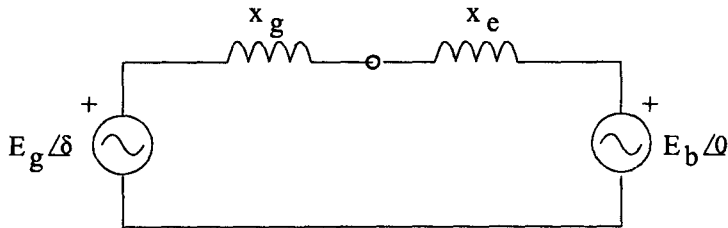
Figure 2.2: Equivalent circuit of the system shown in Fig. 2.1

For the classical model of the generator, the only differential equation relates to the motion of the rotor.

The Swing Equation

The motion of the rotor is described by the following second order equation

$$J\frac{d^2\theta_m}{dt^2} = T_m - T_e \tag{2.1}$$

where

J is the moment of inertia
θ_m is the angular position of the rotor with respect to a stationary axis
T_m is the net mechanical input torque and
T_e is the electromagnetic torque

By multiplying both sides of the Eq. (2.1) by the nominal (rated) rotor speed, ω_m, we get

$$M\frac{d^2\theta_m}{dt^2} = P_m - P_e \tag{2.2}$$

where $M = J\omega_m$ is the angular momentum. It is convenient to express θ_m as

$$\theta_m = \omega_m t + \delta_m \tag{2.3}$$

where ω_m is the average angular speed of the rotor. δ_m is the rotor angle with respect to a synchronously rotating reference frame with velocity ω_m. Substituting Eq. (2.3) in Eq. (2.2) we get

$$M\frac{d^2\delta_m}{dt^2} = P_m - P_e \tag{2.4}$$

This is called the swing equation. Note that M is strictly not a constant. However the variation in M is negligible and M can be considered as a constant. (termed inertia constant).

It is convenient to express Eq. (2.4) in per unit by dividing both sides by base power S_B. Eq. (2.4) can be expressed as

$$\frac{M}{S_B}\frac{d^2\delta_m}{dt^2} = \bar{P}_m - \bar{P}_e \tag{2.5}$$

where $\bar{P}_m$ and $\bar{P}_e$ are expressed in per unit. The L.H.S. of Eq. (2.5) can be written as

$$\frac{M}{S_B}\frac{d^2\delta_m}{dt^2} = \frac{J\omega_m}{S_B}\left(\frac{\omega_B}{\omega_B}\right)\left(\frac{2}{P}\right)\frac{d^2\delta}{dt^2} = \frac{J\omega_m^2}{S_B\omega_B}\frac{d^2\delta}{dt^2} = \left(\frac{2H}{\omega_B}\right)\frac{d^2\delta}{dt^2} \tag{2.6}$$

where

δ is the load angle $= \delta_m \dfrac{P}{2}$

P is the number of poles

ω_B is the electrical angular frequency $= \dfrac{P}{2}\omega_m$

H is also termed as the inertia constant given by

$$H = \frac{1}{2}\frac{J\omega_m^2}{S_B} = \frac{kinetic\ \ energy\ \ stored\ \ in\ \ megajoules}{Rating\ \ in\ \ MVA}$$

The inertia constant H has the dimension of time expressed in seconds. H varies in a narrow range (2-10) for most of the machines irrespective of their ratings.

From Eq. (2.6), the per unit inertia is given by

$$\bar{M} = \frac{M}{S_B} = \frac{2H}{\omega_B} \tag{2.7}$$

The above relation assumes that δ is expressed in radians and time in seconds. If δ is expressed in electrical degrees, then the per unit inertia is

$$M' = \frac{2H}{\omega_B}\cdot\frac{\pi}{180} = \frac{2H}{2\pi f_B}\cdot\frac{\pi}{180} = \frac{H}{180 f_B} \tag{2.8}$$

where f_B is the rated frequency in Hz.

For convenience, in what follows, all quantities are expressed in per unit and no distinction will be made in the symbols to indicate per unit quantities. Thus, Eq. (2.4) is revised and expressed in p.u. quantities as

$$M\frac{d^2\delta}{dt^2} = P_m - P_e \tag{2.9}$$

From Fig. 2.2, the expression for P_e is obtained as

$$P_e = \frac{E_g E_b}{(x_g + x_e)}\sin\delta \tag{2.10}$$

The swing equation, when P_e is expressed using Eq. (2.10), is a nonlinear differential equation for which there is no analytic solution in general. For $P_m = 0$, the solution can be expressed in terms of elliptic integrals [1]. It is

to be noted that the swing equation reduces to the equation of a nonlinear pendulum when $P_m = 0$.

Invariably, numerical methods have to be used for solving the swing equation. However simple techniques exist for the testing of system stability when subjected to small and large disturbances. These will be taken up in the following sections.

2.2 Some Mathematical Preliminaries [3, 4]

A nonlinear continuous time dynamic system is denoted by the state equation

$$\dot{x} = f(x, u) \tag{2.11}$$

where x and f are column vectors of dimension 'n'. u is a vector of dimension 'r' in general. u can be viewed as input vector. If u is a constant vector, the system is said to be autonomous. If the elements of u are explicit functions of time, t, then the system is said to be non-autonomous. If the initial condition is specified, i.e.

$$x(t_o) = x_o \tag{2.12}$$

then the solution to Eq. (2.11) is expressed as $\phi_t(x_o)$ to show explicitly the dependence on initial condition. (Note that since u is constant it can be treated as parameter and the dependence of the solution on u need not be shown explicitly)

f is called the **vector field** and $\phi_t(x_o)$ is called the **trajectory** through x_o. $\phi_t(x)$ where $x \in R^n$ is called the **flow**

For non-autonomous systems, the trajectory is also a function of time t and is expressed as $\phi_t(x_o, t_o)$ which indicates the solution passes through x_o at t_o.

In what follows, the attention will be focussed only on autonomous systems as power systems can be modelled as autonomous systems.

With some mild restrictions on f, the solution of Eq. (2.11) has the following properties

1. The solution exists for all t

2. At any time t, $\phi_t(x) = \phi_t(y)$ if and only if $x = y$. Also as $\phi_{(t_1+t_2)} = \phi_{t_1} \cdot \phi_{t_2}$, it follows that a trajectory of an autonomous system is uniquely specified by its initial condition and that distinct trajectories do not intersect.

3. The derivative of a trajectory with respect to the initial condition exists and is nonsingular. For t and t_o fixed, $\phi_t(x_o)$ is continuous with respect to initial state x_o.

Equilibrium Points (EP)

An equilibrium point x_e of an autonomous system is a constant solution such that

$$x_e = \phi_t(x_e) \tag{2.13}$$

This implies that equilibrium point satisfies

$$0 = f(x_e, \, u) \tag{2.14}$$

Eq. (2.14) shows that x_e is a function of u.

In general, there are several equilibrium points which are obtained as real solutions of Eq. (2.14).

Stability of Equilibrium Point

An equilibrium point, x_e is said to be asymptotically stable if all nearby trajectories approach x_e as $t \to \infty$. It is unstable if no nearby trajectories remain nearby. An unstable equilibrium point is asymptotically stable in reverse time (as $t \to -\infty$). An equilibrium point is non-stable (also called saddle point) if at least one of the nearby trajectories approach x_e in forward time (as $t \to \infty$) and if at least one trajectory approaches x_e in reverse time (as $t \to -\infty$).

The stability of an equilibrium point can be judged by the solution of the linearized system at x_e.

Letting

$$x = x_e + \Delta x \tag{2.15}$$

and substituting in Eq. (2.11) gives

$$\dot{x} = \dot{x}_e + \Delta\dot{x} = f(x_e, \, u) + \left[\frac{\partial f(x,u)}{\partial x}\right]_{x\,=\,x_e} \Delta x \tag{2.16}$$

From Eqs. (2.14) and (2.16) we get

$$\Delta\dot{x} = [A(x_e, \, u)] \, \Delta x \tag{2.17}$$

where A is a $n x n$ matrix whose elements are functions of x_e and u. The ij^{th} element of $[A]$ is given by

$$A_{ij}(x_e, \, u) = \frac{\partial f_i}{\partial x_j}(x_e, \, u) \tag{2.18}$$

For a given x_e and u, the matrix A is constant. The solution of the linearized state equation (2.17) is given by

$$\Delta x(t) \;=\; e^{A(t-to)}\Delta x(t_o) \tag{2.19}$$

$$\;=\; c_1 e^{\lambda_1 t}v_1 + c_2 e^{\lambda_2 t}v_2 + \cdots + c_n e^{\lambda_n t}v_n \tag{2.20}$$

where c_1, $c_2 \ldots c_n$ are constants depending on the initial conditions. λ_i and v_i are the ith eigenvalue and the corresponding eigenvector of matrix $[A]$. It is assumed that all eigenvalues are distinct.

From Eq. (2.20) it can be seen that if $\Re[\lambda_i] < 0$ for all λ_i, then for all sufficiently small perturbations from the equilibrium point x_e, the trajectories tend to x_e as $t \to \infty$. Hence, x_e is asymptotically stable.

If $\Re[\lambda_i] > 0$ for all λ_i then any perturbation leads to the trajectory leaving the neighbourhood of x_e. Hence x_e is unstable. If there exists i and j such that $\Re[\lambda_i] < 0$ and $\Re[\lambda_j > 0]$ then x_e is a saddle point. If $\Re[\lambda_i] \neq 0$ for all λ_i then the equilibrium point is said to be hyperbolic.

No conclusion can be drawn regarding stability of an equilibrium point if it is not hyperbolic and has no λ_i with real part greater than zero.

A stable or unstable equilibrium point with no complex eigenvalues is called a 'node'.

Remarks

1. For all practical purposes, an equilibrium point which is not stable, can be termed as unstable. For a hyperbolic equilibrium point, the number of eigenvalues with positive real parts determines its type. A type 1 Unstable EP (UEP) has one eigenvalue in the RHP of the 's' plane. An EP with all eigenvalues in the R.H.P. is called a source.

2. Equilibrium points are also termed as fixed points. A Stable EP (SEP) is also called a sink.

Steady-state Behaviour

The steady state behaviour of an autonomous system is obtained from the asymptotic behaviour of the system trajectories assuming that the difference between the trajectory and its steady state is called 'transient'.

It is obvious that stable equilibrium points are subsets of steady state behaviour. In addition, a system may also exhibit **limit cycles**. A limit cycle is an isolated periodic solution (with the trajectory forming a closed curve in state space).

There can be more complex behaviour such as chaos which does not have any fixed pattern in the steady state solution. In general, chaotic systems exhibit sensitive dependence on initial conditions and the spectrum of the steady state solution has a broad-band noise like component [4].

2.3   Analysis of Steady State Stability

The swing equation for system shown in Fig. 2.1 is

$$M\frac{d^2\delta}{dt^2} + D\frac{d\delta}{dt} = P_m - P_{max}\sin\delta \tag{2.21}$$

where

$$P_{max} = \frac{E_g E_b}{(x_g + x_e)} \tag{2.22}$$

Equation (2.21) is same as Eq. (2.9) except for the addition of a damping term $D\dfrac{d\delta}{dt}$. It is assumed that D is small but positive. It can be ignored when the solution of the swing equation is required only for a short period (say 1 to 2 seconds) following a disturbance. Hence D can be neglected in transient stability analysis but needs to be considered in steady state stability analysis.

Equation (2.21) can be expressed in the state space form as

$$\begin{aligned}
\frac{dx_1}{dt} &= x_2 \\
\frac{dx_2}{dt} &= -\frac{D}{M}x_2 - \frac{P_{max}}{M}\sin x_1 + \frac{P_m}{M}
\end{aligned} \tag{2.23}$$

where

$$x_1 = \delta, \ x_2 = \frac{d\delta}{dt}$$

The equilibrium points for the sytem of Eq. (2.23) are given by

$$\left.\begin{aligned}
x_2 &= 0 \\
x_1 &= \sin^{-1}\frac{P_m}{P_{max}}
\end{aligned}\right\} \tag{2.24}$$

From the power angle curves shown in Fig. 2.3, it can be seen that there are two values of δ corresponding to a specified value of P_m (when $P_m < P_{max}$) when the range of δ is confined to $-180^o < \delta < 180^o$. Thus, there are two equilibria given by

$$\left.\begin{aligned}
x_e^1 &= x_s = (\delta_s, 0) \\
x_e^2 &= x_u = (\delta_u, 0)
\end{aligned}\right\} \tag{2.25}$$
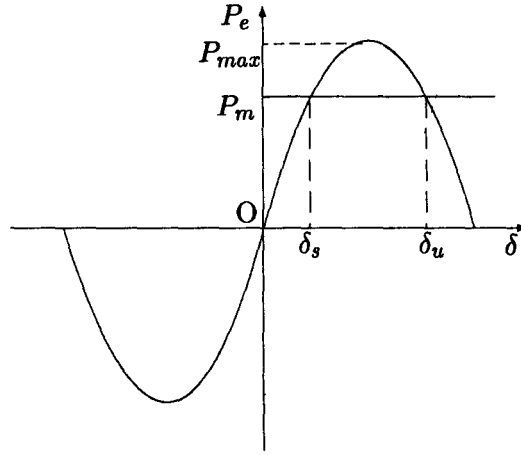
Figure 2.3: Power angle curve

It can be shown by linearizing Eq. (2.23) that x_s is a stable equilibrium point and x_u is the unstable equilibrium point. The criterion for stability is an algebraic one given by

$$\frac{dP_e}{d\delta} > 0 \tag{2.26}$$

Proof : Let $y_1 = \Delta x_1$, $y_2 = \Delta x_2$
Then,

$$\begin{bmatrix} \dot{y}_1 \\ \dot{y}_2 \end{bmatrix} = \begin{bmatrix} 0 & 1 \\ -\dfrac{K}{M} & -\dfrac{D}{M} \end{bmatrix} \begin{bmatrix} y_1 \\ y_2 \end{bmatrix} \tag{2.27}$$

where

$$K = P_{max} \cos \delta_e \tag{2.28}$$

δ_e is the angle at equilibrium (δ_s or δ_u)

The eigenvalues of the linearized system are given by

$$\lambda = -\frac{D}{2M} \pm \sqrt{\frac{D^2}{4M^2} - \frac{K}{M}} \tag{2.29}$$

If K is positive then both eigen values have negative real parts. If K is negative one of the eigenvalues is positive real. For small D, and $K > 0$ eigenvalues are complex given by

$$\lambda = -\sigma \pm j\omega \tag{2.30}$$

where

$$\sigma = \frac{D}{2M}, \quad \omega = \sqrt{\frac{K}{M} - \frac{D^2}{4M^2}}$$

Hence, for the stability of the equilibrium point, a necessary condition is

$$K > 0 \tag{2.31}$$

Remarks

1. The expression for K in the general case is given by

$$K = \frac{dP_e}{d\delta}(\delta_e) \tag{2.32}$$

   This shows explicitly the dependence of K on (δ_e). In general, P_e can be a non-sinusoidal function of δ, although for the special case considered (neglecting losses and saliency) the power angle curve is sinusoidal.

2. For $\delta_e = \delta_s$, $K > 0$ while for $\delta_e = \delta_u$, $K < 0$. Hence x_s is a stable equilibrium point while x_u is unstable (a saddle point).

3. The two equilibrium points come closer as P_m (also equal to the steady state power output of the generator) is increased. The maximum power supplied by the generator (steady-state stability limit) is equal to P_{max} and occurs at $\delta^* = 90^o$ (in this particular case). The condition for stability can also be stated as

$$\delta_s < \delta^* \tag{2.33}$$

   The loci of eigenvalues in the s plane as P_m is varied is shown in Fig. 2.4. Fig. 2.4 (a) shows the loci of eigenvalues calculated at SEP (Stable Equilibrium Point). The eigenvalues are initially complex and split into two real values. One of them reaches origin as P_m is increased to P_{max} (when $K = 0$). The other eigenvalue approaches $\left(\frac{-D}{M}\right)$.

   Figure 2.4 (b) shows the loci for UEP (Unstable Equilibrium Point). Here both eigenvalues are real. As P_m increases, both move towards the origin. At $P_m = P_{max}$ one of the values is exactly zero while the other is $\left(-\frac{D}{M}\right)$.

It is to be noted that for $P_m > P_{max}$ there is no equilibrium.

Comments

1. The stability criterion given in (2.26) is an algebraic one. While this is simple and convenient (avoids computation of eigenvalues) it is to be

(a) at SEP   (b) at UEP
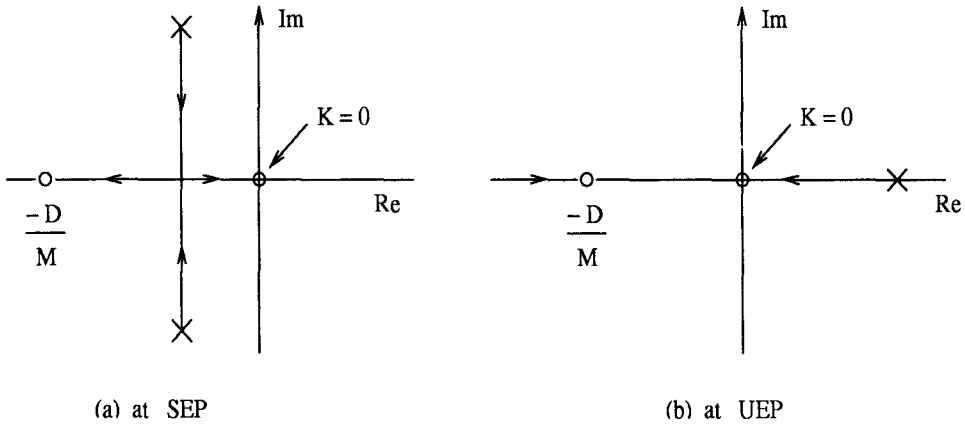
Figure 2.4: Loci of eigenvalues

noted that this is derived from dynamic analysis. Hence the extension of this criterion to more complex dynamics (with the relaxation of some of the assumptions given earlier) is not valid. For the general case, the mathematical analysis involving linearization of the system and checking of the system stability cannot be avoided. (It is to be noted that in simple cases, the stability of linear systems can be directly determined, without recourse to eigenvalue computations, i.e. Routh-Hurwitz and Nyquist criteria. However, these still require the knowledge of system equations).

2. It is interesting to note that the limit of steady state stability using the classical model is also equal to the maximum power transferred in the network (neglecting losses). In other words the steady state stability limit is also the network limit. As it would be practical to maintain stability margin, the network limit must be larger than the maximum power output of the generator.

3. The criterion of $\frac{dP_e}{d\delta} > 0$, can also be derived from 'physical' arguments. If P_m is suddenly increased by a small amount, the rotor initially accelerates (as δ cannot change suddenly). As the velocity and consequently δ increase, the electric power output also increases (if the system is stable) for an equilibrium to be reached. For this to be possible, P_e should increase with increase in δ . Similar arguments apply if P_m is suddenly decreased.

It is to be noted that such 'physical' arguments, although intuitively appealing, can sometimes lead to false conclusions. It will be shown in chapter 7 that the consideration of detailed model of the synchronous generator leads to different criteria for stability than given by (2.26).
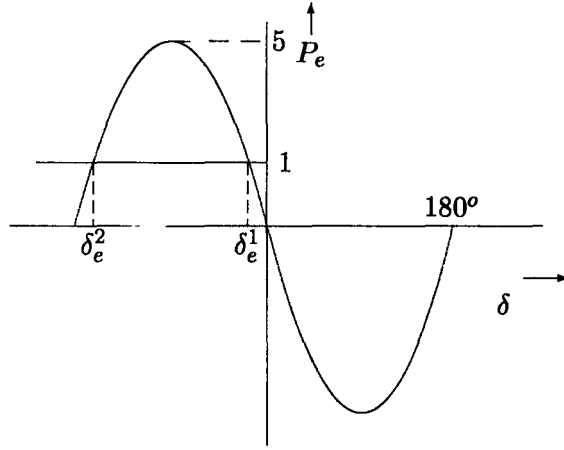
Figure 2.5: Power angle curve for Example 2.1

Example 2.1

A generator is connected to an infinite bus through an external impedance of jx_e. The generator is represented by a voltage source $E_g \angle \delta$ in series with a reactance x_g. If $E_g = E_b$ (infinite bus voltage) = 1.0, $x_e = -0.5$, $x_g = 0.3$ (all in p.u.), for $P_b = 1.0$ p.u., find the equilibrium values of δ, in the range of $(-\pi, \pi)$. Test their stability (P_b is the received power at the infinite bus). Assume infinite bus angle as zero.

Solution

The expression for the electrical power output, P_e is given by

$$P_e = \frac{E_g E_b \sin \delta}{(x_e + x_g)} = P_b$$

Substituting the values for E_g, E_b, x_e and x_g,

$$P_e = -5 \sin \delta$$

The power angle curve is shown if Fig. 2.5. For $P_b = P_e = 1.0$ pu., the equilibrium points are

$$\delta_e^1 = -11.54^o, \quad \delta_e^2 = -168.46^o$$

Testing for stability, .

$$\left. \frac{dP_e}{d\delta} \right|_{\delta=\delta_e^1} = -5 \, \cos \delta_e' \; < \; 0$$

$$\left. \frac{dP}{d\delta} \right|_{\delta=\delta_o^2} = -5 \, \cos \delta_e^2 \; > \; 0$$

Hence, $\delta_e^1 = -11.54^o$ is an unstable equilibrium point (UEP) and $\delta_e^2 = -168.46^o$ is a stable equilibrium point (SEP).

Note that whenever $(x_e + x_g) > 0$, the SEP corresponds to the solution with smaller absolute value of δ, while for $(x_e + x_g) < 0$, SEP corresponds to the solution with larger absolute value of δ. The current supplied by the generator (and losses) are higher for the case with larger (absolute) angle. Hence, it is fortunate that, for all practical purposes, the external reactance is positive (inductive), viewed from generator terminals. This results in lower losses as compared to the case if the net reactance was capacitive.

Note that, negative x_e can result from overcompensation of the transmission line reactance using series capacitors (although this is never done in practice).

Example 2.2

Repeat example (2.1) if the external impedance connected to the generator, $Z_e = 0.1 + j0.2$. The rest of the data is same as before.

Solution

The expression for the received power, P_b, can be obtained as

$$P_b = \frac{E_g E_b \sin(\delta + \alpha)}{\mid Z \mid} - \frac{E_b^2 R}{\mid Z \mid^2}$$

where $Z = Z_e + jx_g = R + jX = \mid Z \mid \angle \phi$, $\alpha = 90 - \phi$.

Note: $\tan \alpha = \dfrac{R}{X}$, $\mid Z \mid = (R^2 + X^2)^{\frac{1}{2}}$, $\phi = \tan^{-1} \dfrac{X}{R}$

The sending end power, P_e is given by $P_e = \dfrac{E_g^2 R}{\mid Z \mid^2} + \dfrac{E_g E_b}{\mid Z \mid} \sin(\delta - \alpha)$

Substituting values for $E_g = E_b = 1.0$, $R = 0.1$, $X = 0.5$, $\mid Z \mid = 0.51$, $\alpha = 11.3^o$ we get two values for $(\delta + \alpha)$ as

$$\begin{aligned} \delta_e^1 + \alpha &= 44.9^o &\implies& \delta_e^1 = 33.6^o \\ \delta_e^2 + \alpha &= 135.1^o &\implies& \delta_e^2 = 123.8^o \end{aligned}$$

It can be checked that $\dfrac{dP_e}{d\delta}(\delta = \delta_e^1) > 0$ while $\dfrac{dP}{d\delta}(\delta = \delta_e^2) < 0$. Hence $\delta_e^1 = 33.6^o$ is a SEP while $\delta_e^2 = 123.8^o$ is an UEP.

Example 2.3

Repeat example 2.2 if $P_b = 1.546$

Solution

The equilibrium values for δ, in this case are
$$\delta_e^1 = 80^o - 11.3^0 = 68.7^o$$
$$\delta_e^2 = 100^0 - 11.3^o = 88.7^o$$

It can be checked that at both values of δ, the system is stable. There are two SEPs in this case.

Note: The system is stable for $\delta \leq 90^o + \alpha = 101.3^o$, while the maximum received power corresponds to $\delta = 90 - \alpha = 78.7^o$.

Example 2.4

Find the level of series compensation that will maximize the received power in a single machine system shown in Fig. 2.6. The generator impedance is assumed to be $Z_g = R_g + jx_g$.
Assume $E_g = E_b = 1.0$, $R_e = 0.1$, $x_e = 1.0$, $x_g = 0.1$, $R_g = 0.0$.
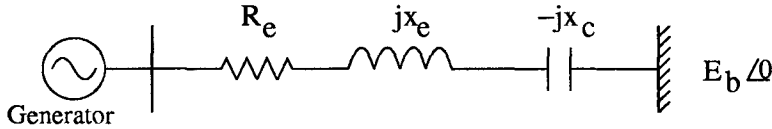
Figure 2.6: System diagram for Example 2.4

Solution

Let $Z = R + jX = Z_e + Z_g = (R_g + R_e) + j(x_g + x_e - x_c)$. The receiving end power is maximum when
$$\delta = 90 - \alpha, \quad \alpha = \tan^{-1}\frac{R}{X}$$

Hence, P_b for this condition is given by
$$P_{bm} = \frac{E_g E_b}{|Z|} - \frac{E_b^2 R}{(|Z|)^2} = \frac{E^2}{R}[\cos\phi - \cos^2\phi]$$

where $E_g = E_b = E$ and $|Z| = R/\cos\phi$

P_{bm} is a function of ϕ which is variable as x_c varies. P_{bm} is maximized for $\cos\phi^* = \frac{1}{2}$ or $\phi^* = 60^o$. The maximum received power is given by

$$P_{bmax} = \frac{E^2}{4R} = \frac{1.0}{4 \times 0.1} = 2.5 \text{ pu}$$

This corresponds to $\delta^* = 90 - \alpha^* = 90 - 30^o = 60^o$. The optimum value of x_c is given by

$$x_c^* = -R \tan \phi^* + x_e + x_g = -\sqrt{3}R + x_e + x_g = 0.927 \quad \text{pu}$$

Example 2.5

Consider the system shown in Fig. 2.7. The generator G has negligible impedance while the SVC can be represented by a voltage source E_s in series with a reactance X_s. Obtain expression for $\mid V \mid$ and P_e as function of E, E_s and δ.

Solution

At the SVC bus, the system external to the SVC can be represented by a Thevenin's equivalent shown in Fig. 2.8(a). The combined equivalent circuit of the external system and the SVC is shown in Fig. 2.8(b).
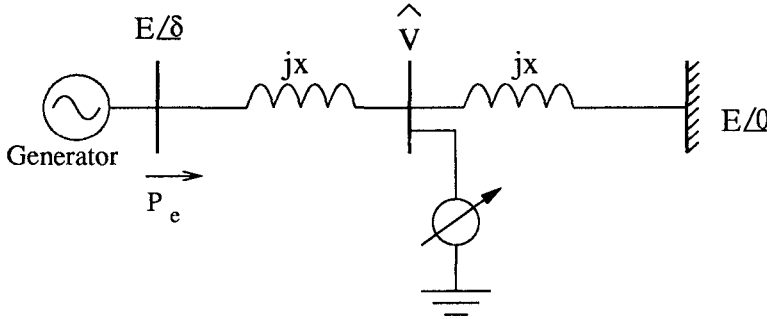
Figure 2.7: System diagram for Example 2.5

The current flowing into SVC is I_s. Since this current is purely reactive (there are no losses), the phase angle of $\hat{E}_s$ is same as that of $\hat{V}_{Th}$. It can be shown that

$$\hat{V}_{Th} = E \cos(\delta/2) \angle \delta/2$$

(The phasor diagram for the condition when SVC is open circuited is shown in Fig. 2.9). The current magnitude is given by

$$\mid I_s \mid = \frac{(E \cos(\delta/2) - E_s)}{(x_s + x/2)}$$

The voltage $\hat{V}$ has the phase angle of $\delta/2$ and its magnitude is given by
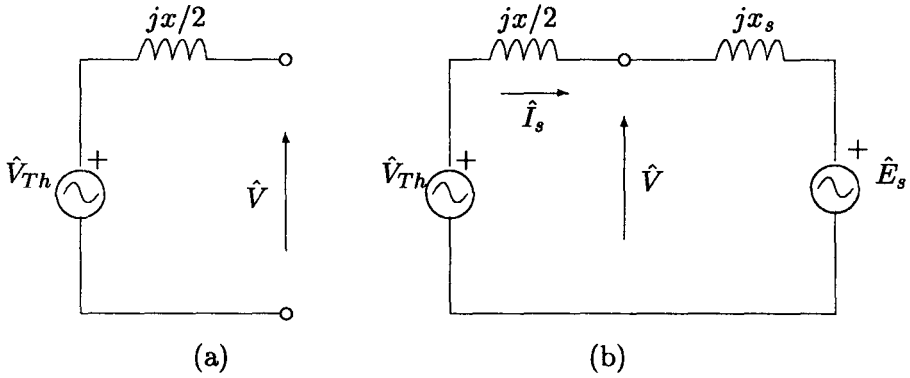
Figure 2.8: (a) Thevenin's equivalent for the external system (Example 2.5) (b) Combined equivalent circuit including SVC
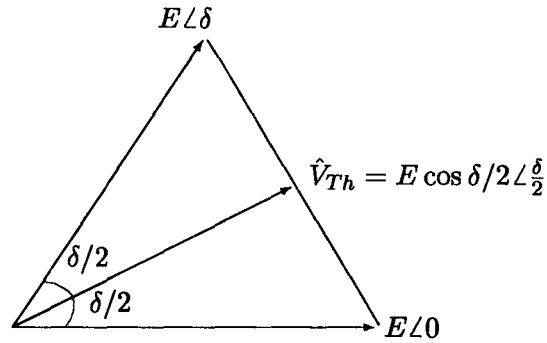
Figure 2.9: Phasor diagram with SVC on open circuit (Example 2.5)

$$V = E_s + \mid I_s \mid x_s = \frac{E_s \dfrac{X}{2}}{(x_s + x/2)} + \frac{E x_s \cos(\delta/2)}{(x_s + x/2)}$$

The expression for P_e is

$$P_e = \frac{EV \sin(\delta/2)}{x}$$

Substituting the expression of V in the above expression gives

$$P_e = \frac{EE_s}{(x + 2x_s)} \sin(\delta/2) + \frac{E^2 x_s \sin\delta}{x(2x_s + x)}$$

Note that if $x_s = 0$, then P_e reduces to

$$P_e = \frac{EE_s}{x} \sin(\delta/2)$$

Comparing this with the expression for P_e in the absence of SVC, given by

$$P_e = \frac{E^2}{2x} \sin \delta$$

it is seen that the SVC results in doubling of the maximum power if $E_s = E$. (Note that $x_s = 0$ corresponds to an ideal SVC).

Example 2.6

In the above example, if $E = E_s = 1.0$, $x = 0.5$, $x_s = 0.2$. Find the stability limit for P_e and the corresponding δ. Repeat for the case when $x_s = 0.0$.

Solution

(a) $P_e = A \sin(\delta/2) + B \sin \delta$

where $A = \dfrac{E\,E_s}{x + 2x_s} = 1.111$, $B = \dfrac{E^2 x_s}{x(x + 2x_s)} = 0.444$

The power is maximum when

$$\frac{dP}{d\delta} = 0 = \frac{1}{2} A \cos(\delta/2) + B \cos \delta$$

Let $x = \cos(\delta/2)$, then

$$\frac{dP}{dt} = 0 \implies 2Bx^2 + \frac{A}{2}x - B = 0$$

The solution of this quadratic equation for x is given by

$$x = \frac{-\dfrac{A}{2} + \sqrt{\dfrac{A^2}{4} + 8B^2}}{4B}$$

(only the positive solution for x is considered so that $\delta/2$ remains less than 90°). Substituting the values,

$$x^* = \cos \frac{\delta^*}{2} = 0.4606 \implies \delta^* = 125.2^o$$

and

$$P_{emax} = 1.111 \sin \frac{125.2}{2} + 0.444 \, \sin 125.2 = 1.3492 \quad \text{p.u.}$$

The power angle curves for this case is shown in Fig. 2.10. (Curve a)
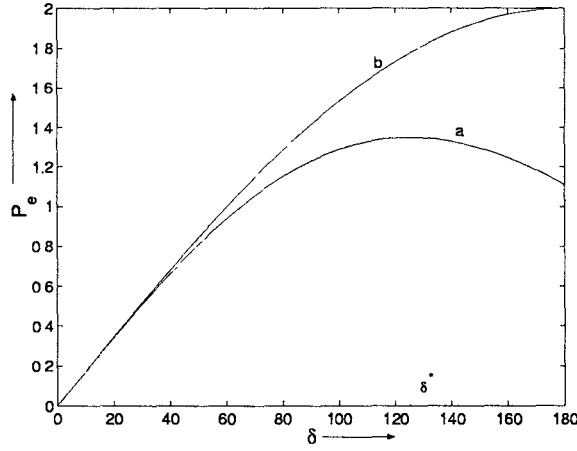
Figure 2.10: Power angle curve for Example 2.6

(b) For $x_s = 0.0$,

$$P_e = \frac{EE_s}{x} \sin \frac{\delta}{2} = 2 \sin \frac{\delta}{2}$$

P_e is maximum when $\delta = 180^o$ and the maximum power at stability limit is

$$P_{emax} = 2.0 \ p.u.$$

The power angle curve for this case is also shown in Fig. 2.10. (Curve b)

Example 2.7

A generator is supplying power to a load centre through a transmission line as shown in Fig. 2.1. The power output of the generator is increased slowly while maintaining the magnitudes of the voltages V_1 and V_2 constants at 1.0 p.u. by manual control (of both generator excitation and infinite bus voltage). Find the steady state stability limit of power that can be transmitted. Assume $x_t = 0.1$, $x_l = 0.4$, $Z_T = j0.1$, $x_g = 0.3$.

Solution

The equivalent circuit for the system is shown in Fig. 2.11 where

$$x_1 = x_g, \quad x = x_t + x_l, \quad x_2 = \Im[Z_T]$$

Note that the system is lossless. The expression for power P_e is given by

$$P_e = \frac{E_g E_b \sin \delta}{(x_1 + x + x_2)}$$
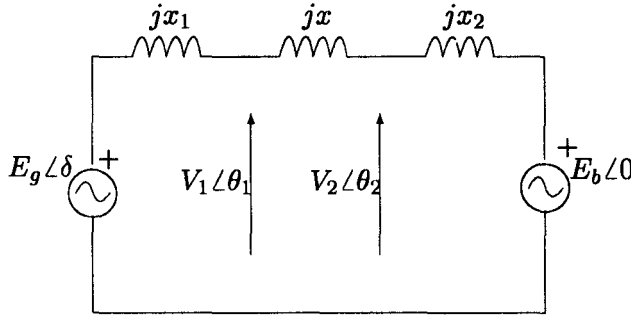
Figure 2.11: Equivalent circuit for Example 2.7

However, the above expression cannot be used directly as E_g and E_b are unknown. The phasor diagram at the stability limit ($\delta = 90^o$) is shown in Fig. 2.12. It is easy to see that at the stability limit,

$$P_e = \frac{E_g V_1}{x_1} \sin(90 - \theta_1) = \frac{E_g V_2}{(x + x_1)} \sin(90 - \theta_2)$$

from which,

$$\frac{V_1}{x_1} \cos \theta_1 = \frac{V_2}{(x + x_1)} \cos \theta_2 \qquad (A)$$

Also,

$$P_e = \frac{E_b V_1 \sin \theta_1}{(x + x_2)} = \frac{E_b V_2 \sin \theta_2}{x_2}$$

from which,

$$\frac{V_1 \sin \theta_1}{(x + x_2)} = \frac{V_2 \sin \theta_2}{x_2} \qquad (B)$$

From the two relations (A) and (B) we have

$$\left. \begin{array}{l} \sin \theta_1 = a \sin \theta_2 \\ \cos \theta_1 = b \cos \theta_2 \end{array} \right\} \qquad (C)$$

where

$$a = \frac{V_2}{V_1} \frac{(x + x_2)}{x_2}, \quad b = \frac{V_2}{V_1} \frac{x_1}{(x + x_1)}$$

Substituting (C) in the following equation

$$\sin^2 \theta_1 + \cos^2 \theta_1 = 1 \qquad (D)$$
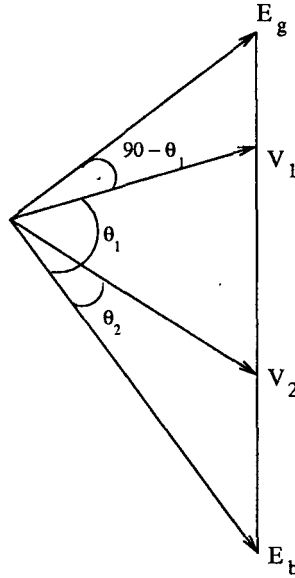
Figure 2.12: Phasor diagram at stability limit (example 2.7)

we get,

$$a^2 \sin^2 \theta_2 + b^2 \cos^2 \theta_2 = 1$$
$$(a^2 - b^2) \sin^2 \theta_2 = 1 - b^2$$

In the example, $x_1 = 0.3$, $x_2 = 0.1$, $x = 0.5$, $V_1 = V_2 = 1.0$

$$a = \frac{0.5 + 0.1}{0.1} = 6.0, \quad b = \frac{0.3}{0.8} = 0.375$$

$$\sin \theta_2 = \sqrt{\frac{(1 - b^2)}{(a^2 - b^2)}} = 0.1548, \quad \theta_2 = 8.91^o$$

$$\sin \theta_1 = 6 \sin \theta_2 = 0.9288, \quad \theta_1 = 68.25$$

The stability limit is also given by

$$P_{emax} \quad = \quad \frac{V_1 V_2}{x} \sin(\theta_1 - \theta_2)$$

$$= \quad \frac{1.0}{0.5} \sin(68.25^0 - 8.91^o) = 1.7204 \quad \text{pu.}$$

E_g and E_b can be calculated from

$$P_{emax} = \frac{E_g V_1}{x_1} \cos \theta_1 = \frac{E_b V_1 \sin \theta_1}{(x + x_2)}$$

The values are $E_g = 1.393$, $E_b = 1.111$. It can be verified that

$$P_{emax} = \frac{E_g E_b}{(x_1 + x + x_2)}$$

2.4   Analysis of Transient Stability

The transient stability pertains to stability under large disturbances. Hence the nonlinearities of the model have to be considered in the analysis. As analytic solutions are not available for the swing equation, numerical methods have to be used.

2.4.1   Numerical solution - Point-by-Point Method:

Point-by-point (also called step-by-step) solution allows the numerical solution of the swing equation. In this method, one or more variables are assumed to remain constant or to vary according to assumed laws throughout a short interval of time Δt.

The swing equation, neglecting damping term can be written as

$$\left.\begin{array}{rcl} \dfrac{d\delta}{dt} & = & \omega \\[3mm] \dfrac{d\omega}{dt} & = & \dfrac{P_a}{M} \end{array}\right\} \tag{2.34}$$

where $P_a = P_m - P_e$ is the accelerating power.

If over an interval (say k^{th}, defined from the instant $t_{(k-3/2)}$ to $t_{(k-1/2)}$) the accelerating power P_a is assumed to be constant (at the value computed at $t_{(k-1)}$) then

$$\omega_{(k-1/2)} = \omega_{(k-3/2)} + \frac{\Delta t}{M} P_{a(k-1)} \tag{2.35}$$

If the speed calculated at $t_{(k-1/2)}$ is assumed to be constant throughout the interval from $t_{(k-1)}$ to t_k (see Fig. 2.13), then

$$\delta_k = \delta_{(k-1)} + \omega_{(k-1/2)} \Delta t \tag{2.36}$$

Defining

$$\Delta \delta_k = \delta_k - \delta_{(k-1)}$$

(a)   (b)
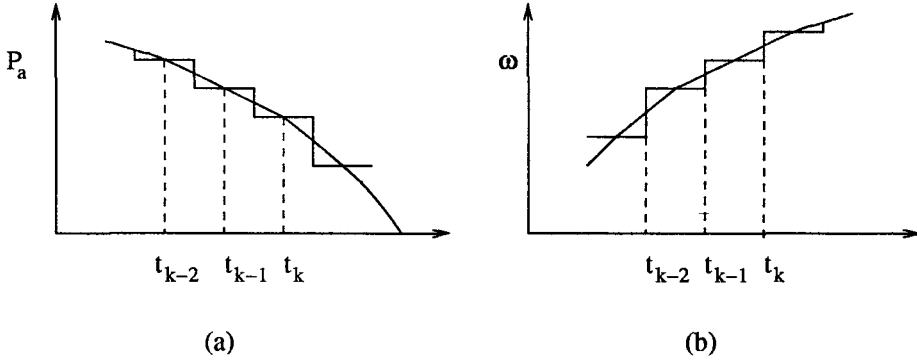
Figure 2.13: Discretization of accelerating power and speed (point by point method)

we can express

$$\Delta \delta_k = \Delta \delta_{(k-1)} + \frac{(\Delta t)^2}{M} P_{a(k-1)} \qquad (2.37)$$

Eq. (2.37) enables the computation of angle directly without recourse to the computation of the speed.

In executing step-by-step method, it is to be noted that if a discontinuity in the accelerating power occurs at the beginning of the interval (due to fault or switching action) then average value of P_a must be used. For example, if a fault occurs at t_o, then

$$\Delta \delta_1 = \frac{(\Delta t)^2}{M} \frac{P_a(t_o^+)}{2} \qquad (2.38)$$

2.4.2 Equal area Criterion

To check the stability of a single machine infinite bus (SMIB) system, there is a simple and direct method which does not require the solution of the swing equation following disturbance(s). This method is known as equal-area criterion for stability. The assumptions used in applying this criterion are

1. Constant mechanical power

2. No damping

3. Classical machine model

The basis for this method is that if the system is stable (in the first swing)the rotor angle (after the disturbance) reaches a maximum value (assum-

ing that the rotor initially accelerates) and then oscillates about the final steady state value. (It is also assumed that a stable steady state equilibrium exists for the post-disturbance system). Hence the stability is checked by monitoring the deviation of the rotor speed $\left(\dfrac{d\delta}{dt}\right)$ and ensuring that it becomes zero following the disturbance.

Let the swing equation be given by

$$M\frac{d^2\delta}{dt^2} = P_a = P_m - P_e \tag{2.39}$$

Multiplying both sides by $\dfrac{d\delta}{dt}$ and integrating with respect to time, we get

$$M\int_{t_o}^{t} \frac{d\delta}{dt}\frac{d^2\delta}{dt^2}dt = \int_{t_o}^{t}(P_m - P_e)\frac{d\delta}{dt}dt \tag{2.40}$$

or

$$\frac{1}{2}M\left(\frac{d\delta}{dt}\right)^2 = \int_{\delta_o}^{\delta}(P_m - P_e)d\delta \tag{2.41}$$

It is assumed at $t = t_o$, the system is at rest (equilibrium state) and the speed deviation is zero. The R.H.S. of Eq. (2.41) can be interpreted as the area between the curves P_m versus δ and the curve P_e versus δ . P_m versus δ is a horizontal line as P_m is assumed to be constant. The curve of P_e versus δ (power angle curve) is shown in Fig. 2.14. If the system is to be stable, then

$$\left.\frac{d\delta}{dt}\right|_{\delta=\delta_{max}} = 0, \tag{2.42}$$

This implies that the area denoted by

$$A = \int_{\delta_o}^{\delta_{max}}(P_m - P_e)d\delta \tag{2.43}$$

must have a positive portion A_1 for which $P_m > P_e$ and a negative portion A_2 for which $P_m < P_e$. The magnitudes A_1 and A_2 must be same as

$$A = A_1 - A_2 = 0 \tag{2.44}$$

Hence the nomenclature of equal-area criterion for stability.

Remarks

1. The equal area criterion is also applicable for a two machine system (without an infinite bus) as it can be converted into a single machine equivalent.
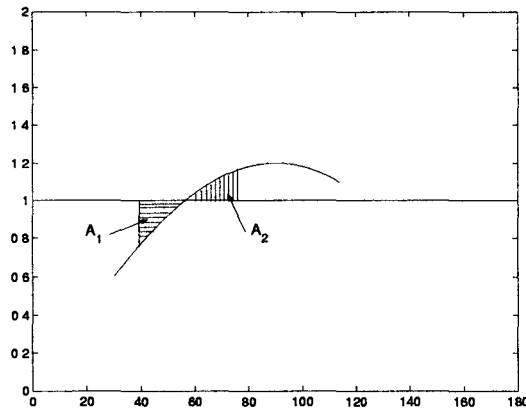
Figure 2.14: Equal area criterion for stability

2. It will be shown later (in chapter 13) that equal- area criterion for stability is a special case of the direct method for stability evaluation using energy functions.

3. Mathematically, the problem of determination of transient stability can be viewed as checking whether the initial system state for the post-fault condition, lies in the region of stability surrounding the post-fault stable equilibrium point. Every SEP has a region of stability (which may be unbounded) or attraction, in which a trajectory approaches SEP as $t \to \infty$. A trajectory starting outside the region of stability will not approach SEP and may even be unbounded. The determination of stability boundary is a complex task. The use of energy functions (discussed in chapter 13) helps to approximate the stability boundary for a given fault or disturbance.

Example 2.8

Transform a two machine system shown in Fig. 2.15 to an equivalent single machine system
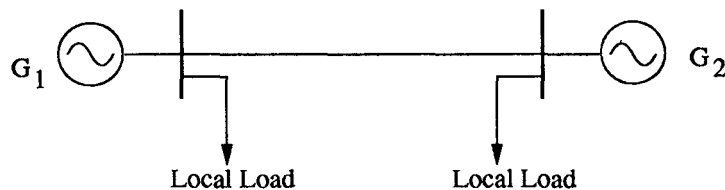
Figure 2.15: A two machine system (Example 2.8)

Solution

The swing equations for the two machines are

$$M_1 \frac{d^2\delta_1}{dt^2} = P_{m1} - P_{e1} \qquad (A)$$

$$M_2 \frac{d^2\delta_2}{dt^2} = P_{m2} - P_{e2} \qquad (B)$$

It can be shown, in general, that both P_{e1} and P_{e2} are functions of a single variable $(\delta_{12} = \delta_1 - \delta_2)$. The expressions can be derived from the equivalent circuit shown in Fig. 2.16 where loads are represented as constant admittances Y_1 and Y_2. Neglecting local loads and losses in the transmission line $(Z = jx)$, the expressions for P_{e1} and P_{e2} are given by

$$P_{e1} = -P_{e2} = \frac{E_{g1}E_{g2}}{(x_{g1} + x + x_{g2})} \sin \delta_{12}$$

Multiplying both sides of the Eq. (A) by M_2 and Eq. (B) by M_1 and subtracting, we get

$$M_1 M_2 \frac{d^2\delta_{12}}{dt^2} = (M_2 P_{m1} - M_1 P_{m2}) - (M_2 P_{e1} - M_1 P_{e2}) \qquad (C)$$

If $P_{e1} = -P_{e2}$, we can simplify (C) as
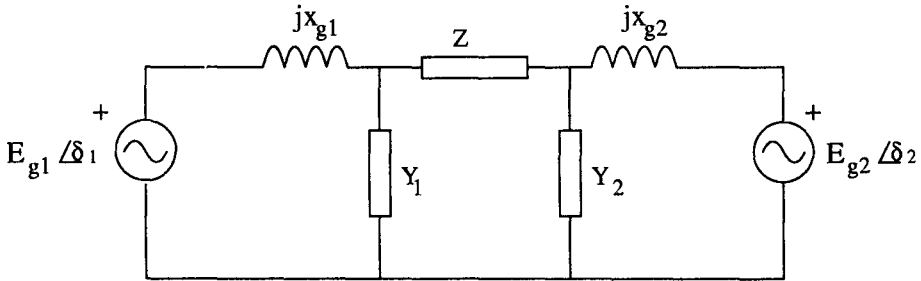
Figure 2.16: Eqivalent circuit (Example 2.8)

$$M_{eq} \frac{d^2\delta_{12}}{dt^2} = P_m^{eq} - P_e^{eq}$$

where

$$M_{eq} = \frac{M_1 M_2}{M_1 + M_2}, \quad P_m^{eq} = \frac{M_2 P_{m1} - M_1 P_{m2}}{M_1 + M_2}, \quad P_e^{eq} = P_{e1} = -P_{e2}$$

Note that if x_{g1} and x_{g2} are small compared to x, the local loads can be accounted by subtracting them from the respective mechanical powers.

Example 2.9

A single machine is connected to a load centre through a transmission line as shown in Fig. 2.17. The load centre is represented by a reactance connected to an infinite bus. The generator is initially operating with $P_e = 1.0$ pu. and the magnitude of voltages V_1 and V_2 are 1.0 p.u. each. Find the maximum step increase in the mechanical power that will not cause transient instability. Use equal area criterion. Assume $x_g = 0.3$, $x_t = 0.1$, $x = 0.4$, $x_2 = 0.1$.
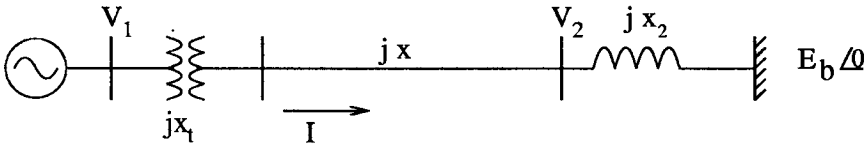
Figure 2.17: System diagram for Example 2.9

Solution

At the initial operating point,

$$P_e = \frac{V_1 V_2}{(x_t + x)} \sin(\theta_1 - \theta_2)$$

where θ_1 and θ_2 are angles of the voltages $\hat{V}_1$ and $\hat{V}_2$. Substituting values of $P_e = 1.0$, $V_1 = V_2 = 1.0$, $x_t + x = 0.5$, we get

$$\theta_1 - \theta_2 = 30^o$$

The current $\hat{I}$ in the line, referred to $\hat{V}_2$ is

$$\hat{I}e^{-j\theta_2} = \frac{1.0\angle 30 - 1.0\angle 0}{j0.5} = 1.0 + j0.27$$

$$E_b e^{-j\theta_2} = V_2 - jx_2\hat{I}e^{-j\theta_2} = 1.0 - j0.1(1.0 + j0.27)$$
$$= 1.032\angle -5.56^o$$

Hence, $\theta_2 = 5.56^o$ and $\theta_1 = 35.56^o$.

$$E_g\angle\delta = \hat{V}_1 + jx_g\hat{I} = 1.0\angle 35.56 + j0.3(1.0 + j0.27)\,e^{j5.56}$$
$$= 1.121\angle 51.1^o$$

The power P_e is given by the expression
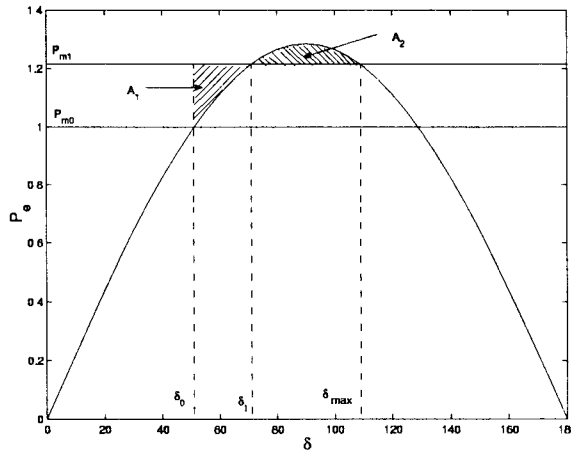
Figure 2.18: Application of equal area criterion (Example 2.9)

$$P_e = P_{max} \sin \delta \quad \text{where} \quad P_{max} = 1.121 \; . \; 1.032/0.9 = 1.285$$

The initial value of $P_m = P_{mo} = 1.0$. If P_m is increased from P_{mo} to P_{m1}, the stable equilibrium value of δ changes from $\delta_o(51.1^o)$ to δ_1 (see Fig. 2.18).

When there is a step increase in P_m the machine accelerates and over-shoots the equilibrium angle δ_1. Let the maximum angle reached be δ_{max}. For critically stable case, $\delta_{max} = \pi - \delta_1$ (see Fig. 2.18). From equal area criterion, the ares A_1 and A_2 are equal

$$
\begin{aligned}
A_1 &= \int_{\delta_o}^{\delta_1} (P_{m1} - P_{max} \sin \delta) d\delta \\
&= -P_{max}[\cos \delta_o - \cos \delta_1] + P_{m1}(\delta_1 - \delta_o) \\
A_2 &= \int_{\delta_1}^{\pi - \delta_1} (P_{max} \sin \delta - P_{m1}) d\delta \\
&= 2P_{max} \cos \delta_1 - P_{m1}(\pi - 2\delta_1)
\end{aligned}
$$

Equating A_1 and A_2, we get

$$P_{m1}(\pi - \delta_1 - \delta_o) = P_{max}[\cos \delta_1 + \cos \delta_o]$$

Since,

$$
\begin{aligned}
P_{m1} &= P_{max} \sin \delta_1, \\
\sin \delta_1(\pi - \delta_1 - \delta_o) &= (\cos \delta_1 + \cos \delta_o)
\end{aligned}
$$

The solution of this nonlinear equation is

$$\delta_1 \simeq 71^o, \quad P_{m1} = 1.215$$

The maximum step increase $= 0.215$ p.u.

Example 2.10

Find the critical clearing angle and time for a three phase fault at the generator terminals in Example 2... The generator is initially supplying power of 1.0 p.u. Assume that the postfault system is identical to the pre-fault system. Additional data: $H = 4 \quad f_B = 50Hz$.

Solution

The power angle curve is shown in Fig. 2.19. During fault, $P_e = 0$ and after the fault is cleared

$$P_e = P_{max} \sin \delta, \quad P_{max} = 1.285$$

For the critically cleared fault, the two areas A_1 and A_2 (shown in Fig. 2.19)
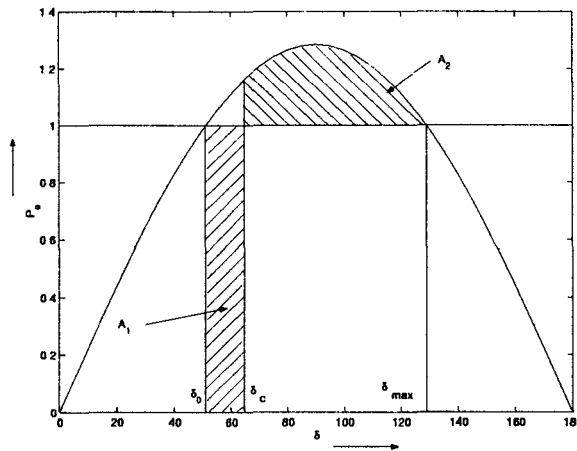
Figure 2.19: Application of equal area criterion (Example 2.10)

must be equal and $\delta_{max} = \pi - \delta_o$

$$A_1 = \int_{\delta_o}^{\delta_c} P_m d\delta = P_m(\delta_c - \delta_o) = P_{max} \sin \delta_o(\delta_c - \delta_o)$$

$$A_2 = \int_{\delta_c}^{\pi-\delta_o} (P_{max} \sin \delta - P_m)d\delta = P_{max}[\cos \delta_c + \cos \delta_o] - P_m(\pi - \delta_o - \delta_c)$$

Equating A_1 and A_2,

$$\sin \delta_o(\delta_c - \delta_o) = [\cos \delta_c + \cos \delta_o] - \sin \delta_o(\pi - \delta_o - \delta_c)$$

Solving for δ_c (critical clearing angle), we get

$$\cos \delta_c = \sin \delta_o(\pi - 2\delta_o) - \cos \delta_o$$

Substituting $\delta_o = 0.892$ rad, we can solve for δ_c as

$$\delta_c = 64.6^o = 1.127 \;\; rad$$

During the fault,

$$\delta = \delta_o + \frac{1}{2}\frac{P_m t^2}{M}, \quad M = \frac{H}{\pi f_B}$$

Substituting $\delta = \delta_c$, we can solve for the critical clearing time, t_c

$$t_c = \sqrt{\frac{2H(\delta_c - \delta_o)}{\pi P_m f_B}} = 0.11 \;\; \text{sec}$$

2.5 Simplified Representation of Excitation Control

In the 'classical' approach for dynamic analysis, the excitation controllers were neglected. This is in view of the fact that slow manual control was used till early fifties for voltage regulation. With the introduction of electronic regulators and field forcing, it was necessary to include the effect of continuous excitation control using automatic voltage regulators based on feedback principle.

The terminal voltage V_g, in general, varies as a function of the power output P_e of the generator. An approximate linear relationship between V_g and P_e can be expressed as

$$V_g = V_{go}(1 - b_p P_e) \tag{2.45}$$

where b_p may be termed as power regulation coefficient of the network. Note that $b_p > 0$, as the voltage decreases with increase in power. The coefficient b_p depends on the method of regulation used. Under ideal conditions with fast (instantaneous) regulation of the terminal voltage, $b_p = 0$. However, the voltage regulation has to act through the field circuit having a large time constant and b_p is non-zero.

Assuming that the generator is connected to an infinite bus (of voltage E_b) through (net) reactance of x_e, the power transmitted is given by

$$
\begin{aligned}
P_e &= \frac{V_g E_b}{x_e} \sin \theta \\[2mm]
&= \frac{V_{go}(1 - b_p P_e) E_b \sin \theta}{x_e} \\[2mm]
&= \frac{V_{go} E_b \sin \theta}{x_e} - \frac{V_{go} E_b}{x_e} b_p P_e \sin \theta
\end{aligned}
\tag{2.46}
$$

where θ is the angle between the terminal voltage and infinite bus.

The expressions for P_e can be obtained from Eq. (2.46) as

$$
P_e = \frac{P_{Nmax} \sin \theta}{1 + P_{Nmax} b_p \sin \theta}
\tag{2.47}
$$

P_e is maximum when $\theta = 90^o$ and is given by

$$
P_{emax} = \frac{P_{Nmax}}{1 + b_p P_{Nmax}}
\tag{2.48}
$$

where

$$
P_{Nmax} = \frac{V_{go} E_b}{x_e}
$$

The maximum power that can be delivered by the generator increases as P_{Nmax} (the maximum power flow in the network) increases and b_p decreases. The variation of P_{emax} as a function of b_p is shown in Fig. 2.20 for two different values of x_e. The maximum value of P_{emax} occurs at $b_p = 0$ and is equal to P_{Nmax}.

The voltage regulation can be accounted by modelling the generator as a voltage source E_g behind a reactance x_g. In the absence of AVR (manual control) $x_g = x_d$. For ideal regulator, $x_g = 0$. For electronic regulators, $x_g \simeq x_d'$.

It is possible to relate x_g to b_p and other system parameters. This follows from the Eq. (2.48) and the following equation.

$$
P_{emax} = \frac{E_g E_b}{(x_e + x_g)}
\tag{2.49}
$$

Given the operating conditions, such as the values of E_b and the power factor, it is possible to express x_g as a function of b_p. The typical variation of
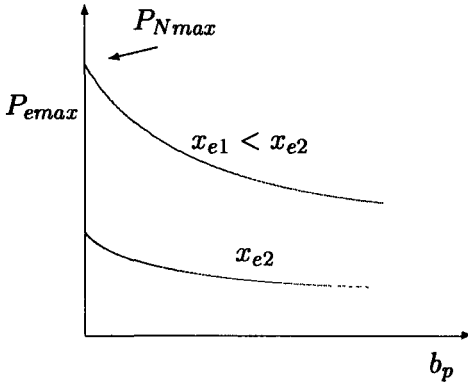
Figure 2.20: Variation of P_{emax} with b_p
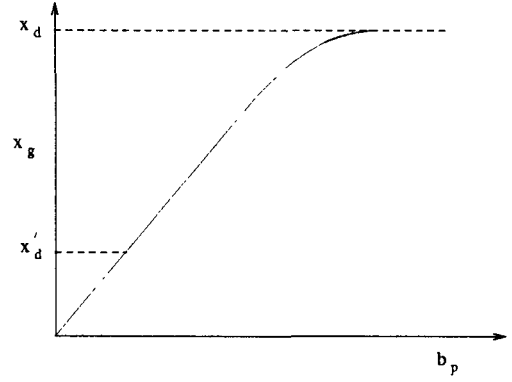
Figure 2.21: Variation of x_g with b_p

x_g with b_p is shown in Fig. 2.21.

Remarks

This approach of reducing the equivalent reactance of the synchronous machine from x_d to x_g to account for voltage regulation is only accurate in determining the power limit in the absence of oscillatory instability. It will be shown in chapter 7 that systems with fast acting exciters and high gain AVR are usually prone to oscillatory instability. This implies that the simplified analysis of excitation controllers is not valid and detailed generator models need to be considered. The detailed component models - synchronous machine, excitation and prime-mover controllers, loads, transmission lines and SVC are taken up in the next three chapters.

Example 2.11

Find the steady state stability limit of power delivered if $x_d = 1.0$, $x_q = 1.0$, $x_e = 1.0$, $E_b = 1.0$. The terminal voltage V_g is maintained at 1.0 p.u. Assume ideal regulator. The phasor diagram is shown in Fig. 2.22. The expression for power P_e is

$$P_e = \frac{E_q E_b \sin \delta}{(x_q + x_e)} = \frac{V_g E_b}{x_e} \sin \theta \qquad (A)$$

E_q is the voltage behind x_q. E_q from phasor diagram is given by

$$E_q = \frac{V_g \cos \dfrac{\theta}{2}}{\cos \left(\delta - \dfrac{\theta}{2} \right)} \qquad (B)$$
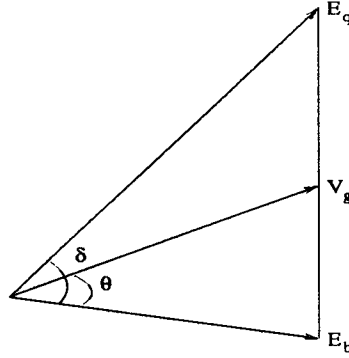
Figure 2.22: Phasor diagram for Example 2.11

From (A),

$$E_q = \frac{V_g(x_q + x_e)}{x_e} \frac{\sin\theta}{\sin\delta} \qquad (C)$$

P_e is maximum when $\theta = 90^o$. For this case, Equating the two expressions for E_q, we get

$$\frac{\cos\dfrac{\theta}{2}}{\cos(\delta - \dfrac{\theta}{2})} = \frac{(x_q + x_e)}{x_e}\frac{\sin\theta}{\sin\delta}$$

$$\frac{x_e}{(x_q + x_e)}\sin\delta = 2\sin\frac{\theta}{2}\cos(\delta - \frac{\theta}{2}) = \sin\delta - \sin(\delta - \theta)$$

$$\frac{x_q}{(x_q + x_e)}\sin\delta = \sin(\delta - \theta)$$

For the data given,

$$\delta^* = 116.6^o, \quad P_{emax} = 1.0 \;\text{p.u.}$$

$$\tan\delta^* = -\frac{(x_q + x_e)}{x_q}, \quad 90^o < \delta^* < 180^o$$

It is interesting to note that the critical angle (corresponding to stability limit) is greater than 90°. The power angle curve, P_e versus δ is shown in Fig. 2.23.
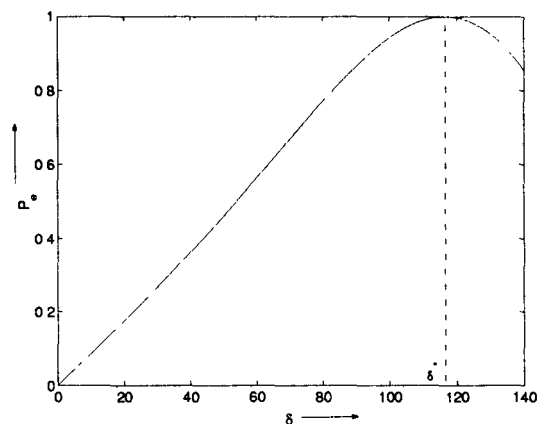
Figure 2.23: Power angle curve (Example 2.11)

References

1. E.W. Kimbark, **Power System Stability, Volume I: Elements of Stability Calculations**, John Wiley (New York), 1948

2. S.B. Crary, **Power System Stability, Volume I: Steady State Stability**, John Wiley, New York, 1945

3. V.A. Venikov, **Transient Phenomena in Electrical Power Systems**, Pergamon Press, Oxford, 1964

4. T.S. Parker and L.O. Chua, **Practical Numerical Algorithms for Chaotic Systems**, Springer-Verlag, New York, 1989

5. J. Guckenheimer and P. Holmes, **Nonlinear Oscillations, Dynamical Systems and Bifurcations of Vector Fields**, Springer-Verlag, New York, 1983

"This page is Intentionally Left Blank"

Chapter 3

Modelling of Synchronous Machine

3.1   Introduction

Simple models of the synchronous generators are not adequate for accurate description of the power system dynamics. In this chapter, detailed models of synchronous machine are developed from the basic equations using phase variables and application of Park's transformation. Park's transformation results in time-invariant machine equations which are easier to handle. Also there is a close connection between Park's variables and the phasors describing voltages and currents in steady state.

In this chapter, the derivation of the machine model is accompanied by its representation using per unit quantities and equivalent circuits on d- and q-axes. Measurement of machine parameters and representation of saturation are also discussed. The application of the model for transient analysis is outlined at the end.

The literature on synchronous machines dates back to several decades. However, there are certain aspects on which there is no universal acceptance. Firstly there are two conventions - originally proposed and modified (according to IEEE committee report [11] published in 1969) on the orientation of axes and direction of currents. In this book, the latter convention is used along with power-invariant Park's transformation. A more serious problem is the lack of unanimity in the definition of transient reactances and time constants when more than one damper winding (in the q-axis) is used. This can lead to confusion. We have used definitions according to IEC recommendations. This appears to be accepted more widely. The assumptions previously used in the computation of machine parameters based on test data can also be dispensed with, according to Canay [21].
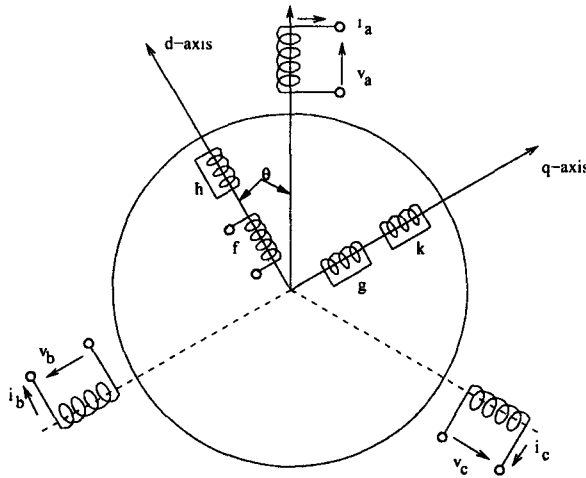
Figure 3.1: Synchronous machine

3.2 Synchronous Machine

The synchronous machine considered is shown in Fig. 3.1. This shows a three phase armature windings (a, b and c) on the stator and four windings on the rotor including the field winding '*f*'. The amortisseur (or damper) circuits in the salient pole machine or the eddy-current effects in the rotor are represented by a set of coils with constant parameters. Three damper coils, '*h*' in the d-axis and g, k on the q-axis are shown in Fig. 3.1. The number of damper coils represented can vary from zero (in the simplest model) to five or more using Jackson-Winchester model [7]. However the most detailed model used extensively in power system dynamic studies is limited to 3 damper coils. (It is also easier to obtain the parameters of this and simpler models).

The following assumptions are used in the derivation of the basic equations of the machine.

1. The mmf in the airgap is distributed sinusoidally and the harmonics are neglected.

2. Saliency is restricted to the rotor. The effect of slots in the stator is neglected.

3. Magnetic saturation and hysteresis are ignored.

The representation of the saturation will be considered later in this chapter.

In what follows, the machine is assumed to have two poles. There is no loss of generality in doing this as the rotor angle θ (with respect to a stationary axis) is assumed to be the electrical angle and the equations are invariant with respect to the number of poles. The mechanical angle θ_m is related to θ by

$$\theta_m = \frac{2}{P}\theta \tag{3.1}$$

3.2.1 Flux Linkage Equations

The stator and rotor flux linkages are given by

$$\psi_s = [L_{ss}]i_s + [L_{sr}]i_r \tag{3.2}$$

$$\psi_r = [L_{rs}]i_s + [L_{rr}]i_r \tag{3.3}$$

where

$$
\begin{aligned}
i_s^t &= [i_a \ i_b \ i_c], & \psi_s^t &= [\psi_a \ \psi_b \ \psi_c] \\
i_r^t &= [i_f \ i_h \ i_g \ i_k]; & \psi_r^t &= [\psi_f \ \psi_h \ \psi_g \ \psi_k]
\end{aligned}
$$

The matrices $[L_{ss}]$ and $[L_{rr}]$ are symmetric and also $[L_{rs}] = [L_{sr}]^t$. From two reaction theory, it is possible to express the inductance coefficients as follows.

$$
[L_{ss}] = \begin{bmatrix} L_{aao} & L_{abo} & L_{abo} \\ L_{abo} & L_{aao} & L_{abo} \\ L_{abo} & L_{abo} & L_{aao} \end{bmatrix} +
$$

$$
L_{aa2} \begin{bmatrix} \cos 2\theta & \cos\left(2\theta - \frac{2\pi}{3}\right) & \cos\left(2\theta + \frac{2\pi}{3}\right) \\ \cos\left(2\theta - \frac{2\pi}{3}\right) & \cos\left(2\theta + \frac{2\pi}{3}\right) & \cos 2\theta \\ \cos\left(2\theta + \frac{2\pi}{3}\right) & \cos 2\theta & \cos\left(2\theta - \frac{2\pi}{3}\right) \end{bmatrix} \tag{3.4}
$$

$$
[L_{rr}] = \begin{bmatrix} L_f & L_{fh} & 0 & 0 \\ L_{fh} & L_h & 0 & 0 \\ 0 & 0 & L_g & L_{gk} \\ 0 & 0 & L_{gk} & L_k \end{bmatrix} \tag{3.5}
$$

$$[L_{sr}] = \begin{bmatrix} M_{af}\cos\theta & M_{ah}\cos\theta \\ M_{af}\cos\left(\theta - \dfrac{2\pi}{3}\right) & M_{ah}\cos\left(\theta - \dfrac{2\pi}{3}\right) \\ M_{af}\cos\left(\theta + \dfrac{2\pi}{3}\right) & M_{ah}\cos\left(\theta + \dfrac{2\pi}{3}\right) \end{bmatrix}$$

$$\begin{matrix} M_{ag}\sin\theta & M_{ak}\sin\theta \\ M_{ag}\sin\left(\theta - \dfrac{2\pi}{3}\right) & M_{ak}\sin\left(\theta - \dfrac{2\pi}{3}\right) \\ M_{ag}\sin\left(\theta + \dfrac{2\pi}{3}\right) & M_{ak}\sin\left(\theta + \dfrac{2\pi}{3}\right) \end{matrix} \tag{3.6}$$

Note that $[L_{sr}]$ is a function of θ and is time varying if the rotor rotates at constant speed. $[L_{ss}]$ is also a function of θ if $L_{aa2} \neq 0$. This is true for salient pole machines.

3.2.2 Voltage Equations

The voltage equations for the stator and rotor coils are given below.

$$-\frac{d\psi_s}{dt} - [R_s]i_s = v_s \tag{3.7}$$

$$-\frac{d\psi_r}{dt} - [R_r]i_r = v_r \tag{3.8}$$

where

$$v_s^t = [v_a \;\; v_b \;\; v_c], \qquad\qquad v_r^t = [-v_f \;\; 0 \;\; 0 \;\; 0]$$

$$\begin{bmatrix} R_s \end{bmatrix} = \begin{bmatrix} R_a & 0 & 0 \\ 0 & R_a & 0 \\ 0 & 0 & R_a \end{bmatrix} = R_a[U_3]$$

$$\begin{bmatrix} R_r \end{bmatrix} = \begin{bmatrix} R_f & 0 & 0 & 0 \\ 0 & R_h & 0 & 0 \\ 0 & 0 & R_g & 0 \\ 0 & 0 & 0 & R_k \end{bmatrix}$$

$[U_3]$ is a unit matrix of dimension 3.

Note: Generator convention is used in expressing the voltage equations. The currents are assumed to be leaving the coil at the terminals and the terminal voltages are assumed to be voltage drops in the direction of the currents. This is contrary to the motor convention (see Fig. 3.2)

(a) Generator convention   (b) Motor convention
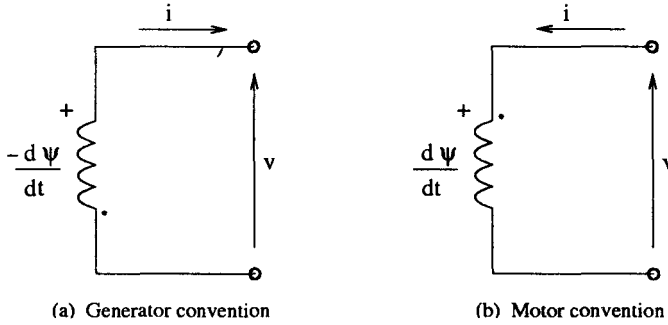
Figure 3.2: Generator and motor conventions

Because of the generator convention, the sign associated with v_f is negative (to sustain a field current in steady state). Note that both v_f and i_f are assumed to be positive in steady state.

3.2.3 Torque Equation

It is assumed that the inertia of the turbines (prime mover) can be clubbed with that of the generator rotor (by assuming the shaft to be rigid). In this case, the equation of motion of the rotor is given by

$$J\frac{d^2\theta_m}{dt^2} + D\frac{d\theta_m}{dt} = T_m - T_e \tag{3.9}$$

where

$\quad J \quad$ is the combined moment of inertia of the rotor
$\quad D \quad$ is the damping (assumed to be viscous) coefficient
$\quad T_m \quad$ is the mechanical torque in the direction of rotation
$\quad T_e \quad$ is the electrical torque opposing the mechanical torque

Note that for a two pole machine, $\theta_m = \theta$. For $P \neq 2$, the Eq. (3.9) can be transformed to

$$\frac{2}{P}\left(J\frac{d^2\theta}{dt^2} + D\frac{d\theta}{dt}\right) = T_m - T_e \tag{3.10}$$

The electrical torque T_e is given by

$$T_e = -\frac{\partial W'}{\partial \theta_m} = -\frac{P}{2}\frac{\partial W'}{\partial \theta} = \frac{P}{2}T_e' \qquad (3.11)$$

where

$T_e' = -\frac{\partial W'}{\partial \theta}$ is the electrical torque of the equivalent two pole machine,

W' is the co-energy expressed as

$$W' = \frac{1}{2}\begin{bmatrix} i_s^t & i_r^t \end{bmatrix}\begin{bmatrix} L_{ss} & L_{sr} \\ L_{rs} & L_{rr} \end{bmatrix}\begin{bmatrix} i_s \\ i_r \end{bmatrix} \qquad (3.12)$$

Substituting Eq. (3.12) in Eq. (3.11) and noting that $[L_{rr}]$ is a constant matrix, we get

$$T_e' = -\frac{1}{2}\left[i_s^t\left[\frac{\partial L_{ss}}{\partial \theta}\right]i_s + 2i_s^t\left[\frac{\partial L_{sr}}{\partial \theta}\right]i_r \right] \qquad (3.13)$$

Substituting Eq. (3.11) in Eq. (3.10) we get

$$J'\frac{d^2\theta}{dt^2} + D'\frac{d\theta}{dt} = T_m' - T_e' \qquad (3.14)$$

where

$$J' = J.\left(\frac{2}{P}\right)^2 \text{ is the equivalent inertia}$$

$$D' = D.\left(\frac{2}{P}\right)^2 \text{ is the equivalent damping coefficient}$$

$$T_m' = \frac{2T_m}{P}, \text{ is the mechanical torque of the equivalent two pole machine}$$

The above equation represents the transformation of 'P' pole machine to a 2 pole machine. The mechanical torque is reduced by a factor of $\frac{2}{P}$. The inertia and damping are reduced by factor of $\left(\frac{2}{P}\right)^2$. However, since all the equations are expressed in per unit (to be introduced later) there is no loss of generality in assuming that the machine has two poles (as stated earlier).

3.3   Park's Transformation

The combined voltage equations (for the stator and the rotor) can be expressed as

$$\left. \begin{array}{rcl} \dfrac{d\psi}{dt} &=& -[R][L]^{-1}\psi - v \\[2mm] i &=& [L]^{-1}\psi \end{array} \right\} \tag{3.15}$$

where

$$\left[\, L \,\right] = \begin{bmatrix} L_{ss} & L_{sr} \\ L_{rs} & L_{rr} \end{bmatrix}, \qquad\qquad \left[\, R \,\right] = \begin{bmatrix} R_s & 0 \\ 0 & R_r \end{bmatrix}$$

$$\psi^t = [\psi_s^t \ \ \psi_r^t] \qquad\qquad i^t = [i_s^t \ \ i_r^t]$$

$$v^t = [v_s^t \ \ v_r^t]$$

Alternatively, the voltage equations can also be expressed as

$$\left. \begin{array}{rcl} \dfrac{di}{dt} &=& [L]^{-1}\left[-[R]i - \dfrac{d\theta}{dt}\left[\dfrac{\partial L}{\partial\theta}\right]i - v \right] \\[3mm] \psi &=& [L]i \end{array} \right\} \tag{3.16}$$

Although it is possible to solve the Eqs. (3.15) or (3.16) numerically, it is almost impossible to obtain analytical solution even when $\dot{\theta} = \dfrac{d\theta}{dt}$ is constant. This is due to the fact that the inductance matrix [L] is time varying and the computation of inverse of $[L]$ is required.

It would be advantageous if the time-varying machine equations can be transformed to a time invariant set. This would result in the simplification of the calculations both for steady state and transient conditions. R.H.Park [6] introduced the following transformation

$$\begin{bmatrix} f_a \\ f_b \\ f_c \end{bmatrix} = [C_P] \begin{bmatrix} f_d \\ f_q \\ f_o \end{bmatrix} \tag{3.17}$$

where f_α can be either stator voltage, current or flux linkage of the stator winding α ($\alpha = a$, b or c). $[C_P]$ is defined by

$$[C_P] = \begin{bmatrix} k_d \cos\theta & k_q \sin\theta & k_o \\[3mm] k_d \cos\left(\theta - \dfrac{2\pi}{3}\right) & k_q \sin\left(\theta - \dfrac{2\pi}{3}\right) & k_o \\[3mm] k_d \cos\left(\theta + \dfrac{2\pi}{3}\right) & k_q \sin\left(\theta + \dfrac{2\pi}{3}\right) & k_o \end{bmatrix} \tag{3.18}$$

where k_d, k_q and k_o are constants appropriately chosen. In original Park's transformation $k_d = 1.0$, $k_q = -1.0$ and $k_o = 1$

The inverse transformation is given by

$$
\begin{bmatrix} f_d \\ f_q \\ f_o \end{bmatrix} = [C_P]^{-1} \begin{bmatrix} f_a \\ f_b \\ f_c \end{bmatrix}
\tag{3.19}
$$

where

$$
[C_P]^{-1} = \begin{bmatrix} k_1 \cos\theta & k_1 \cos(\theta - 2\pi/3) & k_1 \cos(\theta + 2\pi/3) \\ k_2 \sin\theta & k_2 \sin(\theta - 2\pi/3) & k_2 \sin(\theta + 2\pi/3) \\ k_3 & k_3 & k_3 \end{bmatrix}
$$

$$
k_1 = \frac{2}{3k_d}, \quad k_2 = \frac{2}{3k_q}, \quad k_3 = \frac{1}{3k_o}
$$

3.3.1   Transformation of Flux Linkages

$$
\begin{bmatrix} \psi_s \\ \psi_r \end{bmatrix} = \begin{bmatrix} C_P & 0 \\ 0 & U_4 \end{bmatrix} \begin{bmatrix} \psi_{dqo} \\ \psi_r \end{bmatrix}
\tag{3.20}
$$

where U_4 is a unit matrix of order 4 and $\psi_{dqo}^t = [\psi_d \ \ \psi_q \ \ \psi_o]$

The L.H.S. of Eq. (3.20) can be expressed as

$$
\begin{bmatrix} \psi_s \\ \psi_r \end{bmatrix} = \begin{bmatrix} L_{ss} & L_{sr} \\ L_{rs} & L_{rr} \end{bmatrix} \begin{bmatrix} C_P & 0 \\ 0 & U_4 \end{bmatrix} \begin{bmatrix} i_{dqo} \\ i_r \end{bmatrix}
\tag{3.21}
$$

where $i_{dqo}^t = [i_d \ \ i_q \ \ i_o]$

Substituting (3.21) in (3.20) we get

$$
\begin{aligned}
\begin{bmatrix} \psi_{dqo} \\ \psi_r \end{bmatrix} &= \begin{bmatrix} C_P^{-1} & 0 \\ 0 & U_4 \end{bmatrix} \begin{bmatrix} L_{ss} & L_{sr} \\ L_{rs} & L_{rr} \end{bmatrix} \begin{bmatrix} C_P & 0 \\ 0 & U_4 \end{bmatrix} \begin{bmatrix} i_{dqo} \\ i_r \end{bmatrix} \\[2mm]
&= \begin{bmatrix} C_P^{-1} L_{ss} C_P & C_P^{-1} L_{sr} \\ L_{rs} C_P & L_{rr} \end{bmatrix} \begin{bmatrix} i_{dqo} \\ i_r \end{bmatrix} \\[2mm]
&= \begin{bmatrix} L'_{ss} & L'_{sr} \\ L'_{rs} & L_{rr} \end{bmatrix} \begin{bmatrix} i_{dqo} \\ i_r \end{bmatrix}
\end{aligned}
\tag{3.22}
$$

where

$$[L'_{ss}] = \begin{bmatrix} L_d & 0 & 0 \\ 0 & L_q & 0 \\ 0 & 0 & L_o \end{bmatrix}$$

$$\left. \begin{aligned} L_d &= L_{aao} - L_{abo} + \frac{3}{2}L_{aa2} \\ L_q &= L_{aao} - L_{abo} - \frac{3}{2}L_{aa2} \\ L_o &= L_{aao} + 2L_{abo} \end{aligned} \right\} \tag{3.23}$$

$$[L'_{sr}] = \begin{bmatrix} \left(\dfrac{M_{af}}{k_d}\right) & \left(\dfrac{M_{ah}}{k_d}\right) & 0 & 0 \\ 0 & 0 & \left(\dfrac{M_{ag}}{k_q}\right) & \left(\dfrac{M_{ak}}{k_q}\right) \\ 0 & 0 & 0 & 0 \end{bmatrix} \tag{3.24}$$

$$[L'_{rs}] = \begin{bmatrix} \left(\dfrac{3}{2}M_{af}k_d\right) & 0 & 0 \\ \left(\dfrac{3}{2}M_{ah}k_d\right) & 0 & 0 \\ 0 & \left(\dfrac{3}{2}M_{ag}k_q\right) & 0 \\ 0 & \left(\dfrac{3}{2}M_{ak}k_q\right) & 0 \end{bmatrix} \tag{3.25}$$

Remarks

1. $[L'_{rs}]^t \neq [L'_{sr}]$ unless

$$k_d^2 = \frac{2}{3}, \quad k_q^2 = \frac{2}{3} \tag{3.26}$$

2. The mutual inductance terms between the stator and rotor coils in the q-axis are negative for $k_q < 0$ unless M_{ag} and M_{ak} are both negative. It is to be noted that when the q-axis is lagging the direct axis (in the direction of rotation) as assumed in Fig. 3.1, M_{ag} and M_{ak} are positive. These terms are negative only if q-axis is assumed to be leading the d-axis.
Hence, if d-axis is assumed to lead q-axis, it would be convenient to choose positive value of k_q.

3. Note that there is no transformation of the rotor currents and flux linkages. Hence the self inductance matrix of rotor coils is not altered.

4. Eq. (3.22) shows that stator coils 'a', 'b' and 'c' are replaced by fictitious 'd', 'q' and 'o' coils from Park's transformation. Out of these, 'o' coil (in which zero-sequence current i_o flows) has no coupling with the rotor coils and may be neglected if $i_o = 0$. Since the (transformed) mutual inductance terms between d, q coils and the rotor coils are constants, it can be interpreted that d and q coils rotate at the same speed as the rotor. Furthermore, as mutual inductances between the d-coil and the rotor coils on the q-axis are zero, it can be assumed that d-coil is aligned with the d-axis. Similarly, it can be assumed that q coil is aligned along with the q-axis. This is shown in Fig. 3.3.

5. The following trigonometric identities are useful in the derivation of the transformed equations

$$\cos\theta + \cos\left(\theta - \frac{2\pi}{3}\right) + \cos\left(\theta + \frac{2\pi}{3}\right) \quad = \quad 0$$

$$\sin\theta + \sin\left(\theta - \frac{2\pi}{3}\right) + \sin\left(\theta + \frac{2\pi}{3}\right) \quad = \quad 0$$

$$\cos^2\theta + \cos^2\left(\theta - \frac{2\pi}{3}\right) + \cos^2\left(\theta + \frac{2\pi}{3}\right) \quad = \quad \frac{3}{2}$$

$$\sin^2\theta + \sin^2\left(\theta - \frac{2\pi}{3}\right) + \sin^2\left(\theta + \frac{2\pi}{3}\right) \quad = \quad \frac{3}{2}$$

Although the physical interpretation of Park's transformation is useful in gaining an intuitive understanding of its implications, it must be understood that it is not essential in the mathematical analysis of the synchronous machine. This is true of any mathematical transformation whose main objective is to simplify the analysis. From this point of view, the major benefit of Park's transformation is to obtain the machine equations in time-invariant form which simplifies the analysis. The transformation of stator voltage equations will clarify this point.
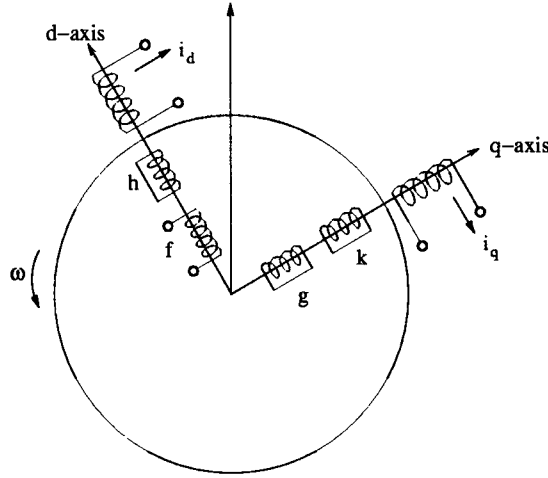
Figure 3.3: Synchronous machine with rotating armature windings

3.3.2 Transformation of Stator Voltage Equations

Applying Park's transformation, Eq. (3.7) can be rewritten as

$$-\frac{d}{dt}[C_P \psi_{dqo}] - [R_s][C_P]i_{dqo} = [C_P]v_{dqo} \qquad (3.27)$$

The first term on the L.H.S. of Eq.(3.27) can be expressed as

$$-\frac{d}{dt}[C_P \psi_{dqo}] = -\dot{\theta}\frac{d[C_P]}{d\theta}\psi_{dqo} - [C_P]\frac{d}{dt}\psi_{dqo} \qquad (3.28)$$

where,

$$\frac{dC_P}{d\theta} = \begin{bmatrix} -k_d \sin\theta & k_q \cos\theta & 0 \\ -k_d \sin\left(\theta - \frac{2\pi}{3}\right) & k_q \cos\left(\theta - \frac{2\pi}{3}\right) & 0 \\ -k_d \sin\left(\theta + \frac{2\pi}{3}\right) & k_q \cos\left(\theta + \frac{2\pi}{3}\right) & 0 \end{bmatrix} = [C_P][P_1] \qquad (3.29)$$

where

$$[P_1] = \begin{bmatrix} 0 & \dfrac{k_q}{k_d} & 0 \\ -\dfrac{k_d}{k_q} & 0 & 0 \\ 0 & 0 & 0 \end{bmatrix}$$

Substituting (3.28) in (3.27), we get

$$-[C_P]\frac{d\psi_{dqo}}{dt} - \dot{\theta}[C_P][P_1]\psi_{dqo} - [R_s][C_P]i_{dqo} = [C_P]v_{dqo} \qquad (3.30)$$

From (3.30), we obtain

$$-\frac{d\psi_{dqo}}{dt} - \dot{\theta}[P_1]\psi_{dqo} - [C_P]^{-1}[R_s][C_P]i_{dqo} = v_{dqo}$$

$$-\frac{d\psi_{dqo}}{dt} - \dot{\theta}[P_1]\psi_{dqo} - R_a i_{dqo} = v_{dqo} \qquad (3.31)$$

after substituting for $[R_s] = R_a[U_3]$

Eq. (3.31) can be expanded as

$$\left.\begin{array}{rcl} -\dfrac{d\psi_d}{dt} - \dot{\theta}\dfrac{k_q}{k_d}\psi_q - R_a i_d &=& v_d \\[3mm] -\dfrac{d\psi_q}{dt} + \dot{\theta}\dfrac{k_d}{k_q}\psi_d - R_a i_q &=& v_q \\[3mm] -\dfrac{d\psi_o}{dt} - R_a i_o &=& v_o \end{array}\right\} \qquad (3.32)$$

The rotor voltage equations are unchanged and can be written in the expanded form from Eq. (3.8) as

$$\left.\begin{array}{rcl} \dfrac{d\psi_f}{dt} + R_f i_f &=& v_f \\[3mm] \dfrac{d\psi_h}{dt} + R_h i_h &=& 0 \\[3mm] \dfrac{d\psi_g}{dt} + R_g i_g &=& 0 \\[3mm] \dfrac{d\psi_k}{dt} + R_k i_k &=& 0 \end{array}\right\} \qquad (3.33)$$

3.3.3   Transformation of the Torque Equation

After applying Park's transformation to Eq. (3.13) the electrical torque is expressed as

$$T_e = -\frac{1}{2}\left[i_{dqo}^t[C_P]^t\left[\frac{\partial L_{ss}}{\partial \theta}\right][C_P]i_{dqo} + 2i_{dqo}^t[C_P]^t\left[\frac{\partial L_{sr}}{\partial \theta}\right]i_r\right] \qquad (3.34)$$

$$\left[\frac{\partial L_{ss}}{\partial \theta}\right] = -2L_{aa2} \begin{bmatrix} \sin 2\theta & \sin\left(2\theta - \frac{2\pi}{3}\right) & \sin\left(2\theta + \frac{2\pi}{3}\right) \\[2em] \sin\left(2\theta - \frac{2\pi}{3}\right) & \sin\left(2\theta + \frac{2\pi}{3}\right) & \sin 2\theta \\[2em] \sin\left(2\theta + \frac{2\pi}{3}\right) & \sin 2\theta & \sin\left(2\theta - \frac{2\pi}{3}\right) \end{bmatrix} \quad (3.35)$$

$$\left[\frac{\partial L_{sr}}{\partial \theta}\right] = \begin{bmatrix} -M_{af}\sin\theta & -M_{ah}\sin\theta \\[1.5em] -M_{af}\sin\left(\theta - \frac{2\pi}{3}\right) & -M_{ah}\sin\left(\theta - \frac{2\pi}{3}\right) \\[1.5em] -M_{af}\sin\left(\theta + \frac{2\pi}{3}\right) & -M_{ah}\sin\left(\theta + \frac{2\pi}{3}\right) \end{bmatrix}$$

$$\begin{matrix} M_{ag}\cos\theta & M_{ak}\cos\theta \\[1.5em] M_{ag}\cos\left(\theta - \frac{2\pi}{3}\right) & M_{ak}\cos\left(\theta - \frac{2\pi}{3}\right) \\[1.5em] M_{ag}\cos\left(\theta + \frac{2\pi}{3}\right) & M_{ak}\cos\left(\theta + \frac{2\pi}{3}\right) \end{matrix} \quad (3.36)$$

$$\left[\frac{\partial L_{ss}}{\partial \theta}\right][C_P] = -3L_{aa2}[C_P][P_2]$$

where

$$[P_2] = \begin{bmatrix} 0 & \frac{k_q}{k_d} & 0 \\[0.8em] \frac{k_d}{k_q} & 0 & 0 \\[0.8em] 0 & 0 & 0 \end{bmatrix} \quad (3.37)$$

$$[C_P]^t\left[\frac{\partial L_{sr}}{\partial \theta}\right] = \begin{bmatrix} 0 & 0 & \frac{3}{2}k_d M_{ag} & \frac{3}{2}k_d M_{ak} \\[0.8em] -\frac{3}{2}k_q M_{af} & -\frac{3}{2}k_q M_{ah} & 0 & 0 \\[0.8em] 0 & 0 & 0 & 0 \end{bmatrix} \quad (3.38)$$

After some manipulations, the expression for electrical torque reduces to

$$T_e = \frac{3}{2}k_d k_q \left[i_q \left(\frac{M_{af}}{k_d}i_f + \frac{M_{ah}}{k_d}i_h + \frac{3}{2}L_{aa2}i_d \right) - i_d \left(\frac{M_{ag}}{k_q}i_g + \frac{M_{ak}}{k_q}i_k - \frac{3}{2}L_{aa2}i_q \right) \right]$$

(3.39)

Since

$$\psi_d = L_d i_d + \frac{M_{af}}{k_d}i_f + \frac{M_{ah}}{k_d}i_h$$

(3.40)

$$\psi_q = L_q i_q + \frac{M_{ag}}{k_q}i_g + \frac{M_{ak}}{k_q}i_k$$

(3.41)

Utilizing (3.40) and (3.41) in Eq. (3.39),

$$T_e = \frac{3}{2}k_d k_q \left[i_q \left\{ \psi_d - \left(L_d - \frac{3}{2}L_{aa2} \right) i_d \right\} - i_d \left\{ \psi_q - \left(L_q + \frac{3}{2}L_{aa2} \right) i_q \right\} \right]$$

(3.42)

$$= \frac{3}{2}k_d k_q [i_q \psi_d - i_d \psi_q]$$

(3.43)

as

$$L_d - \frac{3}{2}L_{aa2} = L_q + \frac{3}{2}L_{aa2} = L_{aa0} - L_{ab0}$$

3.3.4 Choice of constants k_d, k_q and k_o

The transformation $[C_P]$ defined by Eq. (3.18) is most general as no assumptions are made regarding the constants k_d, k_q and k_o . However, original Park's transformation used
$k_d = 1$, $k_q = -1$, $k_o = 1$

Since same transformation is applied for currents and voltages, it can be shown that in general,

$$p = v_a i_a + v_b i_b + v_c i_c = \frac{3}{2} \left(k_d^2 v_d i_d + k_q^2 v_q i_q \right) + 3k_o^2 v_o i_o$$

(3.44)

Proof: L.H.S. of Eq. (3.44) can be expressed as

$$v_{abc}^t i_{abc} = v_{dqo}^t [C_P]^t [C_P] i_{dqo}$$

(3.45)

$[C_P]^t[C_P]$ is a diagonal matrix given below

$$[C_P]^t[C_P] = \begin{bmatrix} \frac{3}{2}k_d^2 & 0 & 0 \\ 0 & \frac{3}{2}k_q^2 & 0 \\ 0 & 0 & 3k_o^2 \end{bmatrix} \tag{3.46}$$

Power Invariant Transformation

A transformation $[C_P]$ is said to be power invariant if it is orthogonal, i.e.

$$[C_P]^t = [C_P]^{-1} \tag{3.47}$$

The choice of k_d, k_q and k_o to get power invariant transformation are

$$k_d = \pm\sqrt{\frac{2}{3}}, \quad k_q = \pm\sqrt{\frac{2}{3}}, k_o = \pm\sqrt{\frac{1}{3}} \tag{3.48}$$

We will assume only positive values of the constants thereby defining a power invariant Park's transformation given by

$$[C_P] = \frac{1}{\sqrt{3}} \begin{bmatrix} \sqrt{2}\cos\theta & \sqrt{2}\sin\theta & 1 \\ \sqrt{2}\cos\left(\theta - \frac{2\pi}{3}\right) & \sqrt{2}\sin\left(\theta - \frac{2\pi}{3}\right) & 1 \\ \sqrt{2}\cos\left(\theta + \frac{2\pi}{3}\right) & \sqrt{2}\sin\left(\theta + \frac{2\pi}{3}\right) & 1 \end{bmatrix} \tag{3.49}$$

The major advantage of a power invariant transformation is that the mutual inductances in the transformed network are equal.

For example

$$M_{df} = \frac{M_{af}}{k_d} \quad \text{and} \quad M_{fd} = \frac{3}{2}M_{af}k_d$$

For $k_d = \sqrt{\frac{2}{3}}$, $M_{df} = M_{fd} = \sqrt{\frac{3}{2}}M_{af}$

In what follows, we will use a power invariant transformation by selecting the following values

$$k_d = \sqrt{\frac{2}{3}} = k_q, \quad k_o = \sqrt{\frac{1}{3}}$$

As mentioned earlier, the positive value of k_q indicates that q-axis is lagging the direct axis, whereas in the original transformation by Park, q-axis is assumed to lead d-axis. Although an IEEE committee report in 1969 [11] recommended a revision of the old convention (of q leading d) usage in power industry is often based on the old convention.

It should also be noted here that the use of generator convention in expressing the stator voltage equations is consistent with the choice of d-axis leading q-axis. Similarly the earlier motor convention is consistent with q-axis leading d-axis. To summarize, the basic differences in the two conventions are shown in Table 3.1.

Table 3.1   Comparison Between Conventions

Features	Convention	
	Original	Revised
Current direction	motor	generator
Orientation of axes	'q' leading 'd'	'd' leading 'q'
Constants	$k_d = 1.0, k_q = -1$	$k_d = k_q = \sqrt{2/3}$

Note that although the armature currents, even in the original convention, are considered to flow out of the generator, the signs associated with these currents (in flux calculations) are negative (consistent with the motor convention). As mentioned before, the revised convention is adopted in the book.

3.4   Analysis of Steady State Performance

The major advantage of Park's transformation is that the machine equations are reduced to time-invariant form which simplifies their solution. Thus, Park's transformation can be considered as a particular case of transformation based on Floquet-Liapunov theory which applies to linear time-varying system with periodic coefficients [16]. (Note that the system equations for the stator and rotor windings are linear if the rotor velocity $\dot{\theta}$ is assumed to be constant and magnetic saturation is neglected) Park's transformation results in linear time-invariant form (with the assumption $\dot{\theta}$=constant) given in Eqs. (3.32) and (3.33).

If the applied voltages v_d, v_q and v_f are constants, the flux linkages and currents (in Park's variables using d-q reference frame) are also constants in steady state. Consequently, the electrical torque, T_e, is also a constant in steady state. If the applied torque T_m (constant) is equal to T_e, then (neglecting damping the assumption of constant velocity in steady state is valid.

3.4.1 Analysis of an Unloaded Generator

In steady state, for an unloaded generator,

$$i_d = i_q = 0, \quad i_g = i_h = i_k = 0, \quad i_f = \frac{v_f}{R_f} \tag{3.50}$$

The flux linkages, from Eq. (3.22) are

$$\left. \begin{aligned}
\psi_d &= L_d i_d + M_{df} i_f + M_{dh} i_h \\
\psi_f &= M_{df} i_d + L_f i_f + L_{fh} i_h \\
\psi_h &= M_{dh} i_d + L_{fh} i_f + L_h i_h
\end{aligned} \right\} \tag{3.51}$$

$$\left. \begin{aligned}
\psi_q &= L_q i_q + M_{qg} i_g + M_{qk} i_k \\
\psi_g &= M_{qg} i_q + L_g i_g + L_{gk} i_k \\
\psi_k &= M_{qk} i_q + L_{gk} i_g + L_k i_k
\end{aligned} \right\} \tag{3.52}$$

where

$$M_{df} = \sqrt{\frac{3}{2}} M_{af}, \quad M_{dh} = \sqrt{\frac{3}{2}} M_{ah}$$

$$M_{qg} = \sqrt{\frac{3}{2}} M_{ag}, \quad M_{qk} = \sqrt{\frac{3}{2}} M_{ak}$$

Note that the reciprocity of these mutual inductances ($M_{df} = M_{fd}$ etc.) results from the use of power-invariant Park's transformation (In original Park's transformation $M_{df} = M_{af}$ while $M_{fd} = \frac{3}{2} M_{af}$. The reciprocity is achieved only in per unit quantities with the choice of appropriate base quantities for the stator and rotor circuits. The selection of the per unit quantities is discussed in the next section).

Substituting (3.50) in (3.51) and (3.52), we have, in steady state

$$\left. \begin{aligned}
\psi_f = \psi_{fo} = L_f \frac{v_{fo}}{R_f}, \quad &\psi_{ho} = L_{fh} \frac{v_{fo}}{R_f} \\
\psi_d = \psi_{do} = \frac{M_{df} v_{fo}}{R_f}, \quad &\psi_{qo} = 0, \quad \psi_{go} = \psi_{ko} = 0
\end{aligned} \right\} \tag{3.53}$$

Substituting (3.53) in (3.32), we get

$$\left. \begin{aligned}
v_{do} &= 0 \\
v_{qo} &= \omega_o \psi_{do} = \frac{\omega_o M_{df}}{R_f} v_{fo}
\end{aligned} \right\} \tag{3.54}$$

where $\omega = \omega_o$ in steady state. Note that the subscript 'o' indicates the value at the operating point. It is also assumed that under normal conditions, $\omega_o = \omega_B$ (the rotor runs at the rated speed).

The induced voltages in the stator are given by

$$
\begin{aligned}
v_a &= \sqrt{\frac{2}{3}} \left[v_{do} \cos(\omega_o t + \delta) + v_{qo} \sin(\omega_o t + \delta) \right] \\
v_b &= \sqrt{\frac{2}{3}} \left[v_{do} \cos\left(\omega_o t + \delta - \frac{2\pi}{3}\right) + v_{qo} \sin\left(\omega_o t + \delta - \frac{2\pi}{3}\right) \right] \quad (3.55) \\
v_c &= \sqrt{\frac{2}{3}} \left[v_{do} \cos\left(\omega_o t + \delta + \frac{2\pi}{3}\right) + v_{qo} \sin\left(\omega_o t + \delta + \frac{2\pi}{3}\right) \right]
\end{aligned}
$$

where $\delta = \theta - \omega_o t =$ constant in steady state (Note that $v_o = i_o = \psi_o = 0$). The induced voltages in the stator are equal to the terminal voltages under no-load conditions. From Eq. (3.54), only the second terms in R.H.S. of Eq. (3.55) are non-zero. The voltages are sinusoidal and balanced. The magnitude (rms value) of the line to line voltage is

$$
V_{L-L} = \frac{\omega_o M_{df}}{R_f} v_{fo} \quad (3.56)
$$

The electrical torque in an unloaded generator in steady state is zero. (as currents are zero).

3.4.2   Analysis of a Loaded Generator

A synchronous machine connected to a sinusoidal balanced voltage source delivers electric power determined by the prime-mover output. The currents and flux linkages in the machine are functions of T_m and V (rms line-to-line voltage at the terminals).

Without loss of generality, let the voltage sources at the generator terminals be defined as

$$
\left.
\begin{aligned}
v_a &= \sqrt{\frac{2}{3}} V \sin \omega_o t \\
v_b &= \sqrt{\frac{2}{3}} V \sin\left(\omega_o t - \frac{2\pi}{3}\right) \\
v_c &= \sqrt{\frac{2}{3}} V \sin\left(\omega_o t + \frac{2\pi}{3}\right)
\end{aligned}
\right\} \quad (3.57)
$$

Defining

$$
\theta = \omega_o t + \delta \quad (3.58)
$$

the d- and q-axis components of the terminal voltages can be calculated as

$$v_{do} = -V \sin \delta, \quad v_{qo} = V \cos \delta \tag{3.59}$$

Neglecting armature resistance,

$$\omega_o \psi_{do} = v_{qo}, \quad -\omega_o \psi_{qo} = v_{do} \tag{3.60}$$

Since $i_h = i_g = i_k = 0$ in steady state,

$$i_{qo} = -\frac{v_{do}}{\omega_o L_q}, \quad i_{do} = \frac{1}{\omega_o L_d} \left[v_{qo} - \omega_o M_{df} \frac{v_{fo}}{R_f} \right] \tag{3.61}$$

The operating value of T_e is

$$T_{eo} = \psi_{do} i_{qo} - \psi_{qo} i_{do} \tag{3.62}$$

Substituting from (3.59) to (3.61) in the above expression and assuming $\omega_o = \omega_B$,

$$
\begin{aligned}
T_{eo} &= -\frac{v_{do} x_{df} v_{fo}}{\omega_B x_d R_f} - \frac{v_{do} v_{qo}(x_d - x_q)}{\omega_B x_d x_q} \\
&= \frac{V E_{fdo} \sin\delta}{\omega_B x_d} + \frac{V^2 \sin 2\delta (x_d - x_q)}{2\omega_B x_d x_q}
\end{aligned} \tag{3.63}
$$

where

$$
\begin{aligned}
E_{fdo} &= \frac{x_{df}}{R_f} v_{fo}, \quad x_{df} = \omega_B M_{df} \\
x_d &= \omega_B L_d, \quad x_q = \omega_B L_q
\end{aligned}
$$

Since, $T_e = T_m$ in steady state, the angle δ can be evaluated from the knowledge of T_m, V and E_{fdo}.

Remarks

1. The expression for T_{eo} in (3.63) is identical to the expression for power output in steady state divided by the rated frequency ω_B.

2. The currents i_a, i_b and i_c in the armature are sinusoidal as i_d and i_q are constants.

3. If the voltages at the terminal are unbalanced, v_d and v_q are no longer constants and contain second harmonic components. In such a case, the currents i_d, i_q also contain second harmonic components. The phase currents contain third harmonic components.

3.5   Per Unit Quantities

It is common to express voltages, currents and impedances in per unit by choosing appropriate base quantities. The advantages of an appropriate per unit system are

1. The numerical values of currents and voltages are related to their rated values irrespective of the size of the machine.

2. The per unit impedances on the machine base lie in a narrow range for a class of machines of similar design.

3. The number of parameters required is minimized.

It is to be noted that the base quantities for the stator and rotor circuits can be independently chosen with certain restrictions which result in per unit mutual reactances being reciprocal. If power invariant Park's transformation is used, the constraints imply selecting the same base power for all the circuits.

3.5.1   Stator Base Quantities

The base quantities for the stator d-q windings are chosen as follows

$$
\begin{aligned}
\text{Base power, } S_B \quad &= \quad \text{Three phase rated power} \\
\text{Base voltage, } V_B \quad &= \quad \text{Rated line to line voltage (RMS)} \\
\text{Base current, } I_B \quad &= \quad \sqrt{3} \text{ x Rated line current} \\
\text{Base impedance, } Z_B \quad &= \quad \frac{V_B}{I_B} = \frac{Rated\ line\ to\ neutral\ voltage}{Rated\ line\ current} \\
\text{Base flux linkages, } \psi_B \quad &= \quad \frac{V_B}{\omega_B} \\
\text{Base inductance, } L_B \quad &= \quad \frac{\psi_B}{I_B} = \frac{Z_B}{\omega_B}
\end{aligned}
$$

ω_B is the base angular frequency in radians/sec. (This is also the rated angular speed for a 2 pole machine)

The stator equations in per unit, based on the quantities defined above, are

$$
\left.
\begin{aligned}
-\frac{1}{\omega_B}\frac{d\bar{\psi}_d}{dt} - \frac{\omega}{\omega_B}\bar{\psi}_q - \bar{R}_a\bar{i}_d &= \bar{v}_d \\[2mm]
-\frac{1}{\omega_B}\frac{d\bar{\psi}_q}{dt} + \frac{\omega}{\omega_B}\bar{\psi}_d - \bar{R}_a\bar{i}_q &= \bar{v}_q
\end{aligned}
\right\}
\tag{3.64}
$$

where the per unit quantities are indicated by the bar over the variables. For

example

$$\bar{i}_d = \frac{i_d}{I_B}, \quad \bar{v}_d = \frac{v_d}{V_B}, \quad \bar{\psi}_d = \frac{\psi_d}{\psi_B}$$

Remarks

1. The base voltage and current used in the previous literature are

   V_B = Peak rated voltage per phase

   I_B = Peak rated line current

   The choice of these base quantities are consistent with the original Park's transformation. This is because the per unit voltage (or current) in the old system is identical to that in the revised system defined above (which is consistent with the power-invariant version of Park's transformation)

2. The base impedances in both systems are identical. This fact combined with the identity of per unit quantities implies that the equations (in per unit) in both systems are identical (except for the differences in the orientation of d- and q-axes) thus eliminating the confusion about different versions of Park's transformation.

3. Anderson and Fouad [19] use different base quantities for voltage and current along with power-invariant Park's transformation. They define V_B as (rms) rated line to neutral voltage and I_B as rms line current. Although this results in identical base impedance as defined before, the per unit voltages, currents and fluxes are different which leads to different equations using inconvenient factors (of $\sqrt{3}$).

4. The choice of base quantities for the rotor is related to the choice of stator base quantities. Although in the original Park's transformation, the mutual inductances are not reciprocal, the selection of appropriate base quantities for the rotor will result in reciprocal per unit mutual inductances.

5. The expression for the base three phase power in the old system is

   $$P_B = S_B = \frac{3}{2} V_B I_B$$

   which leads to per unit power expression of

   $$\bar{P} = \frac{P}{P_B} = \bar{v}_d \bar{i}_d + \bar{v}_q \bar{i}_q$$

   (It is assumed that the zero sequence power is zero). In the revised (new) system,

   $$P_B = S_B = V_B I_B$$

   which leads to the same per unit power expression given above.

6. If the operating frequency is same as the base frequency, the per unit inductances are identical to per unit corresponding reactances. Then $\bar{x}_d = \bar{L}_d$, $\bar{x}_{df} = \bar{M}_{df}$ etc.

3.5.2   Rotor Base Quantities

The base power and frequency are same as for the stator circuits. The base currents for the rotor circuits in the d-axis are chosen such that the base field current or base d-axis damper current (in h coil) produce the same mutual flux (in the airgap) as produced by base current flowing in the stator d-axis coil. Similar conditions apply for q-axis coils. The mutual flux linkages in the d-axis are given by

$$\psi_{ad} = (L_d - L_{a\sigma})I_B = M_{df}I_{fB} = M_{dh}I_{hB} \qquad (3.65)$$

where $L_{a\sigma}$ is the leakage inductance of the stator. I_{fB} and I_{hB} are the base currents in the field and damper windings (in d-axis).

From Eq. (3.65),

$$I_{fB} = \frac{L_{ad}}{M_{df}}I_B, \quad I_{hB} = \frac{L_{ad}}{M_{dh}}I_B \qquad (3.66)$$

where $L_{ad} = L_d - L_{a\sigma}$

The base flux linkages for the rotor circuits are chosen that

$$\psi_{fB}I_{fB} = \psi_B I_B = \psi_{hB}I_{hB} \qquad (3.67)$$

Similar relations apply for q-axis coils also. The base currents and flux linkages for the g and k coils are given by

$$I_{gB} = \frac{L_{aq}}{M_{qg}}I_B, \quad I_{kB} = \frac{L_{aq}}{M_{qk}}I_B \qquad (3.68)$$

$$\psi_{gB} = \frac{\psi_B I_B}{I_{gB}}, \quad \psi_{kB} = \frac{\psi_B I_B}{I_{kB}} \qquad (3.69)$$

where

$$L_{aq} = L_q - L_{a\sigma}$$

Remarks

1. The per unit system is chosen such that the per unit mutual reactances M_{df} and M_{dh} are equal and can be expressed as

$$\bar{M}_{df} = \bar{M}_{dh} = \bar{L}_{ad} = \bar{L}_d - \bar{L}_{a\sigma}$$

Similarly

$$\bar{M}_{qg} = \bar{M}_{qk} = \bar{L}_{aq} = \bar{L}_q - \bar{L}_{a\sigma}$$

2. The choice of rotor base quantities is not unique. In general, the per unit mutual inductances can be expressed as

$$\begin{aligned} \bar{M}_{df} &= \bar{M}_{dh} = \bar{L}_d - \bar{L}_{c1} \\ \bar{M}_{qg} &= \bar{M}_{qk} = \bar{L}_q - \bar{L}_{c2} \end{aligned}$$

where $\bar{L}_{c1}$ and $\bar{L}_{c2}$ can be arbitrarily chosen (assuming magnetic linearity). It is only when representing saturation that it is convenient to define the per unit mutual inductances as given earlier. The leakage inductance of the stator $L_{a\sigma}$, is normally assumed to be constant (unaffected by saturation) while the mutual inductances are functions of the mutual flux linkages (considering saturation).

3. The selection of base quantities for the rotor circuits can be avoided if it is assumed that the rotor quantities can be referred to the stator using appropriate turns ratio (which are not always uniquely defined). The equivalent circuit referred to the stator can then be described in per unit quantities (on the stator base). This is explained in the next section.

3.5.3 An Alternative Approach

Consider a set of 'n' coupled coils. The flux linkage of kth coil is given by

$$\psi_k = \sum_{j=1}^{n} L_{kj} i_j \tag{3.70}$$

By expressing ψ_k and i_j in per unit given by

$$\bar{\psi}_k = \frac{\psi_k}{\psi_{kB}}, \quad \bar{i}_j = \frac{i_j}{I_{jB}} \tag{3.71}$$

Eq. (3.70) can be rewritten as

$$\bar{\psi}_k = \sum_{j=1}^{n} \left(\frac{L_{kj}}{\psi_{kB}} I_{jB} \right) \bar{i}_j = \sum_{j=1}^{n} \bar{L}_{kj} \bar{i}_j \tag{3.72}$$

where $\bar{L}_{kj}$ is the per unit mutual inductance given by

$$\bar{L}_{kj} = \frac{L_{kj}}{\psi_{kB}} I_{jB} \tag{3.73}$$

Similarly the per unit $\bar{L}_{jk}$ is given by

$$\bar{L}_{jk} = \frac{L_{jk}}{\psi_{jB}} I_{kB} \tag{3.74}$$

If $\bar{L}_{jk} = \bar{L}_{kj}$, the reciprocity in per unit mutual inductances require

$$\frac{I_{jB}}{\psi_{kB}} = \frac{I_{kB}}{\psi_{jB}} \quad \forall\, j,\ \forall\, k \tag{3.75}$$

which implies same base power for all the coils. It is assumed that the base frequency is same for all the coils.

If it is assumed that the measurements are carried out at the terminals of one coil (which may be labelled as 1 without loss of generality), the mutual flux between coils 1 and j can be expressed as

$$\psi_{1j} = L_{1j}\left(\frac{I_{jB}}{I_B}\right)\left(\frac{I_B}{I_{jB}}\right)i_j = L'_{1j}i'_j \tag{3.76}$$

where

$$i'_j = \left(\frac{I_B}{I_{jB}}\right)i_j = \left(\frac{N_j}{N_1}\right)i_j, \quad j = 2,\ 3,\ldots,n$$

can be considered as the current in coil j referred to coil 1 using the turns ratio $(\frac{N_j}{N_1})$. The base current and flux in coil are defined as I_B and ψ_B dropping the subscript 1. Equation (3.76) suggests the possibility of first referring the quantities to coil 1 using turns ratio (if specified) and then expressing them in per unit with respect to the base quantities defined for coil 1. Thus $\bar{L}_{1j}$ is expressed as

$$\bar{L}_{1j} = \frac{L'_{1j}}{\psi_B}I_B \tag{3.77}$$

Remarks

1. If turns ratios are known, the base currents (and fluxes) for coil j ($j = 2,\ 3,\ldots,\ n$) are defined in terms of the base quantities for coil 1 and the turns ratios.

2. If turns ratio are not explicitly defined, it is possible to choose base quantities such that

$$L'_{1j} = L_1 - l_1, \quad j = 2,\ 3,\ldots,\ n$$

   where l_1 is the leakage inductance of coil 1. The advantage of this choice is that the $(n-1)$ per unit mutual inductances are made equal and the total number of circuit parameters are reduced.

3. From equations (3.73) and (3.74), it is obvious that per unit mutual inductances can be made equal even if $L_{kj} \neq L_{jk}$ by proper choice of base quantities.

Example : A two winding transformer

Consider a two winding transformer shown in Fig. 3.4. The transformer is assumed to be lossless. The equivalent circuit of the transformer is shown in Fig. 3.5. The following equation applies for the secondary circuit of the ideal transformer

$$
\begin{aligned}
v_2 &= e_2 + l_2 \frac{di_2}{dt} \\
&= \frac{e_1 N_2}{N_1} + l_2 \frac{N_1}{N_2} \frac{di_2'}{dt}
\end{aligned}
\qquad (3.78)
$$

In the above equation, the relationships of the ideal transformer, namely

$$
e_2 = \frac{N_2}{N_1} e_1, \quad i_2' = \frac{N_2}{N_1} i_2
$$

are used.

The equation for the primary side of the transformer is

$$
v_1 = L_1 \frac{di_1}{dt} + M \frac{di_2}{dt} = L_1 \frac{di_1}{dt} + M' \frac{di_2'}{dt} = l_1 \frac{di_1}{dt} + e_1
\qquad (3.79)
$$

where

$$
\begin{aligned}
M' &= M \left(\frac{N_1}{N_2} \right) = L_1 - l_1 \\
e_1 &= M' \left(\frac{di_1}{dt} + \frac{di_2'}{dt} \right)
\end{aligned}
$$

Expressing (3.78) and (3.79) in per unit and selecting

$$
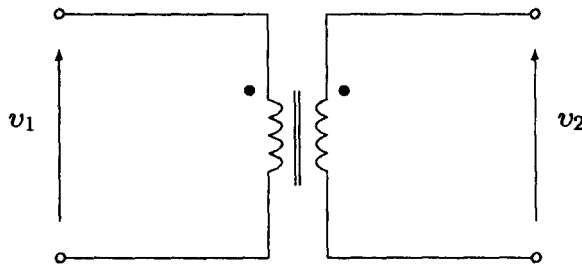V_{2B} = \frac{N_2}{N_1} V_{1B}, \quad I_{2B} = \frac{N_1}{N_2} I_{1B}
$$

$$
N_1 : N_2
$$

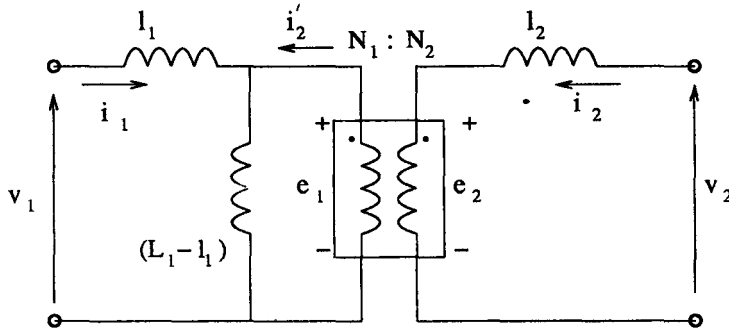Figure 3.4: A two winding transformer

Figure 3.5: Equivalent circuit of two winding transformer

we get

$$\left. \begin{array}{rcl} \bar{v}_1 & = & \bar{l}_1 \dfrac{d\bar{i}_1}{dt} + \bar{e}_1 \\[2mm] \bar{v}_2 & = & \bar{e}_1 - \bar{l}'_2 \dfrac{d\bar{i}_2}{dt} \end{array} \right\} \qquad (3.80)$$

where

$$\bar{e}_1 = \bar{M}' \frac{d}{dt}(\bar{i}_1 + \bar{i}_2)$$

$$l'_2 = \left(\frac{N_1}{N_2}\right)^2 l_2, \quad Z_{1B} = \frac{V_{1B}}{I_{1B}}, \quad \bar{l}_1 = \frac{l_1}{Z_{1B}}, \quad \bar{l}'_2 = \frac{l'_2}{Z_{1B}}, \quad \bar{M}' = \frac{M'}{Z_{1B}}$$

where l'_2 is the leakage inductance of the secondary referred to the primary. From Eq. (3.80) the equivalent circuit of Fig. 3.5, simplifies to that shown in Fig. 3.6.

The above analysis shows that the application of per unit system can be viewed as first referring all the secondary quantities to the primary side by utilizing the turns ratio and then scaling the variables with base quantities defined on the primary side. This interpretation relates the base quantities on both sides using the turns ratio.

In coupled coils, it is not always necessary nor feasible to determine the turns ratio (For example, the damper windings 'h', 'g' and 'k' are fictitious and introduced to represent the effects of eddy currents induced in the generator rotor). In such cases, the effective turns ratio can be defined as

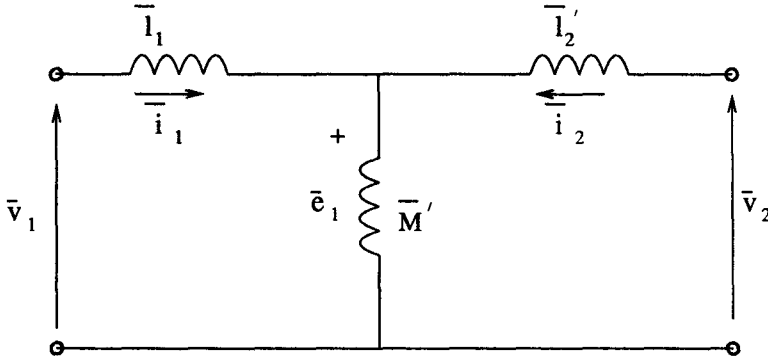$$n_{eff} = \frac{N_2}{N_1} = \frac{M}{(L_1 - l_1)} \qquad (3.81)$$

Figure 3.6: Equivalent circuit in per unit quantities

where l_1 is the leakage inductance of the primary winding. If magnetic saturation is not to be considered, there is no significance in defining a separate leakage inductance l_1 and it can be arbitrarily chosen (even equal to zero). The leakage inductance l_2' can be obtained as

$$l_2' = (L_1 - l_1) \left[\frac{L_2(L_1 - l_1)}{M^2} - 1 \right] \tag{3.82}$$

3.6 Equivalent Circuits of Synchronous Machine

There are two equivalent circuits corresponding to the two axes d and q. On the d-axis there are three coupled coils namely, armature d-coil, field winding, f, and damper winding, h. As explained earlier, by application of per unit system, all the quantities get referred to the armature side. The equivalent circuit on the d-axis is shown in Fig. 3.7.

All the reactances are expressed in per unit. $x_{a\sigma}$ is the armature leakage reactance. x_{fc} and x_{hc} can be viewed as the leakage reactances of the field and the damper winding (h) respectively. x_{rc} represents the fact that per unit mutual reactance x_{fh} (between the field and damper) is not equal to x_{ad}. Actually

$$x_{fh} = x_{ad} + x_{rc} = x_d - x_{a\sigma} + x_{rc} \tag{3.83}$$

It can be shown that the equivalent circuit of Fig. 3.7 can be transformed to the simplified form shown in Fig. 3.8. Here k is defined as

$$k = \left(\frac{x_d - x_c}{x_{ad}} \right)^2 \tag{3.84}$$
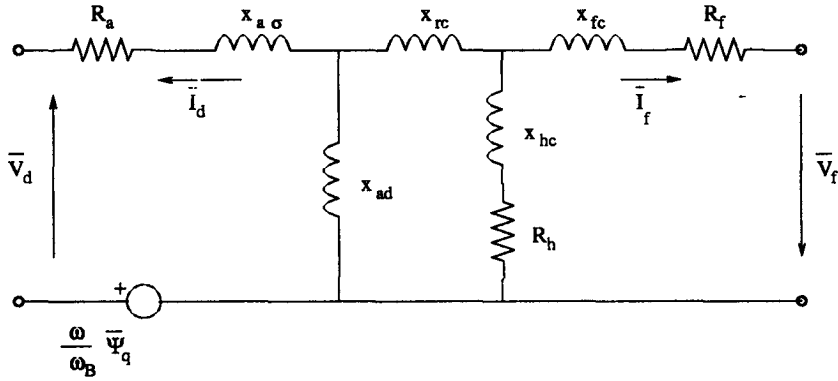
Figure 3.7: Equivalent circuit -d axis
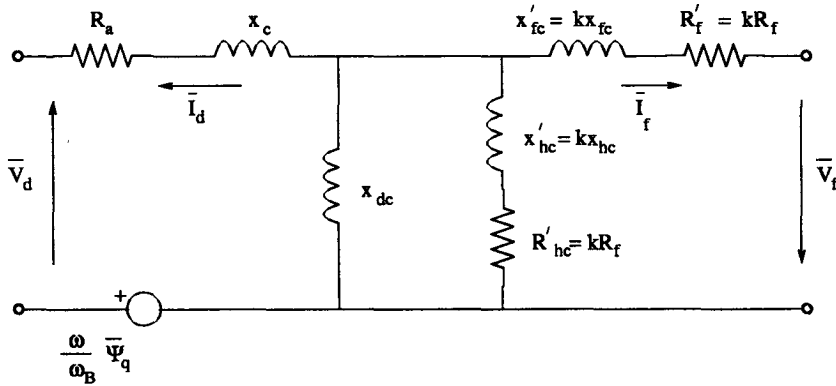
Figure 3.8: Transformed d-axis equivalent circuit

and x_c is obtained from

$$\frac{1}{x_c - x_{a\sigma}} = \frac{1}{x_{ad}} + \frac{1}{x_{rc}} \tag{3.85}$$

Instead of $x_{a\sigma}$, a new reactance x_c appears and the mutual reactances x_{fh}, x_{dh} and x_{df} are all equal to x_{dc}. While this simplified equivalent circuit is often used, error is committed by assuming $x_c \simeq x_{a\sigma}$. This is inaccurate and gives wrong results in predicting field quantities [20, 21]. For example, for turbo alternators x_c is much larger than $x_{a\sigma}$ and for salient pole machines x_c can be negative [21]. Canay [21] has proposed a simple test for the determination of x_c.

The equivalent circuit on the q-axis is shown in Fig. 3.9. Here, as both

Figure 3.9: Equivalent circuit- q-axis

damper windings are short circuited, there is no loss of generality in assuming

$$x_{qg} = x_{qk} = x_{gk} = x_{aq} = x_q - x_{a\sigma} \tag{3.86}$$

Also, for linear magnetic circuits, $x_{a\sigma}$ can be arbitrarily selected. This follows from the fact that the only quantity of interest in the q-axis is the driving point (operational) impedance defined by
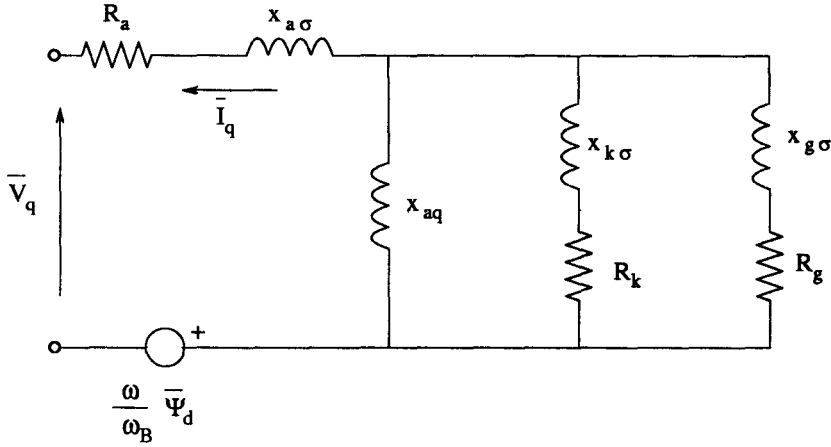
$$\frac{\Psi_q(s)}{I_q(s)} = \frac{x_q(1 + sT'_q)(1 + sT''_q)}{(1 + sT'_{qo})(1 + sT''_{qo})} = X_q(s) \tag{3.87}$$

where T'_{qo} and T'_q are the open and short circuit transient time constants, T''_{qo} and T''_q are the open and short circuit subtransient time constants. Eq. (3.87) shows that only five parameters (including x_q) are required to define the operational impedance and the equivalent circuit (neglecting armature resistance). Thus the role of leakage reactance $x_{a\sigma}$ is only required in accurately representing magnetic saturation. In the absence of saturation, any value of $x_{a\sigma}$ can be used.

This argument does not hold for the d-axis equivalent circuit where x_c is uniquely defined. This is because of the presence of field circuit excitation. The d-axis flux linkage $\Psi_d(s)$ can be expressed as

$$\Psi_d(s) = X_d(s)I_d(s) + G(s)E_{fd}(s) \tag{3.88}$$

where

$$X_d(s) = \frac{x_d(1 + sT'_d)(1 + sT''_d)}{(1 + sT'_{do})(1 + sT''_{do})}$$

T''_{do}, T''_d are open and short circuit subtransient time constants. T'_{do} and T'_d are open and short circuit transient time constants.

$G(s)$ is defined by

$$G(s) = \frac{(1 + sT''_{dc})}{(1 + sT'_{do})(1 + sT''_{do})} \tag{3.89}$$

In Eq. (3.88), E_{fd} is related to v_f by

$$E_{fd} = \frac{x_{df}}{R_f} v_f \tag{3.90}$$

This scaling of the field voltage is done for convenience - and has the effect of equating the generator open circuit voltage (in steady state) to E_{fd} (1 pu E_{fd} results in 1 pu generated voltage on open circuit).

The calculation of self and mutual (per unit) reactances from the equivalent circuit parameters is straight forward and is given below

$$
\begin{aligned}
x_{df} &= x_{dh} = x_{ad} = x_d - x_{a\sigma} \\
x_{fh} &= x_{ad} + x_{rc}, \quad x_f = x_{fh} + x_{fc}, \quad x_h = x_{fh} + x_{hc} \\
x_{qg} &= x_{qk} = x_{gk} = x_{aq} = x_q - x_{a\sigma} \quad . \\
x_g &= x_{aq} + x_{g\sigma}, \quad x_k = x_{aq} + x_{k\sigma}
\end{aligned}
$$

3.7 Determination of Parameters of Equivalent Circuits

It is assumed that R_a, $x_{a\sigma}$ (leakage reactance of the armature) and x_d, x_q (synchronous reactances) are known. In addition there are five parameters in the d-axis equivalent circuit:

$$x_{rc}, \ x_{hc}, \ x_{fc}, \ R_h \quad \text{and} \quad R_f$$

and four parameters of the equivalent circuit in the q-axis:

$$x_{g\sigma}, \ x_{k\sigma}, \ R_g \quad \text{and} \quad R_k$$

3.7.1 Direct Axis Equivalent Circuit

The transient and subtransient quantities can be determined from measurements according to IEC or ASA recommendations. These are

$$x_d', \; x_d'', \; T_d' \quad \text{and} \quad T_d''$$

where x_d' and x_d'' are transient and subtransient reactances of the machine in d-axis. The transfer function $X_d(s)$ is completely defined by the quantities $x_d', x_d'', \; T_d', \; T_d''$ and x_d. This follows from the expression for the inverse of $X_d(s)$ given below which represents the basic definition of x_d' and x_d'' in accordance with IEC or ASA standards

$$\frac{1}{X_d(s)} = \frac{1}{x_d} + \left(\frac{1}{x_d'} - \frac{1}{x_d}\right) \frac{sT_d'}{1 + sT_d'} + \left(\frac{1}{x_d''} - \frac{1}{x_d'}\right) \frac{sT_d''}{1 + sT_d''} \tag{3.91}$$

Relating (3.91) to

$$X_d(s) = \frac{x_d(1 + sT_d')(1 + sT_d'')}{(1 + sT_{do}')(1 + sT_{do}'')} \tag{3.92}$$

We have the following relations

$$T_{do}' + T_{do}'' = \frac{x_d}{x_d'} T_d' + \left(1 - \frac{x_d}{x_d'} + \frac{x_d}{x_d''}\right) T_d'' \tag{3.93}$$

$$T_{do}' T_{do}'' = T_d' T_d'' \frac{x_d}{x_d''} \tag{3.94}$$

These equations can be used to exactly calculate T_{do}' and T_{do}'' if T_d' and T_d'' are known or vice versa. There is no need to make any simplifying assumptions.

It can be shown that

$$X_d(s) + x_e = \frac{x_{de}(1 + sT_{de}')(1 + sT_{de}'')}{(1 + sT_{do}')(1 + sT_{do}'')} = X_{de}(s)$$

where

$$x_{de} = x_d + x_e \tag{3.95}$$

$$T_{de}' + T_{de}'' = \frac{x_d(T_d' + T_d'') + x_e(T_{do}' + T_{do}'')}{x_d + x_e} \tag{3.96}$$

$$T_{de}' T_{de}'' = T_{do}' T_{do}'' \frac{(x_d'' + x_e)}{(x_d + x_e)} \tag{3.97}$$

It is also possible to calculate x_{de}' and x_{de}'' (from the expression for the inverse of $X_{de}(s)$) and these are

$$x_{de}' = \frac{x_{de}(T_{de}' - T_{de}'')}{T_{do}' + T_{do}'' - \left(1 + \dfrac{x_{de}}{x_{de}''}\right) T_{de}''} \tag{3.98}$$

$$x_{de}'' = x_d'' + x_e \tag{3.99}$$

It is to be noted that $x'_{de} \neq (x'_d + x_e)$. It is convenient to determine the parameters for the simpler equivalent circuit (shown in Fig. 3.8) and compute the parameters of Fig. 3.7 based on the relations (3.84) and (3.85). It is necessary that x_c (which is not a leakage reactance) is determined from design calculations or measurements.

Eq. (3.91) represents the admittance of the equivalent circuit shown in Fig. 3.10. In this circuit, the voltage corresponds to $\psi_d(s)$ and the current is $I_d(s)$. The circuit shown in Fig. (3.10) is also equivalent to that shown in Fig. (3.11) where x_c is included in series and

$$x_{dc} = x_d - x_c, \quad x''_{dc} = x''_d - x_c \tag{3.100}$$

By using relations (3.95) to (3.99) where $-x_c$ is substituted for x_e, the quantities $x'_{dc}, x''_{dc}, T'_{dc}$ and T''_{dc} are obtained. The expressions for $x'_{fo}, R'_{fo}, x'_{ho}$ and R'_{ho} are
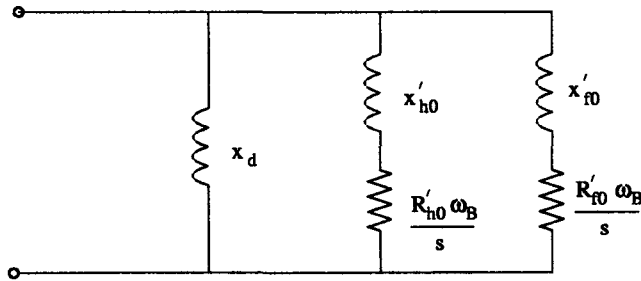

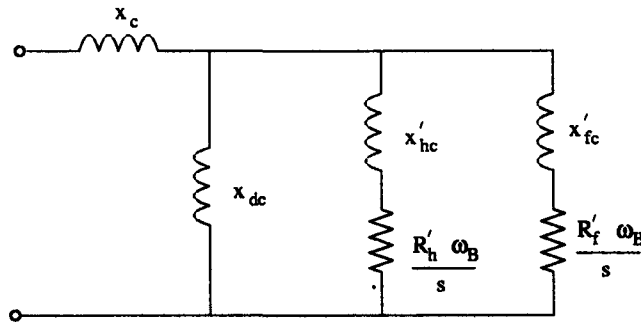Figure 3.10: Representation of $X_d(s)$ by an equivalent circuit

Figure 3.11: Alternate representation of $X_d(s)$

$$x'_{fo} \;=\; \frac{x_d x'_d}{x_d - x'_d}, \quad R'_{fo} = \frac{x'_{fo}}{\omega_B T'_d} \tag{3.101}$$

$$x'_{ho} \;=\; \frac{x'_d x''_d}{x'_d - x''_d}, \quad R'_{ho} = \frac{x'_{ho}}{\omega_B T''_d} \tag{3.102}$$

The expressions for x'_{fc}, R'_f, x'_{hc} and R'_h (for the equivalent circuit of Fig. 3.8 or 3.11) are

$$x'_{fc} \;=\; \frac{x_{dc} x'_{dc}}{x_{dc} - x'_{dc}}, \quad R'_f = \frac{x'_{fc}}{\omega_B T'_{dc}} \tag{3.103}$$

$$x'_{hc} \;=\; \frac{x'_{dc} x''_{dc}}{x'_{dc} - x''_{dc}}, \quad R'_h = \frac{x'_{hc}}{\omega_B T''_{dc}} \tag{3.104}$$

The calculations of the parameters of the equivalent circuit in Fig. 3.8 are summarized below

Step 1: Compute T'_{do} and T''_{do} from Eqs, (3.93) and (3.94)

Step 2: Compute

$$x_{dc} \;=\; x_d - x_c$$
$$x''_{dc} \;=\; x''_d - x_c$$

Step 3: Compute T'_{dc} and T''_{dc} from

$$T'_{dc} + T''_{dc} \;=\; (T'_d + T''_d)\, x_d/x_{dc} - (T'_{do} + T''_{do})\, x_c/x_{dc}$$
$$T'_{dc} T''_{dc} \;=\; T'_{do} T''_{do} x''_{dc}/x_{dc}$$

Step 4: Calculate x'_{dc} from

$$x'_{dc} = \frac{x_{dc}(T'_{dc} - T''_{dc})}{T'_{do} + T''_{do} - \left(1 + \dfrac{x_{dc}}{x''_{dc}}\right) T''_{dc}}$$

Step 5: Calculate the parameters

$$x_{rc} \;=\; (x_c - x_{ao})\frac{x_{ad}}{x_{dc}}$$

$$x_{hc} \;=\; \frac{x'_{dc} x''_{dc}}{(x'_{dc} - x''_{dc})}\left(\frac{x_{ad}}{x_{dc}}\right)^2$$

$$x_{fc} \;=\; \frac{x_{dc} x'_{dc}}{(x_{dc} - x'_{dc})}\left(\frac{x_{ad}}{x_{dc}}\right)^2$$

$$R_h \;=\; \frac{x_{hc}}{\omega_B T''_{dc}}$$

$$R_f \;=\; \frac{x_{fc}}{\omega_B T'_{dc}}$$

It can be shown that the time constant T_{dc}'' in the expression (3.89) is given by

$$T_{dc}'' = \frac{x_{hc}}{R_h \omega_B} \tag{3.105}$$

Calculation of Transient and Subtransient Quantities from Equivalent Circuit Parameters

The open circuit time constants T_{do}' and T_{do}'' can be calculated from the equivalent circuit parameters of Fig. 3.8. These are obtained as the negative reciprocals of the roots of a characteristic equation

$$1 + \frac{s}{\omega_B}\left(\frac{x_f'}{R_f'} + \frac{x_h'}{R_h'}\right) + \frac{s^2}{\omega_B^2}\left[\frac{x_{dc}(x_{fc}' + x_{hc}') + x_{fc}'x_{hc}'}{R_f'R_h'}\right] = 0 \tag{3.106}$$

If it is assumed that $R_h' >> R_f'$, then

$$T_{do}' \simeq \frac{x_f'}{\omega_B R_f'} = \frac{x_{fc}' + x_{dc}}{\omega_B R_f'} \tag{3.107}$$

$$T_{do}'' \simeq \frac{1}{\omega_B R_{hc}'}\left[x_{hc}' + \frac{x_{fc}'x_{dc}}{(x_{dc} + x_{fc}')}\right] \tag{3.108}$$

The transient reactance, x_d' can also be approximated as

$$x_d' = x_d - \frac{x_{dc}^2}{x_f'} = x_c + \frac{x_{dc}x_{fc}'}{x_{dc} + x_{fc}'} \tag{3.109}$$

The short circuit transient time constant T_d' can be approximated as

$$T_d' = T_{do}'\frac{x_d'}{x_d} \tag{3.110}$$

Many publications use the approximations (3.107) to (3.110) without examining their validity. The basic assumptions behind these approximations are

1. In computing transient quantities, the damper circuit is assumed to be open, i.e. $R_h \to \infty$

2. In computing the subtransient quantities, the field circuit is assumed to have zero resistance.

Obviously these assumptions are not valid in all the cases. Unfortunately, the old practices (of using the approximations) still continue in industry. F.P. DeMello

and L.H. Hannett [24] even claim that it is a matter of definitions, the only requirement being consistent with the definitions. For example, they state that T'_{do} and T''_{do} are to be defined by the expressions given in (3.107) and (3.108) rather than as the roots of the characteristic equation (3.106) which govern the response of the machine fluxes under open circuit. While this argument is certainly valid, it does create confusion to have two sets of definitions. There is a need for standard definitions of T'_{do} and T''_{do}. Recent literature [21, 22, 23, 25, 27] stress the use of logical definition of the time constants based on the machine responses.

3.7.2 Quadrature Axis Equivalent Circuit

The parameters of the q-axis equivalent circuits that are to be determined are

$$x_{g\sigma}, \ x_{k\sigma}, \ R_g \quad \text{and} \quad R_k$$

These are obtained from the measured or calculated data on x'_q, x''_q, T'_q and T''_q. It is assumed that x_q and $x_{a\sigma}$ are known. The procedure for calculation of the q-axis equivalent circuit parameters is similar to that given for the d-axis equivalent circuit parameters. The steps are given below:

Step 1: Compute

$$x_{aq} \ = \ x_q - x_{a\sigma}$$
$$x''_{q\sigma} \ = \ x''_q - x_{a\sigma}$$

Step 2: Compute T'_{qo} and T''_{qo} from

$$T'_{qo} + T''_{qo} \ = \ \frac{x_q}{x'_q}T'_q + \left(1 - \frac{x_q}{x'_q} + \frac{x_q}{x''_q}\right)T''_q$$
$$T'_{qo}T''_{qo} \ = \ T'_q T''_q \frac{x_q}{x''_q}$$

Step 3: Compute $T'_{q\sigma}$ and $T''_{q\sigma}$ from

$$T'_{q\sigma} + T''_{q\sigma} \ = \ (T'_q + T''_q)\frac{x_q}{x_{aq}} - (T'_{qo} + T''_{qo})\frac{x_{a\sigma}}{x_{aq}}$$
$$T'_{q\sigma}T''_{q\sigma} \ = \ T'_{qo}T''_{qo}\frac{x''_{q\sigma}}{x_{aq}}$$

Step 4:

$$x'_{q\sigma} = \frac{x_{aq}(T'_{q\sigma} - T''_{q\sigma})}{T'_{qo} + T''_{qo} - \left(1 + \dfrac{x_{aq}}{x''_{q\sigma}}\right) T''_{q\sigma}}$$

Step 5: Calculate the parameters

$$x_{k\sigma} = \frac{x'_{q\sigma} x''_{q\sigma}}{x'_{q\sigma} - x''_{q\sigma}}$$

$$x_{g\sigma} = \frac{x_{aq} x'_{q\sigma}}{x_{aq} - x'_{q\sigma}}$$

$$R_k = \frac{x_{k\sigma}}{\omega_B T''_{q\sigma}}$$

$$R_g = \frac{x_{g\sigma}}{\omega_B T'_{q\sigma}}$$

Remarks

1. The open circuit time constants T'_{qo} and T''_{qo} can be determined from the equivalent circuit parameters. These are obtained as negatives of the reciprocals of the roots of the characteristic equation

$$1 + \frac{s}{\omega_B} \left(\frac{x_g}{R_g} + \frac{x_k}{R_k}\right) + \frac{s^2}{\omega_B^2} \left[\frac{x_{aq}(x_{g\sigma} + x_{k\sigma}) + x_{g\sigma} x_{k\sigma}}{R_g R_k}\right] = 0 \qquad (3.111)$$

If $R_g \gg R_k$, T'_{qo} and T''_{qo} can be approximated as

$$T'_{qo} \simeq \frac{x_g}{\omega_B R_g} = \frac{x_{g\sigma} + x_{aq}}{\omega_B R_g}$$

$$T''_{qo} \simeq \frac{1}{\omega_B R_k} \left[x_{k\sigma} + \frac{x_{g\sigma} x_{aq}}{(x_{aq} + x_{g\sigma})}\right]$$

   The assumptions are similar to that used in connection with the calculation of transient and subtransient quantities in the d-axis. However the justification for these assumptions for the q-axis is suspect as the difference between T'_{qo} and T''_{qo} is much less than the difference between T'_{do} and T''_{do}

2. Unfortunately, the practice of making the assumptions both for d- and q-axis parameters, appears to continue. This can lead to inaccurate results in the prediction of machine performance.

One way out of this difficulty is the determination of transfer function $X_d(s)$ and $X_q(s)$ directly from measurements using frequency response tests [29-32]

3. A most frequently used assumption is that $x_{fh} = x_{ad}$. This is inaccurate as $x_{ad} = x_d - x_{a\sigma}$. In the absence of magnetic saturation, there is no restriction in selecting

$$x_{fh} = x_{df} = x_{dh} = x_{dc} = x_d - x_c$$

(all the three mutual reactances are assumed to be equal). However, the value of x_c must be accurately determined either by calculations or test (Note that for some machines x_c may be even be negative).

For the q-axis equivalent circuit there is no restriction on the choice of

$$x_{gk} = x_{qg} = x_{qk} = x_{ag} = x_q - x_{a\sigma}$$

Neglecting saturation, $x_{a\sigma}$ can even be assumed to be zero or selected arbitrarily.

3.7.3 Measurement of Characteristic Reactance x_c

x_c can be determined from measurements during 3-phase sudden short circuit test on the machine. Immediately after the short circuit applied at $t = 0^+$, the field current variation with time is shown in Fig. 3.12. The AC component has a frequency of ω_B. Defining the ratio,

$$a = \frac{I_p\,(t = 0^+)}{I_{fo}} \tag{3.112}$$

where I_p is the peak (amplitude) value of the AC component and I_{fo} is the initial (prefault) current in the field winding.

It can be shown (with approximations, $x'_{dc} \simeq x'_d - x_c$ and $\omega_B T'_{dc} >> 1$), that

$$a \simeq \frac{(x_d - x'_d)}{x''_d} \frac{(x''_d - x_c)}{(x'_d - x_c)} \tag{3.113}$$

x_c can be solved from (3.113) as

$$x_c = x''_d \left[1 - \frac{(x'_d - x''_d)}{(x_d - x'_d)\left(\dfrac{c}{a}\right) - x''_d} \right] \tag{3.114}$$
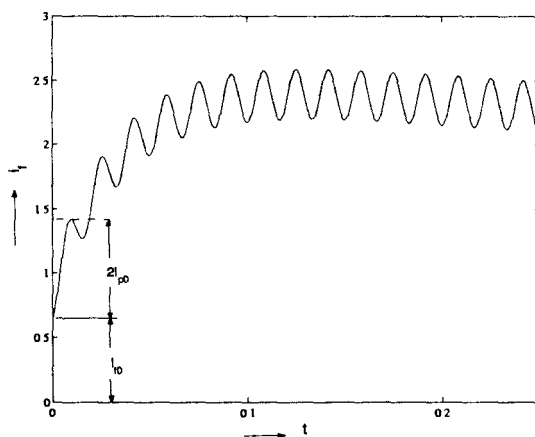
Figure 3.12: Field current variation following sudden short circuit

where

$$c = \sqrt{1 + \left[\frac{x_d - x_d' - ax_d''}{ax_d'T_d''\omega_B}\right]^2}$$

A check on the measurement is that the AC component of the field current cannot be too small. The ratio a has a minimum value given by

$$a_{min} \simeq \frac{x_d - x_d'}{x_d'}\frac{1}{T_d''\omega_B}$$

3.7.4   Examples

Example 3.1

In the IEEE First Benchmark model for SSR [50], the generator has the following data.
$x_d = 1.79$, $x_{a\sigma} = 0.13$, $x_d' = 0.169$, $x_d'' = 0.135$, $T_{do}' = 4.3$, $T_{do}'' = 0.032$,
$x_q = 1.71$, $x_q' = 0.228$, $x_q'' = 0.2$, $T_{qo}' = 0.85$, $T_{qo}'' = 0.05$, $f_B = 60$ Hz.

Compute the equivalent circuit parameters using (a) exact calculation and (b) approximate method (also termed as standard method [22]).

Solution

Even in the exact method, since x_c is not specified, it is assumed that $x_c = x_{a\sigma}$.
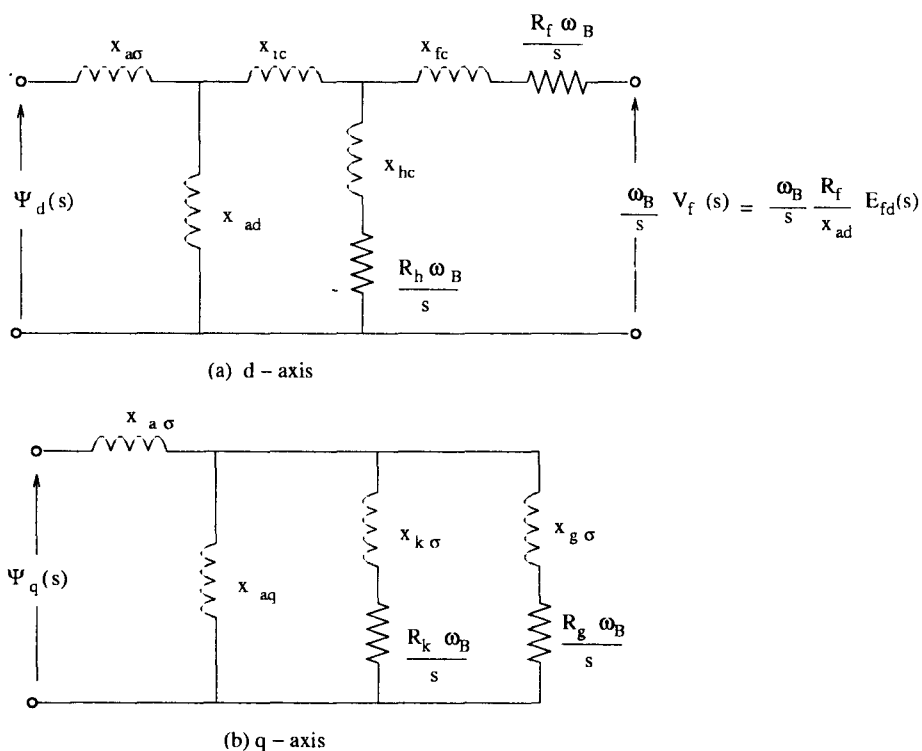
(a) d – axis

(b) q – axis

Figure 3.13: Equivalent Circuits

The equivalent circuits for both d- and q-axis are shown in Fig. 3.13. The approximate (standard) method uses the assumptions

1. In computing the transient quantities, the damper winding in the d-axis (or the high resistance damper in the q-axis) is assumed to be open

2. In computing the subtransient quantities, the resistance of field winding (or the low resistance damper winding in the q-axis) is neglected

The calculation of the equivalent circuit parameters based on these assumptions are given in Table 3.2

The results are shown in Table 3.3.

Example 3.2 [21]

A salient pole machine has the following data in the d-axis.
$x_d = 1.77$, $x'_d = 0.254$, $x''_d = 0.155$, $x_{a\sigma} = 0.089$, $x_c = -0.0776$, $T'_d = 0.87$,
$T''_d = 0.07$, $f_B = 50$ Hz.

Table 3.2   Equivalent circuit Parameters-Standard Method

d-axis	q-axis
$x_{ad} = x_d - x_{a\sigma}$	$x_{aq} = x_q - x_{a\sigma}$
$x_{f\sigma} = \dfrac{(x_d' - x_{a\sigma})}{(x_d - x_d')}x_{ad}$	$x_{g\sigma} = \dfrac{(x_q' - x_{a\sigma})}{(x_q - x_q')}x_{aq}$
$x_{h\sigma} = \dfrac{(x_d'' - x_{a\sigma})}{(x_d' - x_d'')}(x_d' - x_{a\sigma})$	$x_{k\sigma} = \dfrac{(x_q'' - x_{a\sigma})}{(x_q' - x_q'')}(x_q' - x_{a\sigma})$
$R_f = \dfrac{1}{\omega_B T_d'} \cdot \dfrac{x_d'}{x_d} \cdot \dfrac{x_{ad}^2}{(x_d - x_d')}$	$R_g = \dfrac{1}{\omega_B T_q'} \cdot \dfrac{x_q'}{x_q} \cdot \dfrac{x_{aq}^2}{(x_q - x_q')}$
$R_h = \dfrac{1}{\omega_B T_d''} \cdot \dfrac{x_d'}{x_d''} \cdot \dfrac{(x_d' - x_{a\sigma})^2}{(x_d' - x_d'')}$	$R_k = \dfrac{1}{\omega_B T_q''} \cdot \dfrac{x_q}{x_q'} \cdot \dfrac{(x_q' - x_{a\sigma})}{(x_q' - x_q'')}$

Table 3.3   Numerical Values of Parameters (Example 3.1)

d-Axis Parameters	Standard	Exact with assumption $x_c = x_{a\sigma}$	q-Axis Parameters	Standard	Exact
$x_{h\sigma}$	0.00574	0.00546	$x_{k\sigma}$	0.245	0.329
$x_{f\sigma}$	0.0399	0.0618	$x_{g\sigma}$	0.104	0.0942
R_h	0.00371	0.00407	R_k	0.0182	0.0141
R_f	0.00105	0.00141	R_g	0.00526	0.00819

Calculate the equivalent circuit parameters for the d-axis using

a) standard method

b) Exact method with the assumption $x_c = x_{a\sigma}$

c) Exact method

Solution

The results are shown in Table 3.4. (Note that for the exact method, the subscript c should substitute for σ) Note also that x_c and x_{rc} are negative in this case. In general, this is true for salient pole machines.

Example 3.3 [21]

(a) Obtain the expressions for $X_d(s)$ and $G(s)$ in terms of circuit parameters in d-axis

(b) Calculate the time constants T_{do}', T_{do}'', T_d' and T_d'' if $x_d = 1.803$, $x_{df} = x_{dh} = x_{ad} = 1.571$, $x_{fh} = 1.6624$, $x_f = 1.8334$, $x_h = 1.674$, $R_f = 0.000856$, $R_h = 0.00871$, $f_B = 60$ Hz Also compute x_d' and x_d''.

Table 3.4 d-Axis Parameters (Example 3.2)

Parameters	Standard	Exact	Exact $x_c = x_{a\sigma}$
x_{rc}	–	-0.152	–
$x_{h\sigma}(x_{hc})$	0.110	0.672	0.105
$x_{f\sigma}(x_{fc})$	0.183	0.328	0.200
R_h	0.00763	0.0266	0.00736
R_f	0.000979	0.000956	0.00106

Solution

(a) The expression for $X_d(s)$ can be obtained as

(i)

$$X_d(s) = \frac{\psi_d(s)}{I_d(s)}\bigg|_{E_{fd}=0}$$

$$= \frac{x_d(1 + a_1 s + a_2 s^2)}{(1 + b_1 s + b_2 s^2)} = x_d \frac{(1 + sT_d')(1 + sT_d'')}{(1 + sT_{do}')(1 + sT_{do}'')}$$

From the equivalent circuit in Fig. 3.13, we have

$$X_d(s) = x_{a\sigma} + \cfrac{1}{\cfrac{1}{x_{ad}} + \cfrac{1}{\left(x_{h\sigma} + \cfrac{R_h \omega_B}{s}\right)} + \cfrac{1}{\left(x_{f\sigma} + \cfrac{R_f \omega_B}{s}\right)}}$$

$$= \frac{x_d(1 + a_1 s + a_2 s^2)}{(1 + b_1 s + b_2 s^2)}$$

where

$$b_1 = \frac{(x_{ad} + x_{f\sigma})}{\omega_B R_f} + \frac{(x_{ad} + x_{h\sigma})}{\omega_B R_h} = \frac{x_f}{\omega_B R_f} + \frac{x_h}{\omega_B R_h}$$

$$b_2 = \frac{1}{R_f R_h \omega_B^2}[x_{ad}(x_{f\sigma} + x_{h\sigma}) + x_{f\sigma} x_{h\sigma}]$$

$$a_1 = x_{a\sigma} b_1 + x_{ad}\left(\frac{x_{f\sigma}}{R_f \omega_B} + \frac{x_{h\sigma}}{R_h \omega_B}\right)$$

$$a_2 = x_{a\sigma} b_2 + \frac{x_{ad} x_{f\sigma} x_{h\sigma}}{R_f R_h \omega_B^2}$$

T'_{do} and T''_{do} are obtained as the negative reciprocals of the roots of the equation

$$1 + b_1 s + b_2 s^2 = 0$$

Similarly T'_d and T''_d are obtained as the negative reciprocals of the roots of the equation

$$1 + a_1 s + a_2 s^2 = 0$$

Note: The calculations are identical if in the equivalent circuit of Fig. 3.13, $x_{a\sigma}$ is replaced by x_c and $x_{h\sigma}$ and $x_{f\sigma}$ are replaced by x'_{hc} and x'_{fc} respectively.

(ii)

$$G(s) = \frac{\psi_d(s)}{E_{fd}(s)} \Big|_{I_d = 0}$$

From the equivalent circuit of Fig. 3.13, we can obtain

$$G(s) = \frac{R_f \omega_B}{x_{ad} s \left(x_{f\sigma} + \dfrac{R_f \omega_B}{s} \right)} \times$$

$$\left[\frac{1}{\dfrac{1}{x_{ad}} + \left(x_{f\sigma} + \dfrac{R_f \omega_B}{s} \right) + \left(x_{h\sigma} + \dfrac{R_h \omega_B}{s} \right)} \right]$$

$$= \frac{\left(1 + s \dfrac{x_{h\sigma}}{R_h \omega_B} \right)}{(1 + b_1 s + b_2 s^2)} = \frac{(1 + sT_1)}{(1 + sT'_{do})(1 + sT''_{do})}$$

where

$$T_1 = \frac{x_{h\sigma}}{R_h \omega_B}$$

(b) Substituting the values, the time constants are obtained as

$$T'_d = 1.497 \ \text{sec}, \quad T''_d = 0.035, \quad \text{sec} \quad T_1 = 0.00353 \ \text{sec}$$
$$T'_{do} = 6.14 \ \text{sec}, \quad T''_{do} = 0.047 \ \text{sec}$$

The reactances, x'_d and x''_d are obtained by applying Eqs. (3.93) and (3.94).

These are $x''_d = 0.327$, $x'_d = 0.442$

3.8   Measurements for Obtaining Data

The synchronous machine data mainly refer to the parameters of the equivalent circuits on the two axes. Test procedures are designed to obtain this data. Most of these presume that there are only two rotor windings per axis (model 2.2)

Classification of Machine Models [32]

Depending on the degree of complexity, the machine models are classified depending upon the number of rotor circuits on each axis. Model (i, j) refers to a synchronous machine having 'i' number of rotor circuits on the d-axis and 'j' number of rotor circuits on the q-axis. Thus model (1.0) refers to the case when all damper windings are neglected and only the field winding (on the d-axis) is considered. Model (2.2) is the most commonly used detailed model although models (3.2) and (3.3) have also been proposed [7,32]. On the other hand, model (0.0) refers to the classical model neglecting flux decay and damper windings.

Short Circuit Tests [26]

IEEE Standard No.115 [26] describes in detail the short circuit tests which were first proposed in 1948. The latest revision of the test code was done in 1983.

A typical test is a three phase short circuit applied to the terminals of a synchronous machine which is running at rated speed on open circuit. The open circuit voltage can be chosen at any value within specifications. For determination of the reactances, the tests are performed for several voltage levels in a range typically up to about 0.5 to 0.6 p.u. of rated terminal voltage. The oscillograms of the armature currents are obtained and the variations in the peak to peak current magnitudes with time are plotted on semi-logarithmic paper. Generally, two slopes in the current variation are identified. The projection of each slope to zero time (when the fault is applied) will determine the initial magnitude of the current, which, when divided into the voltage magnitude before the fault, gives a reactance. The initial, smaller value is the subtransient reactance (x_d'') and the second larger value is the transient resistance (x_d'). The slopes are also used to derive the time constants T_d' and T_d''. There is no procedure in IEEE Standard No.115 for a similar test to obtain quantities in the q-axis.

Decrement Tests: [23, 24, 27]

These tests involve sudden changes imposed on either stator or field windings. In the method described in [24], the machine armature currents are interrupted

under two initial operating conditions (i) $i_d = 0$ and (ii)$i_q = 0$. The conditions can be achieved by under-exciting or over exciting the machine at some percentage of the full load. Achieving an exact loading condition for either $i_d = 0$ or $i_q = 0$ is unnecessary provided an accurate measurement of the rotor angle is available.

Decrement tests proposed by Shackshaft [23, 27] have been used at Central Electricity Generating Board in U.K. There are two types of tests

a) Stator decrement tests

b) Rotor decrement tests

In a stator decrement test, the machine under test is operated at zero load and is excited totally from the power system, i.e. its field current is zero. The generator is then suddenly disconnected from the system and the subsequent variation of stator voltage and the current in the field winding (if closed) can be used to determine the machine parameters.

In a rotor decrement test with the stator on open circuit, the machine is excited via its field winding and the excitation supply is then suddenly shorted out. From the decay of the field current and stator voltage, some of the parameters can be obtained.

Frequency Response Tests [25, 29-32]

An alternative approach to the determination of machine parameters is through frequency response testing. Both (a) standstill and (b) on-line frequency response tests are used.

Conceptually, this approach involves viewing the machine model as a two port network in the d-axis and one port network in the q-axis. (See Fig. 3.14.) This representation enables even the most detailed model (3.3) to be considered. Also, these networks can be viewed as linear R-C networks whose immittance functions have certain properties. For example the function $X_d(s)$ can be expressed as

$$X_d(s) = \frac{x_d(1 + sT_1)(1 + sT_2)(1 + sT_3)}{(1 + sT_4)(1 + sT_5)(1 + sT_6)} \qquad (3.115)$$

with 3 rotor windings in d-axis. From the properties of the immittance function, we have

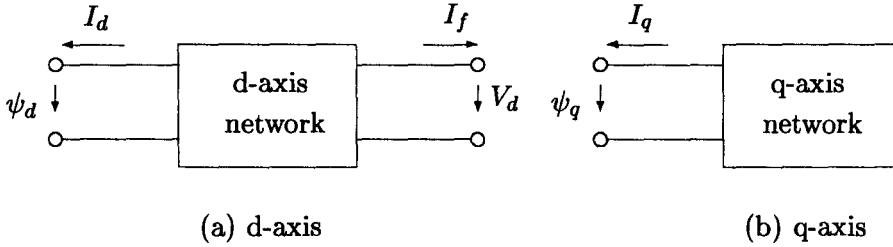$$T_3 < T_6 < T_2 < T_5 < T_1 < T_4$$

(a) d-axis (b) q-axis

Figure 3.14: Representation of d-axis and q-axis models

For model (2.2), the above inequality can be expressed as

$$T_d'' < T_{do}'' < T_d' < T_{do}'$$

Similarly for the q-axis, we have

$$T_q'' < T_{qo}'' < T_q' < T_{qo}'$$

The standstill frequency response (SSFR) test is convenient to use and the details are given in [29]. In addition to the determination of the transfer functions $\frac{V_d}{I_d}(s)$, $\frac{V_q}{I_q}(s)$, with field winding shorted, Coultes and Watson [29] also recommend the measurement of two more transfer function $\frac{V_f}{I_d}(s)$ and $\frac{I_f}{I_d}(s)$, the former with the field winding open and the latter with the field shorted. The measurements also enable the computation of x_{rc} in the d-axis equivalent circuit of Fig. 3.7.

The direct axis operational impedance, $\frac{V_d}{I_d}(s)$ is measured using any one of the two possible connections shown in Fig. 3.15. In the first connection (a), the magnetic axes of phase a and field are aligned ($\theta = 0$). In the second connection (b), the magnetic axis of field winding is at 90° to that of phase a ($\theta = 90^o$).

It can be shown for connection (a) that,

$$\frac{V_d(s)}{I_d(s)} = -\frac{2}{3}\frac{V}{I}(s) = -Z_d(s) \tag{3.116}$$

$$X_d(s) = \frac{\omega_B}{s}\left[Z_d(s) - R_a\right] \tag{3.117}$$

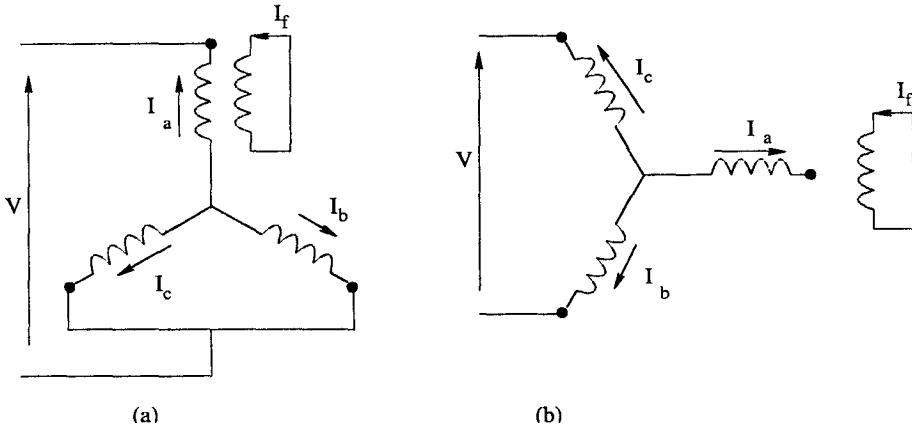(a)   (b)

Figure 3.15: Two connections for measuring direct axis impedances

Proof

From the stator equations, with $\omega = 0$, we have

$$-\frac{s}{\omega_B}\Psi_d(s) - R_a I_d(s) = V_d(s) \qquad (3.118)$$

$$-\frac{s}{\omega_B}\Psi_q(s) - R_a I_q(s) = V_q(s) \qquad (3.119)$$

With field winding shorted, we have

$$\Psi_d(s) = X_d(s)I_d(s) \qquad (3.120)$$

Substituting (3.120) in (3.118), we get

$$\frac{V_d(s)}{I_d(s)} = \frac{-s}{\omega_B}X_d(s) + R_a \qquad (3.121)$$

From Fig. 3.15 (a), we have

$$\left.\begin{array}{rcl} V_b(s) & = & V_c(s) \\ V(s) & = & V_a(s) - V_b(s) \end{array}\right\} \qquad (3.122)$$

$$\left.\begin{array}{rcl} I_a(s) & = & -I(s) \\ I_b(s) & = & I_c(s) = \frac{1}{2}I(s) \end{array}\right\} \qquad (3.123)$$

Since $\theta = 0$,

$$\begin{array}{rcl} I_d & = & \sqrt{\frac{2}{3}}\left[-I\cos(0^o) + \frac{I}{2}\cos(-120^o) + \frac{I}{2}\cos(120^o)\right] \\ & = & -\sqrt{\frac{3}{2}}I \end{array} \qquad (3.124)$$

$$I_q = \sqrt{\frac{2}{3}} \left[-I\sin(0) + \frac{I}{2}\sin(-120^o) + \frac{I}{2}\sin(120^o) \right]$$
$$= 0 \qquad (3.125)$$

$$V_d = \sqrt{\frac{2}{3}} \left[V_a\cos(0) + V_b\cos(-120^o) + V_c\cos(120^o) \right]$$
$$= \sqrt{\frac{2}{3}} [V_a - V_b] = \sqrt{\frac{2}{3}}V \qquad (3.126)$$

$$V_q = \sqrt{\frac{2}{3}} \left[V_a\sin(0) + V_b\sin(-120^o) + V_c\sin(120^o) \right]$$
$$= 0 \qquad (3.127)$$

From, (3.124) and (3.126) we get

$$\frac{V_d(s)}{I_d(s)} = -\frac{2}{3}\frac{V(s)}{I(s)} = -Z_d(s)$$

Substituting in (3.121), we also have

$$X_d(s) = \frac{\omega_B}{s} [Z_d(s) - R_a]$$

For quadrature axis measurement, the rotor is turned 90° electrically ($\theta = 90^o$). It can be shown in this case, that

$$\frac{V_q(s)}{I_q(s)} = -Z_q(s) = -\frac{s}{\omega_B}X_q(s) - R_a \qquad (3.128)$$

3.9 Saturation Models

Magnetic materials used in the stator and rotor of synchronous machine exhibit saturation. This implies that the machine inductances are not constants but depend on the levels of flux in different parts of the machine. An exact analysis of saturation can be very complex and impractical to use in large scale system studies [32, 41].

There are several saturation models proposed in the literature [34-43] but they tend to be highly empirical and lack theoretical justification although recent developments [33, 41, 42] are aimed at achieving better representation of saturation in a machine. Sauer [33] has presented algebraic constraints that must be satisfied by saturation models of lossless fields. This has relevance to the

development of theoretically sound saturation models based on fundamental laws that lead to a typical dynamic model. Harley et al [43] present a comparative study of the saturation models used in stability studies involving synchronous machines.

Most of the different methods proposed in the literature consider that the mutual inductances in a machine are subject to saturation. Thus,

$$x_{ads} = S_d x_{ad} \qquad\qquad (3.129)$$

$$x_{aqs} = S_q x_{aq} \qquad\qquad (3.130)$$

where the subscript 's' indicates saturated value while x_{ad} and x_{aq} are unsaturated (linear) reactances. S_d and S_q are nonlinear factors that depend on flux levels. The assumptions are that the leakage inductances are unaffected by saturation. However, some methods consider saturation of field flux leakage path while assuming only constant armature leakage reactance.

Saturation factor S_d, is normally derived from open circuit saturation curve. Since data on S_q is generally not available, it is assumed that $S_q = 1$ for salient pole machines and $S_d = S_q$ for round rotor machines. The determination of S_d is explained with reference to the O.C.C. and air-gap line shown in Fig. 3.16. The abscissa represents the mmf (F_d). At no load, F_d depends only on I_f (the field current). The ordinate represents the flux level ψ_{ad} which corresponds to an internal voltage component E_q behind a leakage or Potier reactance (Note that the open circuit voltage is identical to E_q).
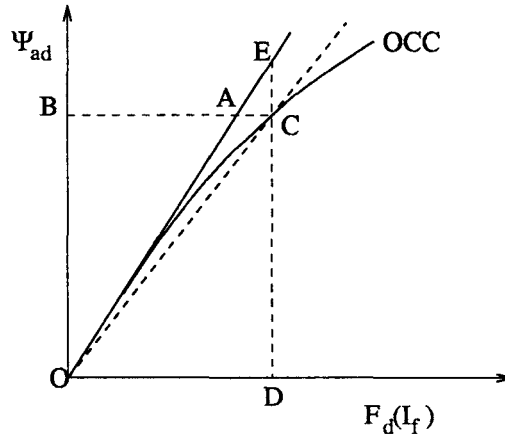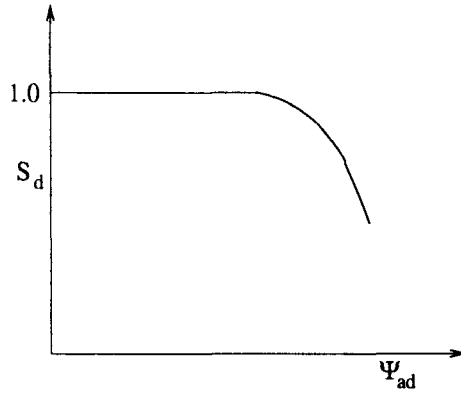

Figure 3.16: Direct axis open circuit characteristics

The value of unsaturated x_{ad} is given by

$$x_{ad} = \frac{DE}{OD} \qquad\qquad (3.131)$$

Figure 3.17: Variation of S_d

The saturated reactance, x_{ads} is given by the slope of the line OC, when $OB = \psi_{ad} = E_q$.

$$x_{ads} = \frac{DC}{OD} = x_{ad}\frac{DC}{DE} = S_d \cdot x_{ad} \tag{3.132}$$

which gives

$$S_d = \frac{DC}{DE} = \frac{BA}{BC} \tag{3.133}$$

Similar procedure can be used to determine S_q if the saturation curve is available. The variation of S_d with $\psi_{ad}(E_q)$ is shown in Fig. 3.17. Some saturation models consider S_d as a function of the total airgap flux ψ_t, given by

$$\psi_t = \sqrt{\psi_{ad}^2 + \psi_{aq}^2} \tag{3.134}$$

Minnich et al [41] have proposed that the reactances x_{ads} and x_{qs} can be expressed in terms of product of two nonlinear functions, i.e.

$$x_{ads} = x_{ad} \cdot F_{d1}(\mid V_P \mid) \cdot F_{d2}(\psi_{qp}) \tag{3.135}$$

$$x_{qs} = x_q \cdot F_{q1}(\mid V_P \mid) \cdot F_{q2}(\psi_{qp}) \tag{3.136}$$

$\mid V_P \mid$ is the magnitude of the total voltage or flux behind an internal reactance (called for convenience as the Potier reactance, although it is not the same defined originally). V_P and ψ_{qp} are defined by

$$V_P = V_t + jI_a x_p \tag{3.137}$$

$$\psi_{qp} = \psi_q - I_q x_p = -V_d - I_q x_p \tag{3.138}$$

as in steady state, (at rated speed),

$$\psi_q = -V_d$$

It has been observed that saturation is a strong function of the voltage $|V_P|$. In [41] the authors fit the saturation function F_2 using a quadratic, while F_1 is defined by a look-up table (as power series fit is inadequate).

Instead of using saturation factors to modify the inductance values, some models introduce a 'saturation current' which reduces the d-axis mmf for salient pole machines or the total mmf for round rotor machines. However this model is not preferred as it fails to distinguish between the degrees of saturation in the two axes [43].

The effect of saturation on x_q is important from the point of view of determining the correct rotor angle. The accurate modelling of saturation (in both axes) is also necessary for the accurate prediction of field excitation required for a specified generator power output.

An important phenomenon resulting from saturation is the cross-coupling between d- and q-axis coils (termed as the cross-magnetizing phenomenon). Due to saturation, d-axis current I_d produces q-axis flux linkages and vice versa. Also, the field and the q-axis coil in the armature get coupled. The cross-magnetization arises from the fact that when the machine is loaded, the permeability is not symmetric around d-axis. The effects of various saturation models on generator swing curves are investigated in [43] and the results are interesting. Although the studies were carried out without considering machine controllers (both excitation and governor), the conclusions indicate that using saturated, but constant values of reactances gives reasonably accurate results. Thus, the complication of modifying the reactances at every solution step may not be essential. While this result is significant particularly for large scale system studies, it needs to be checked thoroughly with extensive experimentation. Unfortunately, there are no detailed reports of comparative studies on saturation models in synchronous machines.

3.10 Transient Analysis of a Synchronous Machine

The transient response of a synchronous machine can be considered under the following conditions

(a) connected to a voltage source

(b) connected to an external network

When the machine is running at constant speed and saturation is neglected, the machine equations are linear. Neglecting the armature resistance, and assuming

the machine is running at rated speed they are

$$
\left.
\begin{aligned}
-\frac{1}{\omega_B}\frac{d\psi_d}{dt} - \psi_q &= v_d \\
-\frac{1}{\omega_B}\frac{d\psi_q}{dt} + \psi_d &= v_q
\end{aligned}
\right\}
\tag{3.139}
$$

$$
\left.
\begin{aligned}
\frac{1}{\omega_B}\frac{d\psi_f}{dt} &= -R_f i_f + \frac{R_f}{x_{df}} E_{fd} \\
\frac{1}{\omega_B}\frac{d\psi_h}{dt} &= -R_h i_h
\end{aligned}
\right\}
\tag{3.140}
$$

$$
\left.
\begin{aligned}
\frac{1}{\omega_B}\frac{d\psi_g}{dt} &= -R_g i_g \\
\frac{1}{\omega_B}\frac{d\psi_k}{dt} &= -R_k i_k
\end{aligned}
\right\}
\tag{3.141}
$$

Machine connected to a voltage source

If it is assumed that the machine is connected to a balanced sinusoidal voltage of rated frequency, then v_d and v_q are constants. It is seen that the equation (3.139) is not coupled to the rest and can be solved as

$$
\psi_d(t) = c_1 \cos \omega_B t + c_2 \sin \omega_B t + v_q \tag{3.142}
$$

$$
\psi_q(t) = -c_2 \cos \omega_B t + c_1 \sin \omega_B t - v_d \tag{3.143}
$$

c_1 and c_2 are determined from the initial conditions of ψ_d and ψ_q as

$$
\begin{aligned}
c_1 &= \psi_d(0) - v_q \\
c_2 &= -\psi_q(0) - v_d
\end{aligned}
$$

Eqs. (3.140) and (3.141) can be solved independently by substituting for the rotor currents in terms of flux linkages. The relevant equations are

$$
\begin{bmatrix} \psi_d \\ \psi_f \\ \psi_h \end{bmatrix}
=
\begin{bmatrix} x_d & x_{df} & x_{dh} \\ x_{df} & x_f & x_{fh} \\ x_{dh} & x_{fh} & x_h \end{bmatrix}
\begin{bmatrix} i_d \\ i_f \\ i_h \end{bmatrix}
\tag{3.144}
$$

$$
\begin{bmatrix} \psi_q \\ \psi_g \\ \psi_k \end{bmatrix}
=
\begin{bmatrix} x_q & x_{qg} & x_{qk} \\ x_{qg} & x_g & x_{gk} \\ x_{qk} & x_{gk} & x_k \end{bmatrix}
\begin{bmatrix} i_q \\ i_g \\ i_k \end{bmatrix}
\tag{3.145}
$$

From (3.144) and (3.145), it is possible to obtain

$$
\left.
\begin{aligned}
i_f &= a_1 \psi_f + a_2 \psi_h + b_1 \psi_d \\
i_h &= a_2 \psi_f + a_3 \psi_h + b_2 \psi_d
\end{aligned}
\right\}
\tag{3.146}
$$

$$i_g = a_4\psi_g + a_5\psi_k + b_3\psi_q \atop i_k = a_5\psi_g + a_6\psi_k + b_4\psi_q \Bigg\} \tag{3.147}$$

If,

$$x_{df} = x_{dh} = x_{fh} = x_{dc} = x_d - x_c \atop x_f = x_{dc} + x_{fc}, \quad x_h = x_{dc} + x_{hc} \Bigg\} \tag{3.148}$$

then

$$a_1 = \frac{1}{x_{fc}} - \frac{x_1}{x_{fc}^2} \frac{x_{dc}}{(x_{dc} + x_1)}$$

$$a_2 = -\frac{x_{dc}}{(x_{dc} + x_1)} \frac{x_1}{x_{fc} x_{hc}}$$

$$a_3 = \frac{1}{x_{hc}} - \frac{x_1}{x_{hc}^2} \frac{x_{dc}}{(x_{dc} + x_1)}$$

$$b_1 = -\frac{x_{dc}}{(x_{dc} + x_1)} \frac{x_1}{x_c x_{fc}}, \quad b_2 = -\frac{x_{dc}}{(x_{dc} + x_1)} \frac{x_1}{x_c x_{hc}}$$

where

$$\frac{1}{x_1} = \frac{1}{x_c} + \frac{1}{x_{fc}} + \frac{1}{x_{hc}}$$

Similarly, if

$$x_{qg} = x_{qk} = x_{gk} = x_{aq} = x_q - x_{a\sigma} \atop x_g = x_{aq} + x_{g\sigma}, \quad x_k = x_{aq} + x_{k\sigma} \Bigg\} \tag{3.149}$$

then,

$$a_4 = \frac{1}{x_{g\sigma}} - \frac{x_2}{x_{g\sigma}^2} \frac{x_{aq}}{(x_{aq} + x_2)}$$

$$a_5 = -\frac{x_2}{x_{g\sigma} x_{k\sigma}} \frac{x_{aq}}{(x_{aq} + x_2)}$$

$$a_6 = \frac{1}{x_{k\sigma}} - \frac{x_2}{x_{k\sigma}^2} \frac{x_{aq}}{(x_{aq} + x_2)}$$

$$b_3 = -\frac{x_2}{x_{g\sigma} x_{a\sigma}} \frac{x_{aq}}{(x_{aq} + x_2)}$$

$$b_4 = -\frac{x_2}{x_{k\sigma} x_{a\sigma}} \frac{x_{aq}}{(x_{aq} + x_2)}$$

where

$$\frac{1}{x_2} = \frac{1}{x_{a\sigma}} + \frac{1}{x_{g\sigma}} + \frac{1}{x_{k\sigma}}$$

Substituting Eqs. (3.146) and (3.147) in (3.140) and (3.141), we obtain,

$$\left. \begin{array}{rcl}
\dfrac{d\psi_f}{dt} &=& -\omega_B R_f[a_1\psi_f + a_2\psi_h] - \omega_B R_f b_1\psi_d + \dfrac{\omega_b R_f}{x_{df}} E_{fd} \\[3mm]
\dfrac{d\psi_h}{dt} &=& -\omega_B R_h[a_2\psi_f + a_3\psi_h] - \omega_B R_f b_2\psi_d
\end{array} \right\} \qquad (3.150)$$

$$\left. \begin{array}{rcl}
\dfrac{d\psi_g}{dt} &=& -\omega_B R_g[a_4\psi_g + a_5\psi_k] - \omega_B R_g b_3\psi_q \\[3mm]
\dfrac{d\psi_k}{dt} &=& -\omega_B R_k[a_5\psi_g + a_6\psi_k] - \omega_B R_k b_4\psi_q
\end{array} \right\} \qquad (3.151)$$

Eqs. (3.150) and (3.151) are decoupled and can be solved independently. Here ψ_d, ψ_q and E_{fd} are treated as input variables. The solutions for the rotor flux linkages also include sinusoidal terms at fundamental frequency in light of Eqs. (3.142) and (3.143). The solution for the currents i_d and i_q are obtained in terms of flux linkages as

$$i_d = C_1\psi_d + C_2\psi_f + C_3\psi_h \qquad (3.152)$$

$$i_q = C_4\psi_q + C_5\psi_g + C_6\psi_k \qquad (3.153)$$

If the reactances are as defined in (3.148) and (3.149), then

$$C_1 = \frac{1}{x_c} - \frac{x_1}{x_c^2} \frac{x_{dc}}{(x_{dc} + x_1)}, \quad C_2 = -\frac{x_1}{x_{fc}x_c} \frac{x_{dc}}{(x_{dc} + x_1)}$$

$$C_3 = -\frac{x_1}{x_{hc}x_c} \frac{x_{dc}}{(x_{dc} + x_1)}, \quad C_4 = \frac{1}{x_{a\sigma}} - \frac{x_2}{x_{a\sigma}^2} \frac{x_{aq}}{(x_{aq} + x_2)}$$

$$C_5 = -\frac{x_2}{x_{a\sigma}x_{g\sigma}} \frac{x_{aq}}{(x_{aq} + x_2)}, \quad C_6 = -\frac{x_2}{x_{a\sigma}x_{k\sigma}} \frac{x_{aq}}{(x_{aq} + x_2)}$$

The electrical torque can be computed from

$$T_e = \psi_d i_q - \psi_q i_d \qquad (3.154)$$

It can be seen that the torque consists of sinusoidal components of fundamental frequency and second harmonic in addition to constant components.

Remarks

1. The analysis assumed the armature resistance as zero which enabled the machine equations to be decoupled. First, ψ_d and ψ_q are solved and the solution is utilized to solve for the rotor flux linkages in the direct axis and quadrature axis separately.

2. If armature resistance is to be considered, then the machine equations cannot be decoupled. The three sets of Equations (six in all), (3.139) to (3.141) have to be solved simultaneously.

   The armature resistance is never zero, hence the sinusoidal components in the flux linkages and torque eventually decay to zero. If the solution is required for a short period immediately following a disturbance, it is in order to simplify the solution by assuming $R_a = 0$ as the armature resistance is usually very small.

3. The sinusoidal component in i_d and i_q result in second harmonic components in the armature currents i_a, i_b and i_c in addition to the dc components. It is usually presumed that this so called dc component decays with the time in the presence of armature resistances.

   However, it can be shown that the sinusoidal components in i_d and i_q have a frequency slightly differing from the rated frequency. This implies that the 'dc' components in the armature currents are not really dc (unidirectional) but decaying sinusoidal components of very low frequency (say 0.02 Hz). Note that the radian frequency of oscillation in i_d and i_q is obtained as the imaginary part of the complex eigenvalue of the matrix $[F]$ defined by the machine equations expressed as

$$\dot{x} = [F]x + [G]u \qquad (3.155)$$

where the state vector x and input vector u are defined by

$$
\begin{aligned}
x^t &= [\psi_d \quad \psi_q \quad \psi_f \quad \psi_h \quad \psi_g \quad \psi_k] \\
u^t &= [v_d \quad v_q \quad E_{fd}]
\end{aligned}
$$

Note also that the choice of state vector is not unique. The currents can also be chosen as state variables. However, the simplification that arises when $R_a = 0$, is not obvious in this case.

4. The 'dc' components in the armature currents lead to sinusoidal components of rated frequency (or very close to rated) in the electrical torque. Generally, fast variations in the torque have little influence on the motion of the rotor (due to its inertia) unless shaft torsional modes are considered.

   In stability studies, where swing curves (variation of rotor angle δ with time) are of importance, it is acceptable to ignore the transients in the stator. In this case, the stator is described by algebraic equations. Neither ψ_d, ψ_q or i_d, i_q can be considered as state variables as they can change suddenly in response to step changes in the terminal voltages v_d and v_q.

Analysis of Machine connected to an External Network

In most of the cases, the normal operation of a synchronous machine in a power system is when it is connected to an external network consisting of transmission lines, transformers, loads and other components. In such cases, it is not possible to assume that the terminal voltages are specified or known. The network can be modelled by an electrical circuit consisting of lumped elements of linear R, L and C. Thus it is advantageous to obtain a circuit equivalent for the machine stator which can then be combined with the equivalent circuits for the external network.

A circuit model for a synchronous machine which is applicable for transient analysis is given in [13]. The stator is represented by a three phase equivalent circuit shown in Fig. 3.18 . The inductance matrix for the circuit is defined as

$$[L_s''] = [L_{ss}] - [L_{sr}][L_{rr}]^{-1}[L_{rs}] \tag{3.156}$$
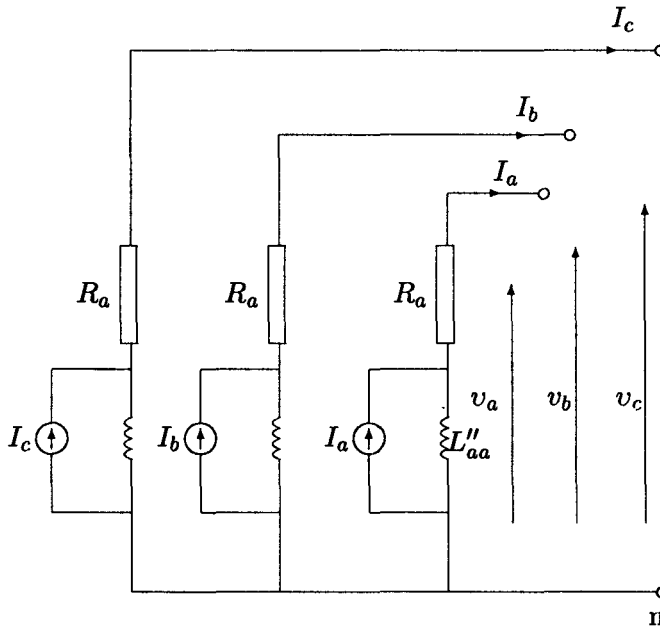
Figure 3.18: Equivalent circuit of stator

It can be shown that if subtransient saliency is absent, i.e. $x_d'' = x_q'' = x''$, then the elements of $[L_s'']$ are constants (independent of the rotor angle). Also, $[L_s'']$ is a cyclic symmetric matrix with all the off-diagonal terms as L_{ab}''. It can

also be shown that the subtransient inductance is given by

$$L''_d = L''_q = L'' = L''_{aa} - L''_{ab} \qquad (3.157)$$

When subtransient saliency is present, by introducing a 'dummy' rotor coil in the q-axis, (or d-axis) with appropriately chosen parameters, it is possible to modify $[L''_s]$ (which is dependent on θ in the presence of subtransient saliency) and obtain a new constant matrix. Note that the introduction of an open 'dummy' coil has no effect on the machine performance.

The current source I_s in Fig. 3.18 is defined by

$$-I_s = [L''_s]^{-1}[L_{sr}][L_{rr}]^{-1}\psi_r, \quad I^t_s = [I_a \quad I_b \quad I_c] \qquad (3.158)$$

in the absence of a dummy coil, and modified to

$$-I_s = [L''_s]^{-1}\{[L_{sr}][L_{rr}]^{-1}\psi_r + [M_c]L_c^{-1}[M_c]^t i_s\} \qquad (3.159)$$

in the presence of a dummy coil. $[M_c]$ is the vector of mutual inductances between the dummy coil and the stator windings. L_c is the self inductance of the dummy coil.

It can be shown [16] that the subtransient saliency results when

$$L_{aa2} - \frac{s_1 - s_2}{2} \neq 0 \qquad (3.160)$$

where

$$s_1 = \frac{(M_{af}L_h - M_{ah}L_{fh})M_{af} + (M_{ah}L_f - M_{af}L_{fh})M_{ah}}{L_f L_h - L_{fh}^2} \qquad (3.161)$$

$$s_2 = \frac{(M_{ag}L_k - M_{ak}L_{gk})M_{ag} + (M_{ak}L_g - M_{ag}L_{gk})M_{ak}}{L_g L_k - L_{gk}^2} \qquad (3.162)$$

The inductances used in the above expressions are defined in section 3.2.

The vector $[M_c]$ is defined as

$$[M_c]^t = \left[M_{ac}\sin\theta \quad M_{ac}\sin\left(\theta - \frac{2\pi}{3}\right) \quad M_{ac}\sin\left(\theta + \frac{2\pi}{3}\right) \right]$$

(It is assumed that the dummy rotor coil is on q-axis)

With the dummy coil considered, the saliency is avoided if

$$s_2 + \frac{M_{ac}^2}{L_c} = s_1 - 2L_{aa2} \qquad (3.163)$$

This equation determines the parameters of the dummy coil. As there is only one equation in two parameters, one of the parameters, say L_c can be arbitrarily assigned a value, say L_q. Then M_{ac} is determined from Eq. (3.163).

The current vector I_s can be viewed as vector of dependent current sources (dependent on the rotor flux linkages and stator currents). The dependence on stator currents may be problematic; in such a case, the dummy coil can be treated as closed with a high resistance. The current vector I_s can be expressed as

$$-I_s = [L_s'']^{-1}\{[L_{sr}][L_{rr}]^{-1}\psi_r + [M_c]L_c^{-1}\psi_c\} \tag{3.164}$$

where ψ_c, the flux linkage of the dummy coil becomes an additional state variable.

Remarks

1. It is assumed in the derivation of Eqs. (3.159) and (3.164) that the dummy coil has no coupling with other rotor coils (for convenience).

2. Note that when the dummy coil is open, then

$$\psi_c = [M_c]^t i_s \tag{3.165}$$

3. The assumption about closed dummy coil is an approximation; however the degree of approximation (or accuracy) is controlled by selecting arbitrarily large resistance for the dummy coil.
   It is convenient to define an (open circuit) time constant T_c for the dummy coil which should be theoretically zero, but can be given an arbitrarily small value. Numerical experiments on realistic systems indicate a value of $T_c < 0.001$ sec is adequate for transient analysis while $T_c < 0.01$ sec is satisfactory for stability studies.

4. The equivalent circuit of Fig. 3.18 can be combined with the external stationary network to obtain the differential equations. If network (and stator) transients are ignored, then the resulting equations are algebraic.

Torque Equation

The electrical torque in the machine can be derived as [13]

$$T_e = -i_s^t [L_s''] I_t \tag{3.166}$$

where

$$I_t = [L_s'']^{-1} \left\{ \left[\frac{\partial L_{sr}}{\partial \theta}\right][L_{rr}]^{-1}\psi_r + \left[\frac{\partial M_c}{\partial \theta}\right]L_c^{-1}\psi_c \right\} \tag{3.167}$$

It is assumed that $[L_s'']$ is a constant matrix (as discussed earlier).

Example 3.4

A synchronous generator is operating at rated speed and on no-load. The open circuit voltage is 1.0 pu. There is a sudden three phase short circuit at the generator terminals at $t = 0$.

(a) Obtain expression for i_d, i_q, i_f and T_e as function of time. Assume that the transients in the armature are neglected. Also neglect armature resistance.

(b) Repeat (a) if transients in the armature are considered (with $R_a = 0$)

(c) Plot i_d, i_q, i_f and T_e as functions of time for the data in Example 3.3(b). Assume $x_q'' = x_d''$

Solution

The fault at the generator terminals is simulated by considering the superposition of two voltage sources; the first is the prefault voltage at the terminals (v_{do} and v_{qo}) and the second is equal and opposite to the first (see Fig. 3.19)

$$\Delta V_d = -v_{do}, \quad \Delta V_q = -v_{qo}$$

The net currents are obtained by superposition of the currents due to the two sources taken one at a time. The first source (v_{do} and v_{qo}) result in prefault currents, Under no load conditions, these are

$$i_{do} = 0, \quad i_{qo} = 0, \quad i_{fo} = \frac{E_{fdo}}{x_{df}}$$

(a) Neglecting transients in the armature and with $R_a = 0$,
$\psi_{do} = v_{qo} = E_{fdo}, \ \psi_{qo} = -v_{do} = 0$
The response due to ΔV_d and ΔV_q are obtained from

$$
\begin{aligned}
\Delta I_d(s) &= \frac{\Delta \Psi_d}{X_d(s)} = \frac{\Delta V_q}{sX_d(s)} \\
&= \frac{\Delta V_q}{s} \left[\frac{1}{x_d} + \left(\frac{1}{x_d'} - \frac{1}{x_d} \right) \frac{sT_d'}{1 + sT_d'} + \left(\frac{1}{x_d''} - \frac{1}{x_d'} \right) \frac{sT_d''}{1 + sT_d''} \right] \\
\Delta I_q(s) &= \frac{\Delta \Psi_q}{X_q(s)} = 0
\end{aligned}
$$

It can be derived that

$$\Delta I_f(s) = -G'(s)\Delta I_d(s)$$

(a) Faulted generator

(b) Equivalent network
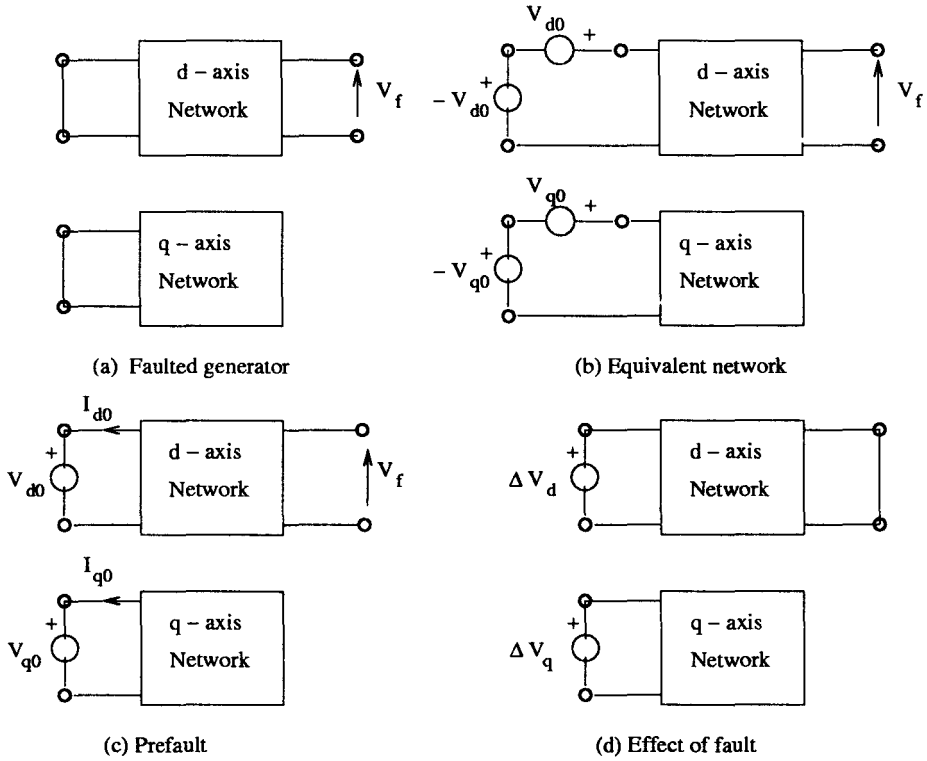
(c) Prefault

(d) Effect of fault

Figure 3.19: Application of superposition theorem (Example 3.4)

where

$$G'(s) = \frac{x_{ad}}{\omega_B R_f} \frac{s(1 + T_1 s)}{(1 + sT'_{do})(1 + sT''_{do})}, \quad T_1 = \frac{x_h - x_{fh}}{\omega_B R_h}$$

Substituting for $I_d(s)$,

$$\Delta I_f(s) = -\frac{\Delta V_q x_{ad}}{\omega_B R_f x_d} \frac{(1 + sT_1)}{(1 + sT'_d)(1 + sT''_d)}$$

Taking inverse Laplace transforms, we get

$$\Delta i_d(t) = -\left[\frac{1}{x_d} + \left(\frac{1}{x'_d} - \frac{1}{x_d}\right) e^{-\frac{t}{T'_d}} + \left(\frac{1}{x''_d} - \frac{1}{x'_d}\right) e^{-\frac{t}{T''_d}}\right] v_{qo}$$

as

$$\Delta V_q = -v_{qo} = -E_{fdo}$$

$$\Delta i_q(t) = 0$$

$$\Delta i_f(t) = \frac{v_{qo}x_{ad}}{\omega_B R_f x_d}\left[c_1 e^{-\frac{t}{T_d'}} + c_2 e^{-\frac{t}{T_d''}}\right]$$

$$c_1 = \frac{1}{T_d'}\left(1 - \frac{T_1}{T_d'}\right) \div \left(1 - \frac{T_d''}{T_d'}\right) \simeq \frac{1}{T_d'}$$

$$c_2 = \frac{1}{T_d''}\left(1 - \frac{T_1}{T_d''}\right) \div \left(1 - \frac{T_d'}{T_d''}\right) \simeq -\frac{1}{T_d'}\left(1 - \frac{T_1}{T_d''}\right)$$

$$i_d(t) = i_{do} + \Delta i_d(t) = \Delta i_d(t), \quad i_q(t) = i_{qo} + \Delta i_q(t) = 0$$

$$\psi_d(t) = \psi_{do} + \Delta\psi_d(t), \quad \psi_q(t) = \psi_{qo} + \Delta\psi_q(t) = 0$$

$$T_e = \psi_d i_q - \psi_q i_d = 0$$

(b) Neglecting armature resistance,

$$s\Delta\Psi_d(s) + \omega_B\Psi_q(s) = -\Delta V_d(s) = 0$$

$$s\Delta\Psi_q(s) - \omega_B\Psi_d(s) = -\frac{\omega_B}{s}\Delta V_q = \frac{\omega_B}{s}v_{qo}$$

From the above equations, we get

$$\Delta\Psi_d(s) = -\frac{\omega_B^2 v_{qo}}{s(s^2 + \omega_B^2)}$$

$$\Delta\Psi_q(s) = \frac{v_{qo}\omega_B}{s^2 + \omega_B^2}$$

Taking inverse Laplace Transform,

$$\Delta\psi_d(t) = v_{qo}[-1 + \cos\omega_B t]$$

$$\Delta\psi_q(t) = v_{qo}\sin\omega_B t$$

$$\Delta I_d(s) = \frac{\Delta\psi_d(s)}{X_d(s)}$$

$$= -\frac{\omega_B^2 v_{qo}}{(s^2 + \omega_B^2)} \times$$

$$\left[\frac{1}{sx_d} + \left(\frac{1}{x_d'} - \frac{1}{x_d}\right)\frac{1}{1 + \varepsilon T_d'} + \left(\frac{1}{x_d''} - \frac{1}{x_d'}\right)\frac{1}{1 + sT_d''}\right]$$

from which

$$\Delta i_d(t) \simeq \left[-\left[\frac{1}{x_d} + \left(\frac{1}{x_d'} - \frac{1}{x_d} \right) e^{-\frac{t}{T_d'}} + \left(\frac{1}{x_d''} - \frac{1}{x_d'} \right) e^{-\frac{t}{T_d''}} \right] \times \right.$$
$$\left. + \frac{1}{x_d''} \cos \omega t \right] v_{qo}$$

$$\Delta I_q(s) = \frac{\Delta \Psi_q(s)}{X_q(s)}$$
$$= \frac{v_{qo}\omega_B}{s^2 + \omega_B^2} \left[\frac{1}{x_q} + \left(\frac{1}{x_q'} - \frac{1}{x_q} \right) \frac{sT_q'}{1 + sT_q'} + \left(\frac{1}{x_q''} - \frac{1}{x_q'} \right) \frac{sT_q''}{1 + sT_q''} \right]$$

From which

$$\Delta i_q(t) \approx \frac{v_{qo} \sin \omega_B t}{x_q''}$$

$$\Delta I_f(s) = -\frac{x_{ad}}{\omega_B R_f} \frac{s(1 + sT_1)}{(1 + sT_{do}')(1 + sT_{do}'')} \Delta I_d(s)$$
$$= \frac{\omega_B v_{qo} x_{ad}}{x_d R_f (s^2 + \omega_B^2)} \frac{(1 + sT_1)}{(1 + sT_d')(1 + sT_d'')}$$

from which

$$\Delta i_f(t) = \frac{v_{qo} x_{ad}}{\omega_B T_d' R_f x_d} \left[e^{-\frac{t}{T_d'}} - \left(1 - \frac{T_1}{T_d''} \right) e^{-\frac{t}{T_d''}} - \frac{T_1}{T_d''} \cos \omega_B t \right]$$

Since,
$$v_{qo} = x_{ad} i_{fo}$$

and
$$\frac{x_{ad}^2}{\omega_B R_f T_d'} \simeq \frac{(x_d - x_d')}{x_d'}$$

$$\Delta i_f(t) \simeq i_{fo} \frac{(x_d - x_d')}{x_d'} \left[e^{-\frac{t}{T_d'}} - \left(1 - \frac{T_1}{T_d''} \right) e^{-\frac{t}{T_d''}} - \frac{T_1}{T_d''} \cos \omega_B t \right]$$

The electrical torque is expressed as

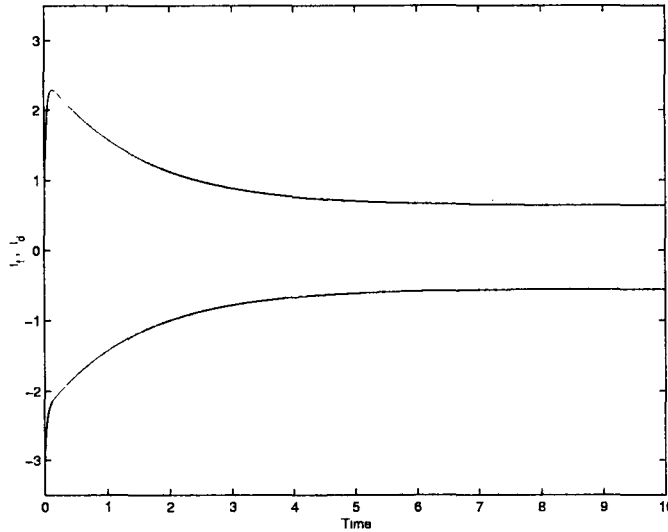$$T_e = (\psi_{do} + \Delta \psi_d)(i_{qo} + \Delta i_q) - (\psi_{qo} + \Delta \psi_q)(i_{do} + \Delta i_d)$$

Figure 3.20: Variation of i_d and i_f with armature transients neglected (Example 3.4)

(c) The variations of i_d and i_f with time, when armature transients are neglected are shown in Fig. 3.20. The variations of i_d, i_q, i_f and T_e with armature transients considered are shown in Fig. 3.21.

The following points can be noted from the example

(i) The field current and torque have sinusoidal components of fundamental frequency. The latter also has a second harmonic component.
The armature currents $i_a, i\ i_b$ and i_c also have second harmonic components.

(ii) The electrical torque during short circuit is zero if armature transients are neglected. This implies if $T_m > 0$ (in a loaded generator) the rotor continues to accelerate from the instant of fault.
However, with armature transients included, the initial torque can be of such value that the machine initially decelerates. This is termed as 'backswing' [51]. The effect of this phenomenon is that the critical clearing time for a fault is higher than what is computed neglecting the backswing.

(iii) The effect of the armature resistance (which was neglected in the example) can be considered approximately, by noting that the machine response (with armature transients) includes a term determined by the mode (eigenvalue) calculated from the equation [2]

$$s^2 + 2\alpha s + \omega_B^2 = 0$$
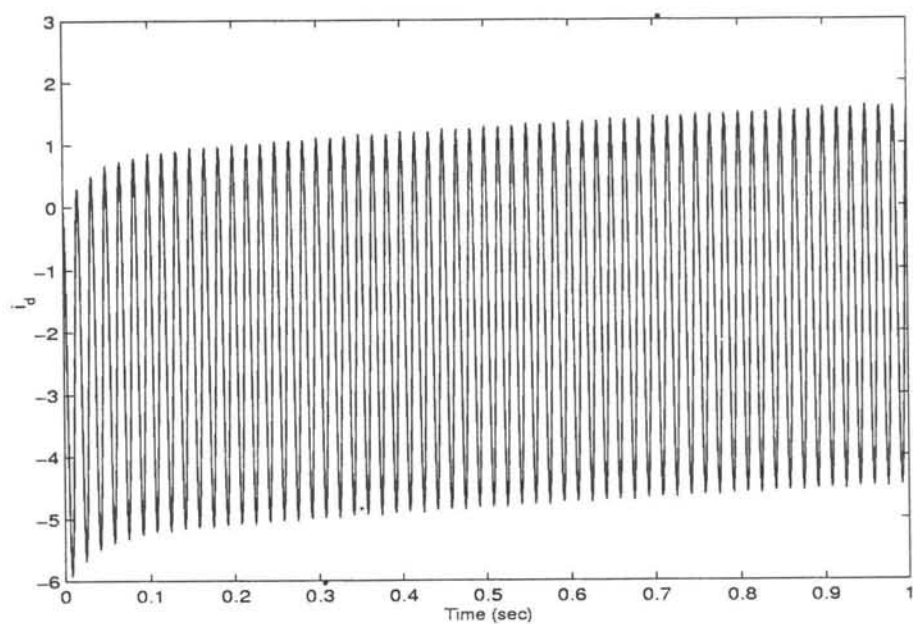
(a) Variation of i_d
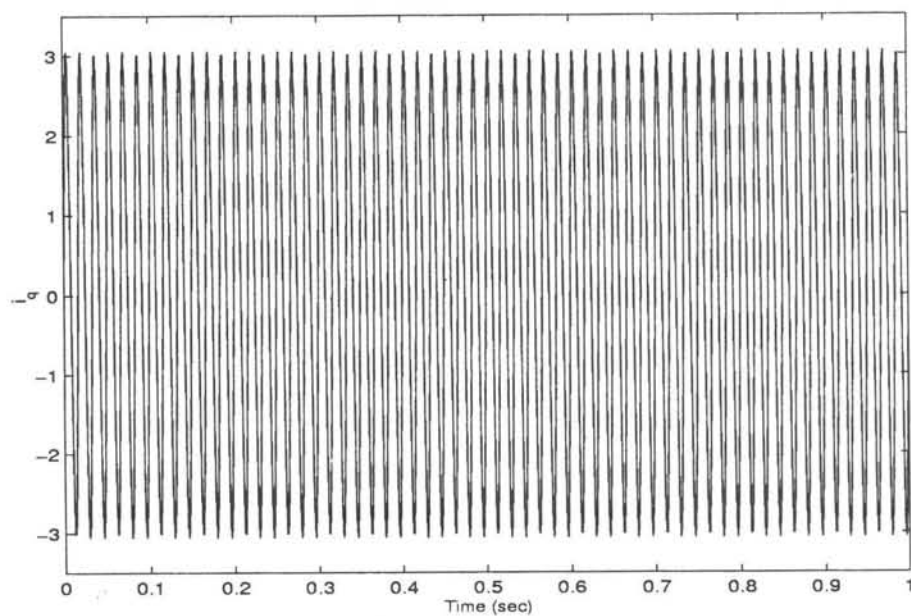
(b) Variation of i_q
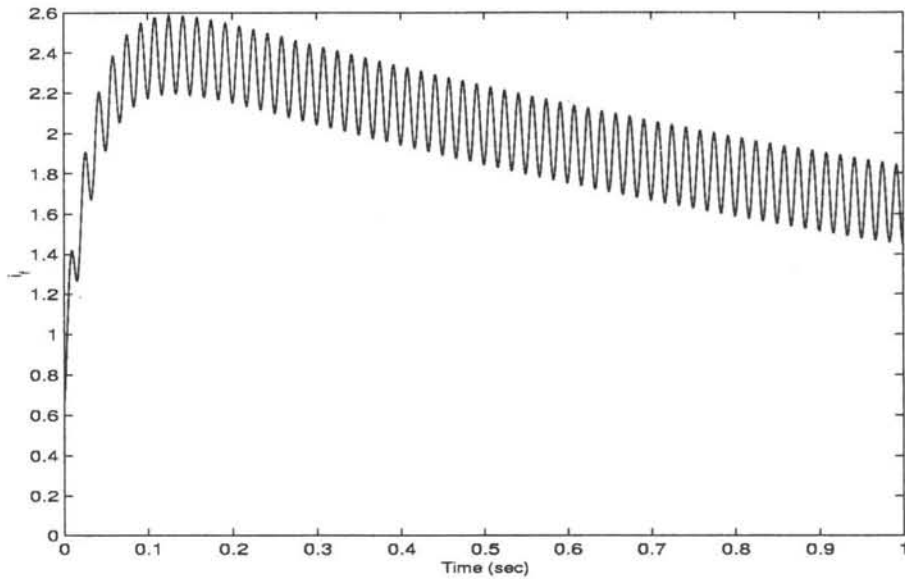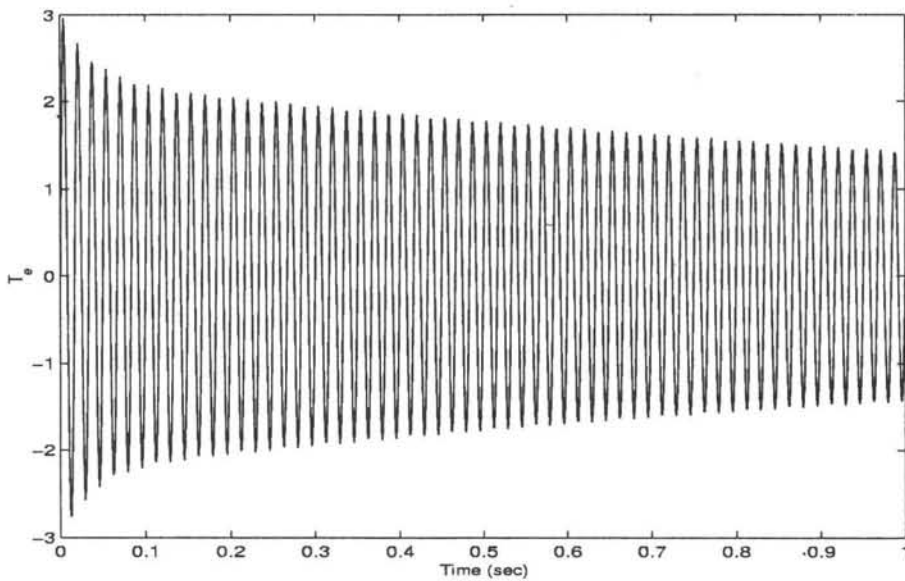
(c) Variation of i_f

(d) Variation of T_e

Figure 3.21: With armature transients considered (Example 3.4)

where

$$\alpha = \frac{\omega_B R_a}{2}\left(\frac{1}{x_d''} + \frac{1}{x_q''}\right) = \frac{1}{T_a}$$

The roots of the quadratic equation are

$$s = -\alpha \pm j\sqrt{\omega_B^2 - \alpha^2} = -\alpha \pm j\omega$$

The response for i_d and i_q includes terms

$$e^{-\alpha t}\cos\omega t \quad \text{and} \quad e^{-\alpha t}\sin\omega t$$

It is to be noted that $\omega < \omega_B$. The armature currents i_a, i_b and i_c include terms

$$e^{-\alpha t}\cos(\omega_B - \omega)t \quad \text{and} \quad e^{-\alpha t}\sin(\omega_B - \omega)t$$

which are not unidirectional.

References and Bibliography

A. Synchronous Machine Theory, Modelling

1. E.W. Kimbark, **Power System Stability: Vol. 3 - Synchronous Machines**, John Wiley, New York, 1956

2. B. Adkins and R.G. Harley, **The General Theory of Alternating Current Machines:Application to Practical Problems**, Chapman and Hall, London, 1975

3. A.E. Fitzgerald, C.Kingsley and S.D. Umans, **Electric Machinery**, McGraw-Hill, New York, 1983

4. C. Concordia, **Synchronous Machines**, John Wiley, New York, 1951

5. P.C. Krause, **Analysis of Electric Machinery**, McGraw-Hill, New York, 1987

6. R.H. Park, "Two-Reaction theory of synchronous machines -Part I; Generalized method of analysis", AIEE Trans. Vol. 48, July 1929, pp. 716-730

7. W.B. Jackson and R.L. Winchester, "Direct and quadrature axis equivalent circuits for solid-rotor turbine generators", IEEE Trans. Vol. PAS-88, No. 7, 1969, pp. 1121-1136

8. S.N. Nasar, "Electromechanical energy conversion in nm-winding double cylindrical structures in presence of space harmonics", IEEE Trans. Vol. PAS-87, No. 4, 1968, pp. 1099-1106

9. G. Kron, "Non-Riemannian dynamics of rotating electrical machinery", J. Math & Phys, Vol. 13, 1934, pp. 51-102

10. J.L. Willems, "A system theory approach to unified electrical machine analysis", Int. J. of Control, Vol. 15, No. 3, 1972, pp. 401-418

11. IEEE Committee Report, "Recommended phasor diagram for synchronous machines", IEEE Trans. Vol. PAS-88, Nov. 1969, pp. 1593-1610

12. J.C. Dunfield and T.H. Barton, "Effect of m.m.f. and permeance harmonics in electrical machines - with special reference to a synchronous machine", Proc. IEE, Vol. 114, No. 10, 1967, pp. 1143-1450

13. R.S. Ramshaw and K.R. Padiyar, "Generalized system model for slipring machines", Proc. IEE (London), Vol. 120, No. 6, 1973, pp. 647-658

14. P.L.Dandeno, P.Kundur and R.P. Schultz, "Recent trends and progress in synchronous machine modelling in the electric utility industry", Proc. IEEE, Vol. 62, No. 7, 1974, pp. 941-950

15. M. Riaz, "Hybrid-parameter models of synchronous machines", IEEE Trans. Vol. PAS-93, June 1974, pp. 849-858

16. K.R. Padiyar and R.S. Ramshaw, "Transformations in rotating electric machines based on Floquet-Liapunov theory", Seventh Annual Southeastern Symposium on Circuit Theory, Auburn, U.S.A., March 1975

B. Testing and Determination of Parameters

17. C. Concordia and F.J. Maginnis, "Inherent errors in the determination of synchronous-machine reactances by test", AIEE Trans. Vol. 64, June 1945, pp. 288-294

18. A.W. Rankin, "Per-unit impedances of synchronous machines", AIEE trans., Vol. 64, August 1945, pp. 569-573

19. P.M. Anderson and A.A. Fouad, **Power System Control and Stability**, Iowa State Univ. Press, Ames, Iowa, 1977

20. I.M. Canay, "Causes of discrepancies on calculation of rotor quantities and exact equivalent diagrams of synchronous machine", IEEE Trans. Vol. PAS-88, No. 7, 1969, pp. 1114-1120

21. I.M. Canay, "Determination of model parameters of synchronous machines", IEE Proc., Vol. 130, Pt.B, No. 2, 1983, pp. 86-94

22. IEEE Task Force, "Supplementary definitions and associated test methods for obtaining parameters for synchronous machine stability study simulations", IEEE Trans. Vol. PAS-99, No. 4, 1980, pp. 1625-1633

23. G. Shackshaft, "New approach to the determination of synchronous-machine parameters from test", Proc. IEE, Vol. 121, No. 11, 1974, pp. 1385-1392

24. F.P. DeMello and L.H. Hannet, "Validation of synchronous machine model and derivation of model parameters from tests", IEEE Trans. Vol. PAS-100, 1981, pp. 662-672

25. S.D. Umans, J.A. Mallick and G.L. Wilson, "Modelling of solid rotor turbogenerators, Part I: Theory and Techniques, Part II: Example of model derivation and use in digital simulation", IEEE Trans. Vol. PAS-97, No. 1, 1978, pp. 278-291

26. IEEE, **Test Procedures for synchronous machines**, (115), 1983

27. G. Shackshaft and A.T. Poray, "Implementation of new approach to determination of synchronous machine parameters from tests", Proc. IEE (London), Vol. 124, No. 12, 1977, pp. 1170-1178

28. R.P. Schultz, W.D. Jones and D.N. Ewart, "Dynamic models of turbine generators derived from solid rotor equivalent circuits", IEEE Trans. Vol. PAS-92, May-June 1973, pp. 926-933

29. M.E, Coultes and W.Watson, "Synchronous machine models by standstill frequency response tests", IEEE Trans. Vol. PAS-100, April 1981, pp. 1480-1489

30. P.L. Dandeno, P.Kundur, A.T. Poray and H.M. Zein El-Din, "Adaptation and validation of turbogenerator model parameters through on-line frequency response measurements", IEEE Trans. Vol. PAS-100, April 1981, pp. 1658-1664

31. P.L. Dandeno, P. Kundur, A.T. Poray and M. Coultes, "Validation of turbogenerator stability models by comparison with power system tests", IEEE Trans. Vol. PAS-100, April 1981, pp. 1637-1645

32. IEEE Task Force, "Current usage & suggested practices in power system stability simulations for synchronous machines", IEEE Trans. on Energy Conversion, Vol. EC-1, No. 1, 1986, pp. 77-93

C. Saturation Modelling

33. P.W. Sauer, "Constraints on saturation modeling in AC machines", Paper 91 SM 408-5 EC, IEEE PES Summer Meeting, July 1991

34. G.R. Slemon, "Analytical models for saturated synchronous machines", IEEE Trans. Vol. PAS-90, No. 2, 1971, pp. 409-417

35. C.C. Young, "Equipment and system modeling for large scale stability studies", IEEE Trans. Vol. PAS-91, No. 1, 1972, pp. 99-109

36. F.P. DeMello and L.N. Hannett, "Representation of saturation in synchronous machines", IEEE Trans. on Power Systems, PWRS-1, No. 4, 1986, pp. 8-18

37. R.S. Ramshaw and G. Xie, "Nonlinear model of nonsalient synchronous machines", IEEE Trans. Vol. PAS-103, No. 7, 1984, pp. 1809-1815

38. G. Xie and R.S. Ramshaw, " Nonlinear model of synchronous machines with saliency", IEEE Trans. on Energy Conversion, Vol. EC-1, No. 3, 1986, pp. 198-203

39. S.H. Minnich, "Small signals large signals and saturation in generator modeling", IEEE Trans. on Energy Conversion, Vol. EC-1, No.1, 1986, pp. 94-102

40. K.P. Kovacs, "On the theory of cylindrical rotor A.C. machines including main flux saturation", IEEE Trans. Vol. PAS-103, No. 4, 1984, pp. 754-761

41. S.H. Minnich et al, "Saturation functions for synchronous generators from finite elements", IEEE Trans. on Energy conversion, Vol. EC-2, No. 4, 1987, pp. 680-692

42. A.M. El-Serafi et al, "Experimental study of the saturation and cross-magnetizing phenomenon in saturated synchronous machines", IEEE Trans. on Energy Conversion, Vol. EC-3, No. 4, 1988, pp. 815-823

43. R.G. Harley, D.J. Limebeer and E. Chirricozzi, "Comparative study of saturation methods in synchronous machine models", IEE Proc., (London), Vol. 127, Pt.B, No. 1, 1980, pp. 1-7

D. Transient Analysis, Applications

44. P.W. Sauer, S. Ahmed-Zaid and M.A. Pai, "Systematic inclusion of stator transients in reduced order synchronous machine models", IEEE Trans. Vol. PAS-103, No. 3, 1984, pp. 1348-1354

45. G.C. Verghese, J.H. Lang and L.F. Casey, "Analysis of instability in electrical machines", IEEE Trans. on Industry Applications, Vol. IA-22, No. 5, 1986, pp. 853-864

46. C. Concordia et al, "Synchronous starting of motor from generator of small capacity", IEEE Trans. Vol. PAS-86, Oct. 1967, pp. 1215-1226

47. R.S. Ramshaw and K.R. Padiyar, "Synchronous starting in pumped storage plants", Conf. Digest, IEEE Canadian Conf. on Communications and Power, Montreal, Canada, Nov. 1974

48. K.R. Padiyar and R.S. Ramshaw, "A generalized synchronous machine model for large scale power system studies", Conf. Proc., Power Industry Computer Application (PICA), IEEE, Boston, U.S.A., May 1971

49. R.S. Ramshaw and K.R. Padiyar, "Applications of a synchronous machine circuit model", (summary), Proc. IEE (London), Vol. 121, August 1974

50. IEEE Task Force, "First Benchmark model for computer simulation of subsynchronous resonance", IEEE Trans. Vol. PAS-96, 1977, pp. 1565-1572

51. R.G. Harley and B. Adkins, "Calculation of angular backswing following a short circuit of a loaded alternator", Proc. IEE (London), Vol. 117, 1970, pp. 377

"This page is Intentionally Left Blank"

Chapter 4

Excitation and Prime Mover Controllers

The synchronous generator is provided with two automatic (feedback) controllers for the regulation of the terminal voltage and frequency. These controllers indirectly influence the reactive power and active power outputs of the generator respectively. The regulation of the voltage is the faster of the two controllers and has bearing on the system stability much more than the regulation of speed.

In this chapter, we will look at the modelling of the excitation and prime mover controllers for the purposes of stability analysis of power systems. For each control system, the models are grouped into a few standard types which are conveniently handled in computer simulation and analysis [1-3]. The block diagram structure of each standard type is well defined such that an equipment belonging to that type is characterized by a set of parameters.

4.1 Excitation System

The main objective of the excitation system is to control the field current of the synchronous machine. The field current is controlled so as to regulate the terminal voltage of the machine. As the field circuit time constant is high (of the order of a few seconds), fast control of the field current requires field forcing. Thus exciter should have a high ceiling voltage which enables it to operate transiently with voltage levels that are 3 to 4 times the normal. The rate of change of voltage should also be fast. Because of the high reliability required, unit exciter scheme is prevalent where each generating unit has its individual exciter.

There are three distinct types of excitation systems based on the power source for exciter.

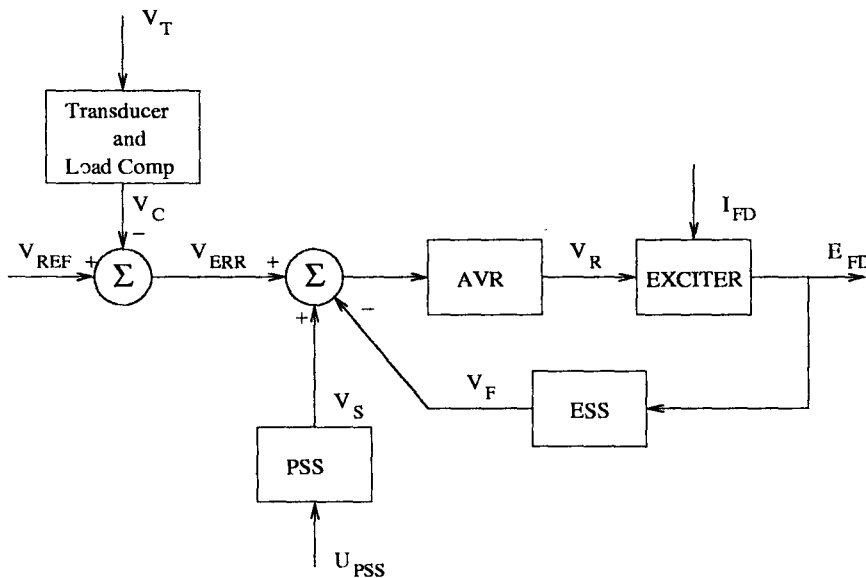1. **DC Excitation Systems** (DC) which utilize a DC generator with commutator.

Figure 4.1: Functional block diagram of excitation control system

2. **AC Excitation Systems** (AC) which use alternators and either stationary or rotating rectifiers to produce the direct current needed.

3. **Static Excitation Systems** (ST) in which the power is supplied through transformers and rectifiers.

   The first two types of exciters are also called rotating exciters which are mounted on the same shaft as the generator and driven by the prime mover.

4.2 Excitation System Modelling

The general functional block diagram of an excitation system (for all the three types defined earlier) is shown in Figure 4.1. The modelling of the various components of the excitation system is described below.

4.2.1 Terminal voltage Transducer and load compensation

This is shown in Figure 4.2. The terminal voltage of the generator is sensed and transformed to a dc quantity. Although the filtering associated with the voltage transducer may be complex, it is usually modelled as a single time constant T_R. In many systems, T_R is very small and can be assumed to be zero for simplicity.
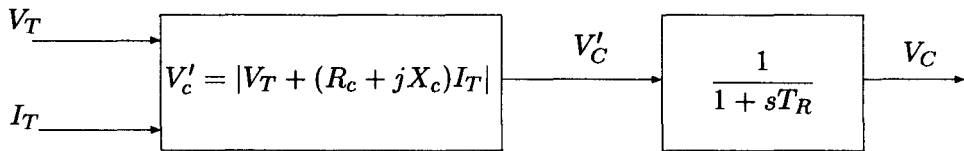
Figure 4.2: Transducer and Load Compensation

The purpose of the load compensation is to synthesize a voltage which differs from the terminal voltage by the voltage drop in an impedance $(R_c + jX_c)$. Both voltage and current phasors must be used in computing V_c. The objectives of the load compensation are as follows.

a) sharing of reactive power among units which are bussed together with zero impedance between them. In this case, R_c and X_c are positive and the voltage is regulated at a point internal to the generator.

b) when the generating units are connected in parallel through unit transformers, it may be desirable to regulate voltage at a point beyond the machine terminals to compensate for a portion of the transformer impedance. In this case both R_c and X_c are negative values.

In most cases, R_c is negligible and can be ignored.

4.2.2   Exciters and Voltage Regulators

The modelling of various excitation systems has been reported in two IEEE Committee reports [1, 2]. Modern Automatic Voltage Regulators (AVR) are continuously acting electronic regulators with high gain and small time constants.

The exciters can be of the following types

1. Field controlled dc generator - commutator

2. a) Field controlled alternator with non-controlled rectifier (using diodes)

    i) with slip rings and brushes (stationary rectifier)

    ii) brushless, without sliprings (rotating rectifier)

   b) Alternator with controlled rectifier

3. Static exciter with

   a) potential source controlled rectifier in which the excitation power is supplied through a potential transformer connected to generator terminals

   b) Compound source (using both current and voltage transformers at
      the generator terminals) with
      (i) non-controlled rectifier (control using magnetic elements such as
          saturable reactors)
      (ii) controlled rectifier (for controlling the voltage)

Historically, DC generator-commutator exciters were first to be used.
The DC generator may be self-excited or separately excited (using a pilot ex-
citer). The voltage regulator for DC excitation systems were based on rotating
amplifier (amplidyne) or magnetic amplifiers.

AC and static excitation systems invariably use electronic regulators
which are fast acting and result in the phase control of the controlled recti-
fiers using thyristors. In type 2(a) exciters, field control of the alternator is
achieved using controlled rectifier with power source derived from the alternator
output. With brushless exciters, the field circuit of the alternator is mounted
in the stationary member and is supplied through a controlled rectifier from a
permanent magnet generator. The armature of the alternator is on the rotor and
connected directly to rotating diode rectifier and thus sliprings are eliminated.

The performances of the exciters type 2(b) and 3(a) are expected to
be similar as in both systems, the generator field is directly supplied through
controlled rectifiers which have fast response. The only difference is that of the
power source for the rectifiers (and the generator field) - in 2(b) it comes from the
alternator (hence a part of the AC excitation systems) and in 3(a) it comes from
static elements (potential transformer) and thus belongs to the static excitation
systems.

In the first IEEE committee report published in 1968 [1], excitation
systems were classified not according to their power source but in an arbitrary
manner. However the IEEE Type 1 excitation system defined in that report
represents a majority of the excitation systems in service and is widely used.
It essentially represents rotating exciters but with some modifications can also
represent static exciters. This is shown in Figure 4.3. Here, V_R is the output of
the regulator, which is limited. The regulator transfer function has single time
constant T_A and a positive gain of K_A. The saturation function $S_E = f(E_{FD})$
represents the saturation of the exciter.

It is to be noted that the limits on V_R also imply limits on E_{FD}. Actually
the latter are usually specified, and the former can be found from the equation
(in steady state)

$$\left. \begin{array}{l} V_R - (K_E + S_E)E_{FD} = 0 \\ E_{FDmin} \leq E_{FD} \leq E_{FDmax} \end{array} \right\} \tag{4.1}$$
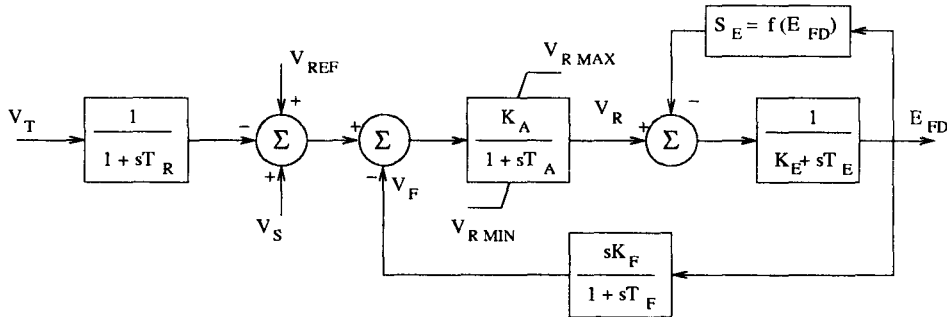
Figure 4.3: IEEE Type 1 Excitation system

IEEE Type 1 can also represent the static excitation system (3(a)) by specifying the following parameters

$$K_E = 1, \ T_E = 0, \ S_E = 0 \quad and \quad V_{RMAX} = K_P V_T \qquad (4.2)$$

Eq. (4.2) shows that the upper limits on the regulator and exciter outputs are directly related to the terminal voltage (V_T) of the generator.

4.2.3 Excitation System Stabilizer (ESS) and Transient Gain Reduction (TGR)

This is used for increasing the stable region of operation of the excitation system and permit higher regulator gains. It is to be noted that feedback control systems, of which the excitation system is an example, often require lead/lag compensation or derivative (rate) feedback.

The feedback transfer function for ESS is shown in Figure 4.4. This can be realized by a transformer (assumed to be ideal) whose secondary is connected to a high impedance (see Figure 4.5). The turns ratio of the transformer and the time constant (L/R) of the impedance determine K_F and T_F according to the relations
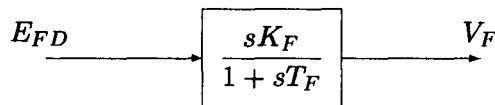
Figure 4.4: Excitation System Stabilizer(ESS)
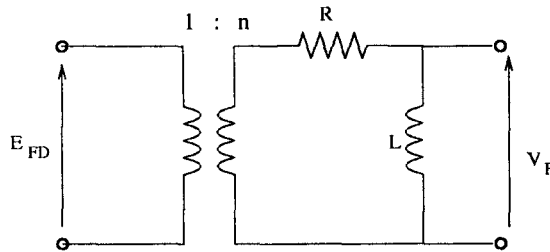
Figure 4.5: Realization of ESS

$$T_F = \frac{L}{R} \tag{4.3}$$

$$K_F = \frac{nL}{R} \tag{4.4}$$

The time constant is usually taken as 1 second. Instead of feedback compensation for ESS, a series connected lead/lag circuit can also be used as shown in Figure 4.6. Here T_C is usually less than T_B. Hence, this means of stabilization is termed as Transient Gain Reduction (TGR). The objective of TGR is to reduce the transient gain or gain at higher frequencies, thereby minimizing the negative contribution of the regulator to system damping. However if Power System Stabilizer (PSS) is specifically used to enhance system damping, the TGR may not be required. A typical value of the transient gain reduction factor (T_B/T_C) is 10.
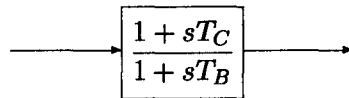
Figure 4.6: Transient Gain Reduction(TGR)

4.2.4   Power System Stabilizer (PSS)

The stabilization provided by PSS is not to be confused with that by ESS. While ESS is designed to provide effective voltage regulation under open or short circuit conditions, the objective of PSS is to provide damping of the rotor oscillations whenever there is a transient disturbance. The damping of these oscillations (whose frequency varies from 0.2 to 2.0 Hz) can be impaired by the provision of

high gain AVR, particularly at high loading conditions when a generator is connected through a high external impedance (due to weak transmission network).

While detailed discussion of PSS will be taken up separately in chapter 8, it is worth noting here that the input signal for PSS is derived from speed/ frequency, or accelerating power or a combination of these signals. The PSS design in a multi-machine environment can be complex, as several rotor oscillation frequencies have to be considered. In any case, the stabilizer is designed to have zero output in steady state. Also the output is limited in order not to adversely affect the voltage control. The stabilizer output V_S is added to the terminal voltage error signal.

4.3 Excitation Systems- Standard Block Diagram

The second IEEE committee report published in 1981 [2], distinguished between the excitation systems based on their power source. This classification is more logical and can avoid gross approximations in the representation of different excitation systems.

4.3.1 DC Excitation System

The type DC 1 which represents field controlled DC commutator exciters with continuously acting voltage regulators, is shown in Figure 4.7. This is similar to the IEEE Type 1 excitation system . The block with the transfer function $(1 + sT_C)/(1 + sT_B)$ represents Transient Gain Reduction (TGR) as $T_B > T_C$. This has the similar function as Excitation System Stabilizer (ESS) which is used in the feedback path. Normally, either TGR (in the forward path) or ESS is used. By choosing $T_B = T_C$, the TGR is neglected. Similarly by choosing $K_F = 0$, ESS is avoided.

4.3.1.1 Derivation of the Transfer Function for separately Excited DC Generator

Consider the DC exciter shown in Figure 4.8. The equation for the field circuit of the exciter is

$$E_s = I_f R_f + \frac{d\psi_f}{dt} = I_f R_f + L_f \frac{dI_f}{dt} \tag{4.5}$$

The exciter voltage E_x is a nonlinear function of I_f as shown in Figure 4.9. The speed of the exciter is assumed to be constant as it is normally driven by the generator shaft.
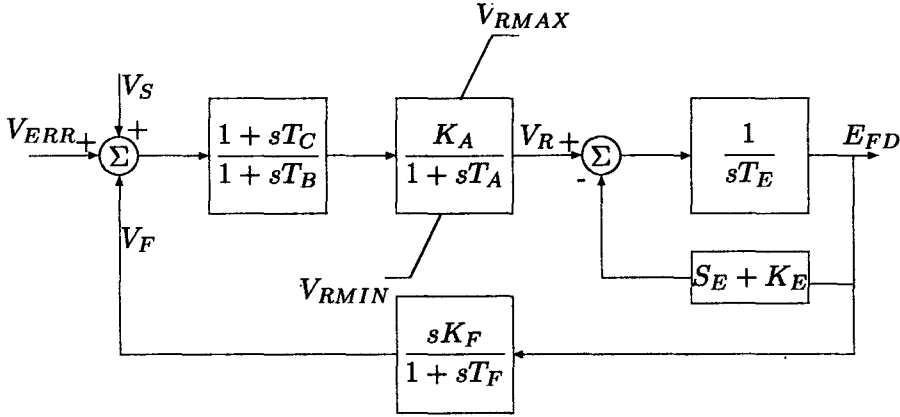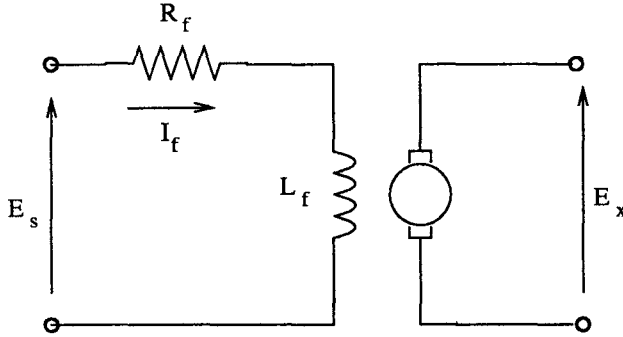
Figure 4.7: Type DC1-DC commutator exciter

Figure 4.8: Separately excited DC generator

From Figure 4.9, we can express

$$I_f = \frac{E_x}{R_g} + \Delta I_f \qquad (4.6)$$

$$\Delta I_f = S_e E_x \qquad (4.7)$$

R_g is the slope of the exciter saturation curve near $E_x = 0$. It is convenient to express I_f in per unit of I_{fb} where

$$I_{fb} = \frac{E_{xb}}{R_g} \qquad (4.8)$$

E_{xb} is the rated voltage which is defined as the voltage which produces rated open circuit voltage in the generator neglecting saturation.
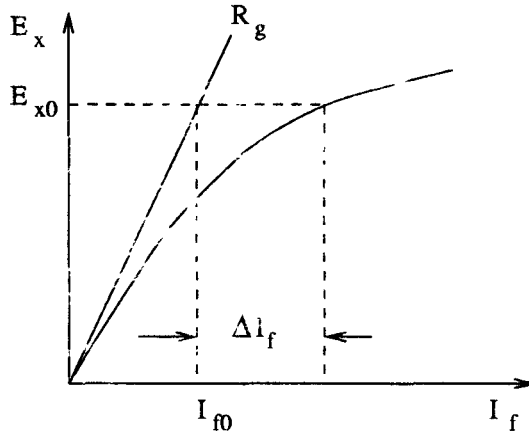
Figure 4.9: Exciter load saturation curve

Thns, in per unit quantities, Eqs. (4.6) and (4.5) are reduced to

$$\bar{I}_f = \bar{E}_x + S'_E \bar{E}_x \tag{4.9}$$

$$\bar{E}_s = \bar{I}_f \frac{R_f}{R_g} + \frac{K_f}{R_g} \frac{d\bar{E}_x}{dt} \tag{4.10}$$

where

$$S'_E = R_g S_e$$

$$K_f = L_f \frac{d\bar{I}_f}{d\bar{E}_x}$$

Since

$$\bar{E}_s = V_R$$

equations (4.9) and (4.10) represent the exciter block diagram shown in Figure 4.10. Here

$$T_E = \frac{K_f}{R_g} \tag{4.11}$$

$$S_E = \frac{R_f S'_E}{R_g} \tag{4.12}$$

$$K_E = \frac{R_f}{R_g} \tag{4.13}$$

$$E_{FD} = \bar{E}_x \tag{4.14}$$
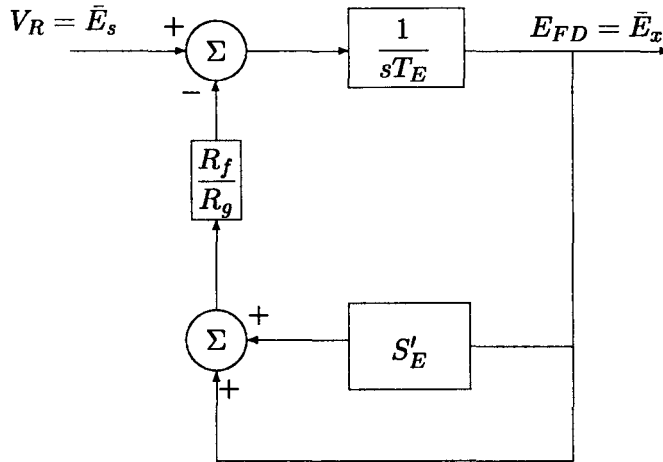
Figure 4.10: Block diagram of separately excited DC generator

4.3.1.2   Self Excited DC Generators

Figure 4.11 shows the schematic diagram of the self-excited exciter.' E_a represents the voltage of the amplifier in series with the exciter shunt field. Hence,

$$\bar{E}_s = \bar{E}_x + \bar{E}_a \tag{4.15}$$

Using this relation along with the block diagram given in Figure 4.10 and noting
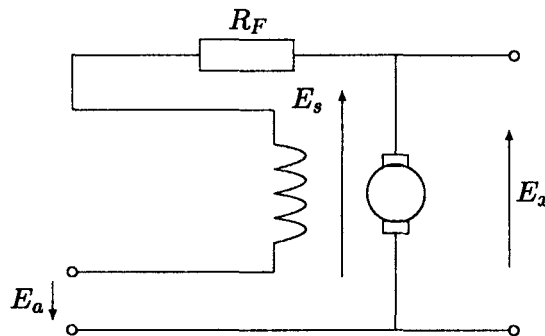
Figure 4.11: Self Excited DC Generator

that

$$\bar{E}_a = V_R \tag{4.16}$$

We can reduce the block diagram of the self-excited exciter to that given in Figure 4.10 with the modified value of K_E as

$$K_E' = \frac{R_f}{R_g} - 1 \tag{4.17}$$

The field resistance R_f is periodically adjusted to maintain $V_R = 0$ in steady state. For this case, from Eq. (4.1), we get

$$K_E = -S_{Eo} \tag{4.18}$$

where S_{Eo} is the value of saturation function S_E at the initial operating point. It is to be noted that K_E is generally negative for self-excited exciter.

4.3.2 AC Excitation System

Type AC 1 (Field controlled alternator rectifier, with non-controlled rectifiers) excitation system is shown in Figure 4.12. This is different from earlier representation [1] in that a) the armature reaction of the alternator ($K_D I_{FD}$) and b) rectifier regulation (F_{EX}) are considered. The constant K_D is a function of the
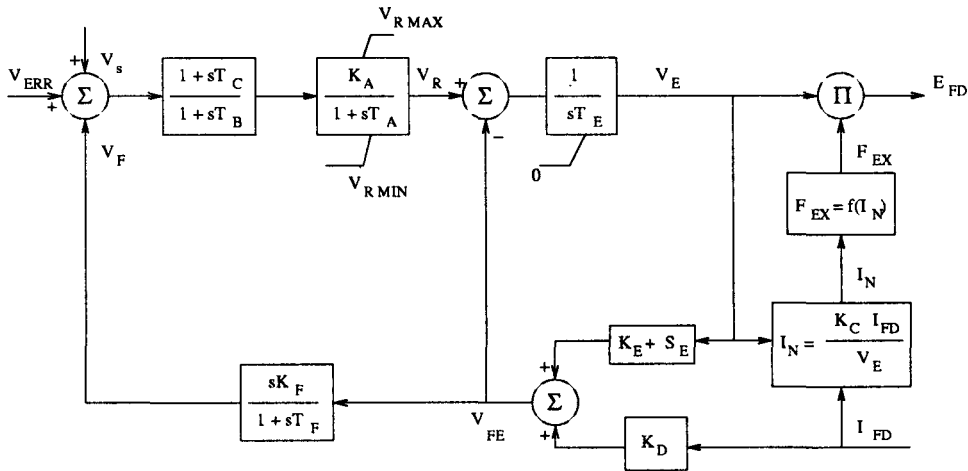
Figure 4.12: Type AC1-Alternator-rectifier excitation system

alternator synchronous and transient reactances. The constant K_C is a function of the commutating reactance. The function F_{EX} is defined as follows

$$F_{EX} = 1 - \frac{I_N}{\sqrt{3}} \quad if \quad I_N \leq \frac{\sqrt{3}}{4}$$
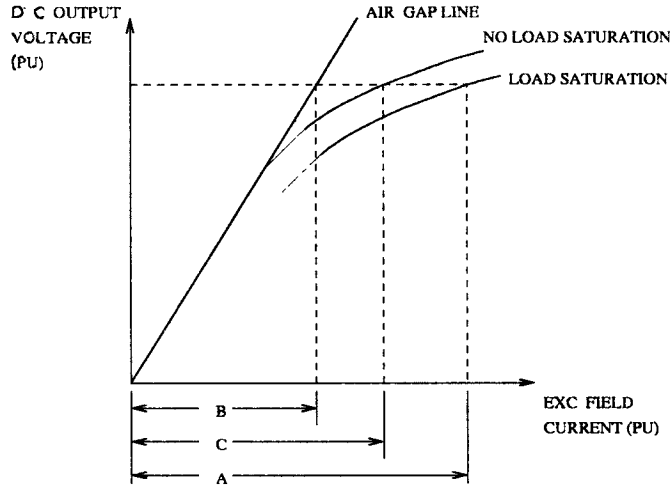
Figure 4.13: Exciter Saturation Characteristics

$$= \sqrt{\frac{3}{4} - I_N^2} \quad if \quad \frac{\sqrt{3}}{4} < I_N < \frac{3}{4} \tag{4.19}$$

$$= \sqrt{3}(1 - I_N) \quad if \quad I_N \geq \frac{3}{4}$$

The signal V_{FE} is proportional to the exciter field current. This signal is also used as input to the Excitation System Stabilizer (ESS).

4.3.3   Saturation Function

The exciter saturation function S_E is defined as a multiplier of per unit exciter voltage to represent the increase in exciter field current (expressed in per unit) due to saturation. It applies both to DC and AC exciter. The exciter saturation characteristics are shown in Figure 4.13. At a given exciter voltage (E_{FD}), the quantities A, B and C are defined as the exciter field currents required on (a) constant resistance load saturation curve (b) air-gap line and (c) no-load saturation curve respectively. For DC-commutator exciters, S_E is defined as

$$S_E = \frac{A - B}{B} \tag{4.20}$$

  When exciter field resistance is significantly different from the base resistance value, the adjusted value of S_E' should be used instead of S_E (Note: S_E' is defined in 4.9).

    For alternator-rectifier exciters, S_E is defined using no-load saturation

curve, as

$$S_E = \frac{C - B}{B} \tag{4.21}$$

The no-load saturation curve is used in the case of alternator-rectifier exciters as the exciter regulation effects are taken into account by the synchronous reactance and commutating reactance voltage drops, considered separately.

Mathematically the saturation function, S_E, is modelled as

$$S_E = A_x e^{B_x E_{FD}} \tag{4.22}$$

The constants A_x and B_x can be found if S_E is specified at two different values of E_{FD}. Usually, S_E is specified at or near ceiling voltage and at a lower value, commonly at 75% of that level.

4.3.4 Static Excitation System

In these systems, transformers are used to convert voltage (and also current in compounded systems) to the required level of the field voltage.Controlled or uncontrolled rectifiers are then used to provide the dc voltage for the generator field. Although negative field voltage forcing is used, many of the excitation systems used do not permit negative field current. This aspect is normally ignored in computer simulation but can be significant sometimes (particularly in asynchronous operation). As the exciter ceiling voltage tends to be high in static exciters, field current limiters are used to protect the exciter and field circuit. However, this protection is also not modelled except in special cases.

The block diagram of the potential source, controlled- rectifier excitation system is shown in Figure 4.14. The internal limiter following the summing junction can be neglected, but field voltage limits which are dependent on both V_T and I_{FD} must be considered. For transformer fed systems K_C is small and can be neglected.

The block-diagram given in Figure 4.14 is also similar to that of alternator supplied controlled rectifier excitation system. The only difference is that the field voltage limits are not dependent on the generator terminal voltage V_T in the case of alternator supplied system.

4.4 System Representation by State Equations

For digital computer simulation (and also for state space analysis of the overall system), it is necessary to describe the system by state equations. Given the
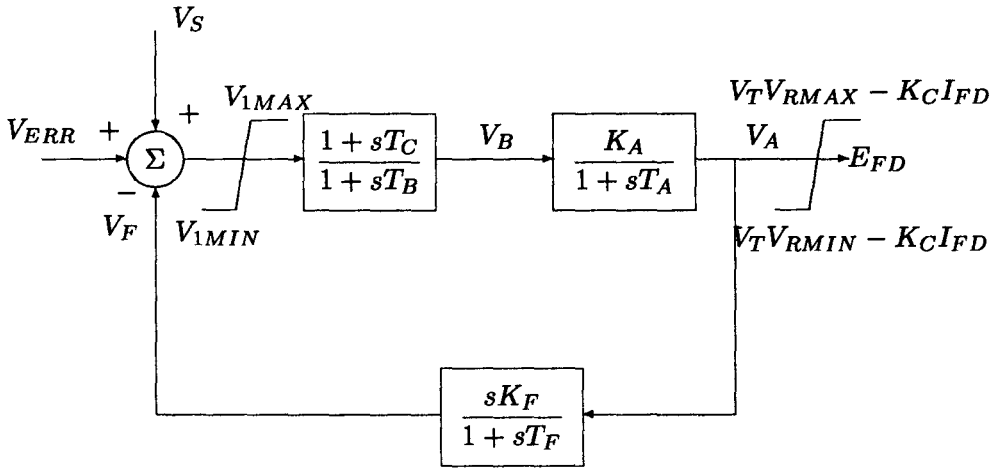
Figure 4.14: Type ST1-Potential source controlled rectifier exciter

block diagram representation of the system, it is possible to derive the state equations.

The choice of the state variables is not unique for a given transfer function. However, the minimum number of state variables required, is invariant. If the zeroes of the transfer function do not coincide with the poles, the minimum number of state variables is equal to the total number of poles.

4.4.1   Derivation of State Equations from Transfer Functions

It is assumed that the number of zeroes of a transfer function does not exceed the number of poles. Any general function can be expressed as a product of simpler functions with not more than two poles and two zeroes. These can be real or complex. Let the second order transfer function be expressed as

$$\frac{Y}{U}(s) = F(s) = \frac{K(1 + a_1 s + a_2 s^2)}{(1 + b_1 s + b_2 s^2)} \tag{4.23}$$

This can also be expressed as

$$Y(s) = (1 + a_1 s + a_2 s^2) Z(s) \tag{4.24}$$

and

$$Z(s) = \frac{K U(s)}{1 + b_1 s + b_2 s^2} \tag{4.25}$$

Defining the state variables as

$$x_1 = z \tag{4.26}$$
$$x_2 = \dot{x}_1 = \dot{z}$$

the Eq. (4.25) represents a simplified block diagram (or signal flow graph) in which the dynamic blocks are only integrators. This is shown in Figure 4.15. The state equations are readily written below as

$$\dot{x}_1 = x_2 \tag{4.27}$$

$$\dot{x}_2 = \left(-\frac{1}{b_2}\right) x_1 - \left(\frac{b_1}{b_2}\right) x_2 + \left(\frac{K}{b_2}\right) u \tag{4.28}$$

From Eq.(4.24), we get

$$y = (x_1 + a_1 x_2 + a_2 \dot{x}_2) \tag{4.29}$$

Substituting from Eq. (4.28), (4.29) can be finally expressed as
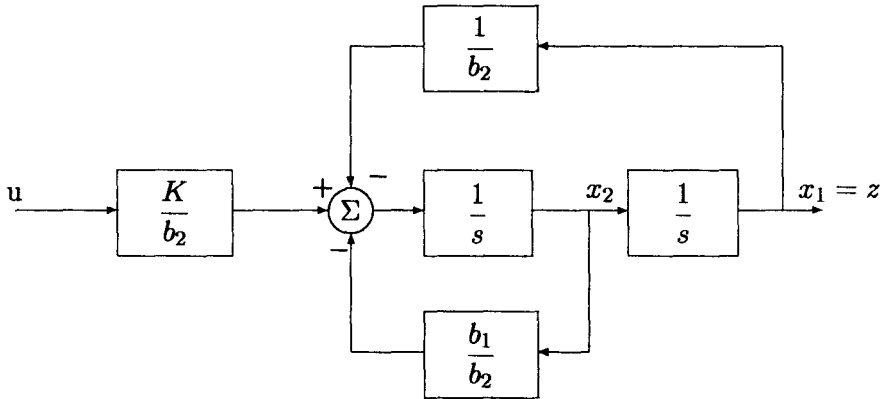
Figure 4.15: Block diagram representation of Eqn 4.25

$$y = \left(1 - \frac{a_2}{b_2}\right) x_1 + \left(a_1 - \frac{a_2}{b_2} b_1\right) x_2 + \frac{K a_2}{b_2} u \tag{4.30}$$

If all the poles and zeroes of a transfer function are real, the simplest transfer function (as a factor of the overall transfer function) is given by

$$T(s) = \frac{K(1 + sT_1)}{(1 + sT_2)} \tag{4.31}$$

This function can be represented by a block diagram shown in Figure 4.16. From the diagram, the equations are

$$\dot{x} = \frac{1}{T_2}\left(-x + \frac{K(T_2 - T_1)u}{T_2}\right) \tag{4.32}$$

$$y = x + \left(K\frac{T_1}{T_2}\right)u \tag{4.33}$$

It is to be noted that if $T_1 = 0$ then

$$y = x \tag{4.34}$$

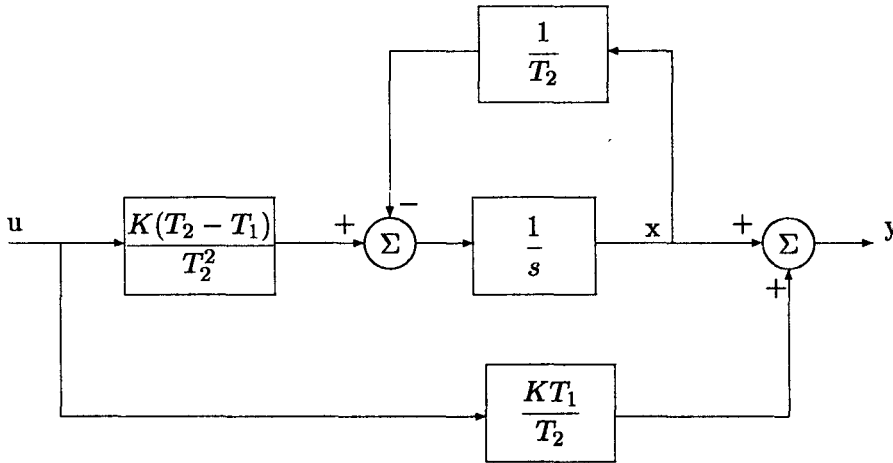It is also to be noted if $T_1 = T_2$, there is a pole-zero cancellation. In this case $x = 0$ and $y = Ku$.

Figure 4.16: Block diagram representation of Eq.(4.31)

4.4.2 Inclusion of Limits

There are two types of limiters

1. Windup Limiter

2. Non-Windup Limiter

As the behaviour of these limiters are different, it is necessary to indicate the type of the limiter in the block diagram using the convention shown in Figure 4.17.

In the case of the windup limiter, the output variable (y) of the transfer function is not limited and is free to vary. In this case the limiter can be treated as a separate block whose input is y and the output is z. If

$$F(s) = \frac{1}{1 + sT}$$

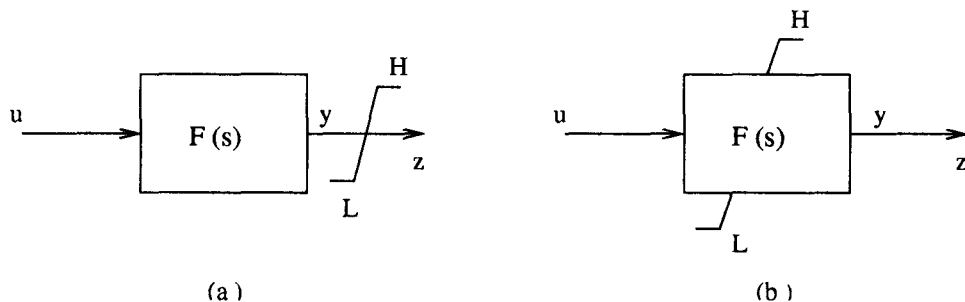the equations with the windup limiter are

(a)   (b)

Figure 4.17: (a) Windup limiter (b)Non-windup limiter

$$\frac{dy}{dt} = \frac{u - y}{T} \qquad (4.35)$$

If

$$\left. \begin{array}{lll} L \leq y \leq H, & \text{then} & z = y \\ y > H, & \text{then} & z = H \\ y < L, & \text{then} & z = L \end{array} \right\} \qquad (4.36)$$

In the case of the non-windup limiter, the output of the transfer function is limited and there is no separate block for the limiter. The equations in this case are

$$f = (u - y)/T \qquad (4.37)$$

If
$$\begin{array}{llll} y = H & \text{and} & f > 0, \\ y = L & \text{and} & f < 0, \end{array}$$

then,
$$\frac{dy}{dt} = 0$$

otherwise,
$$\frac{dy}{dt} = f$$

and

$$L \leq y \leq H \qquad (4.38)$$

Note that

1. Windup limiter can result in slow response as the output z of the limiter does not change until y comes within the limits.

2. Generally, all integrator blocks have non-windup limits.

4.4.3 Examples

Example 1: IEEE Type 1 Excitation System

This system is shown in Figure 4.3 and has been widely used. The equations for the system are given below

$$\frac{dE_{FD}}{dt} = \frac{1}{T_E}\left(-\left[K_E + S_E(E_{FD})\right]E_{FD} + V_R\right) \qquad (4.39)$$

$$\frac{dV_2}{dt} = \frac{1}{T_F}\left[-V_2 + \frac{K_F}{T_F}E_{FD}\right] \qquad (4.40)$$

$$\frac{dV_1}{dt} = \frac{1}{T_R}\left[-V_1 + V_T\right] \qquad (4.41)$$

$$V_{ERR} = V_{REF} - V_1 \qquad (4.42)$$

$$V_F = \frac{K_F}{T_F}E_{FD} - V_2 \qquad (4.43)$$

$$F_R = \frac{1}{T_A}\left[-V_R + K_A(V_{ERR} + V_S - V_F)\right] \qquad (4.44)$$

$$\left.\begin{array}{l}
\text{If } V_R > V_{RMAX} \quad \text{set} \quad V_R = V_{RMAX} \\
\text{If } V_R = V_{RMAX} \quad \text{and} \quad F_R > 0, \quad \text{set} \quad \frac{dV_R}{dt} = 0 \\
\text{If } V_R < V_{RMIN} \quad \text{set} \quad V_R = V_{RMIN} \\
\text{If } V_R = V_{RMIN} \quad \text{and} \quad F_R < 0, \quad \text{set} \quad \frac{dV_R}{dt} = 0 \\
\text{Otherwise ,} \quad \frac{dV_R}{dt} = F_R
\end{array}\right\} \qquad (4.45)$$

It is to be noted that the limiter is represented as a non-windup limiter.

Example 2 : Static Excitation System

This is shown in Figure 4.14. Many modern excitation systems can be represented by the block diagram shown in the figure. The equations are given

below for the case neglecting K_C. The internal limits are also neglected. The system includes TGR instead of ESS.

$$V_I = V_{ERR} + V_S \qquad (4.46)$$

$$\frac{dV_1}{dt} = \frac{1}{T_B}\left[-V_1 + \frac{(T_B - T_C)}{T_B}V_I\right] \qquad (4.47)$$

$$V_B = V_1 + \frac{T_C}{T_B}V_I \qquad (4.48)$$

$$\frac{dV_A}{dt} = \frac{1}{T_A}\left[-V_A + K_A V_B\right] \qquad (4.49)$$

If

$$V_T V_{RMIN} \leq V_A \leq V_T V_{RMAX}, \quad then$$
$$E_{FD} = V_A \qquad (4.50)$$

If $V_A > V_T V_{RMAX}$, then $E_{FD} = V_T V_{RMAX}$
If $V_A < V_T V_{RMIN}$, then $E_{FD} = V_T V_{RMIN}$

4.5 Prime-Mover Control System

The regulation of frequency in the system requires the speed control of prime-mover using governor. However, parallel operation of generators requires a droop characteristic incorporated in the speed-governing system to ensure stability and proper division of load. Hence, to maintain constant frequency, an auxiliary control is required which responds to a load unbalance. Also, it is necessary for the prime-mover control to adjust the generation according to economic dispatch.

Thus, different prime-mover controls are classified as (a) primary (speed-governor), (b) secondary (load frequency control) and (c) tertiary (involving economic dispatch). With increase in the system size due to interconnections, the frequency variations (in normal conditions) become less and less and load frequency control assumes importance. However, the role of speed governors in rapid control of frequency cannot be underestimated.

In stability studies, the secondary and tertiary controls are usually neglected. Only speed-governing systems including turbines need to be represented. In this section, both turbine and governor models are presented based on the IEEE report published in 1973 [3].
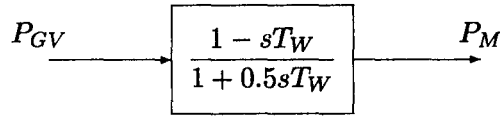
Figure 4.18: Hydroturbine model

4.5.1 Modelling of Turbines

4.5.1.1 Hydraulic Turbine

The hydraulic turbine is approximately represented by the block diagram shown in Figure 4.18. The time constant T_W is called the water starting time or water time constant. The equation for T_W is

$$T_W = \frac{LV}{H_T g} \tag{4.51}$$

where L is the length of the penstock, V is the water velocity, H_T is the total head and g is the acceleration due to gravity. For more accurate models, travelling wave phenomenon in penstock need to be considered. However, this is not required in stability studies.

The input P_{GV} for the turbine comes from the speed-governor. It is the gate opening expressed in per unit. Values for T_W lie in the range of 0.5 to 5.0 seconds with the typical value around 1.0 sec.

It is to be noted that hydroturbine has non-minimum phase characteristic and results in slower response. The response to a unit step input is shown in Figure 4.19 and is compared to the response, if the zero in the R.H.P. for the transfer function shown in Figure 4.18, did not exist.

4.5.1.2 Steam Turbine System

There are six common steam turbine systems given below

  (i) Nonreheat
 (ii) Tandem Compound, Single Reheat
(iii) Tandem Compound, Double Reheat
 (iv) Cross Compound, Single Reheat with two LP turbines
  (v) Cross Compound, Single Reheat with single LP turbine
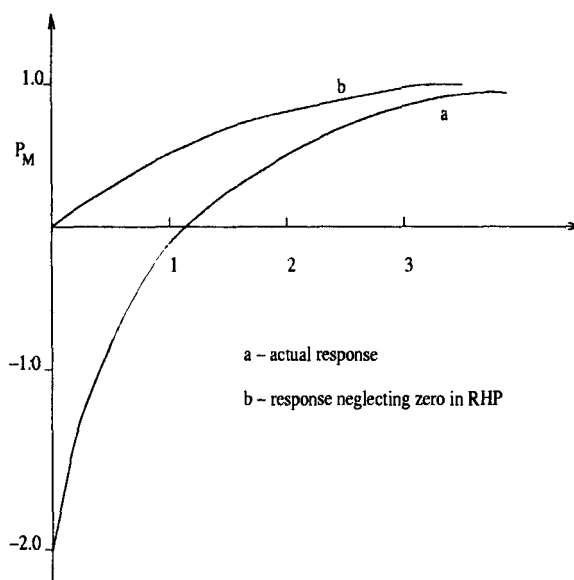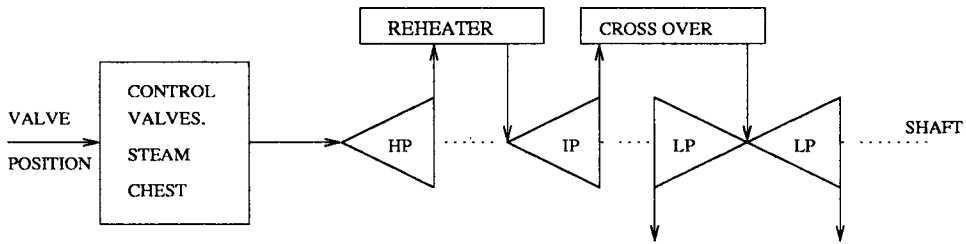 (vi) Cross Compound, Double Reheat

Figure 4.19: Response of a hydroturbine to a unit step input

Tandem compound has only one shaft on which all the turbines, High Pressure (HP), Intermediate Pressure (IP) and Low Pressure (LP) turbines are mounted. Sometimes there is a Very High Pressure (VHP) turbine also. Cross compound systems have two shafts driving two independent generators. The configurations corresponding to (ii) Tandem Compound, Single Reheat and (iii) Cross Compound, Single Reheat are shown in Figure 4.20. This does not show the extraction of steam taken at various turbine stages to heat feedwater, as this has no major significance in stability studies. The block diagrams for the steam turbine systems given in Figure 4.20 are shown in Figure 4.21. All compound steam turbines use governor controlled valves at the inlet to the high pressure turbine, to control the steam flow. The steam chest, reheater and crossover piping all introduces delays. The time constants T_{CH} and T_{RH} and T_{CO} represent these delays. The fractions F_{HP}, F_{IP}, F_{LP} represent fractions of the total turbine power developed, in the HP,IP and LP turbines respectively. Typical values for T_{CH}, T_{RH} and T_{CO} are

$$T_{CH} = 0.1 - 0.4\ s$$
$$T_{RH} = 4 - 11\ s$$
$$T_{CO} = 0.3 - 0.5\ s$$

The typical values of F_{HP}, F_{IP} and F_{LP} are 0.3, 0.3 and 0.4 respectively, the sum adding to unity.

(a) Tandem compound, single reheat
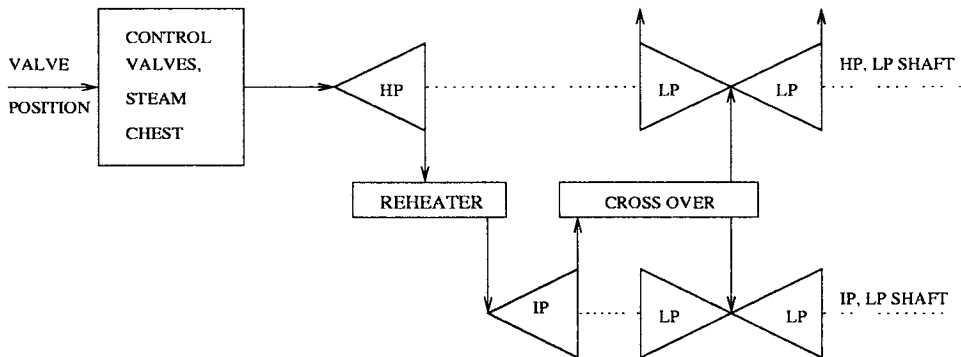
(b) Cross compound, single reheat

Figure 4.20: Steam system configurations

4.5.2   Speed-Governing Systems

There are two types of speed-governing systems, namely

 a) Mechanical-Hydraulic
 b) Electro-Hydraulic

In both types, hydraulic motors are used for positioning the valve or gate control-ling steam or water flow. The speed sensing and conditioning (at low power) for electro-hydraulic governors is done using electronic circuits while for mechanical-hydraulic governors, it is done using mechanical components.

4.5.2.1   Hydroturbines

The mechanical-hydraulic speed-governing system for a hydroturbine consists of a speed-governor, a pilot valve and servomotor, a distributor valve and gate
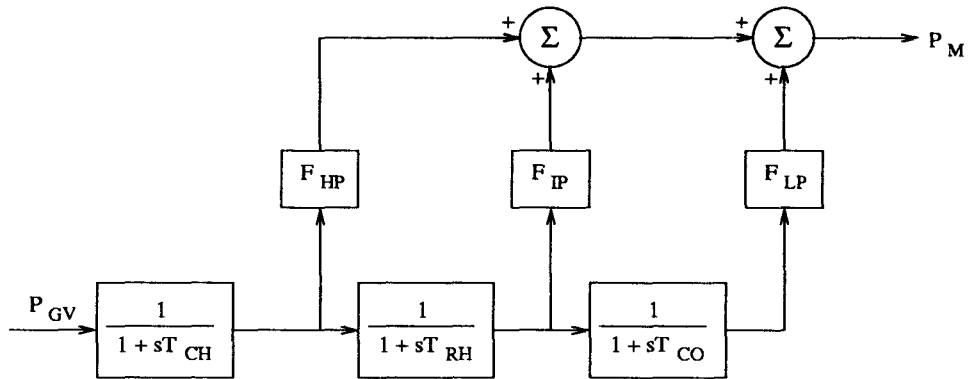
(a) Tandem compound, single reheat
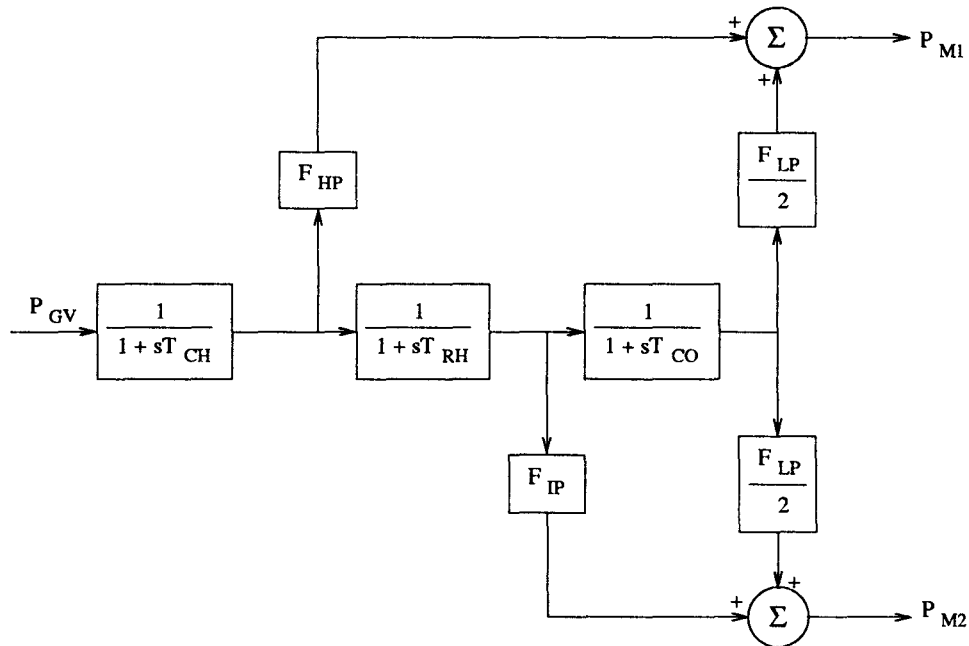
(b) Cross compound, single reheat

Figure 4.21: Steam turbine models

servomotor and governor controlled gates. A functional block diagram is shown in Figure 4.22. Because of the effects of water inertia on hydroturbine, a dashpot feedback is required for stable performance.
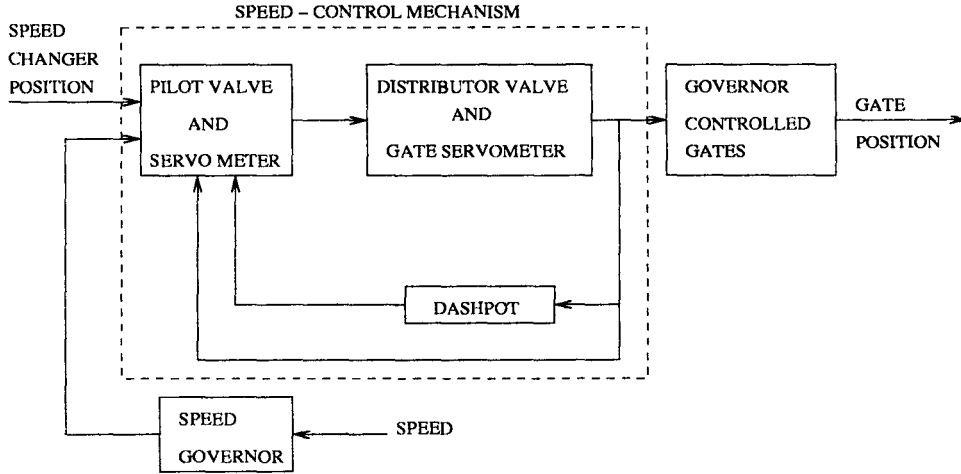
Figure 4.22: Speed governing system for hydroturbines-functional block diagram

An approximate nonlinear model for the hydro-governing system is shown in Figure 4.23. The typical values and ranges of parameters are given in Table 4.1. It is to be noted that T_R and δ are computed from

$$T_R = 5T_W \quad , \quad \delta = 1.25T_W/H$$

where H is generator inertia constant, T_W is the water starting time.

Table 4.1   Typical Values of Parameters
for Governors of Hydroturbines

Parameter	Typical Value	Range
T_R	5.0	2.5-25
T_G	0.2	0.2-0.4
T_P	0.04	0.03-0.05
δ	0.3	0.2-1.0
σ	0.05	0.03-0.06

The electro-hydraulic governor has essentially same dynamic performance as that of mechanical-hydraulic governor. Hence a common simplified block diagram for the speed governing system for hydro-turbine is employed in stability studies and is shown in Figure 4.24. The parameters of this block diagram can be determined from those defined in Figure 4.23.

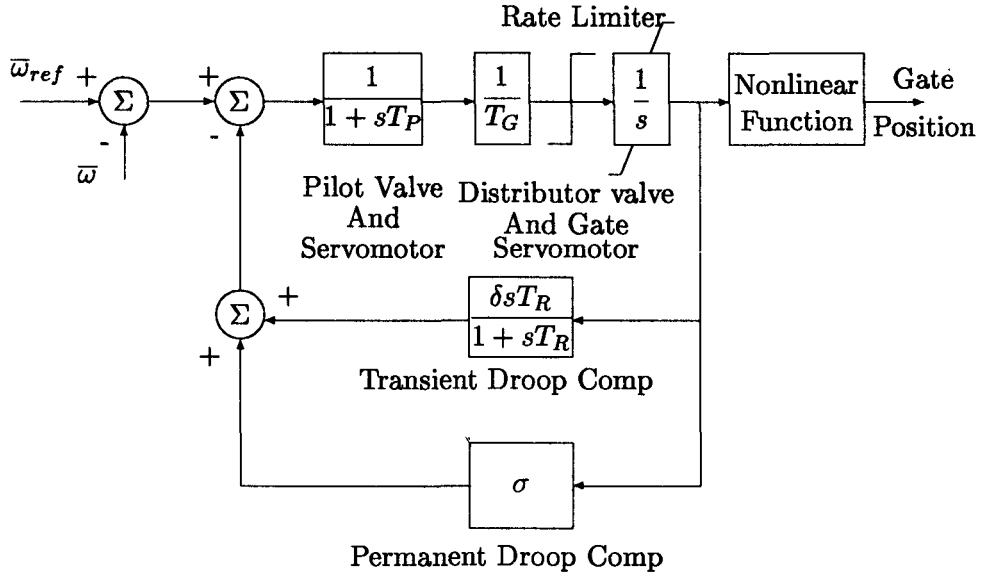$$T_1, T_3 = \frac{T_B}{2} \pm \sqrt{\frac{T_B^2}{4} - T_A} \tag{4.52}$$

Figure 4.23: Model of Speed governing system for hydroturbines

where

$$T_A = \left(\frac{1}{\sigma}\right) T_R T_G$$

$$T_B = \left(\frac{1}{\sigma}\right) [(\sigma + \delta)T_R + T_G]$$

The other parameters are given as

$$K = \frac{1}{\sigma} \quad , \quad T_2 = 0 \tag{4.53}$$

P_o is the initial power (load reference determined from automatic generation control). The output of the governor is P_{GV} which is expressed as power reference in per unit. It is to be noted that K is the reciprocal of σ (steady state speed regulation expressed in per unit).

4.5.2.2   Steam Turbines

The mechanical-hydraulic governing system for a steam turbine consists of a speed governor, a speed relay, a hydraulic servomotor and governor controlled valves. A functional block diagram is given in Figure 4.25.

A functional block diagram for the electro-hydraulic governor is shown in Figure 4.26. The feedback from steam flow (or pressure in the first stage
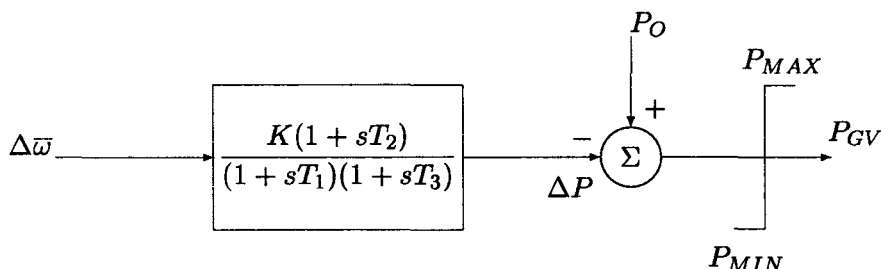
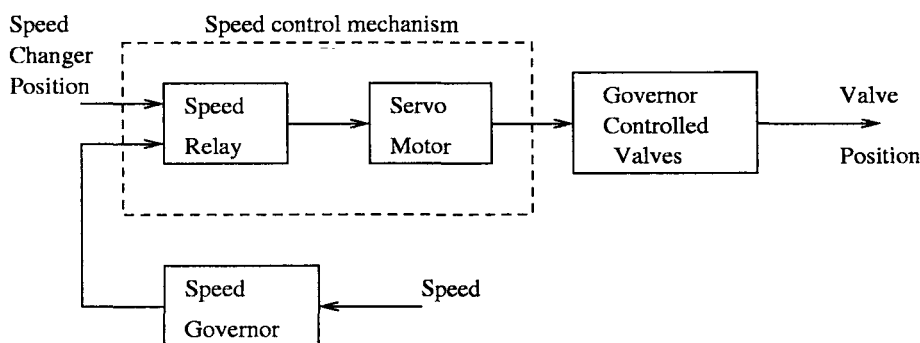Figure 4.24: General model of speed governor of hydroturbines

Figure 4.25: Mechanical-hydraulic speed governing system for steam turbines-functional block diagram

turbine) and the servomotor feedback loop provide for improved linearity over the mechanical-hydraulic governor system.

A simplified, general model for the speed-governing systems for steam turbine is shown in Figure 4.27. Typical values of time constants (in seconds) are given below.

Mechanical-hydraulic governor : $T_1 = 0.2 - 0.3$, $T_2 = 0$, $T_3 = 0.1$
Electro-hydrualic governor   : $T_1 = T_2$, $T_3 = 0.025 - 0.15$

Note that when $T_1 = T_2$, the value of T_1 or T_2 has no effect as there is pole-zero cancellation. For studies involving the dynamic performance for midterm and long term, it is essential also to model boiler controls in addition to automatic generation control (AGC). In this context, it is relevant to note that there are two basic modes of energy control in fossil fueled steam generator units -
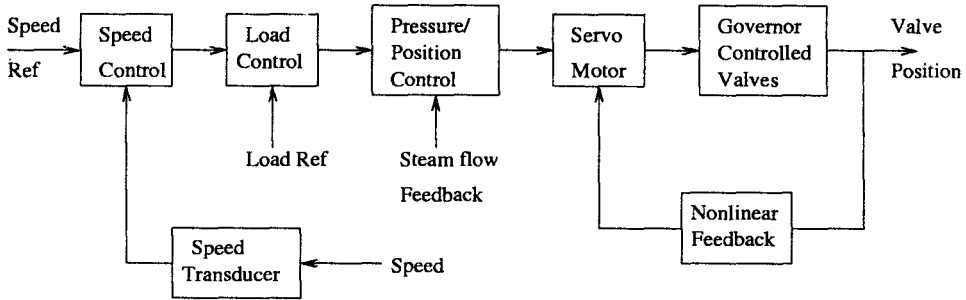
Figure 4.26: Electro-hydraulic speed governing system for steam turbines-functional block diagram
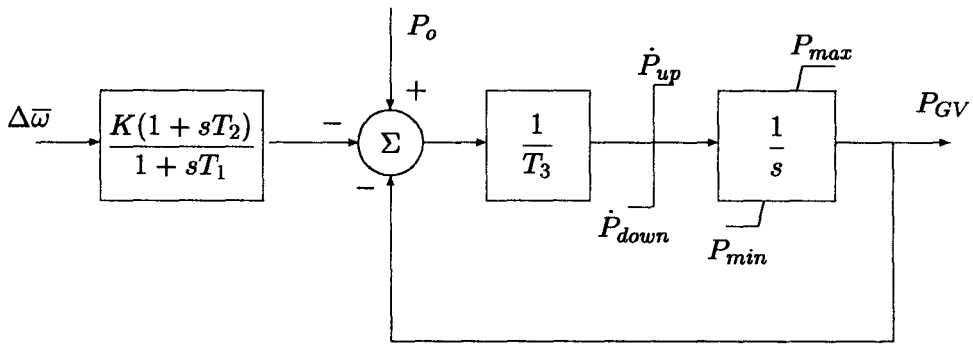

Figure 4.27: General model for speed governor for steam turbine

1. Boiler following (or turbine leading) mode
2. Turbine following (or boiler leading) mode

In the first mode of control which is applicable to many drum-type boilers (and also a few once-through boilers), changes in the power are initiated by turbine control valves and boiler controls respond to changes in steam flow and pressure. The response to small changes in power demand are rapid as turbine utilizes the stored energy in the boiler. However large changes can be detrimental to the boiler operation as large excursions in steam pressure and flow result following changes in the valve position.

In the second mode of control, (boiler leading turbine) the turbine control valves are made to regulate boiler pressure and changes in generation are made through boiler controls. The fast action of the turbine control valves can be utilized to maintain the boiler pressure almost constant. However, in this mode, the response of the turbine power to a change in load demand is slow as the
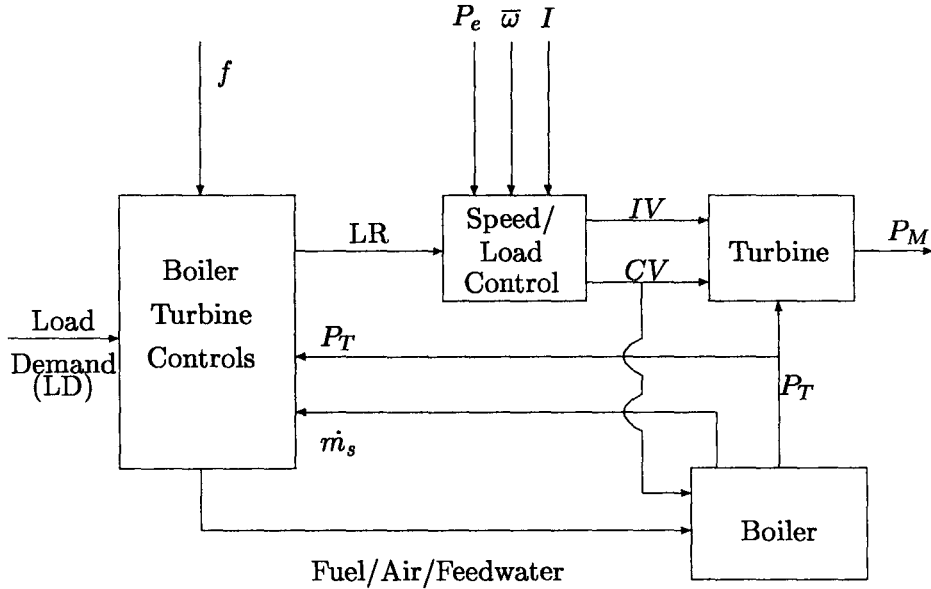
Figure 4.28: Basic structure of prime mover and energy supply system

lags in the fuel system and boiler storage affect the response. A compromise between the two desired objectives - (a) fast response and (b) constraints of regulating pressure and temperatures for maintaining boiler safety is achieved by the adoption of control modes termed as coordinated, integrated or direct energy balance. The need for close coordination between boiler and turbine controls is more crucial for once - through boilers than drum type boilers [14]. A recent development is to use turbine leading mode for small changes in steam pressure and switch to boiler leading mode for large changes.

The basic structure of the overall prime mover and energy supply controls is shown in Figure 4.28. The mechanical power P_m is a function of the steam pressure (P_T), control valve flow area (CV) and intercept valve flow area (IV). The boiler outputs, P_T and $\dot{m}_s$ (steam flow rate) are modelled as functions of CV and fuel, air and feedwater flows. The pressure effects of the reheater are included in the turbine model.

The speed/load control block represents the turbine control logic in response to changes in speed/load reference (LR), speed($\bar{\omega}$), steam pressure (P_T) and possibly in the case of fast valving applications, in response to changes in the electrical power (P_e) and generator current (I).

The boiler turbine controls establish the load reference LR in response

to the load demand (LD) set either manually or by AGC. Other inputs to the control logic are plant frequency (f), P_T and $\dot{m}_s$. In its simplest form, the boiler and turbine controls are decoupled, with power changes implemented directly through load reference (LR) and boiler controls responding to changes in P_T and $\dot{m}_s$.

4.6 Examples

Example 4.1

A generator equipped with a static excitation system is on no load (open circuited). The terminal voltage V_T in this case, is related to E_{FD} by the transfer function

$$V_T = \frac{1}{1 + sT'_{do}} E_{FD}$$

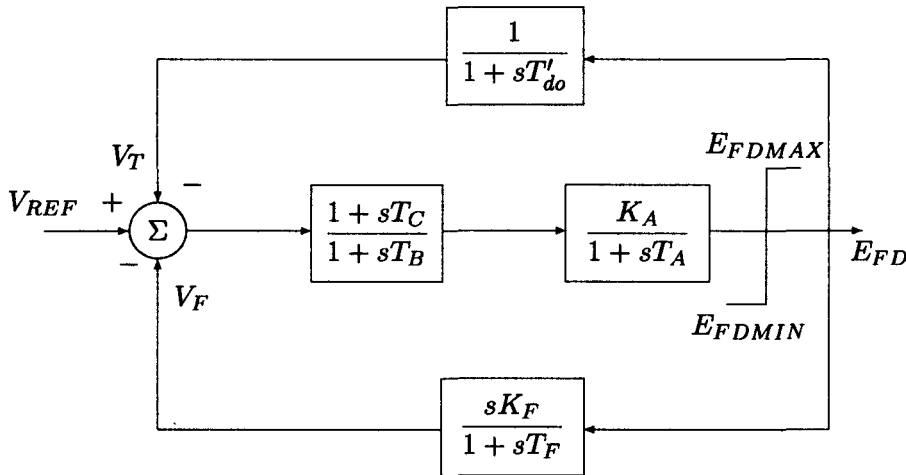The overall system block diagram is shown in Figure 4.29. The system is initially

Figure 4.29: System block diagram(Example 4.1)

in steady state with $E_{FD} = V_T = 1.0$. Obtain the response of E_{FD} for a step increase in V_{REF} by 0.2 pu, for the two cases
(a) $T'_{do} = 5\ s$ (b)$T'_{do} = 1\ s$
The excitation system data : $K_A = 400$, $T_A = 0.025s$, $T_B = 10s$,
$E_{FDMAX} = 6.0$, $E_{FDMIN} = -6.0$, $T_F = 1.0s$

(i) $K_F = 0.0$, $T_C = 10\ s$ (No TGR or ESS)

(ii) $K_F = 0.0$, $T_C = 1\ s$ (No ESS, only TGR)

(iii) $K_F = 0.03$, $T_C = 10\ s$ (No TGR, only ESS)

(iv) $K_F = 0.03$, $T_C = 1\ s$ (TGR and ESS are included)

(Note that with $K_F = 0.0$, the effect of ESS is not considered, with $T_B = T_C$, there is a pole zero cancellation and TGR is not considered)

Solution

The system equations can be obtained from the block diagram representation given in Figure 4.30 which is equivalent to that shown in Figure 4.29. These are

$$\frac{dV_A}{dt} = \frac{1}{T_A}[-V_A + K_A V_B] \tag{4.54}$$

$$V_B = x_B + \frac{T_C}{T_B}V_I \tag{4.55}$$

$$V_I = V_{REF} - V_F - V_T \tag{4.56}$$

$$\frac{dV_T}{dt} = \frac{1}{T'_{do}}[-V_T + E_{FD}] \tag{4.57}$$

$$V_F = \frac{K_F}{T_F}E_{FD} - x_F \tag{4.58}$$

$$\frac{dx_F}{dt} = \frac{1}{T_F}\left[-x_F + \frac{K_F}{T_F}E_{FD}\right] \tag{4.59}$$

$$\frac{dx_B}{dt} = \frac{1}{T_B}\left[-x_B + \left(1 - \frac{T_C}{T_B}\right)V_I\right] \tag{4.60}$$

$$\left.\begin{aligned} E_{FD} &= V_A \quad \text{if}\ E_{FDMIN} \le E_{FD} \le E_{FDMAX}\\ &= E_{FDMIN} \quad \text{if}\ E_{FD} < E_{FDMIN}\\ &= E_{FDMAX} \quad \text{if}\ E_{FD} > E_{FDMAX} \end{aligned}\right\} \tag{4.61}$$

The initial conditions for the four state variables are obtained as

$$V_A(0) = E_{FD}(0) = 1.0, \quad x_B(0) = \frac{V_A(0)}{K_A}\left[1 - \frac{T_C}{T_B}\right]$$

$$x_F(0) = \frac{K_F}{T_F}E_{FD}(0), \quad V_T(0) = 1.0$$

The reference voltage V_{REF} is calculated as
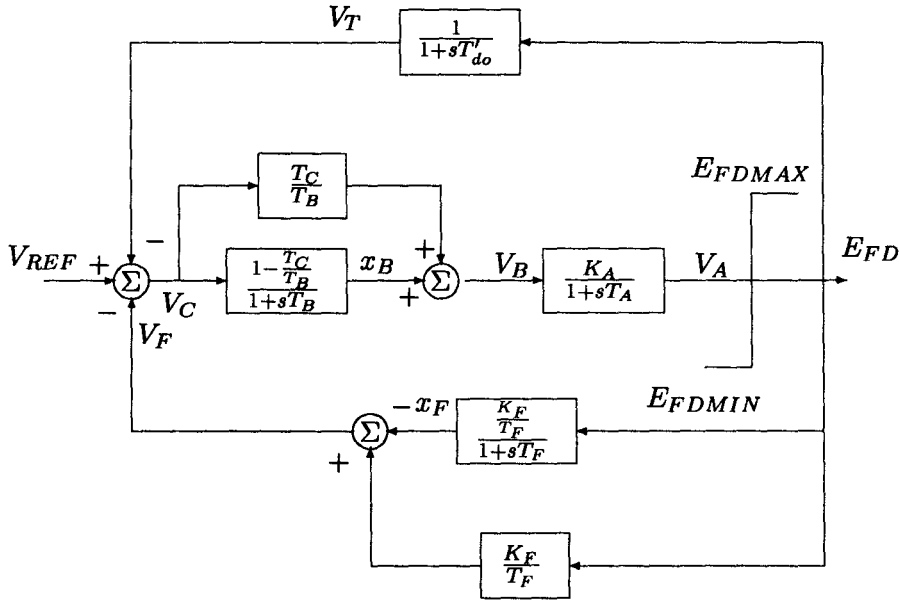
$$V_{REF} = V_T(0) + \frac{V_A(0)}{K_A}$$

Figure 4.30: Block diagram indicating state variables (Example 4.1)

The system equations can be simulated using any numerical integration method (say modified Euler's method). The results (variation on E_{FD} with time) for case (a) are shown in Figure 4.31 while for case (b) are shown in Figure 4.32. The disturbance is initiated at $t = 0.5$ s. Each figure shows the results for the four different conditions, namely (i) with no TGR or ESS (ii) with TGR (iii) with ESS (iv) with both TGR and ESS.

The results show that either TGR or ESS is necessary to improve the response which tends to be oscillatory and takes more time to settle (particularly for case (b)) without TGR and ESS . For this example, ESS gives slightly better results compared to TGR. There is no real advantage in having both TGR and ESS . The presence of both TGR and ESS has the effect of preventing the AVR hitting the upper limit during the transient but the settling time is actually increased, particularly for case (a).

It is interesting to observe that the response time of the excitation system is within 0.5s even when $T'_{do} = 5$ s. The use of TGR or ESS helps in reducing the settling time when T'_{do} is small. Although this example refers to the noload operation of the generator, the results can be related to system operation under
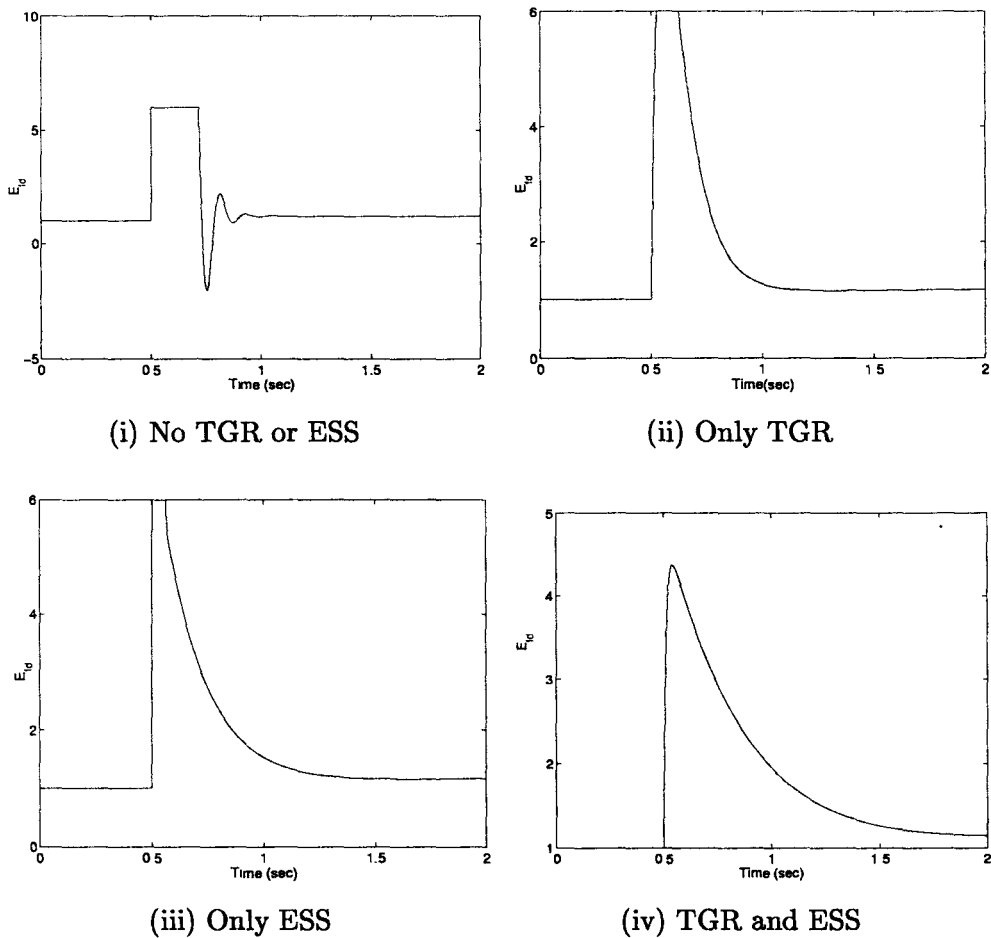
(i) No TGR or ESS

(ii) Only TGR

(iii) Only ESS

(iv) TGR and ESS

Figure 4.31: Variation of E_{fd} (Example 4.1 - case (a))

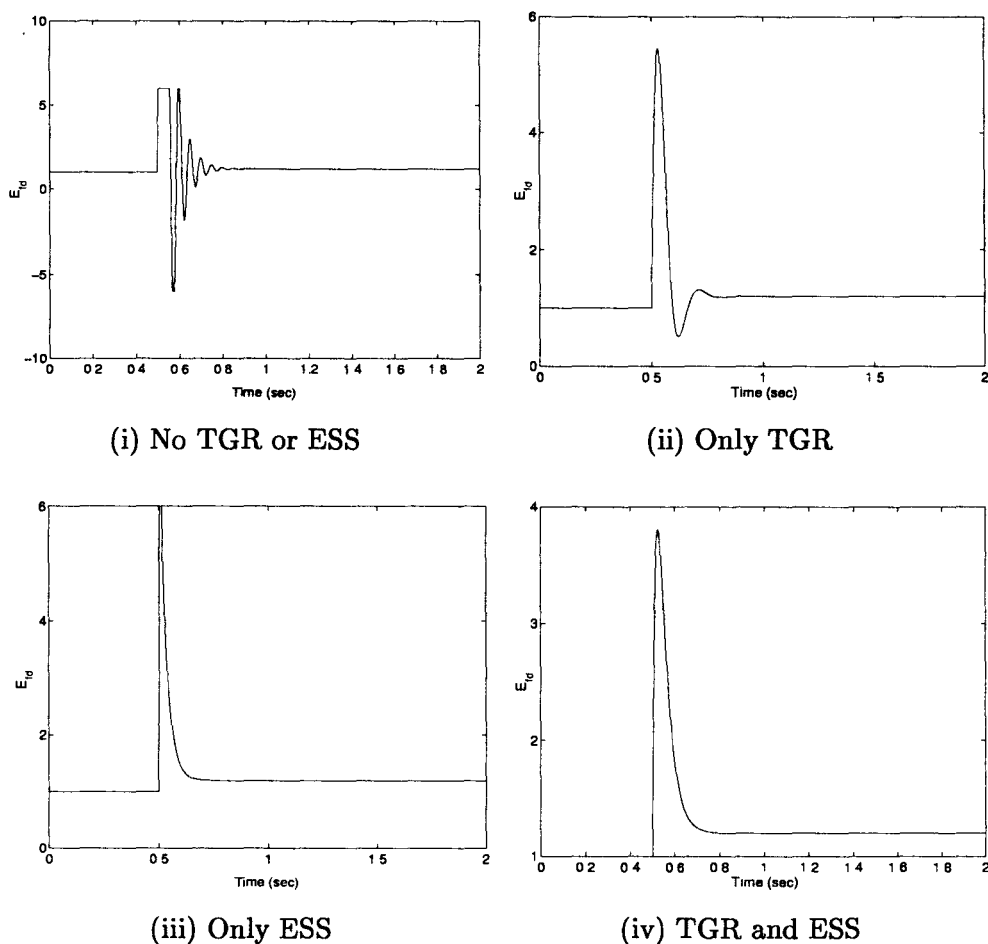load. In this case T'_{do} is to be replaced by a generator time constant T_G, where

$$T'_d < T_G < T'_{do}$$

The final steady state value of E_{FD} or V_T is given by the relation

$$V_{REF} = V_T + \frac{E_{FD}}{K_A} = E_{FD}\left(1 + \frac{1}{K_A}\right)$$

Substituting the value of $V_{REF} = 1.2025$, we get

$$E_{FD} = V_T = 1.20$$

(i) No TGR or ESS

(ii) Only TGR

(iii) Only ESS

(iv) TGR and ESS

Figure 4.32: Variation of E_{fd} (Example 4.1 - case (b))

Example 4.2

The generator is initially operating with $V_T = 1.0$, $E_{FD} = 2.2$, while supplying load. The generator breaker trips suddenly at $t = 0$. Obtain the response of the excitation system. The data is as given in Example 4.1 with $K_F = 0.0$ and (i) $T_C = 10 \ s$ (no TGR) (ii) $T_C = 1 \ s$ (with TGR).

Solution

The reference voltage in this example is given by

$$V_{REF} = V_T(0) + \frac{E_{FD}(0)}{K_A} = 1.0055$$

The initial conditions for the state variables are

$$V_A(0) = 2.2, \quad x_B(0) = 0.00495 \quad \text{(with TGR)}$$
$$V_T(0) = 1.0, \quad x_F(0) = 0$$

The results of the simulation for cases (a) and (b) are shown in Figure 4.33 and 4.34 respectively. The variations of both E_{FD} and V_T are shown. It is interesting to observe that although the response is non-oscillatory with TGR, it is slow compared to the case without TGR (particularly for $T'_{do} = 5$ s) Also the peak values reached are higher in the case with TGR. Thus the advantages of using TGR are suspect.
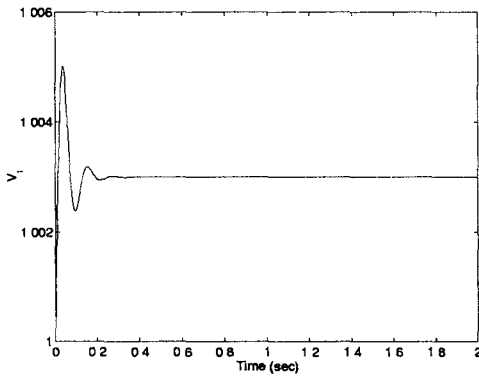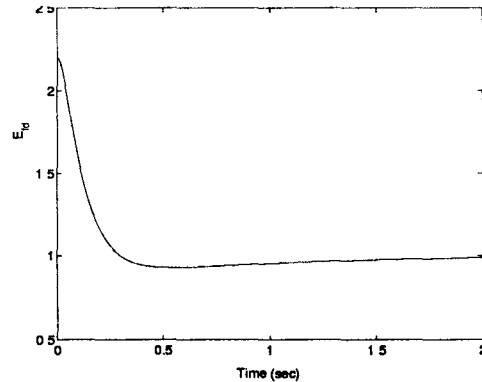

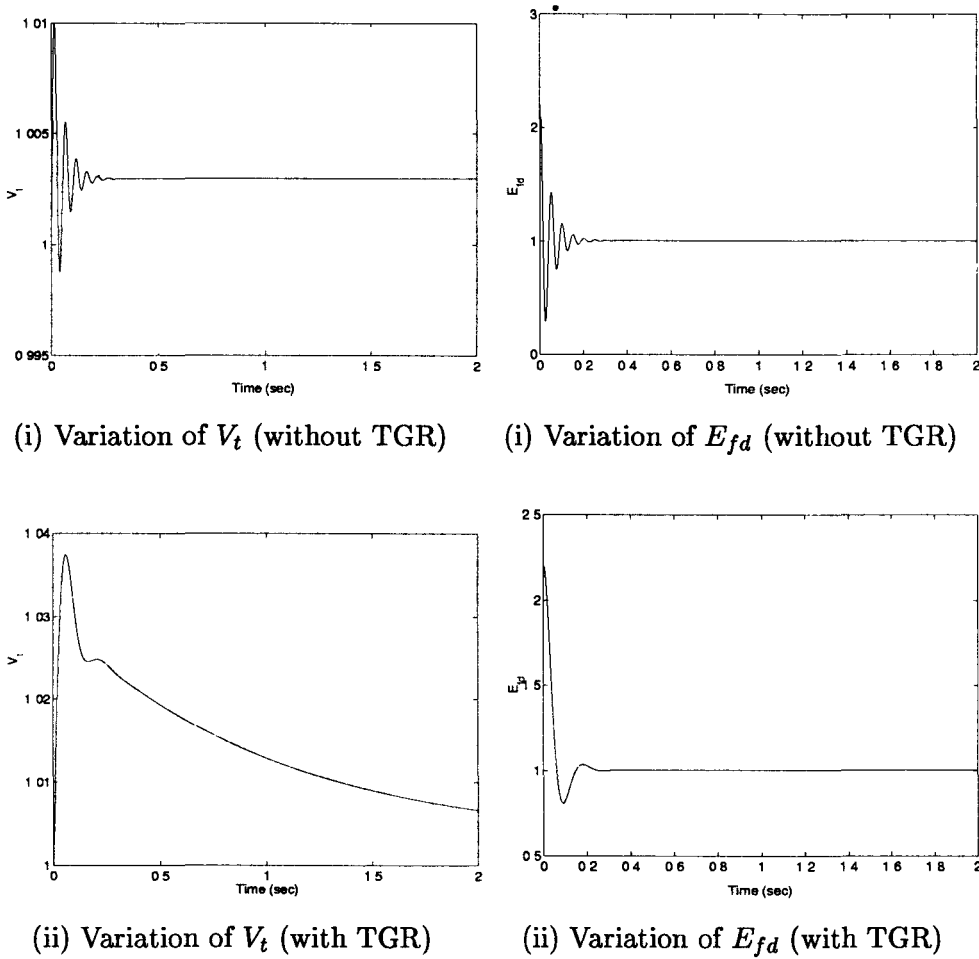(i) Variation of V_t (without TGR)   (i) Variation of E_{fd} (without TGR)
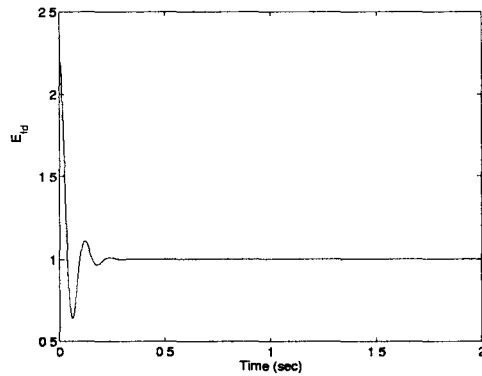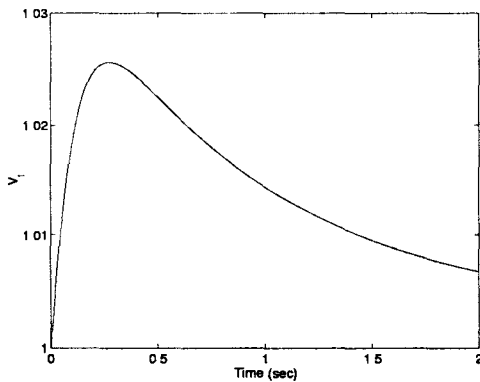
(ii) Variation of V_t (with TGR)   (ii) Variation of E_{fd} (with TGR)

Figure 4.33: Variation of E_{fd} (Example 4.2 - case (a))

(i) Variation of V_t (without TGR)

(i) Variation of E_{fd} (without TGR)

(ii) Variation of V_t (with TGR)

(ii) Variation of E_{fd} (with TGR)

Figure 4.34: Variation of E_{fd} (Example 4.2 - case (b))

It is to be noted that without AVR the terminal voltage would have reached the value of 2.2 pu (the same as $E_{fd}(0)$), neglecting saturation.

Example 4.3

A generator is driven by a hydroturbine and is delivering a constant power load. The governor input $\Delta\bar{\omega}$ (incremental per unit speed) is determined from the differential equation

$$2H\frac{d\bar{\omega}}{dt} = P_m - P_e \qquad (4.62)$$

The overall system representation (neglecting limits) including the governor,

turbine and generator rotor is shown in Figure 4.35. The permanent speed droop is neglected in modelling the governor. For the system to be stable, show that

$$\beta < \frac{1 - 1.5\alpha}{1 - \alpha} \qquad (4.63)$$

where

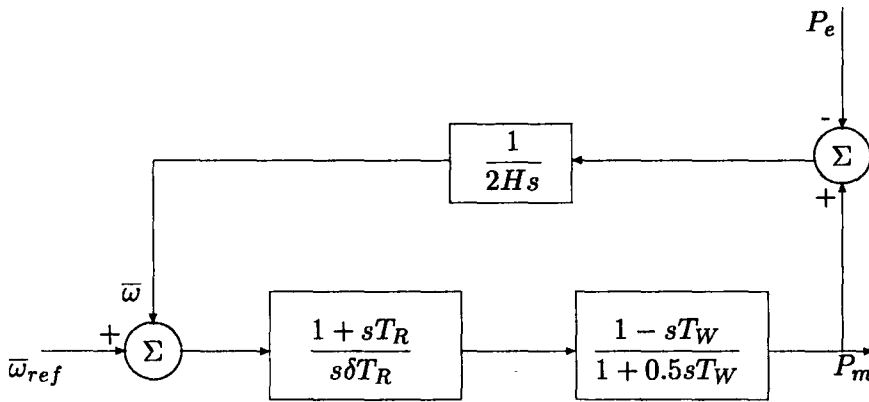$$\alpha = \frac{T_W}{T_R}, \quad \beta = \frac{T_W}{2\delta H}$$

Figure 4.35: Block diagram (Example 4.3)

Solution

From small signal analysis (using incremental quantities) the characteristic equation for the third order system shown in Figure 4.35 can be expressed as

$$\delta T_R H T_W s^3 + T_R(2H\delta - T_W')s^2 + (T_R - T_W)s + 1 = 0 \qquad (4.64)$$

Applying Routh-Hurwitz criterion, the condition for stability can be obtained as

$$(T_R - T_W) - \frac{\delta T_R H T_W}{T_R(2H\delta - T_W)} > 0 \qquad (4.65)$$

$$(2H\delta - T_W) > 0 \qquad (4.66)$$

$$(T_R - T_W) > 0 \qquad (4.67)$$

As $T_R > 0$, $H > 0$, the inequalities (4.66) and (4.67) imply

$$\delta > 0, \quad \alpha < 1, \quad \beta < 1$$

The inequality (4.65) can be expressed as

$$1 - \alpha - \frac{0.5\alpha}{1 - \beta} > 0$$

After some manipulations, the above criterion can be reduced to

$$\beta < \frac{1 - 1.5\alpha}{1 - \alpha}$$

Remarks

1. The governor transfer function shown in Figure 4.35 is an approximation of what is shown in Figure 4.23. This can be seen from the fact that a system with feedback transfer function $H(s)$ can be approximated as

$$T(s) = \frac{G(s)}{1 + G(s)H(s)} \approx \frac{1}{H(s)} \tag{4.68}$$

where $T(s)$ is the overall transfer function, $G(s)$ is the transfer function in the forward path.

Applying this to the block diagram in Figure 4.23, the governor transfer function is approximately given by

$$T(s) \approx \frac{1}{\sigma + \dfrac{\delta s T_R}{1 + s T_R}}$$

Letting $\sigma = 0$ (neglecting permanent speed droop), the transfer function is same as that given in Figure 4.35.

References and Bibliography

1. IEEE Committee Report, "Computer representation of excitation systems", IEEE Trans. Vol. PAS-87, June 1968, pp. 1460-1464

2. IEEE Committee Report, "Excitation system models for power system stability studies", IEEE Trans. Vol. PAS-100, No. 2, 1981, pp. 494-509

3. IEEE Committee Report, "Dynamic Models for steam and hydro turbines in power system studies", IEEE Trans. Vol. PAS-92, Nov/Dec. 1973, pp. 1904-1915

4. IEEE Committee Report, "Excitation system dynamic characteristics", IEEE Trans. Vol. PAS-92, Jan/Feb. 1973, pp.64-75

5. K.R. McClymont, G. Manchur, R.J. Ross and R.J. Wilson, "Experience with high-speed rectifier excitation systems", IEEE Trans. Vol. PAS-87, June 1968, pp. 1464-1470

6. E.C. Hartung, E.H. Lenfest and G.R. Meloy, "A rotating thyristor excitation system for hydraulic generators", IEEE Trans. Vol. PAS-91, Sept./Oct. 1972, pp. 2171-2178

7. M.L. Crenshaw, W.J. Miller, R.P. Schulz and M. Temoshok, "Althyrex excitation system with power stabilizer", IEEE Paper 70 CP 563-PWR, 1970

8. T.L. Dillman, J.W. Skoogland, F.W. Keay, W.H. South and C. Raczowski, "A high initial response brushless excitation system", IEEE Trans. Vol. PAS-90, Sept/Oct.1971, pp. 2089-2094

9. D.G. Ramey and J.W. Skoogland, "Detailed hydrogovernor representation for system stability studies", IEEE Trans. Vol. PAS-89, Jan 1970.

10. C. Concordia, "Effect of prime-mover speed control characteristics on electric power system performance", IEEE Trans. Vol. PAS-88, May 1969, pp. 752-756

11. J.M. Undrill and J.W. Woodward, "Nonlinear hydro governing model and improved calculation for determining temporary droop", IEEE Trans. Vol. PAS-86, April 1967, pp.443-452

12. L.M. Hovey, "Optimum adjustment of hydro governors on Manitoba hydro system", AIEE Trans. Vol. 81, Part III, Dec. 1962, pp. 581-587

13. T.H. Einstein, "Generalized representation of generator excitation power requirements", IEEE Trans. Vol. PAS-91, Sept/Oct 1972, pp. 1840-1847

14. IEEE Committee Report, "Dynamic models for fossil fueled steam units in power system studies", IEEE Trans. on Power Systems, Vol. 6, No. 2, 1991, pp. 753-761

15. IEEE Working Group Report, "Hydraulic turbine and turbine control models for system dynamic studies", IEEE Trans. on Power Systems, Vol. 7, No. 1, 1992, pp. 167-179

Chapter 5

Transmission Lines, SVC and Loads

In this chapter, the modelling of the elements of the AC network, external to synchronous generators, is discussed. The AC network primarily consists of transformers, transmission lines, shunt and series reactive compensation devices and loads. In power system modelling, a transformer is represented by leakage impedances connected in series. Shunt reactors, shunt and series capacitors are also represented by linear impedances.

In recent times, Static Var Compensators (SVC) are used for fast reactive power control in power systems. The major benefits are improvement of system stability and voltage regulation. It is necessary to model these devices in stability studies.

5.1 Transmission Lines

Transmission lines are basically distributed parameter devices. For the study of fast switching transients, it is necessary to model them in some detail. For example, the frequency response of a line can be approximated by cascaded connection of π networks - a lumped parameter model. However for power system dynamic performance studies involving frequencies below fundamental (synchronous frequency), the representation by a single π circuit is adequate. As a matter of fact, for studies involving low frequency transients, the transmission lines can be assumed to be in quasi-steady state - the voltages and currents can be assumed to be sinusoidal with slowly varying amplitudes and phase angles.

A basic assumption in the modelling of three phase transmission lines is that they are symmetric. This implies that the self impedances of all the three phases are equal. Also, the mutual impedances between any two phases are equal. An additional assumption is that the line parameters are constant - the network is linear. It can be shown that, in steady state, a symmetric three phase linear network connected to synchronous generators has only fundamental frequency voltages or currents. On the other hand, a lack of symmetry leads to

unbalanced currents (with negative sequence components) which can result in third harmonic voltage generation.

The symmetry is disturbed during unbalanced faults such as single line to ground or line to line faults. However, their duration is brief and the presence of harmonics can be neglected.

5.1.1   Modelling of Transmission Network

A single phase π equivalent of a transmission line is shown in Fig. 5.1. However it is to be noted that the coefficient matrices, inductance $[L]$, resistance $[R]$ and capacitance $[C]$ are all 3x3 matrices. These are defined as
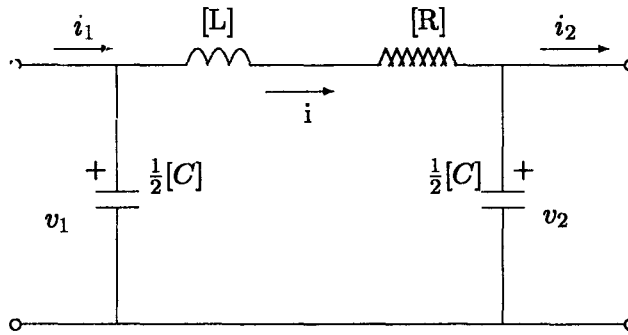

Figure 5.1: A single phase π equivalent of a transmission line

$$[L] = \begin{bmatrix} L_s & L_m & L_m \\ L_m & L_s & L_m \\ L_m & L_m & L_s \end{bmatrix}, \ [R] = \begin{bmatrix} R_s & R_m & R_m \\ R_m & R_s & R_m \\ R_m & R_m & R_s \end{bmatrix}, \ [C] = \begin{bmatrix} C_s & C_m & C_m \\ C_m & C_s & C_m \\ C_m & C_m & C_s \end{bmatrix}$$

The network equations are

$$[L]\frac{di}{dt} + [R]i = v_1 - v_2 \tag{5.1}$$

$$\frac{1}{2}[C]\frac{dv_1}{dt} = i_1 - i \tag{5.2}$$

$$\frac{1}{2}[C]\frac{dv_2}{dt} = i - i_2 \tag{5.3}$$

where v_1, v_2, i_1, i_2 and i are three dimensional vectors, with phase variables as elements. For example,

$$i^t = [i_a \quad i_b \quad i_c],$$
$$v_1^t = [v_{1a} \quad v_{1b} \quad v_{1c}]$$
$$v_2^t = [v_{2a} \quad v_{2b} \quad v_{2c}]$$

5.1.2   Transformation to D-Q components

If generator is described by variables in d-q components, using Park's transformation, it stands to reason that the external network equations should also be expressed in d-q components. However, there is one problem and that is Park's transformation is not unique and each generator has individual d-q components (corresponding to the individual transformation).

For a connected network, it is obvious that the entire network is to be transformed using a single transformation with reference to a common, synchronously rotating reference frame. Such a transformation is termed as Kron's transformation defined as

$$
\begin{bmatrix} f_a \\ f_b \\ f_c \end{bmatrix} = \sqrt{\frac{2}{3}} \begin{bmatrix} \cos\theta_o & \sin\theta_o & \frac{1}{\sqrt{2}} \\ \cos(\theta_o - \frac{2\pi}{3}) & \sin(\theta_o - \frac{2\pi}{3}) & \frac{1}{\sqrt{2}} \\ \cos(\theta_o + \frac{2\pi}{3}) & \sin(\theta_o - \frac{2\pi}{3}) & \frac{1}{\sqrt{2}} \end{bmatrix} \begin{bmatrix} f_D \\ f_Q \\ f_o \end{bmatrix} \tag{5.4}
$$

$$
= [C_K] f_{DQo}
$$

where $f^t_{DQo} = [f_D \quad f_Q \quad f_o]$

It is to be noted that f can be any variable, voltage or current. θ_o is defined as

$$
\theta_o = \omega_o t + \gamma \tag{5.5}
$$

where ω_o is the average (synchronous) frequency in the network in steady state and γ is a constant. The difference between Kron's transformation $[C_K]$ and Park's transformation $[C_P]$ lies in θ_o being replaced by θ in Park's transformation. θ is defined by

$$
\theta = \omega_o t + \delta \tag{5.6}
$$

It is to be noted that δ is dependent on the generator and not a common variable. $[C_K]$ is defined such that

$$
[C_K]^{-1} = [C_K]^t \tag{5.7}
$$

In other words, $[C_K]$ is an orthogonal matrix and satisfies the condition for a power invariant transformation.

The relationship between $[C_P]$ and $[C_K]$ is given by

$$
[C_P] = [C_K][T_1] \tag{5.8}
$$

where

$$
[T_1] = \begin{bmatrix} \cos\delta & \sin\delta & 0 \\ -\sin\delta & \cos\delta & 0 \\ 0 & 0 & 1 \end{bmatrix} \tag{5.9}
$$

It is to be noted that $[T_1]$ is also an orthogonal matrix. Actually, $[T_1]$ defines the transformation between Park's and Kron's variables, as

$$
\begin{bmatrix} f_D \\ f_Q \\ f_o \end{bmatrix} = [T_1] \begin{bmatrix} f_d \\ f_q \\ f_o \end{bmatrix}
\tag{5.10}
$$

where f_d, f_q are Park's components and f_D, f_Q are Kron's components (with respect to a synchronously rotating reference frame). Note that subscripts D,Q are associated with Kron's transformation. This convention will be followed throughout.

Applying Kron's transformation to Eq. (5.1) results in

$$
L_1 \frac{di_D}{dt} + \omega_o L_1 i_Q + R_1 i_D = v_{1D} - v_{2D}
\tag{5.11}
$$

$$
L_1 \frac{di_Q}{dt} - \omega_o L_1 i_D + R_1 i_Q = v_{1Q} - v_{2Q}
\tag{5.12}
$$

$$
L_o \frac{di_o}{dt} + R_o i_o = v_{1o} - v_{2o}
\tag{5.13}
$$

The last equation can be neglected if no zero sequence voltages or currents are present. L_1, R_1, L_o and R_o are defined by

$$
L_1 = L_s - L_m, \quad L_o = L_s + 2L_m
$$
$$
R_1 = R_s - R_m, \quad R_o = R_s + 2R_m
$$

It is to be noted that L_1 and R_1 are positive sequence (or negative sequence) quantities. Applying Kron's transformation to Eqs. (5.2) and (5.3) gives

$$
\frac{1}{2} C_1 \frac{dv_{1D}}{dt} + \frac{\omega_o}{2} C_1 v_{1Q} = i_{1D} - i_D
\tag{5.14}
$$

$$
\frac{1}{2} C_1 \frac{dv_{1Q}}{dt} - \frac{\omega_o}{2} C_1 v_{1D} = i_{1Q} - i_Q
\tag{5.15}
$$

$$
\frac{1}{2} C_1 \frac{dv_{2D}}{dt} + \frac{\omega_o}{2} C_1 v_{2Q} = i_D - i_{2D}
\tag{5.16}
$$

$$
\frac{1}{2} C_1 \frac{dv_{2Q}}{dt} - \frac{\omega_o}{2} C_1 v_{2D} = i_Q - i_{2Q}
\tag{5.17}
$$

The zero sequence variables are normally neglected and their equations can be omitted. C_1 is positive sequence capacitance given by

$$
C_1 = C_s - C_m
$$

Denoting

$$\hat{i} = i_Q + j i_D, \quad \hat{v}_1 = v_{1Q} + j v_{1D}, \quad \hat{v}_2 = v_{2Q} + j v_{2D} \tag{5.18}$$

Eqs. (5.11) and (5.12) can be expressed as

$$L_1 \frac{d\hat{i}}{dt} + (R_1 + j\omega_o L_1)\hat{i} = \hat{v}_1 - \hat{v}_2 \tag{5.19}$$

¹rom Eq. (5.10), we have

$$\left. \begin{array}{rcl} f_D & = & \cos\delta f_d + \sin\delta f_q \\ f_Q & = & -\sin\delta f_d + \cos\delta f_q \end{array} \right\} \tag{5.20}$$

ⁱrom Eq. (5.20), we can obtain

$$f_Q + j f_D = e^{j\delta}(f_q + j f_d) \tag{5.21}$$

From Eq. (5.21), we can express Eq. (5.19) as

$$e^{j\delta}\left[L_1 \frac{d\hat{i}'}{dt} + j\frac{d\delta}{dt}L_1\hat{i}' + (R_1 + j\omega_o L_1)\hat{i}'\right] = (\hat{v}_1' - \hat{v}_2')\, e^{j\delta} \tag{5.22}$$

where

$$\hat{i}' = i_q + j i_d, \quad \hat{v}_1' = v_{1q} + j v_{1d}, \quad \hat{v}_2' = v_{2q} + j v_{2d}$$

ₛimplifying Eq. (5.22) we get

$$L_1 \frac{d\hat{i}'}{dt} + (R_1 + j\omega L_1)\hat{i}' = \hat{v}_1' - \hat{v}_2' \tag{5.23}$$

ₙhere

$$\omega = \omega_o + \frac{d\delta}{dt}$$

Eq. (5.23) can also be derived directly from applying Park's transformation. Eq. (5.21) is a very useful relation and can be represented by a phasor diagram shown in Fig. 5.2.

5.1.3 Steady State Equations

neglecting transients, the equations that are applicable in steady state are obtained by neglecting variations in D-Q components. These complex equations ₐre

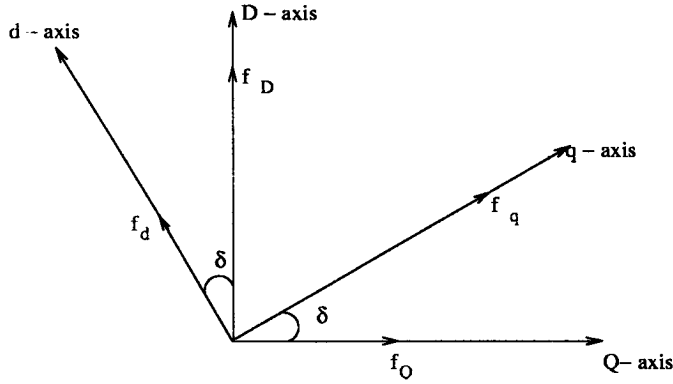$$(R_1 + j\omega_o L_1)\hat{I} = \hat{V}_1 - \hat{V}_2 \tag{5.24}$$

Figure 5.2: Phasor diagram showing relationship between dq and DQ variables

$$jw_o\frac{C_1}{2}\hat{V}_1 = \hat{I}_1 - \hat{I} \tag{5.25}$$

$$jw_o\frac{C_1}{2}\hat{V}_2 = \hat{I} - \hat{I}_2 \tag{5.26}$$

These equations describe a single phase circuit shown in Fig. 5.3 with sinusoidal excitation. (It is to be noted that the constancy of i_D and i_Q implies sinusoidal currents in the line). In Fig. 5.3, Z and Y are defined by

$$Z = R_1 + jw_oL_1, \quad Y = jw_oC_1$$

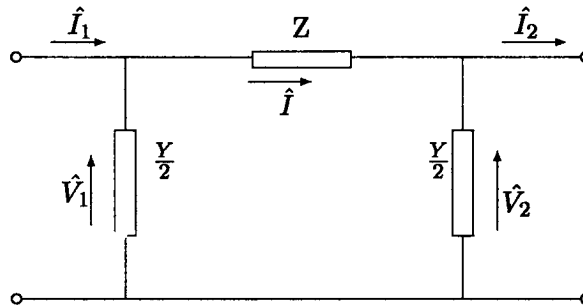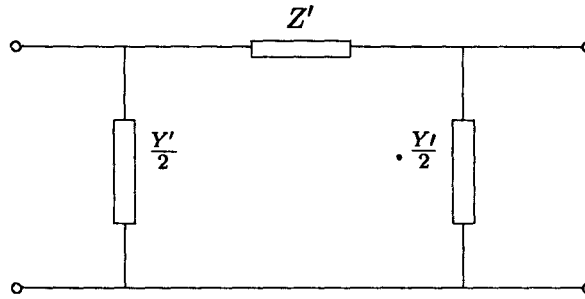For long transmission lines, an exact π equivalent shown in Fig. 5.4 is applicable

Figure 5.3: Positive sequence cercuit for steady state

in steady state, where

$$Z' = \frac{Z\sinh\sqrt{ZY}}{\sqrt{ZY}}, \quad Y' = \frac{Y\tanh(\sqrt{ZY}/2)}{(\sqrt{ZY}/2)}$$

Figure 5.4: An exact π equivalent for steady state

R_1, L_1 and C_1 are calculated by multiplying the positive sequence R, L and C parameters per unit length by the length of the line.

The AC system consisting of transmission lines, transformers and other impedance elements can be represented by a single phase equivalent network (in positive sequence parameters). The equations for such a network are expressed conveniently using a bus admittance matrix as

$$[Y]V = I \tag{5.27}$$

where I are current injections at the nodes. At generator nodes, I consists of armature currents and at load nodes, I consists of load currents (treated as injections). At a given bus, both the generators and loads may be present in which case, algebraic sum of generator and load currents is to be considered.

5.2 D-Q Transformation using $\alpha - \beta$ Variables

Stationary three phase symmetric matrices can be decoupled through transformation involving constant real matrices. The most well known among these is Clarke's transformation using $\alpha - \beta$ variables. Using a power invariant transformation given by

$$\begin{bmatrix} f_a \\ f_b \\ f_c \end{bmatrix} = [C_C] \begin{bmatrix} f_\alpha \\ f_\beta \\ f_o \end{bmatrix} \tag{5.28}$$

where

$$[C_C] = \begin{bmatrix} \sqrt{\dfrac{2}{3}} & 0 & \dfrac{1}{\sqrt{3}} \\[2mm] -\dfrac{1}{\sqrt{6}} & -\dfrac{1}{\sqrt{2}} & \dfrac{1}{\sqrt{3}} \\[2mm] -\dfrac{1}{\sqrt{6}} & \dfrac{1}{\sqrt{2}} & \dfrac{1}{\sqrt{3}} \end{bmatrix}$$

Eq. (5.1) is transformed to three decoupled equations given below

$$L_1 \frac{di_\alpha}{dt} + R_1 i_\alpha = v_{1\alpha} - v_{2\alpha} \tag{5.29}$$

$$L_1 \frac{di_\beta}{dt} + R_1 i_\beta = v_{1\beta} - v_{2\beta} \tag{5.30}$$

$$L_o \frac{di_o}{dt} + R_o i_o = v_{1o} - v_{2o} \tag{5.31}$$

The advantage of using Clarkes α, β, o components is that a three phase network is transformed to three decoupled networks 'α', 'β' and zero sequence. Out of these, the 'α' and 'β' networks are identical and zero sequence network can be generally neglected (in the absence of zero sequence currents). Thus, the circuit shown in Fig. 5.1 is transformed to two decoupled circuits shown in Fig. 5.5. Although the two circuits are identical, it is to be noted that the currents and voltages are different in the 'α' and 'β' circuits.

(a) α– sequence   (b) β– sequence
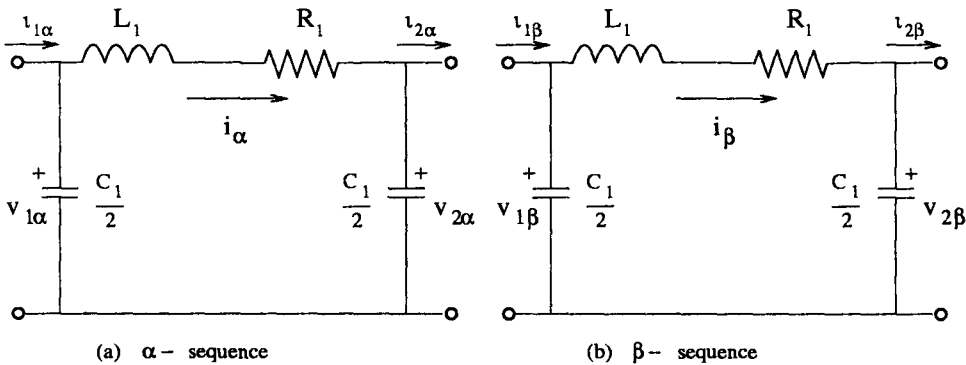
Figure 5.5: Sequence Networks

The transformation from $\alpha\beta o$ to DQo components is given by

$$\begin{bmatrix} f_\alpha \\ f_\beta \\ f_o \end{bmatrix} = [T_2] \begin{bmatrix} f_D \\ f_Q \\ f_o \end{bmatrix} \tag{5.32}$$

where

$$[T_2] = \begin{bmatrix} \cos\theta_o & \sin\theta_o & 0 \\ -\sin\theta_o & \cos\theta_o & 0 \\ 0 & 0 & 1 \end{bmatrix}$$

It is to be noted that $[T_2]$ is similar to $[T_1]$ in that δ is replaced by θ_o. It is not difficult to see that transformation from $\alpha\beta o$ to dqo component is given by

$$\begin{bmatrix} f_\alpha \\ f_\beta \\ f_o \end{bmatrix} = [T_3] \begin{bmatrix} f_d \\ f_q \\ f_o \end{bmatrix} \tag{5.33}$$

where

$$[T_3] = \begin{bmatrix} \cos\theta & \sin\theta & 0 \\ -\sin\theta & \cos\theta & 0 \\ 0 & 0 & 1 \end{bmatrix}$$

The advantage of using $\alpha\beta$ variables for a stationary network is that the state (differential) equations for the network can be obtained on a single phase basis. For the single phase 'α' network, the general equations are

$$\dot{x}_\alpha = [A_N]x_\alpha + [B_N]u_\alpha \tag{5.34}$$

where x_α are the state variables which consist of inductor currents and capacitor voltages (Note that only those inductors which form part of cotree (links) and capacitors which form part of tree are considered). The equations for 'β' network can be expressed as

$$\dot{x}_\beta = [A_N]x_\beta + [B_N]u_\beta \tag{5.35}$$

The structure of Eq. (5.35) follows from the fact that 'β' network is identical to the 'α' network. u_α and u_β are input variables (in α, β components) which may include voltage and current sources in the network. It is convenient to apply D-Q transformation to Eqs. (5.34) and (5.35). Expressing x_α and x_β in terms of x_D and x_Q as

$$\left. \begin{array}{rl} x_\alpha &= \cos\theta_o x_D + \sin\theta_o x_Q \\ x_\beta &= -\sin\theta_o x_D + \cos\theta_o x_Q \end{array} \right\} \tag{5.36}$$

the transformed network equations are

$$\dot{x}_D = [A_N]x_D - \omega_o x_Q + [B_N]u_D \tag{5.37}$$

$$\dot{x}_Q = [A_N]x_Q + \omega_o x_D + [B_N]u_Q \tag{5.38}$$

where u_D and u_Q are input variables transformed to D-Q components.

5.3   Static Var compensators

Fast control of reactive power is important for maintaining security during power system operation. Traditionally, the reactive power control depended on mechanically switched shunt capacitors and reactors which only help in maintaining the desired voltage profile in the system during slowly changing load conditions. However, disturbances such as faults followed by line switching or generator tripping can result in system stability and voltage problems. If the system has to operate close to stability limits in steady state, (with minimum margins), fast control of reactive power is essential. In the past, dynamic shunt compensators such as synchronous condensers and saturable reactors were used, although infrequently as the transmission systems were conservatively designed with large stability margins.

In recent years, thyristor controlled static var compensators are being used for fast reactive power control [1-8]. Advances in high power semiconductors, microelectronics and digital controls which are already used in HVDC transmission systems have made this improvement possible. SVCs were originally developed for power factor compensation of fast changing loads (such as arc furnaces) in early 1970's but later (before the end of the decade) were adapted for dynamic shunt compensation of AC transmission lines. They are extremely fast in response (about 2-3 cycles) and free from the problems of synchronous condensers (such as loss of synchronism and increased maintenance due to rotating parts).

SVCs are used for

1. Increasing power transfer in long lines

2. Stability improvement (both steady state and transient) with fast acting voltage regulation

3. Damping of low frequency oscillations (corresponding to electromechanical modes)

4. Damping of subsynchronous frequency oscillations (due to torsional modes)

5. Control of dynamic overvoltages

5.3.1   Types of SVC and Controllers

There are three basic types of SVCs [5]

(a) Variable impedance type

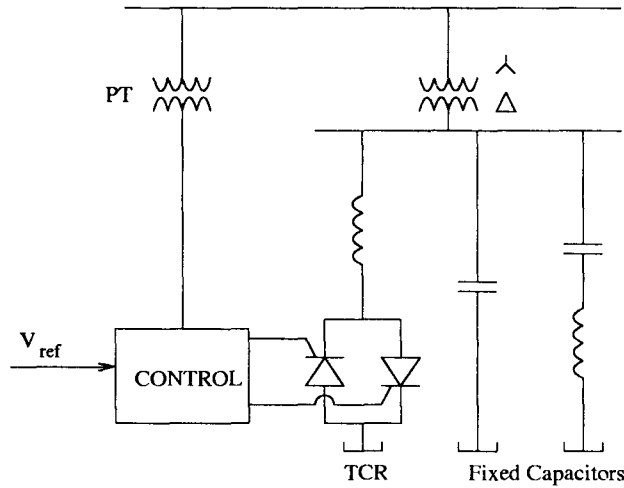(b) Current source type

(c) Voltage source type

Figure 5.6: Schematic diagram of FC-TCR

5.3.1.1 Variable Impedance Type SVC

The SVCs in use to-day are variable impedance type made of Thyristor Controlled Reactor (TCR) in parallel with either Fixed Capacitor (FC) or Thyristor Switched Capacitor (TSC). A FC-TCR type of SVC is shown in Fig.5.6. Both FC and TCR are supplied from a step down transformer. TCR is phase controlled by controlling the firing angle α in the range from 90° to 180°. A typical waveform of phase current is shown in Fig. 5.7.

The instantaneous current i_{TCR} over half a cycle is given by

$$\left. \begin{aligned} i_{TCR} &= \frac{\sqrt{2}V}{X_L}(\cos\alpha - \cos\omega t), \quad \alpha < \omega t < \alpha + \sigma \\ &= 0, \quad \alpha + \sigma < \omega t < \alpha + \pi \end{aligned} \right\} \tag{5.39}$$

where V is the rms voltage, X_L is the fundamental frequency reactance of the reactor, α is the delay angle, σ is the conduction angle. The fundamental frequency current I_1 can be obtained as
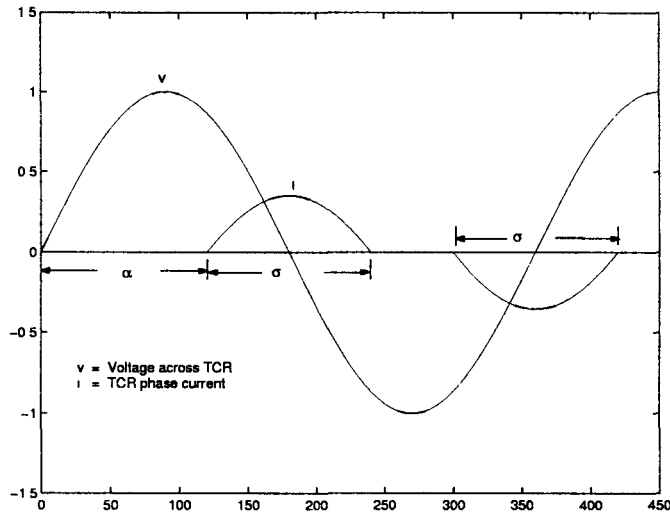
$$I_1 = B_{TCR}(\sigma)V \tag{5.40}$$

Figure 5.7: TCR current waveform

where

$$B_{TCR}(\sigma) = \frac{\sigma - \sin \sigma}{\pi X_L} \qquad (5.41)$$

It is to be noted that σ, given by

$$\sigma = 2 \left(\pi - \alpha \right)$$

can vary from 0 to π radians as α is decreased from π to $\pi/2$.

TCR produces odd harmonics. To eliminate triplen harmonics, TCR is connected in delta. The line current harmonics are of the order $6n \pm 1$ where n is an integer. To reduce harmonic content further, twelve pulse operation is used in which there are two branches of TCR, fed from two transformer secondaries, one connected in star and the other connected in delta. To prevent remaining harmonics from entering the system, some of the fixed capacitor banks can be connected as series tuned filters.

Instead of fixed capacitors, thyristor switched capacitors (TSC) can be used which result in the reduction in the reactor size (and consequently harmonics) and better performance of SVC under system fault conditions.

5.3.1.2   Voltage Source Type SVC

A basic scheme is shown in Fig. 5.8. This shows a six pulse Voltage Source Converter (VSC) with capacitor on its DC side. VSC produces a set of three

AC voltages from the input DC (capacitor) voltage. By controlling the switching instants of the GTO devices, the magnitude of the output voltages can be controlled. The voltages are essentially in phase with the supply voltage. By varying the magnitude of the output voltage, the reactive current can be regulated.
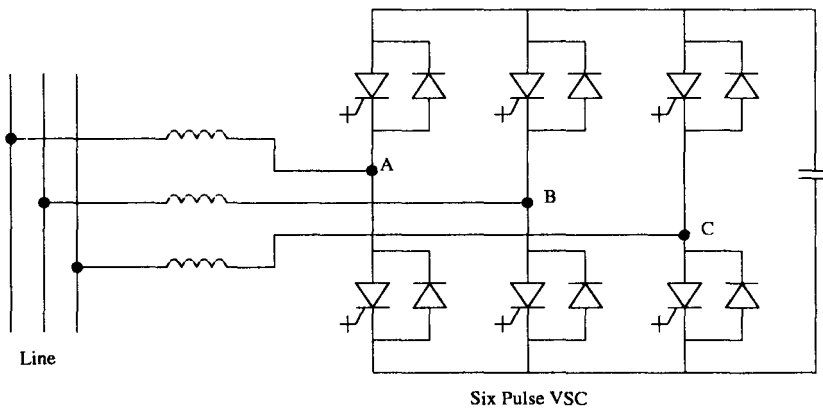

Figure 5.8: Advanced SVC using voltage source converter

A six pulse VSC produces a set of three square voltage waveforms. The voltage waveforms are shown in Fig. 5.9. The output voltages contain harmonics. By combining a number of six pulse VSC into a multi-pulse configuration, voltage distortion can be reduced.

This type of SVC has been termed as an advanced type SVC [9,10] and also as Static Condenser (STATCON) [11]. The variable impedance type SVC is also said to belong to the first generation FACTS (Flexible AC Transmission System) controllers. STATCON is a second generation FACTS controller and is expected to be commercially available before the year 2000 [12].

5.3.2 SVC Control Characteristics

The steady state control characteristics of a variable impedance type SVC is shown in Fig. 5.10. Here, the voltage is measured at the high voltage side of the transformer (or network bus) feeding the SVC and the current is the reactive current, considered to be positive when SVC is inductive (absorbing reactive power). In the control range, the SVC voltage is not maintained constant. The slope of the control characteristics is positive (3 to 5%) and helps in (a) stable parallel operation of more than one SVC connected at the same or neighbouring buses and b) prevent SVC hitting the limits too frequently.
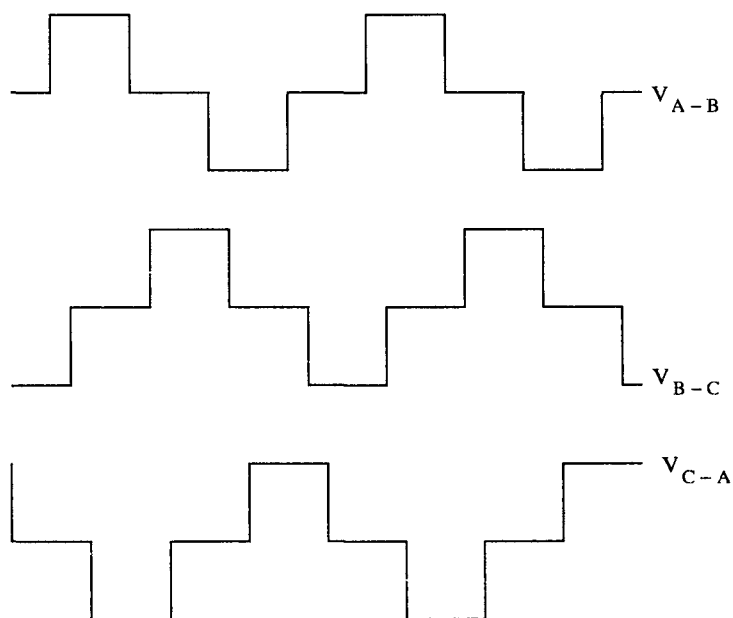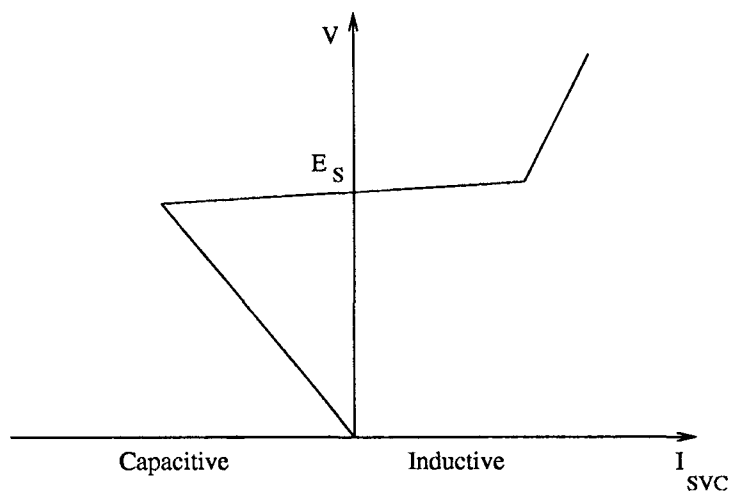
Figure 5.9: Voltage waveforms in a six pulse VSC

Figure 5.10: Steady state control characteristics of variable impedance SVC

The reference voltage of the SVC is chosen such that, under normal operating conditions, SVC delivers close to zero reactive power so that the full control range of SVC is available for use whenever there is a transient. Thus, slow coordination between a SVC and other reactive power control devices (such as mechanically switched capacitors and reactors) is necessary.
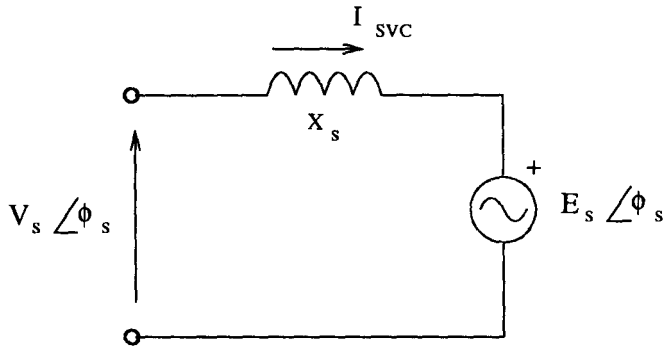

Figure 5.11: Equivalent circuit for SVC in control range

It is to be noted that when the SVC hits the capacitive limit, it behaves like a fixed capacitor. Similarly, when it hits the inductive limit, it behaves as a fixed inductor. In the control range, the SVC can be modelled as a nonlinear voltage source E_s in series with a fictitious, fixed inductor X_s (see Fig. 5.11). The phase angle of the voltage source is same as that of the bus voltage V_s. The value of the inductor is related to the slope of the control characteristic.

The block diagram of SVC control is shown in Fig. 5.12. Both terminal voltage and SVC current are used as control signals (K is the slope of the control characteristic shown in Fig. 5.10) The auxiliary control signal V_F is used for damping of oscillations. It can be derived from bus frequency, line current, or synthesized generator rotor velocity. The regulator is proportional-integral type with provision for gain reduction in case of control instability under abnormal system conditions. The linearizer transfer function $F^{-1}(\alpha)$ is the inverse of

$$F(\alpha) = \frac{2(\pi - \alpha) + \sin 2\alpha}{\pi X_L} \qquad (5.42)$$

GPG is the gate pulse generator which produces firing pulses for individual TCR valves synchronized with the supply voltage.

The steady state control characteristic for a STATCON is shown in Fig. 5.13. The reactive current can be maintained constant even at low voltages. Also a STATCON can be designed with higher transient ratings than steady state
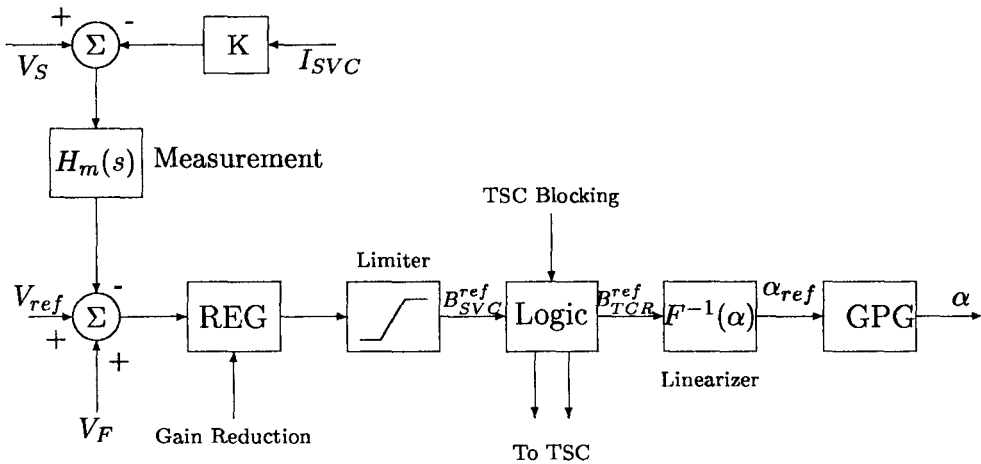
Figure 5.12: Block diagram of SVC controller

and deliver more reactive power compared to a SVC (FC-TCR type) where the reactive power is severely limited by the size of the capacitor and the bus voltage level.

5.3.3   Modelling of SVC

For steady state analysis, it is adequate to model the steady state control characteristics of SVC. Even for transient stability studies, where low frequency phenomena are of interest, and AC network transients are neglected, steady state representation of SVC may be adequate as a first approximation. However to model the damping contribution of SVC, it is necessary to consider the dynamics of SVC controller. A typical transfer function modelling of the SVC controller is shown in Fig. 5.14. Here the output is B_{SVC} and the delays introduced by the GPG are modelled approximately by the transfer function

$$G_c(s) = \frac{e^{-sT_d}}{1 + sT_s}$$ (5.43)

where T_d is approximately $T/12$ for a six pulse converter and T_s is $T/4$ where T is the period of supply voltage. T_m represents the transducer time constant. Filters are neglected in this model.

The output of SVC is a time-varying susceptance B_{SVC}. The inclusion of this in the network results in a time varying admittance matrix which can be problematic. The inclusion of a single SVC in the network can be handled by
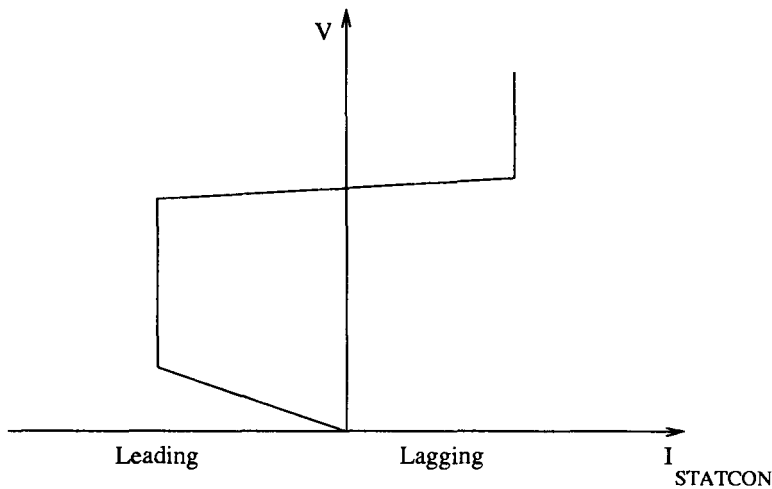
Figure 5.13: Steady state control characteristics of STATCON

the use of compensation theorem which enables the calculation of SVC current using Thevenin's equivalent of the network at the SVC bus. This equivalent has to be updated at every time step when SVC current is to be calculated.

5.4 Loads

The importance of load modelling in stability studies is well known. However, the major problem in the evaluation of power system dynamic performance is not posed by the complexity in load models, but the difficulty in obtaining data. Hence, in the early days, when AC network analyzers were used for study, the simplicity in load representation (by treating them as constant impedances) was common for convenience in calculations. Even when AC network analyzers were replaced by digital computer programs, the practice of modelling loads as constant impedances was continued and justified for the following reasons.

(i) For the study of first swing stability of generators feeding radially into a load centre, the load representation is less critical.

(ii) The use of constant impedance loads result in linear network equations which simplify the solution

(iii) Data on the response of system loads to disturbances are not available and difficult to obtain on the system

Regarding the last item, it is to be noted that several attempts have been made by different utilities to obtain the load data by measurements at high voltage substations [13-17].
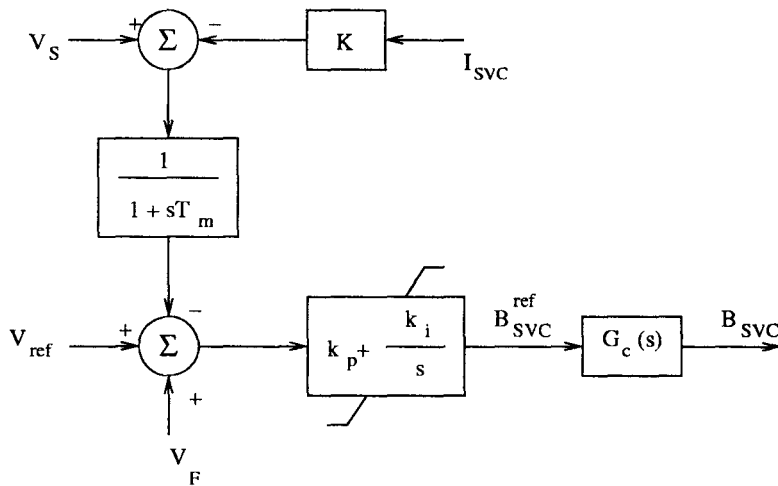
Figure 5.14: Model of SVC controller

The significance of load modelling is keenly felt in voltage stability analysis. The problem of voltage collapse is critically dependent on the response of the system load.

The system load is a mix of the following classes (or components)

(a) Residential

(b) Commercial

(c) Industrial

(d) Agricultural (irrigation pumps)

(e) Power plant (auxiliary motors)

Each class of loads listed above can be further subdivided into subclasses. For example, the industrial loads consist of (i) aluminium refining pot lines (ii) steel mills with arc furnaces (iii) large motors and (iv) small industrial motors.

The advantage of a component based approach is the possibility of using standard model for each component and avoiding the need for system measurements.

The load models can also be divided into

A) static loads

B) dynamic loads

In general, motor loads are treated as dynamic loads.

5.4.1 Static Load Representation

At any given bus, it is of importance to develop an aggregated static model. There are two ways of static load represention.

1.   Polynomial Representation

Both active and reactive power loads are represented by quadratic polynomials given by

$$\frac{P}{P_o} = a_o + a_1 \left(\frac{V}{V_o}\right) + a_2 \left(\frac{V}{V_o}\right)^2 \tag{5.44}$$

$$\frac{Q}{Q_o} = b_o + b_1 \left(\frac{V}{V_o}\right) + b_2 \left(\frac{V}{V_o}\right)^2 \tag{5.45}$$

where P_o, Q_o are initial values of power and reactive power at initial value of voltage V_o. The coefficients a_o, a_1 and a_2 are the fractions of the constant power, constant current and constant impedance components in the active power loads. Similar comments apply to the coefficients b_o, b_1 and b_2. Also it is to be noted that

$$a_o + a_1 + a_2 = 1$$
$$b_o + b_1 + b_2 = 1$$

The problem with constant power type loads is that it is not applicable for cases involving severe voltage drops. As voltage approaches zero, the load current is also expected to reach zero. Hence exponential load representation is more valid for a larger voltage excursion.

2.   Exponential Representation

This can include not only voltage dependence but also the effect of frequency variations. In general, the active power can be represented as [20]

$$\frac{P}{P_o} = c_1 \left(\frac{V}{V_o}\right)^{m_{p1}} (1 + k_p \Delta f) + (1 - c_1) \left(\frac{V}{V_o}\right)^{m_{p2}} \tag{5.46}$$

where
c_1 is the frequency dependent fraction of active power load
m_{p1} is the voltage exponent for frequency dependent component of active power load
m_{p2} is the voltage exponent for frequency independent component of active power load
Δf is the per unit frequency deviation (from nominal)
k_p is the frequency sensitivity coefficient for the active power load.

The reactive power load is expressed as

$$\frac{Q}{P_o} = c_2 \left(\frac{V}{V_o}\right)^{m_{q1}} (1 + k_{q1}\Delta f) + \left(\frac{Q_o}{P_o} - c_2\right) \left(\frac{V}{V_o}\right)^{m_{q2}} (1 + k_{q2}\Delta f) \quad (5.47)$$

where
c_2 is the reactive load coefficient-ratio of initial uncompensated reactive load to total initial active power load P_o.
m_{q1} is the voltage exponent for the uncompensated reactive load
m_{q2} is the voltage exponent for the reactive compensation term
k_{q1} is the frequency sensitivity coefficient for the uncompensated reactive power load
k_{q2} is the frequency sensitivity coefficient for reactive compensation

The second term on the R.H.S. of Eq. (5.47) represents to a first approximation, the effect of reactive compensation and losses in the subtransmission and distribution system between the bus and the various loads. The first term is made up of individual load components using their power factors. The second term is based on the difference between this value and the initial reactive power at the bus (specified in the power flow data).

It is to be noted that the reactive power is normalized by dividing by P_o rather than Q_o. This is done to avoid difficulty when $Q_o = 0$ due to cancellation of reactive power consumption by shunt capacitance.

5.4.2   Dynamic Load Representation

5.4.2.1   Induction Motor Model

The simplest induction motor model is to consider only the dynamics of the rotor inertia described by

$$\frac{d\omega_m}{dt} = \frac{1}{2H}[T_E(S) - T_M(\omega_m)] \quad (5.48)$$

where ω_m is the per unit motor speed. The per unit mechanical torque T_M is a function of ω_m given by

$$T_M = T_{Mo}(A\omega_m^2 + B\omega_m + c)$$

The per unit electrical torque T_E is a function of the motor slip S and is computed from the steady state equivalent circuit shown in Fig. 5.15. H is the inertia constant of the motor. T_E is given by the expression
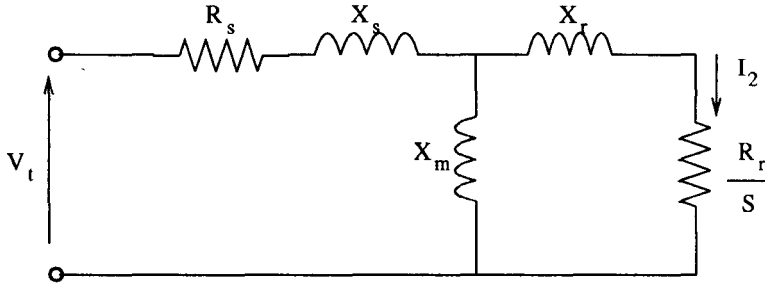
$$T_E = I_2^2 \frac{R_r}{S}$$

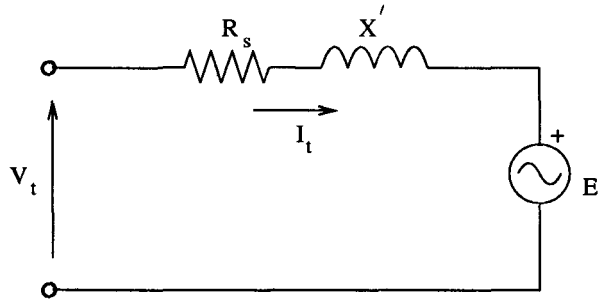Figure 5.15: Steady state equivalent circuit of an induction motor

Figure 5.16: Stator equivalent circuit for an induction motor

If rotor flux transients are to be included, the model is modified. The stator equivalent circuit is shown in Fig. 5.16 where E' is a complex voltage source defined by

$$\frac{dE'}{dt} = -j2\pi f S E' - \frac{1}{T_o}[E' - j(X - X')I_t] \tag{5.49}$$

where

$$T_o = \frac{X_r + X_m}{2\pi f R_r}, \quad I_t = \frac{V_t - E'}{R_s + jX'} = i_Q + ji_D$$

f is the operating frequency, X and X' are given by

$$X = X_s + X_m, \quad X' = X_s + \frac{X_m X_r}{X_m + X_r}$$

Using D-Q components, Eq. (5.49) can also be expressed in terms of real variables E'_D and E'_Q as

$$\left.\begin{array}{l} \dfrac{dE'_D}{dt} = -(\omega_s - \omega_m)E'_Q + \dfrac{1}{T_o}(X - X')i_Q - \dfrac{1}{T_o}E'_D \\[4mm] \dfrac{dE'_Q}{dt} = (\omega_s - \omega_m)E'_D - \dfrac{1}{T_o}(X - X')i_D - \dfrac{1}{T_o}E'_Q \end{array}\right\} \qquad (5.50)$$

where $\omega_s = 2\pi f$

The electrical torque T_E is given by

$$T_E = E'_D i_D + E'_Q i_Q \qquad (5.51)$$

5.4.2.2   General Load Model

The dynamic response of loads to step changes in the bus voltage (particularly for small changes) can be measured and a general (aggregated) load model can be formulated. A typical response of active power load to a voltage step is shown in Fig. 5.17. This does not show the long term response affected by the automatic tap changers on low voltage transformers.
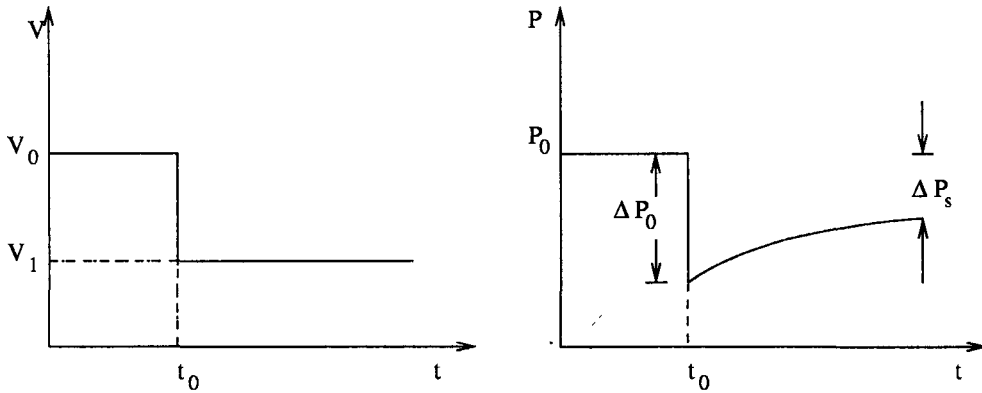

Figure 5.17: Load responce for a step change in voltage

The differential equation describing this response can be expressed as [27]

$$T_P \frac{dP}{dt} + P = P_s(V) + k_P(V)\frac{dV}{dt} \qquad (5.52)$$

The load behaviour is determined by two load functions and a time constant T_P. P_s is called the static load function and is applicable in steady state. k_P is called the dynamic load function.

The transient and steady state power increments ΔP_o and ΔP_s (shown in Fig. 5.17) can be obtained as

$$\Delta P_o = P(t_o^-) - P(t_o^+) = \frac{1}{T_P}[K_P(V_o) - K_P(V_1)]$$

$$\Delta P_s = P(t_o^-) - P(\infty) = P_s(V_o) - P_s(V_1)$$

where

$$K_P(V) = \int_0^V k_p(\sigma)d\sigma$$

References and Bibliography

1. T.J.E. Miller, **Reactive Power Control in Electric Systems**, John Wiley (New York), 1982

2. L. Barthold et al, "Static shunt device for reactive power control", CIGRE, Paper 31-08, 1974

3. K. Reichert, "Controllable reactive compensation", Int. J. of Electric Power and Energy Systems, Vol. 4, No. 1, 1982, pp. 51-61

4. L.Gyugyi, "Power electronics in electric utilities : Static var compensators", Proc. IEEE, Vol. 76, No. 4, 1988, pp. 483-494

5. L. Gyugyi, "Reactive power generation and control by thyristor circuits", IEEE Trans. on Ind. Applications, Vol. IA-15, No. 5, 1979, pp. 521-531

6. R.L. Hauth and R.J. Moran, "Introduction to static var systems for voltage and var control", IEEE Tutorial Course, 'Power Electronics Applications in Power Systems', 78, EH 0135-4-PWR, 1978

7. M.M. Govrilovic et al, "Bibliography of static var compensators", IEEE Trans. on Power Apparatus and Systems, Vol. PAS-102, No. 12, 1983, pp. 3744-3752

8. D. Mc Gillis et al, "Role of static compensations particular to James Bay System", Proc. IEE, Vol. 128, Pt. C, No. 6, 1981, pp. 389-393

9. C.W. Edwards et al, "Advanced static var generator employing GTO thyristors", IEEE Trans. on Power Delivery, PWRD-3, No. 4, 1988, pp. 1622-1627

10. L. Gyugyi et al, "Advanced static var compensator using gate turn-off thyristors for utility applications", CIGRE Paper 23-203, 1990

11. H. Mehta et al, "Static condenser for flexible AC transmission systems", FACTS EPRI Workshop, May 1992

12. J. Douglas, "FACTS - The delivery system of the future", EPRI Journal, Oct/Nov. 1992, pp. 5-11

13. M.H. Kent et al, "Dynamic modelling of loads in stability studies", IEEE Trans. Vol. PAS-88, No. 5, 1969, pp. 756-763

14. C.T. Nguyen et al, "Determination of power system load characteristics using a digital data-acquisition system", CIGRE Conf., Paper 31-05, 1978

15. C.T. Nguyen et al, "Load characteristics and stability of the Hydro-Quebec system", Paper A79 438-3 presented at IEEE PES Summer Meeting, July 1979

16. M.S. Chen et al, "Determining the static and dynamic characteristics of power system loads", CIGRE Conf., Paper 31-11, 1978

17. K. Srinivasan et al, "Closed loop load response to random perturbations", IEEE Trans. Vol PAS-98, No. 5, 1979, pp. 1591-1595

18. G. Shackshaft et al, "A general-purpose model of power system loads", Proc. IEE, Vol. 124, No. 8, 1977, pp. 715-723

19. G. Shackshaft and P.H. Ashmole, "The influence of load characteristics on power system performance-A CEGB viewpoint", CIGRE Conf., Paper 31-02, 1978

20. **Load Modelling for Power Flow and Transient Stability Computer Studies**, Vol. 1, EPRI Report, EL-5003, Jan. 1987

21. F. Iliceto et al, "Behaviour of loads during voltage dips encountered stability studies, field and laboratory tests", IEEE Trans. Vol. PAS-9 Nov/Dec 1972, pp. 2470-2479

22. D.S. Brereton et al, "Representation of induction motor loads during pow system stability studies", AIEE Trans. Vol. 76, Part III, 1957, pp. 451-46

23. F. Iliceto and A. Capasso, "Dynamic equivalents of asynchronous moto: loads in system stability studies", IEEE Trans. Vol. PAS-93, 1974, pp. 1650-1659

24. R. Ueda and S. Takata, "Effects of induction motor load on power systems", IEEE Trans. Vol. PAS-100, May 1981, pp. 2555-2562

25. K.R. Padiyar and P. Rajasekharam, "Effects of induction motor load on dynamic stability of power systems", Int. J. of Elec. Machines and Power Systems, Vol. 9, 1984, pp. 269-283

26. K.R. Padiyar and N. Prabhakaran, "Digital simulation of three phase induction motors using hybrid models", J. of Inst. of Enggrs (I), Vol. 63, pt EL1, Aug. 1982, pp. 23-31

27. D.J. Hill, "Nonlinear dynamic load models with recovery for voltage stability studies", IEEE Trans. on Power Systems, Vol. 8, No. 1, 1993, pp. 166-176

`

"This page is Intentionally Left Blank"

Chapter 6

# Dynamics of a Synchronous Generator Connected to Infinite Bus

Chapters 3, 4 and 5 presented the models of the major components of the power system that determine its dynamic behaviour. The most important component is the synchronous generator with its associated controls - excitation and prime mover. If the major objectives of dynamic analysis are to predict system stability, then it is often adequate to consider only the excitation system and ignore the prime-mover controls.

In this chapter, the dynamics of a synchronous generator is illustrated by taking up the example of a single machine connected to an infinite bus (SMIB). Although this is the simplest system example that can be considered, it is not entirely unrealistic. For example, a remote power station connected to a load centre through a long transmission line can be approximated by SMIB system. Although a power station consists of more than one generator, it is acceptable to assume that, for disturbances external to the power station, the generators can be represented by an equivalent machine. Also, in a multi-machine system, it is possible to ignore the dynamics of other machines than the one under study, as a first approximation. This is conveniently done by representing the external system for a generator by its Thevenin's equivalent. While the accuracy of this approximation depends on the system data, type of the study considered etc, the simplification of a SMIB system enables one to gain insights into the dynamic behaviour of a synchronous generator.

6.1   System Model

The system considered is shown in Fig. 6.1. This shows the external network (represented by a black box) with two ports. One port is connected to the generator terminals while the second port is connected to a voltage source $E_b \angle 0$ (representing the infinite bus). Both the magnitude E_b and the phase angle of the voltage source are assumed to be constants. Also, there is no loss of generality in assuming the phase angle of the bus voltage as zero (reference bus). (However,

in a general case, where the voltage source is Thevenin's equivalent, both the voltage magnitude and angle may be treated as variable).
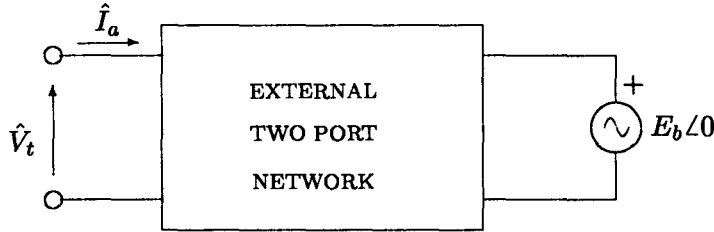
$$\hat{V}_t = (v_q + jv_d)e^{j\delta}, \quad \hat{I}_a = (i_q + ji_d)e^{j\delta}$$

Figure 6.1: External two port network

One of the major assumptions in the analysis of dynamic performance involving low frequency (< 5 Hz) behaviour of the system, is to neglect the transients in the external network. This simplifies the analysis as the network is modelled by algebraic equations based on single phase representation (see chapter 5). The network equations are conveniently expressed using voltage (and current) phasors with D-Q components (expressed on a synchronously rotating or Kron's reference frame).

If network transients are to be neglected, it is logical to ignore the transients in the stator windings of the synchronous machine, which are connected to the external network. This implies that stator equations are also reduced to algebraic. The use of stator flux linkages or currents as state variables is not possible. Thus the equations given in Chapter 3 have to be modified. Also, the degree of detail used in modelling a synchronous machine can vary depending on the requirements and the data available.

6.2   Synchronous Machine Model

6.2.1   Stator Equations

The stator equations in Park's reference frame are described in Chapter 3. Expressed in per unit, these are

$$-\frac{1}{\omega_B}\frac{d\psi_d}{dt} - \frac{\omega}{\omega_B}\psi_q - R_a i_d = v_d \tag{6.1}$$

$$-\frac{1}{\omega_B}\frac{d\psi_q}{dt} + \frac{\omega}{\omega_B}\psi_d - R_a i_q = v_q \tag{6.2}$$

It is assumed that the zero sequence currents in the stator are absent. If stator transients are to be ignored, it is equivalent to ignoring the $p\psi_d$ and $p\psi_q$ terms in Eqs. (6.1) and (6.2) (Note that p is the differential operator $\frac{d}{dt}$). In addition, it is also advantageous to ignore the variations in the rotor speed ω. This can be justified on the grounds that under disturbances considered the variations in the speed are negligible. (Actually, in some cases neglecting $p\psi_d$ and $p\psi_q$ terms go together with neglecting variations in ω - see Ex. 6.1) With these assumptions, Eqs. (6.1) and (6.2) can be expressed as

$$-(1 + S_{mo})\psi_q - R_a i_d \;=\; v_d \qquad (6.3)$$

$$(1 + S_{mo})\psi_d - R_a i_q \;=\; v_q \qquad (6.4)$$

where S_{mo} is the initial operating slip defined as

$$S_{mo} = \frac{\omega_o - \omega_B}{\omega_B} \qquad (6.5)$$

Example 6.1

Prove that, if the armature flux linkage components, with respect to a synchronously rotating reference frame, are constants, then the transformer emf terms ($p\psi_d$ and $p\psi_q$) and terms introduced by the variations in the rotor speed cancel each other.

Solution

Let ψ_D and ψ_Q be the components of armature flux linkages w.r.t. a synchronously rotating reference frame (rotating at speed ω_o). The flux linkage components in d-q axes are related to ψ_D and ψ_Q by

$$(\psi_q + j\psi_d)e^{j\delta} = \psi_Q + j\psi_D \qquad (A)$$

Taking derivatives, we get

$$(p\psi_q + jp\psi_d)e^{j\delta} + j(\psi_q + j\psi_d)\frac{d\delta}{dt}e^{j\delta} = 0 \qquad (B)$$

From the above, we can derive, (by separating real and imaginary parts)

$$\left.\begin{array}{rcl} \frac{1}{\omega_B}p\psi_q - (S_m - S_{mo})\psi_d &=& 0 \\[2mm] \frac{1}{\omega_B}p\psi_d + (S_m - S_{mo})\psi_q &=& 0 \end{array}\right\} \qquad (C)$$

In deriving these equations, $\frac{d\delta}{dt}$ is expressed as

$$\frac{d\delta}{dt} = \omega_B(S_m - S_{mo})$$

The stator differential equations (6.1) and (6.2) can be written as

$$-\frac{1}{\omega_B}\frac{d\psi_d}{dt} - (1 + S_m)\psi_q - R_a i_d = v_d$$

$$-\frac{1}{\omega_B}\frac{d\psi_q}{dt} + (1 + S_m)\psi_d - R_a i_q = v_q$$

Utilizing (C) in the above, we get Eqs. (6.3) and (6.4) which shows that transformer emfs cancel with the changes in the rotational emfs due to variation in the rotor speed (or slip S_m).

In most of the cases, it will be assumed that the initial operating slip is zero [the operating frequency is the rated (nominal) frequency].

6.2.2   Rotor Equations

Since the stator Eqs. (6.3 and 6.4) are algebraic (neglecting stator transients), it is not possible to choose stator currents i_d and i_q as state variables (state variables have to be continous functions of time, whereas i_d and i_q can be discontinuous due to any sudden changes in the network - this point will be made clear later). As rotor windings either remain closed (damper windingss) or closed through finite voltage source (field winding), the flux linkages of these windings cannot change suddenly. This implies that if i_d changes suddenly, the field and damper currents also change suddenly in order to maintain the field and damper flux linkages continuous. The flux linkage immediately after a disturbance remains constant at the value just prior to the disturbance. (This property is termed as the theorem of constant flux linkages in the literature - see Kimbark [1]).

The previous discussion shows that rotor winding currents cannot be treated as state variables when stator transients are neglected. The obvious choice of state variables are rotor flux linkages or transformed variables which are linearly dependent on the rotor flux linkages.

Depending on the degree of detail used, the number of rotor windings and corresponding state variables can vary from one to six. In a report published in 1986 by an IEEE Task Force [2], following models are suggested based on varying degrees of complexity.

1. Classical model (Model 0.0)

2. Field circuit only (Model 1.0)

3. Field circuit with one equivalent damper on q-axis (model 1.1)

4. Field circuit with one equivalent damper on d-axis

   (a) Model 2.1 (one damper on q-axis)
   (b) Model 2.2 (two dampers on q-axis)

5. Field circuit with two equivalent damper circuits on d-axis

   (a) Model 3.2 (with two dampers on q-axis)
   (b) Model 3.3 (with three dampers on q-axis)

It is to be noted that in the classification of the machine models, the first number indicates the number of windings on the d-axis while the second number indicates the number of windings on the q-axis. (Alternately, the numbers represent the number of state variables considered in the d-axis and q-axis). Thus, the classical model which neglects damper circuits and field flux decay, ignores all state variables for the rotor coils and is termed model (0.0).

In Chapter 3, it was assumed that the synchronous machine is represented by model (2.2). This model is widely used in the literature and for which data are supplied by manufacturers of machines or obtained by tests described in IEEE Standard No. 115 [3]. Model 3.3 is claimed to be the most detailed model applicable to turbo alternators, while models (2.1) and (1.1) are widely used for hydro generators [2]. It is to be noted that while higher order models provide better results for special applications, they also require an exact determination of parameters. With constraints on data availability and for study of large systems, it may be adequate to use model (1.1) if the data is correctly determined [4].

In what follows, model (1.1) is assumed for the representation of synchronous machine.

6.3 Application of Model 1.1

The stator and rotor flux linkages are given by

$$\psi_d = x_d i_d + x_{ad} i_f \qquad (6.6)$$

$$\psi_f = x_{ad} i_d + x_f i_f \qquad (6.7)$$

$$\psi_q = x_q i_q + x_{aq} i_g \qquad (6.8)$$

$$\psi_g = x_{aq} i_q + x_g i_g \qquad (6.9)$$

Solving (6.7) and (6.9) for i_f and i_g, we get

$$i_f = \frac{\psi_f}{x_f} - \frac{x_{ad}}{x_f} i_d \tag{6.10}$$

$$i_g = \frac{\psi_g}{x_g} - \frac{x_{aq}}{x_g} i_q \tag{6.11}$$

Substituting Eqs. (6.10) and (6.11) in (6.6) and (6.8) respectively, we get

$$\psi_d = x_d' i_d + E_q' \tag{6.12}$$

$$\psi_q = x_q' i_q - E_d' \tag{6.13}$$

where

$$x_d' = x_d - \frac{x_{ad}^2}{x_f} \tag{6.14}$$

$$x_q' = x_q - \frac{x_{aq}^2}{x_g} \tag{6.15}$$

$$E_q' = \frac{x_{ad}\psi_f}{x_f} \tag{6.16}$$

$$E_d' = -\frac{x_{aq}\psi_g}{x_g} \tag{6.17}$$

The voltage equations for the rotor windings are

$$\frac{1}{\omega_B} \frac{d\psi_f}{dt} = -R_f i_f + v_f \tag{6.18}$$

$$\frac{1}{\omega_B} \frac{d\psi_g}{dt} = -R_g i_g \tag{6.19}$$

Substituting Eqs. (6.10) and (6.16) in Eq. (6.18), we get

$$\frac{1}{\omega_B} \frac{x_f}{x_{ad}} \frac{dE_q'}{dt} = -\frac{R_f E_q'}{x_{ad}} + \frac{R_f x_{ad}}{x_f} i_d + v_f \tag{6.20}$$

$$\frac{dE_q'}{dt} = \frac{\omega_B R_f}{x_f} \left[-E_q' + \frac{x_{ad}^2}{x_f} i_d + \frac{x_{ad}}{R_f} v_f \right] \tag{6.21}$$

$$= \frac{1}{T_{do}'} [-E_q' + (x_d - x_d') i_d + E_{fd}] \tag{6.22}$$

In deriving the above Eq. (6.14) and the following relations are used

$$E_{fd} = \frac{x_{ad}}{R_f} v_f \tag{6.23}$$

$$T'_{do} = \frac{x_f}{\omega_B R_f} \tag{6.24}$$

Substituting Eqs. (6.11), (6.17) in Eq. (6.19) it is possible to obtain the following equation after some manipulations

$$\frac{dE'_d}{dt} = \frac{1}{T'_{qo}} \left[-E'_d - (x_q - x'_q) i_q \right] \tag{6.25}$$

where

$$T'_{qo} = \frac{x_g}{\omega_B R_g} \tag{6.26}$$

It is to be noted that in model 1.1, it is convenient to define the equivalent voltage sources E'_d and E'_q which are used as state variables instead of ψ_f and ψ_g. The advantages of this will be self evident when we consider the stator and torque equations.

Stator Equations

Substituting Eqs. (6.12) and (6.13) in Eqs. (6.3) and (6.4) and letting $S_{mo} = 0$, we get

$$E'_q + x'_d i_d - R_a i_q = v_q \tag{6.27}$$

$$E'_d - x'_q i_q - R_a i_d = v_d \tag{6.28}$$

If transient saliency is neglected by letting

$$x'_d = x'_q = x' \tag{6.29}$$

we can combine Eqs. (6.27) and (6.28) into a single complex equation given by

$$(E'_q + jE'_d) - (R_a + jx')(i_q + ji_d) = v_q + jv_d \tag{6.30}$$

The above equation represents an equivalent circuit of the stator shown in Fig. 6.2(a). This shows a voltage source $(E'_q + jE'_d)$ behind an equivalent impedance $(R_a + jx')$.

The variables (D-Q) in Kron's frame of reference are related to the variables (d-q) in Park's frame of reference by

$$(f_Q + jf_D) = (f_q + jf_d) e^{j\delta} \tag{6.31}$$
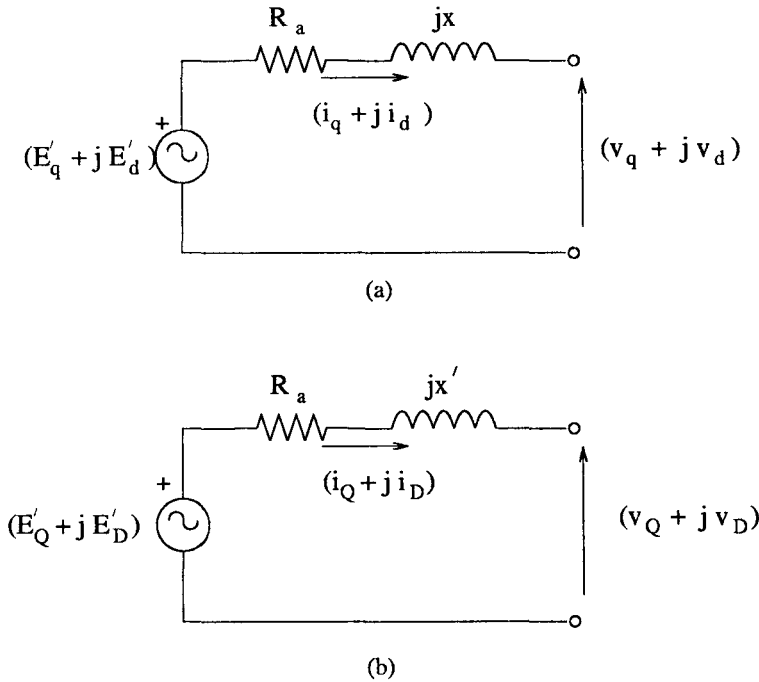
(a)

(b)

Figure 6.2: Stator equivalent circuits

where f can represent voltage or current. Applying (6.31) to (6.30), we get

$$(E'_Q + jE'_D) - (R_a + jx')(i_Q + ji_D) = v_O + jv_D \qquad (6.32)$$

Eq. (6.32) also represents an equivalent circuit of the stator shown in Fig. 6.2 (b).

Unfortunately no equivalent circuit for the stator exists when transient saliency is considered. This can pose a problem in the network calculations in multimachine systems. The ways of handling saliency will be discussed in chapter 12. For a single machine system however, saliency does not pose any problem.

Rotor Mechanical Equations

The rotor mechanical equations in per unit can be expressed as

$$M\frac{d^2\delta}{dt^2} + D'\frac{d\dot{\delta}}{dt} = T_m - T_e \qquad (6.33)$$

where $M = \frac{2H}{\omega_B}$, T_e is electrical torque given by

$$T_e = \psi_d i_q - \psi_q i_d \tag{6.34}$$

D is the damping term and T_m is the mechanical torque acting on the rotor. Substituting Eqs. (6.12) and (6.13) in (6.34), we get,

$$T_e = E'_d i_d + E'_q i_q + (x'_d - x'_q) i_d i_q \tag{6.35}$$

If transient saliency is ignored ($x'_d = x'_q$) then the third term in the above expression is identically zero.

Eq. (6.33) can be expressed as two first order equations as

$$\frac{d\delta}{dt} = \omega_B(S_m - S_{mo}) \tag{6.36}$$

$$2H\frac{dS_m}{dt} = -D(S_m - S_{mo}) + T_m - T_e \tag{6.37}$$

where the generator slip, S_m is defined below

$$S_m = \frac{\omega - \omega_B}{\omega_B} \tag{6.38}$$

Note that $\frac{d\delta}{dt}$ is defined as

$$\frac{d\delta}{dt} = \omega - \omega_o \tag{6.39}$$

Normally, the operating speed is considered to be the same as the nominal or rated speed. In this case, $S_{mo} = 0$. D is the per unit damping, given by

$$D = \omega_B D' \tag{6.40}$$

Network Equations

It is assumed that the external network connecting the generator terminals to the infinite bus is linear two port. This includes any complex representation of the external system with several transmission lines, transformers and loads. The loads are assumed to be of constant impedance type. A typical network is shown in Fig. 6.3 which shows a generator transformer, a transmission line, a shunt load and a Thevenin's impedance, Z_b connected between the end of the line and infinite bus (equivalent voltage source). The shunt load is connected somewhere between the two ends of the line. The transmission can be made up of several lines connected in parallel. Equivalent circuit of the system of Fig. 6.3 is shown in Fig. 6.4. z_t is the leakage impedance of the generator
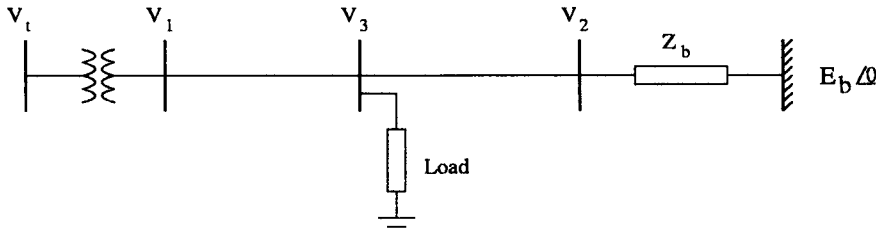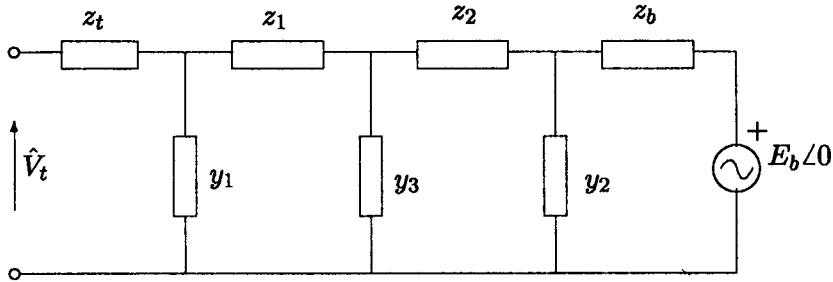
Figure 6.3: A typical network diagram

Figure 6.4: Equivalent circuit of the system in Figure 6.3

transformer, z_1 and z_2 are series impedances of the two line sections, y_1 and y_2 are the shunt admittances of the line sections (represented by π equivalents). y_3 includes both line and load admittances. Actually y_1 and y_2 can also include the admittances of load connected at the sending end and receiving end of the line respectively.

Whatever may be the configuration of the external network, it can be represented by the two port network parameters. As only the first port, connected to the generator terminals is of interest, the voltage there can be expressed as

$$\hat{V}_t = \frac{\hat{I}_a}{y_{11}} + h_{12}\hat{E}_b \tag{6.41}$$

where y_{11} is the short circuit self admittance of the network, measured at the generator terminals, h_{12} is a hybrid parameter (open circuit voltage gain). In general, both y_{11} and h_{12} are complex. For a simple network consisting of only series impedance $(R_e + jx_e)$, it is not difficult to see that

$$\frac{1}{y_{11}} = R_e + jx_{e}, \qquad\qquad h_{12} = 1.0 + j0.0 \tag{6.42}$$

In the general case, let

$$\frac{1}{y_{11}} = z_R + jz_I, \qquad h_{12} = h_1 + jh_2 \qquad (6.43)$$

Eq. (6.41) can be expressed as

$$(v_q + jv_d)e^{j\delta} = (z_R + jz_I)(i_q + ji_d)e^{j\delta} + (h_1 + jh_2)E_b \qquad (6.44)$$

Multiplying both sides of the above equation by $e^{-j\delta}$, we get

$$(v_q + jv_d) = (z_R + jz_I)(i_q + ji_d) + (h_1 + jh_2)E_b e^{-j\delta} \qquad (6.45)$$

Equating real and imaginary parts, we get

$$v_q = z_R i_q - z_I i_d + h_1 E_b \cos \delta + h_2 E_b \sin \delta \qquad (6.46)$$
$$v_d = z_I i_q + z_R i_d + h_2 E_b \cos \delta - h_1 E_b \sin \delta \qquad (6.47)$$

The above equations can be substituted in Eqs. (6.27) and (6.28) and solved for i_d and i_q in terms of state variables E'_d, E'_q and δ.

Solution of Network Equations : An example

The simplest external network is a series impedance $(R_e + jx_e)$. If $R_e = 0$, then

$$z_R = 0, \qquad z_I = x_e, \qquad h_1 = 1.0, \qquad h_2 = 0 \qquad (6.48)$$

Substituting these values in Eqs. (6.46) and (6.47) we get,

$$v_q = -x_e i_d + E_b \cos \delta \qquad (6.49)$$
$$v_d = x_e i_q - E_b \sin \delta \qquad (6.50)$$

If $R_a = 0$, the substitution of the above equations in Eqs. (6.27) and (6.28) gives

$$i_d = \frac{E_b \cos \delta - E'_q}{(x_e + x'_d)} \qquad (6.51)$$

$$i_q = \frac{E_b \sin \delta + E'_d}{(x_e + x'_q)} \qquad (6.52)$$

Eqs. (6.51) and (6.52) can be substituted in Eqs. (6.22), (6.25) and (6.35) to eliminate the non-state variables and express the equations in the form

$$\dot{x}_m = f_m(x_m, u_m) \qquad (6.53)$$

where

$$x_m^t = [\delta \quad S_m \quad E'_q \quad E'_d]$$
$$u_m^t = [E_{fd} \quad T_m]$$

It is to be noted that E_b is treated as a parameter. E_{fd} and T_m are inputs from the excitation and turbine-governor system respectively. If the dynamics of the controllers are ignored, then E_{fd} and T_m are also treated as parameters. Otherwise E_{fd} and T_m are treated as outputs of dynamic systems represented by differential equations which are to be appended to Eq. (6.53).

6.4   Calculation of Initial Conditions

The system equations (6.53) are nonlinear and have to be solved numerically. In solving these equations it is assumed that the system is at a stable equilibrium point (SEP) till time t=0, and a disturbance occurs at t=0 or later. It is necessary to calculate the initial conditions x_o at time t=0 based on the system operating point determined from load (power) flow.

From power flow calculations in steady state, we get the real and reactive power (P_t and Q_t), the voltage magnitude (V_t) and angle (θ) at the generator terminals. Here θ is the angle with respect to the slack (infinite) bus.

In steady state, the derivatives of all the state variables, $\dot{x} = 0$. From this condition, we get

$$E'_{qo} = E_{fdo} + (x_d - x'_d)i_{do} \tag{6.54}$$

$$E'_{do} = -(x_q - x'_q)i_{qo} \tag{6.55}$$

$$T_{mo} = T_{eo} = E'_{qo}i_{qo} + E'_{do}i_{do} + (x'_d - x'_q)i_{do}i_{qo} \tag{6.56}$$

In the above equations, the subscript 'o' indicates the operating values. It is to be noted that, in general, the initial slip S_{mo} cannot be determined from Eq. (6.36). It has to be specified separately. As mentioned earlier, it can be taken as zero.

Substituting Eqs. (6.54) and (6.55) in Eqs. (6.27) and (6.28), we get

$$E_{fdo} + x_d i_{do} - R_a i_{qo} = v_{qo} \tag{6.57}$$

$$-x_q i_{qo} - R_a i_{do} = v_{do} \tag{6.58}$$

From the above, one can obtain

$$\begin{aligned} E_{fdo} + (x_d - x_q)i_{do} &= (v_{qo} + jv_{do}) + (R_a + jx_q)(i_{qo} + ji_{do}) \\ &= \hat{V}_t \angle{-\delta} + (R_a + jx_q)\hat{I}_a \angle{-\delta} \end{aligned} \tag{6.59}$$

Defining

$$E_q \angle \delta = \hat{V}_t + (R_a + jx_q)\hat{I}_a \tag{6.60}$$

We can express,

$$E_{fdo} = E_{qo} - (x_d - x_q)i_{do} \tag{6.61}$$

Eq. (6.60) can be used to fix the position of q-axis. The phasor diagram shown in Fig. 6.5 represents the Eqs. (6.60) and (6.61). The d- and q-axis components of the armature current (i_d, i_q) and the terminal voltage (v_d, v_q) are also shown in the diagram.
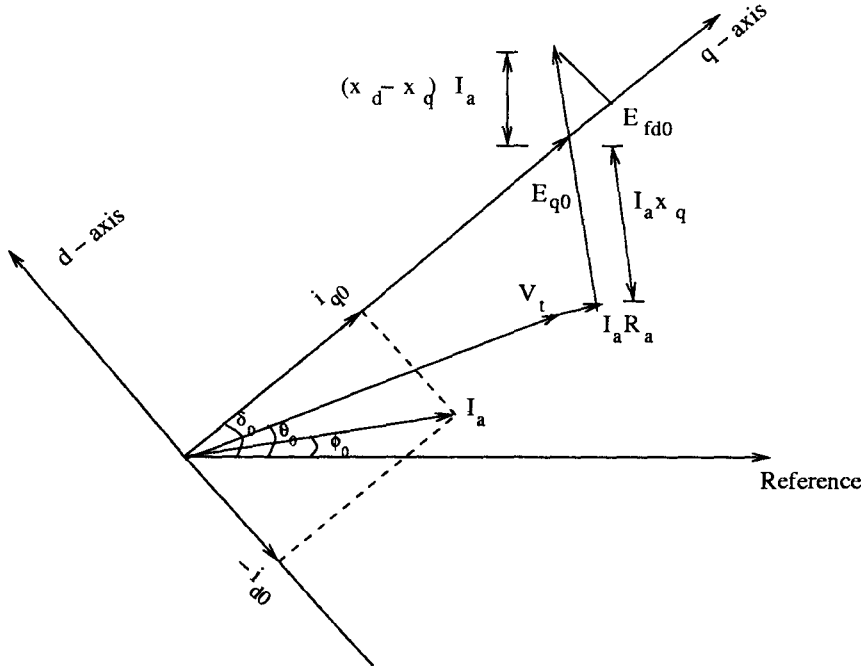

Figure 6.5: Phasor Diagram

The procedure for the computation of the initial conditions is given below

1. Compute $\hat{I}_{ao}$ from

$$\hat{I}_{ao} = I_{ao}\angle\phi_o = \frac{P_t - jQ_t}{V_{to}\angle-\theta_o}$$

2. Compute E_{qo} and δ_o from

$$E_{qo}\angle\delta_o = V_{to}\angle\theta_o + (R_a + jx_q)I_{ao}\angle\phi_o$$

(Note that P_t, Q_t, V_{to} and θ_o are obtained from the power flow analysis in steady state)

3. Compute

$$i_{do} = -I_{ao}\sin(\delta_o - \phi_o)$$
$$i_{qo} = I_{ao}\cos(\delta_o - \phi_o)$$
$$v_{do} = -V_{to}\sin(\delta_o - \theta_o)$$
$$v_{qo} = V_{to}\cos(\delta_o - \theta_o)$$

4. Compute

$$E_{fdo} = E_{qo} - (x_d - x_q)i_{do}$$
$$E'_{qo} = E_{fdo} + (x_d - x'_d)i_{do}$$
$$E'_{do} = -(x_q - x'_q)i_{qo}$$
$$T_{eo} = E'_{qo}i_{qo} + E'_{do}i_{do} + (x'_d - x'_q)i_{do}i_{qo} = T_{mo}$$

Example 6.2

A generator is connected to an infinite bus through an external impedance of jx_e. If $E_b = V_{to} = 1.0$ p.u. $P_t = 1.0$ p.u. Find the initial conditions. Assume $x_e = 0.25$ p.u.
The generator data: $x_d = 1.8$, $x_q = 1.7$, $x'_d = 0.17$, $x'_q = 0.23$, $R_a = 0.0$,
$T'_d = 0.4$ sec, $T'_q = 0.1$ sec, $H = 4$ sec, $f_B = 60$ Hz.

Solution

The generator terminal bus angle θ_o is found from

$$P_t = \frac{V_t E_b \sin\theta_o}{x_e}$$

Substituting values,

$$\sin\theta_o = 0.25, \quad \theta_o = 14.48^o$$

$$\hat{I}_a = \frac{\hat{V}_t - E_b\angle 0}{jx_e} = \frac{1.0\angle 14.48^o - 1.0\angle 9^o}{j0.25} = 1.008\angle 7.24^o$$
$$\hat{E}_{qo} = V_t\angle\theta_o + jx_q\hat{I}_a$$
$$= 1.0\angle 14.48^o + j1.7 \ . \ 1.008\angle 7.24^o$$
$$= 2.090\angle 68.91^o = E_{qo}\angle\delta_o$$
$$E_{qo} = 2.090, \quad \delta_o = 68.91^o$$

The initial armature current components are

$$i_{do} = -I_a\sin(\delta_o - \phi_o) = -1.008\sin(68.91 - 7.24)$$

$$
\begin{aligned}
&= -0.8873 \\
i_{qo} &= I_a \cos(\delta_o - \phi_o) = 1.008 \cos(68.91 - 7.24) \\
&= 0.4783 \\
E_{fdo} &= E_{qo} - (x_d - x_q)i_{do} = 2.090 + 0.1 \cdot 0.8873 \\
&= 2.179 \\
E'_{qo} &= E_{fdo} + (x_d - x'_d)i_{do} = 0.7327 \\
E'_{do} &= -(x_q - x'_q)i_{qo} = -0.7031 \\
T_{eo} &= E'_{qo}i_{qo} + E'_{do}i_{do} + (x'_d - x'_q)i_{do}i_{qo} \\
&= 1.0
\end{aligned}
$$

(Check: $T_{eo} = P_t + I_a^2 R_a$)
The initial slip, S_{mo} can be assumed to be equal to zero.

6.5   System Simulation

The synchronous machine is represented by model 1.1. Magnetic saturation is either neglected or considered by using saturated values of mutual inductances, x_{dc} (or x_{ad}) and x_{aq}. (In chapter 3, it was mentioned that the saturation modelling during dynamic simulation may not be significant).

The machine equations are

$$
\frac{d\delta}{dt} = \omega_B(S_m - S_{mo}) \tag{6.62}
$$

$$
\frac{dS_m}{dt} = \frac{1}{2H}\left[-D(S_m - S_{mo}) + T_m - T_e\right] \tag{6.63}
$$

$$
\frac{dE'_q}{dt} = \frac{1}{T'_{do}}\left[-E'_q + (x_d - x'_d)i_d + E_{fd}\right] \tag{6.64}
$$

$$
\frac{dE'_d}{dt} = \frac{1}{T'_{qo}}\left[-E'_d - (x_q - x'_q)i_q\right] \tag{6.65}
$$

The electrical torque, T_e is expressed in terms of state variables E'_d and E'_q and non-state variables i_d and i_q. The expression for T_e is

$$
T_e = E'_d i_d + E'_q i_q + (x'_d - x'_q)i_d i_q \tag{6.66}
$$

The non-state variables i_d and i_q can be obtained from the stator algebraic Eqs. (6.27), (6.28) and the network Eqs. (6.46) and (6.47). Substituting the former in the latter, we can solve for i_d and i_q from the following linear

equations

$$\begin{bmatrix} (x'_d + z_I) & -(R_a + z_R) \\ -(R_a + z_R) & -(x'_q + z_I) \end{bmatrix} \begin{bmatrix} i_d \\ i_q \end{bmatrix} = \begin{bmatrix} f_1(\delta) - E'_q \\ f_2(\delta) - E'_d \end{bmatrix} \tag{6.67}$$

where

$$f_1(\delta) = h_1 E_b \cos \delta + h_2 E_b \sin \delta$$
$$f_2(\delta) = h_2 E_b \cos \delta - h_1 E_b \sin \delta$$

$(z_R + jz_I)$ is the input impedance of the external network viewed from the generator terminals with the infinite bus shorted. $(h_1 + jh_2)$ is the voltage gain at the generator terminals with armature open circuited. (Alternatively, $(h_1 + jh_2)\hat{E}_b$ is Thevenin voltage source viewed from the generator terminals). The use of these hybrid parameters enables the consideration of any complex network connected between the generator and the infinite bus.

Example 6.3

Obtain the hybrid parameters for the two port network shown in Fig. 6.4. Define

$$Z_2 = \cfrac{1}{y_2 + \cfrac{1}{Z_b}} + z_2$$

$$Z_1 = \cfrac{1}{y_3 + \cfrac{1}{Z_2}} + z_1$$

Then,

$$z_R + jz_I = \cfrac{1}{y_1 + \cfrac{1}{Z_1}} + z_t$$

Define

$$H_3 = \frac{1/y_2}{(1/y_2 + Z_b)}$$

$$H_2 = \frac{1/y_3}{(1/y_3 + Z_2)}$$

$$H_1 = \frac{1/y_1}{(1/y_1 + Z_1)}$$

Then,

$$h_1 + jh_2 = H_1 H_2 H_3$$

The machine equations, eliminating non-state variables (from Eq. 6.67) can be expressed as Eq. (6.53) which is reproduced below.

$$\dot{x}_m = f_m(x_m, \ u_m)$$

where

$$x_m^t \ = \ [\delta \ \ S_m \ \ E_q' \ \ E_d']$$
$$u_m^t \ = \ [E_{fd} \ \ T_m]$$

If the generator controllers (excitation and prime-mover) are neglected then there are no additional dynamic equations. If controller dynamics are considered, then the following equations are to be included along with Eq. (6.53)

$$\left. \begin{array}{rcl} \dot{x}_e & = & f_e(x_e, \ u_e) \\ E_{fd} & = & E_{fd}(x_e) \end{array} \right\} \tag{6.68}$$

$$\left. \begin{array}{rcl} \dot{x}_p & = & f_p(x_p, \ u_p) \\ T_m & = & T_m(x_p) \end{array} \right\} \tag{6.69}$$

The inputs to the excitation controller, u_e, are generally, the terminal voltage V_t, reference voltage V_{ref} and slip S_m (if PSS is to be considered). The inputs to prime-mover controller u_p, are slip S_m and speed reference ω_{ref}. Combining Eqs. (6.53), (6.68) and (6.69) and eliminating non-state variable, V_t, we can write the overall system equations as

$$\dot{x}_g = f(x_g, \ u_g) \tag{6.70}$$

where

$$x_g^t \ = \ [x_m^t \ \ x_e^t \ \ x_p^t]$$
$$u_g^t \ = \ [V_{ref} \ \ \omega_{ref}]$$

If prime-mover controller is not considered then

$$x_g^t \ = \ [x_m^t \ \ x_e^t]$$
$$u_g^t \ = \ [V_{ref} \ \ T_m]$$

Actually, Eq. (6.53) can be viewed as a special case of Eq. (6.70) which is applicable for a detailed model of the generator including controllers.

Numerical Integration of System Equations

It is assumed that the system is initially in steady state with operating conditions determined from power flow analysis. With the knowledge of P_t, Q_t (power output at the terminals of the generator), V_t and θ (voltage magnitude and phase angle), it is possible to determine the initial conditions (see section 6.4). The initial operating values of x_g and u_g satisfy

$$0 = f(x_{go}, u_{go}) \tag{6.71}$$

The disturbances that can be considered are

(a) step change in u_g

(b) step change in network parameters caused by faults and switching

(c) step change in E_b

The system responses to the disturbances is obtained by numerical integration of the nonlinear system differential equations. There are several numerical methods and a brief discussion is given in Appendix A. A simple explicit method is the modified Euler (also called as Heun's method) outlined below.

This is a single step method in which, given the initial values for an interval (t_{n-1}, t_n), the end values are obtained as follows

1. Predict $x_g(t_n)$ from

$$x_{gp}(t_n) = x_g(t_{n-1}) + hf(x_g^{n-1}, u_g^{n-1}) \tag{6.72}$$

(The superscript indicates the instant at which the variables are evaluated)

2.

$$x_g(t_n) = x_g(t_{n-1}) + \frac{h}{2}[f(x_{gp}^n, u_g^n) + f(x_g^{n-1}, u_g^{n-1})] \tag{6.73}$$

h is the step size which should be sufficiently small both from the accuracy and numerical stability considerations.

It is to be noted that the state variables are continuous, although the currents and voltages in the network can be discontinuous when a fault or switching occurs.

Example 6.4

In example 6.2, Z_e (the electrical impedance) changes to $j0.5$ at $t = 0$. Find i_d, i_q and $\dfrac{d^2\delta}{dt^2}$ at $t = 0^+$.

Solution

The expressions for i_d and i_q (with lossless network) are given in (6.51) and (6.52).

At $t = 0^+$, $\delta = 68.91^o$, $E'_q = 0.7324$, $E'_d = -0.7031$

$$i_d(t = 0^+) = \frac{E_b \cos \delta - E'_q}{(x_e + x'_d)} = \frac{\cos 68.91 - 0.7327}{(0.5 + 0.17)} = -0.5565$$

$$i_q(t = 0^+) = \frac{E'_d + E_b \sin \delta}{(x_e + x'_q)} = \frac{\sin 68.91 - 0.7031}{(0.5 + 0.23)} = 0.3150$$

$$T_e = 0.7327 \cdot 0.3150 + 0.5565 \cdot 0.7031 + 0.06 \cdot 0.5565 \cdot 0.3150$$

$$= 0.6326$$

$$\frac{d^2\delta}{dt^2}(t = 0^+) = \frac{\omega_B}{2H}(T_m - T_e) = \frac{377(1.0 - 0.6326)}{(2 \cdot 4)} = 17.31 \ rad/sec^2$$

Example 6.5

The system is shown in Fig. 6.6. The switch is closed at $t = 0$. $x_e = 0.192$ (with switch open) and $x_e = 0.055$ with switch closed.
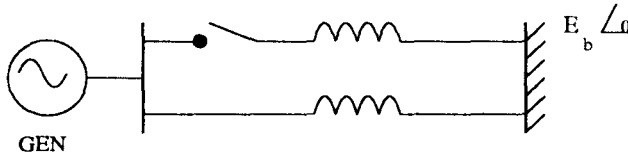
Figure 6.6: System diagram (Example 6.5)

The generator data : $x_d = 1.93$, $x_q = 1.77$, $x'_d = 0.23$, $x'_q = 0.50$, $T'_{do} = 5.2$ sec, $T'_{qo} = 0.81$ sec, $H = 3.74$
Assume $E_b = 1.0$. Calculate swing curves for the following cases

  (i) $P_t = 0.9$, $Q_t = 0.6$

 (ii) $P_t = 0.9$, $Q_t = -0.02$

(iii) $P_t = 0.3$, $Q_t = 0.02$

(iv) $P_t = 0.3$, $Q_t = -0.36$

(The data is taken from Dunlop and Parikh[5])

Solution

The results (swing curves) are shown in Figs. 6.7 to 6.10 for all the 4 cases considered. The variations of the terminal voltage are also shown in the Figures. The initial values of state variables and i_d, i_q, E_{fd} and V_t are given in Table 6.1

(a) Swing Curve   (b)Variation of terminal voltage
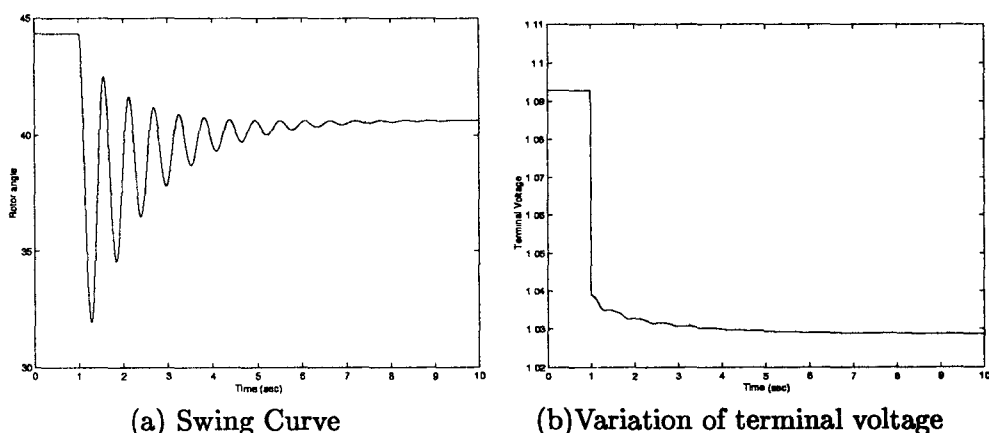
Figure 6.7: Case (i) (Example 6.5).

(a) Swing Curve   (b)Variation of terminal voltage
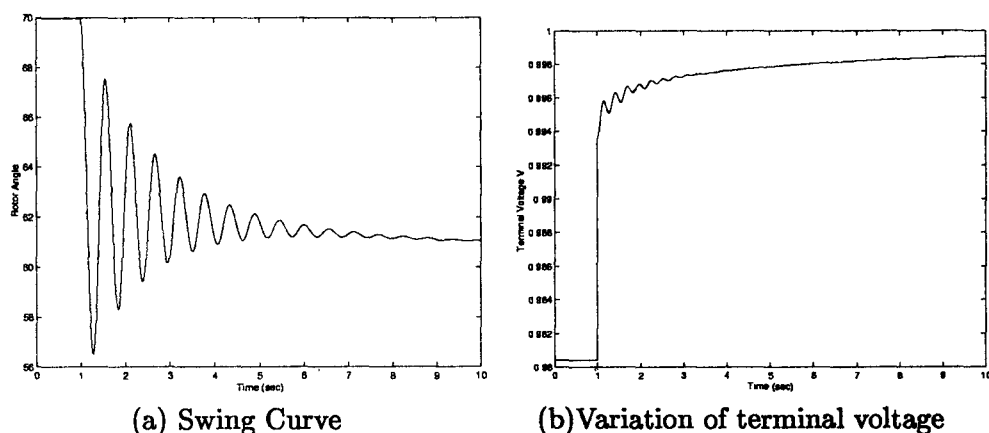
Figure 6.8: Case (ii) (Example 6.5).

It is interesting to observe that

(a) the responses of the rotor angle (following the disturbance) are mainly oscillatory in all the cases. However, there is also a significant unidirectional

(a) Swing Curve   (b)Variation of terminal voltage
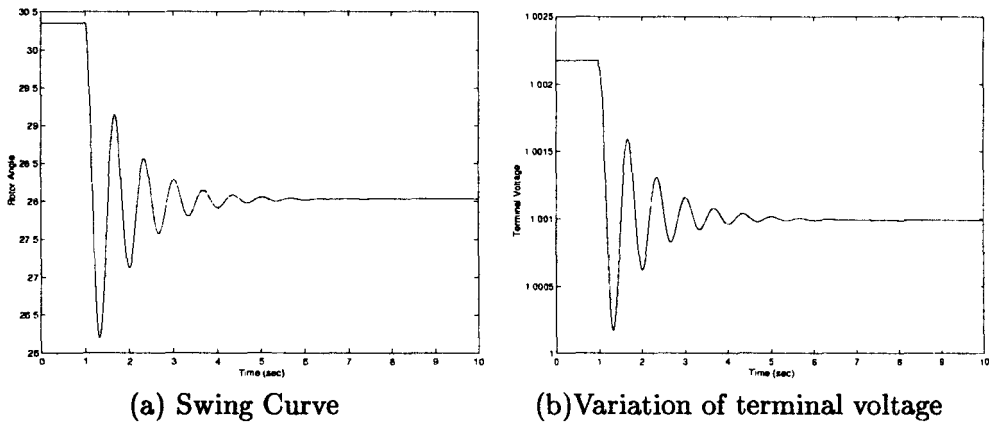
Figure 6.9: Case (iii) (Example 6.5).

(a) Swing Curve   (b)Variation of terminal voltage
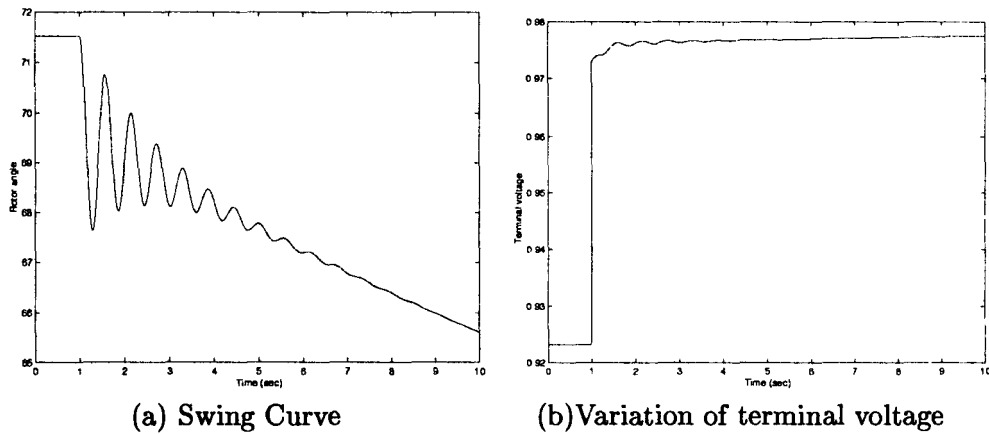
Figure 6.10: Case (iv) (Example 6.5).

Table 6.1 Initial Values for Example 6.5

Variable	Case (i)	Case (ii)	Case (iii)	Case (iv)
δ	44.10^o	69.73^o	30.27^o	71.38^o
E_q'	1.111	0.6813	0.9312	0.3893
E_d'	-0.4568	-0.6126	-0.3273	-0.6145
i_d	-0.9221	-0.7813	-0.1536	-0.1535
i_q	0.3597	0.4824	0.2577	0.4838
E_{fd}	2.6787	2.0094	1.1923	0.6503
V_t	1.0928	0.9804	1.0022	0.9232

component in case (iv). The oscillations are damped in all the cases and the decay is fastest in case (iii).

(b) The response of the terminal voltage has mainly a slowly varying unidirectional component in all the cases except (iii)

(c) While the rotor angle is reduced (in steady state) in all the cases, the terminal voltage is reduced in cases (i) and (iii) while increased in cases (ii) and (iv) following the disturbance. The rotor angle is reduced as the external reactance is reduced as the power transfer remains at the same level as before. However Q_t is increased as the reactance is reduced, since E_{fd} remains at the same level as before. With positive Q_t, the increase in Q_t has the effect of reducing the terminal voltage, while with negative Q_t, the increase (implying the reduction in the magnitude) has the effect of increasing the voltage magnitude.

Example 6.6

A single line diagram of the system is shown in Fig. 6.11. The system data (on a 1000 MVA base) are given below.

Generator : $R_a = 0.00327$, $x_d = 1.7572$, $x_q = 1.5845$ $x'_d = 0.4245$, $x'_q = 1.04$,
          $T'_{do} = 6.66$, $T'_{qo} = 0.44$, $H = 3.542$, $f_B = 50$ Hz.
Transformer : $R_t = 0.0$, $x_t = 0.1364$
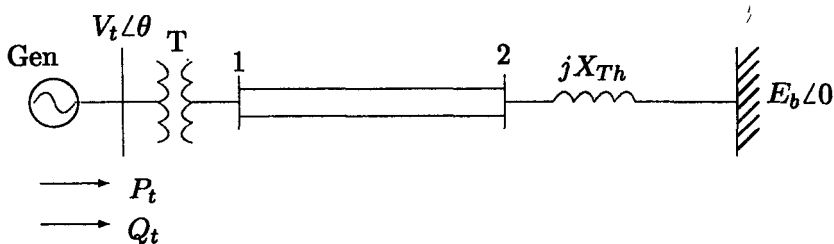
Figure 6.11: System diagram (Example 6.6)

Transmission line : (per circuit) $R_l = 0.08593$, $x_l = 0.8125$, $B_c = 0.1184$
(These parameters are representative of a 400 kV, 400 km long line with 50% shunt compensation)
Excitation System : Static exciter with single time constant AVR is used.
$K_A = 400$, $T_A = 0.025$, $E_{fdmax} = 6.0$, $E_{fdmin} = -6.0$
Operating Data : $E_b = 1.0$, $P_t = 0.6$, $Q_t = 0.02224$, $V_t = 1.05$, $\theta = 21.65^o$
$X_{Th} = 0.13636$ (represents Thevenin's impedance of the receiving end system).
Simulate the system response for the following conditions

A. Step increase in V_{ref} by 0.1 pu

B. Step increase in T_m by 0.1 pu

C. Step increase in E_b by 0.1

D. A three phase fault at the sending end of one of the circuits of the transmission line followed by clearing at the end of 4 cycles (The faulted line connecting buses 1 and 2 is tripped to clear the fault).

Solution

The initial conditions are calculated as $\delta_o = 61.5^o$, $S_{mo} = 0.0$, $E'_{qo} = 0.9699$, $E'_{do} = -0.2316$, $i_{do} = -0.3823$, $i_{qo} = 0.4253$
The variations of δ, S_m, E'_q, E'_d, E_{fd}, V_t and T_e for the four cases (A to D) are shown in Figures 6.12 to 6.15.

It is interesting to observe that

(a) The disturbances (B) and (D) result in the net system damping becoming negative. For the case (B) the power output is increased by 0.1 pu and for case (D) the transmission is weakened after the fault clearing.
It will be seen in chapter 8 that the Power System Stabilizer (PSS) can help damp the low frequency oscillations.

(b) For case (D), if a switching station is provided at the midpoint of the transmission line and only one line section connecting the midpoint to bus 1 is tripped following the fault clearing, it is seen from the swing curve for this case (shown in Fig. 6.16) that the net damping is positive.

(c) For case (C) it is seen that the rotor angle increases with increase in E_b. This may appear to be surprising. Actually if there is no AVR and the field voltage E_{fd} is maintained constant, then the rotor angle decreases with increase in E_b. (see Fig. 6.17). Without AVR, the terminal voltage rises, but with AVR it is held constant which requires reduction of the field voltage in steady state. It is clear, that with increase in E_b, reactive power output of the generator reduces (and becomes negative).

# 6.6 Consideration of other Machine Models

Sections 6.3 to 6.5 considered the application of synchronous machine model 1.1 as this is considered to be reasonably adequate. Simpler models are conveniently considered as special cases with the modification of machine parameters. This is simpler than writing separate sets of equations for each model.
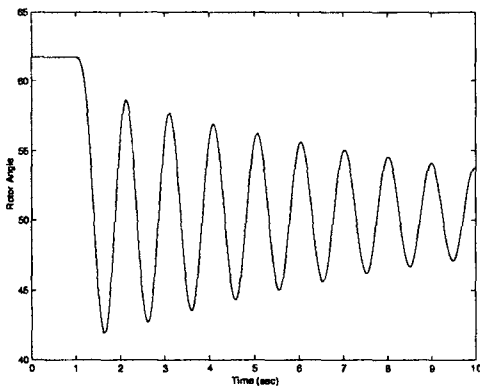
(a) Variation of rotor angle (δ)
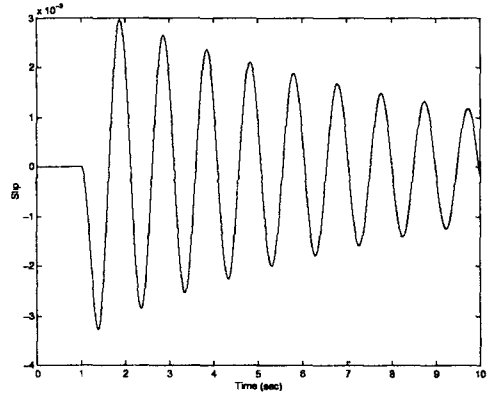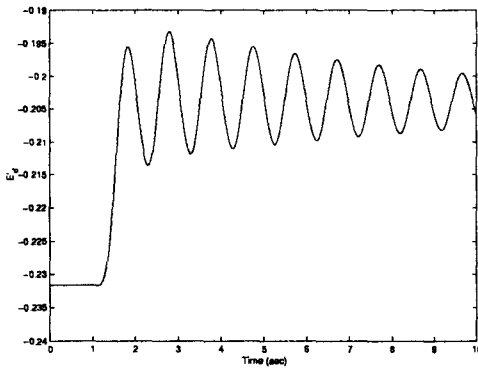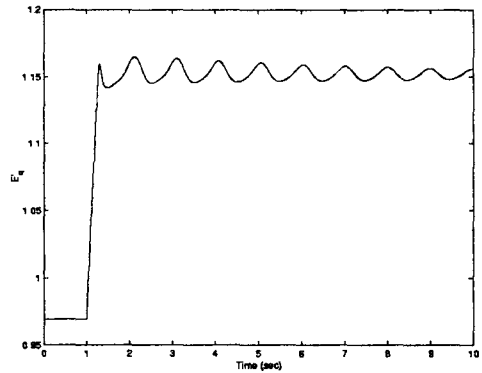
(b) Variation of slip (S_m)

(c) Variation of E_d'
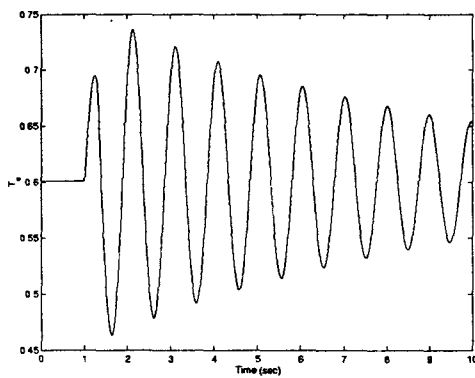
(d) Variation of E_q'

(e) Variation of electrical torque
(T_e)
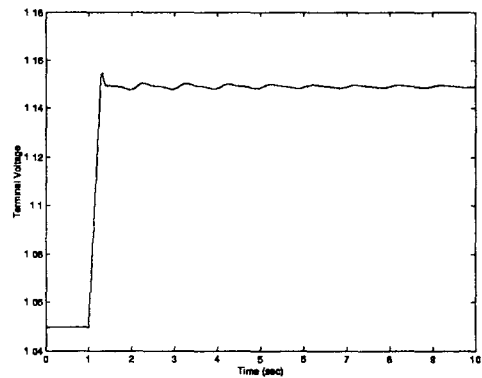
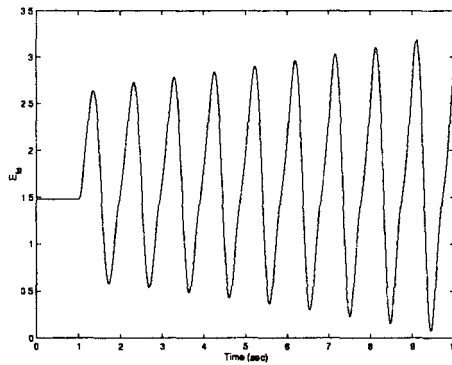(f) Variation of terminal voltage
(V_T)
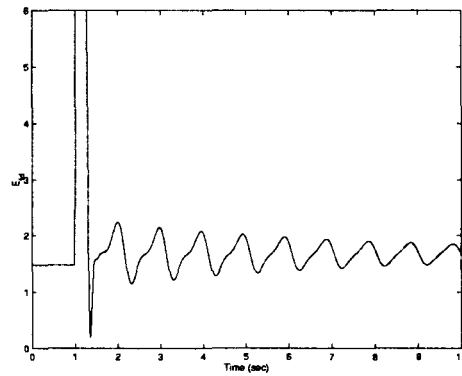
(g)Variation of terminal voltage (E_{fd})

Figure 6.12: Response to step increase in V_{ref} (Example 6.6 - Case A)
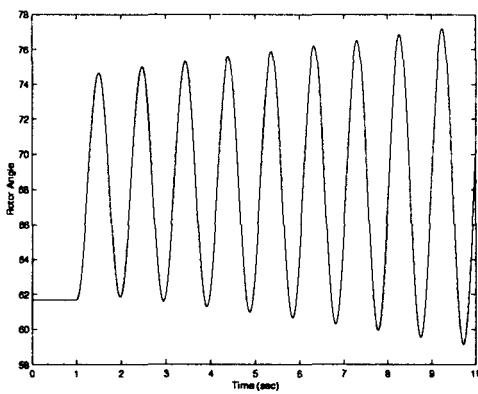
(a) Variation of rotor angle (δ)
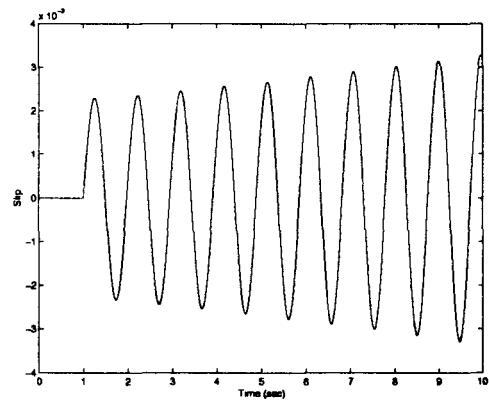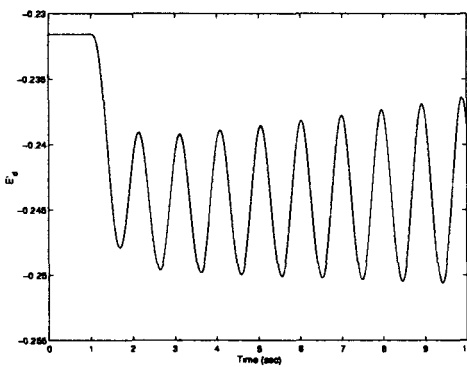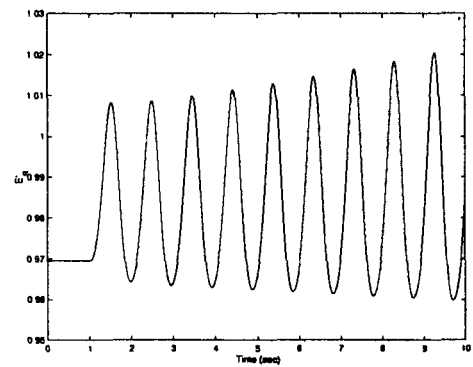
(b)Variation of slip (S_m)

(c)Variation of E_d'
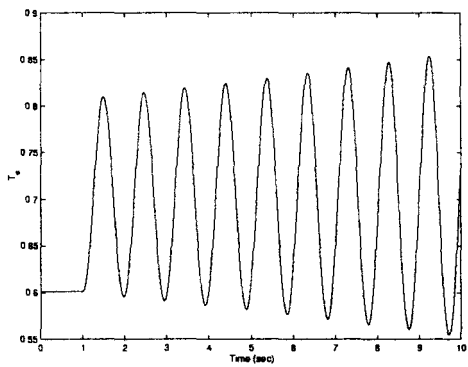
(d)Variation of E_q'

(e)Variation of electrical torque
(T_e)
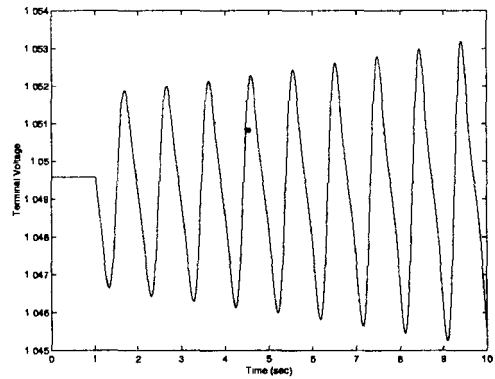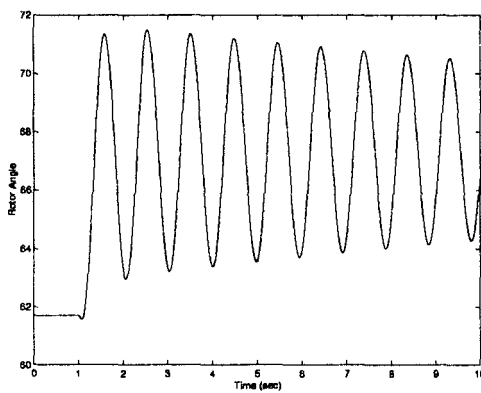

(f)Variation of terminal voltage
(V_T)

(g) Variation of E_{fd}

Figure 6.13: Response to step increase in T_m (Example 6.6 - Case B)

(a) Variation of δ
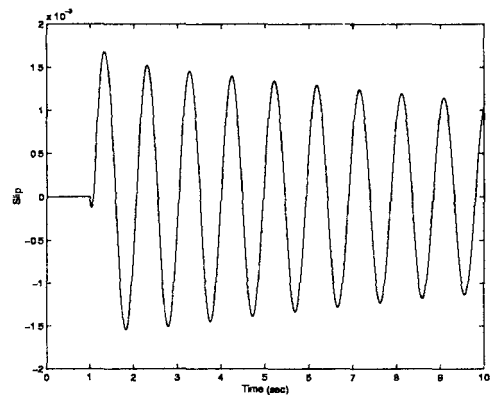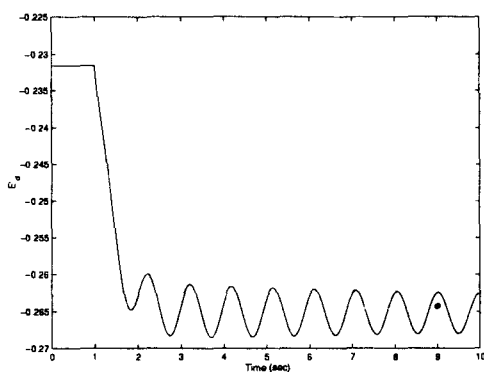
(b) Variation of S_m

(c) Variation of E_d'

(d) Variation of E_q'
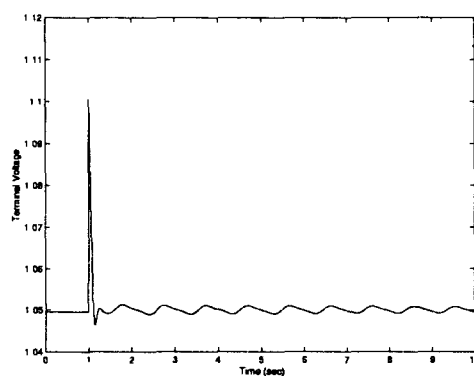
(e) Variation of T_e
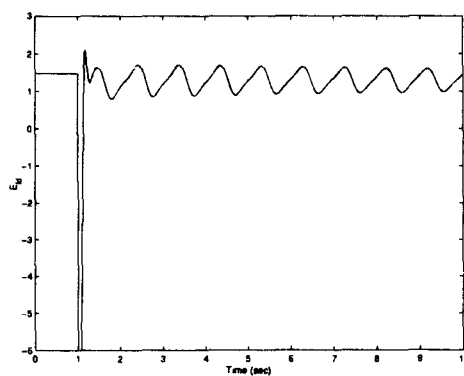
(f) Variation of V_T

(g) Variation of E_{fd}

Figure 6.14: Response to step increase in E_b (Example 6.6 - Case C)

(a) Variation of δ

(b) Variation of S_m

(c) Variation of E_d'

(d) Variation of E_q'

(e) Variation of T_e

(f) Variation of V_T

(g) Variation of E_{fd}
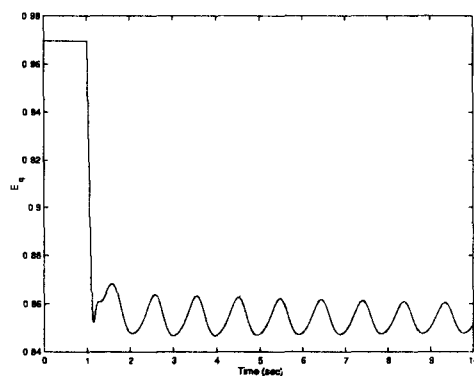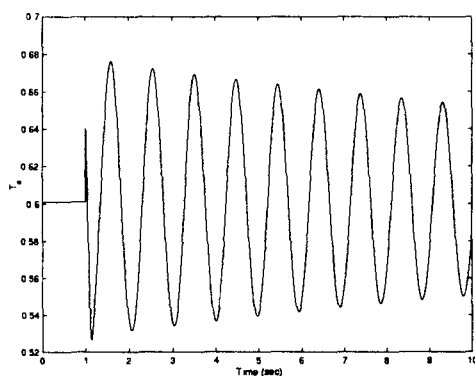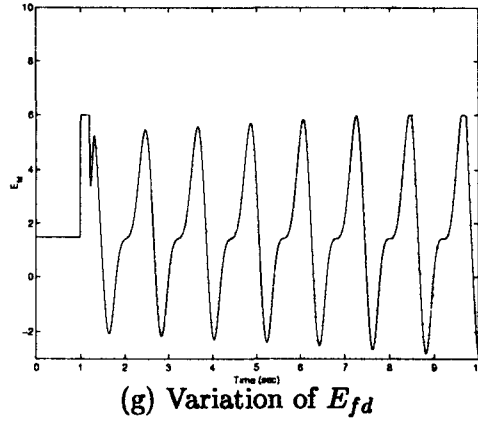
Figure 6.15: Response to a three phase fault (Example 6.6 - Case D)
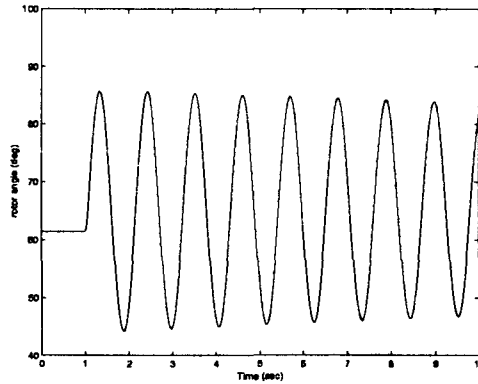
Figure 6.16: Swing curve with line sectioning (Example 6.6 - Case D)

6.6.1 Simpler Models

Model (1.0) can be handled by letting

$$x'_q = x_q, \quad T'_{qo} \neq 0 \tag{6.74}$$

Note that with $x'_q = x_q$, Eq. (6.65) reduces to

$$\frac{dE'_d}{dt} = \frac{1}{T'_{qo}}[-E'_d], \quad E'_{do} = -(x_q - x'_q)i_{qo} = 0$$

With the initial condition at zero, E'_d remains at zero throughout the simulation as long as $T'_{qo} > 0$. The actual value of T'_{qo} is unimportant and can be set at any arbitrary (convenient) value (say 1.0 sec).

(a) Variation of δ (b) Variation of V_T
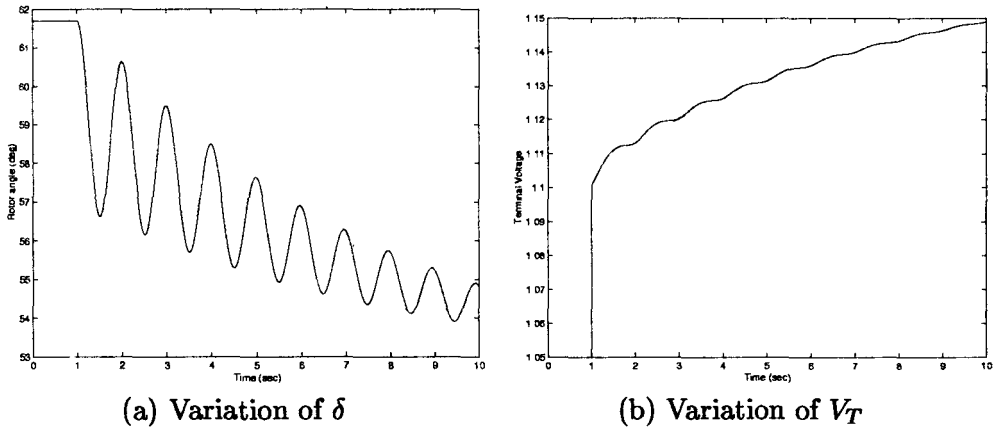
Figure 6.17: Response to step increase in E_b without AVR (Example 6.6)

For the consideration of classical model (0.0) in addition to the constraints (6.74) it is necessary to set

$$T'_{do} = \text{large value (say 1000 sec)} \tag{6.75}$$

If saliency is not to be considered, then it is necessary to set

$$x'_q = x_q = x'_d \tag{6.76}$$

With the constraints (6.74) to (6.76), the model reduces to that of a voltage source E'_q behind a transient reactance of x'_d. The large value of T'_{do} ensures that E'_q remains practically constant (neglecting flux decay).

Note that the constraint (6.76) can also be included in model (1.0) and has the effect of neglecting saliency while considering flux decay. The term 'saliency' has been used rather loosely here. The normal definition of saliency applies when $x_d \neq x_q$. The saliency that we need to consider in dynamic analysis, depends on the model used. The 'dynamic saliency' has been defined [11] in this context to distinguish it from the usual definition of saliency. Table 6.2 indicates the constraints which have to be satisfied for no dynamic saliency with different machine models.

Note: With one rotor winding on the q-axis there is only one reactance and one time constant (open circuit) which can be defined. Logically (in relation to d-axis), these should be labelled as x'_q (transient reactance) and T'_{qo}. However many authors use the symbols x''_q (subtransient reactance) and T''_{qo} with model (2.1).

Table 6.2. Constraints for No Dynamic Saliency

Machine Model	Constraints
Classical (0.0)	$x_q = x'_q = x'_d$
1.0	$x_q = x'_q = x'_d$
1.1	$x'_q = x'_d$
2.1	$x''_q = x''_d$
2.2	$x''_q = x''_d$

6.6.2 Application of Model 2.2

The appropriate rotor state variables in this case are the rotor flux linkages; although several authors use hybrid versions (E'_q and E'_d in addition to ψ_k and ψ_h) [12]

Stator Equations

The stator flux linkages are given by

$$\psi_d = x_d i_d + x_{df} i_f + x_{dh} i_h \tag{6.77}$$

$$\psi_q = x_q i_q + x_{qg} i_g + x_{qk} i_k \tag{6.78}$$

It is possible to eliminate i_f and i_h from Eq. (6.77) by expressing them in terms of ψ_f, ψ_h and i_d. The expressions for i_f and i_h are obtained from

$$\begin{bmatrix} i_f \\ i_h \end{bmatrix} = \begin{bmatrix} x_f & x_{fh} \\ x_{fh} & x_h \end{bmatrix}^{-1} \left\{ \begin{bmatrix} \psi_f \\ \psi_h \end{bmatrix} - \begin{bmatrix} x_{df} \\ x_{dh} \end{bmatrix} i_d \right\} \tag{6.79}$$

Similarly i_g and i_k in Eq. (6.78) can be substituted from

$$\begin{bmatrix} i_g \\ i_k \end{bmatrix} = \begin{bmatrix} x_g & x_{gk} \\ x_{gk} & x_k \end{bmatrix}^{-1} \left\{ \begin{bmatrix} \psi_g \\ \psi_k \end{bmatrix} - \begin{bmatrix} x_{qg} \\ x_{qk} \end{bmatrix} i_q \right\} \tag{6.80}$$

Eliminating rotor currents, Eq. (6.77) and (6.78) reduce to

$$\psi_d = x''_d i_d + \psi''_d \tag{6.81}$$

$$\psi_q = x''_q i_q + \psi''_q \tag{6.82}$$

where

$$\begin{aligned} \psi''_d &= \frac{(x_{df} x_h - x_{dh} x_{fh})}{(x_f x_h - x^2_{fh})} \psi_f + \frac{(x_{dh} x_f - x_{df} x_{fh})}{(x_f x_h - x^2_{fh})} \psi_h \\ &= C_1 \psi_f + C_2 \psi_h \end{aligned} \tag{6.83}$$

$$\psi_q'' = \frac{(x_{qg}x_k - x_{qk}x_{gk})}{(x_g x_k - x_{gk}^2)}\psi_g + \frac{(x_{qk}x_g - x_{qg}x_{gk})}{(x_g x_k - x_{gk}^2)}\psi_k$$

$$= C_3\psi_g + C_4\psi_k \tag{6.84}$$

$$x_d'' = x_d - C_1 x_{df} - C_2 x_{dh} \tag{6.85}$$

$$x_q'' = x_q - C_3 x_{qg} - C_4 x_{qk} \tag{6.86}$$

In comparison with Eqs. (6.12) and (6.13), Eqs. (6.81) and (6.82) could be expressed as

$$\psi_d = x_d'' i_d + E_q'' \tag{6.87}$$

$$\psi_q = x_q'' i_q - E_d'' \tag{6.88}$$

Substituting the above in Eqs. (6.3) and (6.4) and letting $S_{mo} = 0$, we get

$$E_q'' + x_d'' i_d - R_a i_q = v_q \tag{6.89}$$

$$E_d'' - x_q'' i_q - R_a i_d = v_d \tag{6.90}$$

If subtransient saliency is neglected, i.e. $x_q'' = x_d'' = x''$ then the above equations represent an equivalent circuit shown in Fig. 6.18.
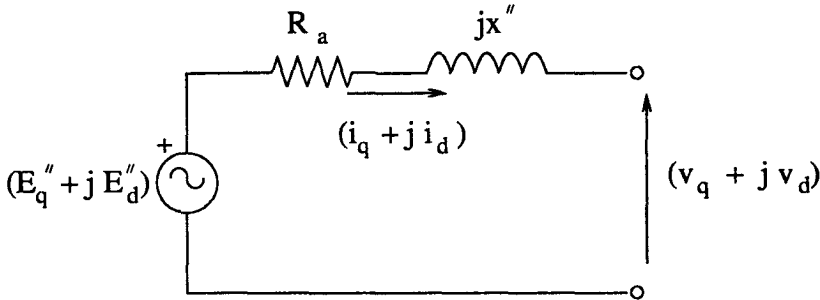
Figure 6.18: Stator equivalent circuit (model 2.2)

Although Eqs.(6.89) and (6.90) are similar to Eqs. (6.27) and (6.28), there is no specific advantage in selecting E_d'' and E_q'' as state variables. Some authors use combinations of E_d', E_d'' and E_q', E_q'' as state variables [13, 14]. Although this is acceptable, it is to be noted that the equations for E_q' and E_d' will be different, in general, from Eqs. (6.64) and (6.65). The terms involving other state variables will also enter into the equations. In specific cases, it is

possible that $C_1 = 0$ (implying that the damper winding in the d-axis completely shields the field winding from d-axis winding in the armature). Similarly $C_3 = 0$ when 'k' winding acts as a perfect shield between q-winding and g-winding. In such cases, $E_q^{''}$ is only a function of ψ_h and $E_d^{''}$ only a function of ψ_k. The significance of this is, that in the event of a fault or disturbance affecting the armature, there is no instantaneous change in the field current (or current in the g-winding).

It is obvious that the machine equations should be formulated for the general case with no assumptions regarding the parameters. Hence, the best choice for state variables is rotor flux linkages which are basic variables as opposed to the derived variables (such as $E_d^{''}$ and $E_q^{''}$). A major problem with formulations of machine equations given in several publications [12-14] is that the equations are expressed using the so called 'stability constants' (transient and subtransient reactances and time constants). From the discussions in chapter 3, it should be clear that such restrictions (the use of stability constants) are unnecessary and confusing (the latter in view of the fact that there is still no agreement on the definitions of $T_{do}^{''}$, $T_{qo}^{''}$ and $x_d^{'}$ and $x_q^{'}$). Hence it would be advisable to use circuit parameters (self and mutual reactances, resistances) in the equations that are derived from fundamental laws.

Rotor Equations

The basic equations in the rotor flux linkages (using per unit quantities) are

$$\left.\begin{aligned} \frac{d\psi_f}{dt} &= \omega_B\left[-R_f i_f + \frac{R_f}{x_{df}}E_{fd}\right] \\ \frac{d\psi_h}{dt} &= -\omega_B R_h i_h \end{aligned}\right\} \qquad (6.91)$$

$$\left.\begin{aligned} \frac{d\psi_g}{dt} &= -\omega_B R_g i_g \\ \frac{d\psi_k}{dt} &= -\omega_B R_k i_k \end{aligned}\right\} \qquad (6.92)$$

Eliminating the rotor currents using Eqs. (6.79) and (6.80), we can express the above equations as

$$\frac{d\psi_f}{dt} = a_1\psi_f + a_2\psi_h + b_1 E_{fd} + b_2 i_d \qquad (6.93)$$

$$\frac{d\psi_h}{dt} = a_3\psi_f + a_4\psi_h + + b_3 i_d \qquad (6.94)$$

$$\frac{d\psi_g}{dt} = a_5\psi_g + a_6\psi_k + + b_4 i_q \qquad (6.95)$$

$$\frac{d\psi_k}{dt} = a_7\psi_g + a_8\psi_k + + b_5 i_q \qquad (6.96)$$

where

$$a_1 = -\frac{\omega_B R_f x_h}{D_1}, \quad a_2 = \frac{\omega_B R_f x_{fh}}{D_1}$$

$$a_3 = \frac{\omega_B R_h x_{fh}}{D_1}, \quad a_4 = -\frac{\omega_B R_h x_f}{D_1}$$

$$D_1 = x_f x_h - x_{fh}^2$$

$$a_5 = -\frac{\omega_B R_g x_k}{D_2}, \quad a_6 = \frac{\omega_B R_g x_{gk}}{D_2}$$

$$a_7 = \frac{\omega_B R_k x_{gk}}{D_2}, \quad a_8 = -\frac{\omega_B R_k x_g}{D_2}$$

$$D_2 = x_g x_k - x_{gk}^2$$

$$b_1 = \frac{\omega_B R_f}{x_{df}}, \quad b_2 = \omega_B R_f C_1, \quad b_3 = \omega_B R_h C_2$$

$$b_4 = \omega_B R_g C_3, \quad b_5 = \omega_B R_k C_4$$

Electrical Torque

The new expression for electrical torque can be obtained by substituting Eqs. (6.81) and (6.82) in the basic expression for the torque given by

$$
\begin{aligned}
T_e &= \psi_d i_q - \psi_q i_d \\
&= \psi_d'' i_q - \psi_q'' i_d + (x_d'' - x_q'') i_d i_q \\
&= E_q'' i_q + E_d'' i_d + (x_d'' - x_q'') i_d i_q
\end{aligned}
\tag{6.97}
$$

ψ_d'' and ψ_q'' can be substituted from expressions (6.83) and (6.84). The final expression for T_e can be written as

$$T_e = (C_1 \psi_f + C_2 \psi_h) i_q - (C_3 \psi_g + C_4 \psi_k) i_d + (x_d'' - x_q'') i_q i_d \tag{6.98}$$

The last term is due to subtransient saliency.

6.6.3 Application of Model 2.1

This model differs from model (2.2) in that only one damper winding (say g) is considered in the q-axis. The equations are identical to those given in the previous section except for the following

$$\psi_q'' = C_3' \psi_g, \quad C_3' = \frac{x_{qg}}{x_g} \tag{6.99}$$

$$\frac{d\psi_g}{dt} = -\frac{\omega_B R_g \psi_g}{x_g} + b_4' i_q, \quad b_4' = \omega_B R_g C_3' \tag{6.100}$$

Also, there is no equation for ψ_k. The torque equation is modified by putting $C_4 = 0$ and substituting C_3' instead of C_3 in Eq. (6.98). The subtransient reactance x_q'' is obtained as

$$x_q'' = x_q - C_3' x_{qg}$$

(Note that transient reactance x_q' is not defined here. As mentioned earlier, this convention appears to be widely used).

6.7   Inclusion of SVC Model

The Static Var Compensator (SVC) is provided in the system to enhance power transfer, improve stability and voltage regulation. As mentioned in Chapter 5, the response of SVC is fast because of thyristor controllers. When only low frequency behaviour is to be studied, it is in order to neglect the SVC controller dynamics and model SVC by its control characteristics shown in Fig. 6.19. This shows three regions of operation
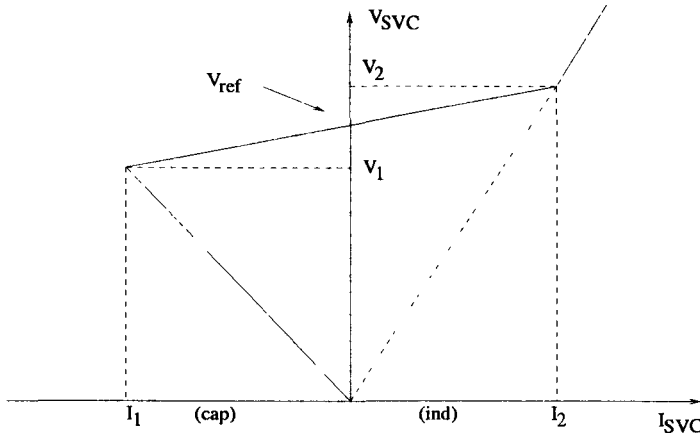
Figure 6.19: SVC control characteristics

(i) **Control region:**
$V_1 < V_{SVC} < V_2, \quad I_1 < I_{SVC} < I_2$

(ii) **Capacitive limit:**
$V_{SVC} < V_1, \quad B_{SVC} = B_C$

(iii) **Inductive limit:**
$V_{SVC} > V_2, \quad B_{SVC} = -(B_L - B_C)$

where $B_L = \frac{1}{X_L} = \max[B_{TCR}]$

All the three regions of operation of SVC can be modelled by an equivalent circuit shown in Fig. 6.20(a). However, the circuit parameters vary depending on the region of operation of SVC as given below.

Region (i):
$$\hat{E}_{SVC} = V_{ref} \angle \phi_{SVC}, \quad X_{SVC} = K \tag{6.101}$$

(K is the slope of the control characteristics in the control region)

Region (ii):
$$\hat{E}_{SVC} = 0, \quad X_{SVC} = -\frac{1}{B_C} \tag{6.102}$$

Region (iii):
$$\hat{E}_{SVC} = 0, \quad X_{SVC} = \frac{1}{B_L - B_C} \tag{6.103}$$

6.7.1   Network Solution with SVC : Application of Compensation Theorem

The model of SVC in control region (i) is nonlinear and with limits considered, it is also time-varying. If one SVC is to be considered, the network solution with SVC can be considerably simplified by applying compensation theorem.

In this approach, the SVC is treated as a time-varying current source which can be computed from the solution of a simple network shown in Fig. 6.20(b). Here the network external to the SVC is modelled by a time-varying Thevenin's equivalent. If the network impedances are constant, Z_{eq} remains constant. Z_{eq} is found as the impedance of the network seen at the SVC terminals when all the sources in the network are removed (the voltage sources are shorted and the current sources are open circuited). V_{Th} is found as the SVC terminal voltage with SVC current set to zero.

From Fig. 6.20(b), the SVC current can be computed as

$$\hat{I}_{SVC} = \frac{\hat{V}_{eq} - \hat{E}_{SVC}}{Z_{eq} + jX_{SVC}} \tag{6.104}$$

The magnitude of the SVC terminal voltage is

$$V_s = |\hat{V}_{SVC}| = |\hat{E}_{SVC} + j\hat{I}_{SVC}X_{SVC}| \tag{6.105}$$

(a) SVC Equivalent circuit

(b) Combined equivalent circuit
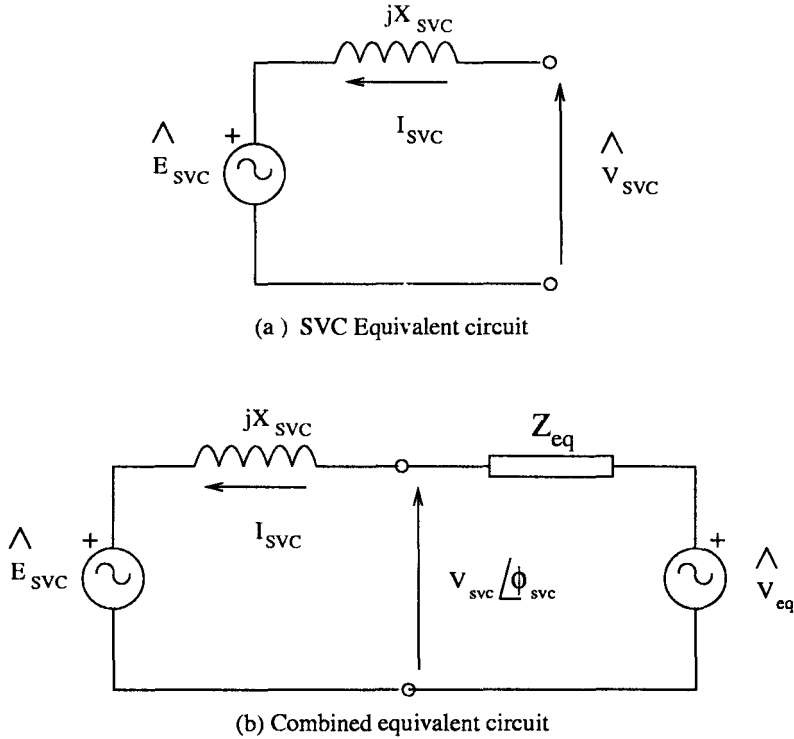
Figure 6.20: Equivalent Circuits

If $\hat{E}_{SVC} = 0$, the solution of Eq. (6.104) is straightforward as $\hat{V}_{eq}$ and $\hat{Z}_{eq}$ are known at any given time instant. The magnitude of $\hat{E}_{SVC}$ for the control region (i) is known but the phase angle is dependent on $\hat{V}_{SVC}$ (see Eq. 6.101).

Calculation of ϕ_{SVC} in Control Region

It can be shown that ϕ_{SVC} is obtained from the solution of a quadratic equation given by

$$a \tan^2 \phi_{SVC} + b \tan \phi_{SVC} + c = 0 \qquad (6.106)$$

Proof

From Eq. (6.104) and (6.105), we can express

$$\hat{V}_{SVC} = (1 - \hat{A})\hat{V}_{eq} + \hat{A}\hat{E}_{SVC} \qquad (6.107)$$

where

$$\hat{A} = \frac{Z_{eq}}{Z_{eq} + jX_{SVC}} = A\angle\alpha \qquad (6.108)$$

Separating real and imaginary components in Eq. (6.107) we get,

$$V_s \cos \phi_{SVC} = x + z \cos(\phi_{SVC} + \alpha) \qquad (6.109)$$

$$V_s \sin\phi_{SVC} \;=\; y + z\sin(\phi_{SVC} + \alpha) \tag{6.110}$$

where

$$x = \Re[(1 - \hat{A})\hat{V}_{eq}], \quad y = \Im[(1 - \hat{A})\hat{V}_{eq}]$$
$$z = \mid \hat{A}\hat{E}_{SVC} \mid$$

From Eqs. (6.109) and (6.110), we get

$$
\begin{aligned}
\tan\phi_{SVC} &= \frac{y + z\cos\alpha\sin\phi_{SVC} + z\sin\alpha\cos\phi_{SVC}}{x + z\cos\alpha\cos\phi_{SVC} - z\sin\alpha\sin\phi_{SVC}} \\[2mm]
&= \frac{y\sec\phi_{SVC} + z\cos\alpha\tan\phi_{SVC} + z\sin\alpha}{x\sec\phi_{SVC} + z\cos\alpha - z\sin\alpha\tan\phi_{SVC}}
\end{aligned}
\tag{6.111}
$$

After some manipulations and using the identity

$$\sec^2\phi = 1 + \tan^2\phi$$

We can finally derive Eq. (6.106), where

$$
\begin{aligned}
a &= x^2 - z^2\sin^2\alpha \\
b &= -2xy \\
c &= y^2 - z^2\sin^2\alpha
\end{aligned}
$$

Once ϕ_{SVC} is found, I_{SVC} is readily calculated.

Network Solution

The network solution is carried out in two steps. In the first step, the voltage solution is obtained by putting $\hat{I}_{SVC} = 0$. The voltage calculated at the SVC bus, at the end of the first step is same as $\hat{V}_{Th}$.

The knowledge of $\hat{V}_{eq}$ and Z_{eq} (which has been calculated in advance and stored) enables the computation of $\hat{I}_{SVC}$ as described earlier.

The network is solved again with the injection of $\hat{I}_{SVC}$ at the SVC bus (all other sources put equal to zero). The second solution does not require much computations as the current vector is sparse.

The voltages at all the buses are obtained from the addition (superposition) of the voltages calculated in the two network solutions.

Remarks

1. It is assumed that the generator stator is represented by a constant impedance (neglecting dynamic saliency). Even if dynamic saliency is present, it

can be handled by the introduction of a dummy rotor coil in the quadrature axis (see Chapter 3). Dynamic saliency results in time-varying impedance (with respect to network or common reference frame). Also, the impedance needs to be expressed (as a 2x2 matrix) in D-Q axes. In this case, it can be shown that ϕ_{SVC} can be obtained by solving a quartic equation.

2. Z_{eq} changes whenever there is a change in the network configuration.

3. If Z_{eq} is a purely reactive (inductive) impedance, then ϕ_{SVC} is identical to the phase angle of $\hat{V}_{eq}$, which is known. This eliminates the need for the solution of the quadratic equation (6.106).
   Even if quadratic equation is to be solved, the correct value of ϕ_{SVC} is obtained as that solution which is closer to the phase angle of $\hat{V}_{eq}$.

Example 6.7

For the system considered in Example 6.6, a SVC of rating ±300 MVAR is connected at the midpoint of the transmission lines. The SVC data are $I_1 = -0.3$, $I_2 = 0.3$ (on a 1000 MVA base), $V_{ref} = 1.03584$, $K = 0.1$.

Simulate the system response for the following conditions

(B) step increase in T_m by 0.1 pu

(D) A three phase fault at the sending end of one of the circuits followed by clearing at the end of 4 cycles (To compare with Example 6.6, both the line sections, one connecting SVC bus to bus 1 and the other connecting SVC bus to bus 2 are assumed to trip. The postfault configuration include only one circuit as in Example 6.6).

The operating data is same as in Example 6.6 as the SVC output before the disturbance is assumed to be zero (Note that V_{ref} is same as the SVC bus voltage in this case).

Solution

The initial conditions for the generator are same as in Example 6.6. The variations of δ, S_m, E'_q, E'_d, E_{fd}, V_t, T_e and V_{SVC} for the cases (B) and (D) are shown in Figures 6.21 to 6.22.

It is interesting to observe that the oscillations are damped in both the cases showing the improvement introduced by SVC. With SVC, more power can be transferred without losing stability. Also, SVC permits operation with weaker AC network (after the fault is cleared).
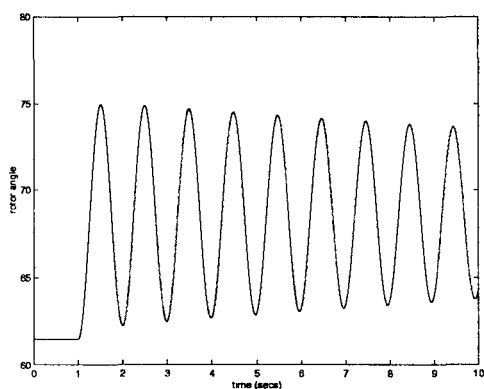
(a) Variation of δ
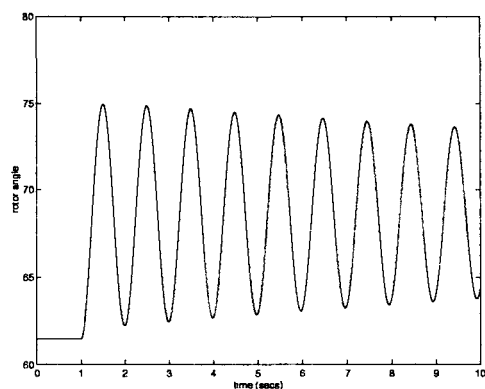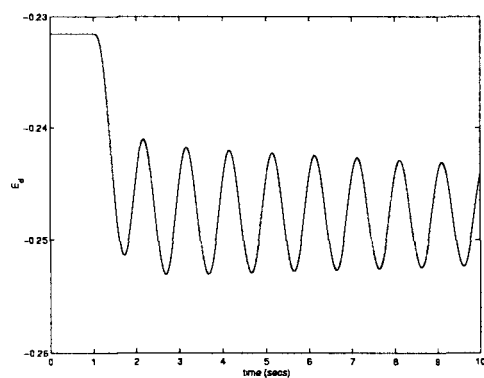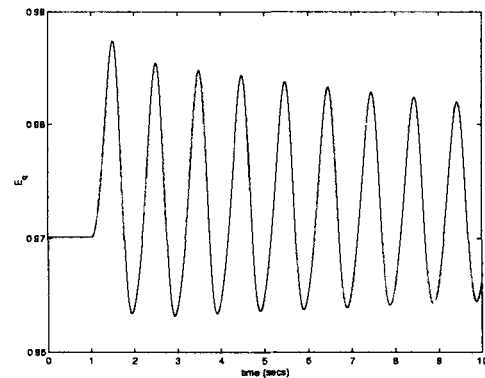
(b) Variation of S_m

(c) Variation of E'_d
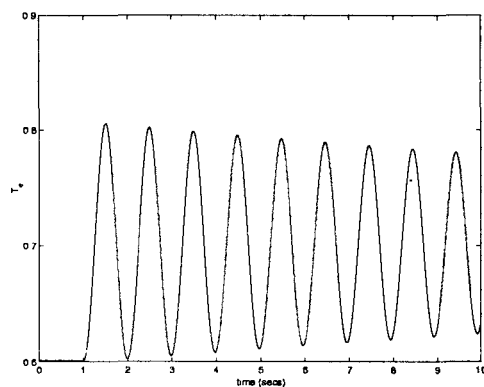
(d) Variation of E'_q
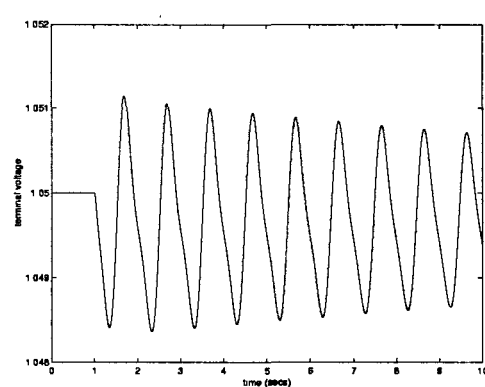
(e) Variation of T_e
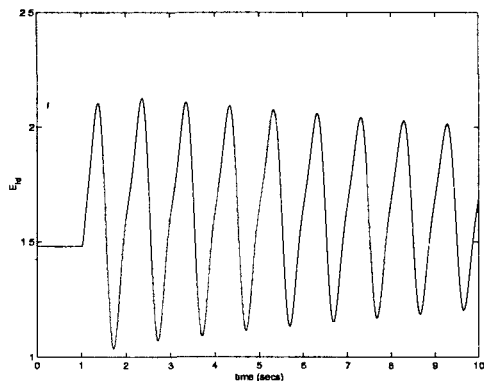
(f) Variation of V_t
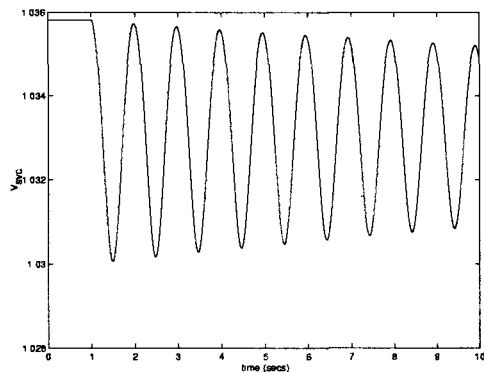
(g) Variation of E_{fd}

(h) Variation of V_{SVC}

Figure 6.21: Response to step increase in T_m with SVC (Example 6.7)

(a) Variation of δ

(b) Variation of S_m

(c) Variation of E'_d

(d) Variation of E'_q
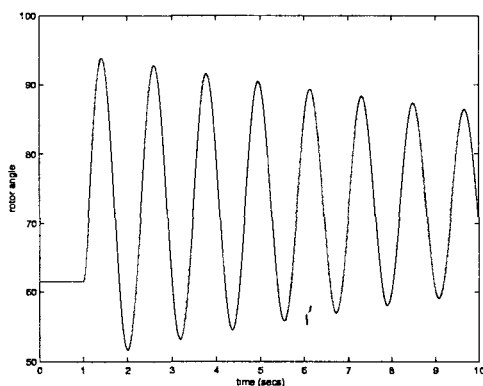
(e) Variation of T_e (f) Variation of V_t
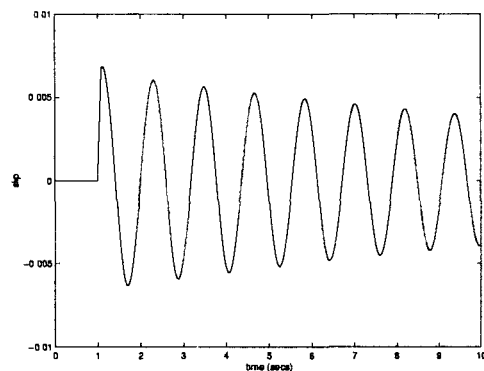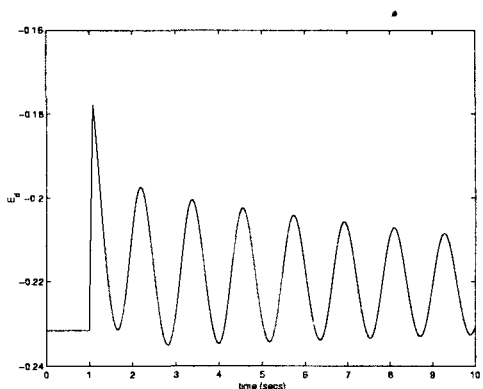
(g) Variation of E_{fd} (h) Variation of V_{SVC}
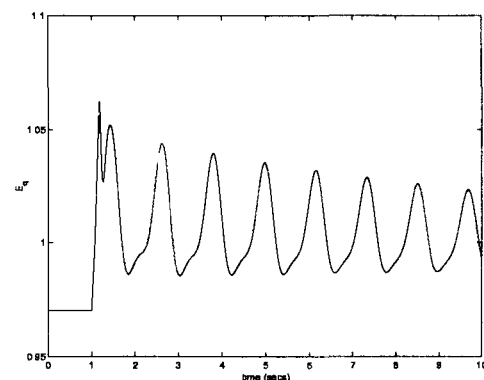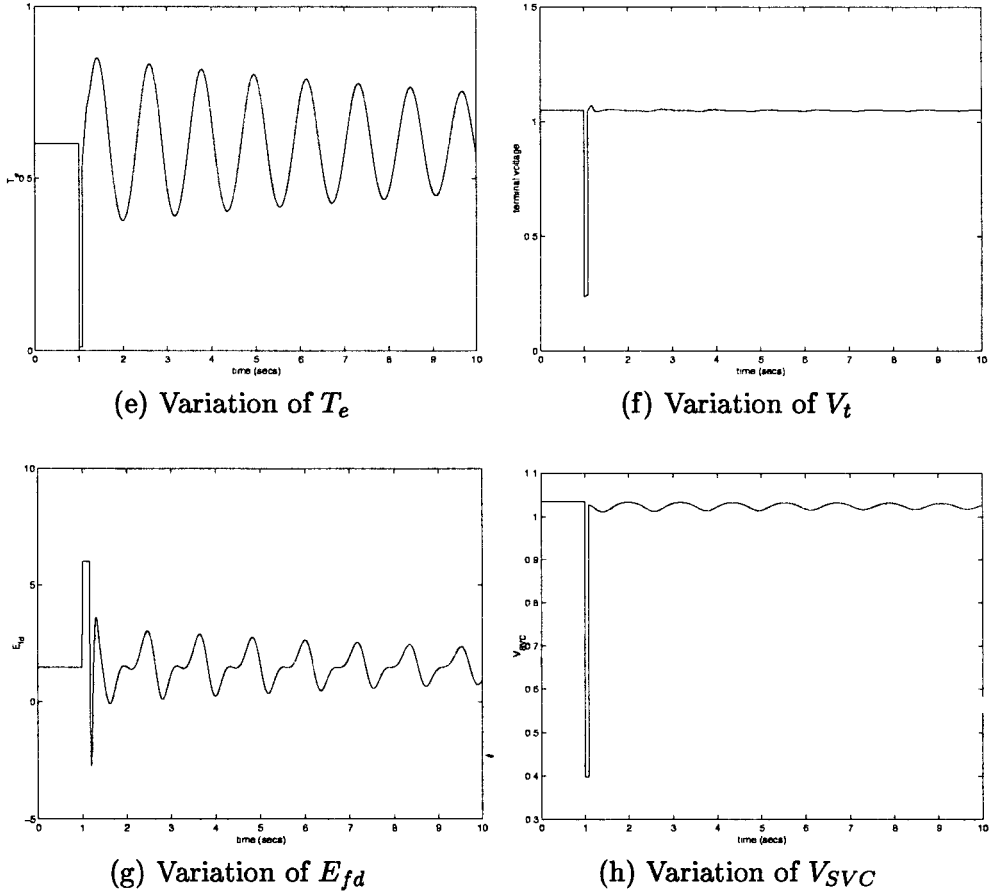
Figure 6.22: Response to three phase fault with SVC (Example 6.7)

References and Bibliography

1. E.W. Kimbark, **Power System Stability, Vol. III:Synchronous Machines**, John Wiley, New York, 1956

2. IEEE Task Force, "Current usage and suggested practices in power system stability simulations for synchronous machines", IEEE Trans. on Energy Conversion, Vol. EC-1, No. 1, 1986, pp. 77-93

3. IEEE, **Test procedures for synchronous machines**, (115), 1983

4. P.L. Dandeno, R.L. Hauth and R.P. Schultz, "Effects of synchronous machine modelling in large scale system studies", IEEE Trans. Vol. PAS-92, March/April 1973, pp. 574-582

5. D.W. Olive, "Digital Simulation of synchronous machine transients", IEEE Trans. Vol. PAS-87, Aug 1968, pp. 1669-1675

6. K. Prabhashankar and W. Janischewskyz, "Digital simulation of multimachine power systems for stability studies", IEEE Trans. Vol. PAS-87, Jan 1968, pp. 73-80

7. K.R. Padiyar and R.S. Ramshaw, "Dynamic analysis of multimachine power systems", IEEE Trans. Vol. PAS-91, March/April 1972, pp. 526-535

8. P. Kundur and P.L.Dandeno, "Implementation of advanced generator models into power system stability programs", IEEE Trans. Vol. PAS-102, No. 7, 1983

9. R.D. Dunlop and A.C. Parikh, "Verification of synchronous machine modeling in stability studies: Comparative tests of digital and physical scale model power system simulations", IEEE Trans. Vol. PAS-98, No. 2, 1979, pp. 369-378

10. L. Lapidus and J.H. Seinfeld, **Numerical Solution of Ordinary Differential Equations**, Academic Press, New York, 1971

11. J.M. Undrill, "Structure in the computation of power system nonlinear dynamical response", IEEE Trans. Vol. PAS-88, No. 1, 1969, pp. 1-6

12. F.P. Demello and L.H. Hannett, "Validation of synchronous machine models and derivation of model parameters and tests", IEEE Trans. Vol. PAS-100, No. 2, 1981, pp. 662-672

13. M. Riaz, "Hybrid-parameter models of synchronous machines", IEEE Trans. Vol. PAS-93, June 1974, pp. 849-858

14. J. Arrillaga, C.P. Arnold and B.J. Harker, **Computer Modelling of Electrical Power Systems**, John Wiley, Chichester, 1983

"This page is Intentionally Left Blank"

Chapter 7

Analysis of Single Machine System

With classical model of the synchronous machine, the steady state instability at the limiting power is characterized by a slow monotonic increase (or decrease) in the rotor angle, resulting in loss of synchronism. With the advent of automatic voltage regulators (AVR) it was felt that the steady state stability limit can be enhanced as the AVR acts to overcome the armature reaction. A simplified representation of the effect of AVR is the reduction of generator reactance from x_d to a much smaller value (around x'_d). It is to be noted that without AVRs modern turbo-generators cannot operate at full rated power, as their synchronous reactances are around 2.0 pu. Also, the transient stability is improved by fast acting exciters with high gain AVRs. Unfortunately, such fast acting excitation systems can result in negative damping of the rotor oscillations induced by small disturbances such as random load changes. Thus, system operators started observing spontaneous power oscillations of low frequency in interconnecting ties or long transmission lines. These oscillations have been observed in several systems and are of major concern in system operation. This is mainly due to the fact that the problem is aggravated at peak loading conditions and high external impedance (connected to a generator).

In this chapter, an analysis of a single machine system is presented. The emphasis is on highlighting the factors that influence the oscillatory instability.

7.1 Small Signal Analysis with Block Diagram Representation

Consider a single machine system shown in Fig. 7.1. For simplicity, we will assume a synchronous machine represented by model 1.0 neglecting damper windings both in the d and q axes. (It is possible to approximate the effects of damper windingss by a nonlinear damping term, if necessary). Also, the armature resistance of the machine is neglected and the excitation system represented by a single time-constant system shown in Fig. 7.2.
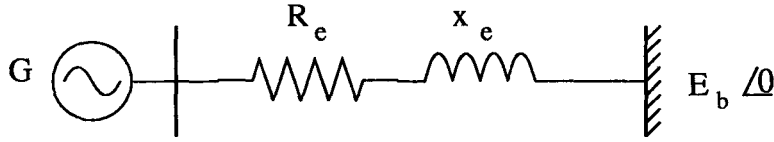
Figure 7.1: A single machine system
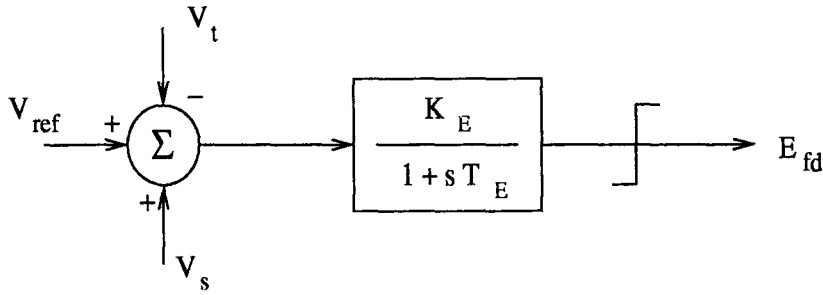
Figure 7.2: Excitation system

The algebraic equations of the stator are

$$E'_q + x'_d i_d = v_q \tag{7.1}$$

$$-x_q i_q = v_d \tag{7.2}$$

The complex terminal voltage can be expressed as

$$v_Q + j v_D = (v_q + j v_d)e^{j\delta} = (i_q + j i_d)(R_e + j x_e)e^{j\delta} + E_b \angle 0$$

From which

$$(v_q + j v_d) = (i_q + j i_d)(R_e + j x_e) + E_b e^{-j\delta} \tag{7.3}$$

Separating real and imaginary parts, Eq. (7.3) can be expressed as

$$v_q = R_e i_q - x_e i_d + E_b \, \cos \delta \tag{7.4}$$

$$v_d = R_e i_d + x_e i_q - E_b \, \sin \delta \tag{7.5}$$

Substituting Eqs. (7.4) and (7.5) in Eqs. (7.1) and (7.2), we get,

$$\begin{bmatrix} (x'_d + x_e) & -R_e \\ -R_e & -(x_q + x_e) \end{bmatrix} \begin{bmatrix} i_d \\ i_q \end{bmatrix} = \begin{bmatrix} E_b \, \cos \delta - E'_q \\ -E_b \, \sin \delta \end{bmatrix} \tag{7.6}$$

The expressions for i_d and i_q are obtained from solving (7.6) and are given below

$$i_d = \frac{1}{A}\left[R_e E_b \sin\delta + (x_q + x_e)(E_b \cos\delta - E_q')\right] \tag{7.7}$$

$$i_q = \frac{1}{A}\left[(x_d' + x_e)E_b \sin\delta - R_e(E_b \cos\delta - E_q')\right] \tag{7.8}$$

where

$$A = (x_d' + x_e)(x_q + x_e) + R_e^2 \tag{7.9}$$

Linearizing Eqs. (7.7) and (7.8) we get

$$\Delta i_d = C_1 \Delta\delta + C_2 \Delta E_q' \tag{7.10}$$

$$\Delta i_q = C_3 \Delta\delta + C_4 \Delta E_q' \tag{7.11}$$

where

$$C_1 = \frac{1}{A}[R_e E_b \cos\delta_o - (x_q + x_e)E_b \sin\delta_o]$$

$$C_2 = -\frac{1}{A}(x_q + x_e)$$

$$C_3 = \frac{1}{A}\left[(x_d' + x_e)E_b \cos\delta_o + R_e E_b \sin\delta_o\right]$$

$$C_4 = \frac{R_e}{A}$$

Linearizing Eqs. (7.1) and (7.2), and substituting from Eqs. (7.10) and (7.11), we get,

$$\Delta v_q = x_d' C_1 \Delta\delta + (1 + x_d' C_2)\Delta E_q' \tag{7.12}$$

$$\Delta v_d = -x_q C_3 \Delta\delta - x_q C_4 \Delta E_q' \tag{7.13}$$

It is to be noted that the subscript 'o' indicates operating value of the variable.

7.1.1 Rotor Mechanical Equations and Torque Angle Loop

The rotor mechanical equations are

$$\frac{d\delta}{dt} = \omega_B(S_m - S_{mo}) \tag{7.14}$$

$$2H\frac{dS_m}{dt} = -DS_m + T_m - T_e \tag{7.15}$$

$$T_e = E_q' i_q - (x_q - x_d')i_d i_q \tag{7.16}$$

Linearizing Eq. (7.16) we get

$$\Delta T_e = [E'_{qo} - (x_q - x'_d)i_{do}]\Delta i_q + i_{qo}\Delta E'_q - (x_q - x'_d)i_{qo}\Delta i_d \qquad (7.17)$$

Substituting Eqs. (7.10) and (7.11) in Eq. (7.17), we can express ΔT_e as

$$\Delta T_e = K_1\Delta\delta + K_2\Delta E'_q \qquad (7.18)$$

where

$$K_1 = E_{qo}C_3 - (x_q - x'_d)i_{qo}C_1 \qquad (7.19)$$
$$K_2 = E_{qo}C_4 + i_{qo} - (x_q - x'_d)i_{qo}C_2 \qquad (7.20)$$

$$E_{qo} = E'_{qo} - (x_q - x'_d)i_{do} \qquad (7.21)$$

Linearizing Eqs. (7.14) and (7.15) and applying Laplace transform, we get

$$\Delta\delta = \frac{\omega_B}{s}\Delta S_m = \frac{\omega_B}{s}\Delta\bar{\omega} \qquad (7.22)$$

$$\Delta S_m = \frac{1}{2Hs}[\Delta T_m - \Delta T_e - D\Delta S_m] \qquad (7.23)$$

The combined Eqs. (7.18), (7.22) and Eq. (7.23) represent a block diagram shown in Fig. 7.3. This represents the torque-angle loop of the synchronous machine.

For classical machine model, $\Delta E'_q = 0$ and the characteristic equation given by

$$2Hs^2 + Ds + K_1\omega_B = 0 \qquad (7.24)$$

For stability, both D and K_1 should be positive. If D is negligible, the roots of the characteristic equations are

$$s_1, s_2 = \pm j\sqrt{\frac{K_1\omega_B}{2H}} = \pm j\omega_n \qquad (7.25)$$

where ω_n is the natural (radian) frequency of oscillation of the rotor. Typically, the frequency of oscillation lies in the range of 0.5 to 2.0 Hz although extreme values of 0.1 Hz at the low end and 4 Hz at the high end are also possible.

7.1.2 Representation of Flux Decay

The equation for the field winding can be expressed as

$$T'_{do}\frac{dE'_q}{dt} = E_{fd} - E'_q + (x_d - x'_d)i_d \qquad (7.26)$$
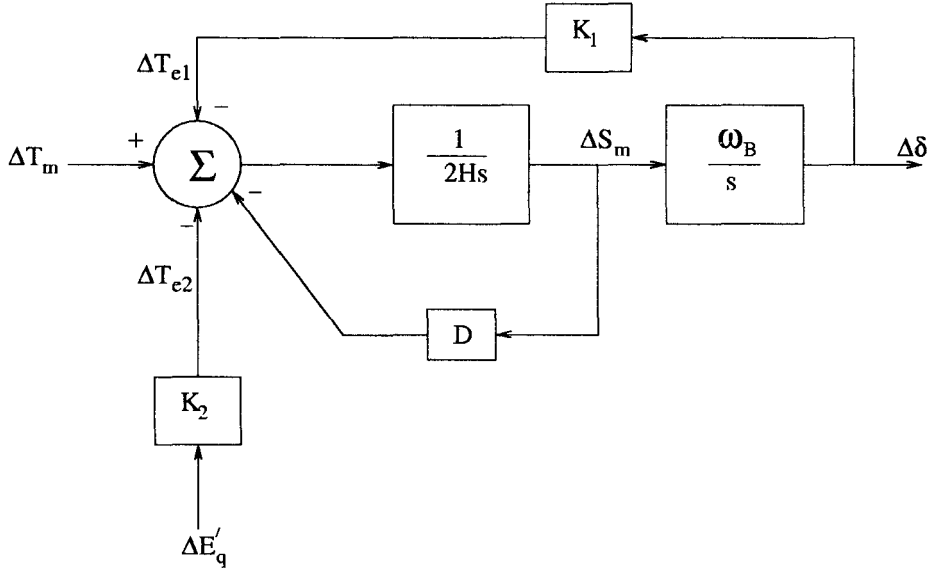
Figure 7.3: Torque-angle loop

Linearizing Eq. (7.26) and substituting from Eq. (7.10) we have

$$T'_{do}\frac{d\Delta E'_q}{dt} = \Delta E_{fd} - \Delta E'_q + (x_d - x'_d)(C_1\Delta\delta + C_2\Delta E'_q) \qquad (7.27)$$

Taking Laplace transform of (7.27) we get,

$$(1 + sT'_{do}K_3)\Delta E'_q = K_3\Delta E_{fd} - K_3K_4\Delta\delta \qquad (7.28)$$

where

$$K_3 = \frac{1}{[1 - (x_d - x'_d)C_2]} \qquad (7.29)$$

$$K_4 = -(x_d - x'_d)C_1 \qquad (7.30)$$

Eq. (7.28) can be represented by the block diagram shown in Fig. 7.4.

7.1.3   Representation of Excitation System

The block diagram of the excitation system considered is shown in Fig. 7.2. The linearized equations of this system can also be represented by the same block diagram omitting the limiter. For the present analysis we can ignore the
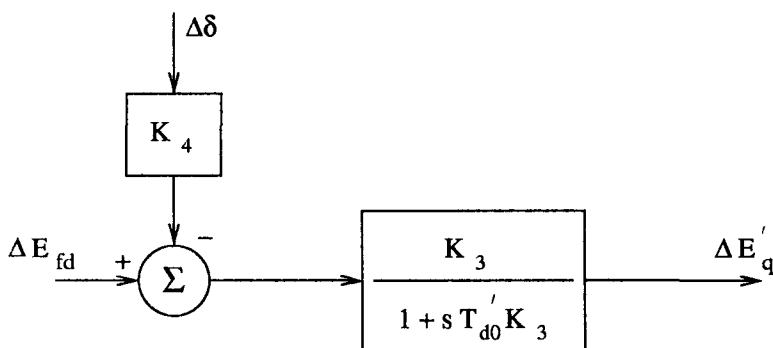
Figure 7.4: Representation of flux decay

auxiliary signal V_s. The perturbation in the terminal voltage V_t can be expressed as

$$\Delta V_t = \frac{v_{do}}{V_{to}} \Delta v_d + \frac{v_{qo}}{V_{to}} \Delta v_q \tag{7.31}$$

Substituting from Eqs. (7.12) and (7.13) in (7.31), we get

$$\Delta V_t = K_5 \Delta \delta + K_6 \Delta E_q' \tag{7.32}$$

where

$$K_5 = -\left(\frac{v_{do}}{V_{to}}\right) x_q C_3 + \left(\frac{v_{qo}}{V_{to}}\right) x_d' C_1 \tag{7.33}$$

$$K_6 = -\left(\frac{v_{do}}{V_{to}}\right) x_q C_4 + \left(\frac{v_{qo}}{V_{to}}\right) (1 + x_d' C_2) \tag{7.34}$$

Using Eq. (7.32) the block diagram of the excitation system is shown in Fig. 7.5. The coefficients K_1 to K_6 defined in Eqs. (7.19), (7.20), (7.29), (7.30), (7.33) and (7.34) are termed as Heffron-Phillips constants. They are dependent on the machine parameters and the operating conditions. Generally K_1, K_2, K_3 and K_6 are positive. K_4 is also mostly positive except for cases when R_e is high. K_5 can be either positive or negative. K_5 is positive for low to medium external impedances $(R_e + jx_e)$ and low to medium loadings. K_5 is usually negative for moderate to high external impedances and heavy loadings.

7.1.4 Computation of Heffron-Phillips Constants for Lossless Network

For $R_e = 0$, the expressions for the constants K_1 to K_6 are simplified. As the armature resistance is already neglected, this refers to a lossless network on the
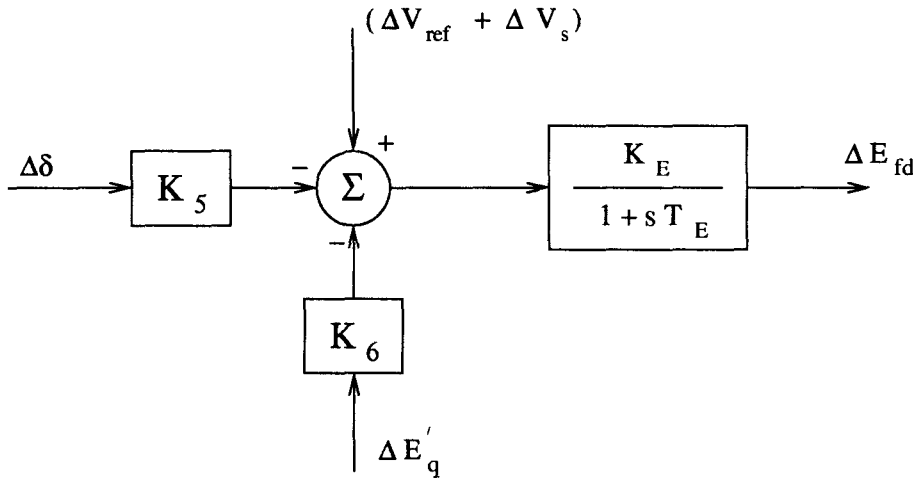
Figure 7.5: Excitation system block diagram

stator side. The expressions are given below.

$$K_1 = \frac{E_b E_{qo} \cos \delta_o}{(x_e + x_q)} + \frac{(x_q - x'_d)}{(x_e + x'_d)} E_b i_{qo} \sin \delta_o$$

$$K_2 = \frac{(x_e + x_q)}{(x_e + x'_d)} i_{qo} = \frac{E_b \sin \delta_o}{(x_e + x'_d)}$$

$$K_3 = \frac{(x_e + x'_d)}{(x_d + x_e)}$$

$$K_4 = \frac{(x_d - x'_d)}{(x'_d + x_e)} E_b \sin \delta_o$$

$$K_5 = \frac{-x_q v_{do} E_b \cos \delta_o}{(x_e + x_q) V_{to}} - \frac{x'_d v_{qo} E_b \sin \delta_o}{(x_e + x'_d) V_{to}}$$

$$K_6 = \frac{x_e}{(x_e + x'_d)} \cdot \left(\frac{v_{qo}}{V_{to}}\right)$$

It is not difficult to see that for $x_e > 0$, the constants K_1, K_2, K_3, K_4 and K_6 are positive. This is because δ_o is generally less than 90° and i_{qo} is positive. K_3 is independent of the operating point and less than unity (as $x'_d < x_d$). Note that x_e is generally positive unless the generator is feeding a large capacitive load (which is not realistic).

It is to be noted that Heffron-Phillips constants can also be defined for any general network connected between the generator and the infinite bus. For a general two-port network, the voltage at the generator port can be expressed

as

$$\hat{V}_t = (v_q + jv_d)e^{j\delta} = \left(\frac{1}{y_{11}}\right)(i_q + ji_d)e^{j\delta} + h_{12}E_b\angle 0$$

where y_{11} is short circuit admittance (at the generator terminals) and h_{12} is a hybrid parameter (open circuit voltage gain). Expressing

$$\frac{1}{y_{11}} = R_e + jx_e, \quad h_{12} = h_1 + jh_2$$

$$\hat{V}_t = (R_e + jx_e)(i_q + ji_d)e^{j\delta} + E_b'\angle\delta_b$$

$$E_b' = \sqrt{h_1^2 + h_2^2}\,E_b, \quad \delta_b = \tan^{-1}\frac{h_2}{h_1} = \text{constant}$$

The expressions for the constants given earlier are still valid if δ_o is replaced by $(\delta_o - \delta_b)$ and E_b replaced by E_b'

7.1.5 System Representation

The system block diagram, consisting of the representation of the rotor swing equations, flux decay and excitation system, is obtained by combining the component blocks shown in Figs. 7.3 to 7.5. The overall block diagram is shown in Fig. 7.6. Here the damping term (D) in the swing equations is neglected for convenience. (Actually D is generally small and neglecting it will give slightly pessimistic results).

From Fig. 7.6, the electrical torque compound ΔT_{e2} is related to $\Delta\delta$ by the following relation

$$\Delta T_{e2}(s) = -\frac{K_2 K_4}{T_{do}'}\left[\frac{s + \frac{1}{T_E}(1 + \frac{K_5 K_E}{K_4})}{s^2 + s(\frac{1}{T_E} + \frac{1}{K_3 T_{do}'}) + (1 + K_3 K_6 K_E)/K_3 T_{do}' T_E}\right]\Delta\delta(s) \tag{7.35}$$

For a static exciter, T_E is very small. If $T_E \simeq 0$, the transfer function $\dfrac{\Delta T_{e2}}{\Delta\delta}$ can be approximated as

$$\frac{\Delta T_{e2}(s)}{\Delta\delta(s)} \simeq -\frac{K_2 K_4}{T_{do}'}\frac{(1 + K_5 K_E/K_4)}{[s + (1 + K_3 K_6 K_E)/K_3 T_{do}']} \tag{7.36}$$

For large values of K_E, Eq. (7.36) can be further approximated as

$$\frac{\Delta T_{e2}(s)}{\Delta\delta(s)} \simeq -\frac{K_2 K_5 K_E}{(T_{do}' s + K_6 K_E)} = -\frac{K_2 K_5/K_6}{s T_{do}'/(K_6 K_E) + 1} \tag{7.37}$$
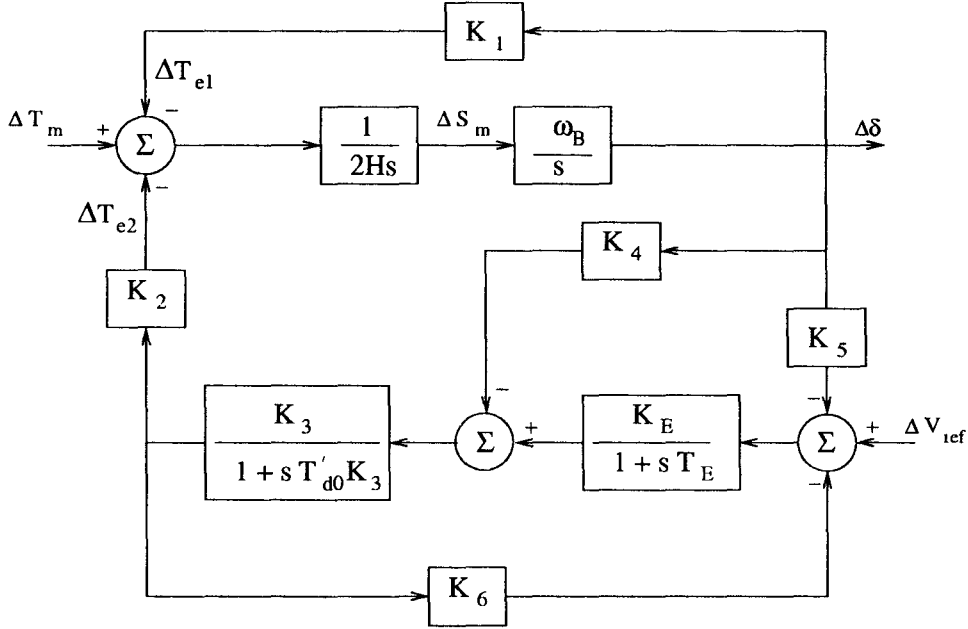
Figure 7.6: Overall block diagram

7.2 Characteristic Equation (CE) and Application of Routh-Hurwitz Criterion

The characteristic equation (CE) for the system shown in Fig. 7.6 can be obtained by combining the transfer function given in Eq. (7.35) with the following equation

$$(2Hs^2 + K_1\omega_B)\Delta\delta(s) = \omega_B(\Delta T_m - \Delta T_{e2}) \tag{7.38}$$

The characteristic equation is a 4th order polynomial expressed as

$$s^4 + a_1 s^3 + a_2 s^2 + a_3 s + a_4 = 0 \tag{7.39}$$

where

$$a_1 = \frac{1}{T_E} + \frac{1}{K_3 T'_{do}}$$

$$a_2 = \frac{(1 + K_3 K_6 K_E)}{K_3 T'_{do} T_E} + \frac{K_1 \omega_B}{2H}$$

$$a_3 = \frac{\omega_B}{2H}\left[\frac{K_1}{T_E} + \frac{K_1}{K_3 T'_{do}} - \frac{K_2 K_4}{T'_{do}}\right]$$

$$a_4 = \frac{\omega_B}{2H} \left[\frac{K_1(1 + K_3 K_6 K_E)}{K_3 T'_{do} T_E} - \frac{K_2 K_4}{T'_{do} T_E}(1 + \frac{K_5 K_E}{K_4}) \right]$$

The application of Routh-Hurwitz criterion enables steady state stability to be determined by the coefficients of the characteristic equation (without having to determine the roots). The application for Eq. (7.39) can indicate limits on the AVR gain K_E.

For static exciters, $T_E \simeq 0$ and the characteristic equation reduces to third degree given by

$$s^3 + b_1 s^2 + b_2 s + b_3 = 0 \tag{7.40}$$

where

$$b_1 = \frac{1 + K_3 K_6 K_E}{K_3 T'_{do}}$$

$$b_2 = \frac{\omega_B K_1}{2H}$$

$$b_3 = \frac{\omega_B}{2H} \left[\frac{K_1(1 + K_3 K_6 K_E)}{K_3 T'_{do}} - \frac{K_2 K_4}{T'_{do}}(1 + \frac{K_5 K_E}{K_4}) \right]$$

The criteria for stability are obtained by forming Routh array given by

$$
\begin{array}{ccc}
s^3 & 1 & b_2 \\
s^2 & b_1 & b_3 \\
s^1 & \alpha & \\
s^o & b_3 &
\end{array}
$$

For steady state stability, b_1, α and b_3 must be positive where

$$\alpha = b_2 - \frac{b_3}{b_1} = \frac{\omega_B K_2 K_3 K_4}{2H(1 + K_3 K_6 K_E)} \left(1 + \frac{K_5 K_E}{K_4} \right)$$

$b_3 > 0$ implies,

$$(K_1 - K_2 K_3 K_4) + K_3 K_E K_6 \left(K_1 - \frac{K_2 K_5}{K_6} \right) > 0$$

The above inequality is applicable as both terms in the L.H.S. are generally positive, i.e.

$$K_1 - K_2 K_3 K_4 \quad > 0 \tag{7.41}$$

$$K_1 - \frac{K_2 K_5}{K_6} \quad > 0 \tag{7.42}$$

Hence the major criterion for stability is that $\alpha > 0$ which implies

$$K_5 + \frac{K_4}{K_E} > 0 \tag{7.43}$$

When K_5 is positive, (7.43) applies and the system is stable. When K_5 is negative the inequality (7.43) puts an upper limit on K_E given by

$$K_E < \frac{K_4}{-K_5} \tag{7.44}$$

In deriving (7.44) it is assumed that $K_4 > 0$. However, it can be seen that for large values of K_E, if $K_5 > 0$, then $\alpha > 0$. This follows from the fact that

$$\alpha \simeq \frac{K_2 K_5}{K_6} \frac{\omega_B}{2H}$$

Thus, the major criterion for stability for large values of K_E is given by

$$K_5 > 0 \tag{7.45}$$

Stability Criterion for System Neglecting AVR

It is worthwhile investigating stability for a system neglecting AVR but considering field flux decay. In this case the equation can be obtained as

$$s^3 + c_1 s^2 + c_2 s + c_3 = 0 \tag{7.46}$$

where

$$c_1 = \frac{1}{T'_{do} K_3}$$

$$c_2 = \frac{\omega_B K_1}{2H}$$

$$c_3 = \frac{\omega_B}{2H} \frac{(K_1 - K_2 K_3 K_4)}{T'_{do} K_3}$$

The application of Routh criterion gives $c_1 > 0$, $c_3 > 0$ and

$$c_2 - \frac{c_3}{c_1} > 0 \tag{7.47}$$

$c_1 > 0$ is applicable as $K_3 > 0$. $c_3 > 0$ implies

$$K_1 - K_2 K_3 K_4 > 0 \tag{7.48}$$

(7.47) can be expressed as

$$\frac{\omega_B}{2H} K_2 K_3 K_4 > 0 \tag{7.49}$$

As $K_2 > 0$, the criterion for stability is

$$K_4 > 0 \tag{7.50}$$

For $R_e = 0$, the expression for K_4 is positive for $\delta_o < 90^o$. However for $R_e \neq 0$, the expression for K_4 can be obtained as

$$K_4 = \frac{E_b(x_d - x_d')}{A} \left[(x_e + x_q) \sin\delta_o - R_e \cos\delta_o \right] \tag{7.51}$$

If,

$$R_e > (x_e + x_q) \tan\delta_o \tag{7.52}$$

then, $K_4 < 0$. However, unless local resistive load is considered at the generator terminals, the external resistance R_e will be less than the limit given above.

For $K_4 < 0$, there will be two roots of the CE in the right half plane (RHP). However for $K_4 > 0$ and $K_1 - K_2 K_3 K_4 < 0$, $(K_1 > 0)$ there will be only one root in the RHP.

7.3   Synchronizing and Damping Torques Analysis

The concepts of synchronizing and damping torques are basic in the power system analysis. Assuming that the generator rotor is oscillating sinusoidally, restoring torques are set up to oppose the motion. The component of torque in phase with the rotor angle δ is called as the synchronizing torque while the component of torque in phase with the rotor velocity deviation (or slip) is termed the damping torque. Mathematically, the synchronizing torque coefficient (T_S) is defined as

$$T_S = \Re \left[\frac{\Delta T_e}{\Delta \delta}(j\omega) \right] \tag{7.53}$$

Similarly, the damping torque coefficient (T_D) is defined as

$$T_D = \Re \left[\frac{\Delta T_e}{\Delta \bar{\omega}}(j\omega) \right] \tag{7.54}$$

Since

$$\frac{\Delta T_e(s)}{\Delta \bar{\omega}(s)} = \frac{\omega_B}{s} \left[\frac{\Delta T_e(s)}{\Delta \delta(s)} \right] \tag{7.55}$$

We can derive

$$T_D = \frac{\omega_B \Im \left[\dfrac{\Delta T_e(j\omega)}{\Delta\delta(j\omega)}\right]}{\omega} \tag{7.56}$$

Similarly, T_S can also be expressed as

$$T_S = -\frac{\omega}{\omega_B} \Im \left[\frac{\Delta T_e(j\omega)}{\Delta\bar{\omega}(j\omega)}\right] \tag{7.57}$$

The significance of the concepts of synchronizing and damping torques is the postulate that the small rotor oscillations are governed by an approximate second order differential equation given by

$$Mp^2\Delta\delta + \frac{T_D}{\omega_B}p\Delta\delta + T_S\Delta\delta = 0 \tag{7.58}$$

where M is the inertia constant $\left(\dfrac{2H}{\omega_B}\right)$, p the differential operator, $\dfrac{d}{dt}$

It is to be noted that the accuracy of this approximation depends on the nature of the electrical network connected to the generator.

The significance of Eq. (7.58) is that for stability of rotor oscillations, both T_S and T_D should be positive calculated at all possible frequencies of oscillations. An initial estimate for the frequency of oscillation is given by Eq. (7.25).

For $T_D < 0$ and $T_S > 0$, there will be two complex roots which will lie in the RHP. For $T_D > 0$ and $T_S < 0$ or for both T_S and T_D negative, there will be one real root in the RHP.

7.3.1   Application : Case 1 : System without AVR

When AVR is not considered, the electrical torque (ΔT_e) is given by the expression

$$
\begin{aligned}
\Delta T_e &= \Delta T_{e1} + \Delta T_{e2} \tag{7.59} \\
&= \left[K_1 - \frac{K_2 K_3 K_4}{1 + sT'_{do}K_3}\right]\Delta\delta
\end{aligned}
$$

From the above, T_S and T_D can be obtained as

$$T_S = K_1 - \frac{K_2 K_3 K_4}{1 + \omega^2 T'^2_{do} K_3^2} \tag{7.60}$$
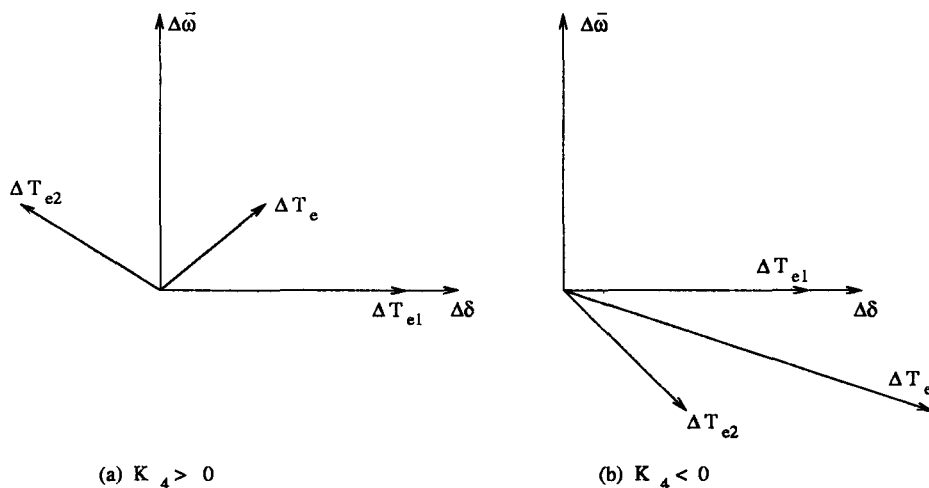
Figure 7.7: Phasor diagram

$$T_D = \frac{K_2 K_3^2 K_4 T'_{do} \omega_B}{1 + \omega^2 T'^2_{do} K_3^2} \tag{7.61}$$

For T_S and T_D to be positive for all frequencies of oscillations, it is necessary that

$$\left.\begin{array}{ccc} K_1 & > & 0 \\ K_1 - K_2 K_3 K_4 & > & 0 \end{array}\right\} for \;\; T_S > 0 \tag{7.62}$$

$$K_4 \;\; > \;\; 0 \;\; for \;\; T_D > 0$$

The first condition applies for high oscillation frequencies such that $\omega T'_{do} K_3 \gg 1$. The second applies for low frequencies such that $\omega T'_{do} K_3 \ll 1$. The third condition applies for all frequencies.

It is to be noted that the above conditions for stability are identical to those given by Routh Criterion. $K_4 < 0$ indicates negative damping. Fig. 7.7 shows the phasors $\Delta\delta$, $\Delta\bar{\omega}$, ΔT_{e1}, ΔT_{e2} and ΔT_e . (a) shows the phasor relations for the case when $K_4 > 0$ and (b) for the case when $K_4 < 0$. It is obvious that with $K_4 < 0$ the damping torque is negative although the synchronizing torque is increased (compared to case (a)). The negative synchronizing torque component introduced by ΔT_{e2} (for $K_4 > 0$) results from the demagnitizing action of the armature reaction which weakens field flux.

7.3.2 Case 2: Fast excitation system ($T_F \simeq 0$)

For $T_E \simeq 0$ the electrical torque (ΔT_e) can be approximated as (see Eq. 7.36)

$$\Delta T_e = \left[K_1 - \frac{K_2 \dfrac{\left(K_5 + \dfrac{K_4}{K_E}\right)}{K_6}}{\dfrac{sT'_{do}}{(K_E K_6)} + 1} \right] \Delta \delta \qquad (7.63)$$

In deriving the above expression, it is assumed that $K_3 K_6 K_E \gg 1$ and hence

$$1 + K_3 K_6 K_E \simeq K_3 K_6 K_E$$

By combining Eq. (7.63) with Eq. (7.59) it is not difficult to get the following conditions for stability

$$\left. \begin{array}{r} K_1 \quad > \ 0 \\[4pt] K_1 - \left(\dfrac{K_2}{K_6}\right)\left(K_5 + \dfrac{K_4}{K_E}\right) \ > \ 0 \end{array} \right\} \quad for \ \ T_S > 0 \qquad (7.64)$$

$$\left(K_5 + \frac{K_4}{K_E}\right) > 0 \ \ for \ \ T_D > 0 \qquad (7.65)$$

For large values of K_E, the conditions reduce to

$$\left. \begin{array}{r} K_1 \quad > \ 0 \\[4pt] K_1 - \dfrac{K_2 K_5}{K_6} \ > \ 0 \end{array} \right\} for \ \ T_S > 0 \qquad (7.66)$$

$$K_5 > 0, \qquad for \ \ T_D > 0 \qquad (7.67)$$

These conditions are related to those obtained by applying Routh's criterion.

Example 7.1

A synchronous generator is connected to an infinite bus through an external reactance $x_e = 0.4$ pu. Compute the Heffron-Phillips constants, K_1 to K_6 at the operating point

(a) $P_g = 0.5$, $V_t = 1.0$, $E_b = 1.0$

(b) $P_g = 1.0$, $V_t = 1.0$, $E_b = 1.0$

The machine data: $x_d = 1.6$, $x_q = 1.55$, $x'_d = 0.32$, $T'_{do} = 6.0$, $H = 5$,
$D = 0$, $f_B = 60$ Hz.

Solution

The data given assumes machine model (1.0). The initial conditions are calculated from the operating point and the constants K_1 to K_6 are obtained from using the expressions given in section 7.1.4.

(a) $\hat{V}_t = 1.0\angle 11.53$, $I_a = 0.5025$, $E_{qo} = 1.3279$, $\delta_o = 47.24^o$, $i_{do} = -0.3328$,
$i_{qo} = 0.3765$, $v_{do} = -0.5836$, $v_{qo} = 0.8120$
$K_1 = 0.9346$, $K_2 = 1.0198$, $K_3 = 0.3600$, $K_4 = 1.3053$, $K_5 = 0.0500$,
$K_6 = 0.4511$

(b) $\hat{V}_t = 1.0\angle 23.57$, $I_a = 1.0215$, $E_{qo} = 2.0382$, $\delta_o = 73.08^o$, $i_{do} = -0.8960$,
$i_{qo} = 0.4906$, $v_{do} = -0.7605$, $v_{qo} = 0.6494$
$K_1 = 1.1060$, $K_2 = 1.3288$, $K_3 = 0.3600$, $K_4 = 1.7009$, $K_5 = -0.1002$,
$K_6 = 0.3608$

Note: K_3 is independent of operating point. K_5 is positive for case (a) and negative for case (b). All other constants are positive. If AVR is not considered, then the conditions for stability are

$$K_1 > 0, \quad K_1 - K_2 K_3 K_4 > 0$$

The value of $(K_1 - K_2 K_3 K_4)$ is 0.4554 for case (a) and 0.2924 for case (b).

If AVR is to be considered, the condition for stability is primarily

$$K_E < \frac{K_4}{-K_5}$$

For case (b), this implies that $K_E < 16.98$

Example 7.2

For the system given in Example 7.1, plot the variations of -
K_1, $(K_1 - K_2 K_3 K_4)$ and K_5 with variations in x_e. (All other parameters having same values as before).

Solution

The variations in K_1, $(K_1 - K_2 K_3 K_4)$ and K_5 are shown in Fig. 7.8. It is interesting to observe that

(i) $K_1 > 0$ for both cases. As expected, K_1 reduces with increase in x_e. The reduction is faster for case (b) $P_g = 1.0$
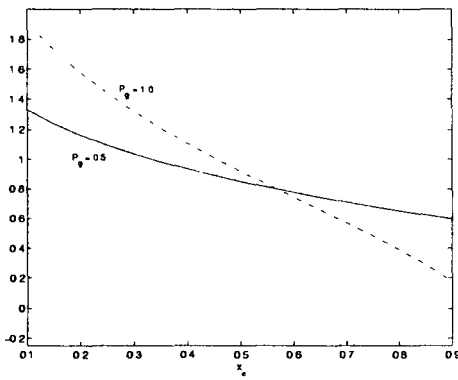
(a) Variation of K_1
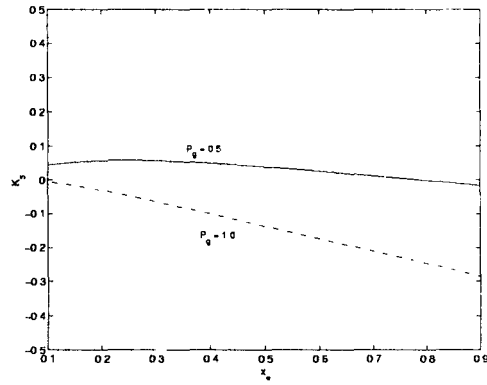
(b) Variation of K_5
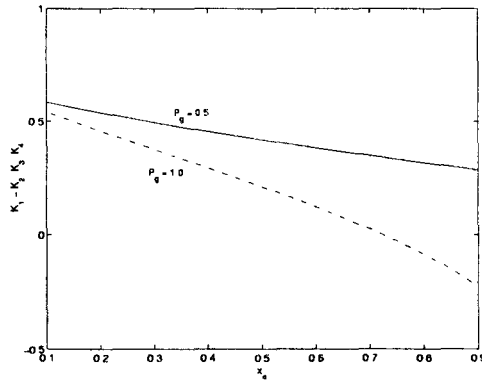
(c) Variation of $(K_1 - K_2K_3K_4)$

Figure 7.8: Variations of parameters with x_e (Example 7.2).

(ii) $(K_1 - K_2K_3K_4)$ is positive for case (a) while for case (b) it becomes negative for x_e exceeding 0.7

(iii) $K_5 > 0$ for case (a) when $x_e < 0.8$. However, $K_5 < 0$ for case (b) even for $x_e = 0.1$. K_5 reduces with increase in x_e.

Example 7.3

Repeat Example 7.2 if $x_e = 0.4$ and P_g is varied from 0.5 to 1.5 p.u.

Solution

The variations of K_1, $(K_1 - K_2K_3K_4)$ and K_5 with variation in P_g are shown in Fig. 7.9. It is interesting to observe that

(i) $K_1 > 0$ and remains practically constant.

(ii) $(K_1 - K_2K_3K_4)$ reduces with increase in P_g. It reaches the value of zero as P_g approaches 1.5 pu.

(iii) K_5 reduces as P_g increases. K_5 crosses zero as P_g approaches the value of 0.7 p.u. and remains negative as P_g is further increased.
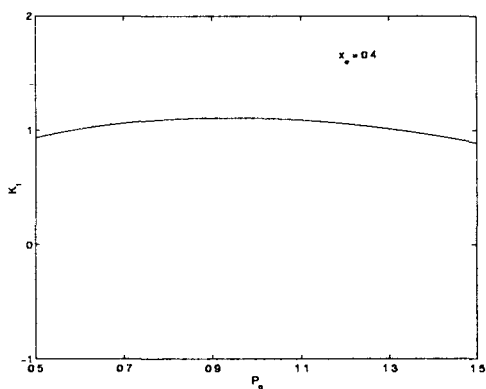
(a) Variation of K_1 (b) Variation of K_5
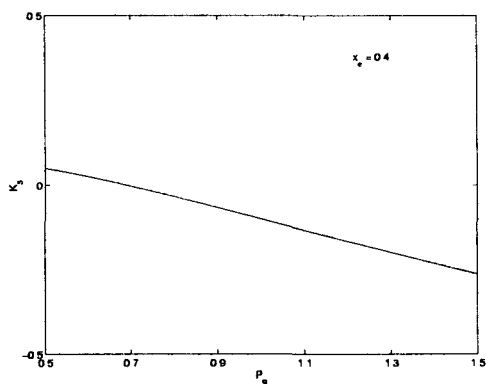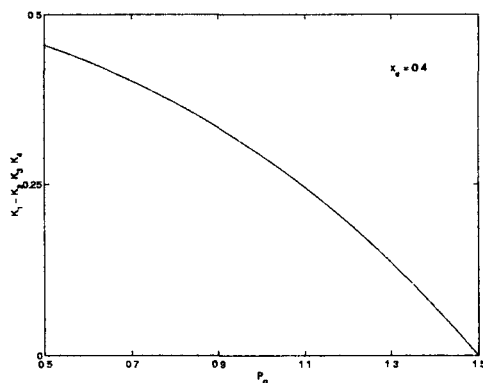
(c) Variation of $(K_1 - K_2K_3K_4)$

Figure 7.9: Variation of parameters with P_g (Example 7.3).

Example 7.4

For the system shown in Fig. 7.10, compute the constants K_1 to K_6 for the two operating points (a) $P_g = 1.0$ (b)$P_g = 1.1$. For both cases, assume that $V_t = E_b = 1.0$. The system data are $R_E = 1.0$, $x_E = 5.0$, the machine data is same as in Example 7.1.
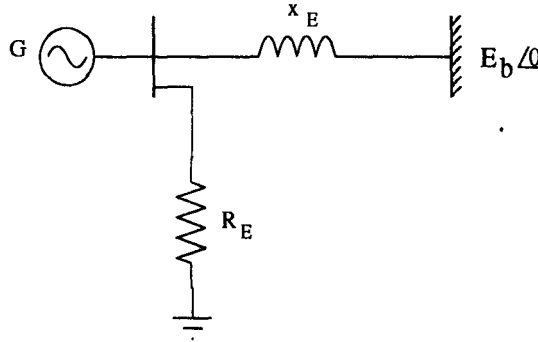
Figure 7.10: System for Example 7.4

Solution

From the discussion given in section 7.1.4, the external network is a special case of a two-port network for which the parameters are calculated as

$$y_{11} = \frac{1}{R_E} + \frac{1}{jx_E} = \frac{1}{R_e + jx_e}, \quad h_{12} = \frac{R_E}{R_E + jx_E}$$

The system shown in Fig. 7.10 is equivalent to the system shown in Fig. 7.1 with infinite bus voltage replaced by

$$E_b' \angle \delta_b = h_{12} E_b$$

(a) The initial conditions are calculated as
$\hat{V}_t = 1.0\angle 0$, $I_a = 1.0$, $E_{qo} = 1.8446$, $\delta_o = 57.17^o$, $i_{do} = -0.8403$,
$i_{qo} = 0.5421$, $v_{do} = -0.8403$, $v_{qo} = 0.5421$
The constants are obtained from using the expressions given in section 7.1.3. They are
$K_1 = 0.1971$, $K_2 = 2.1575$, $K_3 = 0.4490$ $K_4 = 0.2629$, $K_5 = 0.0068$,
$K_6 = 1.0650$

(b) The initial conditions are
$\hat{V}_t = 1.0\angle 30$, $I_a = 1.1003$, $E_{qo} = 1.998$, $\delta_o = 88.58^o$, $i_{do} = -0.9527$,
$i_{qo} = 0.5506$, $v_{do} = -0.8534$, $v_{qo} = 0.5213$
The constants are
$K_1 = 0.0345$, $K_2 = 2.2571$, $K_3 = 0.4490$ $K_4 = 0.1826$, $K_5 = -0.0649$,
$K_6 = 1.0613$

7.4   Small Signal Model: State Equations

7.4.1   Simplified Model

It is possible to express the system equations in the state space form. From the block diagram, shown in Fig. 7.6, the following system equations can be derived

$$\dot{x} = [A]x + [B](\Delta V_{ref} + \Delta V_s) \tag{7.68}$$

where

$$x^t = [\Delta\delta \ \ \Delta S_m \ \ \Delta E'_q \ \ \Delta E_{fd}]$$

$$[A] = \begin{bmatrix} 0 & \omega_B & 0 & 0 \\ -\dfrac{K_1}{2H} & -\dfrac{D}{2H} & -\dfrac{K_2}{2H} & 0 \\ -\dfrac{K_4}{T'_{do}} & 0 & -\dfrac{1}{T'_{do}K_3} & \dfrac{1}{T'_{do}} \\ -\dfrac{K_E K_5}{T_E} & 0 & -\dfrac{K_E K_6}{T_E} & -\dfrac{1}{T_E} \end{bmatrix}$$

$$[B]^t = \begin{bmatrix} 0 & 0 & 0 & \dfrac{K_E}{T_E} \end{bmatrix}$$

The damping term D, is included in the swing equation. The eigenvalues of the matrix should lie in LHP in the 's' plane for the system to be stable. The effect of various parameters (for example, K_E and T_E) can be examined from eigenvalue analysis. It is to be noted that the elements of matrix $[A]$ are dependent on the operating condition.

Example 7.5

For the system considered in Example 7.1, compute the eigenvalues for the two operating conditions and (i) without AVR (ii) with AVR of $T_E = 0.05$ sec, $K_E = 200$.

Solution

The system matrix $[A]$ is defined in Eq. (7.68). The substitution of the parameter values and calculation of eigenvalues using MATLAB program gives the following results

(a) $P_g = 0.5$

    (i) Without AVR

        $-0.1185 \pm j5.9302, \quad -0.2259$

    (ii) With AVR

        $-0.1512 \pm j5.5407, \quad -10.0803 \pm j14.3810$

(b) $P_g = 1.0$

    (i) Without AVR

        $-0.1702 \pm j6.4518, \quad -0.1225$

    (ii) With AVR

        $0.5091 \pm j7.1562, \quad -10.7405 \pm j12.1037$

It is interesting to observe that

(i) The complex pair of eigenvalues corresponding to low frequency rotor oscillations is affected by AVR in different ways for cases (a) and (b). In the first case ($P_g = 0.5$), the damping is slightly increased with AVR while the frequency of oscillation is slightly decreased. This is equivalent to the statement that while AVR can contribute damping torque (with $K_5 > 0$) the synchronizing torque is slightly decreased.

For the case (b), the net damping becomes negative while the frequency of oscillation increases slightly. This is mainly due to the fact that $K_5 < 0$, in this case.

(ii) There is a negative real eigenvalue in the case without AVR which moves towards the origin as P_g is increased. However the inclusion of a single time constant excitation system results in another complex pair in the left half plane, further away from the imaginary axis compared to the rotor mode. The loci of eigenvalues for the case without AVR are shown in Fig. 7.11 as P_g is varied from 0.5 to 1.7 (for $x_e = 0.4$). The variations with x_e (varied from 0.1 to 1.0) for $P_g = 1.0$, are shown in Fig. 7.12. It is interesting to note that while the complex pair remains in the left half plane, the real eigenvalue crosses imaginary axis into RHP as either P_g or x_e is increased. This shows that instability in the case when AVR is absent, is mainly due to monotonic increase (or decrease) in the rotor angle when small perturbations are present.

Example 7.6

For Example 7.5, plot the loci of the critical eigenvalues as K_E is varied from 0 to 400.
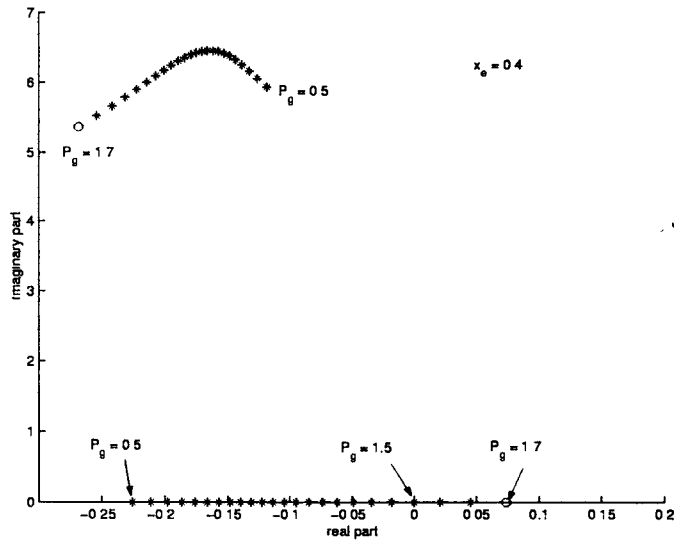
Figure 7.11: Eigenvalue loci for variation in P_g (Example 7.5).
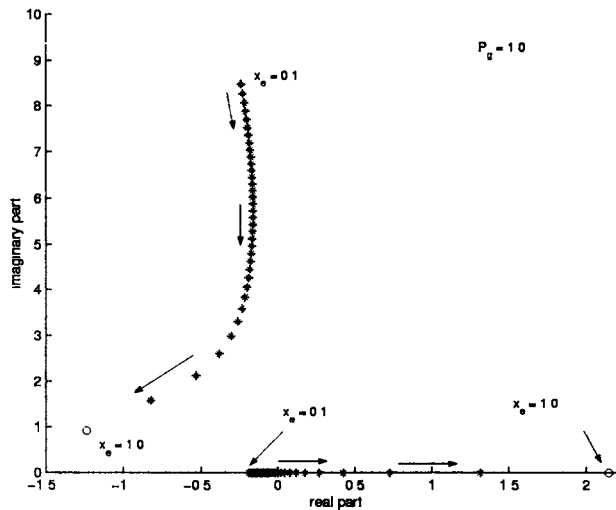
Figure 7.12: Eigenvalue loci for variation in x_e (Example 7.5).

Solution

The loci of the complex critical eigenvalues are shown in Fig. 7.13. For case (a) (with $P_g = 0.5$), the damping increases at first as K_E is increased from zero but starts decreasing as K_E is further increased. However the locus remains
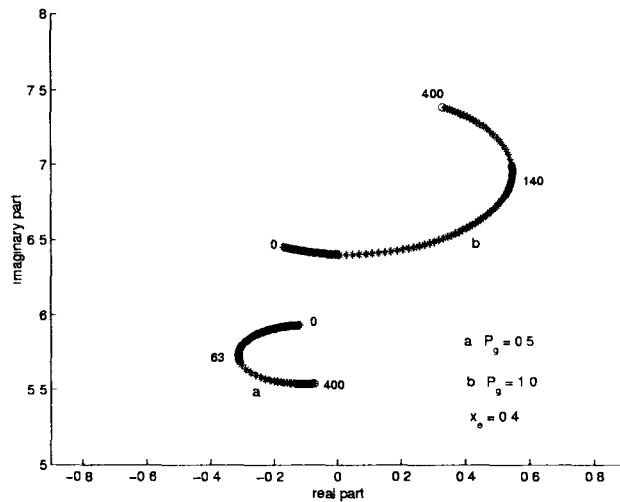
Figure 7.13: Eigenvalue loci for variation in AVR gain(Example 7.6).

in the LHP. For case (b), the damping starts decreasing as K_E is increased from zero and the eigenvalue crosses imaginary axis as K_E is increased beyond 17.0. Although the locus turns around as K_E is further increased, it remains in the RHP.

The difference in the loci for the two cases can be attributed to the fact that while $K_5 < 0$ for case (b) it is positive for case (a). Thus instability is expected in case (b) for sufficiently large values of K_E.

(Note that only one of the critical eigenvalues is shown in Fig. 7.13. The other is the complex conjugate whose locus is the mirror image about the real axis).

Example 7.7

For the system of Example 7.4, compute the eigenvalues (i) without and (ii) with AVR ($K_E = 200, T_E = 0.05$ sec).

Solution

(a) $P_g = 1.0$

    (i) Without AVR
        $-0.2395 \pm j2.7247$, 0.1078

    (ii) With AVR
        $-0.0063 \pm j2.6102$, $-10.1793 \pm j24.7821$

(b) $P_g = 1.1$

    (i) Without AVR
        $-0.6246 \pm j1.4174, \quad 0.8780$

    (ii) With AVR
        $0.0753 \pm j2.5280, \quad -10.2609 \pm j24.6505$

Note that

    (i) Case (a) corresponds to the case with no power transmission on the tie line. (P_g is just adequate to meet the local load). For case (b), the power flow on the line is $\dfrac{1}{10}$ of the local load.

    (ii) The frequency of oscillation is less when compared to the system of Example 7.1. Also the frequency reduces as power flow increases on the line.

    (iii) While AVR stabilizes the system for case (a), the mode of instability for case (b) shifts from one of monotonic instability to oscillatory instability when AVR is present.

Example 7.8

For Example 7.7, plot the loci of the critical eigenvalues as K_E is increased from 0 to 400.

Solution

The loci of the complex critical eigenvalues for the cases (a) and (b) are shown in Fig. 7.14. The results are similar to those shown in Fig. 7.13 in the sense that for the case (operating point) when $K_5 < 0$, the increase in K_E beyond a limit results in oscillatory instability.

7.4.2 Detailed Models

The analysis given above considered only the synchronous machine model 1.0 and simple excitation system model. It is possible to consider more detailed models both for the machine and controllers (both excitation and prime-mover).

In general, the linearized machine model can be expressed as

$$\dot{x}_m = [A_m]x_m + [B_{m1}]\Delta i_m + [B_{m2}]\Delta E_{fd} + [B_{m3}]\Delta T_m \qquad (7.69)$$

where

$$\Delta i_m^t = [\Delta i_d \quad \Delta i_q]$$
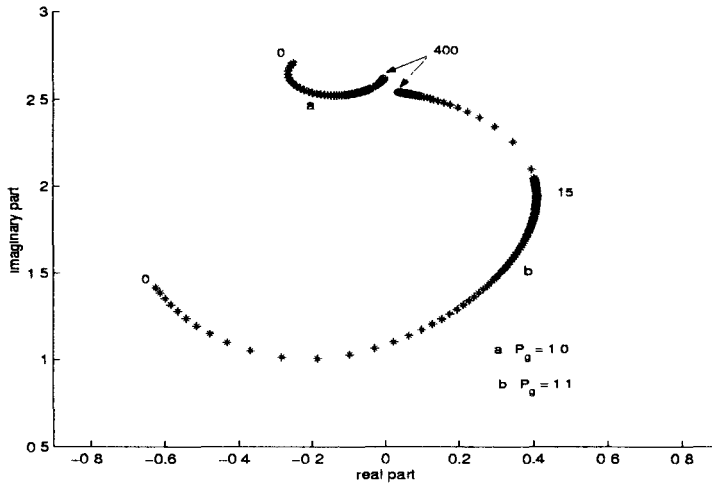
Figure 7.14: Eigenvalue loci for variation in AVR gain (Example 7.8).

For machine model 1.1, the state vector x_m is say

$$x_m^t = [\Delta\delta \;\; \Delta S_m \;\; \Delta E_q' \;\; \Delta E_d']$$

The various coefficient matrices are

$$[A_m] = \begin{bmatrix} 0 & \omega_B & 0 & 0 \\[2mm] 0 & -\dfrac{D}{2H} & -\dfrac{i_{qo}}{2H} & -\dfrac{i_{do}}{2H} \\[4mm] 0 & 0 & -\dfrac{1}{T_{do}'} & 0 \\[4mm] 0 & 0 & 0 & -\dfrac{1}{T_{qo}'} \end{bmatrix}$$

$$[B_{m1}] = \begin{bmatrix} 0 & 0 \\[2mm] \beta_1 & \beta_2 \\[2mm] (x_d - x_d')/T_{do}' & 0 \\[2mm] 0 & -(x_q - x_q')/T_{qo}' \end{bmatrix}$$

$$[B_{m2}]^t = \begin{bmatrix} 0 & 0 & \dfrac{1}{T_{do}'} & 0 \end{bmatrix}$$

$$[B_{m3}]^t = \begin{bmatrix} 0 & \dfrac{1}{2H} & 0 & 0 \end{bmatrix}$$

$$\beta_1 = (E'_{do} + (x'_d - x'_q)i_{qo})/2H$$
$$\beta_2 = (E'_{qo} + (x'_d - x'_q)i_{do})/2H$$

Controller Equations

In general, the controller (including excitation and prime-mover) can be described by the following equations

$$\dot{x}_c = [A_c]x_c + [B_{c1}]\Delta v_m + [B_{c2}]\Delta S_m + [E_c]u_c \qquad (7.70)$$

where x_c is the state vector for the control system and

$$u_c^t = [\Delta V_{ref} \;\; \Delta \omega_{ref}]$$
$$\Delta v_m^t = [\Delta v_q \;\; \Delta v_d]$$

ΔS_m is expressed as

$$\Delta S_m = e_2^t x_m$$

where e_2 is a column vector equal to the second column of the unit matrix of same dimension as that of vector x_m. (It is assumed that irrespective of the machine model, ΔS_m is always the second variable among the state variables corresponding to the machine. The first variable is $\Delta\delta$).

ΔE_{fd} and ΔT_m are outputs of the controllers expressed as

$$\Delta E_{fd} = C_1^t x_c, \quad \Delta T_m = C_2^t x_c$$

where C_1 and C_2 are column vectors of same dimension as that of x_c. There is no loss of generality if x_c vector is so arranged such that

$$C_1^t = [1 \;\; 0 \;\; 0.......0]$$

In other words C_1 is the first column of the unit matrix of same dimension as that of vector x_c.

Note: Power System Stabilizer (PSS) (to be discussed in the next chapter) can also be treated as a part of the excitation controller. Also, if prime-mover controller is ignored, then C_2 can be put equal to zero.

Equations (7.69) and (7.70) can be combined to give

$$\dot{x}_g = [A_g]x_g + [B_{g1}]\Delta i_m + [B_{g2}]\Delta v_m + [E_g]u_c \qquad (7.71)$$

where

$$[A_g] = \begin{bmatrix} A_m & B_{m2}C_1^t + B_{m3}C_2^t \\ B_{c2}e_2^t & A_c \end{bmatrix} \tag{7.72}$$

$$\begin{aligned} B_{g1}^t &= [B_{m1}^t \quad [0]] \\ B_{g2}^t &= [[0] \quad B_{c1}^t] \\ E_g^t &= [[0] \quad E_c^t] \end{aligned}$$

It is to be noted that Δi_m and Δv_m are related by the following equations

$$\Delta v_m = \begin{bmatrix} \Delta v_q \\ \Delta v_d \end{bmatrix} = -[Z_g]\Delta i_m + \begin{bmatrix} \Delta E_q' \\ \Delta E_d' \end{bmatrix} \tag{7.73}$$

where

$$[Z_g] = \begin{bmatrix} -x_d' & R_a \\ R_a & x_q' \end{bmatrix}$$

The armature resistance is usually very small and can be neglected in the above equations.

Network Equations

For a single generator connected to infinite bus through an external network, the following equation in Δv_m can be derived

$$\begin{bmatrix} \Delta v_q \\ \Delta v_d \end{bmatrix} = \begin{bmatrix} Z_{11} & Z_{12} \\ Z_{21} & Z_{22} \end{bmatrix} \begin{bmatrix} \Delta i_d \\ \Delta i_q \end{bmatrix} + \begin{bmatrix} a_{11} & a_{12} \\ a_{21} & a_{22} \end{bmatrix} \begin{bmatrix} -E_b \sin\delta_o \\ -E_b \cos\delta_o \end{bmatrix} \Delta\delta$$

or

$$\Delta v_m = [Z]\Delta i_m + [A]\Delta\delta \tag{7.74}$$

The derivation of Eq. (7.74) is quite straightward for a two port network connecting the generator to the infinite bus. However, the form given in Eq. (7.74) applies even if nonlinear voltage dependent load and SVC are considered at an intermediate bus.

Representation of Nonlinear Load

For example, consider a system shown in Fig. 7.15 which shows a nonlinear load and a SVC at bus 3. The load can be described by

$$P_L = P_{Lo} \left(\frac{V}{V_o} \right)^{m_p} \tag{7.75}$$

$$Q_L = Q_{Lo} \left(\frac{V}{V_o} \right)^{m_q} \tag{7.76}$$

The load current $\hat{I}_L$ can be expressed as
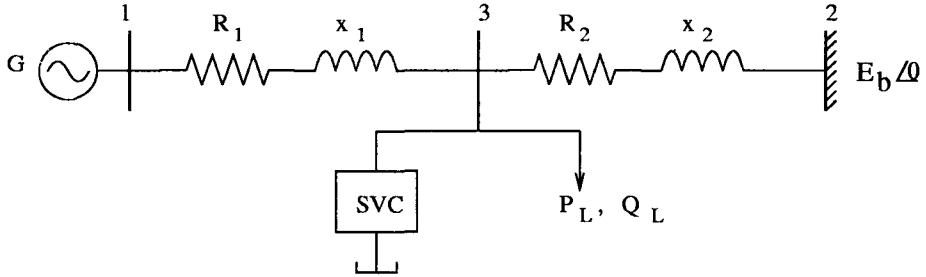
Figure 7.15: System diagram

$$\hat{I}_L = I_{qL} + jI_{dL} = \frac{P_L - jQ_L}{\hat{V}_L^*}$$

$$= \frac{(P_L - jQ_L)}{V^2} \hat{V}_L \tag{7.77}$$

where

$$\hat{V}_L = V_{qL} + jV_{dL},$$

Note that the magnitude of the load bus voltage is denoted by V (without the subscript L).

Substituting Eqs. (7.75) and (7.76) in Eq. (7.77) and linearizing, it is possible to express $\Delta \hat{I}_L$ as

$$\Delta \hat{I}_L = \Delta I_{qL} + j\Delta I_{dL} = (G_{Lo} + jB_{Lo})(\Delta V_{qL} + j\Delta V_{dL})$$

$$+ \frac{1}{\hat{V}_{Lo}^*} [(m_p - 2)P_{Lo} - j(m_q - 2)Q_{Lo}] \frac{\Delta V}{V_o} \tag{7.78}$$

where

$$G_{Lo} + jB_{Lo} = \frac{P_{Lo} - jQ_{Lo}}{V_o^2}$$

Note that if the load is of constant impedance type, both m_p and m_q have value of 2 and the second term is the R.H.S. of Eq. (7.78) is zero.

By expressing ΔV as

$$\Delta V = \left(\frac{V_{dLo}}{V_o}\right)\Delta V_{dL} + \left(\frac{V_{qLo}}{V_o}\right)\Delta V_{qL} \tag{7.79}$$

it is possible to express (7.78) in the form

$$\begin{bmatrix} \Delta I_{dL} \\ \Delta I_{qL} \end{bmatrix} = \begin{bmatrix} B_{Lo} + b_1 & G_{Lo} + g_1 \\ G_{Lo} + g_2 & -B_{Lo} - b_2 \end{bmatrix} \begin{bmatrix} \Delta V_{qL} \\ \Delta V_{dL} \end{bmatrix} \tag{7.80}$$

$$= [Y_L] \begin{bmatrix} \Delta V_{qL} \\ \Delta V_{dL} \end{bmatrix}$$

$$b' = \frac{1}{V_o^2}[(m_p - 2)P_{Lo}\sin\theta_o - (m_q - 2)Q_{Lo}\cos\theta_o]$$

$$b_1 = b'\left(\frac{V_{qLo}}{V_o}\right), \quad g_1 = b'\left(\frac{V_{dLo}}{V_o}\right)$$

$$g' = \frac{1}{V_o^2}[(m_p - 2)P_{Lo}\cos\theta_o + (m_q - 2)Q_{Lo}\sin\theta_o]$$

$$g_2 = g'\left(\frac{V_{qLo}}{V_o}\right), \quad b_2 = -g'\left(\frac{V_{dLo}}{V_o}\right)$$

θ_o is the initial angle of the load bus voltage with respect to q axis. It is to be noted that, $b_1 \neq b_2$ and similarly $g_1 \neq g_2$. Hence Eq. (7.80) cannot be expressed as a single equation in phasors.

Representation of SVC

For a study of the low frequency behaviour of the system, it is not necessary to model the network transients. Similarly, the fast dynamics of SVC controller can be neglected and SVC represented by its steady state control characteristics. Only auxiliary control utilizing bus frequency or other signals need to be considered.

Neglecting auxiliary control, the control characteristics of SVC can be expressed as

$$\hat{I}_{SVC} = -j\left[\frac{V - V_{ref}}{k}\right]\frac{\hat{V}}{V} \tag{7.81}$$

where k is the slope of the control characteristics, $\hat{V}$ is the voltage phasor corresponding to the SVC bus. V is the magnitude of $\hat{V}$. Eq. (7.81) shows that I_{SVC} lags $\hat{V}$ by $90°$ if $V > V_{ref}$.

Eq. (7.81) can be expressed as

$$I_{qS} + jI_{dS} = -\frac{j}{k}\left[1 - \frac{V_{ref}}{V}\right](V_q + jV_d) \qquad (7.82)$$

Linearizing Eq. (7.82), we get

$$\Delta I_{qS} + j\Delta I_{dS} = -j\frac{I_{So}}{V_o}(\Delta V_q + j\Delta V_d) - \frac{jV_{ref}}{kV_o}(\cos\theta_o + j\,\sin\theta_o)\Delta V$$

This can be written as

$$\begin{bmatrix} \Delta I_{dS} \\ \Delta I_{qS} \end{bmatrix} = \begin{bmatrix} -B_S + b_S & g_S \\ g'_S & B_S - b'_S \end{bmatrix}\begin{bmatrix} \Delta V_q \\ \Delta V_d \end{bmatrix} \qquad (7.83)$$

$$= [Y_{SVC}]\begin{bmatrix} \Delta V_q \\ \Delta V_d \end{bmatrix}$$

where

$$B_S = \frac{I_{So}}{V_o}, \quad I_{So} = \frac{V_o - V_{ref}}{k}$$

$$b_S = -\frac{V_{ref}}{kV_o}\cos\theta_o\left(\frac{V_{qo}}{V_o}\right), \quad b'_S = -\frac{V_{ref}}{kV_o}\sin\theta_o\left(\frac{V_{do}}{V_o}\right)$$

$$g_S = -\frac{V_{ref}}{kV_o}\cos\theta_o\left(\frac{V_{do}}{V_o}\right), \quad g'_S = \frac{V_{ref}}{kV_o}\sin\theta_o\left(\frac{V_{qo}}{V_o}\right)$$

As $b_S \neq b'_S$ and $g_S \neq g'_S$, Eq. (7.83) cannot be reduced to a single phasor equation.

Derivation of Eq. (7.74) for system of Fig. 7.15

The Eq. (7.74) can be derived as follows. The generator armature current Δi_m can be expressed as

$$\Delta i_m = [Y_{SVC} + Y_L]\Delta V_3 + [Y_2][\Delta V_3 - \Delta V_2] \qquad (7.84)$$

where

$$\Delta V_3 = \begin{bmatrix} \Delta V_{q3} \\ \Delta V_{d3} \end{bmatrix}, \quad \Delta V_2 = \begin{bmatrix} -E_b\,\sin\delta_o \\ -E_b\,\cos\delta_o \end{bmatrix}\Delta\delta$$

$$[Y_2] = \begin{bmatrix} B_2 & G_2 \\ G_2 & -B_2 \end{bmatrix}$$

$$G_2 + jB_2 = \frac{1}{R_2 + jx_2}$$

Δv_m can be expressed as

$$\Delta v_m = [Z_1]\Delta i_m + \Delta V_3 \qquad (7.85)$$

where

$$[Z_1] = \begin{bmatrix} -x_1 & R_1 \\ R_1 & x_1 \end{bmatrix}$$

Eliminating ΔV_3 from Eq. (7.84), we get

$$\cdot\ \Delta V_3 = [Z']\Delta i_m + [Z'][Y_2]\Delta V_2 \qquad (7.86)$$

where

$$[Z'] = [Y_2 + Y_L + Y_{SVC}]^{-1}$$

Substituting (7.86) in (7.85) we can derive

$$\Delta V_m = [Z_1 + Z']\Delta i_m + [Z'][Y_2] \begin{bmatrix} -E_b \ \sin \delta_o \\ -E_b \ \cos \delta_o \end{bmatrix} \Delta \delta$$

From the above, the coefficients in Eq. (7.74) are easily derived.

Derivation of System Equations

The system equations are obtained by eliminating Δi_m and Δv_m from Eq. (7.71). Eqs. (7.73) and (7.74) are used to eliminate Δi_m and Δv_m. Δi_m can be expressed as

$$\Delta i_m = [F_i]x_g \qquad (7.87)$$

where

$$[F_i] = [Z_T]^{-1}\{[C_E] - [A]e_1\}$$

$$[Z_T] \quad = \quad [Z] + [Z_g]$$

$[C_E]$ and e_1 are defined from

$$\begin{bmatrix} \Delta E'_q \\ \Delta E'_d \end{bmatrix} = [C_E]x_g, \quad \Delta \delta = e_1 x_g$$

Substituting Eq. (7.87) in (7.74) we get

$$\Delta v_m = [F_v]x_g \qquad (7.88)$$

where

$$[F_v] = [Z][F_i] + [A]e_1$$

Substituting Eqs. (7.87) and (7.88) in Eq. (7.71) we get the system equation

$$\dot{x}_g = [A_T]x_g + [E_g]u_c \tag{7.89}$$

where

$$[A_T] = [A_g] + [B_{g1}][F_i] + [B_{g2}][F_v]$$

Example 7.9

A synchronous generator is connected to an infinite bus through a line of reactance ($x_e = 0.6$). At the midpoint of the line, a SVC is connected. The SVC is initially supplying no reactive power. The operating data is:
$E_b = V_t = 1.0$, $P_g = 1.0$.
Plot the loci of the critical eigenvalues as K_E is varied from 0 to 400 for the following cases (i) $k = 0.001$ (ii) $k = 0.1$
Assume $T_E = 0.05$sec. The machine data is same as that given in Example 7.1.

Solution

The initial conditions are calculated as $\hat{V}_t = 1.0\angle 36.87$, $I_a = 1.0541$,
$E_{qo} = 2.1686$, $\delta_o = 82.49$, $i_{do} = -0.9479$, $i_{qo} = 0.4611$, $v_{do} = -0.7148$,
$v_{qo} = 0.6994$.

The loci of the critical eigenvalue for the two cases are shown in Fig. 7.16. This also shows the case when SVC is not considered. The effect of SVC is to reduce the effective length of the line (or reduction of x_e) which results in the eigenvalue locus being shifted to the left.

Without SVC, the critical AVR gain (which results in instability) is around 8; with SVC, the critical gain is 17.0 with $k = 0.1$ and increases to 28.7 with $k = 0.001$. Thus voltage control at SVC is beneficial in reducing the negative damping due to AVR. However, the contribution of the voltage controller at SVC is limited. For improved system damping, additional (auxiliary) control loop has to be used with control signal derived from bus frequency or synthesized from voltage and current signals measured at SVC [12].

7.5   Nonlinear Oscillations - Hopf Bifurcation

The small signal stability analysis based on linearized system models indicates only whether the relevant equilibrium point (or operating point) is stable. It
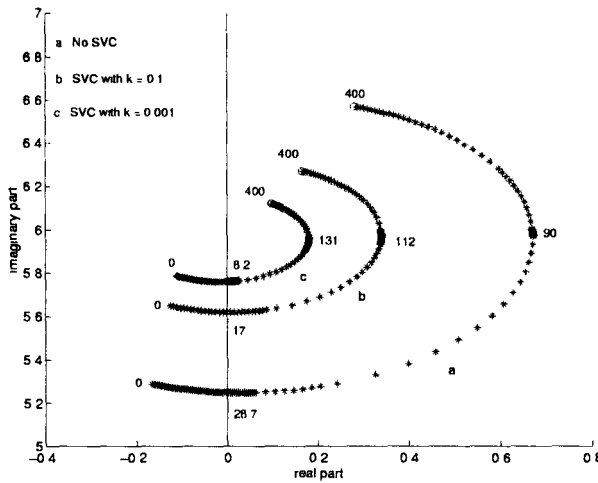
Figure 7.16: Loci of critical eigenvalue with variation in AVR gain (Example 7.9).

does not indicate whether there would be stable (persistent) oscillations if the equilibrium point is unstable. In practical systems, both stable (with finite amplitudes) or unstable (with growing amplitude) oscillations of power flow in transmission lines have been observed. In general, unstable oscillations (due to fast acting static exciters and high gain AVRs) are common. The increasing amplitude of oscillations can lead to loss of synchronism.

The existence of stable nonlinear oscillations is indicated by supercritical Hopf bifurcation [13, 14]. Given the nonlinear equations

$$\dot{x} = f(x, \mu) \tag{7.90}$$

The equilibrium point x_e is a function of μ. Hopf bifurcation is indicated if the linearized system has a complex pair of eigenvalues crossing imaginary axis at $\mu = \mu_o$. The stability of the oscillations is determined from Hopf bifurcation theorem [15]. If the oscillations are stable (stable limit cycle or periodic orbit), the Hopf bifurcation is said to be supercritical, otherwise subcritical. With static excitation systems, the Hopf bifurcation is mostly subcritical. However with high line resistance, the bifurcation could be supercritical. Persistent oscillations have been observed in such cases in the past and damper windingss designed to damp the oscillations.

The problem of oscillatory instability (which can lead to loss of synchronism) introduced by static excitation systems can be solved utilizing Power System Stabilizers (PSS). This is discussed in the next chapter.

References and Bibliography

1. F.P. DeMello and C. Concordia, "Concepts of synchronous machine stability as affected by excitation control", IEEE Trans. Vol. PAS-88, No. 4, 1969, pp. 316-329

2. D.N. Ewart and F.P. DeMello, "A digital computer program for the automatic determination of dynamic stability limits", IEEE Trans. Vol. PAS-86, No. 7, 1967, pp. 867-875

3. W.G. Heffron and R.A. Phillips, "Effects of modern amplidyne Voltage regulators on underexcited operation of large turbine generators", AIEE Trans. (Power Apparatus and Systems), Vol. 71, August 1952, pp. 692-697

4. M.K. El-Sherbiny and D.M. Mehta, "Dynamic system stability, Part I: Investigations of the effect of different loading and excitation systems", IEEE Trans. Vol. PAS-92, No. 5, 1973, pp. 1538-1546

5. F.P. DeMello, and T.F. Laskowski, "Concepts of power system dynamic stability", IEEE Trans. Vol. PAS-94, No. 3, 1975, pp. 827-833

6. M. Mauricio and S. Semlyen, "Effect of load characteristics on the dynamic stability of power systems", IEEE Trans. Vol. PAS-91, pp. 2295-2304

7. D.P. Sen Gupta, N.G. Narahari and J.W. Lynn, "Damping and synchronizing torques contributed by a Voltage regulator to a synchronous generator: A quantitative assessment", Proc. IEE (London),. Vol. 1972, p. 124

8. F.R. Schlief et al,"Excitation control to improve power line stability", IEEE Trans. Vol. PAS-87, June 1968, pp. 1426-1434

9. C.A. Nickle and C.A. Pierce, "Stability of synchronous machines: Effect of armature circuit resistance", AIEE Trans. Vol.49, Jan. 1930, pp. 338-350

10. C. Concordia,"Steady-state stability of synchronous machines as affected by Voltage regulator characteristics", AIEE Trans. Vol. 63, May 1944, pp. 215-220

11. A. Verghese, P.W. Sauer and M.A. Pai, "Synchronous machine block diagram analysis with fast dynamics", Int. J. of Elec. Power & Energy Systems, Vol. 11, No. 4, 1989, pp. 239-247

12. K.R. Padiyar and R.K. Varma, "Damping torque analysis of static VAR system controllers", IEEE Trans. on Power Systems, Vol. 6, No. 2, 1991, pp. 458-465

13. E.H. Abed and P. Varaiya,"Nonlinear oscillations in power systems", Int. J. of Elec. Power & Energy Syst. Vol. 6, Jan 1984, pp. 37-43

14. J.C. Alexander, "Oscillatory solutions of a model system of nonlinear swing equations", Int. J. of Elec. Power & Energy Syst., Vol.8, No. 3, 1986, pp. 130-136

15. B.D. Hassard,N.D. Kazarinoff and Y.H. Wau, **Theory and Applications of Hopf Bifurcation**, Cambridge University Press, 1981

"This page is Intentionally Left Blank"

Chapter 8

Application of Power System Stabilizers

8.1 Introduction

High performance excitation systems are essential for maintaining steady state and transient stability of modern synchronous generators, apart from providing fast control of the terminal voltage. Bus fed static exciters with thyristor controllers are increasingly used for both hydraulic and thermal units [1, 2]. They are characterized by high initial response and increased reliability due to advances in thyristor controllers. The block diagram of a typical static exciter is shown in Fig.8.1. The time constant T_A of the regulator is negligble. The other time constant T_R, in the range of 0.01 to 0.02 sec, is necessary for filtering of the rectified terminal voltage waveform.

The other time constants associated with the exciter are negligible and the voltage regulator and the exciter can be modelled as a gain in series with an optional block of Transient Gain Reduction (TGR). The role of TGR is primarily to provide satisfactory operation on open circuit [3]. The Automatic Voltage Regulator (AVR) gain is typically around 200 pu/pu. The exciter ceiling is typically 8.0 pu. These parameters permit the exciter to reach 90% of the ceiling voltage (from the rated-load field voltage) within 25 ms for a sustained drop in the terminal voltage not exceeding 5%.

It is well established that fast acting exciters with high gain AVR can contribute to oscillatory instability in power systems. This type of instability is characterized by low frequency (0.2 to 2.0 Hz) oscillations which can persist (or even grow in magnitude) for no apparent reason (see Fig. 8.2). There are several instances of such occurrences which have been recorded and studied [4, 5, 6, 7]. This type of instability can endanger system security and limit power transfer. The major factors that contribute to the instability are

(a) loading of the generator or tie line
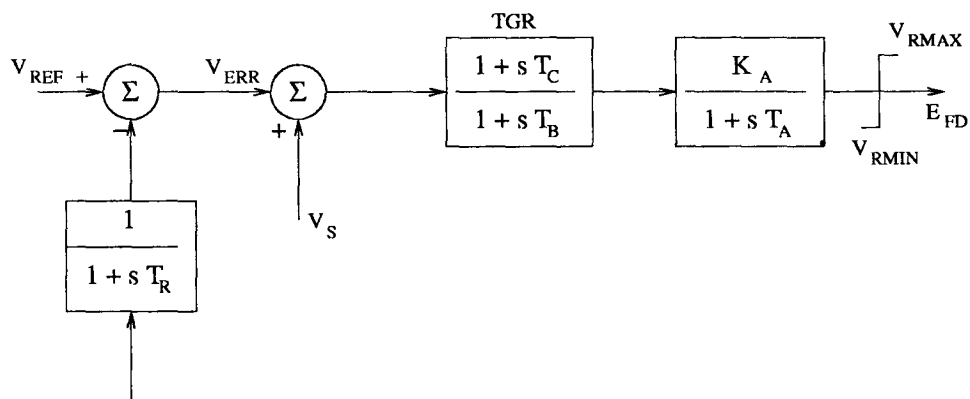
(b) power transfer capability of transmission lines
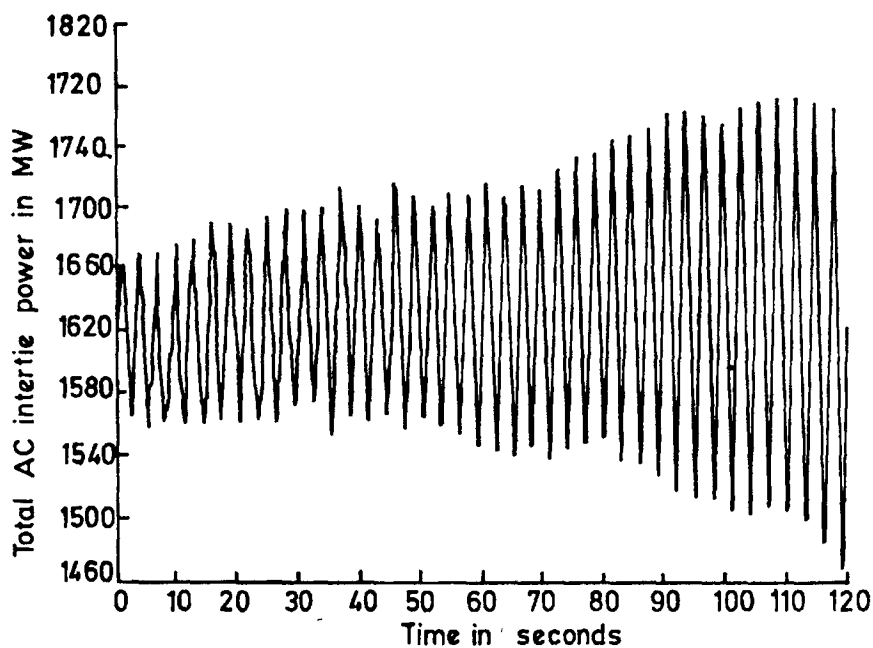
Figure 8.1: Block diagram of static exciter

Figure 8.2: Oscillatory instability [22]

(c) power factor of the generator (leading power factor operation is more problematic than lagging power factor operation)

(d) AVR gain.

A cost efficient and satisfactory solution to the problem of oscillatory instability is to provide damping for generator rotor oscillations. This is conveniently done by providing Power System Stabilizers (PSS) which are supplementary controllers in the excitation systems. The signal V_s in Fig. 8.1 is the output from PSS which has input signal derived from rotor velocity, frequency, electrical power or a combination of these variables. The objective of designing PSS is to provide additional damping torque without affecting the synchronizing torque at critical oscillation frequencies [3].

PSS have been used for over 20 years in Western systems of United States of America and in Ontario Hydro. In United Kingdom, PSS have been used in Scotland to damp oscillations in tie lines connecting Scotland and England [8]. It can be generally said that need for PSS will be felt in situations when power has to be transmitted over long distances with weak AC ties. Even when PSS may not be required under normal operating conditions, they allow satisfactory operation under unusual or abnormal conditions which may be encountered at times. Thus, PSS has become a standard option with modern static exciters and it is essential for power engineers to use these effectively. Retrofitting of existing excitation systems with PSS may also be required to improve system stability.

This chapter presents the various aspects for the application of PSS with emphasis on the tuning procedures. The coverage includes not only on the current practices but also on recent developments and future trends. The stabilization through SVC and HVDC controllers are also discussed.

8.2 Basic concepts in applying PSS

A brief review of the basic concepts of stabilization is undertaken here. The power system, in general, is described by a set of nonlinear differential and algebraic equations. These can be expressed as

$$pX = F(X, Z), \quad p = \frac{d}{dt} \tag{8.1}$$

$$Y = H(X, Z) \tag{8.2}$$

$$0 = G(Y, Z) \tag{8.3}$$

The oscillatory instability can be viewed as stability of the operating point, subjected to small, random perturbations which are always present. The analysis

can be performed by linearizing the system equations around the operating point $(X = X_o, Y = Y_o, Z = Z_o)$. Here X are the state variables, Y represent active and reactive power injections (at buses), Z represent voltage magnitudes and angles at various buses.

Expressing

$$X = X_o + \Delta X, \quad Y = Y_o + \Delta Y, \quad Z = Z_o + \Delta Z. \tag{8.4}$$

it is possible to obtain the following equation

$$p\Delta X = [A]\Delta X \tag{8.5}$$

where

$$[A] = \left[\frac{\partial F}{\partial X} - \frac{\partial F}{\partial Z} \left(\frac{\partial G}{\partial Y} \frac{\partial H}{\partial Z} + \frac{\partial G}{\partial Z} \right)^{-1} \frac{\partial G}{\partial Y} \frac{\partial H}{\partial X} \right] \tag{8.6}$$

It is to be noted that the elements of A are functions of the operating point.

The stability of the operating point can be judged by the location of the eigenvalues of the matrix A. If all the real parts of the eigenvalues are negative, the system is stable. If one or more has positive real part, then the system is unstable. While this criterion of stability is valid for very small perturbations (which may not be true in practice), it is interesting to note that several analytical studies [5, 6, 7] show excellent correlation between theory and field tests. The criterion indicates problem areas but cannot provide estimates for amplitudes of the oscillation observed.

To give more insight into the problem, we can take up a multi-machine system where generators are modelled by the 'classical' model, neglecting flux decay, saliency, damper windings and governor effects. In this case, the linearized system equations can be written as

$$[M]p^2\Delta\delta = -[K]\Delta\delta \tag{8.7}$$

where $[M]$ is diagonal matrix with $M_{jj} = \frac{2H_j}{\omega_B}$ (H_j is the inertia constant of jth synchronous machine). $K_{ij} = \partial P_{ei}/\partial\delta_j$, where P_{ei} is the power output of ith machine, δ_j is the rotor angle of jth machine referred to a rotating reference frame (with the operating speed ω_o). If the network can be reduced by retaining only the internal buses of the generators and the losses in the reduced network can be neglected,

$$K_{ij} = \frac{E_i E_j}{X_{ij}} \cos(\delta_i - \delta_j) \simeq \frac{1}{X_{ij}} \tag{8.8}$$

where X_{ij} is the reactance of the element connecting the generator buses i and j. E_i and E_j are the generator voltages. The approximation assumes that the voltages are around 1.0 pu. and the bus angle difference (in steady-state) are small. The matrix $[K]$ is singular and has rank $\leq (m-1)$ where m is the size of K (also equal to the number of generators). This enables the reduction of the number of angle variables by one by treating relative angles (with respect to a reference machine which can be chosen as the first machine) as state variables.

The solution of equation (8.7) can, in general, be expressed as

$$\Delta\delta^R = \sum_{j=1}^{m-1} V_j(c_j \cos \omega_j t + d_j \sin \omega_j t) \tag{8.9}$$

where $\Delta\delta^R = [\Delta\delta_{21} \quad \Delta\delta_{31}.....\Delta\delta_{m1}]^t$ is the vector of relative angles ($\Delta\delta_{i1}$ $= \Delta\delta_i - \Delta\delta_1$), $c_1,\ldots, c_{m-1}, d_1, d_2,\ldots, d_{m-1}$ are scalars depending on the initial conditions, V_1, V_{m-1} are vectors. The structure of a vector V_j depicts the participation of various machines in the oscillation mode whose frequency is ω_j. It is to be noted that for a 'm' machine system, there are $(m-1)$ oscillatory modes whose frequency varies in the range of (0.2 to 3 Hz). The frequencies are obtained as square roots of the non-zero and real eigenvalues of the matrix $[M]^{-1}[K]$.

In a practical system, the various modes (of oscillation) can be grouped into 3 broad categories [9].

A. Intra-plant modes in which only the generators in a power plant participate. The oscillation frequencies are generally high in the range of 1.5 to 3.0 Hz.

B. Local modes in which several generators in an area participate. The frequencies of oscillations are in the range of 0.8 to 1.8 Hz.

C. Inter area modes in which generators over an extensive area participate. The oscillation frequencies are low and in the range of 0.2 to 0.5 Hz.

The above categorization can be illustrated with the help of a system consisting of two areas connected by a weak AC tie (see Fig. 8.3). Area 2 is represented by a single generator G_4. The area 1 contains 3 generators G_1, G_2, and G_3. The generators G_1 and G_2 are connected in parallel and participate in the intra-plant oscillations which have higher frequency due to the lower reactance between the two machines and also smaller inertias. In local mode oscillation, G_1 and G_2 swing together and against G_3. In oscillations due to inter area mode, all generators G_1 to G_4 participate and have the lowest frequency.
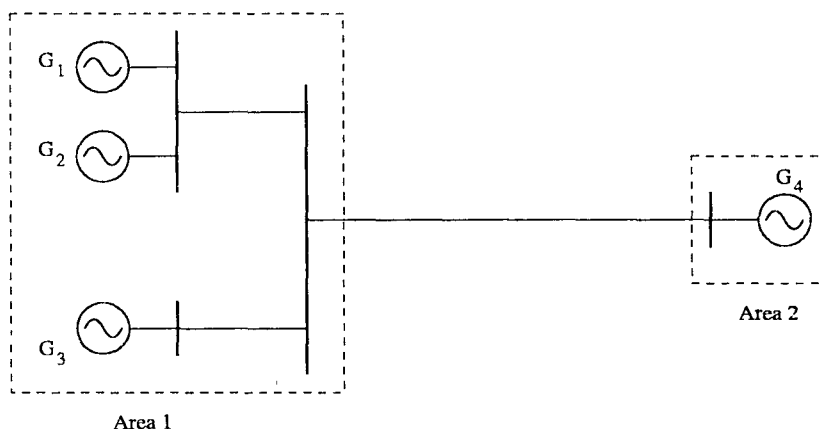
Figure 8.3: A sample power system

It is to be noted that the distinction between local modes and inter area modes applies mainly for those systems which can be divided into distinct areas which are separated by long distances. For systems in which the generating stations are distributed uniformly over a geographic area, it would be difficult to distinguish between local and inter area modes from physical considerations. However, a common observation is that the inter area modes have the lowest frequency and highest participation from the generators in the system spread over a wide geographic area.

The PSS are designed mainly to stabilize local and inter area modes. However, care must be taken to avoid unfavourable interaction with intra-plant modes [10] or introduce new modes which can become unstable.

Depending on the system configuration, the objective of PSS can differ. In Western U.S.A, PSS are mainly used to damp inter area modes without jeopardizing the stability of local modes. In other systems such as Ontario Hydro, the local modes were the major concern. In general, however, PSS must be designed to damp both types of modes. The procedures for tuning of PSS depend on the type of applications.

If the local mode of oscillation is of major concern (particularly for the case of a generating station transmitting power over long distances to a load centre) the analysis of the problem can be simplified by considering the model of a single machine (the generating station is represented by an equivalent machine) connected to an infinite bus (SMIB). With a simplified machine model (1.0), and the excitation system, the analysis can be carried out using the block diagram representation given in Chapter 7. The instability arises due to the negative

damping torque caused by fast acting exciter under operating conditions that lead to $K_5 < 0$. The objective of PSS is to introduce additional damping torque without affecting the synchronizing torque.

8.3 Control Signals

The obvious control signal (to be used as input to the PSS) is the deviation in the rotor velocity. However, for practical implementation, other signals such as bus frequency [11], electrical power [9], accelerating power [12, 13] are also used. The latter signal is actually synthesized by a combination of electrical and mechanical power signals. The mechanical power signal can be obtained from the gate position in a hydraulic turbine or steam pressures in steam turbine. Nevertheless, it is difficult to measure mechanical power. It can be argued that if mechanical power variations are slow, then a signal derived from the electrical power approximates accelerating power. However, this can pose problem during rapid increases of generation for which PSS action leads to depression in the voltage, endangering security.

A recent development is to synthesize accelerating power signal from speed and electrical power signals. This is shown in Fig. 8.4 [13]. A similar approach is used at Ontario Hydro and the PSS utilizing these signals are termed as Delta-P-Omega stabilizers [14]. It is claimed that the new control signal has eliminated the problem of torsional interactions and improved reliability.
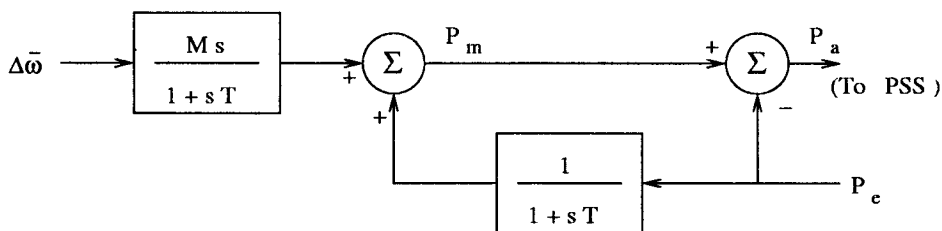

Figure 8.4: Synthesis of accelerating power signal

The choice of control signal for PSS can be based on the following criteria

(a) The signal must be obtained from local measurements and easily synthesized.

(b) The noise content of the signal must be minimal. Otherwise complicated filters are required which can introduce their own problems.

(c) The PSS design based on a particular signal must be robust and reject noise. This implies that lead compensation must be kept to a minimum to avoid amplifying the noise.

All the control signals considered- rotor speed, frequency, electrical power are locally available. The speed signal can be obtained from a transducer using a tooth wheel mounted on the shaft. Alternately it can be obtained from the angle of the internal voltage which can be synthesized. The bus frequency signal can be obtained by measuring the period using zero crossing detection. The power signal can be derived from a Hall effect transducer.

The speed signal is inherently sensitive to the presence of torsional oscillations at frequencies in the range of 8 to 20 Hz. This can lead to negative damping of the torsional mode [15]. An initial solution to this problem was ingenious - to relocate the speed pick up at the node of the first torsional frequency. However, this was not a general solution (for example in 4 pole nuclear units in Ontario Hydro, the node of the first torsional mode of oscillation is located inside the turbine casing and hence inaccessible). A practical solution is to provide a torsional filter tuned to the frequency of the critical mode. However, this filter introduces another mode of oscillation, the damping of which reduces with increasing stabilizer gain [16].

Speed signal can also lead to negative damping of intra-plant modes if the PSS is not properly designed. In reference [10], the average speed instead of individual speed is suggested as a suitable control signal in a plant whenever more than one unit operate.

The frequency signal is insensitive to intra-plant modes and hence there is no danger of destabilising intra-plant modes. The frequency signal is also less sensitive to torsional frequency components. However, the frequency signal is prone to noise caused by nearby loads such as arc furnaces [6, 10].

The acceleration signal (based on accelerating power) results in minimum lead compensation requirements. The signal is also insensitive to torsional modes. Both these factors imply that torsional filters may be dispensed with completely or their design simplified.

8.4   Structure and tuning of PSS

The block diagram of the PSS used in industry is shown in Fig. 8.5. It consists of a washout circuit, dynamic compensator, torsional filter and limiter. The function of each of the components of PSS with guidelines for the selection of parameters (tuning) are given next.
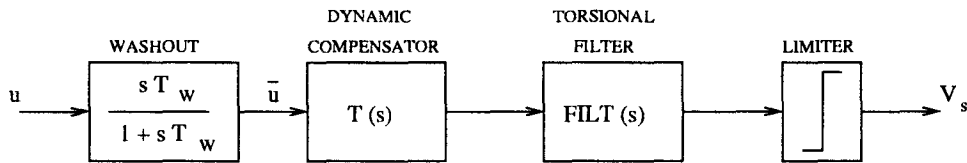
Figure 8.5: Block diagram of PSS

It is to be noted that the major objective of providing PSS is to increase the power transfer in the network, which would otherwise be limited by oscillatory instability. The PSS must also function properly when the system is subjected to large disturbances.

8.4.1   Washout Circuit

The washout circuit is provided to eliminate steady-state bias in the output of PSS which will modify the generator terminal voltage. The PSS is expected to respond only to transient variations in the input signal (say rotor speed) and not to the dc offsets in the signal. This is achieved by subtracting from it the low frequency components of the signal obtained by passing the signal through a low pass filter (see Fig. 8.6).
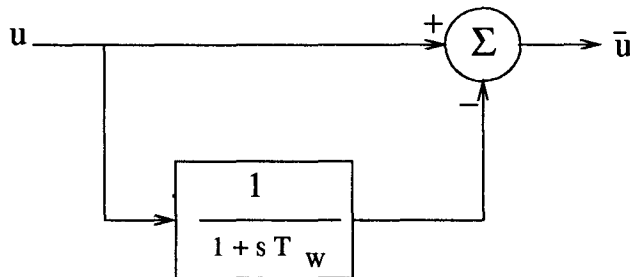
Figure 8.6: Washout circuit

The washout circuit acts essentially as a high pass filter and it must pass all frequencies that are of interest. If only the local modes are of interest, the time constant T_W can be chosen in the range of 1 to 2. However, if inter area modes are also to be damped, then T_W must be chosen in the range of 10 to 20. A recent study [1] has shown that a value of $T_W = 10$ is necessary to improve damping of the inter area modes. There is also a noticeable improvement in the first swing stability when T_W is increased from 1.5 to 10. The higher value of T_W also improved the overall terminal voltage response during system islanding conditions.

8.4.2   Dynamic Compensator

The dynamic compensator used in industry is made up to two lead-lag stages and has the following transfer function

$$T(s) = \frac{K_s(1 + sT_1)(1 + sT_3)}{(1 + sT_2)(1 + sT_4)} \qquad (8.10)$$

where K_s is the gain of PSS and the time constants, T_1 to T_4 are chosen to provide a phase lead for the input signal in the range of frequencies that are of interest (0.1 to 3.0 Hz). With static exciters, only one lead-lag stage may be adequate. In general, the dynamic compensator can be chosen with the following transfer function

$$T(s) = \frac{K_s N(s)}{D(s)} \qquad (8.11)$$

where

$$
\begin{aligned}
N(s) &= 1 + a_1 s + a_2 s^2 + \dots a_p s^p \\
D(s) &= 1 + b_1 s + b_2 s^2 + \dots b_p s^p
\end{aligned}
$$

The zeros of $D(s)$ should lie in the left half plane. They can be complex or real. Some of the zeros of $N(s)$ can lie in the right half plane making it a non-minimum phase.

For design purposes, the PSS transfer function is approximated to $T(s)$, the transfer function of the dynamic compensator. The effect of the washout circuit and torsional filter may be neglected in the design but must be considered in evaluating performance of PSS under various operating conditions.

There are two design criteria.

1. The time constants, T_1 to T_4 in equation (8.10) are to be chosen from the requirements of the phase compensation to achieve damping torque

2. The gain of PSS is to be chosen to provide adequate damping of all critical modes under various operating conditions. It is to be noted that PSS is tuned at a particular operating condition (full load conditions with strong or weak AC system) which is most critical. Although PSS may be tuned to give optimum damping under such condition, the performance will not be optimal under other conditions. The critical modes include not only local and inter area modes, but other modes (termed as control or exciter modes) introduced by exciter and/or torsional filter.

The basis for the choice of the time constants of the dynamic compensator can be explained with reference to the block diagram of the single machine

System without PSS
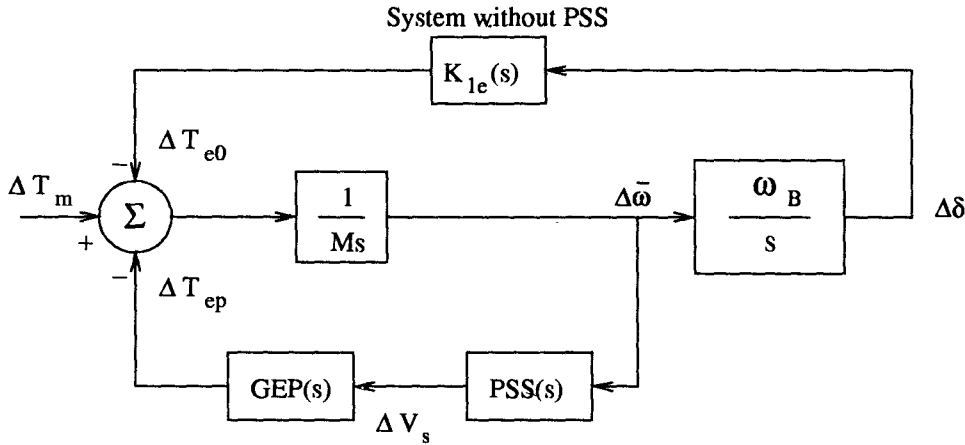
Figure 8.7: Stabilizer with speed input: system block diagram

system when PSS is included (see Fig. 8.7). If PSS is to provide pure damping torque at all frequencies, ideally the phase characteristics of PSS must balance the phase characteristics of GEP at all frequencies. As this is not practical, the following criteria are chosen to design the phase compensation for PSS.

(a) The compensated phase lag (phase of P(s) = GEP(s) PSS(s)) should pass through 90° at frequency around 3.5 Hz (For frequency input signal this can be reduced to 2.0 Hz).

(b) The compensated phase lag at local mode frequency should be below 45°, preferably near 20°

(c) The gain of the compensator at high frequencies (this is proportional to $T_1 T_3/T_2 T_4$) should be minimized.

The first criterion is important to avoid destabilization of intra-plant modes with higher frequencies. It is also preferable to have the compensated phase to be lagging at inter area modes so that PSS provides some synchronizing torque at these frequencies. The time constant of the washout circuit can also affect the compensated phase lag. The third criterion is required to minimize the noise amplification through PSS.

The plots of the phase angle ϕ of the compensator of Eq. (8.10), with variation in frequency are shown in Fig. 8.8 for different values of the centre frequency f_c defined by

$$f_c = \frac{1}{2\pi} \frac{1}{\sqrt{T_1 T_2}} \qquad (8.12)$$

It is assumed that

$$\frac{T_1}{T_2} = \frac{T_3}{T_4} = n$$

The plots of Fig. 8.8 (a) are obtained for $n = 10$. Fig. 8.8 (b) shows similar plots, but for $n = 2$. Since the two lead-lag stages are assumed to be identical, the phase angle ϕ is twice that for a single stage. The figure 8.8 shows the phase angle $(\frac{\phi}{2})$ corresponding to a single stage.

(a) $n = 10$ (b) $n = 2$
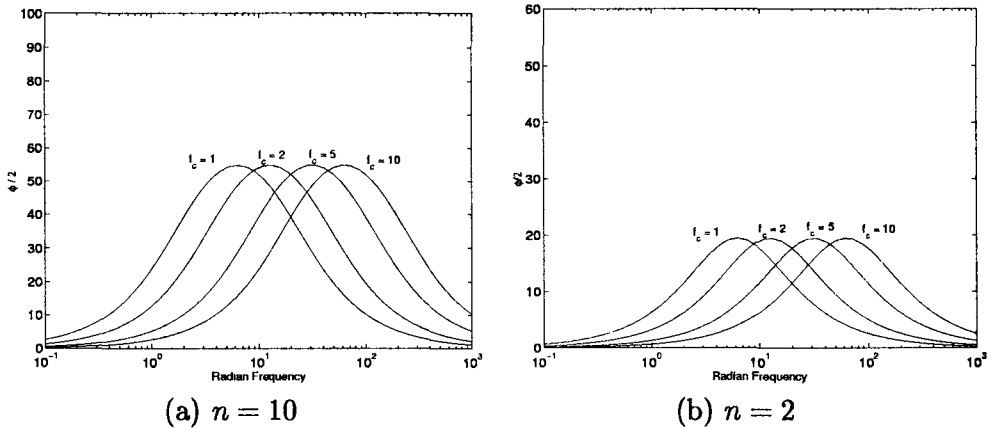
Figure 8.8: Variation of phase angle of compensator

The results given in Fig. 8.8 show that the peak value of the phase lead provided by the compensator occurs at the centre frequency (f_c). Also, increasing n increases the phase lead. Depending on the phase compensation required, f_c and n can be selected. A single stage of lead-lag network is adequate whenever the requirements of the phase lead are moderate.

The determination of the 'plant' transfer function can be done analytically or experimentally from field tests. In the former case, GEP(s) can be obtained from the fact that

$$GEP(s) = \frac{\Delta T_e}{\Delta V_s}\bigg|_{\Delta\bar{\omega} = 0} \tag{8.13}$$

where V_s is the output of the PSS. The condition $\Delta\bar{\omega} = 0$, can be enforced by selecting arbitrarily very high values of inertias and calculating the frequency response over a range of frequencies. There are computer programs to compute eigenvalues or frequency response for a large system [17-19].
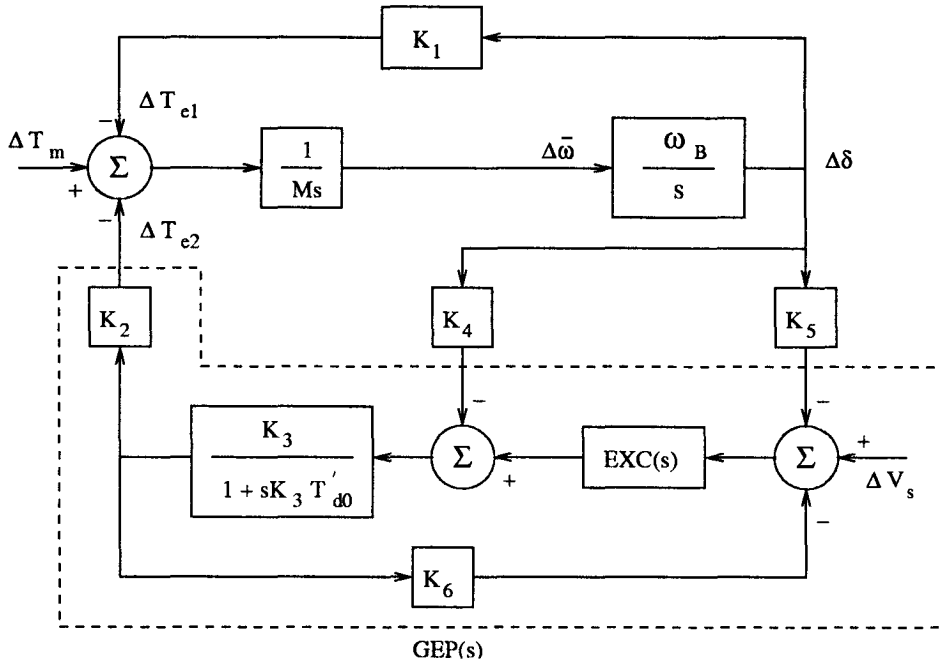
Figure 8.9: Simplified model of SMIB system

For a SMIB system with machine model (1.0), GEP(s) can be determined from the block diagram shown in Fig. 8.9. From this, GEP(s) is obtained as

$$GEP(s) = \frac{K_2 K_3 EXC(s)}{(1 + sT'_{do}K_3) + K_3 K_6 EXC(s)} \tag{8.14}$$

where $EXC(s)$ is the transfer function of the excitation system.

The transfer function GEP(s) cannot be determined exactly from the field tests as the rotor velocity variations can never be avoided in practice. However, it is shown below that GEP(s) can be determined from the following approximate relationship

$$GEP(s) \simeq \frac{K_2}{K_6} \frac{\Delta V_t(s)}{\Delta V_s(s)} \tag{8.15}$$

By measuring the transfer function between the terminal voltage and stabilizer output (V_s) it is possible to experimentally determine the phase characteristics of the plant.

Derivation of Eq. 8.15
The simplified model of the SMIB (single machine infinite bus) without PSS can
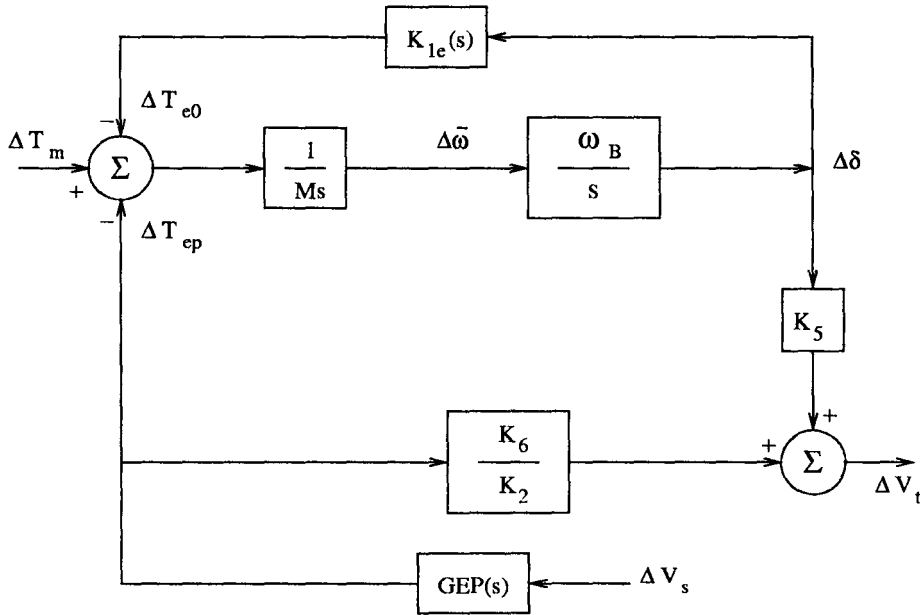
Figure 8.10: Simplified model of SMIB system without PSS

be obtained as shown in Fig. 8.10. From this figure, the transfer function from V_s to V_t can be obtained as

$$\frac{\Delta V_t}{\Delta V_s}(s) = GEP(s) \left[\frac{K_6}{K_2} - \frac{K_5 \omega_B}{Ms^2 + \omega_B K_{1e}(s)} \right] \qquad (8.16)$$

where $M = 2H$

K_{1e} is the effective complex synchronizing torque

If K_5 is zero, then

$$GEP(s) = \frac{K_2}{K_6} \frac{\Delta V_t(s)}{\Delta V_s(s)}$$

K_5 represents the effect of the rotor angle changes in terminal voltage which has the following characteristics.

1. With no load on the generator, K_5 is positive and approaches zero as the transmission system becomes weaker.

2. Under load, K_5 is positive for strong systems but passes through zero and becomes negative as the system becomes weak.

Hence K_5 can be assumed to be zero and the approximation of GEP(s) by R.H.S. of equation (8.15) is valid.

The comparison between the exact and the approximate computation of GEP(s) is shown in Fig. 8.11 for a representative system.
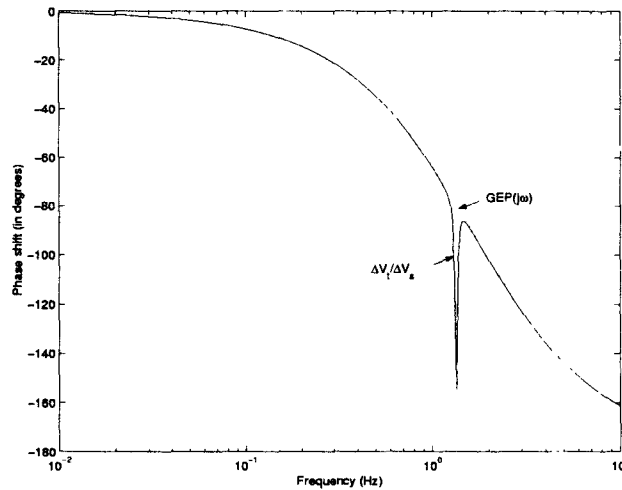
(a) Strong System
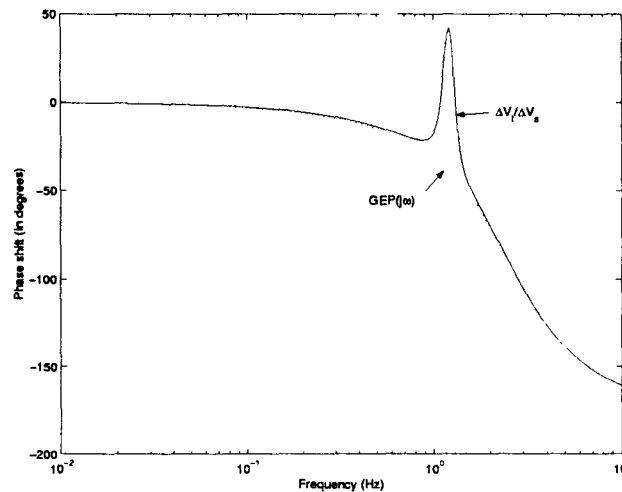
(b) Weak System

Figure 8.11: Phase characteristics of measurable and ideal plant transfer functions
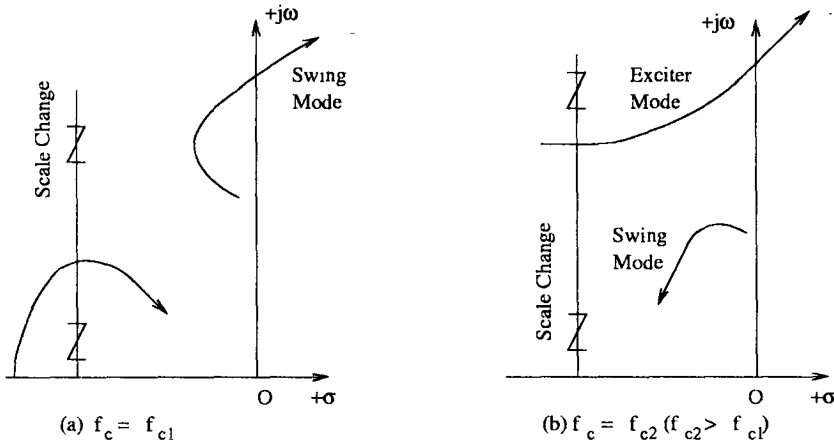
Figure 8.12: Root loci with variation in stabiliser gain

Once GEP(s) is determined, the PSS time constants are adjusted (by trial and error) such that the criteria given earlier are satisfied. The performance of the PSS can also be checked by root locus plots. See Fig. 8.12 for an example. The root loci with variation in stabilizer gain are drawn for two different values of f_c and for a fixed value of the ratio n. In addition to f_c, it is possible to vary the ratio of T_1/T_2 and T_3/T_4 independently to get a better performance. It is observed that either the local mode or the other mode (called the exciter mode irrespective of its source) gets destabilized as the PSS gain K_s is increased.

The studies carried out by Larsen and Swann [9] indicate that depending upon the input signal used, PSS is to be tuned for a particular system condition which has the highest stabilizer loop gain and greatest phase lag. Full load on the generator yields the highest loop gain. For speed and power input stabilizers, the strongest AC system results in the highest loop gain and greatest phase lag. For frequency input stabilizers, the highest loop gain occurs with weakest AC transmission system.

To set the gain of the PSS, root locus analysis is performed. The optimal PSS gain is chosen for the particular tuning condition as the gain that results in the maximum damping of the least damped mode. From studies carried out in [9], the optimum gain (K_{opt}) is related to the value of the gain (K_I) that results in instability. For speed input stabilizers $K_{opt} = 1/3K_I$, for frequency input stabilizers $K_{opt} = 2/3K_I$. For power input stabilizers $K_{opt} = 1/8K_I$. These thumb rules are useful while implementing PSS in the field without having to do root locus studies.

It is to be noted that for input signals other than rotor speed, the block diagram shown in Fig. 8.7 is not valid. In such cases, the diagram is as given in Fig. 8.13, where X is an arbitrarily chosen control (input) signal. $S_X(s)$ is defined as the input signal sensitivity factor and $FB_X(s)$ is defined as the input signal feedback factor. For power input stabilizer,

$$S_p(s) \simeq \frac{\omega_B K_{1e}(s)}{s} \tag{8.17}$$
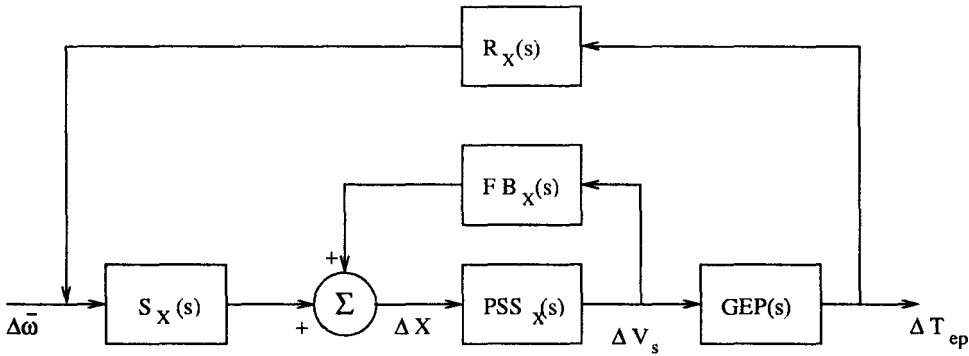
Figure 8.13: Stabilizer loop with arbitrary input X

$$FB_p(s) = GEP(s) \tag{8.18}$$

For the general case, the plant transfer function in the stabilizer path is given by

$$P_X(s) = \frac{\Delta T_{ep}}{\Delta \bar{\omega}}(s) = \frac{S_X(s)PSS_X(s)GEP(s)}{1 - FB_X(s)PSS_X(s)} \tag{8.19}$$

For speed input stabilizer, $S_X = 1.0$, $FB_X = 0$. Hence

$$P_\omega(s) = PSS_\omega(s)GEP(s) \tag{8.20}$$

To summarize, the tuning procedure for the dynamic compensator, the following steps are carried out.

1. Identify the plant GEP(s)

2. Choose the time constants from the phase compensation technique described earlier and from the knowledge of GEP(s).

3. Select the PSS gain such that it is a fraction of the gain corresponding to instability. This can be determined from root loci to maximize the damping of the critical (least damped) mode.

8.4.3   Torsional Filter

The torsional filter in the PSS is essentially a band reject or a low pass filter to attenuate the first torsional mode frequency. The transfer function of the filter can be expressed as

$$FILT(s) = \frac{\omega_n^2}{s^2 + 2\zeta\omega_n s + \omega_n^2} \tag{8.21}$$

For stabilizers derived from accelerating power, torsional filter can have a simple configuration of a low pass filter independent of the frequency of the torsional mode to be filtered out.

Torsional filter is necessitated by the adverse interaction of PSS with the torsional oscillations. This can lead to shaft damage, particularly at light generator loads when the inherent mechanical damping is small. Even if shaft damage does not occur, stabilizer output can go into saturation (due to torsional frequency components) making it ineffective. The criteria for designing of the torsional filter are:

1. The maximum possible change in damping of any torsional mode is less than some fraction of the inherent torsional damping.

2. The phase lag of the filter in the frequency range of 1 to 3 Hz is minimized.

8.4.4   Limiter

The output of the PSS must be limited to prevent the PSS acting to counter the action of AVR. For example, when load rejection takes place, the AVR acts to reduce the terminal voltage when PSS action calls for higher value of the terminal voltage (due to the increase in speed or frequency). It may even be desirable to trip the PSS in case of load rejection.

The negative limit of PSS output is of importance during the back swing of the rotor (after initial acceleration is over). The AVR action is required to maintain the voltage (and thus prevent loss of synchronism) after the angular separation has increased. PSS action in the negative direction must be curtailed more than in the positive direction. Ontario Hydro uses a -0.05 pu. as the lower limit and 0.1 to 0.2 as the higher limit. Recent studies have shown [1] that higher negative limit can impair first swing stability.

It is of interest to note that discontinuous excitation control is employed at Ontario Hydro in order to improve transient stability [2]. This control termed as Transient Stability Excitation Control (TSEC) operates using a signal derived

from the rotor angle and augments the PSS output. The operation is permitted only if the following conditions are satisfied simultaneously

(a) a drop in the terminal voltage in excess of the preset value

(b) field voltage is at positive ceiling

(c) rise in speed above a preset value.

The effect of TSEC is to maintain the maximum permissible terminal voltage over the entire positive swing of the rotor angle. However, the angle signal is used only during the transient period of about 2 seconds following a severe disturbance. The operation of TSEC is discontinued when either the speed drops below a threshold value or the exciter comes out of saturation. The output of the TSEC is allowed to decay exponentially. The reason for discontinuous control arises from the fact that the continuous use of the angle signal is deleterious to steady state stability.

8.5 Field implementation and operating experience

The tuning of power system stabilizer can be performed using extensive analytical studies covering various aspects. While such studies are useful in optimizing the performance of PSS, satisfactory operation of PSS can be obtained by tuning the PSS using field test results as described below [9,20].

1. Measure the open loop frequency response without PSS. This involves obtaining the transfer function between the terminal voltage and the AVR input (V_s) in frequency domain. As described earlier, the transfer function is approximately related to GEP(s).

2. Select PSS time constants by trial and error such that desired phase compensation is obtained. The guidelines for selecting the phase compensation are:

   (a) Check that the compensated system (GEP(s) PSS(s)) has some phase lag at inter area modes

   (b) Verify the stabilizer time constant settings by field test which involves determination of points on a root locus. The local mode oscillations are stimulated by step changes to AVR reference, line switching or low level sinusoidal modulation (at local mode frequency) of the voltage reference. The effect of the PSS can be measured by comparing the damping with zero PSS gain and few low values of the gain which

cause a noticeable change. The waveform recorded can give information on the frequency and damping ratio.

Modern test equipment such as HP 5423A Structural Dynamic Analysis (SDA) which use random noise signals and microprocessor based instrumentation help in simplifying the measurements and reducing the burden on the operator [20].

3. Perform the gain margin test. This consists of slowly increasing the stabilizer gain until instability is observed which is characterized by growing oscillations at a frequency greater than the local mode. The oscillation can be monitored from PSS output. Once instability is detected the stabilizer is switched out of service. Reduction of stabilizer output limits during the test will ensure that safe operation of the generator is maintained.

During the gain margin test, torsional oscillations should be monitored to check that the torsional filter is giving satisfactory performance.

4. The PSS gain can now be set to a lower value and a fraction of the instability gain. Typically the gain is set to 1/3 of the instability gain (for speed input stabilizers).

Operating Experience with PSS

The early operating experience with speed input stabilizers showed the need for torsional filtering to eliminate unfavourable interactions at torsional frequencies. Also, improper design can lead to destabilization of intra-plant modes. The frequency input stabilizers are susceptible to noise generated by arc furnace loads located close to the power stations.

The presence of the torsional filter can introduce additional control (or so called exciter) mode whose damping reduces as stabilizer gain is increased [16]. Replacing speed signal by synthesized accelerating power signal [2] can help overcome this problem.

The overall performance of properly tuned stabilizers is excellent. Ontario Hydro statistics [2] showed a mean time to failure of about 5.7 years in 107 stabilizer years of operation. Built-in protection features have mitigated the consequences of stabilizer failure in recent years. Dynamic test facilities incorporated into the stabilizers permit routine testing.

8.6 Examples of PSS Design and Application

Example 8.1

The system data is taken from Example 7.1 given in chapter 7. The system consists of a single machine connected to an external impedance of $0 + j0.4$. The generator is initially supplying power of 1 pu with terminal voltage at 1.0 pu. The infinite bus voltage is $1.0\angle 0.0^o$. A static exciter with a single time constant AVR is considered ($K_E = 200, T_E = 0.05$). Design a speed input PSS at this operating condition.

Solution

The phase angle of GEP $(j\omega)$ as a function of ω is shown in Fig. 8.14. The phase angle decreases as frequency increases. At the rotor oscillation frequency of about 7 rad/sec, the phase lag is 35°. At the cut off frequency of 3.5 Hz (22 rad/sec), the phase lag is around 120°.
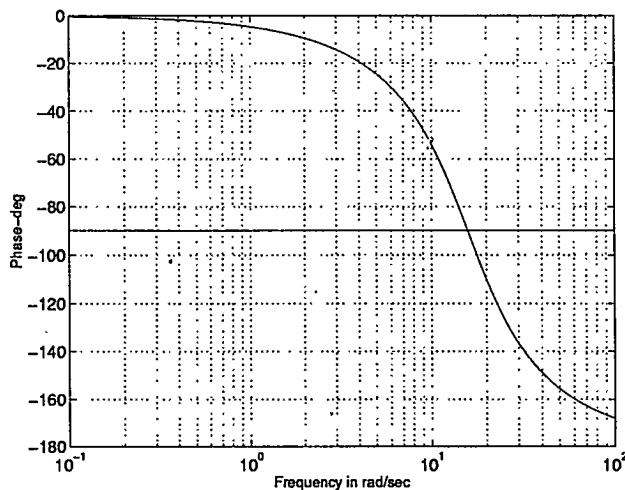
Figure 8.14: Phase angle of GEP$(j\omega)$

A compensator transfer function

$$T(s) = \frac{(1 + sT_1)K_s}{1 + sT_2}$$

with a centre frequency of 3.5 Hz is selected. The maximum phase lead (which occurs at 3.5 Hz) is selected as 30° so that the compensated phase lag is 90° at
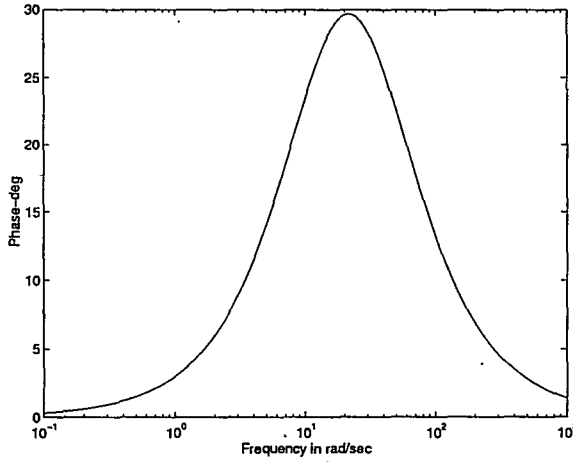
Figure 8.15: Phase angle of compensator $T(j\omega)$

3.5 Hz. The ratio $n = \dfrac{T_1}{T_2}$, has to satisfy

$$\tan^{-1} T_1\omega_c - \tan^{-1} T_2\omega_c = 30^o \tag{8.22}$$

where

$$\omega_c = 2\pi f_c = \frac{1}{\sqrt{T_1 T_2}} = \frac{1}{T_2\sqrt{n}} \tag{8.23}$$

Substituting (8.23) in (8.22), we have

$$\tan^{-1}\sqrt{n} - \tan^{-1}\frac{1}{\sqrt{n}} = 30^o \tag{8.24}$$

The solution of the above equation is $n = 3$. The time constants T_1 and T_2 are selected as

$$T_1 = 0.078 \ s, \quad T_2 = 0.026 \ s$$

The phase lead provided by the PSS at the rotor oscillation frequency is around 19°. This results in the compensated phase lag of about 16° at 7 rad/sec. The phase angle of the compensator is shown in Fig. 8.15 and the compensated phase $\angle T(s)GEP(s)$ is shown in Fig. 8.16. The washout circuit time constant T_W is selected as 2.0 s as the PSS is mainly designed for damping local mode of frequency around 1 Hz. The overall PSS transfer function is

$$PSS(s) = \frac{T_W s}{(1 + sT_W)}\frac{K_s(1 + sT_1)}{(1 + sT_2)}$$
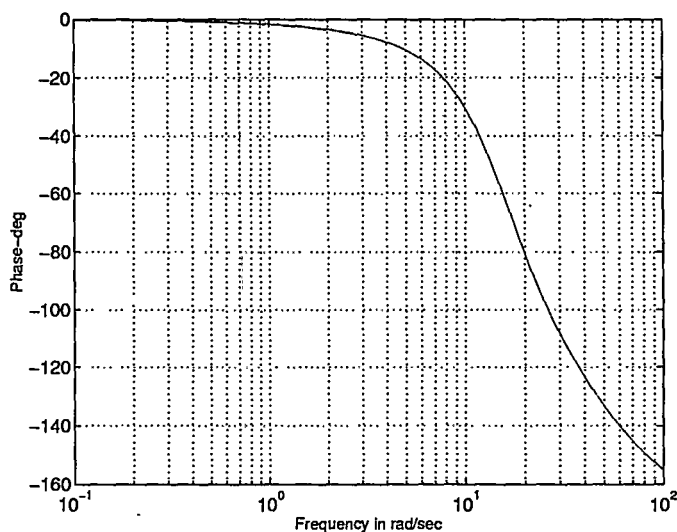
Figure 8.16: Compensated phase angle

To select the appropriate value of the PSS gain (K_s) root locus plot is obtained as K_s is varied. Fig. 8.17 shows the loci of two roots (eigenvalues), one corresponding to the local (rotor) mode and other corresponding to the exciter mode. The root corresponding to the exciter mode moves to the right and crosses imaginary axis at around $K_s = 74$. The root corresponding to the local mode moves to the left as K_s increases from zero and for higher PSS gain, the frequency of oscillation continues to decrease until the complex root splits into two real roots. The optimum PSS gain is chosen such that critical mode has maximum damping ratio. From Fig. 8.17 the optimum PSS gain is 16.

It is to be noted that GEP $(j\omega)$ is a function of the operating point. The plots of the variation of angle of GEP$(j\omega)$ as a function of frequency for three other operating points (a)$P_g = 0.5$, $x_e = 0.4$, (b)$P_g = 0.5$, $x_e = 0.8$, (c)$P_g = 1.0$, $x_e = 0.8$, are shown in Fig. 8.18. The plot for the operating point $P_g = 1.0$, $x_e = 0.4$ (shown in Fig. 8.14) is also given in Fig. 8.18 for comparison. It is seen that the phase lag of GEP $(j\omega)$ is maximum for full load and strong system $(x_e = 0.4)$ conditions. Hence PSS designed for the operating condition $P_g = 1.0$, $x_e = 0.4$ is expected to operate satisfactorily at other operating conditions. The eigenvalues of the system with PSS for the four operating conditions are given in Table 8.1.

Example 8.2

Obtain the responses of the system of Example 8.1 for a three phase fault
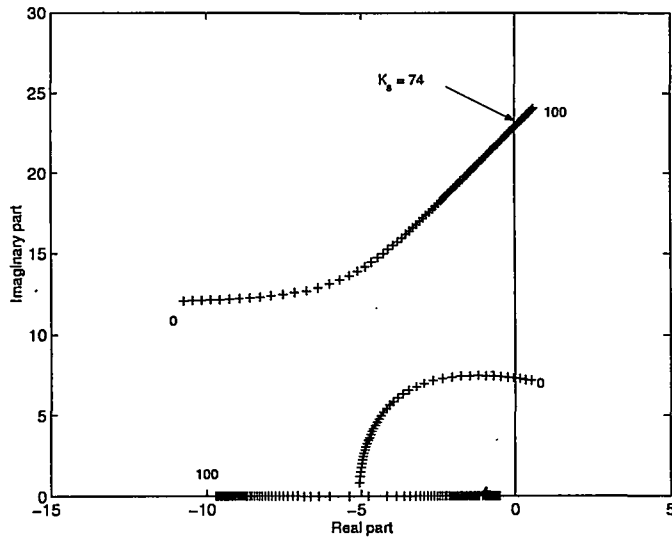
Figure 8.17: Root loci with variation in stabilizer gain
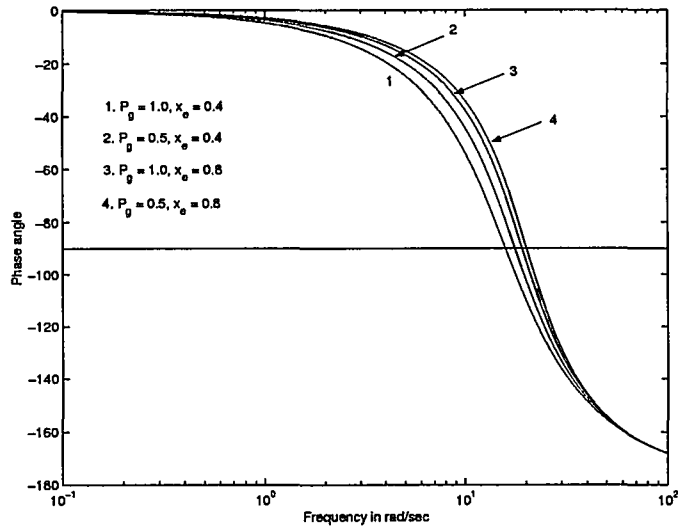
Figure 8.18: Variation of phase of GEP($j\omega$) for different operating points

at the generator terminals followed by clearing after 4 cycles. The operating point is $P_g = 1.0$, $x_e = 0.4$. The system is initially at equilibrium. Compare the responses with and without PSS. Assume the post fault system identical to the pre-fault system. The limits on PSS output are ±0.05 pu and the limits on E_{fd} are ±6.0 pu.

Table 8.1 Eigenvalues with and without PSS (Example 8.1)

Sl. No.	Without PSS $P_g = 1.0$ $x_e = 0.4$	With PSS			
		$P_g = 1.0$ $x_e = 0.4$	$P_g = 1.0$ $x_e = 0.8$	$P_g = 0.5$ $x_e = 0.8$	$P_g = 0.5$ $x_e = 0.4$
1,2	-10.74 $\pm$ j12.10	-5.39 $\pm$ j13.67	-8.29 $\pm$ j16.82	-8.38 $\pm$ 18.02	-7.00 $\pm$ j15.66
3,4	0.51 $\pm$ j7.16	-3.44 $\pm$ j6.56	-1.00 $\pm$ j5.19	-1.06 $\pm$ j 4.68	-2.17 $\pm$ j4.89
5	–	-0.5294	-0.5236	-0.5218	-0.5326
6	–	-39.82	-38.80	-38.49	-39.13

Solution

The results of the simulation without PSS are shown in Fig. 8.19. The fault is assumed to occur at 1 s. The figure shows the variation of rotor angle (δ), E_q', T_e, V_t and E_{fd}.

The plot of the rotor angle shows oscillatory instability as the operating point is unstable. The oscillations in δ, T_e and V_t are increasing in magnitude. The dominant frequency of oscillation is about 1 Hz corresponding to the rotor (swing) mode. There is also a second harmonic component in T_e and V_t. The results of simulation with PSS included are shown in Fig. 8.20. The variation of the PSS output is also given. It is interesting to observe that the oscillations are well damped and steady state is reached in little over 2 s after the occurrence of the disturbance.

Example 8.3

The system diagram and data are given in Example 7.4. The generator represents the equivalent for the area connected to a very strong system (represented by infinite bus) through a tie line of impedance $0 + j5$. The initial power flow over the tie line is 10 % of the local load supplied by the generator. Design a speed input PSS at the operating condition $P_g = 1.1$, $V_t = 1.0$.

Solution

The phase angle of GEP $(j\omega)$ as a function of ω is shown in Fig. 8.21. This shows that the phase lag of GEP $(j\omega)$ is within limits and the PSS does not need to provide any phase lead. The choice of T_1 and T_2 are immaterial provided $n = 1$ (There is a pole-zero cancellation in the compensator).

(a) Variation of rotor angle

(b) Variation of E_q'

(c) Variation of T_e

(d) Variation of V_t

(e) Variation of E_{fd}

Figure 8.19: Simulation results without PSS (Example 8.2)

(a) Variation of rotor angle
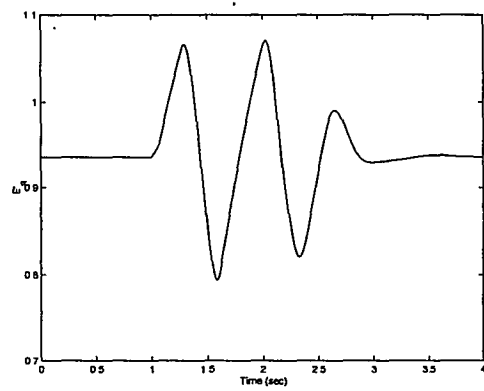
(b) Variation of E_q'

(c) Variation of T_e

(d) Variation of V_t

(e) Variation of E_{fd}

(f) Variation of V_s (PSS output)

Figure 8.20: Simulation results with PSS (Example 8.2)
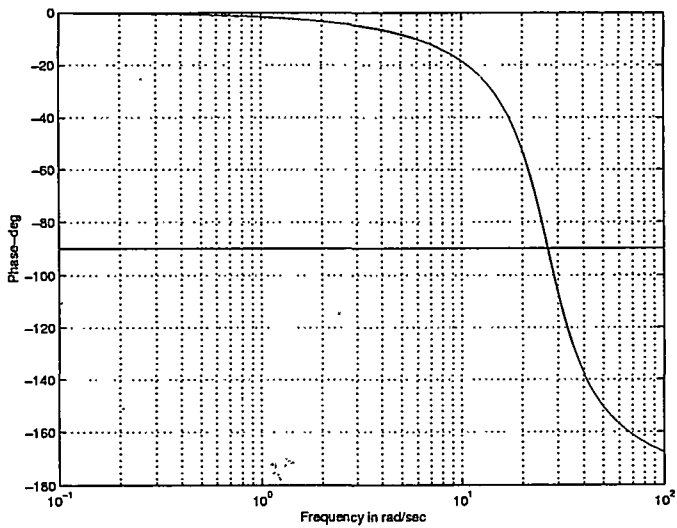
Figure 8.21: Phase angle of GEP($\jmath\omega$) (Example 8.3)
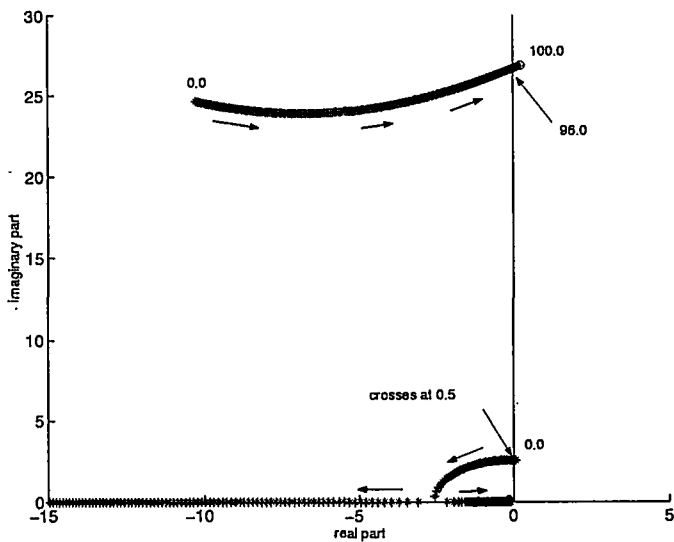
Figure 8.22: Root loci with variation in stabilizer gain (Example 8.3)

Table 8.2 Eigenvalues With and Without PSS (Example 8.3)

Sl.No.	Without PSS	With PSS
1,2	-10.26 ± j 24.65	-9.14 ± j 24.25
3,4	0.075 ± j 2.53	-1.05 ± j 2.34
5	–	-0.1035

The PSS gain is selected from the plot of root loci shown in Fig. 8.22. This shows two modes - a low frequency inter area mode and higher frequency exciter mode which gets destabilized as PSS gain is increased. The optimum gain is $K_s = 10$.

The washout circuit time constant is chosen as 10 s as the inter area mode has a low frequency ($< 0.5Hz$). The PSS transfer function is

$$PSS(s) = \frac{100s}{(1 + 10s)}$$

The system eigenvalues with and without PSS are given in Table 8.2.

Example 8.4

Obtain the response of the system of Example 8.3 for a step increase in V_{ref} by 0.05 pu. The system is initially in equilibrium with $P_g = 1.1$, $x_E = 5.0$. Compare the responses with and without PSS. Assume the limits on V_s (PSS output) as ±0.05 and on E_{fd} as ±6.0 pu.

Solution

The results of the simulation for the case without PSS are shown in Fig. 8.23. The step increase in V_{ref} occurs at 1 sec. The plots of variation of δ, E'_q, T_e, V_t and E_{fd} are given in Fig. 8.23. The results show that the system is marginally unstable and the oscillations continue even beyond 10 s.

The rotor angle decreases as V_{ref} is increased. E'_q and V_t also increase as expected. The electrical torque T_e increases initially and settles down to previous value (neglecting the superimposed oscillations). The field voltage E_{fd} hits the ceiling initially and settles down (neglecting oscillations) to a slightly lower value (compared to the initial operating value) as the demagnetizing current is reduced on account of decrease in the rotor angle.

The results of simulation with PSS considered are given in Fig. 8.24.
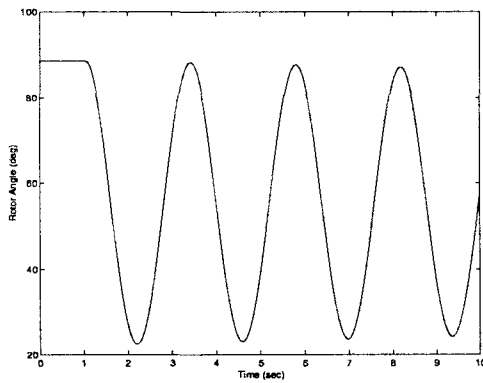
(a) Variation of rotor angle
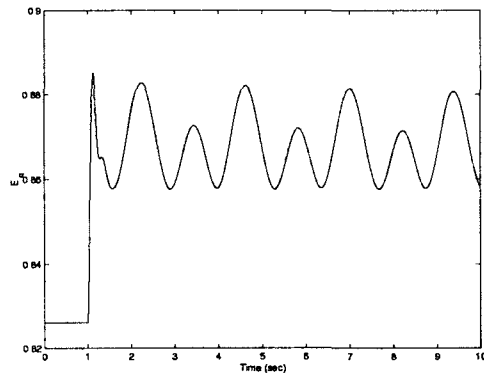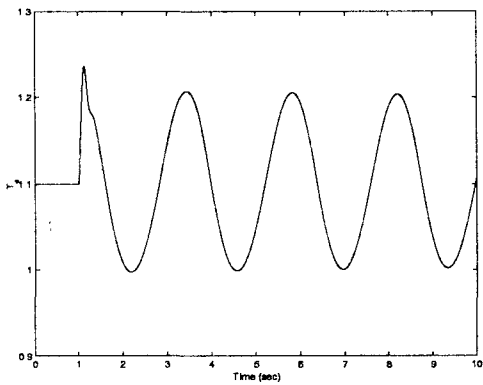
(b) Variation of E_q'
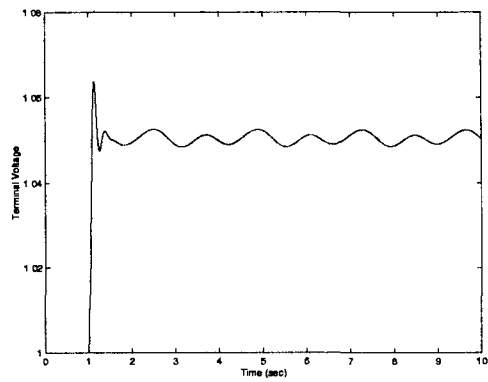
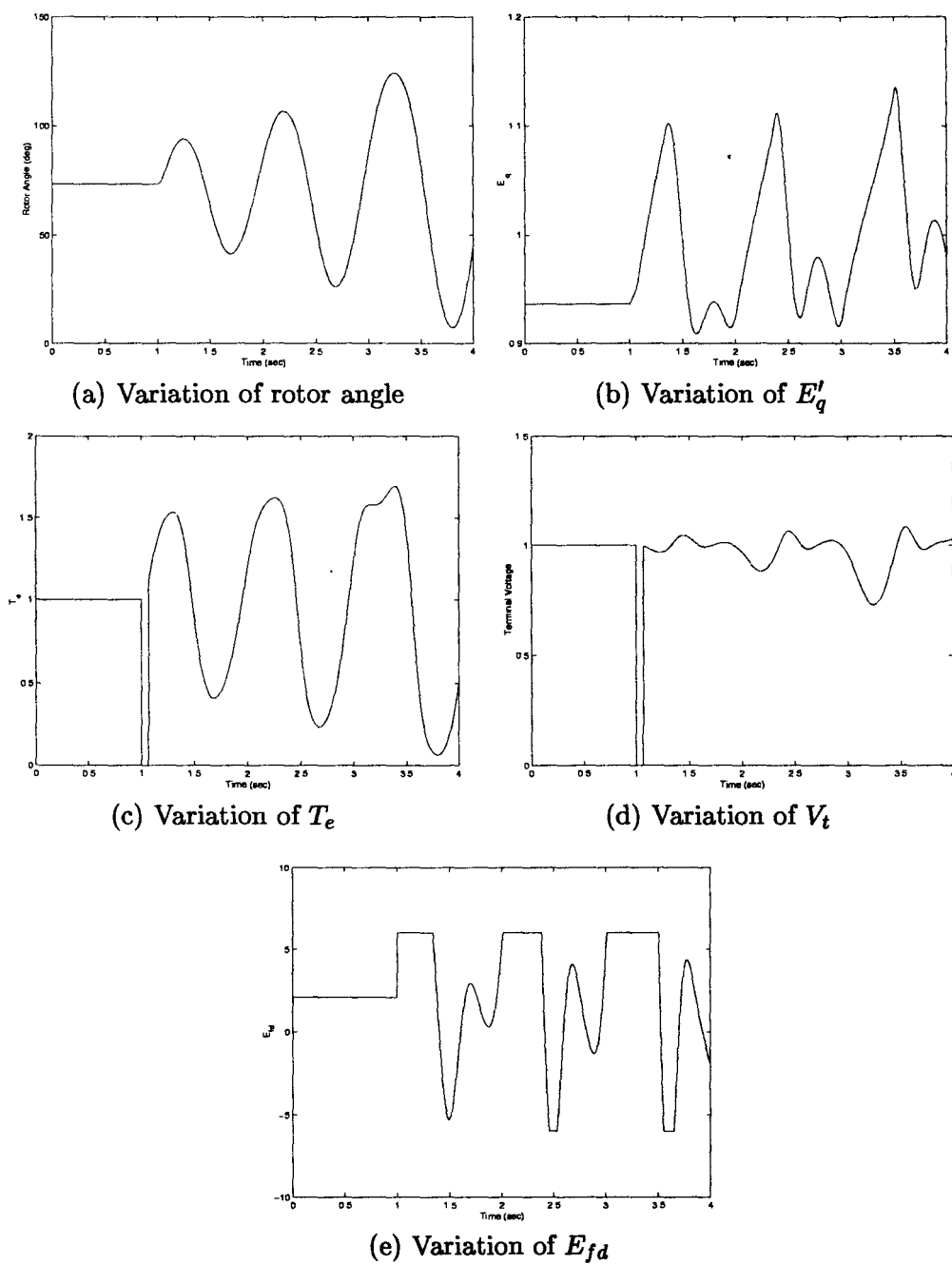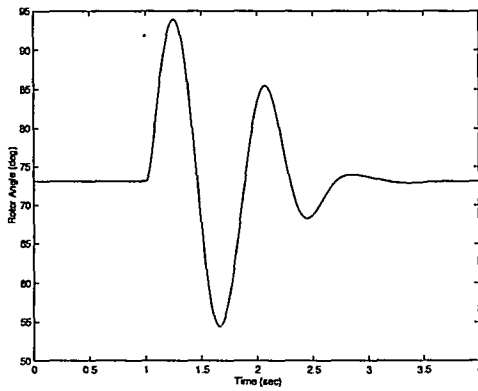(c) Variation of T_e
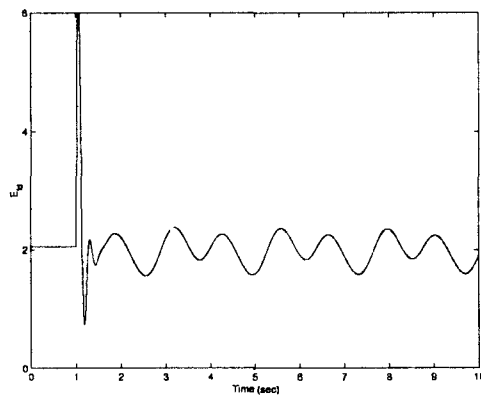
(d) Variation of V_t

(e) Variation of E_{fd}

Figure 8.23: Simulation results without PSS (Example 8.4)
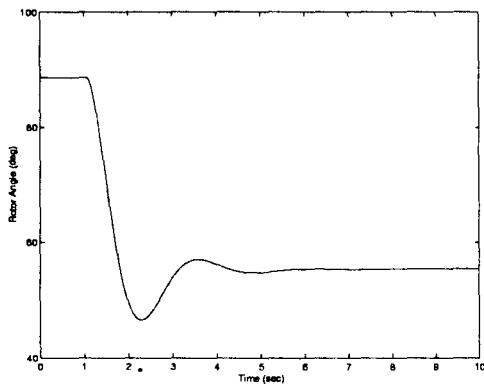
(a) Variation of rotor angle
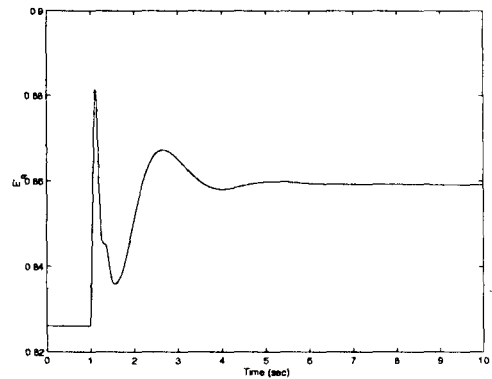
(b) Variation of E'_q

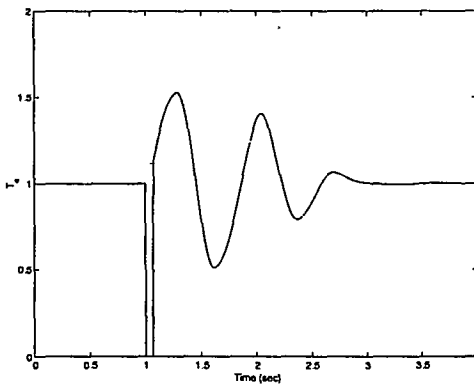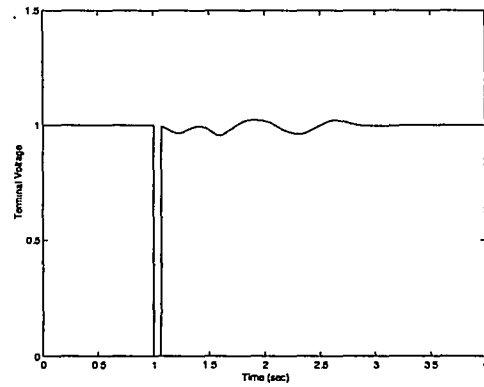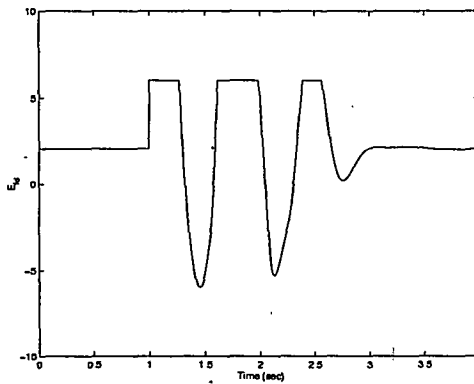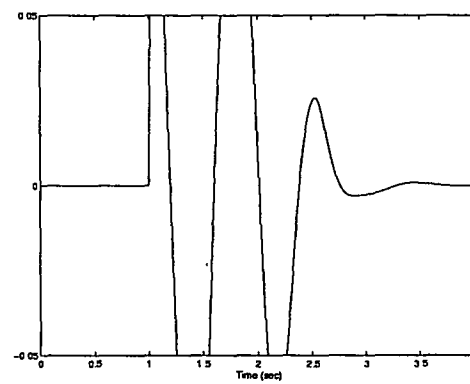(c) Variation of T_e

(d) Variation of V_t

(e) Variation of E_{fd}

(f) Variation of V_s (PSS output)

Figure 8.24: Simulation results with PSS (Example 8.4)

The output of PSS is also given for this case. The oscillations are damped out within 3 s after the occurrence of the disturbance. The PSS output is negative initially as the rotor decelerates following the step increase in V_{ref}. As the action of the PSS is countering the increase in V_{ref}, the initial overshoot in V_t is slightly less than the value reached in the case without PSS. However there is a larger undershoot with PSS on account of the negative output of PSS which lasts for over 1 s. This shows that in damping rotor oscillations PSS can cause some fluctuations in the terminal voltage during the transient. The limiting of PSS output is essential in reducing the voltage fluctuations.

Example 8.5

Consider the system of Example 6.6 (in chapter 6). The generator is assumed to be equipped with a PSS with the following parameters -
$K_s = 15$, $T_1 = 0.75$, $T_2 = 0.3$, $T_W = 10$. Limits on $V_s = \pm 0.05$.
Obtain the responses of the system for case D with PSS included (The disturbance considered is a three phase fault near the sending end of one of the transmission circuits followed by clearing of the fault in 4 cycles by tripping of the line).

Solution

The results of the simulation with PSS considered are shown in Fig. 8.25. The oscillations are well damped and new steady state is reached within 3 sec after the disturbance. The results should be compared with those shown in Fig. 6.15 (without PSS). The system is unstable without PSS. The limits on V_s are active in this case (as in Example 8.2) also as the disturbance is large. However the PSS is effective in spite of the limits imposed on its output. As a matter of fact, the satisfactory limits are essential in reducing voltage fluctuations during the transient following the fault clearing.

(a) Variation of rotor angle   (b) Variation of E_q'
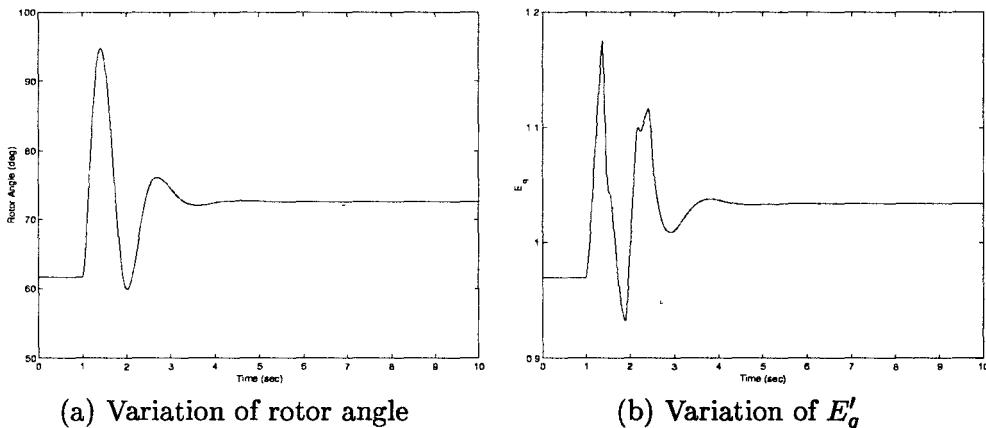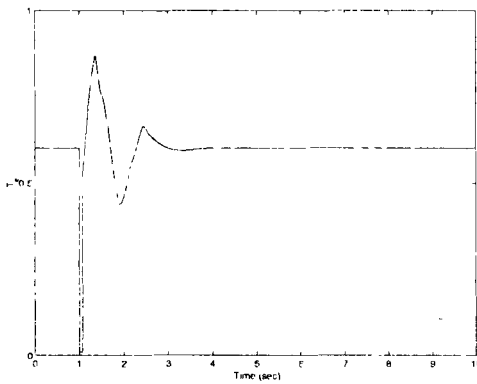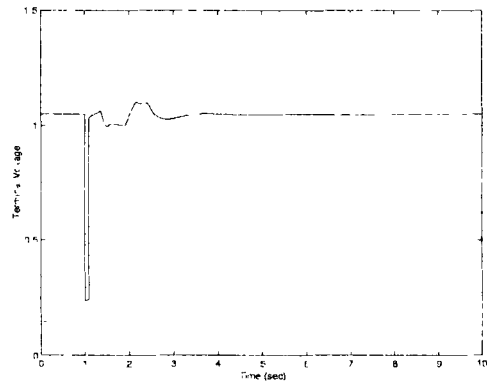
(c) Variation of T_e
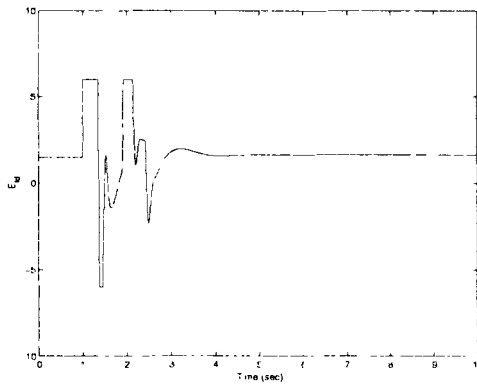
(d) Variation of V_t
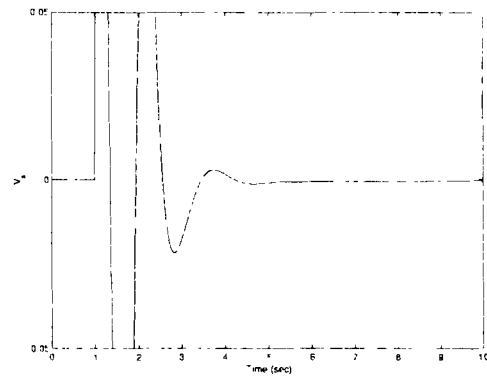
(e) Variation of E_{fd}

(f) Variation of V_s (PSS output)

Figure 8.25: Simulation results with PSS (Example 8.5)

Remarks

1. The optimum gain of PSS is a function of the AVR gain. Smaller AVR gains permit larger PSS gain. However it is advantageous to have large AVR gain for rapid control of voltage during load rejection. High AVR gains and ceilings on the exciter voltage are beneficial in improving transient stability.

2. Phase lead is usually required from PSS. However with static exciters and high gain AVRs, speed input PSS may be required to provide just a pure gain.

3. In practically all the cases, increasing PSS gain results in destabilizing a mode other than the swing (rotor) mode. The results of PSS design given

in both Example 8.1 and 8.3 show an exciter mode that is destabilized at high PSS gains. In example 8.1, the instability gain is $K_S = 74$. The results of the simulation for a three phase fault (see Example 8.2) with PSS gain set at $K_S = 72$, are shown in Fig. 8.26.

It is interesting to observe in this case, that although the rotor oscillations are well damped, there are significant oscillations in V_t, E_q' and E_{fd}. The frequency of these oscillations correspond to the exciter mode of about 3.5 Hz at $K_s = 72$. Such behaviour is typical in cases where exciter mode is poorly damped.

4. The optimal gain $K_S = 16$ in Example 8.1 is little above $\dfrac{1}{5}$ of the instability gain. This shows that the thumb rules given in reference [9] are not general and depend on the type of excitation system considered.
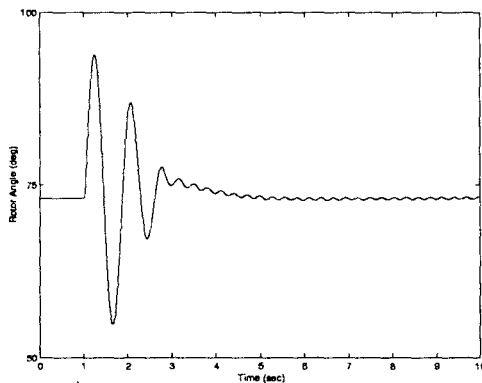
(a) Variation of rotor angle

(b) Variation of E_q'

(c) Variation of T_e
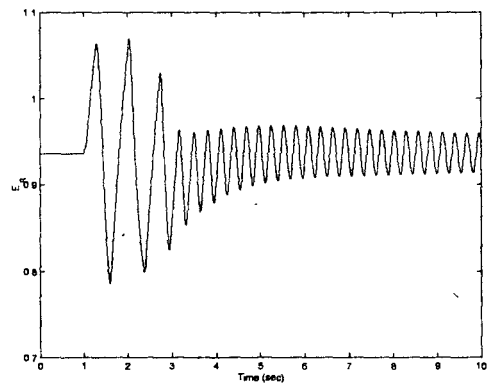
(d) Variation of V_t
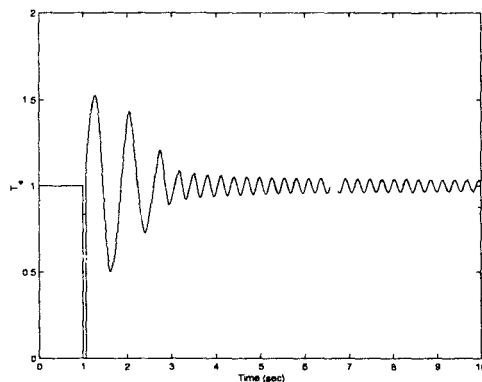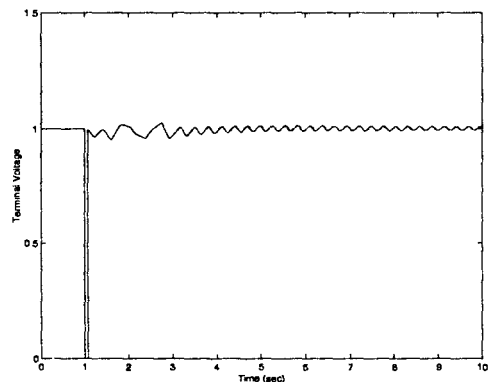
(e) Variation of E_{fd} (f) Variation of V_s (PSS output)
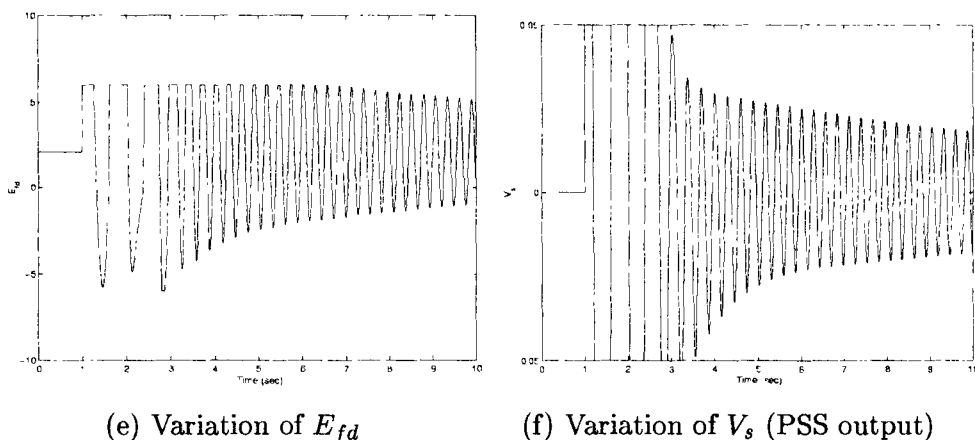
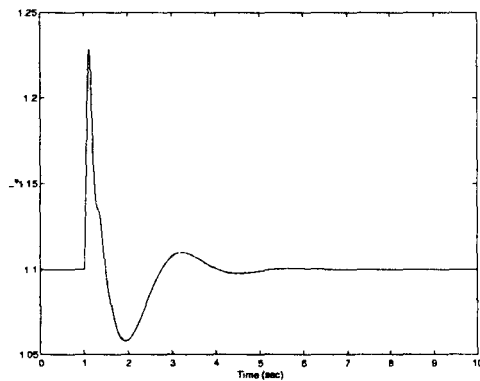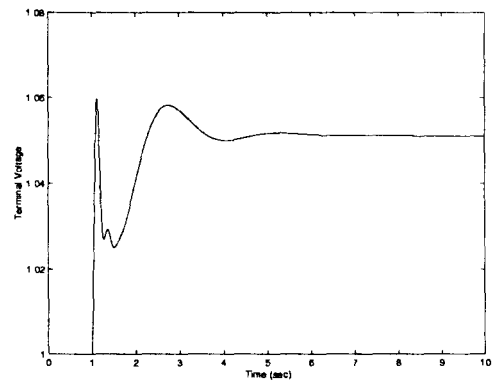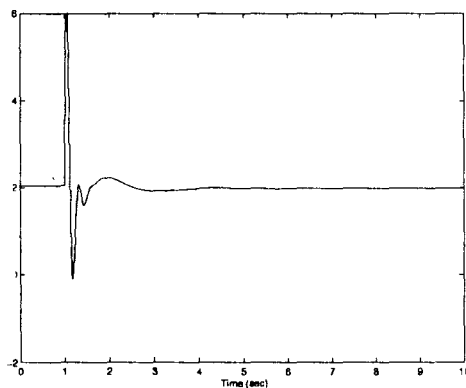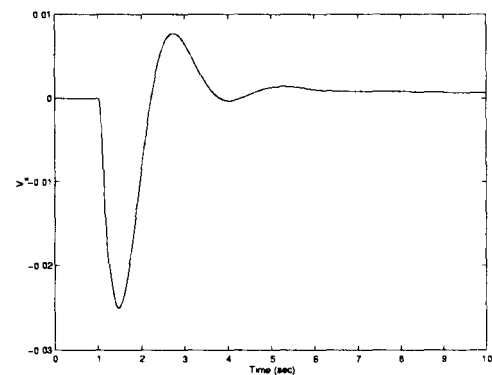Figure 8.26: Simulation results with high PSS gain (Example 8.2)

8.7 Stabilization through HVDC converter and SVC controllers

It is well established now that the stability characteristics of the interconnected systems can be improved by power modulation of DC links [21]. This concept utilizes the fast controllability of power flow in a DC link. The control signals used are bus frequency deviations or power flow in the parallel AC tie. With weak AC systems, active and reactive power modulation can be implemented by providing controllers at both rectifier and inverter stations. The modulation of extinction angle at the inverter in response to the AC voltage (magnitude) signal can avoid voltage instability.

Small signal power modulation implemented at Pacific DC Intertie has helped prevent inter area mode of 1/3 Hz from reducing the power transfer capability of a parallel AC tie [22, 23]. The power or current modulation has now become a standard practice to improve dynamic or transient stability.

Static Var Compensator (SVC) connected at the midpoint of a transmission line can help to increase the power transfer capability of the line. If auxiliary controllers are provided, utilizing signals from locally available measurements, the small signal stability can be improved [24, 25].

8.8 Recent developments and future trends

Research efforts in academic institutions and industry have been directed at better approaches to tuning of PSS using analytical techniques. One such direction

is the applications of modern control theory techniques such as pole assignment and optimal control [26, 27]. It is possible to get better performance from PSS if it is viewed as a dynamic compensator with general structure (with complex poles and zeros with possibility of non-minimum phase characteristics).

Another direction of investigation is the possibility of coordinated tuning of PSS in several locations using the general multi-machine system model. This is of particular relevance in damping of several inter area modes [34, 35]. In this context, it is required to examine the effectiveness of PSS at a particular location. Based on the concept of eigenvalue sensitivities, it is possible to determine the machines where PSS will have the maximum effect on damping of a specific mode [28].

The coordinated tuning of PSS and HVDC/SVC auxiliary controllers would require analytical studies using mathematical models, as tuning based on field tests would be impractical. In a large system, it would be also advantageous to do selective modal analysis [29].

The present practice in tuning PSS is to select a tuning condition (of the system) and select the parameters for satisfactory performance under all possible operating conditions. There can be situations when this is unrealistic. In such cases, self-tuning regulator principle based on constructing a simplified model in real time with parameter estimation and automatic tuning of PSS is desirable [30, 31]. The development of digital control makes it possible to synthesize control signal from sampled (instantaneous) voltage and current measurements [32, 33] and implement adaptive control strategies [34]. With a microcomputer control and static exciters, it should be possible to integrate the functions of voltage regulation and power system stabilization.

References and Bibliography

1. P. Kundur, M. Klein, G.J. Rogers and M.S. Zywno, "Application of power system stabilizers for enhancement of overall system stability", IEEE Trans. on Power Systems, Vol. 4, No. 2, May 1989, pp. 614-626.

2. D.C. Lee and P. Kundur, "Advanced excitation controls for power system stability enhancement", Paper 38-01, CIGRE Conf. Proc. 1986.

3. F.P. Demello and C. Concordia, "Concepts of synchronous machine stability as affected by excitation control", IEEE Trans. Vol. PAS-88, April 1969, pp. 316-329.

4. R.T. Byerly and E.W. Kimbark, (Editors), "Stability of Large Electric Power Systems", IEEE Press, 1974, pp. 261-307.

5. P.A. Rusche, et al., "Investigation of dynamic oscillations of the Ludington pumped storage plant", IEEE Trans. Vol. PAS-95, Nov/Dec. 1976, pp. 1854-1862.

6. E.L. Busby, J.D. Hurley, F.W. Keay and C. Raczkowski, "Dynamic stability improvement at Monticello Station - Analytical study and field tests", IEEE Trans. Vol. PAS-98, No. 3, May/June 1979, pp. 889-901.

7. J.E. Van Ness, F.M. Brasch Jr., G.L. Landgren and S.T. Naumann, "Analytical investigations of dynamic instability occurring at Powerton station", IEEE Trans. Vol. PAS-99, No. 4, July/August 1980, pp. 1386-1395.

8. K.M. Trantor, "Installation of power system stabilisers and the evaluation of settings", IEE Proc., Vol. 135, Pt. C, No. 3, May 1988, pp. 244-250.

9. E.V. Larsen and D.A. Swann, "Applying Power System Stabilizers, Parts I, II and III", IEEE Trans. Vol. PAS-100, June 1981, pp. 3017-3046.

10. F.R. Schlief, R.K. Feeley, W.H. Phillips and R.W. Torluemke, "A power system stabilizer application with local mode cancellation", IEEE Trans. Vol. PAS-98, May/June 1979, pp. 1054-1060.

11. F.R. Schlief, H.D. Hunkins, G.E. Martin and E.E. Hattan, "Excitation control to improve powerline stability", IEEE Trans. Vol. PAS-87, June 1968, pp. 1426-1434.

12. J.P. Bayne, D.C. Lee and W. Watson, "A power system stabilizer for thermal units based on derivation of accelerating power", IEEE Trans. Vol. PAS-96, Nov/Dec. 1977, pp. 1777-1783.

13. F.P. de Mello, L.N. Hannett and J.M. Undrill, "Practical approaches to supplementary stabilizing from accelerating power", IEEE Trans. Vol. PAS-97, No. 5, Sept/Oct. 1978, pp. 1515-1522.

14. D.C. Lee, R.E. Beaulieu and J.R.R. Service, "A power system stabilizer using speed and electrical power inputs - design and field experience", IEEE Trans. Vol. PAS-100, No. 9, Sept. 1981, pp. 4151-4167.

15. W. Watson and M.E. Coultes, "Static exciter stabilizing signals on large generators - mechanical problems", IEEE Trans. Vol. PAS-92, Jan/Feb. 1973, pp. 204-211.

16. P. Kundur, D.C. Lee and H.M. Zein El-Din, "Power system stabilizers for thermal units: analytical techniques and on-site validation", IEEE Trans. Vol. PAS-100, Jan. 1981, pp. 81-95.

17. R.T. Byerly, R.J. Bennon and D.E. Sherman, "Eigenvalue analysis of synchronizing power flow oscillations in large electric power systems", IEEE Trans. Vol. PAS-101, No. 1, Jan. 1982, pp. 235-243.

18. G. Gross, C.F. Imparato and P.M. Look, "A tool for the comprehensive analysis of power system dynamic stability", IEEE Trans. Vol. PAS-101, No. 1, Jan. 1982, pp. 226-234.

19. D.Y. Wong, G.J. Rogers, B. Poretta and P. Kundur, "Eigenvalue analysis of very large power systems", IEEE Trans. on Power Systems, Vol. 3, No. 2, May 1988, pp. 472-480.

20. R.G. Farmer and B.L. Agrawal, "State-of-the-art technique for power system stabilizer tuning", IEEE Trans. Vol. PAS-102, No. 3, March 1983, pp. 699-707

21. IEEE Committee Report, "A description of discrete supplimentary controls for stability", IEEE Trans. Vol. PAS-97, No.1, Jan/Feb. 1978, pp. 149-165

22.. R.L. Cresap and W.A.Mittelstadt, "Small-signal modulation of the Pacific HVDC intertie", IEEE Trans. Vol. PAS-95, No.2, 1976, pp. 536-541

23. R.L. Cresap, W.A. Mittelstadt, D.N. Scott and C.W. Taylor, "Operating experience with modulation of the Pacific HVDC intertie", IEEE Trans. Vol. PAS-97, No.4, July/Aug. 1978

24. K.R. Padiyar and R.K. Varma, "Static VAR system auxiliary controllers for improvement of dynamic stability", Int. J. of Elec. Power and Energy System, Vol. 12, No.4, Oct. 1990, pp. 287-297.

25. K.R. Padiyar and R.K. Varma, "Damping torque analysis of static VAR system controllers", IEEE Trans. on Power Systems, Vol. 6, No. 2, 1991, pp. 458-465

26. K.R. Padiyar, S.S. Prabhu, M.A. Pai and K. Gomathi, "Design of stabilizers by pole assignment with output feedback", Int. J. Elect. Power and Energy Systems, Vol. 2, No. 3, July 1980, pp. 140-146

27. M.A. Pai, K.R. Padiyar and C. Radhakrishna, "Synthesis of damping action in power systems using eigenvalue sensitivities", JIE (India), Pt. EL-4, Vol. 65, 1985, pp. 127-131

28. K.R. Padiyar, S.S. Prabhu and A. Anwar, "Design of power system stabilizers to minimize power fluctuations", J. Indian Inst. of Sci., Vol. 70, Jan-Feb. 1990, pp. 13-21

29. I.J. Perez-Arriaga, G.C. Verghese, F.L. Pagola, J.L. Sancha and F.C. Schweppe, "Developments in selective modal analysis of small-signal stability in electric power systems", Automatica, Vol. 26, No. 2, 1990, pp. 215-231

30. O.P. Malik, G.S. Hope, S.J. Cheng and G. Hancock, "A multi-micro computer based dual rate self tuning power system stabilizer", IEEE Trans. Vol. EC-2, No. 3, 1987, pp. 355-360

31. Q.H. Wu and B.W. Hogg, "Self tuning control for turbogenerators in multimachine power systems", IEEE Proc., Vol. 137, Pt. C, No. 2, March 1990, pp. 146-158

32. F.P.Demello, L.N. Hannett, D.W. Parkinson and J.S. Czuba, "A power system stabilizer design using digital control", IEEE Trans. Vol. PAS-101, No. 8, Aug. 1982, pp. 2860-2868

33. H. Herzog and H. Baumberger, "Digital control of generators", ABB Review, 1, 1990

34. S. Lefebvre, "Tuning of stabilizers in multimachine power systems", IEEE Trans. vol. PAS-102, No.2, 1983, pp. 290-299

35. A. Doi and S. Abe, "Coordinated synthesis of power system stabilizers in multimachine power sytems", IEEE Trans. vol. PAS-103, No. 6, 1984, pp. 1473-1479.

"This page is Intentionally Left Blank"

Chapter 9

Analysis of Multimachine System

The small signal analysis of multimachine power systems is examined in this chapter. The methods for formulation of the system model are presented in some detail. The analysis for large systems has to necessarily concentrate on the critical modes of oscillation (typically interarea modes) which are important. The computational issues in the evaluation of small signal stability are also discussed.

9.1 A Simplified System Model

The electromechanical modes in a system are highlighted by considering only classical models of generators. In addition, the following assumptions simplify the analysis.

1. The losses in transmission lines are neglected.

2. The voltage magnitudes at all buses are constant.

3. The loads are static.

As the voltages at all buses are assumed to be constant, only the real power flow equations need to be considered. At any bus j, (not the generator internal bus), the injected power P_j is given by

$$P_j = -P_{lj} = \sum_{i \in n_j} \frac{V_j V_i}{x_{ij}} \sin(\delta_j - \delta_i) + \sum_{k \in m_j} \frac{V_j E_k}{x'_{dk}} \sin(\delta_j - \delta_k) \qquad (9.1)$$

where n_j is set of load buses connected to bus j, m_j is the set of generator (internal) buses connected to bus j. P_{lj} is the power consumed in the load connected at bus j. x_{ij} is the reactance of the line connecting bus i and j. x'_{dk} is the transient reactance (in direct axis) of generator k. The saliency is neglected in the analysis.

At the kth generator internal bus,

$$P_{ek} = \frac{E_k V_j \ \sin(\delta_k - \delta_j)}{x'_{dk}} \tag{9.2}$$

Linearizing the power flow equations, it is not difficult to see that the deviation in the power flow in a line (ΔP_{ij}) is related to the change in the relative angle across the line, $\Delta\delta_{ij}$.

$$\Delta P_{ij} = g_{ij}\Delta\delta_{ij} \tag{9.3}$$

where

$$g_{ij} = \frac{V_i V_j \ \cos\delta_{ij}}{x_{ij}}$$

Comparing ΔP with current flow and $\Delta\delta$ with voltage drop, the linearized Eqs. (9.1) and (9.2) represent a linear resistive network described by

$$[G]\begin{bmatrix} \Delta\delta_g \\ \Delta\delta_l \end{bmatrix} = \begin{bmatrix} \Delta P_e \\ 0 \end{bmatrix} \tag{9.4}$$

where $\Delta\delta_g$ is a vector of rotor angle deviation corresponding to m (number of generators) internal buses. $\Delta\delta_l$ represents deviations in other bus angles. ΔP_e is the vector of deviations in the electrical power outputs of generators. The second entry on R.H.S. of Eq. (9.4) is zero as the active loads are assumed to be constant on account of constant voltages at load buses. The frequency dependency will be considered later.

It is not difficult to see that the matrix $[G]$ is singular. It represents indefinite conductance matrix of a network with no connection to ground. As an example consider a 3 generator, 4 bus system shown in Fig. 9.1. The linearized power flow equations represent a resistive 7 bus network shown in Fig. 9.2. The $[G]$ matrix for this network is given by

$$[G] = \begin{bmatrix}
g_1 & 0 & 0 & -g_1 \\
0 & g_2 & 0 & 0 \\
0 & 0 & g_3 & 0 \\
-g_1 & 0 & 0 & (g_1 + g_{12} + g_{13}) \\
0 & -g_2 & 0 & -g_{12} \\
0 & 0 & -g_3 & -g_{13} \\
0 & 0 & 0 & 0
\end{bmatrix}$$

$$\begin{bmatrix}
0 & 0 & 0 \\
-g_2 & 0 & 0 \\
0 & -g_3 & 0 \\
-g_{12} & -g_{13} & 0 \\
(g_{12} + g_{23} + g_{24} + g_2) & -g_{23} & -g_{24} \\
-g_{23} & (g_3 + g_{13} + g_{23} + g_{34}) & -g_{34} \\
-g_{24} & -g_{34} & (g_{24} + g_{34})
\end{bmatrix}$$
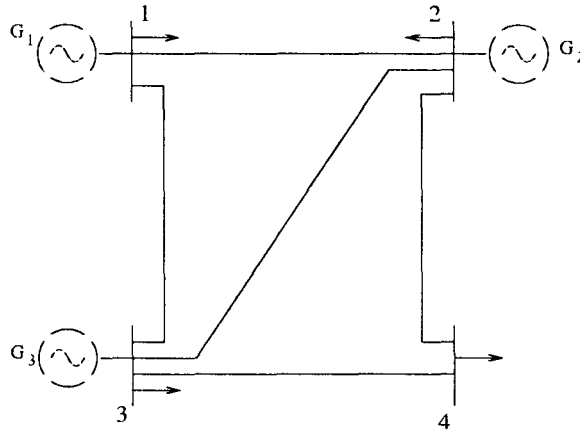
Figure 9.1: System diagram
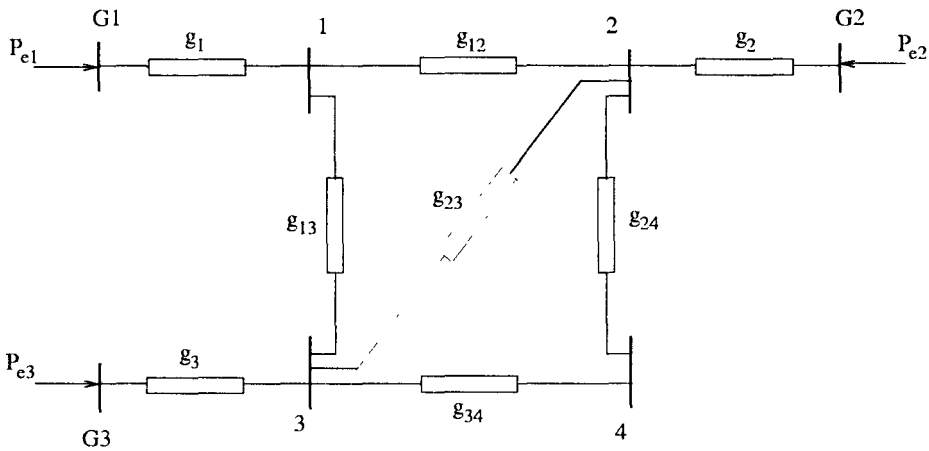
Figure 9.2: A resistive network representing equation 9.4

Each row or column of $[G]$ adds up to zero. From superposition theorem, we can derive an expression for ΔP_{ek} as

$$\Delta P_{ek} = \sum_{j=1}^{m} G_{kj}^{R} \Delta \delta_j \tag{9.5}$$

where G_{kj}^{R} is the short circuit transfer admittance between generator buses j and k. As $\Delta P_{ek} = 0$ if all the angle deviations are equal, i.e. $\Delta \delta_j = \Delta \delta, \quad j = 1, 2 ... m,$

we can obtain,

$$\sum_{j=1}^{m} G_{kj}^{R} = 0 \tag{9.6}$$

G_{kj}^{R} is the element of the reduced conductance matrix $[G^{R}]$ obtained from $[G]$ after eliminating all the buses except the generator internal buses. This follows from Eq. (9.4).

Generator Equations and COI Reference

Utilizing the classical model of generators, the swing equations for generator k can be expressed as

$$M_k \frac{d^2\delta_k}{dt^2} + D'_k \frac{d\delta_k}{dt} = P_{mk} - P_{ek}, \quad k = 1, 2...m \tag{9.7}$$

where

$$M_k = \frac{2H_k}{\omega_B}, \quad D'_k = \frac{D_k}{\omega_B}$$

where D_k is the per unit damping. For simplicity, it will be assumed that the damping is uniform, i.e.

$$\frac{D'_k}{M_k} = \frac{D_k}{2H_k} = \text{constant} = \alpha$$

Defining the Centre of Inertia (COI) whose angle δ_o is defined by

$$\delta_o = \frac{1}{M_T} \left(\sum_{k=1}^{m} M_k \delta_k \right) \tag{9.8}$$

where $M_T = \sum_{k=1}^{m} M_k$ is the total inertia. The equation for COI is given by

$$M_T(p + \alpha)\tilde{\omega}_o = \sum_{k=1}^{m} P_{mk} - \sum_{k=1}^{m} P_{ek} = P_{COI} \tag{9.9}$$

where

$$\tilde{\omega}_o = \frac{d\delta_o}{dt}, \quad p = \frac{d}{dt}$$

In the electrical network,

$$\sum_{k=1}^{m} P_{ek} = \sum_{j=1}^{n} P_{lj} + P_{loss} \tag{9.10}$$

For lossless network and with constant active power loads, P_{COI} is a constant when the mechanical powers are constant. Eq. (9.9) can also be written as

$$M_T(p^2 + \alpha p)\delta_o = P_{COI} \tag{9.11}$$

Substituting Eq. (9.11) in (9.7), we get

$$M_k(p^2 + \alpha p)\theta_k = P_{mk} - P_{ek} - \frac{M_k}{M_T}P_{COI}, \quad k = 1, 2...m \tag{9.12}$$

where θ_k is the rotor angle relative to COI defined by

$$\theta_k = \delta_k - \delta_o \tag{9.13}$$

From the above definition of θ_k, it can be shown that all the relative angles with respect to COI are not independent and the following relation applies.

$$\sum_{k=1}^{m} M_k\theta_k = 0 \tag{9.14}$$

Also,

$$\theta_i - \theta_j = \delta_i - \delta_j \tag{9.15}$$

Linearizing Eq. (9.12), (assuming P_{COI} as constant) we get

$$M_k p^2 \Delta\theta_k + \alpha M_k p\Delta\theta_k = -\Delta P_{ek}, \quad k = 1, 2, ...m \tag{9.16}$$

Utilizing Eq. (9.6), (9.5) can be expressed as

$$\begin{aligned}
\Delta P_{ek} &= \sum_{j=1, j \neq k}^{m} -G_{kj}^R(\Delta\delta_k - \Delta\delta_j) \\
&= \sum_{j=1, j \neq k}^{m} -G_{kj}^R(\Delta\theta_k - \Delta\theta_j)
\end{aligned} \tag{9.17}$$

Eq. (9.15) is utilized in deriving (9.17). If $\alpha = 0$, the linearized system equations can be written in the matrix form as

$$[M]p^2\Delta\theta = -[G]^R\Delta\theta \tag{9.18}$$

in addition to the scalar equation

$$M_T p^2 \Delta\delta_o = 0 \tag{9.19}$$

where $[G]^R$ is a reduced (to generator internal buses) symmetric matrix with elements $G^R(j, k) = G_{jk}^R = G_{kj}^R$. The rank of this matrix is less than or equal to $(m - 1)$.

Remarks

1. For lossless network and constant active power loads

$$\Delta P_{COI} = 0$$

   In this case, we also have (with zero damping)

$$[M]p^2\Delta\delta = -[G]^R\Delta\delta$$

2. In light of Eq. (9.14) the number of independent angle variables on COI reference frame are reduced to only m, namely $\theta_1, \theta_2....\theta_{m-1}$ and δ_o.

3. There are n second order differential equations describing the system. Thus there are $2n$ system eigenvalues out of which two are zero (for zero damping) in light of

$$
\begin{aligned}
p\Delta\delta_o &= \Delta\tilde{\omega}_o \\
p\Delta\tilde{\omega}_o &= -\alpha\Delta\tilde{\omega}_o + \frac{\Delta P_{COI}}{M_T}
\end{aligned}
$$

   If $\alpha \neq 0$, then one of the eigenvalues is $-\alpha$, while the second is zero.

4. Even if $\Delta P_{COI} \neq 0$, it can be shown that

$$\Delta P_{COI} = \sum_{k=1}^{m-1} \gamma_k \Delta\theta_k$$

   The system equations can be written as

$$\Delta\dot{y} = [A]\Delta y$$

   where

$$y^t = [\theta_1, \dot{\theta}_1, \theta_2, \dot{\theta}_2, \ldots, \theta_{m-1},\ \dot{\theta}_{m-1}, \tilde{\omega}_o, \delta_o]$$

$$[A] = \begin{bmatrix} A_{11} & 0 \\ A_{21} & A_{22} \end{bmatrix}$$

   The eigenvalues of $[A]$ are the eigenvalues of $[A_{11}]$ and $[A_{22}]$. The latter is 2x2 matrix given by

$$[A_{22}] = \begin{bmatrix} -\alpha & 0 \\ 1 & 0 \end{bmatrix}$$

   This shows that the system equations on COI reference has the advantage of bringing out the system structure.

5. The assumption about uniform damping is required to decouple the system equations into two sets, when $\Delta P_{COI} = 0$.

Solution of Equation (9.18)

Defining the transformation from θ to β given by

$$[M]^{1/2}\theta = \beta \tag{9.20}$$

Eq. (9.18) can be expressed as

$$
\begin{aligned}
p^2 \Delta\beta &= -[M]^{-1/2}[G]^R[M]^{-1/2}\Delta\beta \\
&= -[K]\Delta\beta
\end{aligned}
\tag{9.21}
$$

where

$$[K] = [M]^{-1/2}[G]^R[M]^{-1/2}$$

is also a symmetric matrix as both $[G]^R$ and $[M]$ are symmetric matrices. $[M]$ is a diagonal matrix of inertia coefficients. The rank of $[K]$ is same as that of $[G]^R$. The eigenvalues of $[K]$ are real and at least one of them is zero. It is to be noted that in the resistive network described by Eq. (9.4), the individual element g_{ij} can be positive, zero or negative depending on whether the magnitude of $(\delta_i - \delta_j)$ is less than, equal or greater than 90° (but less than 180°). It can be shown that if the operating point is a stable equilibrium point, the $(m-1)$ eigenvalues of $[K]$ are each positive. The matrix $[K]$ can be expressed as

$$[K] = [P][\Omega][P]^t$$

where $[P]$ is a matrix of normalized eigenvectors of $[K]$. It is assumed that the eigenvalues of $[K]$ are distinct. $[P]$ is an orthogonal matrix with the property

$$[P]^{-1} = [P]^t$$

Ω is a diagonal matrix of the eigenvalues of $[K]$. It can be shown that each non-zero eigenvalue is equal to square of the radian frequency of an electromechanical (low frequency) oscillatory mode. Thus there are at most $(m-1)$ modes in a m machine system (Note that an infinite bus is an idealization of a large generator with negligible reactance and infinitely large inertia).

Remarks

1. When damping is nonuniform, there will be coupling between Eq. (9.11) and (9.12). However, only $(2m-1)$ variables (θ_1, θ_2 ... θ_{m-1}, $\dot{\theta}_1$, $\dot{\theta}_2$ ... $\dot{\theta}_{m-1}$ and $\tilde{\omega}_o$) need to be considered. The variable δ_o does not appear in the equations and is obtained by integrating $\tilde{\omega}_o$.

2. The frequency dependent load models can be considered where the loads are linearly proportional to bus frequency, i.e.

$$P_{Lj} = P_{Ljo} + k_j \frac{d\delta_j}{dt}$$

where δ_j is the bus angle at load bus j

From the network representation given in Fig. 9.2, $\Delta\delta_j$ can be expressed as

$$\Delta\delta_j = \sum_{k=1}^{m-1} R_{jk} G_{kk}^R \Delta\delta_k$$

where $R_{jk} = R(j,k)$ is the element of the bus resistance matrix $[R]$ defined by

$$[R] = [G']^{-1}$$

where $[G']$ is the matrix derived from $[G]$ by deleting the row and column corresponding to a reference generator (internal bus).

3. The use of COI is not essential in writing state space equations.

Linearized State Space Equations

The linearized state space equations for the system can be obtained from the network analogy with $\Delta\omega$ $(p\Delta\delta)$ analogous to voltage and ΔP analogous to current, the network consists of GLC elements - C (capacitor) corresponding to inertia (M), G (conductance) corresponding to damping (or frequency dependent loads) and L (inductance) corresponding to reciprocal of G_{ij}. As an example, the analogous network for the system shown in Fig. 9.1 is shown in Fig. 9.3. It is assumed that there is a frequency dependent load at bus 4.

The unreduced network is shown in Fig. 9.3(a). The reduced network eliminating buses 1, 2 and 3 is shown in Fig. 9.3 (b). The element $K_{12}, K_{13}, K_{14}, K_{23}, K_{24}$ and K_{34} are reciprocals of inductances (Notice that these are identical to elements of the reduced matrix $[G^R]$ which includes buses G_1, G_2, G_3 and 4). The variable $\Delta\delta$ is analogous to flux linkage. The equations for the network shown in Fig. 9.3 (b) are obtained as

$$M_1 \frac{d}{dt}\Delta\omega_1 + D_1'\Delta\omega_1 = -\Delta P_{e1}$$

$$M_2 \frac{d}{dt}\Delta\omega_2 + D_2'\Delta\omega_2 = -\Delta P_{e2}$$

$$M_3 \frac{d}{dt}\Delta\omega_3 + D_3'\Delta\omega_3 = -\Delta P_{e3}$$
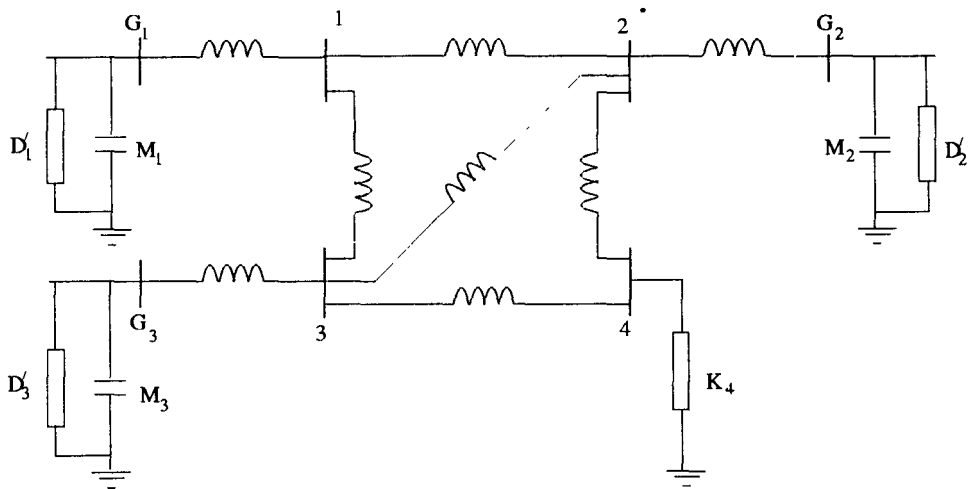
(a) Unreduced network
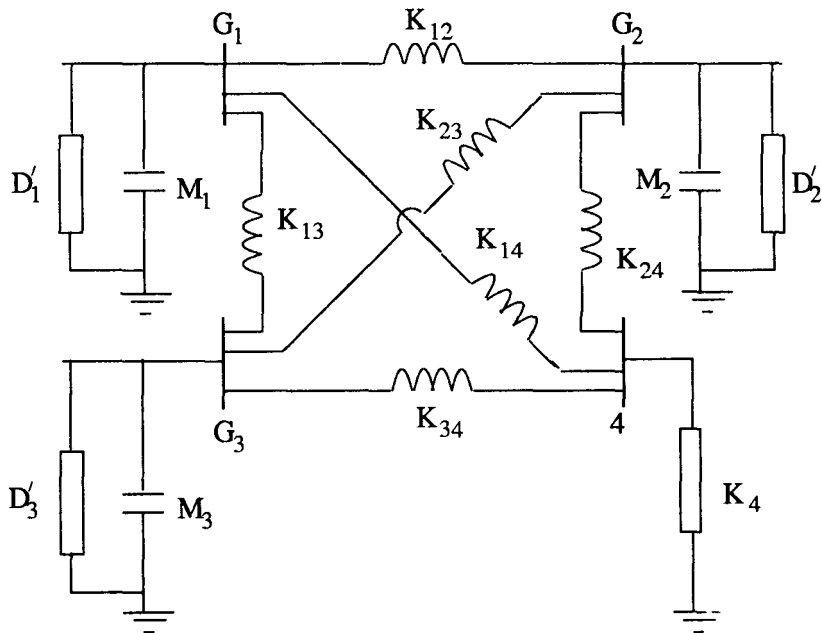
(b) Reduced network

Figure 9.3: An electrical network analogue for small signal analysis

$$\frac{d}{dt}\Delta\delta_{12} = \Delta\omega_1 - \Delta\omega_2$$

$$\frac{d}{dt}\Delta\delta_{13} = \Delta\omega_1 - \Delta\omega_3$$

$$\frac{d}{dt}\Delta\delta_{14} = \Delta\omega_1 - \Delta\omega_4$$

$$\Delta P_{e1} = K_{12}\Delta\delta_{12} + K_{13}\Delta\delta_{13} + K_{14}\Delta\delta_{14}$$

$$\Delta P_{e2} = -K_{12}\Delta\delta_{12} + K_{23}(\Delta\delta_{13} - \Delta\delta_{12}) + K_{24}(\Delta\delta_{14} - \Delta\delta_{12})$$

$$\Delta P_{e3} = -K_{13}\Delta\delta_{13} + K_{23}(\Delta\delta_{12} - \Delta\delta_{13}) + K_{34}(\Delta\delta_{14} - \Delta\delta_{13})$$

$$K_4\Delta\omega_4 = K_{14}\Delta\delta_{14} + K_{24}(\Delta\delta_{14} - \Delta\delta_{12}) + K_{34}(\Delta\delta_{14} - \Delta\delta_{13})$$

The algebraic equations are used to eliminate the non-state variables ΔP_{e1}, ΔP_{e2}, ΔP_{e3} and $\Delta\omega_4$ in the state equations. These are expressed as

$$\dot{x} = [A]x$$

where
$$x^t = [\Delta\omega_1 \quad \Delta\omega_2 \quad \Delta\omega_3 \quad \Delta\delta_{12} \quad \Delta\delta_{13} \quad \Delta\delta_{14}]$$

Remarks

1. The applicability of network analogue for the derivation of system state equations arises on account of the assumptions made earlier that the system is lossless and all buses are PV buses. The latter assumption is quite stringent and can be unrealistic.

2. The frequency dependence of the loads is considered easily from the network analogy.

3. The system is stable if all the damping terms (in generators and loads) are positive and $K_{ij} > 0$ for all i and j. (These are sufficient conditions).

9.2 Detailed Models: Case I

In the previous section, a simplified system model was considered, where generators are represented by classical models. In this section, model 1.0 is assumed for synchronous machines by neglecting damper windings. In addition, the following assumptions are made for simplicity.

1. The loads are represented by constant impedances.

2. Transient saliency is ignored by considering $x_q = x_d'$.

3. Mechanical power is assumed to be constant.

Neglecting saliency, the stator of a synchronous machine is represented by the equivalent circuit shown in Fig. 9.4. The only difference between the classical model and here is that E_q' is treated as a state variable influenced by field excitation.
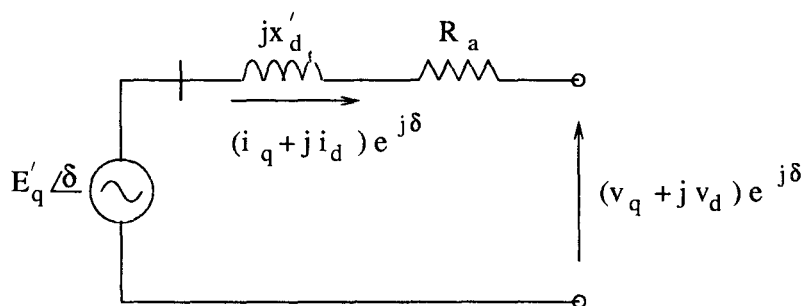
Figure 9.4: Stator equivalent circuit
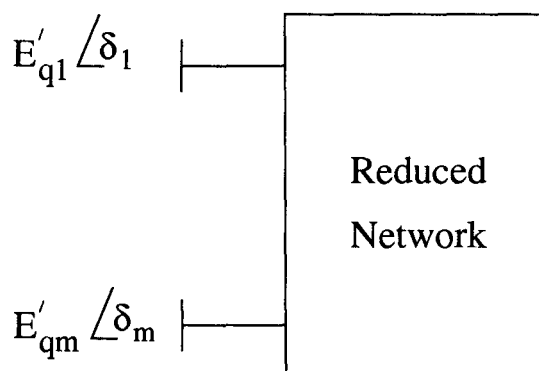
Figure 9.5: Reduced network (with generator internal buses)

From assumption (1), the load buses can be eliminated and the network reduced to only the internal buses of the generator. (see Fig. 9.5)

The electrical power output of generator k is given by

$$P_{ek} = \sum_{j=1}^{m} E_{qk}'[G_{jk} \cos \delta_{kj} + B_{jk} \sin \delta_{kj}] E_{qj}' \qquad (9.22)$$

where $\delta_{kj} = \delta_k - \delta_j$, $(G_{jk} + jB_{jk})$ is an element of the reduced admittance matrix of the network.

Generator Equations

The machine equations (for k^{th} machine) are

$$pE'_{qk} = \frac{1}{T'_{dok}} \left[-E'_{qk} + (x_{dk} - x'_{dk})i_{dk} + E_{fdk} \right] \tag{9.23}$$

$$p\delta_k = \omega_B(S_{mk} - S_{mko}) \tag{9.24}$$

$$pS_{mk} = \frac{1}{2H_k} \left[-D_k(S_{mk} - S_{mko}) + P_{mk} - P_{ek} \right] \tag{9.25}$$

P_{mk} and P_{ek} are used instead of T_{mk} and T_{ek}, for convenience. Actually there is no difference between P_{ek} and T_{ek} as the frequency variations are neglected in the network calculation.

At the generator internal bus, the complex power is given by

$$\begin{aligned} P_{ek} + jQ_{ek} &= E'_{qk}(i_{qk} - ji_{dk}) \\ &= E'_{qk}i_{qk} - jE'_{qk}i_{dk} \end{aligned} \tag{9.26}$$

Thus, i_{dk} is expressed by

$$i_{dk} = \frac{-Q_{ek}}{E'_{qk}} \tag{9.27}$$

where the expression for Q_{ek} is obtained as

$$Q_{ek} = \sum_{j=1}^{m} E'_{qk}[G_{jk} \sin \delta_{kj} - B_{jk} \cos \delta_{kj}]E'_{qj} \tag{9.28}$$

Linearizing Eq. (9.27), we get

$$\Delta i_{dk} = \frac{Q_{eko}}{(E'_{qko})^2}\Delta E'_{qk} - \frac{\Delta Q_{ek}}{E'_{qko}} \tag{9.29}$$

Linearizing Eqs. (9.23) to (9.25), and combining the equations for all the generators we have

$$\dot{X}_g = [A_g]X_g + [B_g]\Delta S_e + [E_g]\Delta E_{fd} \tag{9.30}$$

where
$X_g^t = [\Delta E'_{q1} \ \Delta\delta_1 \ \Delta S_{m1} \dots \Delta E'_{qk} \ \Delta\delta_k \ \Delta S_{mk} \dots \Delta E'_{qm} \ \Delta\delta_m \ \Delta S_{mm}]$
$[A_g] = \text{Diag } [A_{g1} \ A_{g2} \dots A_{gm}]$
$[B_g] = \text{Diag } [B_{g1} \ B_{g2} \dots B_{gm}]$
$[E_g] = \text{Diag } [E_{g1} \ E_{g2} \dots E_{gm}]$
$\Delta S_e^t = [\Delta P_{e1} \ \Delta Q_{e1} \dots \Delta P_{ek} \ \Delta Q_{ek} \dots \Delta P_{em} \ \Delta Q_{em}]$

$$[A_{gk}] = \begin{bmatrix} a_k & 0 & 0 \\ 0 & 0 & \omega_B \\ 0 & 0 & -\dfrac{D_k}{2H_k} \end{bmatrix}$$

$$[B_{gk}] = \begin{bmatrix} 0 & b_k \\ 0 & 0 \\ -\dfrac{1}{2H_k} & 0 \end{bmatrix}, \quad [E_{gk}] = \begin{bmatrix} \dfrac{1}{T'_{dok}} \\ 0 \\ 0 \end{bmatrix}$$

$$a_k = \frac{1}{T'_{do}} \left[-1 + \frac{(x_{dk} - x'_{dk})}{(E'_{qko})^2} Q_{eko} \right], \quad b_k = -\frac{(x_{dk} - x'_{dk})}{T'_{do} E'_{qko}}$$

Linearizing expression (9.22) and (9.28), we can express

$$\Delta S_e = [F_1]\Delta E'_q + [F_2]\Delta \delta \tag{9.31}$$

where $[F_1]$ and $[F_2]$ are $(2m \times m)$ matrices. It is not difficult to see that $[F_2]$ is a singular matrix as all the columns add up to zero. This comes about as the expressions in P_{ek} and Q_{ek} depend only on the differences in the rotor angles. Thus, state space description is simplified by considering the state vector as

$$X^t_G = [\Delta E_{q1} \ \Delta \delta_{1m} \ \Delta S_{m1} \dots \Delta E'_{qk} \ \Delta \delta_{km} \ \Delta S_{mk} \dots \Delta E'_{qm} \ \Delta S_{mm}]$$

Here, $\Delta \delta_{km} = \Delta \delta_k - \Delta \delta_m$ and one of the angle variables is dispensed with. The system equation can be expressed as

$$\dot{X}_G = [A_G]X_G + [B_G]\Delta S_e + [E_G]\Delta E_{fd} \tag{9.32}$$

$[A_G]$ is $(3m - 1) \times (3m - 1)$ matrix, $[B_G]$ is $(3m - 1) \times 2m$ matrix and $[E_G]$ is $(3m - 1) \times m$ matrix. They differ from $[A_g], [B_g]$ and $[E_g]$ in that (a) the entries for $[A_{gm}], [B_{gm}]$ and $[E_{gm}]$ are different and (b) the last column of $[A_G]$ has entries in rows corresponding to $\Delta \delta_{km}$, which are each equal to $-\omega_B$.

$[A_{gm}], [B_{gm}]$ and $[E_{gm}]$ are given by

$$[A_{gm}] = \begin{bmatrix} a_m & 0 \\ 0 & -\dfrac{D_m}{2H_m} \end{bmatrix}, \quad [B_{gm}] = \begin{bmatrix} 0 & b_m \\ -\dfrac{1}{2H_m} & 0 \end{bmatrix}, \quad [E_{gm}] = \begin{bmatrix} \dfrac{1}{T'_{dom}} \\ 0 \end{bmatrix}$$

Using relative angles instead of absolute angles, Eq. (9.31) is reduced to

$$\Delta S_e = [F_1]\Delta E'_q + [F'_2]\Delta \delta' \tag{9.33}$$

where $[F'_2]$ is a $(2m \times m - 1)$ matrix obtained from $[F_2]$ by subtracting the last column of $[F_2]$ from all the remaining columns (and deleting the last column). $\Delta \delta'$ is a vector of relative angles whose k^{th} element is $(\Delta \delta_k - \Delta \delta_m) = \Delta \delta_{km}$.

The final system equations are obtained by substituting Eq. (9.33) in (9.32). We have

$$\dot{X}_G = \{[A_G] + [B_G][F]\}X_G + [E_G]\Delta E_{fd} \tag{9.34}$$

where

$$[F] = [F_1][C_1] + [F_2'][C_2]$$

$[C_1]$ and $[C_2]$ are defined by
$[C_1] = \text{Diag} [C_{11} \ldots C_{1k} \ldots C_{1m}]$
$[C_2] = \text{Diag} [C_{21} \ldots C_{2k} \ldots C_{2(m-1)}]$
C_{1k} and C_{2k} are row vectors of dimension 3, defined by

$$C_{1k} = [1 \quad 0 \quad 0], \quad C_{2k} = [0 \quad 1 \quad 0]$$

C_{1m} is a row vector of dimension 2.

$$C_{1m} = [1 \quad 0]$$

$C_{2(m-1)}$ is a row vector of dimension 5 given by

$$C_{2(m-1)} = [0 \quad 1 \quad 0 \quad 0 \quad 0]$$

If excitation controllers are to be considered, then the system matrix will be augmented by the inclusion of controller dynamics. In this case, ΔE_{fd} is a vector of output variables from the excitation controllers and can be expressed in terms of the state variables of the controllers.

9.3   Detailed Model : Case II

The assumption about loads as constant impedances, is restrictive if nonlinear load characteristics or load dynamics are to be considered. The dynamics of SVC or HVDC controllers can be viewed as part of load dynamics as SVC and HVDC converter buses are treated as load buses. Of course, the controller dynamics are unique and distinct from typical loads such as induction motors.

Generator Equations

In order to preserve the structure of the power system network, (retaining the load buses), the generator representation as given in the previous section needs to be slightly modified. The generator equations are expressed as

$$\dot{x}_g = [A_g]x_g + [B_g]\Delta V_g + [E_g]u_c \qquad (9.35)$$

where u_c is the vector of small perturbations in the reference input variables of the generator controllers (ΔV_{ref} and ΔT_m or $\Delta \bar{\omega}_{ref}$). ΔV_g are the small

deviations in the generator terminal voltage expressed in polar or rectangular coordinates defined below

$$\Delta V_g^p = \begin{bmatrix} V_{go}\Delta\theta_g \\ \Delta \mid V_g \mid \end{bmatrix}$$

$$\Delta V_g^r = \begin{bmatrix} \Delta V_{Qg} \\ \Delta V_{Dg} \end{bmatrix}$$

The two expressions are related by

$$\Delta V_g^p = \frac{1}{V_{go}} \begin{bmatrix} -V_{Dgo} & V_{Qgo} \\ V_{Qgo} & V_{Dgo} \end{bmatrix} \begin{bmatrix} \Delta V_{Qg} \\ \Delta V_{Dg} \end{bmatrix} = [P]\Delta V_g^r$$

It is easy to see that

$$[P]^{-1} = [P]$$

The output variables of the generator can be small deviations in the power output or currents (referred to Kron's reference frame). If currents are used, then

$$\Delta I_g = \begin{bmatrix} \Delta I_{Dg} \\ \Delta I_{Qg} \end{bmatrix} = [C_g]x_g + [D_g]\Delta V_g \qquad (9.36)$$

Example: If synchronous machine is represented by model 1.1, neglecting prime-mover dynamics and considering only a single time constant exciter, the state variables are

$$x_g^t = [\Delta\delta \ \ \Delta S_m \ \ \Delta E_q' \ \ \Delta E_d' \ \ \Delta E_{fd}]$$

The nonzero elements of matrix $[A_g]$ are given by
$A_g(1,2) = \omega_B$

$$A_g(2,1) = -\frac{1}{2H} \left[\frac{E_{qo}'}{x_d'}V_{go} \ \cos(\delta_o - \theta_{go}) - \frac{E_{do}'}{x_q'}V_{go} \ \sin(\delta_o - \theta_{go}) + \right.$$

$$\left. (x_d' - x_q')\frac{V_{go}^2 \ \cos 2(\delta_o - \theta_{go})}{x_d' x_q'} \right]$$

$$A_g(2,2) = \frac{-D}{2H}$$

$$A_g(2,3) = \frac{-V_{go} \, \sin(\delta_o - \theta_{go})}{2H x_d'}$$

$$A_g(2,4) = -\frac{V_{go} \, \cos(\delta_o - \theta_{go})}{2H x_q'}$$

$$A_g(3,1) = -\frac{(x_d - x_d')}{T_{do}' x_d'} \, V_{go} \, \sin(\delta_o - \theta_{go})$$

$$A_g(3,3) = -\frac{1}{T_{do}'} \left[1 + \frac{(x_d - x_d')}{x_d'} \right]$$

$$A_g(3,5) = \frac{1}{T_{do}'}$$

$$A_g(4,1) = -\frac{(x_q - x_q') \, \cos(\delta_o - \theta_{go})}{T_{qo}' x_q'} \, V_{go}$$

$$A_g(4,4) = -\frac{1}{T_{qo}'} \left[1 + \frac{(x_q - x_q')}{x_q'} \right]$$

$$A_g(5,5) = -\frac{1}{T_E}$$

Similarly, the nonzero elements of $[B_g]$ and $[E_g]$ are given by

$$B_g^p(2,1) = \frac{1}{2H} \left[\frac{E_{qo}' \, \cos(\delta_o - \theta_{go})}{x_d'} - \frac{E_{do}' \, \sin(\delta_o - \theta_{go})}{x_q'} + V_{go} \, (x_d' - x_q') \frac{\cos 2(\delta_o - \theta_{go})}{x_d' \, x_q'} \right]$$

$$B_g^p(2,2) = -\frac{1}{2H} \left[\frac{E_{qo}' \, \sin(\delta_o - \theta_{go})}{x_d'} + \frac{E_{do}'}{x_q'} \, \cos(\delta_o - \theta_{go}) + (x_d' - x_q') \frac{V_{go} \, \sin 2(\delta_o - \theta_{go})}{x_d' \, x_q'} \right]$$

$$B_g^p(3,1) = \frac{(x_d - x_d') \, \sin(\delta_o - \theta_{go})}{x_d' \, T_{do}'}$$

$$B_g^p(3,2) = \frac{(x_d - x_d') \; \cos(\delta_o - \theta_{go})}{x_d' \; T_{do}'}$$

$$B_g^p(4,1) = \frac{(x_q - x_q') \; \cos(\delta_o - \theta_{go})}{x_q' \; T_{qo}'}$$

$$B_g^p(4,2) = -\frac{(x_q - x_q') \; \sin(\delta_o - \theta_{go})}{x_q' \; T_{qo}'}$$

$$B_g^p(5,2) = -\frac{K_E}{T_E}$$

$$E_g(5) = \frac{K_E}{T_E}, \quad E_g(2) = \frac{1}{2H}$$

$[E_g]$ is a column vector in this case as u_c is a scalar equal to ΔV_{ref}. K_E and T_E are the gain and time constant of the excitation system. The armature resistance is neglected in deriving the expressions. The superscript p indicates polar coordinates are used.

The nonzero elements of $[C_g]$ and $[D_g]$ are given below

$$C_g(1,1) = I_{Qgo} + \frac{V_{go} \; \sin\delta_o \; \cos(\delta_o - \theta_{go})}{x_q'} - \frac{V_{go} \; \sin(\delta_o - \theta_{go}) \; \cos\delta_o}{x_d'}$$

$$C_g(1,3) = -\frac{\cos\delta_o}{x_d'}$$

$$C_g(1,4) = \frac{\sin\delta_o}{x_q'}$$

$$C_g(2,1) = V_{go} \left[\frac{\sin\delta_o \; \sin(\delta_o - \theta_{go})}{x_d'} + \frac{\cos\delta_o \cos(\delta_o - \theta_{go})}{x_q'} \right] - I_{Dgo}$$

$$C_g(2,3) = \frac{\sin\delta_o}{x_d'}$$

$$C_g(2,4) = \frac{\cos\delta_o}{x_q'}$$

$$D_g^p(1,1) = \frac{\cos\delta_o \; \sin(\delta_o - \theta_{go})}{x_d'} - \frac{\sin\delta_o \; \cos(\delta_o - \theta_{go})}{x_q'}$$

$$D_g^p(1,2) = \frac{\cos \delta_o \cos(\delta_o - \theta_{go})}{x_d'} + \frac{\sin \delta_o \sin(\delta_o - \theta_{go})}{x_q'}$$

$$D_g^p(2,1) = -\frac{\sin \delta_o \sin(\delta_o - \theta_{go})}{x_d'} - \frac{\cos \delta_o \cos(\delta_o - \theta_{go})}{x_q'}$$

$$D_g^p(2,2) = -\frac{\sin \delta_o \cos(\delta_o - \theta_{go})}{x_d'} + \frac{\cos \delta_o \sin(\delta_o - \theta_{go})}{x_q'}$$

If $x_d' = x_q' = x'$, then some of the expressions given above are simplified. These are

$$D_g(1,1) = \frac{-\sin \theta_{go}}{x'}, \quad D_g(1,2) = \frac{\cos \theta_{go}}{x'}$$

$$D_g(2,1) = \frac{-\cos \theta_{go}}{x'}, \quad D_g(2,2) = -\frac{\sin \theta_{go}}{x'}$$

$$C_g(1,1) = I_{Qgo} + \frac{V_{go}}{x'} \sin \theta_{go}$$

$$C_g(2,1) = -I_{Dgo} + \frac{V_{go}}{x'} \cos \theta_{go}$$

The matrices $[B_g^r]$ and $[D_g^r]$ are obtained as

$$[B_g^r] = [B_g^p][P]$$
$$[D_g^r] = [D_g^p][P]$$

The superscript r indicates that rectangular coordinates are used.

Network Equations

The linearized network equations can be expressed either using admittance matrix (and DQ variables) or using Jacobian matrix (obtained from power balance equations). Using the former, we can express as

$$[Y_{DQ}]\Delta V_{QD} = \Delta I_{DQ} \tag{9.37}$$

where each element of $[Y_{DQ}]$ is a 2x2 matrix. For example

$$Y_{DQ}(i,j) = \begin{bmatrix} B_{ij} & G_{ij} \\ G_{ij} & -B_{ij} \end{bmatrix}$$

$\Delta V_{QD}(i)$ and $\Delta I_{DQ}(i)$ are vectors with elements

$$\Delta V_{QD}(i) = \begin{bmatrix} \Delta V_{Qi} \\ \Delta V_{Di} \end{bmatrix}, \quad \Delta I_{DQ}(i) = \begin{bmatrix} \Delta I_{Di} \\ \Delta I_{Qi} \end{bmatrix}$$

Note that the voltages are expressed with ΔV_{Qi} preceding ΔV_{Di}. On the other hand, the currents are expressed with ΔI_{Di} preceding ΔI_{Qi}. This is deliberately done so that the matrix $[Y_{DQ}]$ is a real symmetric matrix (if phase shifting transformers are not considered).

If power balance equations are used, the linearized equations can be expressed as

$$[J]\Delta V^p = \Delta S \qquad (9.38)$$

where J is Jacobian matrix defined by

$$J(i,j) = \begin{bmatrix} \dfrac{1}{V_j}\dfrac{\partial P_i}{\partial \theta_j} & \dfrac{\partial P_i}{\partial V_j} \\[2ex] \dfrac{1}{V_j}\dfrac{\partial Q_i}{\partial \theta_j} & \dfrac{\partial Q_i}{\partial V_j} \end{bmatrix}$$

$$\Delta V^p(i) = \begin{bmatrix} V_i\Delta\theta_i \\ \Delta V_i \end{bmatrix}, \quad \Delta S(i) = \begin{bmatrix} \Delta P_i \\ \Delta Q_i \end{bmatrix}$$

P_i and Q_i are power injections at bus i, θ_i and V_i are the angle and magnitude of the voltage at bus i.

It is also possible to use rectangular coordinates instead of polar coordinates. In this case, Jacobian matrix is different than what is given above.

It is convenient to use Eq. (9.37) as the admittance matrix is unchanged with change in the operating point. On the other hand, Jacobian matrix is dependent on the operating point.

If load dynamics are neglected, the effect of the static loads are considered by modifying the diagonal entries of the matrix $[Y_{DQ}]$. The similar thing applies for the effect of SVC also, when only steady state control characteristics are to be considered.

Derivation of System Equations

Let the number of generators in the system be m_g, the number of loads m_l and the number of static var compensators be m_s. Let the number of buses

in the network be n. Eq. (9.37) can be rewritten as

$$[Y_{DQ}]\Delta V_{QD} = [P_G]\Delta I_G - [P_S]\Delta I_S - [P_L]\Delta I_L \qquad (9.39)$$

where P_G is a $2nx2m_g$ matrix with elements

$$P_G(i,j) = \begin{bmatrix} 1 & 0 \\ 0 & 1 \end{bmatrix}$$

if generator j is connected to bus i, otherwise

$$P_G(i,j) = \begin{bmatrix} 0 & 0 \\ 0 & 0 \end{bmatrix}$$

Similarly $[P_S]$ and $[P_L]$ can be defined. $P_S(i,j)$ or $P_L(i,j)$ is a unit matrix of dimension 2 if SVC 'j' (or load j) is connected to bus i. Otherwise $P_S(i,j)$ or $P_L(i,j)$ is a null matrix. Notice that the signs associated with ΔI_S and ΔI_L are negative as the SVC and load currents are assumed to flow away from the bus (load convention).

From the discussion given in chapter 7, both ΔI_S and ΔI_L can be expressed as

$$\Delta I_S = [Y_S]\Delta V_S \qquad (9.40)$$

$$\Delta I_L = [Y_L]\Delta V_L \qquad (9.41)$$

where both $[Y_S]$ and $[Y_L]$ are block diagonal matrices. ΔV_S and ΔV_L can be expressed as

$$\Delta V_S = [P_S]^t \Delta V_{QD}, \quad \Delta V_L = [P_L]^t \Delta V_{QD}$$

The generator current vector ΔI_G is a collection of the quantities ΔI_{g1}, ΔI_{g2} ... ΔI_{gm_g} and can be expressed as

$$\Delta I_G = [C_G]X_G - [Y_G]\Delta V_G \qquad (9.42)$$

where
$$X_G^t = [x_{g1}^t \ x_{g2}^t...x_{gm_g}^t]$$

$$\Delta V_G^t = [\Delta V_{g1}^t \ \Delta V_{g2}^t...\Delta V_{gm_g}^t]$$

$$\Delta I_G^t = [\Delta I_{g1}^t, \Delta I_{g2}^t...\Delta I_{gm_g}^t]$$

$$[C_G] = Diag[C_{g1} \quad C_{g2}...C_{gm_g}]$$

$$[Y_G] = Diag[-D^r_{g1} \quad - D^r_{g2}... - D^r_{gm_g}]$$

After some manipulations, Eq. (9.39) can be expressed as

$$[Y'_{DQ}]\Delta V_{QD} = [P_G][C_G]X_G \tag{9.43}$$

where

$$[Y'_{DQ}] = [Y_{DQ}] + [P_G Y_G P^t_G] + [P_S Y_S P^t_S] + [P_L Y_L P^t_L]$$

is modified admittance matrix. Actually the modification affects only the diagonal elements corresponding to buses where generator, load or SVC are connected. In deriving this, the following relation is also used

$$\Delta V_G = [P_G]^t \Delta V_{QD} \tag{9.44}$$

After solving for ΔV_{QD} from Eq. (9.43), we can express ΔV_G as

$$\Delta V_G = [P_G]^t[Y'_{DQ}]^{-1}[P_G][C_G]X_G \tag{9.45}$$

The collection of all the generator equations is expressed by

$$\dot{X}_G = [A_G]X_G + [B_G]\Delta V_G + [E_G]U_c \tag{9.46}$$

where
$$[A_G] = \text{Diag } [A_{g1} \quad A_{g2}......A_{gm_g}]$$
$$[B_G] = \text{Diag } [B^r_{g1} \quad B^r_{g2}......B^r_{gm_g}]$$
$$[E_G] = \text{Diag } [E_{g1} \quad E_{g2}......E_{gm_g}]$$
$$U^t_c = [u^t_{c1} \quad u^t_{c2}......u^t_{cm_g}]$$

Substituting Eq. (9.45) in (9.46) gives

$$\dot{X}_G = [A_T]X_G + [E_G]U_c \tag{9.47}$$

where

$$[A_T] = [A_G] + [B_G][P_G]^t[Y'_{DQ}]^{-1}[P_G][C_G]$$

9.4   Inclusion of Load and SVC Dynamics

The dynamics of SVC and load (say induction motor) can be included if necessary, by expressing their equations in the form

$$
\left.
\begin{aligned}
\dot{x}_s &= [A_s]x_s + [B_s]\Delta V_s + [E_s]u_{cs} \\
-\Delta I_s &= [C_s]x_s + [D_s]\Delta V_s
\end{aligned}
\right\}
\tag{9.48}
$$

$$
\left.
\begin{aligned}
\dot{x}_l &= [A_l]x_l + [B_l]\Delta V_l + [E_l]u_{cl} \\
-\Delta I_l &= [C_l]x_l + [D_l]\Delta V_l
\end{aligned}
\right\}
\tag{9.49}
$$

$$
\Delta I_S^t = [\Delta I_{s1}^t \ \ \Delta I_{s2}^t .... \Delta I_{sm_s}^t]
$$
$$
\Delta I_L^t = [\Delta I_{l1}^t \ \ \Delta I_{l2}^t .... \Delta I_{lm_l}^t]
$$

Note that Eqs. (9.48) and Eq. (9.49) are similar in structure to the generator equations except for the sign change associated with the currents.

The system equations can be obtained using similar procedure outlined in the previous section.

The equation (9.43) gets modified to

$$
[Y_{DQ}']\Delta V_{QD} = [P_G][C_G]X_G + [P_S][C_S]X_S + [P_L][C_L]X_L
\tag{9.50}
$$

where $[Y_{DQ}']$ is a modified admittance matrix similar to that defined earlier. $[Y_S]$ and $[Y_L]$ in this case are defined by

$[Y_S] = \text{Diag} \ [-D_{s1} \ \ -D_{s2}..... -D_{sm_s}]$
$[Y_l] = \text{Diag} \ [-D_{l1} \ \ -D_{l2}..... -D_{lm_l}]$

The collection of the generator, SVC and load equations can be expressed as

$$
\left.
\begin{aligned}
\dot{X} &= [A]X + [B]\Delta V + [E]U_c \\
\Delta I &= [C]X + [D]\Delta V
\end{aligned}
\right\}
\tag{9.51}
$$

where
$[A] = \text{Diag} \ [A_G \ \ A_S \ \ A_L]$
$[A_S] = \text{Diag} \ [A_{s1} \ \ A_{s2}...A_{sm_s}]$
$[A_L] = \text{Diag} \ [A_{l1} \ \ A_{l2}...A_{lm_l}]$
$[B] = \text{Diag} \ [B_G \ \ B_S \ \ B_L]$
$[B_S] = \text{Diag} \ [B_{s1} \ \ B_{s2}...B_{sm_s}]$

$$[B_L] = \text{Diag } [B_{l1} \ B_{l2}...B_{lm_l}]$$
$$[C] \ = \text{Diag } [C_G \ C_S \ C_L]$$
$$[C_S] = \text{Diag } [C_{s1} \ C_{s2}...C_{sm_s}]$$
$$[C_L] = \text{Diag } [C_{l1} \ C_{l2}...C_{lm_l}]$$
$$[E] \ = \text{Diag } [E_G \ E_S \ E_L]$$
$$[E_S] = \text{Diag } [E_{s1} \ E_{s2}...E_{sm_s}]$$
$$[E_L] = \text{Diag } [E_{l1} \ E_{l2}...E_{lm_l}]$$
$$\Delta V^t = [\Delta V_G^t \ \Delta V_S^t \ \Delta V_L^t]$$
$$\Delta V_S^t = [\Delta V_{s1}^t \ \Delta V_{s2}^t....\Delta V_{sm_s}^t]$$
$$\Delta V_L^t = [\Delta V_{l1}^t \ \Delta V_{l2}^t....\Delta V_{lm_l}^t]$$

ΔV can be expressed as

$$\Delta V = \begin{bmatrix} P_G^t \\ P_S^t \\ P_L^t \end{bmatrix} \Delta V_{QD} = [P]^t \Delta V_{QD} \qquad (9.52)$$

where

$$[P] = [P_G \ P_S \ P_L]$$

From Eqs. (9.50) and (9.52), we can derive

$$\Delta V = [P]^t [Y_{DQ}']^{-1} [P][C]X \qquad (9.53)$$

This can be substituted in Eq. (9.51) to give

$$\dot{X} = [A_T]X + [E]U_c \qquad (9.54)$$

where

$$[A_T] = [A] + [B][P]^t [Y_{DQ}']^{-1} [P][C]$$

9.5 Modal Analysis of Large Power Systems

In recent years, computer programs for the eigenvalue analysis of large power systems have been developed. Notable among them are

(i) AESOPS (Analysis of Essentially Spontaneous Oscillations in Power Systems) [6]

(ii) PEALS (**P**rogram for **E**igenvalue **A**nalysis of **L**arge **S**ystems) [7]

The first program was developed under sponsorship of Electric Power Research Institute (EPRI) in U.S.A. and is capable of handling systems having upto 200C buses, 3600 lines and 350 generators. The second program is claimed to have the capability of handling systems having up to 12,000 buses and 1000 generators.

The major objective of both programs is to compute low frequency electromechanical (rotor) modes. It is obvious that in a large system, not all the eigenvalues are of interest. Also, the computation of all eigenvalues would require an enormous amount of computer time. Without considering sparsity, the number of computations required in eigenvalue calculation is proportional to n^3 where n is the size of the matrix. Hence only critical eigenvalues (which lie close to the imaginary axis and likely to cross into the RHP as the system operating conditions are changed) need to be determined.

The computation of an eigenvalue and the corresponding vector of matrix $[A_T]$ can be viewed as the solution of a set of nonlinear equations given by

$$[A_T - \lambda_i I_n]v_i = 0 \qquad (9.55)$$

where λ_i is the eigenvalue and v_i is the corresponding eigenvector. $[I_n]$ is a unit matrix of order n. There are n equations in n unknowns – λ_i and $(n-1)$ elements of the eigenvector. (one nonzero element of the vector v_i can be arbitrarily chosen as 1.0). Thus, the solution of Eq. (9.55) which determines λ_i and v_i, is equivalent to solving a load flow. While there may be thousands of state variables (and eigenvalues) there may be only few critical modes which have to be computed.

The formation of system matrix $[A_T]$ in power systems can be viewed as the elimination of non-state variables Z in the following general equations

$$\dot{X} \quad = \quad [A]X + [B]Z \qquad (9.56)$$
$$\underline{0} \quad = \quad [C]X + [D]Z \qquad (9.57)$$

These equations are applicable irrespective of the complexity of the system considered. The matrices $[A], [B]$ and $[C]$ are block diagonal, each block corresponding to the individual dynamic devices. The matrix $[D]$ is obtained from network admittance $[Y]$ and is generally sparse. The system matrix $[A_T]$ is obtained from Eqs. (9.56) and (9.57) as

$$[A_T] = [A] - [B][D]^{-1}[C] \qquad (9.58)$$

The matrix $[A_T]$ is generally full although the matrices on the RHS of (9.56) and (9.57) are sparse. For the determination of an eigenvalue and the eigenvector

it is convenient to express the equations as

$$
\begin{bmatrix} \underline{0} \\ \underline{0} \end{bmatrix} = \begin{bmatrix} [A - \lambda_i I_n] & [B] \\ [C] & [D] \end{bmatrix} \begin{bmatrix} X_i \\ Z_i \end{bmatrix}
\tag{9.59}
$$

where X_i is the eigenvector corresponding to λ_i.

Iterative Scheme for Computation of Eigenvalue

The matrix $[A]$ is block diagonal. If we wish to compute an eigenvalue which has its origin in a block (corresponding to a dynamic device, say a generator), then the matrix can be partitioned as

$$
[A] = \begin{bmatrix} A_1 & 0 \\ 0 & A_R \end{bmatrix}
$$

where R indicates the rest of the blocks. Note that $[A_R]$ is also a block diagonal matrix with number of blocks reduced by one compared to $[A]$. If $[A_1]$ corresponds to a generator with classical model, then there are two state variables (ΔS_{m1} and $\Delta \delta_1$) and $[A_1]$ can be expressed as

$$
[A_1] = \begin{bmatrix} -\dfrac{D_1}{2H_1} & -\dfrac{K_1}{2H_1}\omega_B \\[2ex] \omega_B & 0 \end{bmatrix}
\tag{9.60}
$$

By defining,

$$
[B'] = [[0] \quad [B_1]], \quad [C'] = \begin{bmatrix} [0] \\ [C_1] \end{bmatrix}
$$

$$
[D'(\lambda_i)] = \begin{bmatrix} A_R - \lambda_i I_{n_r} & B_2 \\ C_2 & D \end{bmatrix}
$$

where $[B_1], [B_2], [C_1]$ and $[C_2]$ are defined from

$$
[B] = \begin{bmatrix} B_1 \\ B_2 \end{bmatrix}, \quad [C] = [C_1 \quad C_2]
$$

it is possible to express λ_i as the solution of the equation

$$
det[A_1 - B'D'^{-1}(\lambda_i)C' - \lambda_i I_{n1}] = 0
\tag{9.61}
$$

where *det* stands for the determinant, I_{n_1} is the unit matrix of order n_1 (same as the size of $[A_1]$). Also

$$n = n_1 + n_r$$

The equation (9.61) is based on the assumption that

$$det[D'(\lambda_i)] \neq 0$$

The derivation of Eq. (9.61) follows from Schur's formula for partitioned matrices, according to which,

$$det[F] = det[D] \cdot det[A - BD^{-1}C] = det[A] \, det[D - CA^{-1}B] \qquad (9.62)$$

where

$$[F] = \begin{bmatrix} A & B \\ C & D \end{bmatrix} \qquad (9.63)$$

Schur's formula is applied to the matrix defined in Eq. (9.59) which is rearranged as

$$\begin{bmatrix} A_1 - \lambda_i I_{n1} & B' \\ C' & D'(\lambda_i) \end{bmatrix} \qquad (9.64)$$

Eq. (9.59) can be reduced (using the above matrix) to

$$\lambda_i X_{i1} = [A_1 - B'D'^{-1}(\lambda_i)C']X_{i1} \qquad (9.65)$$

where X_{i1} is the subset of X_i corresponding to the state variables defined in block 1 (A_1). An iterative technique can be used to solve for λ_i and $(n_1 - 1)$ elements of X_{i1} from Eq. (9.65). As a special case, when $n_1 = 1$, Eq. (9.64) reduces to a scalar equation expressed as

$$\lambda_i = A_1 - B'D'^{-1}(\lambda_i)C' \qquad (9.66)$$

One way of solving the above equation is by using a fixed point iteration

$$\lambda_i^{k+1} = A_1 - B'D'^{-1}(\lambda_i^k)C' \qquad (9.67)$$

where k indicates the iteration number. Starting with the initial estimate of λ_i; (9.67) can be used to improve the estimate until convergence is obtained. A better iterative scheme is based on Newton's method. In reference [10] it is shown that the heuristic approaches for the computation of eigenvalues given in AESOPS and PEALS programs are based on approximation of Newton type

algorithm for iterative solution of (9.66). Better algorithms are possible based on better approximations which converge faster.

Selective Modal Analysis [12-14]

Selective Modal Analysis (SMA) is a framework for the study of selected modes for the analysis of small signal stability in large power systems. The modes considered are swing (rotor) modes involving low frequency (0.1-2 Hz) oscillations.

SMA involves model reduction by retaining only the relevant state variables depending on the selected modes and eliminating the rest. For example, if only swing modes are to be considered, then the retained variables are δ (rotor angle) and S_m (slip) for all the machines. In general, the unreduced system can be modelled as

$$\left[\begin{array}{c} \dot{r} \\ \dot{z} \end{array}\right] = \left[\begin{array}{cc} A_1 & A_2 \\ A_3 & A_4 \end{array}\right] \left[\begin{array}{c} r \\ z \end{array}\right] \tag{9.68}$$

where the vector r is the vector of variables retained. In this particular case,

$$r^t = [\Delta\delta^t \quad \Delta S_m^t] \tag{9.69}$$

Eq. (9.68) is represented by the block diagram shown in Fig. 9.6. This shows two subsystems - one significant and the other less significant and their interaction. The transfer function matrix of the less significant dynamics is given by

$$[H(s)] = A_2[sI - A_4]^{-1}A_3 \tag{9.70}$$

The SMA procedure involves the reduction of the system model in an iterative fashion, starting with the crude reduced model

$$\dot{r} = [A_1]r = [A_r^o]r \tag{9.71}$$

At k^{th} stage of iteration, the dynamic block $[H(s)]$ is replaced by a static gain matrix $[M^{k+1}]$. This results in the reduced model

$$\dot{r} = [A_1 + M^{k+1}]r = [A_r^{k+1}]r \tag{9.72}$$

The initial value of $[M]$ is null matrix. If 'm' is the number of modes to be retained in the reduced model ($m \leq n_r$ where n_r is the size of vector r), then $[M^{k+1}]$ is selected to satisfy

$$[M^{k+1}][v_{r1}^k \quad v_{r2}^k \quad v_{rm}^k] = [H(\lambda_1^k)v_{r1}^k ....H(\lambda_m^k)v_{r1}^k] \tag{9.73}$$
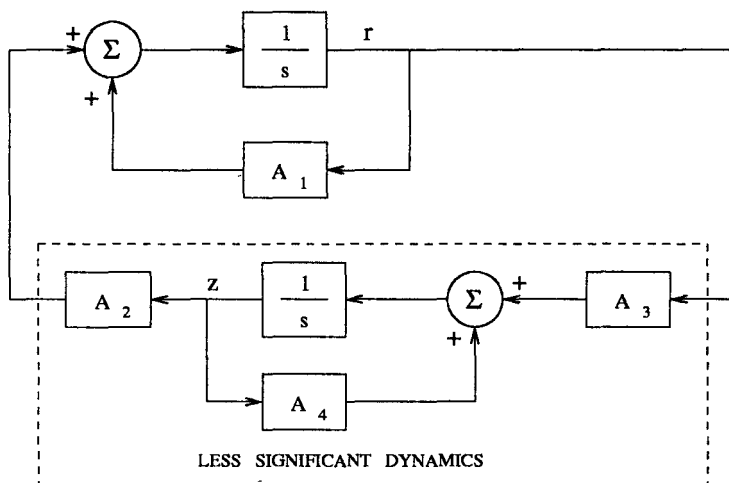
Figure 9.6: Interaction of significant and less significant subsystems

where v_{ri} is the part of the right eigenvector corresponding to the eigenvalue λ_i that is retained with the state variable vector r. If $m = 1$, then

$$[M^{k+1}]v_{r1}^k = [H(\lambda_1^k)]v_{r1}^k$$

This implies that

$$[M^{k+1}] = [H(\lambda_1^k)] \quad for \ m = 1 \tag{9.74}$$

The solution for $[M^{k+1}]$ exists in general as the eigenvectors are independent. There are infinitely many solutions for $m < n_r$. In these cases, the solution can be selected such that it minimizes the sum of the norms of the errors between $[M^{k+1}]$ and $[H(\lambda_i^k)]$ for $i = 1, 2...m$.

The convergence of the SMA procedure depends on the choice of the significant variables. This can be based on the 'participation factors' of the variables for the mode considered. Let i^{th} mode be specified by its eigenvalue λ_i and the associated right and left eigenvectors v_i and w_i respectively. Let the vectors be normalized such that

$$w_i^t v_i = 1$$

The response of the system model given by

$$\dot{x} = [A]x$$

is obtained as

$$x(t) = \sum_{i=1}^n \alpha_i v_i e^{\lambda_i t} \tag{9.75}$$

where α_i are constants determined by $x(0)$. Premultiplying both sides of Eq. (9.75) by w_i^t, we get

$$w_i^t x(t) = \alpha_i (w_i^t v_i) e^{\lambda_i t} = \alpha_i \left(\sum_{k=1}^n [w_i(k) v_i(k)] \right) e^{\lambda_i t} \qquad (9.76)$$

$w_i(t)$ and $v_i(k)$ are the kth entries of the ith left and right eigenvectors. The participation factor p_{ki} of the kth state variable in the ith mode is defined by

$$p_{ki} = w_i(k) v_i(k) \qquad (9.77)$$

As a consequence of the eigenvector normalization defined above, the participation factors sum to unity both across the state variables and across modes. Physically, the term $v_i(k)$ reflects the activity of the kth state variable when i^{th} mode is excited, while the term $w_i(k)$ weighs the contribution of this activity to the ith mode. Mathematically, the participation factor p_{ki} is the sensitivity $\frac{\partial \lambda_i}{\partial a_{kk}}$, where a_{kk} is the kth diagonal element of $[A]$.

The participation ratio, ρ_i in the ith mode is defined as

$$\rho_i = \frac{\sum_r p_{ki}}{\sum_z p_{ki}} \qquad (9.78)$$

where the sums in the numerator and denominator involves participation factors of state variables in vectors r and z respectively. The SMA algorithm converges locally to a mode of the full system if and only if $\mid \rho_i \mid > 1$. This result is proved in reference [12] for case $m = 1$.

For the general case (when $n_r \geq m > 1$) SMA algorithm has good convergence properties when $\mid \rho_i \mid >> 1$ for the m modes of interest and $<< 1$ for the remaining modes [14].

9.6 Case Studies

Two case studies, one on a two area system reported in [15] and [17] and the other on a ten machine system widely reported in the literature, are presented here.

9.6.1 Two Area System

The single line diagram of the system is shown in Fig. 9.7. It is a 4 generator, 10 bus system with a total connected load of 2734 MW. The two areas are
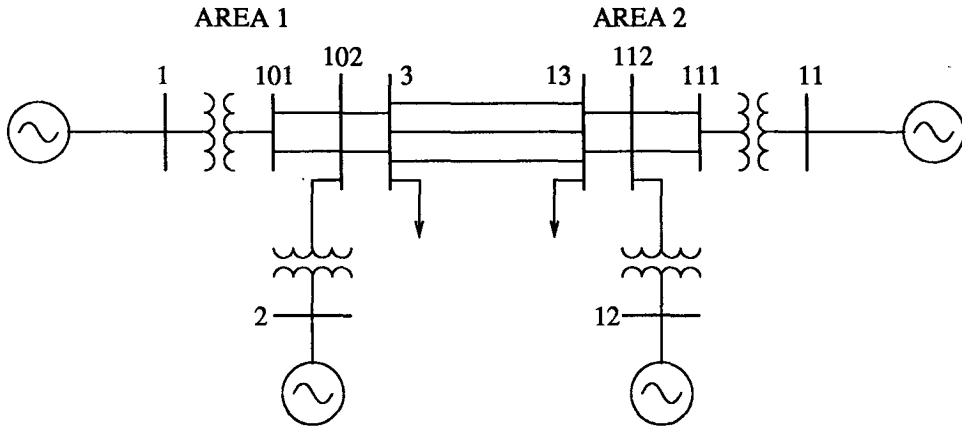
Figure 9.7: A two-area system

connected by three AC tie lines. The system and operating data are given in Tables 9.1 to 9.4. The transmission line data (on 100 MVA base) are given in Table 9.1. The load flow data and results are given in Table 9.2. The machine and excitation system data are given in Tables 9.3 and 9.4 respectively.

Table 9.1: Transmission line data on 100 MVA base

From Bus Number	To Bus Number	Series Resistance (R_s) pu	Series Reactance (X_s) pu	Shunt Susceptance (B) pu
1	101	0.001	0.012	0.00
2	102	0.001	0.012	0.00
3	13	0.022	0.22	0.33
3	13	0.022	0.22	0.33
3	13	0.022	0.22	0.33
3	102	0.002	0.02	0.03
3	102	0.002	0.02	0.03
11	111	0.001	0.012	0.00
12	112	0.001	0.012	0.00
13	112	0.002	0.02	0.03
13	112	0.002	0.02	0.03
101	102	0.005	0.05	0.075
101	102	0.005	0.05	0.075
111	112	0.005	0.05	0.075
111	112	0.005	0.05	0.075

Table 9.2: Load Flow Data and Results

Bus No.	Voltage (mag) (pu)	Angle (deg)	Real Power Gen (pu)	Reactive Power Gen (pu)	Real Power Load (pu)	Reactive Power Load (pu)	Shunt Susceptance (pu)
1	1.03	8.2154	7.0	1.3386	0.0	0.0	0.0
2	1.01	-1.5040	7.0	1.5920	0.0	0.0	0.0
11	1.03	0.0	7.2172	1.4466	0.0	0.0	0.0
12	1.01	-10.2051	7.0	1.8083	0.0	0.0	0.0
101	1.0108	3.6615	0.0	0.0	0.0	0.0	0.0
102	0.9875	-6.2433	0.0	0.0	0.0	0.0	0.0
111	1.0095	-4.6977	0.0	0.0	0.0	0.0	0.0
112	0.9850	-14.9443	0.0	0.0	0.0	0.0	0.0
3	0.9761	-14.4194	0.0	0.0	11.59	2.12	3.0
13	0.9716	-23.2922	0.0	0.0	15.75	2.88	4.0

Table 9.3: Machine data

Variable	Machine at Bus 1	Machine at Bus 2	Machine at Bus 11	Machine at Bus 12
X_l (pu)	0.022	0.022	0.022	0.022
R_a (pu)	0.00028	0.00028	0.00028	0.00028
X_d (pu)	0.2	0.2	0.2	0.2
X_d' (pu)	0.033	0.033	0.033	0.033
T_{do}' (sec)	8.0	8.0	8.0	8.0
X_q (pu)	0.19	0.19	0.19	0.19
X_q' (pu)	0.061	0.061	0.061	0.061
T_{qo}' (sec)	0.4	0.4	0.4	0.4
H (sec)	54.0	54.0	63.0	63.0
D (pu)	0	0	0	0

The loads are modelled as constant impedances. The eigenvalues of the system matrix are shown in Table 9.5. There are 20 eigenvalues as the size of the total system matrix is 20 with 5 state variables per generator. The first column shows the eigenvalues of the full matrix with all the rotor angle deviations included as state variables. Due to errors in the load flow (mismatch in powers $\neq 0$) and other numerical errors in the computations, the two eigenvalues which should be zero are calculated as complex pair of very small magnitude (#18 and #19).

Table 9.4:Excitation system data

Variable	Machine at Bus 1	Machine at Bus 2	Machine at Bus 11	Machine at Bus 12
K_A (pu)	200	200	200	200
T_A (sec)	0.02	0.02	0.02	0.02

Table 9.5: Eigenvalues - Two area System

No.	Eigenvalues		Comments
	Original Matrix	Reduced Matrix	
1	-39.9893	-39.9893	
2	-39.4922	-39.4922	
3,4	-24.5058 ± j20.6749	-24.5058 ± j20.6749	
5,6	-25.0383 ± j11.9973	-25.0383 ± j11.9973	
7	-11.5835	-11.5835	
8	-11.1735	-11.1735	
9,10	-0.7594 ± j7.2938	-0.7594 ± j7.2938	Swing mode 1
11,12	-0.7365 ± j6.6899	-0.7365 ± j6.6899	Swing mode 2
13,14	-0.0044 ± j4.4444	-0.0044 ± j4.4444	Swing mode 3 (interarea mode)
15	-4.5727	-4.5727	
16	-4.4802	-4.4802	
17	-4.1121	-4.1121	
18,19	0.0 ± j 0.0017	0.0 ,(0.0)	
20	-4.2449	-4.2449	

Table 9.6: Participation Factors

Variable	Mode #1 ($\omega_1 = 7.29$)	Mode #2 ($\omega_2 = 6.69$)	Mode #3 ($\omega_3 = 4.44$)
ΔS_{m1}	-0.18 ± j0.14	0.004 ± j0.001	-0.06 ± j0.15
ΔS_{m2}	-0.27 ± j0.14	0.00 ± j 0.00	-0.062 ± j0.07
ΔS_{m3}	-0.00 ±j0.00	0.24 ± j0.03	-0.068 ± j0.13
ΔS_{m4}	-0.04 ±j0.00	0.30 ± j 0.08	-0.061 ± j0.07

The matrix is reduced by deleting the row and column corresponding to $\Delta\delta_1$ and expressing all the other rotor angles relative to that of generator #1. The matrix is also modified by entering $-\omega_B$ in the column for ΔS_{m1} in rows corresponding to $\Delta\delta_i$ $i = 2, 3...m$ where m is the number of generators. The eigenvalues of the

19x19 reduced matrix are also shown in Table 9.5. This shows that the second eigenvalue also comes out as zero (the other zero eigenvalue has been separated by the matrix reduction). It is to be noted that the second eigenvalue is zero due to the damping (D) being zero for all the generators. If damping is non-zero, the second eigenvalue will be real and non-zero.

It is to be noted that for this system with 4 generators, there are three swing modes of frequencies 7.3, 6.7 and 4.4 (all expressed in rad/sec). The last mode is an interarea mode. The participation factors of the variables $S_{mi}, i = 1$ to 4 in all the three swing modes are given in Table 9.6. This shows that generators 1 and 2 participate in mode 1 while the generators 3 and 4 participate in mode 2. Both modes 1 and 2 may be termed as local modes while mode 3 in which all the generators participate, is the interarea mode. It is interesting to observe that while the local modes are damped, the interarea mode is poorly damped and requires stabilization using PSS.

Table 9.7   Eigenvalues-Ten machine system

No.	Eigenvalues		Comments
	Original Matrix	Reduced Matrix	
1,2	-0.2541 $\pm$ j 8.6811	-0.2541 $\pm$ j8.6811	Swing mode 1
3,4	-0.1865 $\pm$ j 8.2509	-0.1865 $\pm$ j8.2509	Swing mode 2
5,6	-0.1823 $\pm$ j 8.3340	-0.1823 $\pm$ j8.3340	Swing mode 3
7,8	-0.1698 $\pm$ j 7.1939	-0.1698 $\pm$ j7.1939	Swing mode 4
9,10	-0.1624 $\pm$ j 6.9901	-0.1624 $\pm$ j6.9901	Swing mode 5
11,12	-0.1636 $\pm$ j 6.3584	-0.1636 $\pm$ j6.3584	Swing mode 6
13,14	-0.1609 $\pm$ j 6.2241	-0.1609 $\pm$ j6.2241	Swing mode 7
15,16	-0.1939 $\pm$ j 5.9474	-0.1939 $\pm$ j5.9474	Swing mode 8
17,18	-0.1560 $\pm$ j 3.6521	-0.1560 $\pm$ j3.6521	Swing mode 9
19	-0.6715	-0.6715	
20,21	0.0084, -0.0012	0.0000,(0.0)	
22	-0.0897	-0.0898	
23	-0.2901	-0.2901	
24	-0.2663	-0.2663	
25,26	-0.1575 $\pm$ j0.0310	-0.1575 , -0.0338	
27	-0.2285	-0.2285	
28	-0.2197	-0.2197	
29	-0.1863	-0.1863	
30	-0.1370	-0.1370	

9.6.2   Ten Machine System

The data for this system is taken from reference [16] and is given in Appendix C. The machines are represented by model 1.0 and the AVR is neglected. The loads are modelled as constant impedances. The eigenvalues of the original (30x30) matrix and the reduced (29x29) matrix are shown in Table 9.7. The first 18 eigenvalues are complex and correspond to 9 swing modes in the system. The radian frequency of oscillation varies from 3.65 to 8.68.

As damping in the machines was neglected, the reduced matrix gives zero eigenvalue correctly instead of the complex pair. The reduced matrix also brings out the real eigenvalues correctly (particularly #25 and 26). There are practically no differences in the complex eigenvalues (corresponding to swing modes) obtained from original or reduced matrix.

References and Bibliography

1. M.A. Laughton, "Matrix analysis of dynamic stability in synchronous multimachine systems", Proc. IEE (London), Vol. 113, Feb. 1966, p. 325

2. J.M. Undrill, "Dynamic stability calculations for an arbitrary number of interconnected synchronous machines", IEEE Trans. Vol. PAS-87, No. 3, 1968, pp. 835-849

3. R.T.H. Alden and P.J. Nolan, "Evaluating alternative models for power system dynamic stability studies", IEEE Trans. Vol. PAS-95, March 1976, pp. 433-440

4. K.R. Padiyar, M.A. Pai and C. Radhakrishna, "A versatile system model for the dynamic stability of power systems including HVDC links", IEEE Trans. Vol. PAS-100, April 1981, pp. 1871-1880

5. G. Gross, C.F. Imperato and P.M. Look, "A tool for the comprehensive analysis of power system dynamic stability", IEEE Trans. Vol. PAS-101, No. 4, 1982, pp. 226-234

6. R.T. Byerly, R.J. Bennon and D.E. Sherman, "Eigenvalue analysis of synchronizing power flow oscillations in large electric power systems", IEEE Trans. Vol. PAS-101, No. 1, 1982, pp. 235-243

7. D.Y. Wong, G.J. Rogers, B. Poretta and P.Kundur, "Eigenvalue analysis of very large power systems", IEEE Trans. on Power systems, Vol. 3, No. 2, 1988, pp. 472-480

8. N. Uchida and T. Nagao, "A new eigen analysis method of steady-state stability studies for large power systems: S matrix method", IEEE Trans. on Power Systems, Vol. PWRS-3, No. 2, 1988, pp. 706-711

9. A. Semlyen and L. Wang, "Sequential computation of the complete eigen-system for the study zone in small signal stability analysis of large power systems", IEEE Trans. on Power systems, Vol. PWRS-3, No. 2, May 1988, pp. 715-725

10. P.W. Sauer,C.Rajagopalan and M.A. Pai, "An explanation and general-ization of the AESOPS and PEALS algorithms", IEEE Trans. on Power Systems, Vol. 6, No. 1, 1991, pp. 293-299

11. N. Martins, "Efficient eigenvalue and frequency response methods applied to power system small signal stability analysis", IEEE Trans. on Power Systems,Vol. PWRS-1, No. 1, 1986, pp. 217-226

12. I.J. Perez-Arriaga, G.C. Verghese and F.C. Schweppe, "Selective modal analysis with applications to electric power systems, Part I: Heuristic in-troduction; Part II: The dynamic stability problem", IEEE Trans. Vol. PAS-101, No. 9, 1982, pp. 3117-3134

13. F.L. Pagola, I.J. Perez-Arriaga and G.C. Verghese, "On sensitivities, resi-dues and participations: Applications to oscillatory stability analysis and control", IEEE Trans. on Power Systems, Vol. PWRS-4, No. 1, 1989, pp. 278-285

14. I.J. Perez-Arriaga, G.C. Verghese, F.L. Pagola, J.L. Sancha and F.C. Schweppe, "Developments in selective modal analysis of small signal stability in electric power systems", Automatica, Vol. 26, No. 2, 1990, pp. 215-231

15. M. Klien,G.J. Rogers and P.Kundur, "A fundamental study of inter-area oscillations in power systems", IEEE Trans. on Power Systems, Vol. 6, No. 3, 1991, pp. 914-921

16. A.K. Behera,**Transient Stability Analysis of Multi-machine Power Systems using Detailed Models**, Ph.D Thesis, University of Illinois at Urbana-Champaign, 1988

17. D.R. Morris, **Analysis of Low Frequency Oscillations in Power Sys-tems**, M.S. Thesis, University of Illinois, at Urbana-Champaign, 1993

18. D.L.Bauer et al, "Simulation of low frequency undamped oscillations in large power systems", IEEE Trans. Vol. PAS-94, No. 2, 1975, pp. 207-213

"This page is Intentionally Left Blank"

Chapter 10

Analysis of Subsynchronous Resonance

The application of series capacitors for long distance power transmission helps in improving power transfer and is economical compared to addition of new lines. Series capacitors have been used extensively in Western U.S.A. and Sweden.

While it has been known that series capacitors can cause self excited oscillations at low frequencies (due to low X/R ratio) or subsynchronous frequencies (due to induction generator effect), the problem of self excited torsional frequency oscillations (due to torsional interactions) was experienced at Mohave power station in U.S.A. in December 1970 and October 1971. The problem of self excitation due to torsional interaction is a serious problem and led to detailed analysis and study.

The general problem of oscillations at subsynchronous frequencies has been termed as SubSynchronous Resonance (SSR). It has been found that this problem can also surface with radial operation of a HVDC link connected to turbine generator [22] and with Static Var Compensator (SVC) [24].

10.1   SSR in Series Compensated Systems

Consider a turbine-generator supplying a series compensated system shown in Figure 10.1. The electrical system has a resonant frequency (f_{er}) given by

$$f_{er} = f_o \sqrt{\frac{X_C}{X'' + X_T + X_E}} \qquad (10.1)$$

where X'' is the subtransient reactance of the generator and X_T is the leakage reactance of the transformer. Since, in general, $X_C < X_E$, f_{er} is less than the synchronous frequency f_o. It is assumed that the reactances are calculated at the frequency f_o.

For more complex systems than the one shown in Figure 10.1, there will be several resonant frequencies. All of these can be calculated with the knowledge of system data.
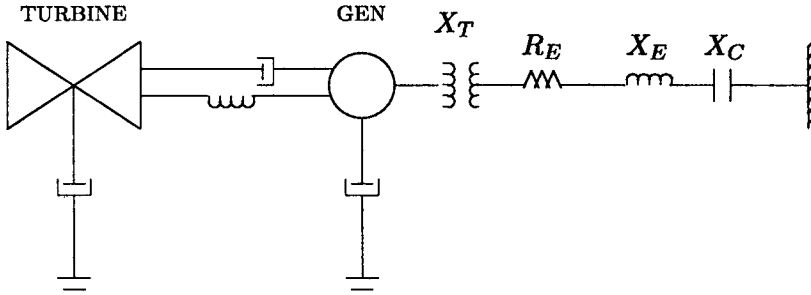

Figure 10.1: A series compensated system

A balanced three phase set of armature currents of frequency f_{er} produce a rotating magnetic field in the air gap, which rotates with same frequency in direction determined by the sequence of currents. Positive sequence currents produce a field which rotates in the same direction as the rotor while negative sequence currents cause a field which rotates in the opposite direction. The frequency of the currents induced in the rotor windings is given by

$$f_r = f_{er} \pm f_o \qquad (10.2)$$

The negative sign is associated with the positive sequence currents while positive sign is associated with the negative sequence currents. The induced rotor currents affect the rotor magnetic field and also result in subsynchronous frequency torques on the rotor (caused by interaction with steady magnetic field of the rotor).

The variations in the rotor magnetic field result in changes in the generator emf even if the rotational speed (ω) remains constant. The emf generated in the stator has frequencies (f_s) given by

$$f_s = f_r \pm f_o \qquad (10.3)$$

Substituting Eq. (10.2) in (10.3) shows that one value of f_s is same as f_{er}. While the other frequency is (f_o+f_r) called the supersynchronous frequency. The emf generated at subsynchronous frequency is of such phase as to tend to sustain the flow of armature currents at the same frequency resulting from an electrical transient. Alternatively it can be said that the generator presents a negative resistance for the flow of subsynchronous frequency currents.

The turbine generator has several rotors corresponding to different stages of steam turbines, generator and rotating exciter (if any). These are connected by shaft sections which are not rigid and act as springs. That is, when an external torque is applied to one end of the shaft it twists. The torque transmitted by the shaft can be assumed to be directly proportional to the difference between the angular positions of the shaft at the two ends. The torsional system consisting of six masses is shown in Figure 10.2. This shows a mechanical system of mass, spring and dash pots. The system, considered in isolation, has resonant frequencies of oscillation termed as torsional modes. (The frequencies usually lie in the range of 10 to 45 Hz). When a transient electrical torque is applied (at the generator mass) the response of the torsional system depends on the frequencies contained in the torque transient. If one of the frequencies in the applied torque is close to one of the torsional frequencies, the oscillations in the generator rotor (with respect to a synchronously rotating reference) have significant amplitudes and result in emfs generated in the stator windings. These emfs also are at sub and super synchronous frequencies and the subsynchronous frequency component tends to sustain the armature currents (and the rotor oscillations).
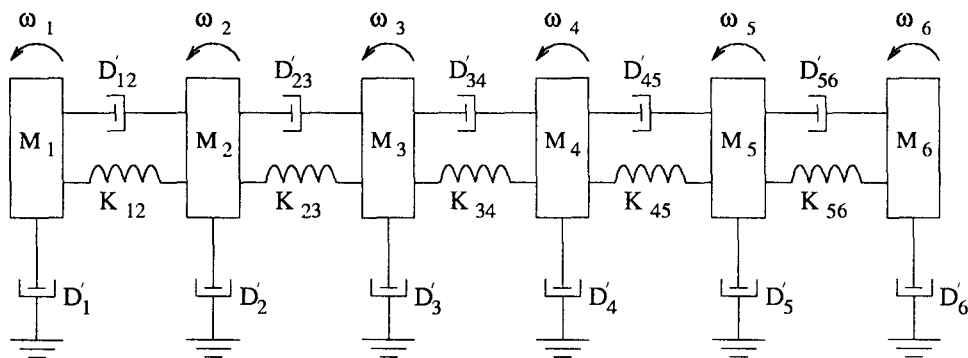

Figure 10.2: Torsional system with six masses

To summarize, it can be said that there is a major problem of subsynchronous resonance (SSR) in series compensated systems. A general definition of SSR has been given in IEEE committee reports [3,4]

Subsynchronous Resonance (SSR)

"Subsynchronous resonance is an electric power system condition where the electric network exchanges energy with a turbine at one or more of the natural frequencies of the combined system below the synchronous frequency of the system".

There are two aspects of the SSR problem. These are

1. Self Excitation (also called steady state SSR)

2. Transient torques (also called transient SSR)

Self Excitation

Subsynchronous frequency currents entering the generator terminals produce subsynchronous frequency terminal voltage components. These voltage components may sustain the currents to produce the effect that is termed as self excitation. There are two types of self excitation, one involving only rotor electrical dynamics and the other involving both rotor electrical and mechanical dynamics. The first one is termed as induction generator-effect while the second one is called torsional interaction.

Induction Generator Effect

As the rotating mmf produced by the subsynchronous frequency armature currents is moving slower than the speed of the rotor, the resistance of the rotor (at the subsynchronous frequency) viewed from the armature terminals is negative (The slip of the machine viewed as an induction generator is negative). When the magnitude of this negative resistance exceeds the sum of the armature and network resistances at a resonant frequency, there will be self excitation.

Torsional Interaction

Generator rotor oscillations at a torsional mode frequency, f_m induce armature voltage components at frequencies (f_{em}) given by

$$f_{em} = f_o \ \pm \ f_m \tag{10.4}$$

When f_{em} is close to f_{er} (electrical resonant frequency defined in Eq. 10.1), the subsynchronous torques produced by the subsynchronous voltage component can be sustained. This interplay between electrical and mechanical systems is termed as torsional interaction.

The torsional interaction can also be viewed as the insertion of negative resistance in the generator armature viewed from the terminals. This effect is much more significant compared to the induction generator effect. This can cause shaft damage as experienced at Mohave generating station.

Transient Torque

System disturbances resulting from switching in the network can excite oscillatory torques on the generator rotor. The transient electrical torque, in

general has many components including unidirectional, exponentially decaying
and oscillatory torques from subsynchronous to multiples (typically second har-
monic) of network frequency. Due to SSR phenomenon, the subsynchronous
frequency components of torque can have large amplitudes immediately follow-
ing the disturbance, although they may decay eventually. Each occurence of
these high amplitude transient torques can result in expenditure of the shaft life
due to fatigue damage. Fatigue is defined as the process of progressive local-
ized permanent structural change occuring in a material subjected to conditions
which produce fluctuating stresses and strains at some point or points and which
may culminate in cracks or complete fracture after a sufficient number of fluctu-
ations. It is a cumulative process when additional events add to previous fatigue
life expenditure. If there are a sufficient number of events causing high transient
torques, the accumulated fatigue may reach a threshold where the probability of
fatigue crack initiation in areas of high stress concentration will be significant.
Once initiated, cracks may propagate to sizes which result in irreversible shaft
damage and eventual break.

The fatigue life N, of a component is defined as the number of stress or
strain cycles of a specified magnitude that can be withstood before failure occurs.
The S-N diagram is a plot of cyclic stress amplitude against the number of cycles
to failure. The fatigue limit (also called endurance limit) is the limiting value
of the median fatigue strength as the number of cycles (N) becomes very large.
Hence stress below fatigue limit results in negligible fatigue life expenditure. A
typical S-N diagram for a particular shaft section is shown in Figure 10.3.
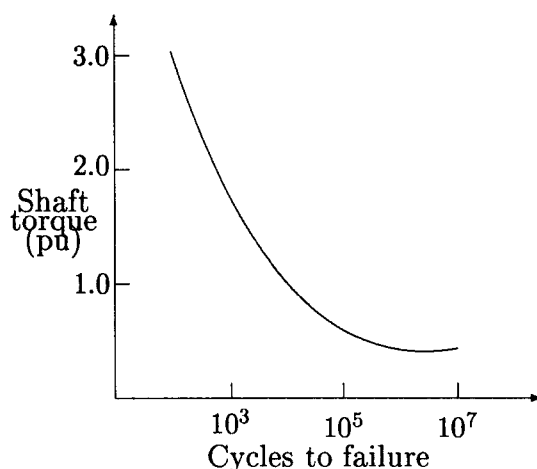

Figure 10.3: A typical S/N curve

The torsional mode damping (defined as the rate of decay of torsional

oscillations at a torsional mode frequency) is the most important factor that is responsible for the shaft life expenditure due to an event causing transient torques. The damping is measured by logarithmic decrement which is defined as the natural logarithmic ratio of the successive peaks of oscillations. The decrement factor (σ) is equal to the mode frequency in hertz multiplied by log-dec.

The damping is either due to mechanical or electrical origin. The mechanical damping includes factors such as windage, bearing friction and hysteresis loss. The damping due to steam forces on the turbine blades results in damping which increases with the load. The net decrement factor (σ) for a mode is the sum of the mechanical damping (σ_m) and electrical damping (σ_e), i.e.

$$\sigma = \sigma_m + \sigma_e$$

σ_e generally tends to be negative with series compensated systems. The problem of transient torques arises from the reduction in σ and the possibility of shaft life expenditure. A major event that can cause high amplitude torques is the reinsertion of capacitors after the clearing of fault (The series capacitors are bypassed during a fault and automatically reinserted after the fault is cleared).

10.2   Modelling of Mechanical System

The mechanical system consisting of rotors of generator, exciter and turbines, shafts can be viewed as a mass-spring-damper system (see Fig. 10.2). The equation for i^{th} mass (connected by elastic shaft sections to mass $(i - 1)$ and mass $(i + 1)$) is given by

$$M_i \frac{d^2\delta_i}{dt^2} + D_i' \frac{d\delta_i}{dt} + D_{i,i-1}' \left(\frac{d\delta_i}{dt} - \frac{d\delta_{i-1}}{dt} \right) + D_{i,i+1}' \left(\frac{d\delta_i}{dt} - \frac{d\delta_{i+1}}{dt} \right) +$$
$$K_{i,i-1}(\delta_i - \delta_{i-1}) + K_{i,i+1}(\delta_i - \delta_{i+1}) = T_{mi} - T_{ei} \tag{10.5}$$

Combining all the equations, for a N mass system,

$$[M]\, p^2\delta + [D']\, p\delta + [K]\, \delta = T_m - T_e = T \tag{10.6}$$

where $[M]$ is a diagonal matrix, $[D']$ and $[K]$ are tridiagonal symmetric matrices. T_m and T_e are the N vectors of mechanical and electrical torques. T_e has only one non-zero element corresponding to the generator rotor (neglecting rotating exciter). Also, the mechanical torque directly acting on the generator rotor is zero. It is not difficult to see that the matrix $[K]$ is singular (the columns add

up to zero). It is to be noted that the damping is usually small and assumed to be viscous. The inertia M_i is given by

$$M_i = \frac{2H_i}{\omega_B}$$

Alternative Representation Using Electrical Analogy

The mechanical system equations can also be written from analogy to an electrical (RLC) network. Defining the per unit slip of a mass (M_i) as

$$S_i = \frac{\omega_i - \omega_B}{\omega_B} \quad . \tag{10.7}$$

We can express

$$\frac{d\delta_i}{dt} = \omega_B(S_i - S_{io}) \tag{10.8}$$

$$2H_i\frac{dS_i}{dt} + D_i(S_i - S_{io}) + D_{i,i-1}(S_i - S_{i-1})$$
$$+ \quad D_{i,i+1}(S_i - S_{i+1}) + T_{i,i-1} + T_{i,i+1} = T_{mi} - T_{ei} \tag{10.9}$$

$$\frac{dT_{i,i-1}}{dt} = K_{i,i-1}(S_i - S_{i-1})\omega_B \tag{10.10}$$

$$\frac{dT_{i,i+1}}{dt} = K_{i,i+1}(S_i - S_{i+1})\omega_B \tag{10.11}$$

where $T_{i,i-1}$ is torque in the shaft section connecting mass i and $(i-1)$. It is not difficult to see that the inertia $(2H)$ is analogous to a capacitance, slip analogous to voltage and torque analogous to current. The spring constant in pu ($K\omega_B$) is analogous to the reciprocal of inductance. The per unit damping coefficient (D) is analogous to conductance. Note that $D_i = D'_i\omega_B$. For the six mass system shown in Fig. 10.2, the electrical analogue is shown in Fig. 10.4. There is no loss of generality in assuming S_{io} (slip at the operating point) as zero. Actually at equilibrium point all the slips will be equal (S_o). If S_o is not zero, it is equivalent to saying that the voltage of the reference bus in Fig. 10.4 is nonzero. This has no effect, particularly when linearized analysis is done.

Note that the state variables for the network shown in Fig. 10.4 are only 11 given by

$$x_m^t = [S_1 \ S_2 \ S_3 \ S_4 \ S_5 \ S_6 \ T_{12} \ T_{23} \ T_{34} \ T_{45} \ T_{56}]$$
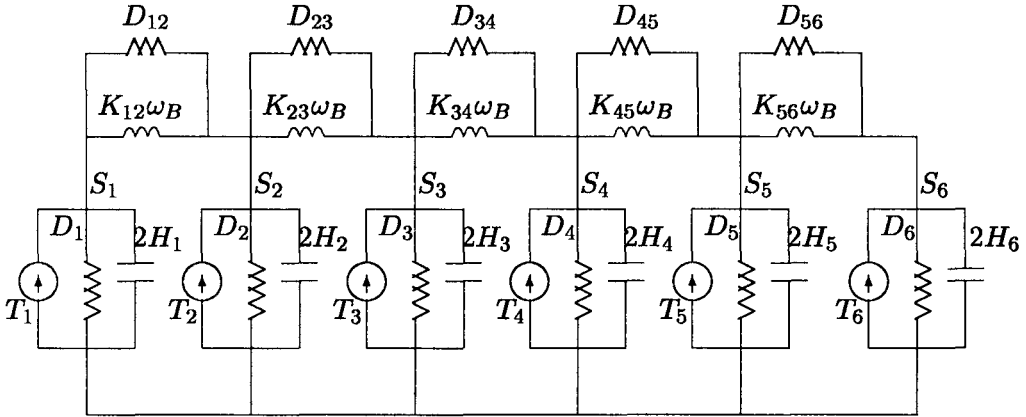
Figure 10.4: An electrical analogue for the torsional system of Fig. 10.2

The additional state variable (required when writing equations for the electrical system) is δ_m (rotor angle corresponding to the generator rotor). The equation for δ_m is given by

$$\frac{d\delta_m}{dt} = \omega_B(S_m - S_{mo}) \tag{10.12}$$

where S_m is the generator rotor slip. (This variable has been used in the previous chapters). In this formulation (using electrical network analogy) only one rotor angle (corresponding to the generator) belongs to the set of state variables. Hence, whenever there is no ambiguity, the subscript 'm' can be dropped for the angle (only δ is used in earlier chapters).

10.3   Analysis of the Mechanical system

10.3.1   Analogy with Electrical Network

Considering only small perturbations around the operating (equilibrium) point, the linearized mechanical system equations are represented by the electrical network shown as in Fig. 10.5. The one port passive network consists of only elements R, L, and C. In deriving this network, the mechanical torques are treated as constants, hence the current sources corresponding to small variations in the torque vanish. The only current source is ΔT_e (connected at the generator bus). The impedance function (in Laplace domain) at the generator bus is defined as

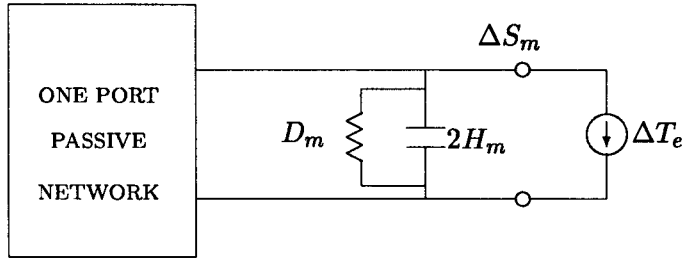$$Z_m(s) = \frac{\Delta S_m(s)}{-\Delta T_e(s)} \tag{10.13}$$

Figure 10.5: Linearized system of Fig. 10.4

If the damping is neglected, the impedance function $Z_m(s)$ corresponds to that of L-C network and can be expressed as

$$Z_m(s) = \frac{(s^2\mu_1^2 + 1)(s^2\mu_2^2 + 1)....(s^2\mu_{N-1}^2 + 1)}{2H_T s(s^2\lambda_1^2 + 1)(s^2\lambda_2^2 + 1)....(s^2\lambda_{N-1}^2 + 1)} \tag{10.14}$$

where

$$H_T = \sum_{i=1}^{N} H_i$$

The poles of this function belong to the set of eigenvalues of the mechanical system. There are $(N-1)$ complex pairs (with real part equal to zero) given by

$$s_k = \pm j\omega_k, \quad \omega_k = \frac{1}{\lambda_k}, \quad k = 1, 2...(N-1) \tag{10.15}$$

where ω_k is the radian frequency. The zeroes of the impedance function occur at (radian) frequencies,

$$\gamma_k = \frac{1}{\mu_k}, \quad k = 1, 2...(N-1) \tag{10.16}$$

It is known from the properties of the impedance function of a L-C network, that

$$0 < \gamma_1 < \omega_1 < \gamma_2 < \omega_2.... < \gamma_k < \omega_k.... < \gamma_{N-1} < \omega_{N-1} \tag{10.17}$$

The impedance function of (10.14) can also be expressed as

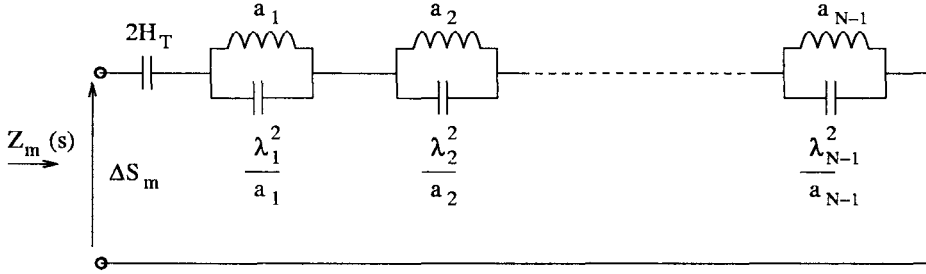$$Z_m(s) = \frac{1}{2H_T s} + \sum_{i=1}^{N-1} \frac{a_i s}{s^2\lambda_i^2 + 1} \tag{10.18}$$

Figure 10.6: Realization of L-C impedance function

All the residues $a_i, i = 1, 2..(N - 1)$ are positive. The impedance function of (10.18) represents the equivalent circuit shown in Fig. 10.6. Here there are N impedances connected in series. For torsional mode i, the impedance consists of an inductance a_i in parallel with a capacitance of $\frac{\lambda_i^2}{a_i}$. The equation for this parallel combination is given by

$$\frac{\lambda_i^2}{a_i} p\Delta S^i + \frac{\Delta\delta^i}{\omega_B a_i} = -\Delta T_e \qquad (10.19)$$

where ΔS^i and $\Delta\delta^i$ are the slip and angle corresponding to the torsional mode i. ΔS^i is the voltage across capacitor (see Fig. 10.7). Noting that
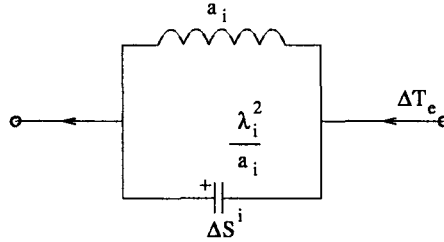
$$p\Delta\delta^i = \omega_B \Delta S^i$$

Figure 10.7: Modal equivalent circuit

We can express Eq. (10.19) as

$$\frac{2H^i}{\omega_B} p^2 \Delta\delta^i + K_i \Delta\delta^i = -\Delta T_e \qquad (10.20)$$

where $H^i = \frac{\lambda_i^2}{2a_i}$ is the modal inertia

$K_i = \frac{1}{\omega_B a_i}$ is the modal spring constant

The generator rotor slip (and angle) can be expressed as

$$\Delta S_m = \Delta S^o + \sum_{i=1}^{N-1} \Delta S^i \qquad (10.21)$$

$$\Delta \delta = \Delta \delta^o + \sum_{i=1}^{N-1} \Delta \delta^i \qquad (10.22)$$

where ΔS^o and $\Delta \delta^o$ are the slip and angle components corresponding to the mode zero.

If damping is present, it is hypothesized that $Z_m(s)$ can be represented as the equivalent circuit shown in Fig. 10.8. D^i is the damping associated with mode i. The damping associated with mode zero is.

$$D_T = \sum_{i=1}^{N} D_i \qquad (10.23)$$

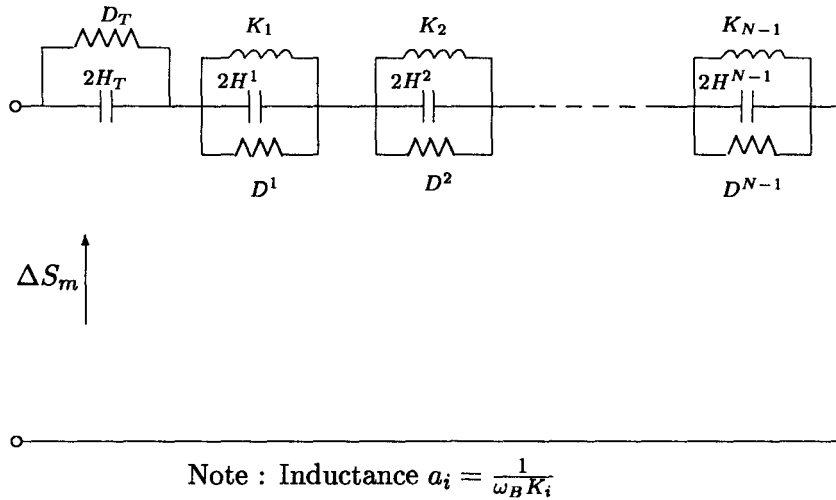Note : Inductance $a_i = \frac{1}{\omega_B K_i}$

Figure 10.8: Realization of R-L-C impedance function

Remarks

1. The mode zero corresponds to the frequency zero (determined from the analysis of the mechanical system alone). However interaction with electrical system results in a nonzero frequency (normally in the range of 0.2 to 2.0 Hz). The low frequency oscillations studied in the chapters 7 to 9

correspond to the mode zero. It is obvious from Eqs. (10.21) and (10.22) that, in the absence of torsional oscillations, only zeroth mode is present in which all rotors participate. As there is no relative motion among rotors (in the absence of torsional oscillations), it is in order to club all the turbine inertias together with the generator rotor. Thus the analysis of mode zero alone is accurately done in the previous chapters.

2. Some authors model the mechanical system in terms of modal parameters (inertias, damping and spring constants). One of the reasons for this is that the damping is normally known in terms of modal damping (determined from decrement tests). Also the 'N' second order equations (for N modes including mode zero) are all uncoupled.

3. Neglecting damping, $Z_m(s)$ has the properties of the immittance function of a single port LC network. These are

   (i) $Z_m(s)$ is an odd function of s, that is $Z_m(s) = -Z_m(-s)$

   (ii) It has only one simple pole at $s = 0$

   (iii) As $s \to \infty$, there is a zero

   (iv) $Z_m(s)$ has only simple poles and zeroes; all are located on the imaginary axis in the 's' plane and they are interlaced

   (v)   The residues at all poles are real and positive

10.3.2   Determination of modal inertia from transformation

The modal inertia (H^i) and spring constant (K_i) of ith mode were defined earlier in terms of the circuit parameters (see Fig. 10.7) determined from the impedance function $Z_m(s)$. This is a novel approach not discussed previously in the literature. The usual method of obtaining the modal parameters is through transformation of Eq. (10.6).

Neglecting damping Eq. (10.6) reduces to

$$[M]p^2\delta + [K]\delta = T \tag{10.24}$$

where T is the applied torque vector.

A transformation defined by

$$\delta = [Q]\delta^m \tag{10.25}$$

can be substituted in Eq. (10.24) and we get

$$[M][Q]p^2\delta^m + [K][Q]\delta^m = T \tag{10.26}$$

Premultiplying both sides of the above equation by $[Q]^t$, we have

$$[Q]^t[M][Q]p^2 {}_\wedge{}^m + [Q]^t[K][Q]\delta^m = [Q]^t T \tag{10.27}$$

or

$$[M^m]p^2\delta^m + [K^m]\delta^m = [Q]^t T = T^1 \tag{10.28}$$

By proper choice of $[Q]$, both $[M^m]$ and $[K^m]$ can be diagonal matrices. However, there is no unique choice of $[Q]$ which has this property (of reducing $[M^m]$ and $[K^m]$ to diagonal matrices).

The transformation matrix $[Q]$ can be obtained from the properties of eigenvectors of real symmetric matrices. A real symmetric matrix (such as $[K]$) has only real eigenvectors (corresponding to real eigenvalues) and these are mutually orthogonal. That is if $[P]$ is a matrix whose columns are eigenvectors of a real symmetric matrix $[K']$ where

$$[K'] = [M]^{-\frac{1}{2}}[K][M]^{-\frac{1}{2}} \tag{10.29}$$

then

$$[P]^t[P] = [D_1]$$

where $[D_1]$ is a diagonal matrix. As eigenvectors are not unique, the matrix $[D_1]$ is also not unique. It can be made a unit matrix if the Euclidean norm of each eigenvector is chosen as unity.

It can also be shown that

$$[K'][P] = [P][\Omega] \tag{10.30}$$

where $[\Omega]$ is a diagonal matrix of eigenvalues of $[K']$ which are actually the squares of the radian frequencies of the torsional modes ($\omega_k^2, k = 1, 2...N$ where $\omega_N = 0$ corresponding to mode zero). Premultiplying both sides of Eq.(10.30) by $[P]^t$ we have,

$$[P]^t[K'][P] = [P]^t[P][\Omega] = [D_1][\Omega] = [\Omega']$$

where $[\Omega']$ is a diagonal matrix.

If $[Q]$ is chosen such that

$$[Q] = [M]^{-\frac{1}{2}}[P] \tag{10.31}$$

then,

$$\begin{aligned}
[Q]^t[M][Q] &= [P]^t[M]^{-\frac{1}{2}}[M][M]^{-\frac{1}{2}}[P] \\
&= [P]^t[P] = [D_1] \tag{10.32}
\end{aligned}$$

Also,

$$
\begin{aligned}
[Q]^t[K][Q] &= [P]^t[M]^{-\frac{1}{2}}[K][M]^{-\frac{1}{2}}[P] \\
&= [P]^t[K'][P] = [\Omega']
\end{aligned}
\tag{10.33}
$$

As $[P]$ is not unique, $[Q]$ is also not unique. However if each vector of $[Q]$ is selected such that its element corresponding to the generator rotor is unity, (which is equivalent to selecting each eigenvector of $[K']$ with element $M_g^{\frac{1}{2}}$ in the row corresponding to the generator rotor) then $[D_1]$ is the diagonal matrix of modal inertias. This is because for each mode, the linearized equation can be expressed as

$$
M^i p^2 \Delta\delta^i + K_i \Delta\delta^i = -\Delta T_e, \quad i = 0, 1, 2 ... (N-1)
\tag{10.34}
$$

(Note that $K_o = 0$, $M^o = \dfrac{2H_T}{\omega_B}$ as superscript o corresponds to mode zero).

Remarks

1. The modal inertias from the above procedure are same as that defined from circuit parameters.

2. Several publications do not stress the importance of unique choice of $[Q]$ matrix for the determination of modal inertias. The importance of the choice is that R.H.S. of Eq.(10.34) is same for all the modes (that is each modal inertia is acted upon by the same (electrical) torque resulting from the generator interaction with the external electrical network.

3. It can be shown that $[Q]$ is also the matrix of eigenvectors of the matrix $[M]^{-1}[K]$. However the latter is not a symmetric matrix. In general, the vectors of matrix $[Q]$ are not orthogonal.

4. The radian frequency of torsional mode i is given by

$$
\omega_i = \sqrt{\frac{\omega_B K_i}{2H^i}}
$$

5. The column vectors of the matrix $[Q]$ are also called mode shapes. The elements of a vector determine the participation of different masses (in relation to that of the generator rotor) in a particular mode of torsional oscillations.

10.3.3 Determination of modal inertias from $Y_m(j\omega)$

It was shown in section (10.3.1) that $Z_m(s)$ can be expressed in terms of partial fractions as

$$Z_m(s) = \frac{1}{2H_T s} + \sum_{i=1}^{N-1} \frac{s}{2H^i(s^2 + \omega_i^2)} \tag{10.35}$$

where H^i is the modal inertia of mode i. The modal spring constant K_i is given by

$$K_i = \frac{2H^i \omega_i^2}{\omega_B}$$

Each factor in the expression (10.35) can be further expressed as

$$\frac{s}{2H^i(s^2 + \omega_i^2)} = \frac{1}{4H^i(s - j\omega_i)} + \frac{1}{4H^i(s + j\omega_i)}$$

When $s = j\omega_i$, the admittance function $Y_m(s)$ (reciprocal of $Z_m(s)$) is zero. Actually $Y_m(j\omega)$ can be expressed as

$$Y_m(j\omega) = jB(\omega) \tag{10.36}$$

The frequencies corresponding to the zero crossing of $B(\omega)$ are the modal frequencies.

H^i can be determined as

$$H^i = \frac{1}{4}\left[\frac{Y_m(s)}{s - j\omega_i}\right]_{s = j\omega_i} \tag{10.37}$$

Let

$$B(\omega) = (\omega - \omega_i)B'(\omega)$$

Eq. (10.37) can be expressed as

$$H^i = \frac{1}{4}B'(\omega_i) = \frac{1}{4}\frac{dB}{d\omega}\bigg|_{\omega=\omega_i} \tag{10.38}$$

Hence the modal inertia is obtained from the slope of $B(\omega)$ at the modal frequency.

10.4   Analysis of the Combined System

The input variable for the (linearized) mechanical system is ΔT_e which is obtained from the electrical system equations. In Laplace domain, the electrical torque ΔT_e can be related to the generator rotor slip by

$$\frac{\Delta T_e(s)}{\Delta S_m(s)} = Y_e(s) \tag{10.39}$$

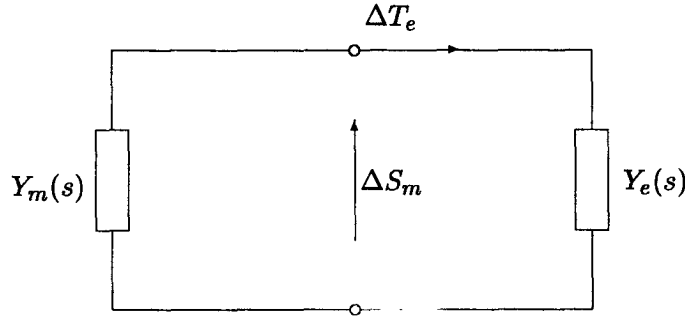The combined system (mechanical and electrical) is represented (at the generator port) as shown in Fig. 10.9. The equations for this equivalent network is given by

Figure 10.9: Combined system (mechanical and electrical)

$$[Y_m(s) + Y_e(s)]\Delta S_m = 0 \tag{10.40}$$

where

$$Y_m(s) = Z_m^{-1}(s)$$

The system eigenvalues are the solutions of the scalar equations

$$Y_m(s) + Y_e(s) = 0 \tag{10.41}$$

For the eigenvalues corresponding to torsional modes, the following approximate equations are applicable

$$Y_m(j\omega_k) + Y_e(j\omega_k) = 0 \tag{10.42}$$

where ω_k is the frequency of the kth torsional mode. Actually,

$$Y_e(j\omega_k) = T_{De}(\omega_k) - j\frac{T_{Se}(\omega_k)}{\omega_k}\omega_B \tag{10.43}$$

where T_{De} and T_{Se} are the damping and synchronizing torque coefficients (calculated from the analysis of the electrical torque). Similarly, one can define

$$Y_m(j\omega_k) = T_{Dm}(\omega_k) - j\frac{T_{Sm}(\omega_k)}{\omega_k}\omega_B \qquad (10.44)$$

Substituting (10.43) and (10.44) in (10.42), one gets

$$T_S(\omega_k) = T_{Sm}(\omega_k) + T_{Se}(\omega_k) = 0 \qquad (10.45)$$

The above equation determines the oscillation frequencies. Variations of T_{Sm} and T_S for a typical case are shown in Fig. 10.10. This shows that T_{Se} has very little effect on the zero crossing of T_S (the determination of oscillation frequencies corresponding to torsional modes). The instability of a torsional mode (ω_k) is determined from the criterion

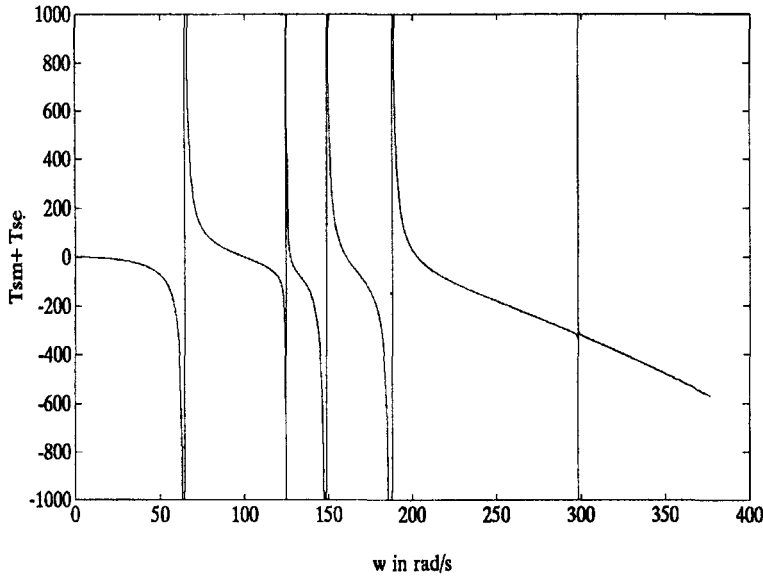$$T_D(\omega_k) = T_{Dm}(\omega_k) + T_{De}(\omega_k) < 0 \qquad (10.46)$$

The above equation is equivalent to the net damping (σ) being negative, that is

$$\sigma = \sigma_m + \sigma_e < 0 \qquad (10.47)$$

where $\sigma = \dfrac{T_D}{4H^i}$, H^i is the modal inertia. The equation (10.47) is approximate and assumes that the oscillation frequency is unaffected by the electrical system [7].
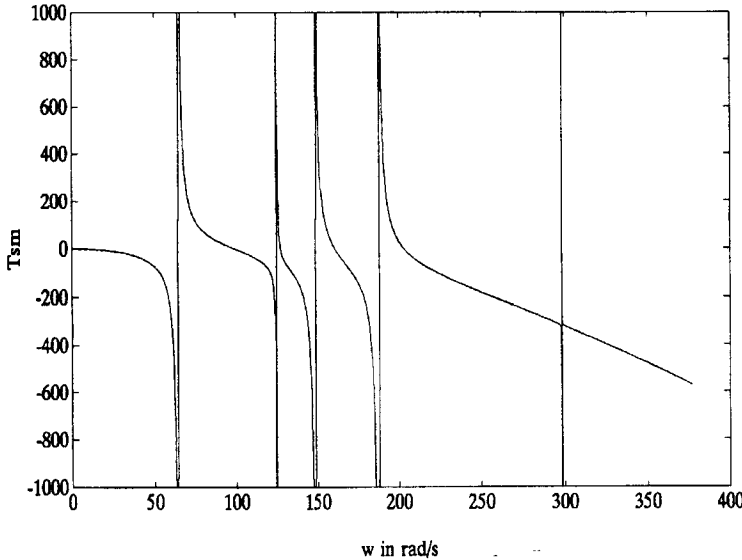
(a) Variation of T_{Sm}

(b) Variation of $T_S = T_{Sm} + T_{Se}$

Figure 10.10: Variations of T_{Sm} and T_S with frequency

10.5   Computation of $Y_e(s)$: Simplified Machine Model

The variation in the electrical torque (ΔT_e) is to be expressed in terms of the variations in generator rotor slip (ΔS_m). For a single machine system, this relationship is easily derived. In order to illustrate the computation, and for simplicity, it is initially assumed that the machine is represented by the simplified model of a frequency dependent voltage source behind a constant inductance. This is equivalent to neglecting flux decay (assuming E_q' as constant), damper circuits and transient saliency $(x_q = x_d' = x')$. Hence

$$\Delta T_e = E' \Delta i_q = E_{qo}' \Delta i_q \qquad (10.48)$$

Since

$$i_q = i_D \sin \delta + i_Q \cos \delta,$$

we have

$$\Delta i_q = \sin \delta_o \Delta i_D + \cos \delta_o \Delta i_Q + i_{do} \Delta \delta \qquad (10.49)$$

as

$$i_d = i_D \cos \delta - i_Q \sin \delta$$

It is convenient to express network equations in D-Q axes (Kron's reference frame). This formulation is also easily extended for multimachine system. For a single machine system, it is possible to write

$$\begin{bmatrix} Z_{DD}(s) & Z_{DQ}(s) \\ Z_{QD}(s) & Z_{QQ}(s) \end{bmatrix} \begin{bmatrix} \Delta I_D(s) \\ \Delta I_Q(s) \end{bmatrix} = \begin{bmatrix} \Delta E_D \\ \Delta E_Q \end{bmatrix} \tag{10.50}$$

For the classical model of the machine

$$\Delta E_Q + j\Delta E_D = E' e^{j\delta_o}(\Delta S_m + j\Delta\delta) \tag{10.51}$$

This follows from the fact that

$$E_Q + jE_D = (1 + S_m)E' e^{j\delta}$$

and E' is a constant (actually E'_q, which does not vary since flux decay is neglected).

Computation of Impedances in the D-Q axes

It is convenient to relate the impedances in the D-Q axes to the impedances in the $\alpha - \beta$ variables by noting

$$\left.\begin{array}{rcl} E_\alpha(s) &=& Z(s)I_\alpha(s) \\ E_\beta(s) &=& Z(s)I_\beta(s) \end{array}\right\} \tag{10.52}$$

E_D and E_Q are related to E_α and E_β by

$$\left.\begin{array}{rcl} E_D &=& E_\alpha \cos\theta_o - E_\beta \sin\theta_o \\ E_Q &=& E_\alpha \sin\theta_o + E_\beta \cos\theta_o \end{array}\right\} \tag{10.53}$$

Taking Laplace transforms on both sides of the above equation, we get

$$E_D(s) = \frac{1}{2}[E_\alpha(s - j\omega_o) + E_\alpha(s + j\omega_o)] - \frac{1}{2j}[E_\beta(s - j\omega_o) - E_\beta(s + j\omega_o)] \tag{10.54}$$

$$E_Q(s) = \frac{1}{2j}[E_\alpha(s - j\omega_o) - E_\alpha(s + j\omega_o)] + \frac{1}{2}[E_\beta(s - j\omega_o) + E_\beta(s + j\omega_o)] \tag{10.55}$$

From the above equations, we get

$$E_Q(s) + jE_D(s) = jE_\alpha(s + j\omega_o) + E_\beta(s + j\omega_o) \tag{10.56}$$

$$E_Q(s) - jE_D(s) = -jE_\alpha(s - j\omega_o) + E_\beta(s - j\omega_o) \tag{10.57}$$

Substituting from Eq. (10. 52) in the above equations, we get

$$
\begin{aligned}
E_Q(s) + jE_D(s) &= jZ(s+j\omega_o)I_\alpha(s+j\omega_o) + Z(s+j\omega_o)I_\beta(s+j\omega_o) \\
&= Z(s+j\omega_o)[I_Q(s) + jI_D(s)] \quad\quad (10.58) \\
E_Q(s) - jE_D(s) &= Z(s-j\omega_o)[I_Q(s) - jI_D(s)] \quad\quad (10.59)
\end{aligned}
$$

From Eqs. (10.58) and (10.59) we can derive

$$
Z_{DD}(s) = Z_{QQ}(s) = \frac{1}{2}[Z(s-j\omega_o) + Z(s+j\omega_o)] \quad\quad (10.60)
$$

$$
Z_{DQ}(s) = -Z_{QD}(s) = \frac{j}{2}[Z(s-j\omega_o) - Z(s+j\omega_o)] \quad\quad (10.61)
$$

Computation of ΔT_e

From the Eqs. (10.48) to (10.61), the following expression can be derived after some manipulations

$$
\begin{aligned}
\Delta T_e(s) &= E'[i_{do} - B(s)E']\Delta\delta(s) + (E')^2 G(s)\Delta S_m \\
&= E'\left\{[i_{do} - B(s)E']\frac{\omega_B}{s} + E'G(s)\right\}\Delta S_m \quad\quad (10.62)
\end{aligned}
$$

where

$$
\begin{aligned}
B(s) &= \Im[Z^{-1}(s+j\omega_o)] \\
G(s) &= \Re[Z^{-1}(s+j\omega_o)]
\end{aligned}
$$

Example: If $\quad Z(s) = R + Ls + \frac{1}{Cs}$, then

$$
B(s) = \frac{\omega_o C[1 - LC(s^2 + \omega_o^2)]}{[1 + RCs + LC(s^2 - \omega_o^2)]^2 + \omega_o^2(2LCs + RC)^2} \quad\quad (10.63)
$$

$$
G(s) = \frac{C\{RC(s^2 + \omega_o^2) + s[1 + LC(s^2 + \omega_o^2)]\}}{[1 + RCs + LC(s^2 - \omega_o^2)]^2 + \omega_o^2(2LCs + RC)^2} \quad\quad (10.64)
$$

Computation of Frequency Response

The $\alpha - \beta$ variables are related to D-Q variables from the relation

$$
f_\beta + jf_\alpha = e^{j\omega_o t}(f_Q + jf_D) \quad\quad (10.65)
$$

where f can be current, voltage or flux.

Let the currents (under balanced conditions) in $\alpha - \beta$ sequence be

$$\left. \begin{array}{rcl} i_\alpha(t) & = & I_p \sin(\omega t + \phi) \\ i_\beta(t) & = & I_p \cos(\omega t + \phi) \end{array} \right\} \tag{10.66}$$

where ω and ϕ are constants. Then

$$i_\beta + j i_\alpha = (I_p e^{j\phi}) e^{j\omega t} \tag{10.67}$$

Applying (10.65), we get

$$(i_Q + j i_D) = (I_p e^{j\phi}) e^{j(\omega - \omega_o)t} \tag{10.68}$$

In Laplace domain, Eq. (10.68) is given by

$$I_Q + j I_D = \frac{(I_p e^{j\phi})}{[s - j(\omega - \omega_o)]} \tag{10.69}$$

If the current is applied to a single port network shown in Fig.10.11, the voltage (response) is given by
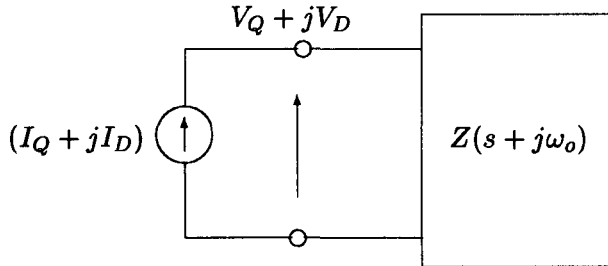
Figure 10.11: A single port network

$$V_Q + j V_D = Z(s + j\omega_o)(I_Q + j I_D)$$

Substituting for the current from Eq.(10.69), we can obtain the steady state response in time domain as

$$v_Q + j v_D = (I_p e^{j\phi}) Z(j\omega) e^{j(\omega - \omega_o)t} \tag{10.70}$$

From the above, we get response in $\alpha - \beta$ quantities

$$v_\beta + j v_\alpha = (I_p e^{j\phi}) Z(j\omega) e^{j\omega t} \tag{10.71}$$

The above Eq. could also have been obtained directly from the response of $\alpha - \beta$ sequence networks.

Eq. (10.70) shows that the frequency response using D-Q variables is computed in the same manner as obtained from the $\alpha - \beta$ sequence networks.

10.6   Computation of $Y_e(s)$: Detailed Machine Model

The computation of torque coefficients using a detailed machine model is outlined below. The synchronous machine stator equations can be expressed as

$$-(p+j\omega)(\psi_q + j\psi_d) = (v_q + jv_d)\omega_B \tag{10.72}$$

where $p = \frac{d}{dt}$, ω is the rotor speed (in radians per second). The armature resistance is neglected in the above equations. Noting that

$$\left.\begin{array}{l} (\psi_q + j\psi_d) = (\psi_Q + j\psi_D)e^{-j\delta} \\ (v_q + jv_d) = (v_Q + jv_D)e^{-j\delta} \end{array}\right\} \tag{10.73}$$

Eq. (10.72) can be expressed in terms of D-Q variables as

$$-(p+j\omega_o)(\psi_Q + j\psi_D) = (v_Q + jv_D)\omega_B \tag{10.74}$$

In deriving (10.74) the following relation is used

$$\omega = \omega_o + \frac{d\delta}{dt}$$

It is interesting to note that Eq. (10.74) is linear while Eq. (10.72) is nonlinear (involving product of ω and flux).

From expressions given in chapter 3,

$$\psi_q = X_q(p)i_q \tag{10.75}$$

$$\psi_d = X_d(p)i_d + G(p)E_{fd} \tag{10.76}$$

Linearizing Eqs. (10.74) to (10.76) and noting that

$$\Delta i_q + j\Delta i_d = -j(i_{qo} + ji_{do})\Delta\delta + e^{-j\delta_o}(\Delta i_Q + j\Delta i_D)$$

$$\Delta\psi_Q + j\Delta\psi_D = j(\psi_{Qo} + j\psi_{Do})\Delta\delta + e^{j\delta_o}(\Delta\psi_q + j\Delta\psi_d)$$

It is possible to express in Laplace domain

$$\begin{bmatrix} F_1(s) \\ F_2(s) \end{bmatrix}\Delta\delta + \begin{bmatrix} Z_1^g(s) & Z_2^g(s) \\ Z_3^g(s) & Z_4^g(s) \end{bmatrix}\begin{bmatrix} \Delta I_D \\ \Delta I_Q \end{bmatrix} + \begin{bmatrix} G_1(s) \\ G_2(s) \end{bmatrix}\Delta E_{fd} = \begin{bmatrix} \Delta V_D \\ \Delta V_Q \end{bmatrix} \tag{10.77}$$

where

$$F_1(s) = \frac{\omega}{\omega_o}\psi_{Do} - \frac{s}{\omega_B}\psi_{Qo} - \frac{1}{\omega_B}(\omega_o\cos\delta_o + s\sin\delta_o)i_{do}X_q(s)$$

$$+ \frac{1}{\omega_B}(-\omega_o\sin\delta_o + s\cos\delta_o)i_{qo}X_d(s)$$

$$F_2(s) = \frac{\omega}{\omega_o}\psi_{Qo} + \frac{s}{\omega_B}\psi_{Do} + \frac{1}{\omega_B}(\omega_o\sin\delta_o - s\cos\delta_o)i_{do}X_q(s)$$

$$- \frac{1}{\omega_B}(\omega_o\cos\delta_o + s\sin\delta_o)i_{qo}X_d(s)$$

$$Z_1^g(s) = -\frac{1}{\omega_B}(\omega_o\cos\delta_o + s\sin\delta_o)\sin\delta_o X_q(s)$$

$$- \frac{1}{\omega_B}(-\omega_o\sin\delta_o + s\cos\delta_o)\cos\delta_o X_d(s)$$

$$Z_2^g(s) = -\frac{1}{\omega_B}(\omega_o\cos\delta_o + s\sin\delta_o)\cos\delta_o X_q(s)$$

$$+ \frac{1}{\omega_B}(-\omega_o\sin\delta_o + s\cos\delta_o)\sin\delta_o X_d(s)$$

$$Z_3^g(s) = \frac{1}{\omega_B}(\omega_o\sin\delta_o - s\cos\delta_o)\sin\delta_o X_q(s)$$

$$+ \frac{1}{\omega_B}(\omega_o\cos\delta_o + s\sin\delta_o)\cos\delta_o X_d(s)$$

$$Z_4^g(s) = \frac{1}{\omega_B}(\omega_o\sin\delta_o - s\cos\delta_o)\cos\delta_o X_q(s)$$

$$- \frac{1}{\omega_B}(\omega_o\cos\delta_o + s\sin\delta_o)\sin\delta_o X_d(s)$$

$$G_1(s) = -\frac{1}{\omega_B}(-\omega_o\sin\delta_o + s\cos\delta_o)G(s)$$

$$G_2(s) = \frac{1}{\omega_B}(\omega_o\cos\delta_o + s\sin\delta_o)G(s)$$

Eq. (10.77) can be combined with the network equation

$$\begin{bmatrix} Z_{DD}(s) & Z_{DQ}(s) \\ Z_{QD}(s) & Z_{QQ}(s) \end{bmatrix} \begin{bmatrix} \Delta I_D \\ \Delta I_Q \end{bmatrix} = \begin{bmatrix} \Delta V_D \\ \Delta V_Q \end{bmatrix} \tag{10.78}$$

to solve for ΔI_D and ΔI_Q in terms of $\Delta\delta$ and ΔE_{fd}.

Note that the elements of the impedance matrix in Eq. (10.78) are defined in (10.60) and (10.61).

The incremental torque ΔT_e is given by

$$\Delta T_e = \psi_{do}\Delta i_q - \psi_{qo}\Delta i_d + i_{qo}\Delta\psi_d - i_{do}\Delta\psi_q \tag{10.79}$$

After some manipulations,

$$\Delta T_e(s) = Y_e(s)\Delta S_m + H(s)\Delta E_{fd} \qquad (10.80)$$

In deriving (10.80), $\Delta i_d, \Delta i_q, \Delta \psi_d$ and $\Delta \psi_q$ are expressed first in terms of $\Delta \delta$ and ΔE_{fd}. Then $\Delta \delta$ is expressed as

$$\Delta \delta(s) = \frac{\omega_B}{s}\Delta S_m(s)$$

10.7 Analysis of Torsional Interaction - A Physical Reasoning

In SSR phenomenon, the torsional interaction (TI) is much more important and complex than the induction generator effect. Thus it is convenient to ignore the flux decay, damper circuits and transient saliency in the analysis of TI.

Assuming that the generator rotor oscillates (about a constant speed of ω_o) sinusoidally the per unit speed ($\bar{\omega}$) is given by

$$\bar{\omega} = \bar{\omega}_o + A\sin\omega_m t \qquad (10.81)$$

where ω_m is the oscillation frequency of the rotor about a synchronously rotating axis in radians per second.

The single phase equivalent circuit (α - sequence) of the generator stator is shown in Fig. 10.12. This consists of a voltage source (e_α) behind a transient inductance. e_α is given by

$$e_\alpha = \bar{\omega}E'\sin(\omega_o t + \delta) \qquad (10.82)$$

Since

$$\frac{d\delta}{dt} = (\bar{\omega} - \bar{\omega}_o)\omega_B$$

Substituting from (10.81) gives

$$\delta = \delta_o - \left(\frac{A\omega_B}{\omega_m}\right)\cos\omega_m t \qquad (10.83)$$

If it is assumed that the amplitude (A) of the rotor oscillation is very small, the induced voltage in the stator, e_α, consists of three sinusoidal components, one of frequency f_o, and other two components of frequencies $f_o \pm f_m$. This follows from substituting Eqs. (10.81) and (10.83) in (10.82) and noting that

$$e_\alpha(t) = \bar{\omega}_o E'\sin(\omega_o t + \delta) + \frac{AE'}{2}\cos[(\omega_o - \omega_m)t + \delta] - \frac{AE'}{2}\cos[(\omega_o + \omega_m)t + \delta]$$
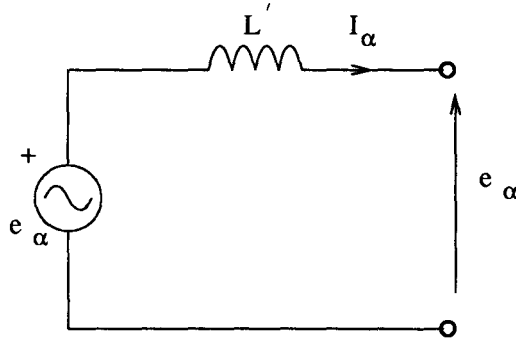
Figure 10.12: α-sequence stator equivalent circuit

We also note that

$$\frac{AE'}{2} \cos[(\omega_o - \omega_m)t + \delta] \approx \frac{AE'}{2} \cos[(\omega_o - \omega_m)t + \delta_o]$$

since,

$$\cos[(\omega_o - \omega_m)t + \delta] \approx \cos[(\omega_o - \omega_m)t + \delta_o] - \frac{A\omega_B}{\omega_m} \sin[(\omega_o - \omega_m)t + \delta_o] \cos \omega_m t$$

Also,

$$\bar{\omega}_o E' \sin(\omega_o t + \delta) \approx \bar{\omega}_o E'[\sin(\omega_o t + \delta_o) + (\delta - \delta_o)\cos(\omega_o t + \delta_o)]$$

$$= \bar{\omega}_o E' \sin(\omega_o t + \delta_o) - \frac{\omega_o AE'}{2\omega_m}\{\cos[(\omega_o - \omega_m)t + \delta_o] + \cos[(\omega_o + \omega_m)t + \delta_o]\}$$

Thus,

$$
\begin{aligned}
e_\alpha(t) \;=\; & \bar{\omega}_o E' \sin(\omega_o t + \delta_o) - \frac{AE'}{2\omega_m}(\omega_o - \omega_m)\cos[(\omega_o - \omega_m)t + \delta_o] \\
& -\frac{AE'}{2\omega_m}(\omega_o + \omega_m)\cos[(\omega_o + \omega_m)t + \delta_o]
\end{aligned}
\tag{10.84}
$$

The subsynchronous frequency component of the voltage source, e_α is

$$e_\alpha^{sub} = -\frac{AE'}{2\omega_m}(\omega_o - \omega_m)\cos[(\omega_o - \omega_m)t + \delta_o]$$

It can be easily derived that

$$e_\beta^{sub} = \frac{AE'}{2\omega_m}(\omega_o - \omega_m)\sin[(\omega_o - \omega_m)t + \delta_o]$$

When these voltages are applied to the α and β sequence networks respectively, the subsynchronous frequency currents flow (in steady state) and are given by the expression

$$(i_\beta^{sub} + ji_\alpha^{sub}) = Z^{-1}[j(\omega_o - \omega_m)](e_\beta^{sub} + je_\alpha^{sub})$$

If $Z(s) = R + Ls + \dfrac{1}{Cs}$

$$Z[j(\omega_o - \omega_m)] = R + j\left[(\omega_o - \omega_m)L - \frac{1}{(\omega_o - \omega_m)C}\right] = Z_{sub}\angle\phi_{sub}$$

If the resonance frequency f_{er} defined by

$$f_{er} = \frac{1}{2\pi\sqrt{LC}}$$

is close to $(f_o - f_m)$, the impedance is small. It is resistive when $(f_o - f_m) = f_{er}$ and capacitive when $f_{er} > (f_o - f_m)$, otherwise it is inductive (when $f_{er} < (f_o - f_m)$).

The d-q component of the currents are given by

$$(i_q + ji_d) = e^{-j(\omega_o t+\delta)}(i_\beta + ji_\alpha)$$

$$i_\alpha^{sub}(t) = -\frac{AE'}{2\omega_m Z_{sub}}(\omega_o - \omega_m)\cos[(\omega_o - \omega_m)t + \delta_o - \phi_{sub}]$$

$$i_\beta^{sub}(t) = \frac{AE'}{2\omega_m Z_{sub}}(\omega_o - \omega_m)\sin[(\omega_o - \omega_m)t + \delta_o - \phi_{sub}]$$

Then

$$i_q^{sub} = -\frac{AE'}{2\omega_m Z_{sub}}(\omega_o - \omega_m)\sin(\omega_m t + \phi_{sub}) \qquad (10.85)$$

The component of the torque T_e^{sub}, due to subsynchronous frequency currents, is given by

$$T_e^{sub} = E'i_q^{sub} = -\frac{A(E')^2}{2\omega_m Z_{sub}}(\omega_o - \omega_m)\sin(\omega_m t + \phi_{sub}) \qquad (10.86)$$

The supersynchronous frequency voltage components e_α^{sup} and e_β^{sup} result in supersynchronous frequency currents given by

$$i_\alpha^{sup} = -\frac{AE'(\omega_o + \omega_m)}{2\omega_m Z_{sup}}\cos[(\omega_o + \omega_m)t + \delta_o - \phi_{sup}]$$

$$i_\beta^{sup} = \frac{AE'(\omega_o + \omega_m)}{2\omega_m Z_{sup}}\sin[(\omega_o + \omega_m)t + \delta_o - \phi_{sup}]$$

where $Z_{sup} \angle \phi_{sup}$ is the network impedance at supersynchronous frequency, viewed from generator (internal) bus. The magnitude of Z_{sup} tends to be large compared to Z_{sub} and ϕ_{sup} is usually positive (the impedance is inductive).

The quadrature axis component (i_q^{sup}) due to the supersynchronous currents can be obtained as

$$i_q^{sup} = \frac{AE'}{2\omega_m Z_{sup}} (\omega_o + \omega_m) \sin(\omega_m t - \phi_{sup}) \tag{10.87}$$

The component of the torque due to the supersynchronous currents, T_e^{sup} is given by

$$T_e^{sup} = E' i_q^{sup} = \frac{A(E')^2 (\omega_o + \omega_m)}{2\omega_m Z_{sup}} \sin(\omega_m t - \phi_{sup}) \tag{10.88}$$

Note that both torque components, T_e^{sub} and T_e^{sup} have same frequency ω_m, the frequency of oscillation of the generator rotor. The damping torque coefficient T_D is given by

$$T_D = -\frac{(E')^2}{2\omega_m} \left[\frac{(\omega_o - \omega_m)}{Z_{sub}} \cos\phi_{sub} - \frac{(\omega_o + \omega_m)}{Z_{sup}} \cos\phi_{sup} \right] \tag{10.89}$$

The net damping tends to be negative due to the fact that

$$Z_{sub} << Z_{sup} \quad \text{and}$$
$$\phi_{sub} \simeq 0 \quad \text{while} \quad \phi_{sup} \simeq 90^o$$

in series compensated system when a torsional oscillation frequency is approximately equal to the complement of the electrical resonance frequency, that is

$$f_o - f_m \simeq f_{er}$$

Fig. 10.13 shows the phasor diagram giving the position of the torque components in relation to the rotor velocity. What is interesting is that the supersynchronous frequency currents in the network give rise to positive damping torque (although of small amplitude). It is the subsynchronous frequency component of network currents that cause negative damping. The smaller the oscillation frequency, higher is the negative damping. Thus the first torsional mode (with the smallest frequency) can cause the most severe problem if network impedance is minimum at that mode.
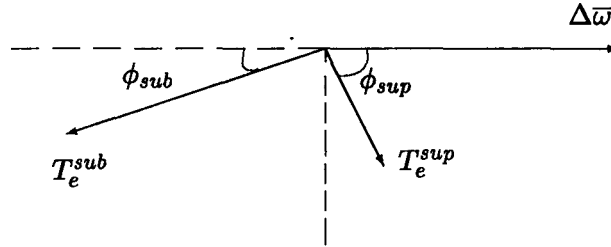
Figure 10.13: Phasor diagram

10.8   State Space Equations and Eigenvalue Analysis

10.8.1   Analysis of Induction Generator Effect

The induction generator effect is present even if the generator rotor is assumed to rotate at constant speed. Hence only the electrical system equations need to be considered for the analysis. In the absence of magnetic saturation and neglecting excitation system (treating E_{fd} as constant) the system equations are linear.

Synchronous Machine

Only the stator and rotor electrical equations are to be considered as the generator angle δ and rotor slip (S_m) are treated as constants.

The stator equations are

$$\left.\begin{array}{l} -\dfrac{1}{\omega_B}p\psi_d - (1 + S_m)\psi_q - R_a i_d = v_d \\[2mm] -\dfrac{1}{\omega_B}p\psi_q + (1 + S_m)\psi_d - R_a i_q = v_q \end{array}\right\} \tag{10.90}$$

The rotor electrical equations (assuming machine model 1.1)

$$\left.\begin{array}{l} pE'_d = \dfrac{1}{T'_{qo}}[-E'_d - (x_q - x'_q)i_q] \\[2mm] pE'_q = \dfrac{1}{T'_{do}}[-E'_q + (x_d - x'_d)i_d + E_{fd}] \end{array}\right\} \tag{10.91}$$

Note that $p = \dfrac{d}{dt}$ in the above equations. Eqs. (10.90) and (10.91) can be expressed as

$$\dot{x}_e = [A_e]x_e + [B_{e1}]u_e + [B_{e2}]E_{fd} \tag{10.92}$$

$$y_e = [C_e]x_e \tag{10.93}$$

where

$$x_e^t = [\psi_d \ \psi_q \ E_d' \ E_q']$$
$$u_e^t = [v_D \ v_Q]$$
$$y_e^t = [i_D \ i_Q]$$

$[A_e]$ is a matrix whose elements depend on S_m. The nonzero elements of $[A_e]$ are given by

$$A_e(1,1) = -\frac{R_a \omega_B}{x_d'}, \quad A_e(1,2) = -\omega_B, \quad A_e(1,4) = \frac{R_a \omega_B}{x_d'},$$

$$A_e(2,1) = \omega_B, \quad A_e(2,2) = -\frac{R_a \omega_B}{x_q'}, \quad A_e(2,3) = -\frac{R_a \omega_B}{x_q'}$$

$$A_e(3,2) = -\frac{1}{T_{qo}'}(\frac{x_q}{x_q'} - 1), \quad A_e(3,3) = -\frac{x_q}{T_{qo}' x_q'}$$

$$A_e(4,1) = \frac{1}{T_{do}'}(\frac{x_d}{x_d'} - 1), \quad A_e(4,4) = -\frac{x_d}{T_{do}' x_d'}$$

The nonzero elements of $[B_{e1}]$ are functions of δ given by

$$B_{e1}(1,1) = -\omega_B \cos \delta, \quad B_{e1}(1,2) = \omega_B \sin \delta$$
$$B_{e1}(2,1) = -\omega_B \sin \delta, \quad B_{e1}(2,2) = -\omega_B \cos \delta$$

The nonzero element of the column vector $[B_{e2}]$ is
$$B_{e2}(4) = \frac{1}{T_{do}'}$$
$[C_e]$ is a 2 x 4 matrix whose elements are functions of δ. They are

$$C_e(1,1) = -C_e(1,4) = \frac{\cos \delta}{x_d'}, \quad C_e(1,2) = C_e(1,3) = \frac{\sin \delta}{x_q'}$$

$$C_e(2,1) = -C_e(2,4) = -\frac{\sin \delta}{x_d'}, \quad C_e(2,2) = C_e(2,3) = \frac{\cos \delta}{x_q'}$$

In deriving Eqs. (10.92) and (10.93) the following expressions are used to eliminate i_d and i_q

$$i_d = \frac{\psi_d - E_q'}{x_d'}, \quad i_q = \frac{\psi_q + E_d'}{x_q'}$$

Network Equations

The network equations can be expressed using D-Q variables. For a two port network with one port connected to an infinite bus, the equations are

$$\dot{x}_N = [A_N]x_N + [B_{N1}]u_{N1} + [B_{N2}]u_{N2} \tag{10.94}$$

where

$$u^t_{N1} = [i_D \ i_Q], \quad u^t_{N2} = [E_D \ E_Q]$$

E_D and E_Q are D and Q components of the infinite bus voltage. For the simple network shown in Fig. 10.14,

$$x^t_N = [v_{CD} \ v_{CQ}],$$

components of the capacitor voltage

$$[A_N] = \begin{bmatrix} 0 & -\omega_B \\ \omega_B & 0 \end{bmatrix}, \quad [B_{N1}] = \begin{bmatrix} \omega_B X_c & 0 \\ 0 & \omega_B X_c \end{bmatrix}, \quad [B_{N2}] = [0]$$
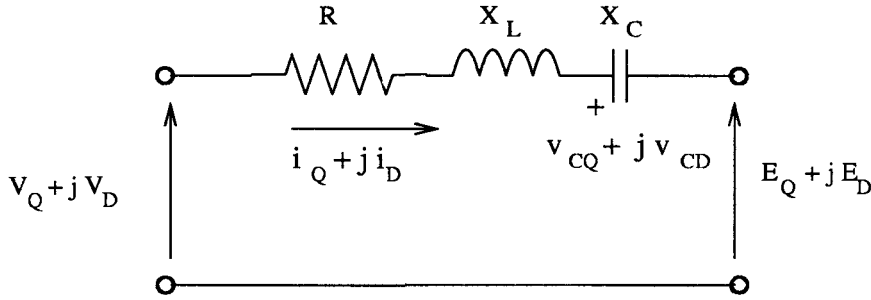
The combined system (machine and network) equations can be obtained after

Figure 10.14: A simple series compensated network

eliminating the variables u_e and u_{N1}. Note that

$$u_{N1} = y_e = [C_e]x_e \tag{10.95}$$

and the expression for u_e depends upon the network. For the network shown in Fig. 10.14, we have

$$\left. \begin{array}{l} v_D = E_D + v_{CD} + Ri_D + \frac{X_L}{\omega_B}pi_D + X_L i_Q \\ v_Q = E_Q + v_{CQ} + Ri_Q + \frac{X_L}{\omega_B}pi_Q - X_L i_D \end{array} \right\} \tag{10.96}$$

The above Eq. can be expressed as

$$u_e = u_{N2} + x_N + [F]y_e + \frac{X_L}{\omega_B}py_e \tag{10.97}$$

where

$$[F] = \begin{bmatrix} R & X_L \\ -X_L & R \end{bmatrix}$$

Noting that,

$$py_e = [C_e]px_e = [C_eA_e]x_e + [C_eB_{e1}]u_e + [C_eB_{e2}]E_{fd} \qquad (10.98)$$

We can derive an expression for u_e, as

$$u_e = [H]\left[x_N + [F_1]x_e + \frac{X_L}{\omega_B}[C_eB_{e2}]E_{fd} + u_{N2}\right] \qquad (10.99)$$

where

$$H = \left\{I - \frac{X_L}{\omega_B}[C_eB_{e1}]\right\}^{-1}, \quad [F_1] = [FC_e] + \frac{X_L}{\omega_B}[C_eA_e], \quad I \text{ is a unit matrix.}$$

The final system equations are

$$\dot{X}_E = [A_E]X_E + [B_{E1}]E_{fd} + [B_{E2}]u_{N2} \qquad (10.100)$$

where

$$X_E^t = [x_e^t \ \ x_N^t]$$

For the network shown in Fig. 10.14, we have

$$[A_E] = \begin{bmatrix} A_{E1} & A_{E2} \\ A_{E3} & A_N \end{bmatrix}$$

$$A_{E1} = [A_e] + [B_{e1} \ HF_1]$$

$$A_{E2} = [B_{e1} \ H], \quad [A_{E3}] = [B_{N1} \ C_e]$$

$$[B_{E1}] = \begin{bmatrix} [B_{e2}] + \dfrac{X_L}{\omega_B}[B_{e1} \ H \ C_e \ B_{e2}] \\ [0] \end{bmatrix}$$

$$[B_{E2}] = \begin{bmatrix} [B_{e1} \ H] \\ [B_{N2}] \end{bmatrix}$$

The eigenvalues of the matrix $[A_E]$ should lie in the left half plane if induction generator effect does not lead to self excitation, that is the sum of network and armature resistances (R and R_a) is greater than the negative resistance (introduced by the induction generator effect) at the electrical resonant frequency.

The inclusion of network transients by considering differential equations for the network is essential in the analysis of both induction generator effect and torsional interactions.

10.8.2   Analysis of Torsional Interactions (TI)

In analyzing TI, it is necessary to model the resonant multimass mechanical system in addition to the electrical system.

The mechanical system equations can be expressed as

$$\dot{x}_m = [A_m]x_m + [B_{m1}]T_e + [B_{m2}]u_m$$
$$y_m = [C_m]x_m$$

where u_m is equal to the vector of mechanical torques applied at different turbine rotors, if prime mover dynamics are not included in the equations. If turbine-governor dynamics are to be considered, u_m is the input variable corresponding to speed reference. T_e is the electromagnetic torque of the generator applied only at the generator rotor mass. (The exciter is either assumed to be static exciter or the electromagnetic torque at the rotating exciter is neglected for simplicity). y_m consists of generator rotor angle and slip.

For a four mass system shown in Fig. 10.15, the state vector x_m is given by

$$x_m^t = [\delta \ \ S_m \ \ T_{LG} \ \ S_{LP} \ \ T_{IL} \ \ S_{IP} \ \ T_{HI} \ \ S_{HP}]$$

where T_{LG}, T_{IL}, T_{HI} are the shaft torques, S_m, S_{LP}, S_{IP} and S_{HP} are the rotor slips (of different rotors) and δ is the generator rotor angle. As discussed earlier the equations can be obtained from analogy with a R-L-C electric circuit.

The nonzero elements of $[A_m]$ are

$$A_m(1,2) = \omega_B$$
$$A_m(2,2) = -\frac{D_m}{2H_m}, \ \ A_m(2,3) = \frac{1}{2H_m}$$
$$A_m(3,2) = -K_{LG}, \ \ A_m(3,4) = K_{LG}$$
$$A_m(4,3) = -\frac{1}{2H_{LP}} = -A_m(4,5), \ \ A_m(4,4) = -\frac{D_{LP}}{2H_{LP}}$$
$$A_m(5,4) = -K_{IL}, \ \ A_m(5,6) = K_{IL}$$
$$A_m(6,5) = -\frac{1}{2H_{IP}} = -A_m(6,7), A_m(6,6) = -\frac{D_{IP}}{2H_{IP}}$$
$$A_m(7,6) = -K_{HI}, \ \ A_m(7,8) = K_{HI}$$
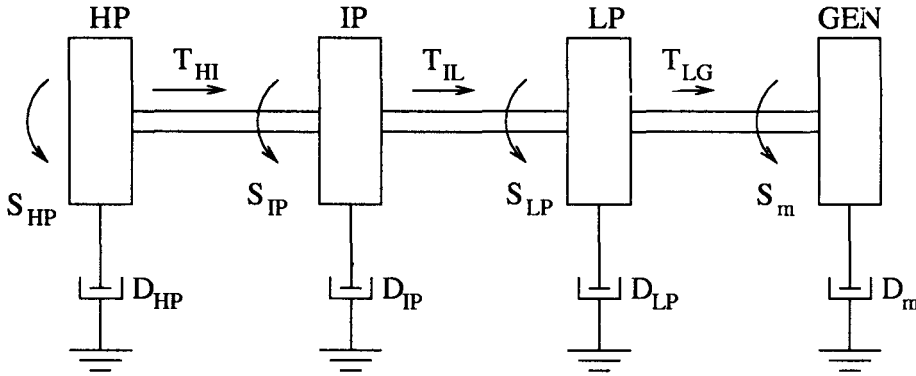$$A_m(8,7) = -\frac{1}{2H_{HP}}, \ \ A_m(8,8) = -\frac{D_{HP}}{2H_{HP}}$$

Figure 10.15: A four mass system

The initial slips are assumed to be zero in deriving the equations. Also the shaft damping terms are neglected (as they are usually small). The column vector, B_{m1} is given by

$$B_{m1}^t = \begin{bmatrix} 0 & -\dfrac{1}{2H_m} & 0 & 0 & 0 & 0 & 0 \end{bmatrix}$$

The matrix $[B_{m2}]$ is not relevant if the mechanical torques are constant (see below).

Derivation of Linearized System Equations

Although the mechanical system equations are linear, the coupling between the mechanical and electrical equations are nonlinear. Hence it is necessary to linearize the equations for small signal stability analysis. The linearized mechanical equations are

$$\Delta \dot{x}_m = [A_m]\Delta x_m + [B_{m1}]\Delta T_e \tag{10.101}$$

The torque equation, in terms of state variables x_e, is given by

$$T_e = \frac{(x_d' - x_q')}{x_d' x_q'}\psi_q \psi_d + \frac{\psi_d E_d'}{x_q'} + \frac{\psi_q E_q'}{x_d'} \tag{10.102}$$

The expression for ΔT_e is given by

$$\Delta T_e = [C_{me}]x_e$$

where $[C_{me}]$ is a row vector whose elements are

$$C_{me}(1) = \frac{(x_d' - x_q')}{x_d' x_q'}\psi_{qo} + \frac{E_{do}'}{x_q'}$$

$$C_{me}(2) = \frac{(x_d' - x_q')}{x_d' x_q'} \psi_{do} + \frac{E_{qo}'}{x_d'}$$

$$C_{me}(3) = \frac{\psi_{do}}{x_q'}, \quad C_{me}(4) = \frac{\psi_{qo}}{x_d'}$$

The linearized machine electrical equations are

$$\Delta \dot{x}_e = [A_e]\Delta x_e + [B_{e1}]\Delta u_e + [B_{e2}]\Delta E_{fd} + [B_{e3}]\Delta y_m \qquad (10.103)$$

$$\Delta y_e = [C_e]\Delta x_e + [C_{em}]\Delta y_m \qquad (10.104)$$

$$\Delta y_m = [C_m]\Delta x_m$$

where

$$[B_{e3}] = \begin{bmatrix} \omega_B v_{qo} & -\omega_B \psi_{qo} \\ -\omega_B v_{do} & \omega_B \psi_{do} \\ 0 & 0 \\ 0 & 0 \end{bmatrix}$$

$$y_m = \begin{bmatrix} \delta \\ S_m \end{bmatrix} = \begin{bmatrix} [I_2] & 0 \end{bmatrix} x_m = [C_m]x_m$$

where $[I_2]$ is a unit matrix of order 2.

$$[C_{em}] = \left[\frac{\partial C_e}{\partial \delta}\right] [P_m], \quad [P_m] = [x_{eo} \quad \underline{0}]$$

Note that P_m consists of two columns. The first column is the operating value of vector x_e. The second column is a null vector. The linearized excitation control system equations (if considered) can be expressed as

$$\Delta \dot{x}_c = [A_c]\Delta x_c + [B_{c1}]\begin{bmatrix} \Delta v_D \\ \Delta v_Q \end{bmatrix} + [B_{c2}]\Delta S_m \qquad (10.105)$$

$$\Delta E_{fd} = e_1^t \Delta x_c \qquad (10.106)$$

where e_1 is a column vector with the first entry at 1 and the rest as zeroes. For a simplified model of a static exciter shown in Fig. 10.16 there are two state variables, the first one corresponding to E_{fd} and the other corresponding to PSS. For the system shown in Fig. 10.16, the various matrices are

$$[A_c] = \begin{bmatrix} -\dfrac{1}{T_A} & \dfrac{K_A K_S}{T_A} \\ 0 & -\dfrac{1}{T_2} \end{bmatrix}, \quad [B_{c2}] = \begin{bmatrix} \dfrac{K_A K_S}{T_A}\dfrac{T_1}{T_2} \\ \left(1 - \dfrac{T_1}{T_2}\right)\dfrac{1}{T_2} \end{bmatrix}$$
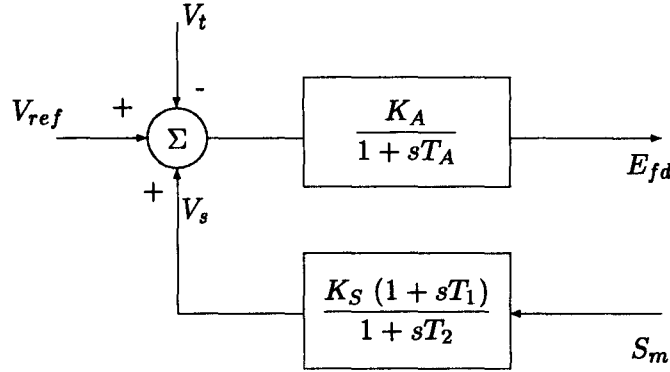
Figure 10.16: A static exciter with PSS

$$[B_{c1}] = \begin{bmatrix} -\dfrac{K_A}{T_A}\dfrac{V_{Do}}{V_{to}} & -\dfrac{K_A}{T_A}\dfrac{V_{Qo}}{V_{to}} \\ \\ 0 & 0 \end{bmatrix}$$

The linearized equations for the generator (including mechanical, electrical and excitation controller) can be expressed as

$$\Delta \dot{x}_G = [A_G]\Delta x_G + [B_G]\Delta u_G \qquad (10.107)$$
$$\Delta y_G = [C_G]\Delta x_G \qquad (10.108)$$

where

$$x_G^t = [x_e^t \ x_c^t \ x_m^t]$$
$$u_G^t = [V_D \ V_Q] = u_e, \quad y_G^t = [i_D \ i_Q] = y_e$$

$$[A_G] = \begin{bmatrix} [A_e] & [B_{e2}e_1^t] & [B_{e3}C_m] \\ \\ [0] & [A_c] & [B_{c2}'C_m] \\ \\ [B_{m1}C_{me}] & [0] & [A_m] \end{bmatrix}, \quad [B_{c2}'] = [\underline{0} \ \ B_{c2}]$$

$$[B_G^t] = [[B_{e1}^t] \ [B_{c1}^t] \ [0]]$$

$$[C_G] = [[C_e] \ [0] \ [C_{em}C_m]]$$

The linearized network equations from Eq. (10.94) are

$$\Delta \dot{x}_N = [A_N]\Delta x_N + [B_{N1}]\Delta u_{N1} \qquad (10.109)$$

$$\Delta u_{N1} = \Delta y_G$$

For the network shown in Fig. 10.14, we can express

$$\Delta u_G = \Delta x_N + [F]\Delta y_G + \frac{X_L}{\omega_B}p\Delta y_G$$

$$p\Delta y_G = [C_G]\Delta \dot{x}_G = [C_G A_G]x_G + [C_G B_G]u_G$$

It is possible to eliminate the variables Δu_G and Δu_{N1} and combine the network and the generator equations. The system equations can be expressed as

$$\dot{x}_T = [A_T]x_T \qquad (10.110)$$

where

$$x_T^t = [x_G^t \ \ x_N^t]$$

The derivation of Eq. (10.110) is left as an exercise. The stability of torsional oscillations can be determined from the eigenvalues of matrix $[A_T]$.

Remarks

1. The use of D-Q variables in describing the network enables extension to systems with multiple generators.

2. The system model is derived by combining component models and the use of appropriate interface variables. The interface between the generator and the network is at the generator terminals and uses voltage and current variables. The generator currents are determined from the generator equations while the voltages are obtained from the network (and generator) equations.

3. The methodology for forming the system matrix is general and flexible to accommodate varying component models and the inclusion of new subsystems (such as SVC or HVDC controllers).

10.9   Simulation of SSR

While steady state SSR problem is conveniently studied by the characterization of operating point stability based on small signal analysis, the study of transient torques requires the consideration of nonlinear models. This is due to the fact that transient torques which can damage shafts arise from large disturbances such as faults and reinsertion of series capacitors.

Since the inclusion of network transients is essential for the analysis of SSR, the simulation used in connection with transient stability evaluation is inadequate. Also it is necessary to model the torsional dynamics considering multimass rotor representation with elastic shafts. Thus, special purpose simulation programs become necessary.

However, in the recent years, EMTP (Electro-Magnetic Transient Program) which was initially developed for the study of high frequency lightning induced transients in transmission lines and subsequently extended for the study of switching transients, has become a general tool for the simulation of power systems whenever network transients have to be modelled. The incorporation of detailed synchronous machine and control system models has now made it possible to simulate transients with subsynchronous frequency oscillations.

10.10   A Case Study

A case study on IEEE First Bench Mark (FBM) model [13] is presented in this section. This consists of a single series compensated transmission line connecting a synchronous generator to a large system. See Fig. 10.17. The network parameters on the generator base of 892.4 MVA are given in Table 10.1. The synchronous machine data are given in Table 10.2. The shaft inertias and the spring constants are given in Table 10.3. There are six inertias corresponding to six rotors-four turbines, generator and rotating exciter.

Table 10.1   Network Parameters in Per Unit on the Generator Base

Parameters	Positive Sequence	Zero Sequence
R	0.02	0.50
X_T	0.14	0.14
X_L	0.50	1.56
X_{sys}	0.06	0.06
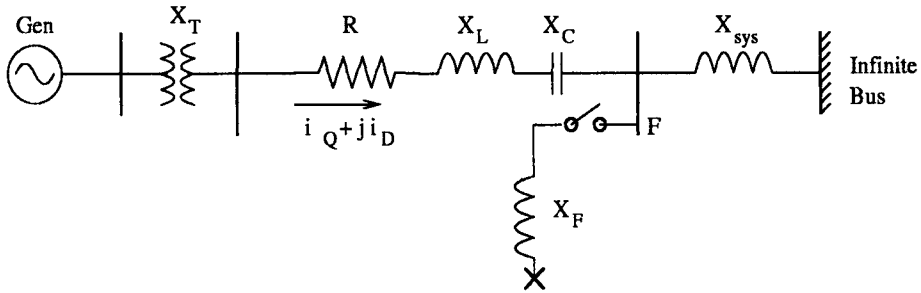
Figure 10.17: IEEE FBM system diagram

Table 10.2 Synchronous Machine Parameters

d-Axis Parameters	Value	q-Axis Parameters	Value
$x_{a\sigma}$	0.130	$x_{a\sigma}$	0.130
x_d	1.790	x_q	1.710
x_d'	0.169	x_q'	0.228
x_d''	0.135	x_q''	0.200
T_{do}'	4.300	T_{qo}'	0.850
T_{do}''	0.032	T_{qo}''	0.050

Table 10.3 Rotor Inertias and Spring Constants

Mass	Inertia Constant (H)	Shaft section	Spring Constant pu Torque/Rad.
HP	0.092897	HP-IP	19.303
IP	0.155589	IP-LPA	34.929
LPA	0.858670	LPA-LPB	52.038
LPB	0.884215	LPB-GEN	70.858
GEN	0.868495	GEN-EXC	2.822
EXC	0.0342165		

The generator is assumed to be operating at no load ($P_g = 0, Q_g = 0$). The infinite bus voltage is assumed to be 1.0 pu. The AVR is neglected in the study. The nominal value of series compensation is assumed to be 70% ($X_c = 0.35$ pu).

10.10.1   Induction Generator Effect

To study the induction generator effect, the system is modelled using state equations as in section 10.8.1. The machine is represented by model (1.1) for simplicity. This requires only the subset of parameters given in Table 10.2 (the subtransient reactances and time constants are not required).

An eigenvalue analysis is carried out with changing level of series compensation. The locus of the critical mode with variation in the level of series compensation is obtained for the three cases given below

(a) with the nominal machine parameters

(b) with $T'_{do} = 0.43$ s, other parameters at nominal values

(c) with $T'_{qo} = 0.085$ s, other parameters at nominal value

The loci for the three cases are shown in Fig. 10.18. All the eigenvalues for $X_c = 0.35$ pu are shown in Table 10.4.

It was observed during eigenvalue analysis that the results are independent of the initial value of the rotor angle (δ_o).

Remarks

1. The radian frequency of the critical network mode reduces with increase in the value of X_c. This frequency (f_r^{sub}) is the complementary frequency defined by

Induction generator effect $T'_{d0} = 4.35, T'_{q0} = 0.855$
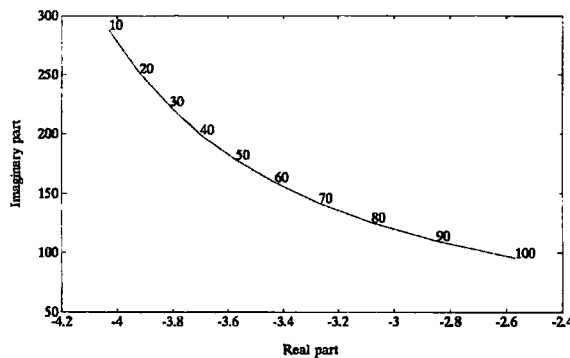
(a) Nominal Parameters
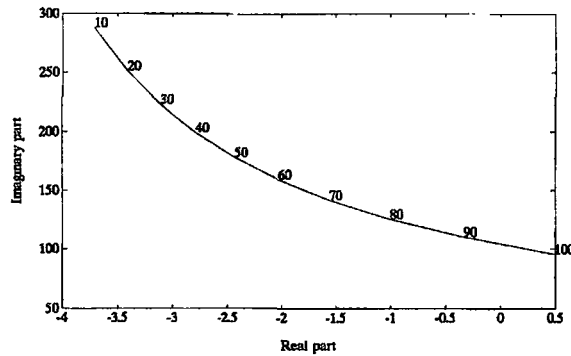
(b) $T'_{d0} = 0.43$
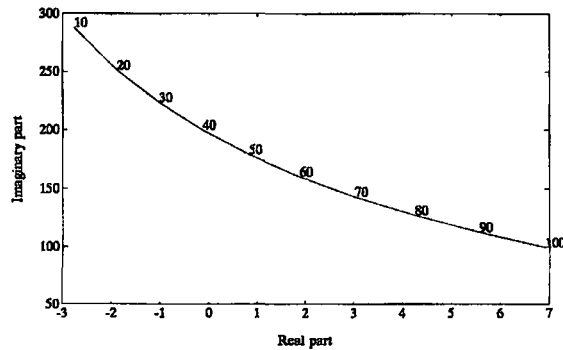
(c) $T'_{q0} = 0.085$

Figure 10.18: Loci of the network mode

$$f_r^{sub} = f_o - f_{er}$$

where the electrical resonant frequency (f_{er}) is defined in Eq. (10.1). As X_c increases, f_{er} increases and f_r^{sub} decreases.

2. The damping of the critical network mode reduces with increase in X_c and can even become negative at higher values of X_c. This is due to the fact that the generator rotor circuits (field and the damper) offer higher negative resistances corresponding to lower values of the slip or rotor frequencies. (Note that the frequency of the currents induced in the rotor circuits is f_r^{sub}).

3. The resistances of the rotor circuits affect the damping of the critical network mode. Higher the resistance, greater the negative damping at increased levels of series compensation (see Fig. 10.18). The quadrature axis damper has a greater effect than the field circuit on the direct axis.

Table 10.4   Eigenvalues (Neglecting mechanical system)

Sl. No.	Case (a) $T'_{do} = 4.3$, $T'_{qo} = 0.85$	Case (b) $T'_{do} = .43$, $T'_{qo} = 0.85$	Case (c) $T'_{do} = 4.3$, $T'_{qo} = 0.085$
1,2	-4.4188 ± j612.37	-4.8076 ± j612.36	-5.9788 ± j612.25
3,4	-3.2674 ± j141.54	-1.5622 ± j141.55	3.0097 ±j142.94
5	-4.1916	-4.1940	-41.123
6	-0.9589	-9.5865	-0.9588

Table 10.5   The Transformation Matrix [Q]

Rotor	Column #1	Column #2	Column #3	Column #4	Column #5	Column #6
HP	-2.0824	-2.9408	6.0260	-1.3927	176.64	1.0000
IP	-1.5644	-1.7303	2.0624	0.0700	-224.25	1.0000
LPA	-0.9178	-0.4019	-1.3839	0.8103	25.399	1.0000
LPB	0.2993	1.0571	-0.5753	-1.6117	-4.7335	1.0000
GEN	1.0000	1.0000	1.0000	1.0000	1.0000	1. 0000
EXE	2.6806	-26.7648	-1.5206	-0.6072	-0.2119	1.0000

Table 10.6   Modal Quantities

	Mode #1	Mode #2	Mode #3	Mode #4	Mode #5	Mode #0
Frequency (rad/sec)	98.7248	126.9921	160.5289	202.8517	298.1878	0.00
Inertia (H^i)	2.70	27.80	6.92	3.92	11297	2.894
Spring constant (K_i)	139.627	2376.4	945.894	856.303	5328600	0.00

10.10.2   Study of Torsional Interaction

The frequency of torsional modes, modal inertias and spring constants were computed using the transformation matrix [Q] given in Table 10.5. The results are shown in Table 10.6. The first five columns of the matrix [Q] are eigenvectors of modes 1 to 5 respectively. The last column is the eigenvector of mode zero.

This shows that all the rotors participate equally in mode zero, as expected. The modal inertia for mode zero is the sum of all the inertias of the six rotors. It is interesting to note that both modal inertia and the spring constant for mode #5 are very large compared to the rest of the modes. Due to this, the external network has negligible influence on mode #5.

The variation of the synchronizing torque coefficient T_{Sm}, which is defined as

$$T_{Sm}(\omega) = -\frac{\omega}{\omega_B}\Im[Y_m(j\omega)] \qquad (10.111)$$

as a function of ω is shown in Fig. 10.19. The zero crossing of $T_{Sm}(\omega)$ occurs at the torsional resonant frequencies. The modal inertia (H^i) can also be determined as

$$H^i = -\frac{\omega_B}{4\omega}\left.\frac{dT_{Sm}}{d\omega}\right|_{\omega = \omega_i}$$

where ω_i is the modal frequency. The above expression follows from (10.38) and the relation (10.111). It is observed from Fig. 10.19 that the pole and zero near the frequency 298 rad/sec are practically indistinguishable.
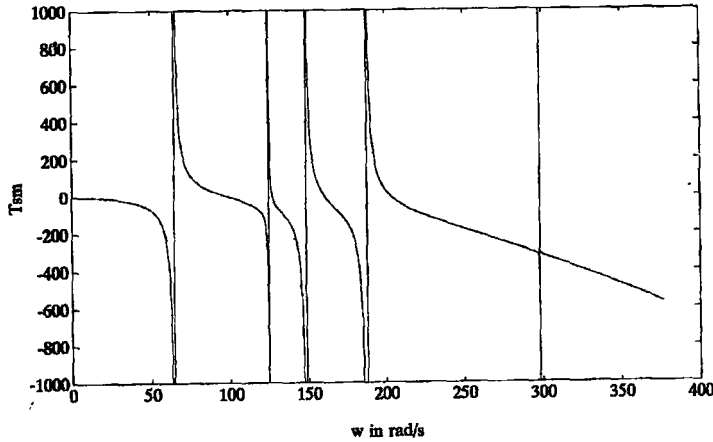
Figure 10.19: Variation of T_{Sm}

The computations of T_{Se} and T_{De} are carried out from the knowledge of $Y_e(s)$ which can be based on either simplified machine model or detailed model. In the simplified machine model (see section 10.5), the flux decay and damper windings are neglected and the stator is represented by a voltage source behind a constant reactance $x' = x'_d$. The variations of T_{Se} and T_{De} as functions of ω are shown in Fig. 10.20.
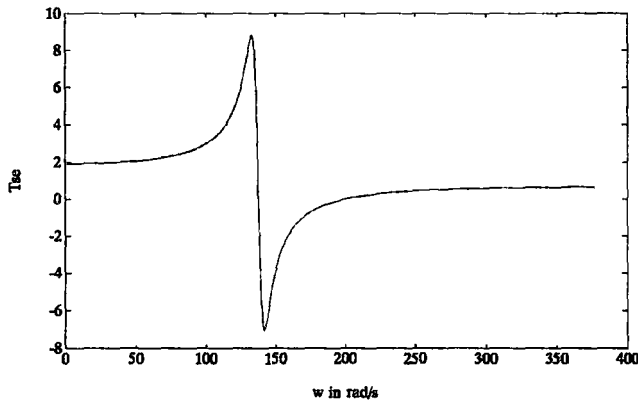
(a) T_{Se} vs ω
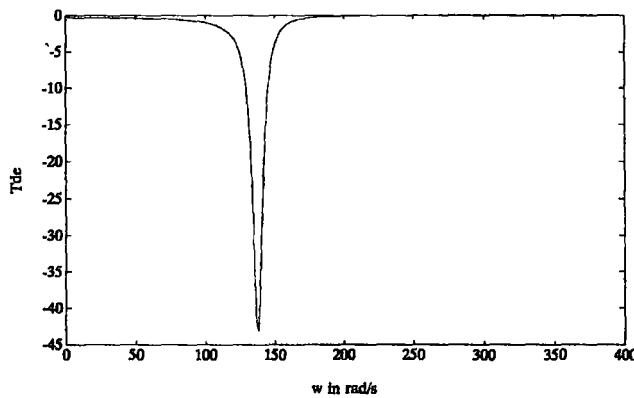
(b) T_{De} vs ω

Figure 10.20: Variation of T_{Se} and T_{De} using simplified model

The variations of T_{Se} and T_{De} when detailed machine model is considered, are shown in Fig. 10.21. It is interesting to observe that the simplified model also gives accurate representation of the negative damping introduced by the network in the vicinity of the frequency 140 rad/sec, which is a function of the series compensation level.

The eigenvalue analysis of the overall system has been carried out. For the nominal value of $X_c = 0.35$ pu all the eigenvalues are given in Table 10.7 for the two cases (i)with machine model (1.1) and (ii)with machine model (2.2).
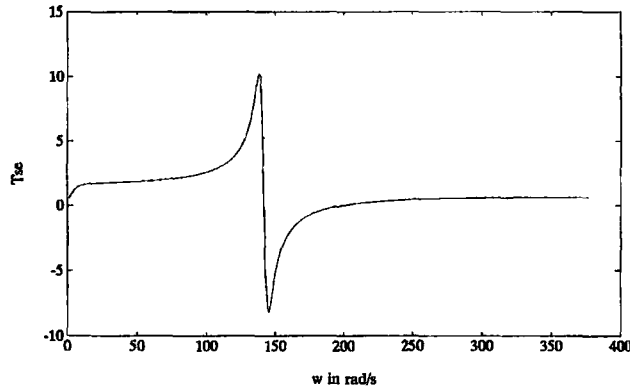
(a) T_{Se} vs ω
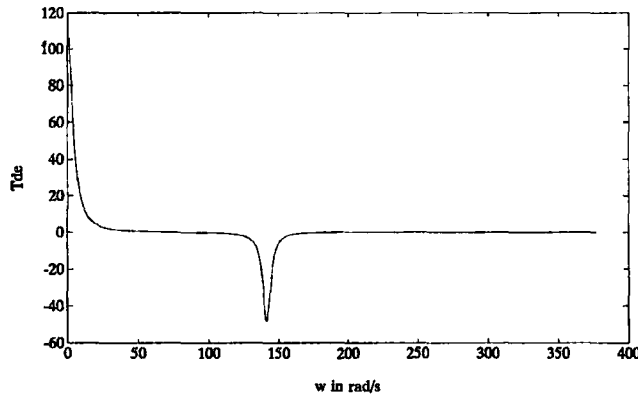
(b) T_{De} vs ω

Figure 10.21: Variation of T_{Se} and T_{De} using detailed machine model(1.1)

It is observed that torsional modes 1 to 4 are negative damped due to torsional interaction. The negative damping of the mode 4 is marginal as its frequency is not close to the critical network mode (#1) frequency. With machine model (1.1), mode 3 is most affected while with model (2.2), the mode 2 is most affected. This is due to the fact the frequency of the network mode #1 depends on the machine model. With machine model (2.2), the network mode has a frequency of 136.93 rad/sec compared to 141.24 rad/sec with machine model (1.1). This shows that the subtransient reactances affect the network mode. The damping of the network mode #1 is also affected by the presence of the additional damper windings due to the induction generator effect.

Table 10.7 Eigenvalues of the combined system

Sr. No.	Machine model (1.1)	Machine model (2.2)	Comments
1,2	-1.4521 ± j10.264	-1.5605 ± j10.431	Torsional mode # 0
3,4	0.02266 ± j 99.626	0.02082 ± j99.812	Torsional mode # 1
5,6	0.02633 ± j127.14	0.04673 ± j127.17	Torsional mode # 2
7,8	0.04135 ± j 160.35	0.02368 ±j160.41	Torsional mode # 3
9,10	0.00241 ± j 202.86	0.00095 ± j202.91	Torsional mode # 4
11,12	0.0000± j 298.18	0.0000 ± j298.19	Torsional mode # 5
13,14	-3.3951 ± j 141.24	-2.9000 ± j 136.93	Network mode # 1
15,16	-4.4197 ± j 612.41	-4.7118 ± j 616.61	Network mode # 2
17	-0.9590	-0.9683	
18	-1.2155	-1.2142	
19	–	-20.259	
20	–	-33.152	

The frequency of the network mode #1 (21.8 Hz) is the complement of the electrical resonant frequency (38.2 Hz) as mentioned earlier. Its frequency is subsynchronous. There is also a supersynchronous network mode (#2) of frequency 98.2 Hz.
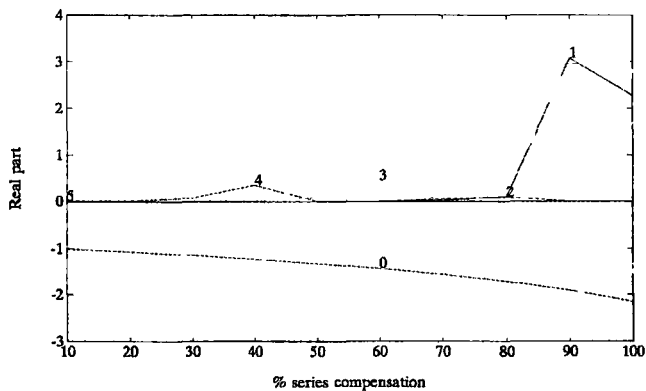
Figure 10.22: Damping of torsional modes (Machine model 2.2)

The variations of the real parts of the eigenvalues corresponding to the torsional modes as series compensation is varied are shown in Figs. 10.22 and 10.23 for machine models (2.2) and (1.1) respectively. The imaginary parts (radian frequencies) are not affected by the external network. The loci of the
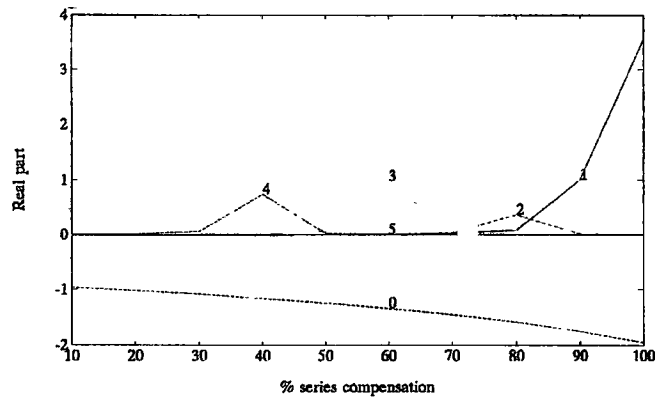
Figure 10.23: Damping of torsional modes (Machine model 1.1)

network mode #1 in the complex plane as series compensation is varied are shown in Figs. 10.24 and 10.25 for machine model (2.2) and (1.1) respectively.
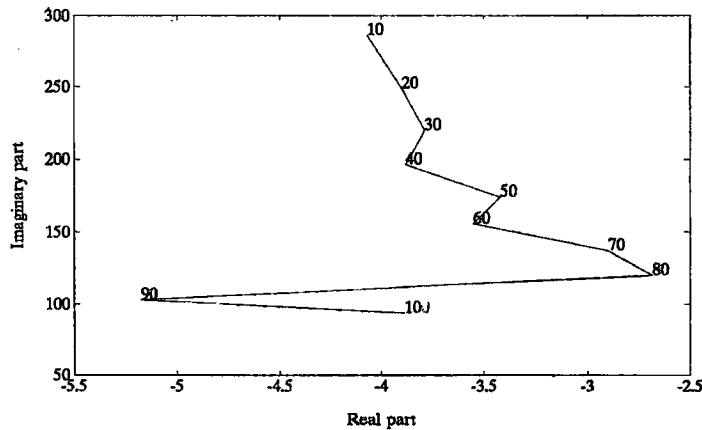
Figure 10.24: Locus of network mode #1 (machine model 2.2)

Remarks

1. Due to Torsional Interaction (TI), the damping of each torsional mode (except mode zero) is significantly affected in the vicinity of a certain level of series compensation (which results in the frequency f_r^{sub} coinciding with the torsional frequency). For mode 1, this occurs at the highest level of series compensation and for mode 4, this occurs at the lowest level of compensation.
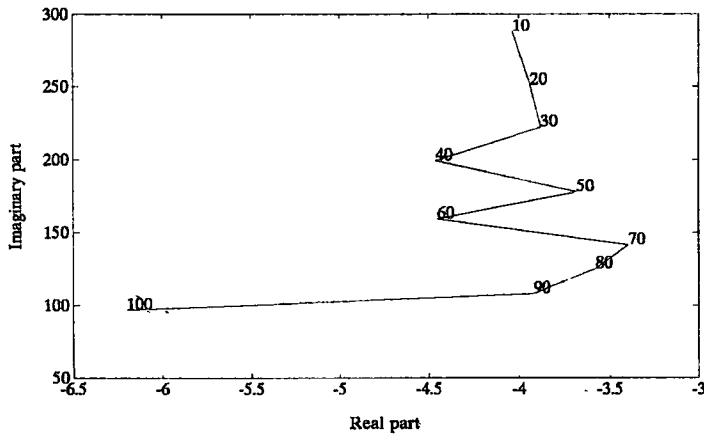
Figure 10.25: Locus of network mode #1 (machine model 1.1)

2. The electrical resonant frequency (f_{er}) and consequently f_r^{sub} depend on the machine model selected. The model (2.2) gives a slightly lower value of f_{er} and consequently a higher value of f_r^{sub} as compared with model (1.1) for the same level of compensation.

3. The negative damping of torsional modes is dependent on the machine model selected. The machine model (1.1) results in slightly higher values of negative damping.

   The damping of zeroth mode increases as the level of compensation is increased. Here also model (2.2) results in slightly better damping compared to model (1.1).

   To summarize, the model (1.1) gives slightly pessimistic results compared to model (2.2) regarding torsional damping.

4. The network mode #1 (f_r^{sub}) is affected both in frequency and damping as compensation level is increased. It is interesting to note that at compensation levels which cause SSR, the network mode has increased (positive) damping.

The maximum TI occurs in the neighbourhood of compensation level of 90% which leads to SSR for mode 1.

It is interesting to compare Fig. 10.25 with Fig. 10.23. The torsional interaction results in damping of the network mode and undamping of the torsional mode.

10.10.3   Simulation

A case study of the system simulation using IEEE First Benchmark Model is
presented here [32]. The simulation is carried out to study the response of
the system to a three phase to ground fault through a reactance at location
F indicated in Fig. 10.17. The fault is initiated at the instant when phase-A
voltage at 'F' is zero. The fault reactance X_F is 0.04 pu in each phase. The fault
in phase A is cleared at the first current zero 75 milliseconds after the initiation
of the fault. Faults in phase B and C are cleared at the subsequent current
zeroes in their respective phases. The series capacitor is selected at $X_c = 0.371$
pu. The generator is initially operating at $P_g = 0.9$ pu at a power factor of 0.9
lagging (at the generator terminals).
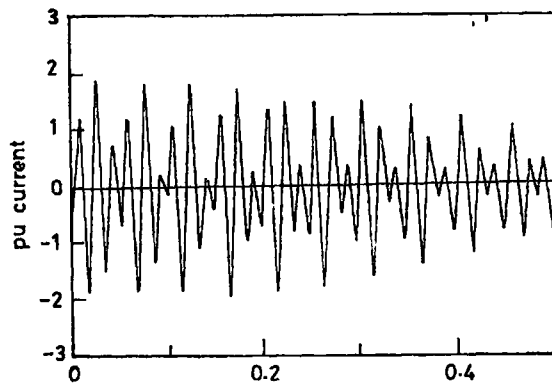
(a) Generator phase current
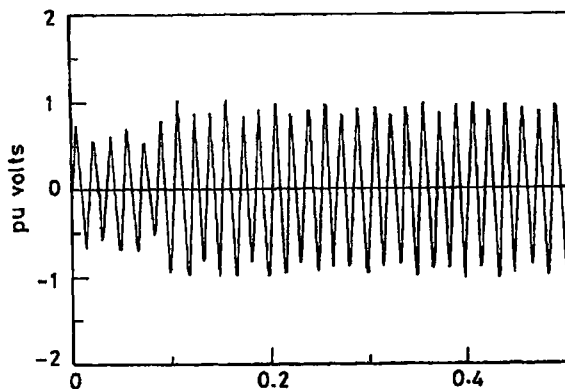
(b) Generator terminal voltage

(c)   Capacitor voltage
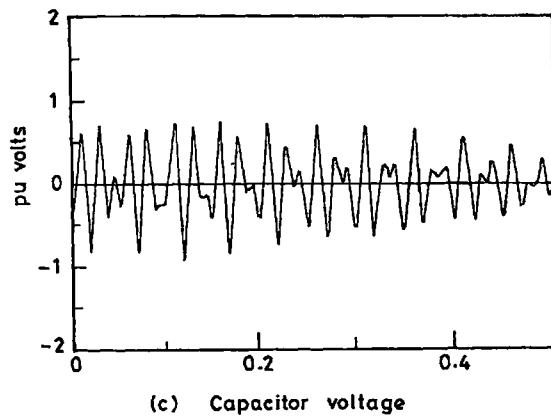
Figure 10.26: Response to a fault IEEE FBM system

(a) Electromagnetic torque
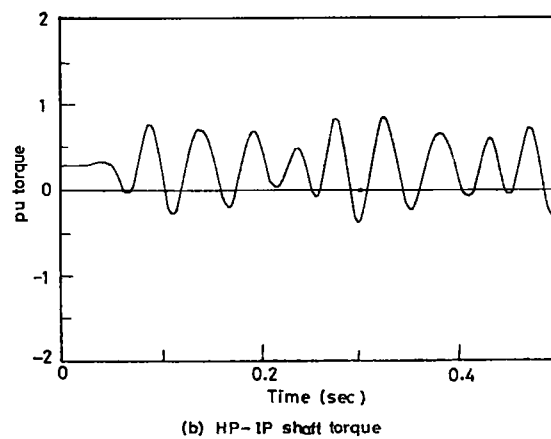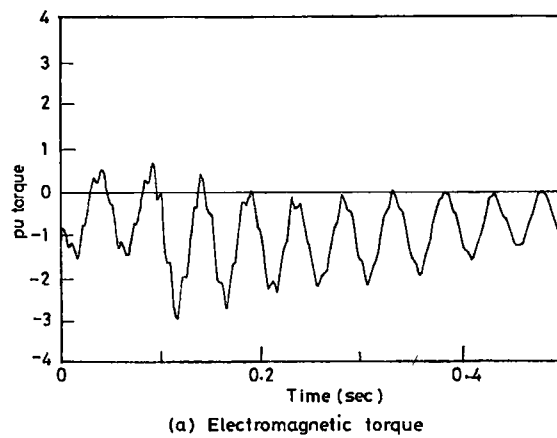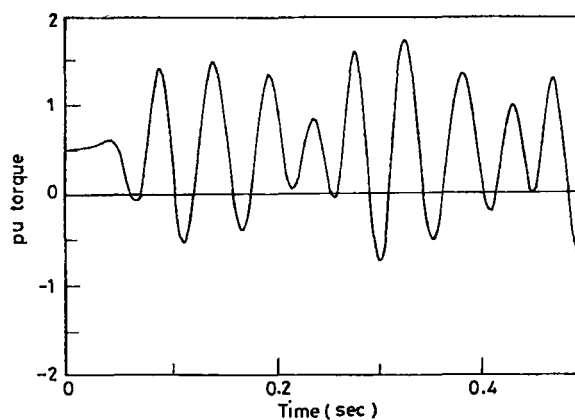
(b) HP-IP shaft torque
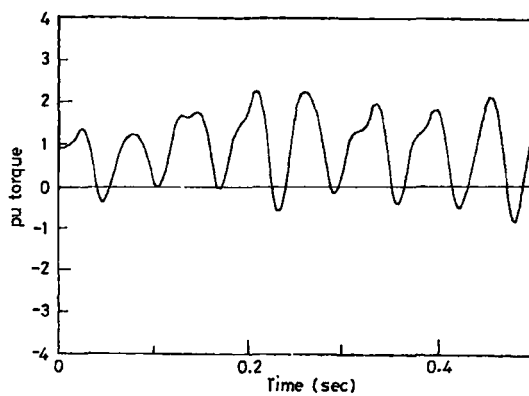
(c) IP-LPA shaft torque
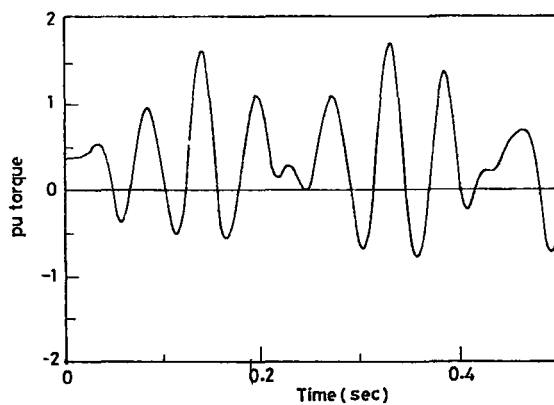
(d) LPA-LPB shaft torque

(e) LPB-GEN shaft torque
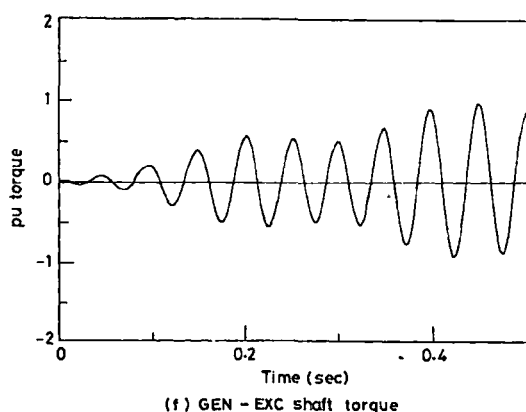
(f) GEN - EXC shaft torque

Fig.10.27 Electromagnetic and shift torques

The generator current, terminal voltage and capacitor voltage all in phase A, are shown in Fig. 10.26. The electromagnetic torque and the shaft torques are shown in Fig. 10.27.

The results show that the shaft torque in GEN-EXC section is increasing with time indicating self excitation due to torsional interaction. The second torsional mode is excited and is undamped. The results given here are agreement with those given in [13].

The simulation can be used to evaluate transient torques in shafts when there is a major disturbance such as fault followed by clearing.

References and Bibliography

1. P.M. Anderson, B.L.Agrawal and J.E. Van Ness, "Subsynchronous Resonance in Power Systems", IEEE Press, New York, 1990.

2. IEEE Publication, "Analysis and Control of Subsynchronous Resonance", IEEE Pub. 76CH1066-0-PWR, New York, 1976

3. IEEE Committee Report, "Proposed Terms, Definitions for Subsynchronous Oscillations", IEEE Trans. Vol. PAS-99, No. 2, 1980, pp. 506-511

4. IEEE Committee Report, "Terms, Definitions and Symbols for Subsynchronous Oscillations", IEEE Trans. Vol. PAS-104, June 1985, pp. 1326-1334

5. IEEE Committee Report, "Effects of switching network, disturbances on turbine-generator shaft systems", IEEE Trans. Vol. PAS-101, No. 9, 1982, pp. 3151-3157

6. D.N. Walker et al, "Results of Sub-synchronous Resonance tests at Mohave", IEEE Trans. Vol. PAS-75, No. 5, 1975, pp. 1878-1889

7. I.M. Canay, "A novel approach to the torsional interaction and electrical damping of the synchronous machine, Part I: Theory, Part II - Application to arbitrary network", IEEE Trans. Vol. PAS-101, No. 10, 1982, pp. 3630-3647

8. C. Concordia and G.K. Carter, "Negative damping of electrical machinery", AIEE Trans. Vol. 60, 1941, pp. 116-119

9. H.M. Rustebakke and C. Concordia, "Self-excited oscillations in transmission system using series capacitors", IEEE Trans. Vol. PAS-89, No. 7, 1970, pp. 1504-1512

10. L.A. Kilgore, L.C. Elliott and E.R. Taylor Jr., "The prediction and control of self-excited oscillations due to series capacitors in power systems", IEEE Trans. Vol. PAS-90, No. 3, 1971, pp. 1305-1311

11. J.W. Ballance and S. Goldberg, "Subsynchronous resonance in series compensated transmission lines", IEEE Trans. Vol. PAS-92, Sept/Oct. 1973, pp. 1649-1648

12. A.A. Fouad and K.T. Khu, "Subsynchronous Resonance zones in the IEEE Benchmark power system", IEEE Trans. Vol. PAS-97, No. 3, 1978, pp. 754-762

13. IEEE Committee Report, "First Benchmark model for computer simulation of Subsynchronous Resonance", IEEE Trans. Vol. PAS-967, Sept/Oct. 1977, pp. 1565-1570

14. IEEE Committee Report, "Second Benchmark model for computer simulation of Subsynchronous Resonance", IEEE Trans. Vol. PAS-104, May 1985, pp. 1057-1066

15. IEEE Committee Report, "A bibliography for the study of Subsynchronous Resonance between rotating machines and power systems", IEEE Trans. Vol. PAS-95, No. 1, 1976, pp. 216-218

16. IEEE Committee Report, "First supplement to a bibliography for the study of Subsynchronous Resonance between rotating machines and power systems", IEEE Trans. Vol. PAS-98, No. 6, Nov.-Dec. 1979, pp. 1872-1875

17. IEEE Committee Report, "Second supplement to a Bibliography for the study of Subsynchronous Resonance between rotating machines and power systems", IEEE Trans. Vol. PAS-104, Feb. 1985, pp. 321-327

18. IEEE Committee Report, "Third supplement to bibliography for the study of subsynchronous Resonance between rotating machines and power systems", IEEE Trans. Vol. 6, No. 2, 1991, pp. 830-834

19. G. Gross and M.C. Hall, "Synchronous machine and torsional dynamic simulation in the computation of electrmagnetic transients", IEEE Trans. Vol. PAS-97, No. 4, 1978, pp. 1074-1086

20. B.L. Agrawal and R.G. Farmer, "Use of frequency scanning techniques for Subsynchronous Resonance", IEEE Trans. Vol. PAS-98, March/April 1979, pp. 341-349

21. W. Watson and M.E. Coltes, "Static exciter stabilizing signals on large generators-mechanical problems", IEEE Trans. Vol. PAS-92, Jan/Feb 1973, pp. 204-211

22. M. Bahrman et al, "Experience with HVDC-turbine generator torsional interaction at Square Butte", IEEE Trans. Vol. PAS-99, May/June 1980, pp. 966-975

23. K. Mortensen, E.V. Larsen and R.J. Piwko, "Field tests and analysis of torsional interaction between the coal-creek turbine-generators and CU HVDC system", IEEE Trans. Vol. PAS-100, Jan. 1981, pp. 336-345

24. N. Rostamkolai et al, "Subsynchronous torsional interactions with Static Var Compensators - concepts and practical solutions", IEEE Trans. on Power Systems, Vol. 5, No. 4, 1990, pp. 1324-1332

25. T.J. Hammons and I.M. Canay, "Effect of damper modelling and fault clearing process on response torque and stressing of turbine-generator shafts", IEEE Trans. on Energy Conversion, Vol. EC-1, No. 1, 1986, pp. 113-121

26. K.R. Padiyar and A.G. Kothari, "Analysis of HVDC turbine generator torsional interactions", Elec. Machines and Power Systems, Vol. 16, 1989, pp. 303-317

27. K.R. Padiyar and R.S. Ramshaw, "State space formulation for transient and dynamic analysis of power systems", Canadian Communications and EHV Conference, Montreal, Nov. 1972

28. K.R. Padiyar and A.G. Kothari, "Study of HVDC torsional interactions through digital dynamic simulation", EHV Machines and Power Systems, Vol. 14, No. 5, 1988

29. K.R. Padiyar and M.K. Geetha, "Analysis of torsional interactions with power system stabilizer", Elec. Machines and Power Systems, Vol. 21, No. 6, 1993, pp. 767-782

30. K.R. Padiyar and M.K. Geetha, "Study of torsional interactions in multi-terminal DC systems through small signal stability analysis", Conf. Publ. No. 345, Fifth Int. Conf. on AC and DC Power Transmission, IEE, London, Sept 1991, pp. 411-413

31. K.R. Padiyar, Sachchidanand and J.Senthil, "Digital computer study of the control of torsional interactions in HVDC turbine generators", Elec. Machines and Power Systems, Vol.22, No. 1, 1994, pp. 87-104

32. J.Senthil, "Simulation of Transients in Synchronous Generators and HVDC Links and Study of Torsional Interactions", Ph.D Thesis, Indian Institute of Technology, Kanpur, September 1990

Chapter 11

Countermeasures for Subsynchronous Resonance

The problem of SSR can be classified as

1. Steady state problem due to self excitation. The causes are

    a. Torsional Interaction
    b. Induction generator effect

2. Transient torques which can cause fatigue damage to rotor shafts.

    The steady state problem should be avoided by proper planning. However it may not be possible to identify all critical operating conditions (which give rise to self excitation) while planning. The problem of transient torques is mainly solved by providing proper filtering (to limit the magnitudes of torques) and damping (with auxiliary devices).

    In addition to the devices required for damping SSR, it is also necessary to provide protective measures and relaying to monitor conditions that can lead to damage.

11.1   System Planning Considerations

There are several things that can be considered during system planning. These are listed below

(i) **Series versus Shunt Compensation**
   The use of shunt compensators do not result in electrical resonant frequencies below synchronous frequency. Actually, it can be shown that resonance due to shunt capacitor is at supersynchronous frequencies. It was shown in chapter 10, that supersynchronous frequency currents result in positive damping of torsional modes. As a matter of fact, the low (and

resistive) network impedance at supersynchronous frequency, increases the damping.

However, the shunt compensation cannot completely replace series compensation. The use of series compensation tends to be economical and more flexible. The location of series capacitors in a line is not critical (compared to that of shunt compensation which should be located at the midpoint of the line for maximum effectiveness). It is advantageous to use both series and shunt compensation where possible. The controllable shunt compensation (using SVC) not only helps to regulate the line voltage but also reduce the level of series compensation required.

(ii) Turbine-Generator Modifications

There are limitations on what can be acheived here. For example, it is impractical (due to constraints on shaft and bearing size) to design machines for which the lowest torsional (mode) frequency is greater than synchronous frequency. The torsional mode frequencies of the turbine-generator can be varied only within small limits. However, this has not much impact on the SSR problem as changes in the network due to future growth/line outages affect the critical electrical resonance frequency.

Another factor that has a critical bearing on SSR problem is the mechanical damping of torsional modes. It would be desirable to increase this damping but is considered as impractical. Another means of limiting shaft torques is through the use of slip couplings which has not been investigated.

Pole-face Amortisseur Windings can be added to reduce the net negative resistance of the generator at subsynchronous frequencies (to control the induction generator effect). It is relatively inexpensive to install pole-face amortisseur windings in new machines. However, retrofitting on old machines is not feasible. Also, the windings are not effective to control torsional interaction and transient torques.

(iii) System Modifications

The steady state SSR problem is mainly due to the coincidence of electrical resonant frequency (f_{er}) with the complement of a torsional mode frequency $(f_o - f_m)$. It is thus possible to adjust the series compensation to avoid this coincidence. As the problem is more severe at lower frequency torsional modes, reducing the level of series compensation helps. This can also be done during system operation by bypassing some capacitor segments.

It is also possible to have **coordinated series capacitor use with loading**. As the mechanical damping decreases with the load, (power output of the generator), it is practical to insert capacitors only when the loading exceeds the minimum loading. As series capacitors are mainly required

at higher loadings, this procedure of coordinating the capacitor use with load is consistent with the dual objectives of improved stability limit and avoidance of steady state SSR problem.

(iv) **Series Capacitor Protection and Reinsertion**

It is not economically feasible to use capacitors that can withstand fault currents. Thus, it is necessary to protect the capacitor banks against overcurrents (and voltages) by bypassing them. In earlier schemes of protection, a spark gap flashes over as the voltage crosses a predetermined level. However, from system stability considerations, it is also necessary to reinsert the capacitors within a few (3 to 5) cycles after fault clearing. This can be done by opening the bypass switch. This process of reinsertion of capacitors produces transient voltages across the capacitors. When these voltages exceed the spark gap setting, the gap may reflash resulting in failure to reinsert the capacitors. The setting of the spark gap determines the protective level of the capacitor. While higher gap setting is desirable for successful reinsertion, lower setting is necessary to reduce the transient torques during faulted period. A dual gap (or extended range dual gap) protection scheme helps, to achieve both objectives of capacitor bypass at lower fault levels (even for remote system fault) and successful reinsertion.

In recent schemes, the capacitor overvoltages are limited by using a highly nonlinear metal oxide resistor in parallel with the capacitor. (see Fig. 11.1). The resistor is sized such that very small currents flow through it during normal capacitor voltages. During faults, the resistor provides parallel path for the current and the voltage across the capacitor reaches a saturation level. Thus, the capacitor is automatically bypassed and reinserted without any hitch. A case study showed that a 15 MW-sec nonlinear resistor applied for 5 cycles reduces the capacitor voltage from 3.5 to 2.2 pu with a corresponding reduction in the peak shaft torque from 3.7 to 1.7 pu.
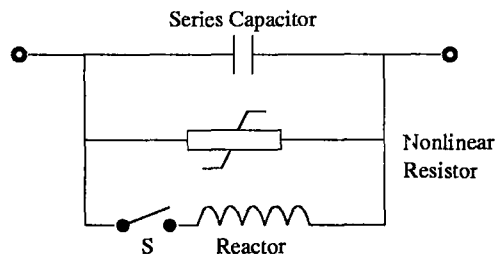

Figure 11.1: Series capacitor protection

11.2   Filtering Schemes

11.2.1 ⁃ Static Blocking Filter (SBF).

This is inserted in series with the generator step-up transformer winding on the neutral end of the transformer high voltage winding (see Fig. 11.2). It can also be placed on the high voltage side of the transformer winding. The SBF is a three phase filter made up of separate filters connected in series. Each section of the filter is a high Q, parallel resonant circuit tuned to block electric currents at (complementary) frequencies corresponding to each of the torsional mode. Thus, this filter provides an excellent transient torque control if properly tuned. The static blocking filter was first installed at Navajo Generating station in Western U.S.A. in 1976.
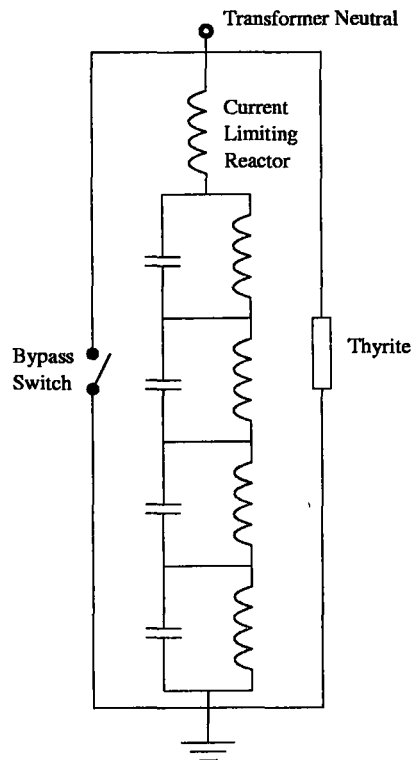
Figure 11.2: Static Blocking Filter

Static blocking filter can provide solution to both steady state and transient torque problems. Since each filter is tuned to protect an individual gen-

erating unit, the filter performance is not much affected by system changes. However, the tuning of the filter is affected by changes in the system frequency and temperature sensitivity of the filter capacitor. A disadvantage of the filters is that they take up space in the switch yard. Also there is the requirement of increased insulation level of the generator transformer.

11.2.2 Bypass Damping Filter

The bypass damping filter is connected in parallel across the series capacitor in each phase (see Fig. 11.3). The filter is useful for countering induction generator effect as it can introduce significant positive resistance in the circuit for subsynchronous oscillation frequencies up to 90% of the system frequency. However, the effectiveness of the filter reduces at the higher frequencies.
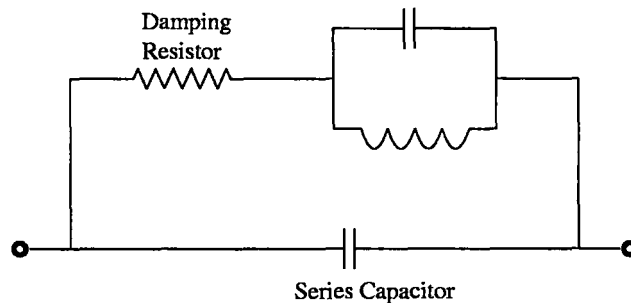
Figure 11.3: Bypass Damping Filter

The damping resistor is connected in series with a parallel combination of a reactor and capacitor which is tuned at the system frequency. Thus the filter has a very high impedance at the system frequency and the power losses in the resistor are limited (under normal conditions). The damping resistor becomes effective at subsynchronous frequencies. The damping filter can be expensive at high voltage levels but in distribution or subtransmission circuits where series capacitors are used (e.g. in resonant link fault current limiting circuits) the filter has been applied.

11.3 Damping Schemes

11.3.1 Supplementary Excitation Damping Control (SEDC)

This is an extension of the PSS concept applied for damping torsional frequency oscillations. It has been mentioned in chapter 8 that PSS used for damping low

frequency oscillations is deleterious for torsional (mode) oscillations. This arises from the fact that the net phase shift between the input speed signal and the electromagnetic torque is such that the damping torque is negative at torsional frequencies.

For damping torsional modes, it is also necessary to utilize the concept of observability. The speed signal can be measured from both ends a)from the rotating exciter and b)the front (standard) end at H.P. turbine. The mode shapes for a particular six mass rotor system are shown in Fig. 11.4. This shows the relative amplitudes of oscillation at different rotors for modes 1 to 5. The modes are numbered in ascending order as their natural frequencies. Thus, the mode 1 has the lowest natural frequency while mode 5 has the highest frequency. Typically, mode 5 is unaffected by torsional interaction.
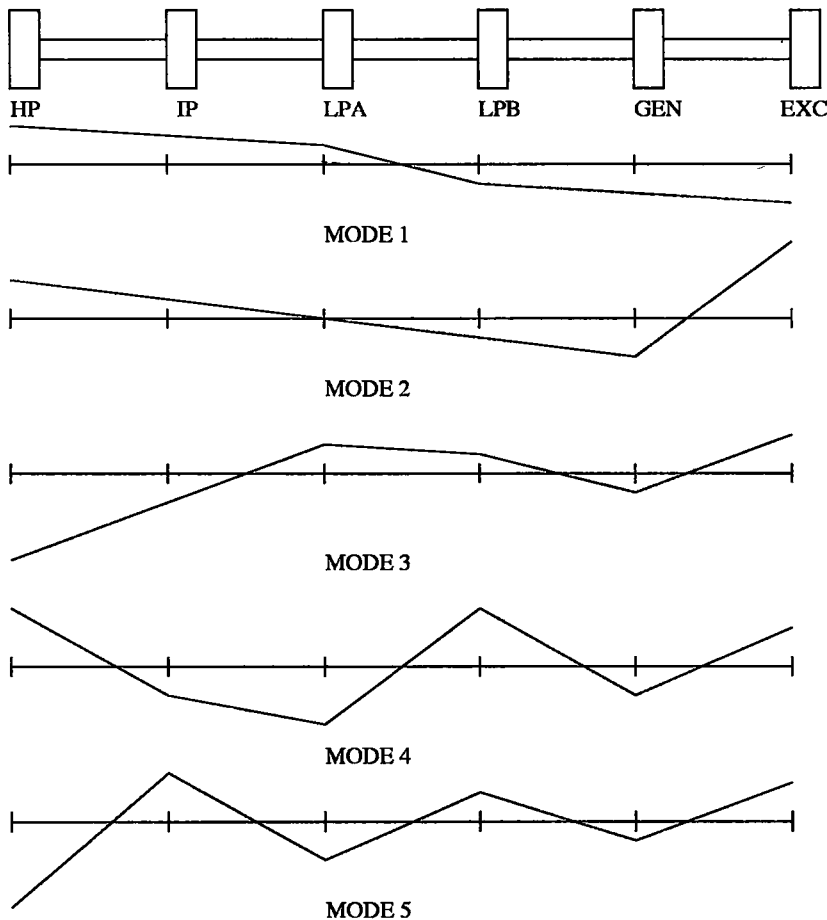
Figure 11.4: Mode shapes for a six mass system

The mode shapes also indicate the phase of the measured variable in relation to the generator speed. For example, the observed variable (at the exciter end) for mode 2 is of opposite phase compared to the generator motion. Also, it is seen from Fig. 11.4, that modes 1 and 2 are best observed from the exicter end while 3 and 4 are best observed from front standard. This will enable maximum signal to noise ratio in the control signals. Thus, although all modes are theoretically observable at each rotor location, from a practical viewpoint, it is advisable to use both control signals (from the two measurements). Also it is impractical to use a single dynamic compensator for damping all the modes.

The control objectives are met by parallel processing each mode as shown in Fig. 11.5. Each mode is isolated from the relevant speed signal measurement, by bandpass filtering at each torsional frequency. The necessary phase and gain compensation are provided individually for each component mode and the output of SEDC is obtained by summing the control signal for all the modes.
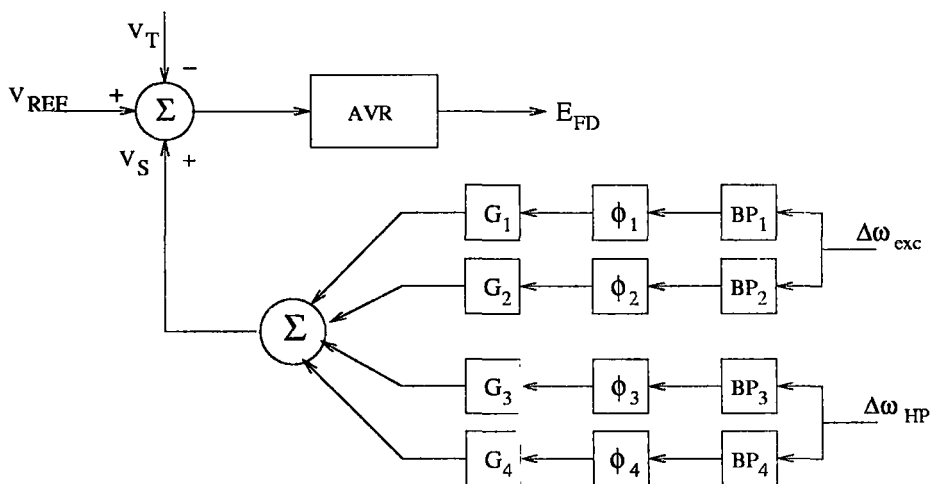
Figure 11.5: SEDC modal control structure

The phase compensation designed at Navajo generating station [7] in 1975, utilized two first order phase delay networks to allow compensation within $\pm 240^o$. Such a large variation was found necessary to account for the variability of phase produced by a bandpass filter around its centre frequency and lack of knowledge of this frequency at the time of its manufacture. The bandpass filter was designed with a sharp cutoff to eliminate interference between adjacent signal channels. A desirable feature in the design of the SEDC is its applicability to turbo-generators of different design. The SEDC tuned for different centre frequencies (of the band pass filters) are required for different generators.

The rating of SEDC required while acting alone, to overcome TI and avoid self excitation at Navojo was found to be equal to the rating of the unit. Hence, the SEDC was designed to supplement the Blocking Filters which were designed as the main countermeasure for SSR problem (both steady state and transient). The use of SEDC improves the margin of torsional stability at the extremes of operating condition.

Tests carried out at Jim Bridger generating station showed that SEDC with optimized phase settings (for resonant conditions) provide greater damping as resonance is approached. (see Fig. 11.6). This is to be compared with the case with no SEDC for radial operation. Fig. 11.6 shows the modal damping versus percentage compensation for (a) without and (b) with SEDC.
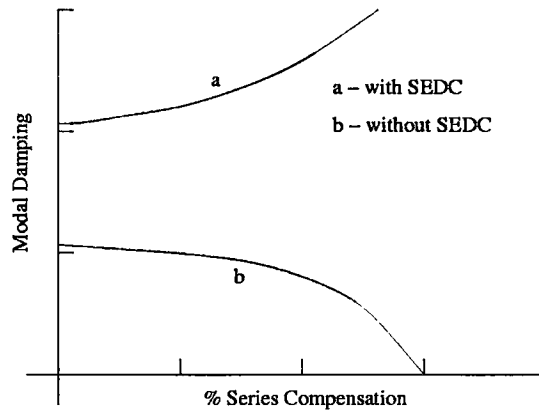
Figure 11.6: Modal damping vs series compensation

11.3.2   NGH Damping Scheme [8, 9]

This scheme was proposed by N.G. Hingorani to damp subsynchronous frequency currents in transmission lines and was first installed at Southern California Edison's Lugo substation in U.S.A. in 1984 [10, 11].

The basic concept of NGH-SSR damping scheme can be explained with reference to Fig. 11.7. If a sinusoidal voltage of frequency f_o is combined with a DC voltage, it is seen that, for the combined voltage, some half cycles are longer than the nominal half cycle period of $\frac{1}{2f_o}$. If a sinusoidal voltage of frequency $f_e < f_o$ is considered instead of the DC voltage, again it is observed that the combined voltage has some half cycles which are longer than $\frac{1}{2f_o}$. Similarly any combination of a base signal of frequency f_o with DC and subsynchronous

frequencies would result in some half cycles longer than the nominal half cycle period.
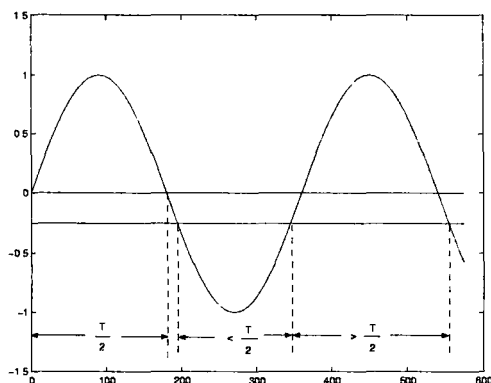
(a) Fundamental frequency combined with DC
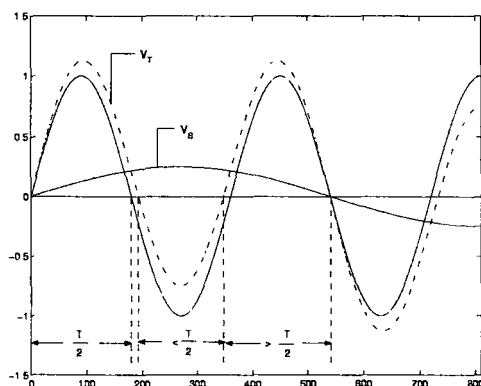
V_S = Subsynchronous, V_T = Total

(b) Fundamental frequency combined with subsynchronous frequency

Figure 11.7: Effect of presence of DC and subsynchronous frequency

The voltage across the series capacitor is a combination of fundamental frequency, DC and subsynchronous frequency components. The basic principle of NGH damping scheme is to dissipate capacitor charges whenever the measured half cycle period exceeds the nominal. This is done by inserting a resistor across the capacitor through thyristor switches (see Fig. 11.8). The thyristor stops conducting whenever the capacitor voltage (and the thyristor current) reaches

zero. Thereafter, the measurement of half cycle period restarts from a new voltage zero. No thyristor fires for half cycles which are shorter than the set period. Two thyristors are needed for the two polarities. For high voltages, the thyristor shown in Fig. 11.8 actually represents a series string of thyristors. The resistor value is not critical although lower its ohmic value, the more effective it is (except when it is too low). It is recommended that the resistor's ohmic value within 5 to 10 percent of the capacitor ohmic value will give satisfactory results.

Thyristor Control   Set Time

Resistor

Capacitor
Voltage

Series Capacitor
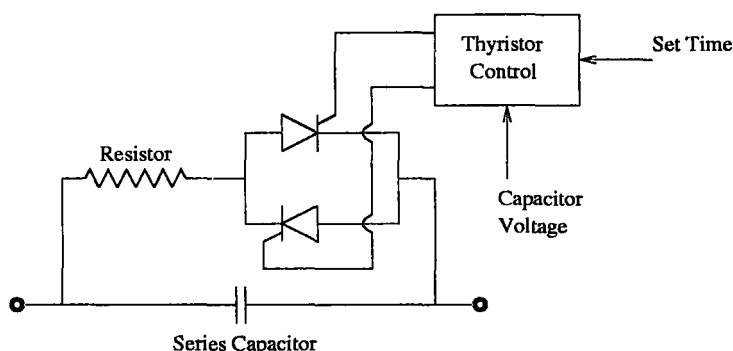
Figure 11.8: Basic NGH - SSR damping scheme

Thyristor Control

A conceptual firing control scheme for thyristors is shown in Fig. 11.9. A pulse generator continuously generates a train of pulses at a rate high enough so that pulse count can be used as a measure of the half cycle period. A signal proportional to the capacitor voltage is fed into an amplifier/clamp which produces a square wave signal between two zero crossings for one polarity of the input wave, thus representing the length of each half wave. The gate allows the pulses to go through for the duration of the half wave. The counter, which is reset by the square wave, counts the number of pulses from voltage zero so that whenever the count exceeds the set value, the counter releases the firing pulse to its thyristor string. A common pulse generator may be used for the two thyristor strings in each phase.

The operation of the controller is independent for each phase. The controller is simple and does not require detection of specific subsynchronous signals. The control signal can be obtained at the platform level. Alternately, it can be generated as the difference of two voltage signals from the measuring devices (on each side of the capacitor) of the voltage with respect to ground. In this case, the control circuitry could be located at the ground level and firing pulses transmitted through optical links.
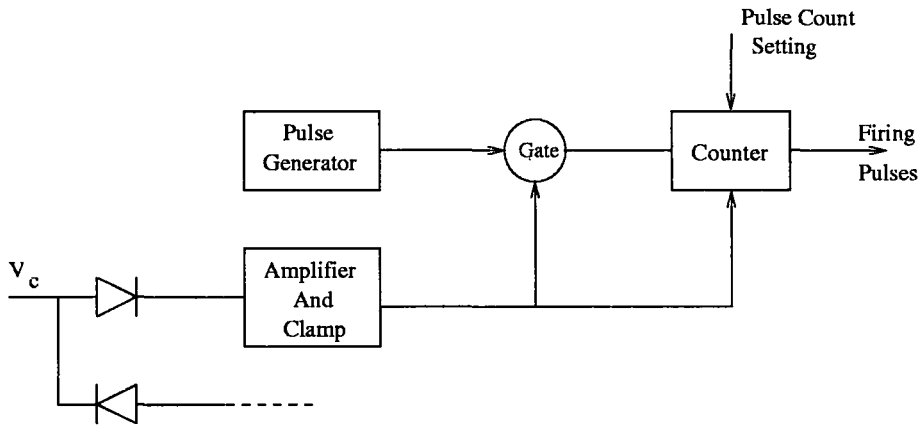
Figure 11.9: Thyristor control for NGH-SSR damping scheme

The objectives of the NGH damping scheme are

a) reduce transient torques

b) suppress steady state (self excitation) SSR problem

c) suppress offset of series capacitors

d) protect the series capacitors

    The scheme may be designed for any or all of the above purposes. If transient torque control is of major concern, the set period can be larger than the nominal half cycle period so that in steady state and with small perturbations the thyristors will not fire. The thyristors will fire only during large disturbances such as faults followed by clearing. If steady state SSR problem is of major concern, the set period can be slightly less than the nominal half period; then the thyristor will conduct during steady state at the tail end of each half cycle of the capacitor voltage; this will provide detuning effect against gradual build up of oscillations. There will be continuous power loss in this case, but is very small and of minor consequence.

    The thyristors can help to protect the capacitors (and themselves) by firing if the instantaneous forward voltage exceeds a set level. The resistor limits the discharge current from the capacitor. The capacitor and thyristor protection can also be implemented by employing nonlinear zinc oxide resistors across the thyristors (see Fig. 11.10). The protection level of the zinc oxide resistor can be selected such that it (in series with the linear resistor) provides

adequate protection for the capacitor. The bypass switch helps to relieve the thyristor/resistor when their duty exceeds safe limits. The bypass switch is also required when capacitor is to be bypassed and reinserted under normal operating conditions.
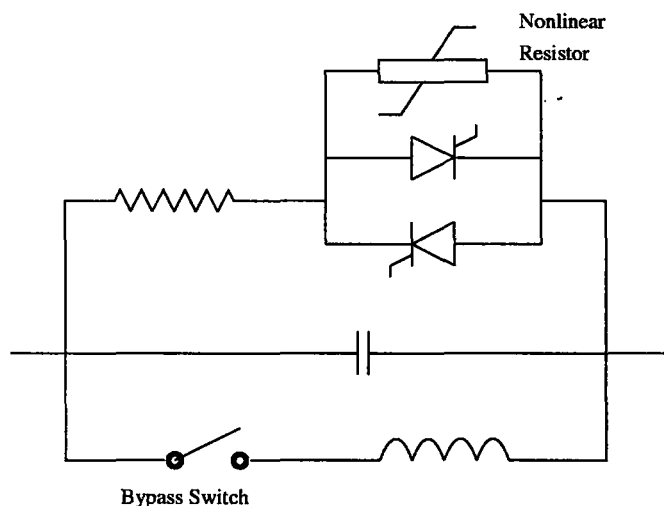

Figure 11.10: Thyristor and capacitor protection

NGH scheme is a passive scheme-it does not require feedback signals. The requirement of thyristors are well within the state of the art. For example, a 1000 A, 30 ohm capacitor may require a 80 kV thyristor string with a resistor duty of 20-50 MJ per phase.

The studies carried out on NGH scheme [9] indicate that it is an effective countermeasure for both steady state and transient SSR problems. However it was found that some undamping can result for torsional modes which are 'off tune' (not in resonance with the electrical system). It is suggested that the use of SEDC can help to overcome this problem. In summary, the studies show that NGH scheme with appropriate SEDC is beneficial in applying series compensation over a wider range (0-75%) whereas SSR problem limited the compensation level to 15%.

11.3.3   Dynamic Stabilizer [12-15]

This is a device based on the use of a modulated shunt reactance connected to the isolated phase bus of a turbine-generator unit. The modulation of the reactance is done with the help of thyristor control which acts in response to a signal based on the generator rotor velocity deviation. See Fig. 11.11.
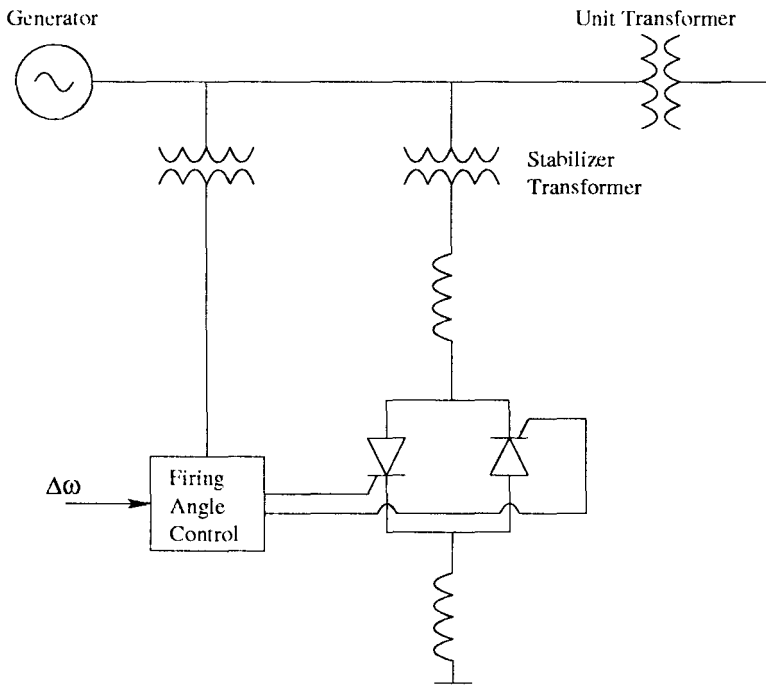
Figure 11.11: Dynamic stabilizer

The shunt susceptance of the TCR (Thyristor Controlled Reactor) is given by the relation

$$B(\sigma) = \frac{\sigma - \sin \sigma}{\pi X_L} \tag{11.1}$$

where σ is the conduction angle, X_L is the reactance (at fundamental frequency) of the shunt reactor. The conduction angle σ is related to the firing angle α by the relation

$$\sigma = 2(\pi - \alpha) \tag{11.2}$$

The firing angle α is modulated around a quiscent point in response to the oscillation of the generator rotor. In the absence of the rotor oscillations, the dynamic stabilizer appears as a continuous reactive load.

The design of the dynamic stabilizer is such that it generates sufficient current of appropriate phase to compensate for the critical subsynchronous frequency currents in the generator armature due to the network resonance. A simple explanation of the working of dynamic stabilizer based on the simplified analysis presented in chapter 10 is given below.

The α-sequence network for a single machine (connected to an infinite bus through a series compensated line) system is shown in Fig. 11.12. This is

based on the assumptions a) flux decay and damper windings are neglected b) transient saliency is neglected ($L_q = L'_d = L'$).
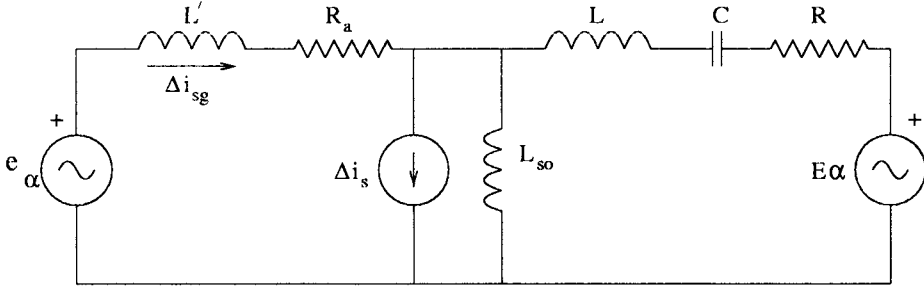

Figure 11.12: α - sequence network

The current through the dynamic stabilizer (in steady state) is given by

$$\hat{I}_s = -jB_s\hat{V}_\alpha \tag{11.3}$$

where $\hat{V}_\alpha$ is the voltage (phasor) at the generator terminals, and

$$B_s = \frac{1}{\omega L_s}$$

If B_s is modulated around a quiscent point, then

$$\Delta\hat{I}_s = -j\Delta B_s\hat{V}_\alpha \tag{11.4}$$

It was shown in chapter 10, that if

$$\bar{\omega} = 1 + A\sin\omega_m t$$

then

$$e_\alpha = E'\sin\omega_o t + e_\alpha^{sub} + e_\alpha^{sup} \tag{11.5}$$

where

$$e_\alpha^{sub} = -\frac{AE'}{2\omega_m}(\omega_o - \omega_m)\cos(\omega_o - \omega_m)t \tag{11.6}$$

and

$$e_\alpha^{sup} = \frac{AE'}{2\omega_m}(\omega_o + \omega_m)\cos(\omega_o + \omega_m)t \tag{11.7}$$

It is assumed that the generator is operating at no load, ($\delta_o = 0$) which is the worst operating condition since modal damping is minimum.

Assuming that the susceptance is modulated using a control signal derived from generator rotor velocity,

$$\Delta B_s = mA \sin \omega_m t \qquad (11.8)$$

where m is the gain to be selected.

The instantaneous current Δi_s is given by

$$\Delta i_s = \Delta B_s E' \sin(\omega_o t - \frac{\pi}{2}) = -\Delta B_s E' \cos \omega_o t \qquad (11.9)$$

In deriving the above expression, the sub and super synchronous frequency components of voltage are ignored (as they are small) and the fundamental frequency terminal voltage is assumed to be same as the fundamental frequency component of e_α (as load current is assumed to be zero).

Substituting Eq. (11.8) in (11.9) we get,

$$\Delta i_s = \Delta i_s^{sub} + \Delta i_s^{sup} \qquad (11.10)$$

where

$$\Delta i_s^{sub} = \frac{mA}{2} E' \sin(\omega_o - \omega_m)t$$

$$\Delta i_s^{sup} = -\frac{mA}{2} E' \sin(\omega_o + \omega_m)t$$

The subsynchronous frequency current Δi_s^{sub} flows through the generator armature and the network. The current Δi_{sg}^{sub} flowing through the armature is given by

$$\Delta i_{sg}^{sub} = \frac{CmAE'}{2} \sin[(\omega_o - \omega_m)t + \phi] \qquad (11.11)$$

where C and ϕ are defined by

$$C \angle \phi = \frac{Z_N^{sub}}{Z_N^{sub} + Z_g^{sub}} \qquad (11.12)$$

Z_N^{sub} is the network impedance, viewed from the generator terminals, computed at subsynchronous frequency, $(\omega_o - \omega_m)$. Similarly, Z_g^{sub} is the generator impedance at subsynchronous frequency. The operating value of the shunt reactance L_{so} can be clubbed with the network. For resonance conditions, Z_N^{sub} is capacitive and

$$Z_N^{sub} + Z_g^{sub} \simeq R \qquad (11.13)$$

(neglecting L_{so} and R_a).

Thus, C is large at resonance and $\phi \simeq -\frac{\pi}{2}$. With $\phi = -\frac{\pi}{2}$,

$$\Delta i_{sg}^{sub} = -\frac{CmAE'}{2}\cos(\omega_o - \omega_m)t$$

The component of the electromagnetic torque due to this component of current, can be shown to be given by

$$\Delta T_e = -\frac{ACm(E')^2}{2\omega_m}(\omega_o - \omega_m)\sin\omega_m t \qquad (11.14)$$

If m is negative, then the torque is entirely damping (in phase with $\Delta\omega$). This shows that the control strategy must be to reduce the shunt reactor current if the speed is increased.

The interesting thing to note about the operation of the dynamic stabilizer is that under the worst (resonant) conditions, even a small modulation in the reactor current results in large oscillating current in the generator armature due to amplification occuring at resonance. The amplification would be maximum if the stabilizer is located at a point in the system when all inductive reactance is on one side of stabilizer while all the capacitive reactance is on other side.

The advantages of dynamic stabilizer are

1. The connection as a shunt device eliminates the requirement to carry continuous generator load current (as compared to blocking filters)

2. The operation is not sensitive to variations in the system frequency or ambient temperature.

3. Maintenance requirements are expected to be minimal.

The disadvantages of dynamic stabilizer are

1. It does not provide protection against induction generator or transient torque problems. The damping is provided only when rotor oscillations are present.

2. Stabilizer introduces harmonic currents which can be minimized by (a) connecting the thyristor controlled reactors (TCR) in delta and (b) providing two secondary windings, one connected in delta and other connected in star to eliminate 5th and 7th harmonics (This arrangement is termed as 12 pulse operation of TCR).

The first dynamic stabilizer was installed at San Juan generating station. This is a 12 pulse TCR and has short time rating of about 20% of that of the generating unit.

The dynamic stabilizer is essentially similar to the Static Var Compensator (SVC). The only difference is that SVC also has fixed or thyristor switched capacitor and voltage control in addition to any auxiliary control. The damping of torsional oscillations can also be done by providing an auxiliary (supplementary) controller with appropriate design. As the SVC is normally installed at a location away from the generator, the required control signal can be synthesized from locally measured variables of line currents and voltages. The generator rotor velocity can also be sensed by computing the frequency of the (internal) generated voltage [20].

11.4   Relaying and Protection

During system operation, care has to be taken to protect the turbine-generator against failures or malfunctioning of filtering and damping devices used as countermeasures for SSR problem. There are two types of relays used to detect dangerous torsional instability conditions and subsynchronous frequency currents and activate the tripping of the generating unit. These are

A. Torsional Motion Relay

B. Armature Current SSR Relay

11.4.1   Torsional Motion Relay

This relay detects excessive mechanical stresses in the turbine-generator (T-G) shaft and operates to disconnect the machine from the transmission network. The input speed signals for the relay are derived from toothed wheels at each end of the T-G shaft. Narrow band filters tuned to the torsional (mode) frequencies are used to obtain signals that are proportional to the respective modal oscillations. From the knowledge of mode shapes and fatigue life of the shaft material, the relay can be used to compare the shaft stress with a predetermined standard. The main objective of this relay is to protect against self excitation caused by torsional interaction (TI). It is too slow to provide protection against high transient torques.

This relay has been applied at Navajo plant in U.S.A. and has protected a generating unit from growing oscillations on one occasion when SEDC malfunctioned.

11.4.2   Armature Current SSR Relay

This relay is used to detect subsynchronous oscillations in armature current and can be applied for protection of generators against both induction generator effect and torsional interaction. It is to be noted that growing armature currents also results in growing shaft torques.

A combined modulation and filtering scheme is used for the extraction of the SSO (Subsynchronous Oscillations) component from the input currents. A functional block diagram of the signal extraction is shown in Fig. 11.13. The multiplier circuits perform synchronous modulation and produce components with frequencies $(f_o - f_{er})$ and $(f_o + f_{er})$ where f_{er} is the frequency of the oscillations present in the currents. The relay is equipped with two level detectors
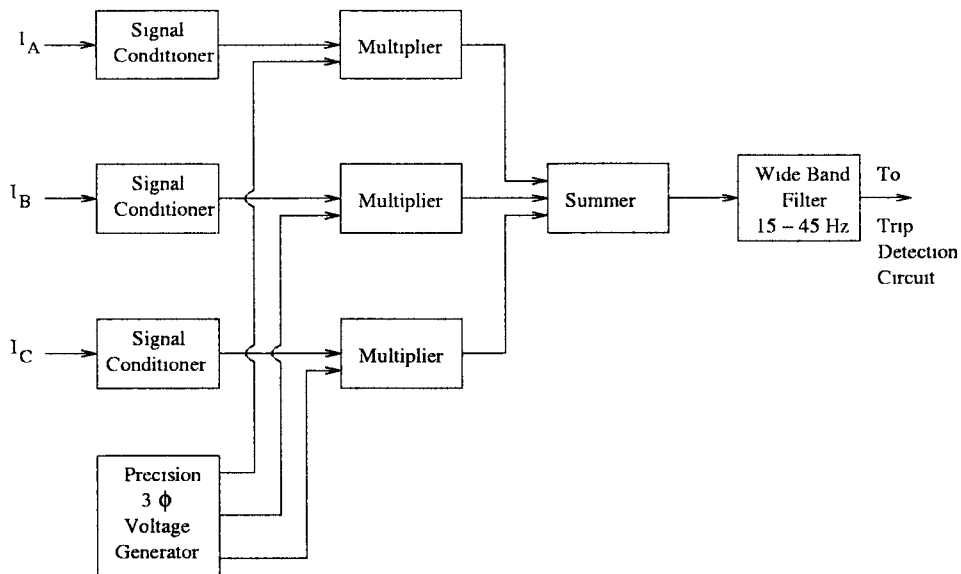
Figure 11.13: Signal extraction for SSO

and adjustable time delay. The minimum pick-up level is about 3% of the rated generator current.

Long time delays are required to avoid unnecessary trips. Thus, the relay cannot provide transient torque protection. Also, the torsional instability caused by PSS is not detected by this relay.

Improvements in the design of the SSR relay provide for selective discrimination of low amplitude sustained or growing SSO and fast response for high amplitude fault currents. For adequate protection, the low amplitude sus-

tained currents should be detected below 0.01 pu of rated armature current and response time within 75 ms for the highest amplitude fault currents (exceeding 3.0 pu).

11.4.3   Torsional Monitor

This device provides data to assess the severity of shaft torsional vibrations resulting from subsynchronous oscillations. The turbine-generator is continuously monitored by the device but no protection is provided.

The first monitor was installed at Navajo plant. The records of shaft torques are generated by the monitor following any transient electrical disturbance. Improvements in the design of monitors provide for estimation of the shaft fatigue damage in addition to the recording of torque oscillations. This helps in restoring to service of the T-G units, that have tripped off line due to SSR relay operation, faster (if the damage is marginal).

References and Bibliography

1. IEEE Committee Report, "Countermeasures to Subsynchronous Resonance problems", IEEE Trans. vol. PAS-99, No.5, 1980, pp.1810-1818

2. IEEE Committee Report, "Series capacitor controls and settings as countermeasures to subsynchronous resonance", IEEE Trans. vol. PAS-101, No.6, 1982, pp.1281-1287

3. R.G. Farmer, A.L. Schwab and Eli Katz,"Navajo project report on subsynchronous resonance analysis and solution", IEEE Trans. vol. PAS-96, No.1, 1977, pp.1226-1232

4. A.L. Courts, N.G. Hingorani and G.E. Stemler, "A new series capacitor protection scheme using nonlinear resistors", IEEE Trans. vol. PAS-97, July/Aug. 1978,pp.1042-1052

5. J.M. Undrill and F.P.Demello,"Subsynchronous oscillations, Part II:Shaft-system dynamic interactions", IEEE Trans. vol. PAS-95, July/Aug. 1976, pp.1456-1464

6. C.E.J. Bowler and D.H. Baker, "Concepts of supplementary torsional damping by excitation modulation", IEEE Publication, 'Symposium on Countermeasures for Subsynchronous Resonance' No.81 TH 0086-9-PWR, 1981

7. C.E.J. Bowler and R.A. Larsen, "Operating experience with Supplementary Excitation Damping Controls", IEEE Publication 'Symposium on

Countermeasures for Subsynchronous Resonance', No. 81 TH 0086-9-PWR,1981

8. N.G. Hingorani, "A new scheme for subsynchronous resonance damping of torsional oscillations and transient torque - Part I", IEEE Trans. vol. PAS-100, No.4, 1981, pp.1852-1855

9. R.A. Hedin, K.B. Stump and N.G. Hingorani,"A new scheme for Subsynchronous Resonance damping of torsional oscillation and transient torque - Part II", IEEE Trans. vol. PAS-100, No.4, 1981, pp.1856-1863

10. N.G. Hingorani et al, "Prototype NGH Subsynchronous Resonance damping scheme - Part I - Field installation and operating experience", IEEE Trans. vol. PWRS-2, No.4, 1987, pp.1034-1039

11. I.S. Benko, B. Bhargava and W.N. Rothenbuhler, "Prototype NGH Subsynchronous Resonance damping Scheme - Part II - Switching and short circuit tests", IEEE Trans. vol. PWRS-2, No.4, 1987, pp.1040-1049

12. T.H. Putman and D.G. Ramey,"Theory of the modulated reactance solution for subsynchronous resonance", IEEE Trans. vol. PAS-101, No.6, 1982, pp.1527-1535

13. O. Wasynczuk,"Damping Subsynchronous Resonance using reactive power control", IEEE Trans. vol. PAS-100, No.3, 1981, pp.1096-1104

14. D.G. Ramey et al, "Dynamic Stabilizer verification tests at San Juan station", IEEE Trans. vol. PAS-100, No.12, 1981, pp.5011-5019

15. A.E. Hammad and M. El Sadek, "Application of a thyristor controlled VAR compensator for damping subsynchronous oscillations in power systems", IEEE Trans. vol. PAS-103, No.1, 1984, pp.198-212

16. O. Wasynczuk,"Damping Subsynchronous Resonance using energy storage", IEEE Trans. vol. PAS-101, No.4, 1982, pp.905-914

17. C.Chen, O. Wasynczuk and N.A. Anwah, "Stabilizing Subsynchronous Resonance using transmission current feedback", IEEE Trans. vol. PWRS-1, No.4, 1986, pp. 34-41

18. Abdel-Aty Edris, "Series compensation schemes reducing the potential of Subsynchronous Resonance", IEEE Trans. on Power Systems, vol. 5, No.1, 1990, pp. 219-226.

19. L.N. Hannett and F.P.DeMello,"Mechanical countermeasures to subsynchronous torsional instability", IEEE Trans. on Power Systems, vol.5, No.4, '990, pp.1146-1150

20. K.R. Padiyar and R.K. Varma, "Static VAR systems auxiliary controllers for damping torsional oscillations", Int. J. Elec. Power and Energy Systems, vol.12, No.4, 1990, pp.271-286

Chapter 12

Simulation for Transient Stability Evaluation

Transient stability of a system refers to the stability (generators remaining in synchronism) when subjected to large disturbances such as faults and switching of lines. Hence, linearized analysis is not applicable and the nonlinear equations of the system have to be solved in stability evaluation. As analytical solutions do not exist even for a simple system, it has been the practice to numerically solve the system equations. In the early days, AC network analyzer was used in conjunction with step by step method of solving swing equations. With the advent of digital computers, several production grade computer programs have been developed which can handle not only large power systems (with hundreds of generators) but also consider detailed generator controller and load models. In addition, models of protection system (relaying) are also incorporated into them such that the present day programs can be termed as simulation programs rather than transient stability programs. In other words, checking transient stability is only one of the many objectives of running a simulation program which can give lot more information such as predict the dynamic performance of the system involving low frequency transients (typically less than 5 Hz).

There are three modes of simulation depending on the varying details of component models. These are

1. Short term simulation (< 10 sec)
2. Mid term simulation (up to 5 minutes)
3. Long term simulation (20 minutes or longer)

Short term simulation has to consider rapidly changing electrical variables (including swinging among generators) while in long term simulation, the slow oscillations in frequency and power (after the fast electrical transients such as inter machine oscillations have decayed) are of importance.

The short term simulation program is usually referred to as transient stability program. The boiler and load frequency controller models are neglected in short term simulation.

In this chapter, techniques for short term simulation are discussed with the objective of evaluating transient stability. While simulation of single machine system has been covered in chapter 6, this chapter considers the simulation of multi-machine systems.

12.1 Mathematical Formulation

The system equations are differential algebraic as the generator stator and network transients are neglected and described by algebraic equations. The generator and controller equations are nonlinear dynamic equations given by

$$\dot{x} = f(x, y) \tag{12.1}$$

where y consists of generator terminal voltages (expressed in rectangular or polar coordinates). It is assumed that the generator voltages are sinusoidal and represented as slowly varying phasors which are determined from network (including stator) algebraic equations given by

$$0 = g(x, y, p) \tag{12.2}$$

where p is a set of parameters (such as load powers). It is to be noted that there are as many equations as the number of unknowns y. Thus Eq. (12.2) refers to power balance in the network and y is the vector of bus voltages (including generator terminal buses). Also, as the network changes due to switching or fault, Eq. (12.2) also changes in structure.

There are two major issues concerning the solution of DAE (Differential Algebraic Equations) of type (12.1) and (12.2) namely

a) Existence of a solution of the algebraic equations (12.2)

b) Methods of solution

It is usually assumed that the solution of differential equation (12.1), given y, exists. It is also assumed that the initial conditions, x_o and y_o (from the operating point) are known at time $t = t_o$. y_o may be determined from power flow analysis (steady state solution) and x_o computed from the knowledge of y_o and power outputs of generators.

If it is assumed that the solution of the algebraic equation (12.2) exists, and y can be solved in terms of x as

$$y = h(x, p) \tag{12.3}$$

The substitution of Eq. (12.3) in (12.1) results in a vector differential equation

$$\dot{x} = f(x, h(x, p)) = F(x, p) \tag{12.4}$$

The solution of Eq. (12.4) by numerical methods is relatively straightforward. Unfortunately, when g is nonlinear, an exact solution of y is not feasible and the reduction to Eq. (12.4) is not practical.

It must be noted that multiplicity of solutions of Eq. (12.2) is not a major problem as the required solution is determined from considerations of continuity. For example, if y_o is the solution at $t = t_o$, the solution at $t = t_o + h$, must be close to y_o as $h \to 0$. The lack of existence of a solution creates problem as the simulation comes to a halt. In such cases, it is fruitful to note that the algebraic equations for the network are actually obtained as approximations to the network models with fast (parasitic) dynamics given by

$$\epsilon \dot{y} = g(x, y, p) \tag{12.5}$$

where ϵ is small and approximated to zero. However, the computer programs available do not provide any special procedures when lack of solution is encountered. Incidentally, the lack of convergence in solving nonlinear equations, using an iterative method does not necessarily indicate lack of solution. Some methods overcome the problem of failure of network solution either by modifying load models or adopting a non-iterative approach for network solution. This will be discussed later.

12.2 Solution Methods

The requirements in the solution method of DAE can be stated as follows [1].

1. Sufficient accuracy for engineering purposes : Typically errors of several percent are tolerable in transient stability studies.

2. Reliability : the numerical methods used should be free from instability and convergence problems. As stated earlier, numerical breakdown results in failure of simulation.

3. Economy of computer storage

4. Flexibility : in terms of modelling details, incorporation of new models, simulation of new components etc.

5. Ease of maintenance : The program should be easy to maintain and update. This feature is related to flexibility given above.

The total computing time depends on the calculations required at each step and step size(s) used. In general, smaller steps are required for better accuracy and improved reliability.

The solution approach to DAE (12.1) and (12.2) can be classified as

A. Partitioned (Alternating)

B. Simultaneous (Combined)

12.2.1   Partitioned Solution of DAE

This is a traditional approach used in most of the available simulation programs. The differential equations (12.1) are solved separately for x by numerical integration and the algebraic equations (12.2) are solved separately for y. These solutions are alternated with each other in some manner. In solving for x, the knowledge of y is required which may be only approximately available. Similarly, in solving for y, x may not be known accurately. This can lead to interface errors, the elimination of which would require iteration of the process of solution at each step. This is not to be confused with iterative solution of either differential or algebraic equations independently. There is strong motivation to reduce the computations at each step and hence the sarface errors are not completely eliminated.

a) Explicit

b) Implicit

A brief discussion of the integration methods is given next.

12.2.2 Numerical Integration of Differential Equations

Consider a continuous time system of equations

$$\dot{x} = f(x, t) \tag{12.6}$$

(Note: If y in (12.1) is expressed as a function of time t then it can be · expressed in the above form).

The solution of the above equation can be expressed as

$$x(t) = \phi_t(x_o, t_o) \tag{12.7}$$

where x_o is the initial value of x at time $t = t_o$.

The integration algorithms generate a sequence of points $x_o, x_1, x_2.....$ at time $t_o, t_1, t_2........$ with approximation

$$x_k \approx \phi_{t_k}(x_o, t_o) \tag{12.8}$$

It is usually assumed that the points are uniformly spaced with size $h > 0$, that is

$$t_k = t_o + hk \quad \text{for} \quad k = 0, 1, 2, ... \tag{12.9}$$

An integration algorithm generates x_{k+1} given x_k at $t = t_k$. The different algorithms vary depending on how $f(x, t)$ is approximated in the interval (t_k, t_{k+1}). The simplest method (Euler) is based on the approximation that f is a constant. This can be done in two ways. In the Forward Euler method, f is approximated as constant evaluated at time t_k. Thus x_{k+1} can be calculated from

$$x_{k+1} = x_k + hf(x_k, t_k) \tag{12.10}$$

In Backward Euler method, f is evaluated at $t = t_{k+1}$. Thus x_{k+1} is given by

$$x_{k+1} = x_k + hf(x_{k+1}, t_{k+1}) \tag{12.11}$$

Forward Euler method belongs to the class of **explicit methods** where x_{k+1} is obtained by explicit calculations and no solution of equations is involved. Backward Euler method belongs to the class of **implicit methods** where solution of equations is required to compute x_{k+1}.

Implicit methods are numerically stable, that is, the propagation of error in the process of integration does not cause the solution to blow up. For explicit methods, numerical stability is guaranteed only if step size h is chosen sufficiently small.

The problems of numerical instability can be illustrated if a system of linear equations

$$\dot{x} = [A]x, \quad x(t_o) = x_o \tag{12.12}$$

is considered.

By applying Forward Euler method, x_{k+1} can be expressed as

$$x_{k+1} = [I + Ah]x_k = [F]x_k \tag{12.13}$$

For numerical stability, the eigenvalues ($\lambda_j, \quad j = 1, 2, ...n$) of the matrix $[F]$ must satisfy

$$\mid \lambda_j \mid < 1 \tag{12.14}$$

Using Backward Euler method, x_{k+1} can be expressed as

$$x_{k+1} = [I - Ah]^{-1}x_k = [H]x_k \qquad (12.15)$$

The eigenvalues of $[H]$ should also lie in a unit circle in the complex plane for stability.

If $[A]$ is a diagonal matrix with elements a_j (j=1,2,......n) which could be complex, the condition (12.14) can be expressed as

$$\mid 1 + ha_j \mid < 1, \quad j = 1, 2, ...n \qquad (12.16)$$

For Backward Euler method, the condition for numerical stability (with $[A]$ diagonal matrix) can be expressed as

$$\mid 1 - a_j h \mid > 1, \quad j = 1, 2, 3, ...n \qquad (12.17)$$

The stability regions for Forward and Backward Euler methods in $a_j h$ plane are shown in Figs. 12.1 and 12.2 respectively. From Fig. 12.2 it is obvious that if a_j (the eigenvalues of $[A]$) lie in left half plane, Backward Euler method is numerically stable for all values of the step size h. On the other hand, the step size for Forward Euler method will be determined by the eigenvalues of the matrix $[A]$ having the largest magnitude. (Note that, for real eigenvalues, the time constant corresponds to the reciproc.d of the eigenvalue. Hence the step size is determined from the smallest time constant of the system). This can be problematic in systems (termed as stiff systems) which have a wide range of eigenvalues. In such systems, the fast dynamics disappear much before steady state is reached (as the settling time is determined from large time constants).

Although implicit methods require more computations per step (due to the requirement of solution of algebraic equation at each step), the step size in stiff systems can be selected on the basis of accuracy only and not determined by considerations of numerical stability. This means that overall computations can be reduced using implicit integration methods.

In power systems, the presence of excitation systems with small time constants can require small time step sizes if explicit methods are used. Hence in the recent times, implicit methods such as trapezoidal rule have become popular and widely used. Using trapezoidal rule of integration, x_{k+1} can be expressed as

$$x_{k+1} = x_k + \frac{h}{2}[f(x_k, t_k) + f(x_{k+1}, t_{k+1})] \qquad (12.18)$$

Another classification of integration methods is based on whether previous values of x are required in integrating over step k. Hence integration methods are
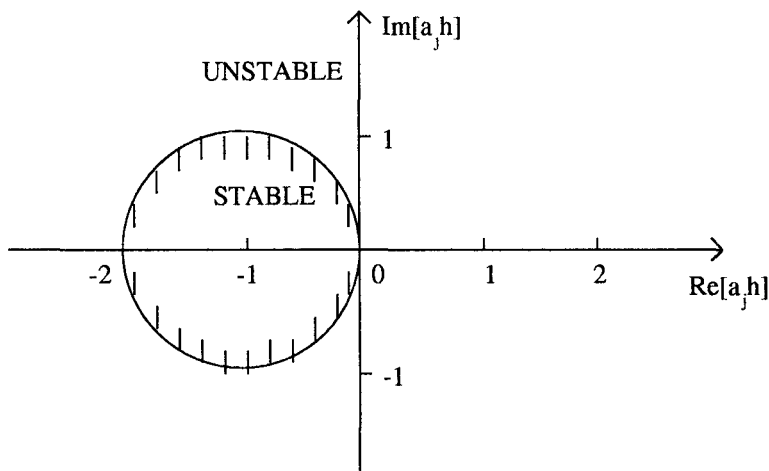
Figure 12.1: Region of Stability - Forward Euler method

termed as (a) single step if only x_k is required in computing x_{k+1} or (b) multi-step if values of x earlier than instant t_k are required in computing x_{k+1}. The advantages of multi-step methods over single step methods are that for a given accuracy, less computations per step are required. However, they are not self starting and the first few values have to be calculated using a single step method. Whenever there is a discontinuity (arising from network switching) the previous values cannot be used and new starting values are to be computed.

12.2.3 Simultaneous Solution of DAE

In this approach, implicit integration is used to convert Eq. (12.1) to an algebraic equation involving variables x_{k+1} and y_{k+1}, the values at the end of the kth interval. These algebraic equations are lumped together with the set (12.2) and solved simultaneously. As Eqs. (12.1) and (12.2) are solved simultaneously, there is no interface error.

12.3 Formulation of System Equations

The major component of system dynamics is contributed by the generator and the associated controllers. The other components described by dynamical equations include induction motor loads, HVDC links and SVC controllers. In what follows, only generator dynamics are considered for simplicity.
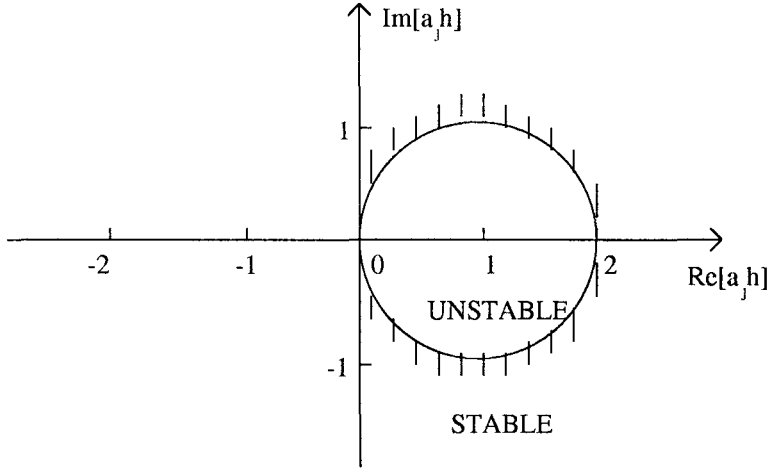
Figure 12.2: Region of Stability - Backward Euler method

12.3.1 Generator Representation

It will be assumed that synchronous machine is represented by model 1.1 (that is considering a field coil on the d-axis and a damper coil on the q-axis). The machine differential equations are (see chapter 6)

$$\frac{dE'_q}{dt} = \frac{1}{T'_{do}}[-E'_q + (x_d - x'_d)i_d + E_{fd}] \tag{12.19}$$

$$\frac{dE'_d}{dt} = \frac{1}{T'_{qo}}[-E'_d - (x_q - x'_q)i_q] \tag{12.20}$$

$$\frac{d\delta}{dt} = \omega_B(S_m - S_{mo}) \tag{12.21}$$

$$\frac{dS_m}{dt} = \frac{1}{2H}[T_m - DS_m - T_e] \tag{12.22}$$

$$T_e = E'_q i_q + E'_d i_d + (x'_d - x'_q)i_d i_q \tag{12.23}$$

Neglecting stator transients, the stator equations are

$$E'_q + x'_d i_d - R_a i_q = v_q \tag{12.24}$$

$$E'_d - x'_q i_q - R_a i_d = v_d \tag{12.25}$$

From the above equations, i_d and i_q are solved as

$$\begin{bmatrix} i_q \\ i_d \end{bmatrix} = \frac{1}{R_a^2 + x'_d x'_q} \begin{bmatrix} R_a & x'_d \\ -x'_q & R_a \end{bmatrix} \begin{bmatrix} E'_q - v_q \\ E'_d - v_d \end{bmatrix} \tag{12.26}$$

These can be substituted in Eqs. (12.19) to (12.20) and the machine rotor electrical equations can be expressed as

$$\dot{x}_R = [A_R]x_R + [B_{R1}]E_{fd} + [B_{R2}]\begin{bmatrix} v_q \\ v_d \end{bmatrix} \qquad (12.27)$$

$$x_R^t = [E_q' \quad E_d']$$

The mechanical equations (12.21) to (12.23) can be expressed as

$$\dot{x}_M = [A_M]x_M + [B_M]T_m - [B_M]T_e \qquad (12.28)$$

$$x_M^t = [\delta \quad S_m]$$

$$T_e = T_e(x_R, v_q, v_d) \qquad (12.29)$$

When Eq. (12.26) is substituted in Eq. (12.23) T_e becomes a nonlinear function of E_q', E_d' and v_d, v_q.

The excitation system including PSS can be represented by the equations

$$\dot{x}_E = [A_E]x_E + [B_{E1}]u_{PSS} + [B_{E2}]V_t \qquad (12.30)$$

$$E_{fd} = E_{fd}(x_E) \qquad (12.31)$$

where u_{PSS} is the input signal to the PSS. If it is derived from rotor velocity then $u_{PSS} = S_m$. V_t is the terminal voltage magnitude. The nonlinearity introduced by non-windup limiters is considered by modifying the coefficient matrices in (12.30). In general E_{fd} is a linear function of x_E except when windup limits on E_{fd} are to be considered.

The turbine-governor system can be represented by the equations

$$\dot{x}_T = [A_T]x_T + [B_{T1}]S_m + [B_{T2}]P_m^{ref} \qquad (12.32)$$

$$T_m = T_m(x_T) \qquad (12.33)$$

where P_m^{ref} is the reference power set by Load Frequency Control (LFC) or Automatic Generation Control (AGC).

The generator equations comprise a) Rotor electrical b) Mechanical c) Excitation system and d) Turbine-governor equations described above. The interconnections among the various subsystems of the generator are shown in Fig. 12.3. It is to be noted that v_q and v_d are derived from the knowledge of the phasor $\hat{I}_a$ (expressed with reference to a common reference frame) and the machine rotor angle δ, as given below

$$(v_q + jv_d) = \hat{V}_t e^{-j\delta} = V_t e^{j(\theta-\delta)} \qquad (12.34)$$

From this we get

$$\left.\begin{array}{l} v_q = V_t \cos(\theta - \delta) \\ v_d = V_t \sin(\theta - \delta) \end{array}\right\} \tag{12.35}$$

and V_t can be expressed as

$$V_t = \sqrt{v_d^2 + v_q^2} \tag{12.36}$$

where θ is the bus angle at the generator terminals (obtained from network solution).

In Fig. 12.3, f_1, f_2 and f_3 are nonlinear functions of the input variables. These can be obtained from equations given earlier.
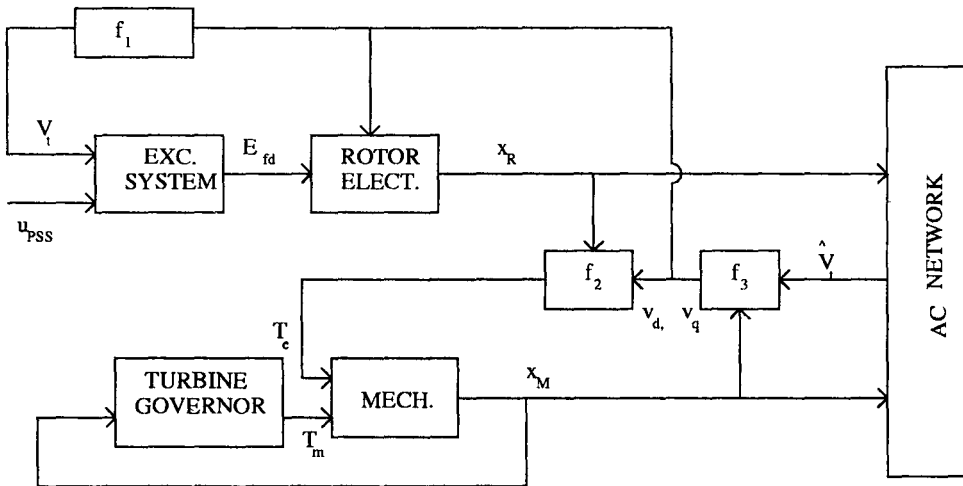
Figure 12.3: Interconnections among subsystems

12.3.2   Inclusion of Generator Stator in the Network

A major assumption in the modelling of AC network is that it is symmetric. Hence for steady state analysis, the network can be represented on a single phase basis using phasor quantities (for slowly varying sinusoidal voltages and currents in the network). Thus the generator stator can also be represented on a single phase basis.

Eq. (12.26) can be expressed as a single equation in phasor quantities if transient saliency is neglected, that is, $x_d' = x_q'$. In this case (see also chapter 6),

$$i_q + ji_d = \frac{1}{R_a + jx'}[(E_q' + jE_d') - (v_q + jv_d)] \tag{12.37}$$
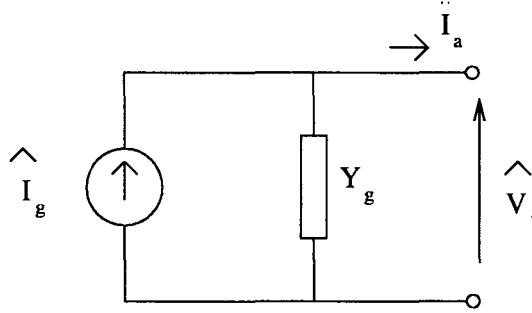
Figure 12.4: Generator equivalent circuit

$$x' = x'_d = x'_q$$

The armature current phasor $\hat{I}_a$ can also be represented on a synchronously rotating reference frame as

$$\hat{I}_a = i_Q + ji_D = (i_q + ji_d)e^{j\delta} = \frac{1}{R_a + jx'}[\hat{E}' - \hat{V}_t] \qquad (12.38)$$

where

$$\begin{aligned}
\hat{E}' &= E'_Q + jE'_D = (E'_q + jE'_d)e^{j\delta} \\
\hat{V}_t &= v_Q + jv_D = (v_q + jv_d)e^{j\delta} = V_t e^{j\theta}
\end{aligned}$$

Eq. (12.38) represents an equivalent circuit shown in Fig. 12.4 where

$$Y_g = \frac{1}{R_a + jx'} \qquad (12.39)$$

$$\hat{I}_g = \hat{E}' Y_g = \frac{(E'_q + jE'_d)e^{j\delta}}{R_a + jx'} \qquad (12.40)$$

It is to be noted that $\hat{I}_g$ is a function of state variables $(E'_q, E'_d$ and $\delta)$ only. Hence it does not change suddenly whenever there is a network switching. The equivalent circuit shown in Fig. 12.4 can be readily merged with the AC network (external to the generator).

12.3.3   Treatment of Transient Saliency

If transient saliency is to be considered, the stator cannot be represented by a single phase equivalent circuit shown in Fig. 12.4. This is because, in general, Eq. (12.26) when transformed to a synchronously rotating reference frame results in

$$\begin{bmatrix} i_Q \\ i_D \end{bmatrix} = [Y_g^{DQ}(t)] \begin{bmatrix} E'_Q - v_Q \\ E'_D - v_D \end{bmatrix} \qquad (12.41)$$

where

$$[Y_g^{DQ}(t)] = \frac{1}{R_a^2 + x_d' x_q'} \begin{bmatrix} \cos\delta & -\sin\delta \\ \sin\delta & \cos\delta \end{bmatrix} \begin{bmatrix} R_a & x_d' \\ -x_q' & R_a \end{bmatrix} \times$$

$$\begin{bmatrix} \cos\delta & \sin\delta \\ -\sin\delta & \cos\delta \end{bmatrix} \qquad (12.42)$$

$[Y_g^{DQ}]$ is a function of δ, and as δ varies with time, is a time varying matrix. This poses problems as the overall network matrix including $[Y_g^{DQ}]$ in real quantities (twice the size of the matrix in complex quatities) is not constant but time varying. This implies the network matrix has to be factored at every step which increases computational complexity.

Hence, there is need for special techniques to handle transient saliency. There are two ways of doing this, namely

(i) Using a dependent source (application of compensation theorem)

(ii) Using a dummy rotor coil

(i) **Use of a dependent source**
The stator equations can be rewritten as

$$\left. \begin{array}{rcl} E_q' + x_d' i_d - R_a i_q & = & v_q \\ E_d' + E_{dc}' - x_d' i_q - R_a i_d & = & v_d \end{array} \right\} \qquad (12.43)$$

where

$$E_{dc}' = -(x_q' - x_d') i_q \qquad (12.44)$$

The above equations can be expressed as a single equation in phasor quantities.

$$E_q' + j(E_d' + E_{dc}') - (R_a + jx_d')(i_q + ji_d) = v_q + jv_d \qquad (12.45)$$

The equivalent circuit of Fig. 12.4 applies if

$$\hat{I}_g = \frac{[E_q' + j(E_d' + E_{dc}')]}{R_a + jx_d'} e^{j\delta} = Y_g \hat{E}' + \hat{I}_{sal} \qquad (12.46)$$

where

$$\hat{I}_{sal} = \frac{jE_{dc}' e^{j\delta}}{R_a + jx_d'}, \quad Y_g = \frac{1}{(R_a + jx_d')}$$

It is to be noted that the transient saliency is replaced by introducing a dependent current source $\hat{I}_{sal}$ which is a function of the terminal voltge $\hat{V}_t$ and δ. It is not difficult to see that, in this approach, the choice of Y_g and correspondingly I_{sal} is not unique. Dommel and Sato [2] choose Y_g as

$$Y_g = \frac{R_a - j\frac{1}{2}(x'_d + x'_q)}{R_a^2 + x'_d x'_q} \qquad (12.47)$$

$\hat{I}_{sal}$ can be derived as

$$\hat{I}_{sal} = -j\frac{1}{2}\frac{(x'_q - x'_d)}{(R_a^2 + x'_q x'_d)}(\hat{E}^* - \hat{V}^*)e^{j2\delta} \qquad (12.48)$$

where '*' denotes complex conjugate.

In reference [2], the saliency is handled by iterative solution (improving on $\hat{I}_{sal}$ until convergence is obtained). It is claimed that the choice of Y_g given in (12.47) speeds up convergence and two or three iterations are normally sufficient. As initial guess for the terminal voltage, the value at the previous instant (say t_k) is used, except that the angle is changed by the same amount by which δ has changed from t_k to t_{k+1}.

(ii) Use of a dummy rotor coil

The motivation for this approach is that if E'_{dc} is a state variable, (proportional to flux linkage of a dummy coil in the q-axis) then the problem of iterative solution for transient saliency is eliminated. In other words, the dependent source $\hat{I}_{sal}$ can be eliminated. This is an approximate treatment of transient saliency, but the degree of approximation can be directly controlled to get acceptable accuracy.

Consider a rotor dummy coil in the q-axis which is linked only with the q-axis coil in the armature, but has no coupling with other coils. Just as E'_d is a fictitious voltage source proportional to $-\psi_q$, E'_{dc} can be considered as another voltage source proportional to the flux linkage $-\psi_c$ of the dummy coil. The differential equation for E'_{dc} can be expressed as

$$\frac{dE'_{dc}}{dt} = \frac{1}{T_c}[-E'_{dc} - (x'_q - x'_d)i_q] \qquad (12.49)$$

where T_c is the open circuit time constant of the dummy coil, which can be arbitrarily selected. In comparing Eq. (12.49) with Eq. (12.44) it is readily seen that the latter is a steady state solution of the former. As T_c tends to zero the solution of (12.49) is given by (12.44). From numerical experiments, it is observed that, T_c need not be smaller than 0.01 sec for acceptable accuracy [10]. This is of similar order as the time constant of a high resistance damper winding. Using implicit integration methods, the step size chosen need not be constrained by the value of T_c chosen.

12.3.4 Load Representation

Loads are represented as static voltage dependent models given by

$$P_L = f_P(V_L) \tag{12.50}$$

$$Q_L = f_Q(V_L) \tag{12.51}$$

where f_P and f_Q are any general nonlinear functions. In many stability pro-
grams, f_P and f_Q are represented as

$$P_L = f_P(V_L) = a_0 + a_1 V_L + a_2 V_L^2 \tag{12.52}$$

$$Q_L = f_Q(V_L) = b_0 + b_1 V_L + b_2 V_L^2 \tag{12.53}$$

If $a_0 = a_1 = b_0 = b_1 = 0$, then we say that loads can be represented by constant
impedances. The load at a bus can be represented by the equivalent circuit
shown in Fig. 12.5 where Y_l is given by

$$Y_l = \frac{P_{Lo} - jQ_{Lo}}{V_{Lo}^2} \tag{12.54}$$

where subscript 'o' indicates operating values, Y_l is chosen such that $\hat{I}_l$ is zero
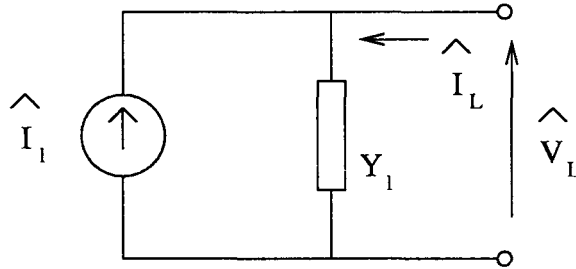
Figure 12.5: Load equivalent circuit

at the operating point. During a transient, $\hat{I}_L$ is calculated from

$$-\hat{I}_L = \frac{f_P(V_L) - jf_Q(V_L)}{V_L^*} - Y_l V_L = \hat{I}_l - Y_l \hat{V}_L \tag{12.55}$$

In general, this is a nonlinear function of V_L and results in the overall network
equations being nonlinear. For constant impedance load models, I_l is identically
equal to zero.

12.3.5   AC Network Equations

The AC network consists of transmission lines, transformers, shunt reactors, capacitors and series capacitors. Only quasi-steady state response of the AC network is considered for stability evaluation, neglecting transients. Also, it is assumed that the network is symmetric. Hence a single phase representation (positive sequence network) is adequate. The network equations can be expressed using bus admittance matrix Y_N as

$$[Y_N]\hat{V} = \hat{I}_N \tag{12.56}$$

where $\hat{V}$ is a vector of complex bus voltages and $\hat{I}_N$ is a vector of current injections. At a bus j, the component of I_N is given by

$$\hat{I}_{Nj} = \hat{I}_{aj} - \hat{I}_{Lj} \tag{12.57}$$

12.3.6   System Algebraic Equations

The generator and load equivalent circuits at all the buses can be integrated into the AC network and the overall system algebraic equations can be obtained as follows

$$[Y]\hat{V} = \hat{I} \tag{12.58}$$

where $[Y]$ is the complex admittance matrix which is obtained from augmenting $[Y_N]$ by inclusion of the shunt admittance Y_g and Y_l at the generator and load buses. $\hat{I}$ is the vector of complex current sources the jth element of which can be expressed as

$$\hat{I}_j = \hat{I}_{gj} + \hat{I}_{lj} \tag{12.59}$$

It is to be noted that in general, $\hat{I}_j$ is a function of bus voltage $\hat{V}_j$. Hence the solution of Eq. (12.58) has to be obtained by an iterative process. The initial estimate for $\hat{V}_k$ can be assumed as $\hat{V}_{k-1}$ (the previous instant). Also if transient saliency is neglected or represented by using a dummy coil, $\hat{I}_{gj}$ is only a function of the state variables E'_{qj}, E'_{dj} and δ_j. In this case, the iterative solution of Eq. (12.58) is required only if loads are nonlinear (not represented by constant impedances).

It must be noted that transient saliency does not introduce nonlinearity. It only results in time varying generator impedance. Nonlinearity of Eq. (12.58) is mainly due to nonlinear voltage dependent loads which are modelled as constant admittances in parallel with nonlinear current sources.

Eq. (12.58) can also be expressed in real variables as

$$[Y^{DQ}]V^{DQ} = I^{DQ} \tag{12.60}$$

where the elements of Y_{ij}^{DQ}, V_j^{DQ} and I_i^{DQ} can be expressed as

$$\left[\ Y_{ij}^{DQ}\ \right] = \left[\begin{array}{cc} B_{ij} & G_{ij} \\ G_{ij} & -B_{ij} \end{array}\right], \quad V_j^{DQ} = \left[\begin{array}{c} V_{Qj} \\ V_{Dj} \end{array}\right], \quad I_i^{DQ} = \left[\begin{array}{c} I_{Di} \\ I_{Qi} \end{array}\right]$$

The arrangement of the variables in Eq. (12.60) is deliberate such that $[Y^{DQ}]$ is a symmetric matrix if $[Y]$ is symmetric (Note $[Y]$ is symmetric if no phase shifting transformers are considered).

12.3.7 System Differential Equations

The differential equations for a generator are expressed as

$$\dot{x}_{gi} = f(x_{gi}, V_{gi}^{DQ}) \tag{12.61}$$

where x_{gi} is a vector of state variables for generator 'i' including machine variables E'_{qi}, E'_{di}, δ_i and other variables corresponding to excitation system and turbine-governor. V_{gi}^{DQ} are the D and Q-axes components of the generator terminal voltage $\hat{V}_{gi}$. It is interesting to note that the generator equations are decoupled and the interconnection is provided through AC network variables.

The equations corresponding to all the generators in the system can be combined and solved either simultaneously (with multiple processors) or sequentially (using a single processor).

If a HVDC link or SVC or any controllable device is considered, the differential equations for these devices can also be expressed in the general form

$$\dot{x}_{cj} = f(x_{cj}, V_{cj}^{DQ}) \quad j = 1, 2 ...... n_c \tag{12.62}$$

where n_c is the number of such devices in the system. The equations for dynamic loads can also be expressed in the above form.

12.4 Solution of System Equations

The algorithm for numerical solution of the system equations has to tackle the problem of computing x_k and V_k at the end of step 'k' given the initial conditions x_{k-1} and V_{k-1}.

12.4.1 Partitioned solution

Explicit or implicit methods are used to numerically integrate the differential equations of the type given in Eqs. (12.61) and (12.62). In doing this values of

V_g and V_c are required in the time interval (t_{k-1}, t_k). In general, the bus voltage vector V is required. One approach is to predict the values of V by extrapolation. One extrapolation formula [1] for V_k, based on two previous values, is

$$V_k = \frac{V_{k-1}^2}{V_{k-2}} \tag{12.63}$$

Extrapolation is necessary to avoid the solution of the algebraic equations more than once in a step. This reduces the computations per step considerably as network solution is a major component in the computational procedure. However the interface error is not eliminated.

The solution of differential equations can be partitioned into subsets corresponding to the subsystems as shown in Fig. 12.3. This procedure not only helps in attaining a flexible program structure, but can also improve the numerical performance particularly when implicit integration method (such as trapezoidal) is used. There can be an optimal sequencing in the integration of the equations which reduces error. For example, solving excitation system first results in the computation of E_{fd} which can be used subsequently in the solution of rotor electrical equations. The solution for E_d' and E_q' can be used to compute electrical torque which is the input to the mechanical system including turbine-governor.

After the solution of x_k, the network equations can be solved from

$$[Y]V_k = I(E_k, V_k) \tag{12.64}$$

Note that the current source vector I is a function of E_k (obtained from a subset of state variables x_k) and V_k. It is convenient to solve (12.64) by factorizing $[Y]$ and expressing (12.64) as

$$[L][U]V_k = I(E_k, V_k) \tag{12.65}$$

Sparsity oriented triangular factorization [5] results in sparse triangular matrices $[L]$ and $[U]$ since $[Y]$ is sparse. The solution for V_k is obtained from forward and backward substitution as

$$[L]W_k = I_k, \quad [U]V_k = W_k \tag{12.66}$$

Whenever I_k is a function of V_k (in case of nonlinear loads) the Eq. (12.64) is conveniently solved using Gauss-Jacobi method where the initial estimate of V_k is used to compute I_k and solve the equation using triangularized admittance matrix. This process is iterated until convergence is obtained in the solution of V_k. The number of iterations are same as in the case when the impedance matrix is used, typically five to seven. However, the use of triangularized admittance

matrix instead of impedance matrix results in less memory and computations. Also if $[Y]$ is symmetric matrix, the lower triangular matrix $[L]$ is the transpose of the upper triangular matrix $[U]$ and need not be computed and stored.

Newton's method can also be used to solve Eq. (12.64). Here the network equations have to be used in the real form (using D-Q variables). At each iteration of Newton's method, the following linear equations have to be solved

$$[J_k]\Delta V_k = F_k = I_k - [Y]V_k \qquad (12.67)$$

where $[J_k]$ is the Jacobian matrix calculated at step k and F_k is the mismatch which should be zero at the solution. The Jacobian matrix differs from $[Y]$ (real admittance matrix) only in the self (diagonal) terms made of 2x2 blocks. However updating the Jacobian matrix at every iteration is not practical. Even updating at every step is not recommended. The use of Very DisHonest Newton (VDHN) method involves maintaining Jacobian matrix constant for several time steps. The updating of Jacobian can be based on the number of iterations required for convergence. Increase in the number of iterations required, signals the need to update Jacobian.

It is to be noted that the use of decoupled Jacobian is not recommended as, in transient stability studies, the decoupling between $P - \theta$ and $Q - V$ is not valid during transient swings caused by large disturbances.

12.5   Simultaneous Solution

The system equations can be expressed as

$$\dot{x} = f(x, V) \qquad (12.68)$$

$$I(x, V) - [Y]V = 0 \qquad (12.69)$$

Implicit method of integration is used to discretize Eq. (12.68). For example, using trapezoidal rule, we get

$$F_{xk} = x_k - x_{k-1} - \frac{h}{2}[f(x_k, V_k) + f(x_{k-1}, V_{k-1})] = 0 \qquad (12.70)$$

Combining this with Eq. (12.69) and linearizing, we get

$$\begin{bmatrix} F_{xk} \\ F_{Vk} \end{bmatrix} = - \begin{bmatrix} A_x^k & B^k \\ C^k & J_N^k \end{bmatrix} \begin{bmatrix} \Delta x_k \\ \Delta V_k \end{bmatrix} = -[J^k] \begin{bmatrix} \Delta x_k \\ \Delta V_k \end{bmatrix} \qquad (12.71)$$

where

$$F_{Vk} = I(x_k, V_k) - [Y]V_k$$

$$A_x^k = \text{Diag}[A_{x1}^k, \ A_{x2}^k, \dots A_{xi}^k, \dots A_{xm}^k] = \frac{\partial F_{xk}}{\partial x_k}$$

$$[B^k] \ = \ [B_1^k, B_2^k, \dots B_i^k, \dots B_m^k] = \frac{\partial F_{xk}}{\partial V_k}$$

$$[C^k] = [C_1^k, C_2^k, \dots C_i^k, \dots C_m^k] = \frac{\partial F_{Vk}}{\partial x_k}$$

$$[J_N^k] = \frac{\partial F_{Vk}}{\partial V_k} = -[Y] + \frac{\partial I_k}{\partial V_k}$$

m is the number of dynamic subsystems (number of generators if no other dynamic devices are considered), J_N is the network Jacobian.

Eq. (12.71) can be solved as follows

$$F'_{Vk} = F_{Vk} - C^k[A_x^k]^{-1}F_{xk} \tag{12.72}$$

$$[L_N] = [J_N^k] - C^k[A_x^k]^{-1}B^k \tag{12.73}$$

$$-[L_N^k]\Delta V_k = F'_{Vk} \tag{12.74}$$

$$\Delta x_k = [A_x^k]^{-1}(F_{xk} - B^k\Delta V_k) \tag{12.75}$$

In exact Newton's method, not only the Jacobian $[J^k]$ varies with each step, but also varies with each iteration in step. However in VDHN method, the Jacobian is not updated unless the system configuration is changed or the number of iterations in a step increase above a threshold value. Although the convergence is slow with VDHN method, there is a significant reduction in the number of computations at each step.

12.6   Case Studies

The results of transient stability evaluation for three test systems are presented in this section. The test systems selected are

(1) IEEE Transient Stability Test Systems [8]

    (a) 17 generator, 162-bus system

    (b) 50 generator, 145-bus system

(2) 10 generator, 39-bus New England Test System [9]

The results are obtained from a PC-based computer program 'STEPS' (Structure preserving (or Sparse) Transient Energy based Program for Stability), specifically developed for power system simulation for transient stability, in which, computation of structure-preserving energy function is an important feature [10]. It will be shown in the next chapter that the scanning of energy function is a much simpler method for monitoring system transient stability compared to scanning a large number of swing curves. In addition, the application of a structure-preserving (or sparse) transient energy function enables direct stability evaluation using potential energy boundary surface or controlling UEP (unstable equilibrium point) method of determining critical energy. The application of energy function methods is considered separately in chapter 13.

12.6.1   17 Generator System

All the generators are represented by classical models and the loads are modelled as constant impedances. The disturbance considered is a three phase fault at bus #75 cleared by opening line between bus #75 and #9. This is a benchmark test reported in [8].

The simulation shows that the critical clearing time lies in the range (0.354-0.355 s). The swing curves (rotor angle with respect to Centre of Inertia) for all the 17 generators are shown in Figures 12.6 to 12.8. The results for both stable and unstable cases are given. The instability arises from generator 16 (connected to bus #130) going out of step. The results are in agreement with those given in [8].

12.6.2   50 Generator System

The generators are represented by classical models and the loads are modelled as constant impedances. The disturbance considered is a three phase fault at bus #7 cleared by opening line between bus #7 and bus #6.

The simulation shows that critical clearing time lies in the range (0.108-0.109 s). The swing curves for critical generators are shown in Fig. 12.9 which displays both stable and unstable cases. The instability is due to machines connected at buses 104 and 111 going out of step with respect to the remaining machines. The results are in agreement with those given in [8].

12.6.3   10 Generator System

The system data is taken from [10]. The machines are represented by two-axis models (1.1). The generators are assumed to be provided with static exciters.

The loads are modelled as constant impedances for simplicity. The disturbance considered is a three phase fault at bus #14 cleared by opening line between bus #14 and bus #34. The critical clearing time lies between 0.34 and 0.35 s. If the machines are represented by classical models, then the critical clearing time reduces to a value between 0.26 and 0.27 s.

The swing curves for all the ten machines represented by classical models are shown in Figs. 12.10 and 12.11. The swing curves in the case when generators are modelled in detail are shown in Figs. 12.12 and 12.13. The variations in the field voltages for all the generators in the latter case are shown in Figs. 12.14 and 12.15.

It is interesting to observe that the mode of instability is unaltered whether the machines are represented by classical or detailed models. In both cases the instability is due to separation of machine 2 which decelerates while other machines accelerate. It is also observed that groups of generators located close to each other or forming a radial system are coherent. Thus generators 1 and 3, 4 and 5, 6 and 7 form three coherent groups. It is interesting to observe that the variations of E_{fd} within coherent groups are similar.

12.7 Dynamic Equivalents and Model Reduction

In large systems, it is not only desirable to reduce the complexity by reducing the order of the model, but is often necessary on account of the computational constraints particularly for on-line applications. In this case, the non-availability of data can also be a problem.

In nonlinear simulations for stability evaluation, we are mainly concerned about the impact of large disturbances in a particular area called the study system. The system external to the study system is not of direct interest in stability studies and is of consequence only insofar as it affects the response of the study system to disturbances within the study system. Hence it is desirable to represent the external system by dynamic equivalents. In the past, Ward type equivalents based on distribution factors used in power flow studies was extended for dynamic studies [11]. Subsequent developments led to two types of dynamic equivalents.

1. Modal equivalents [12,13,17]

2. Coherency-based equivalents [14-16]

(a) Stable (t_{cl}=0.354 s)

(b) Unstable (t_{cl}=0.355 s)
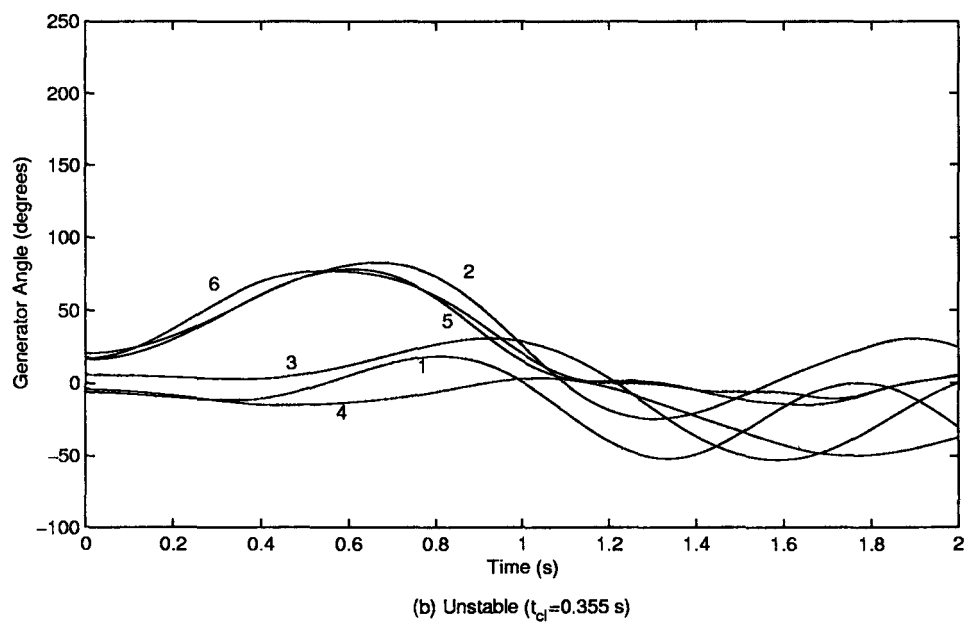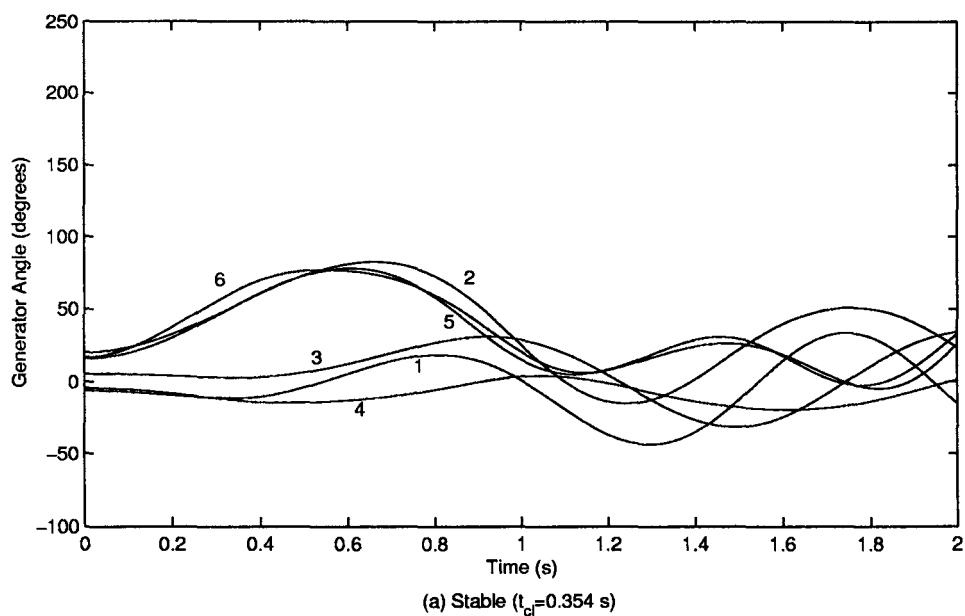
Figure 12.6: Swing Curves - 17 Generator system

(a) Stable (t_{cl}=0.354 s)

(b) Unstable (t_{cl}=0.355 s)
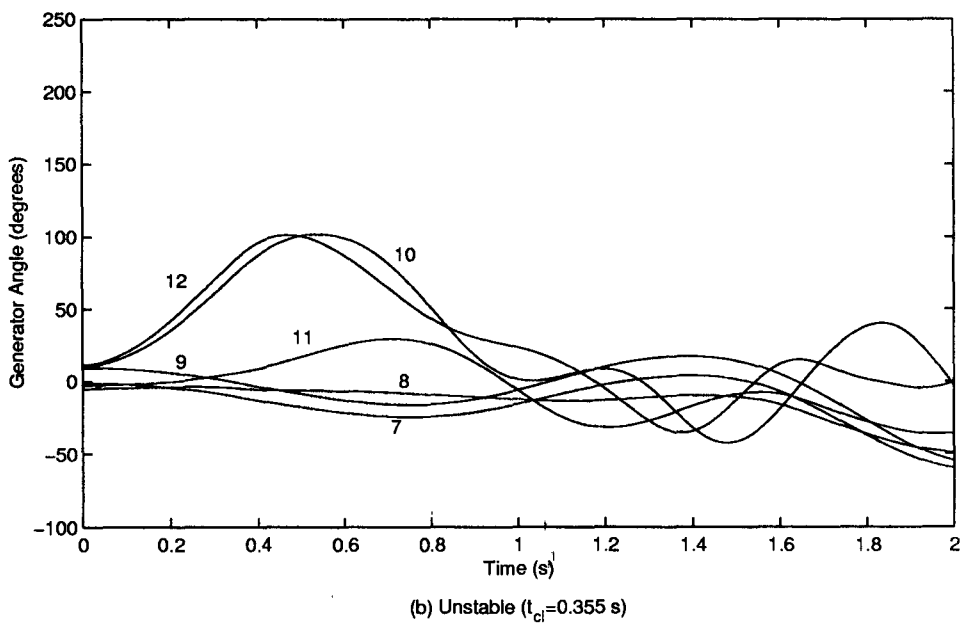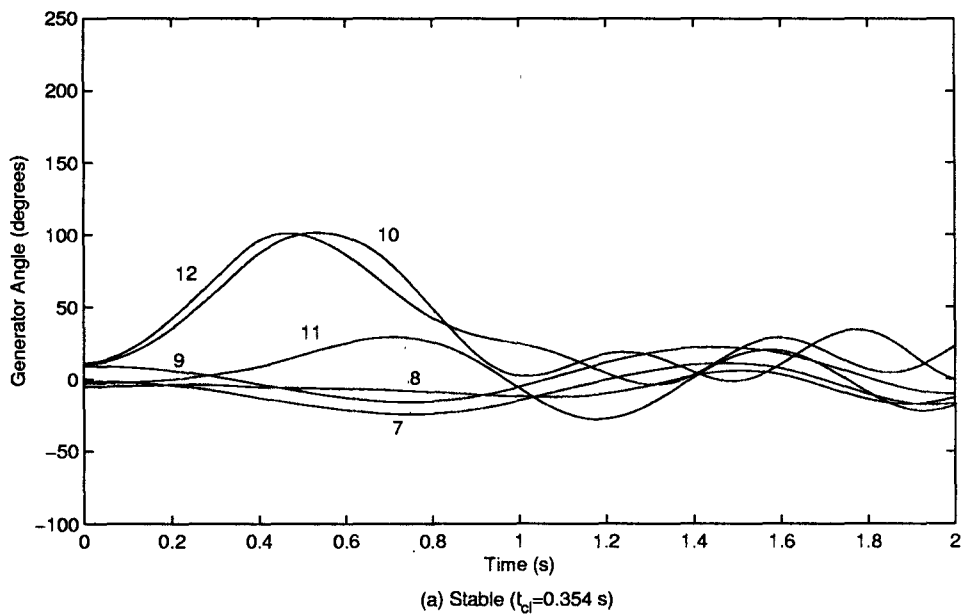
Figure 12.7: Swing Curves - 17 Generator system
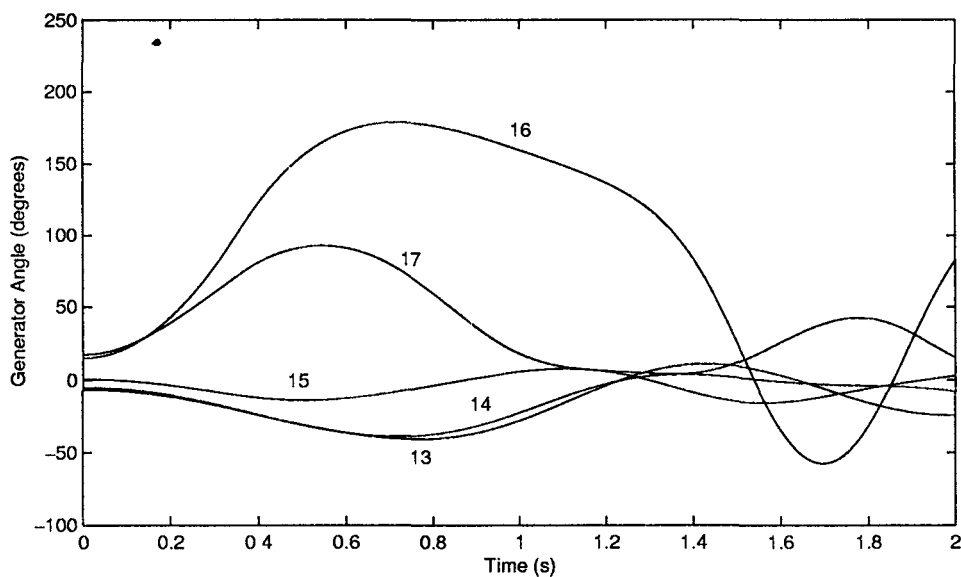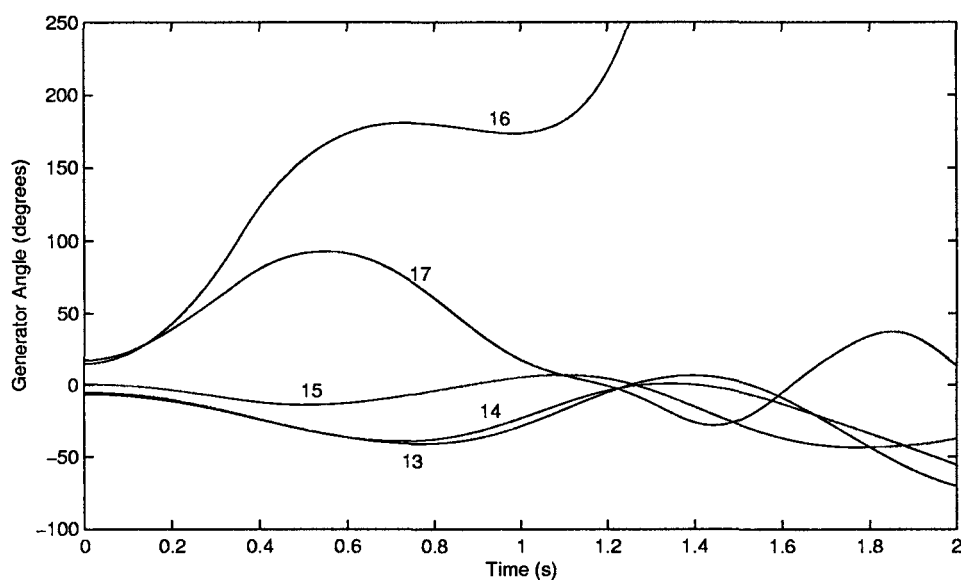
(a) Stable ($t_{cl} = 0.354$ s)

(b) Unstable ($t_{cl} = 0.355$ s)
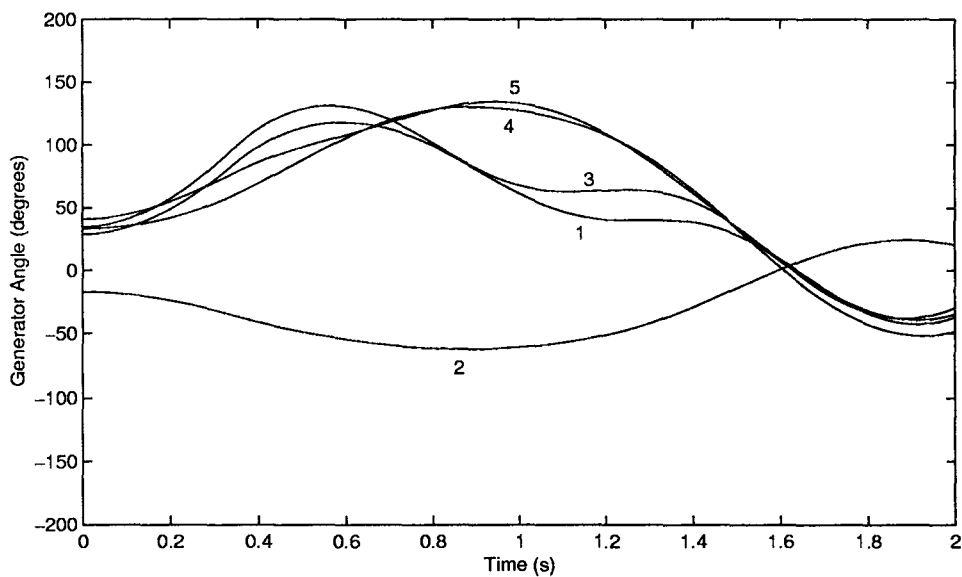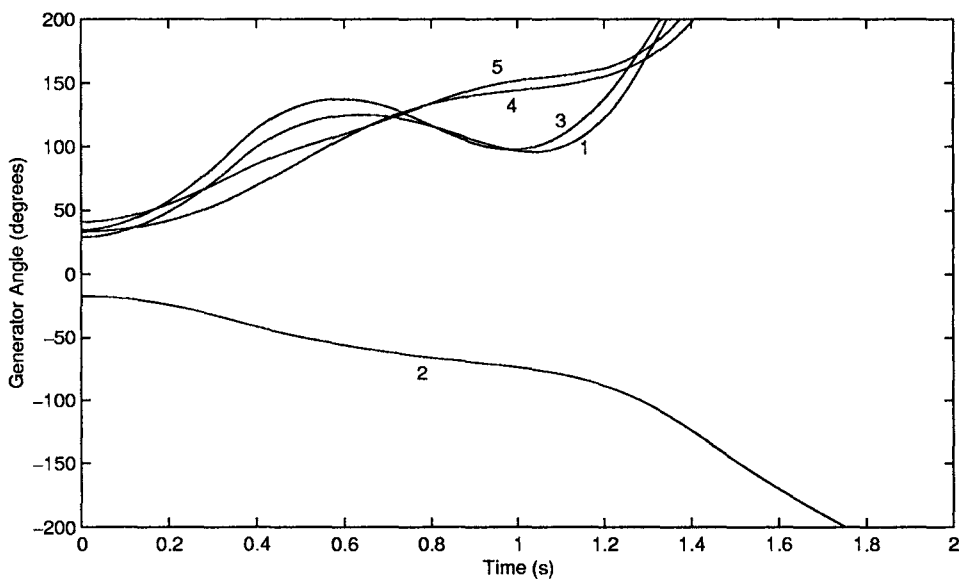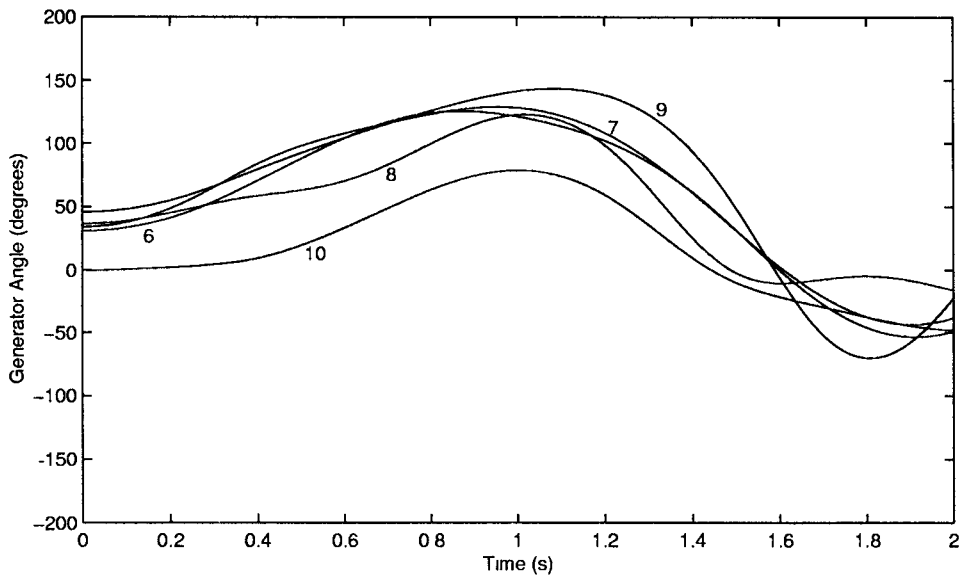
Figure 12.8: Swing Curves - 17 Generator system
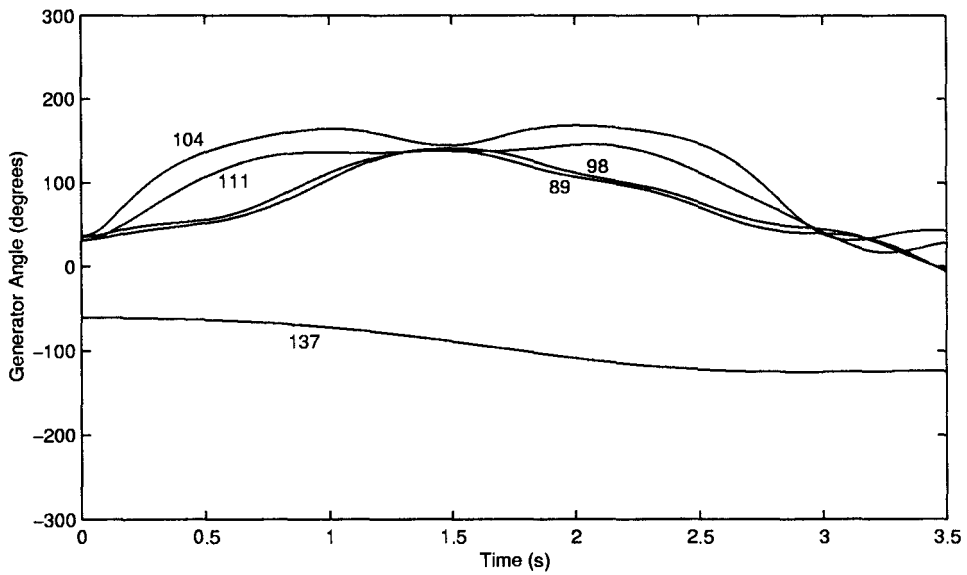
(a) Stable ($t_{cl} = 0.108$ s)
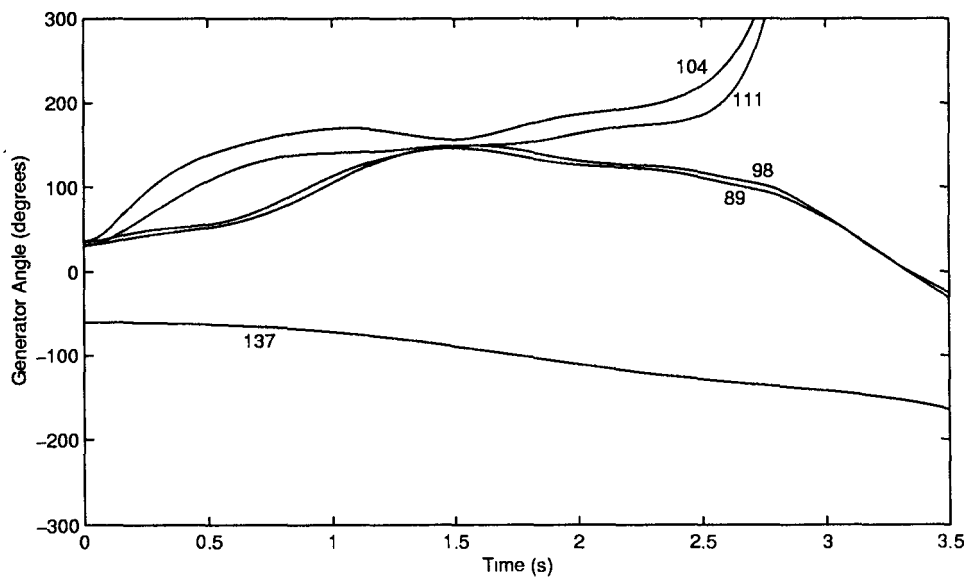
(b) Unstable ($t_{cl} = 0.109$ s)

Figure 12.9: Swing Curves - 50 Generator system

(a) Stable (t_{cl} = 0.26 s)
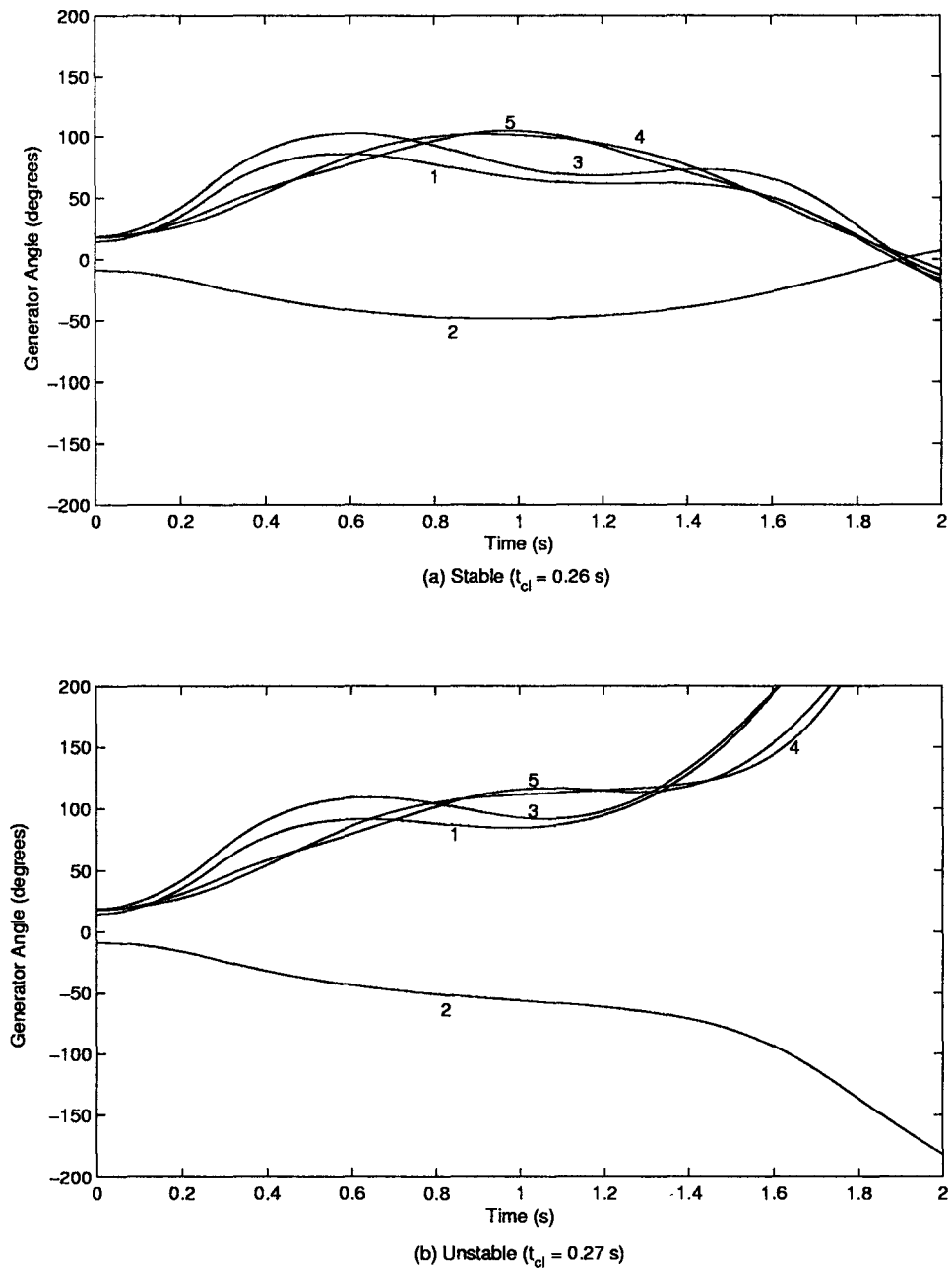
(b) Unstable (t_{cl} = 0.27 s)

Figure 12.10: Swing Curves - 10 Generator system
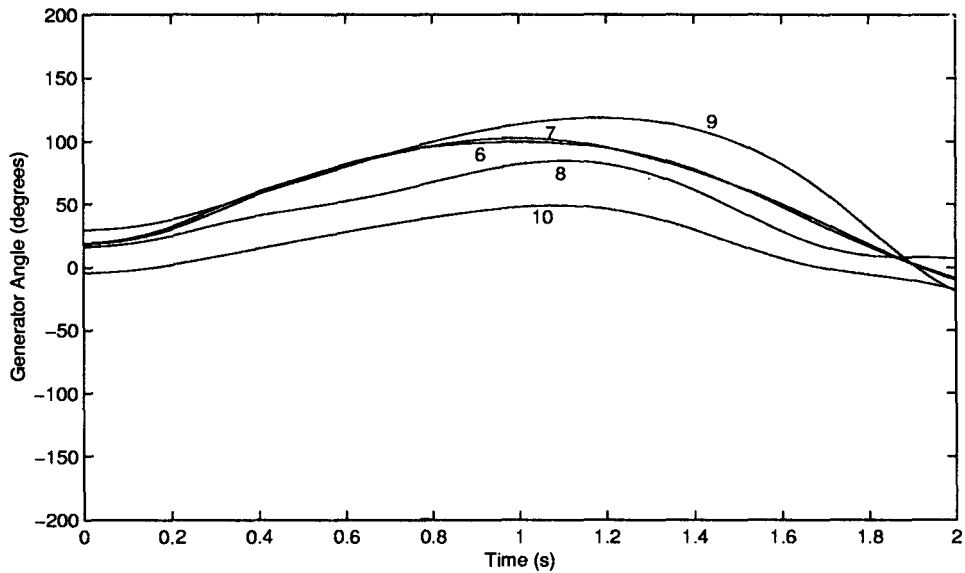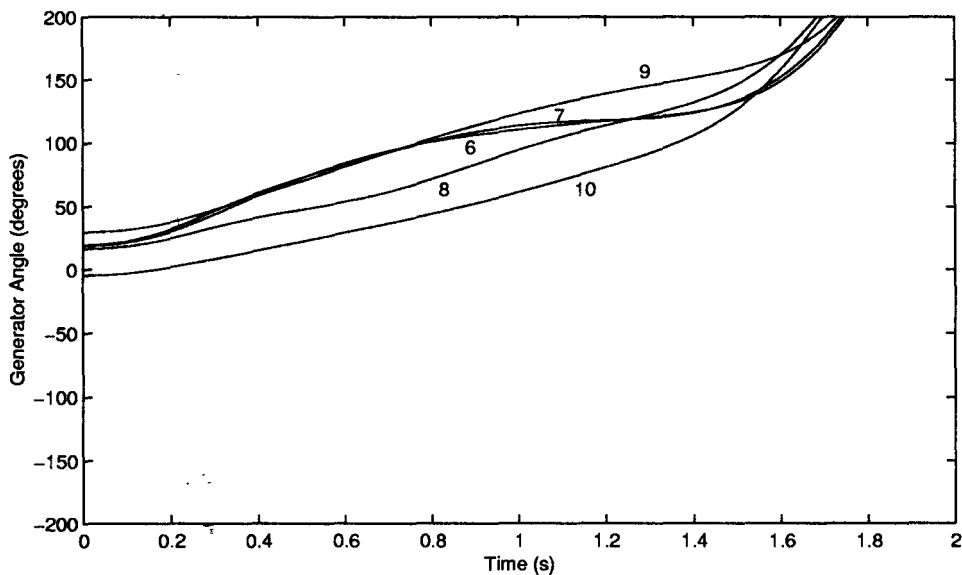
(a) Stable (t_{cl} = 0.26 s)

(b) Unstable (t_{cl} = 0.27 s)

Figure 12.11: Swing Curves - 10 Generator system

(a) Stable ($t_{cl} = 0.34$ s)

(b) Unstable ($t_{cl} = 0.35$ s)

Figure 12.12: Swing Curves - 10 Generator system (Detailed Model)
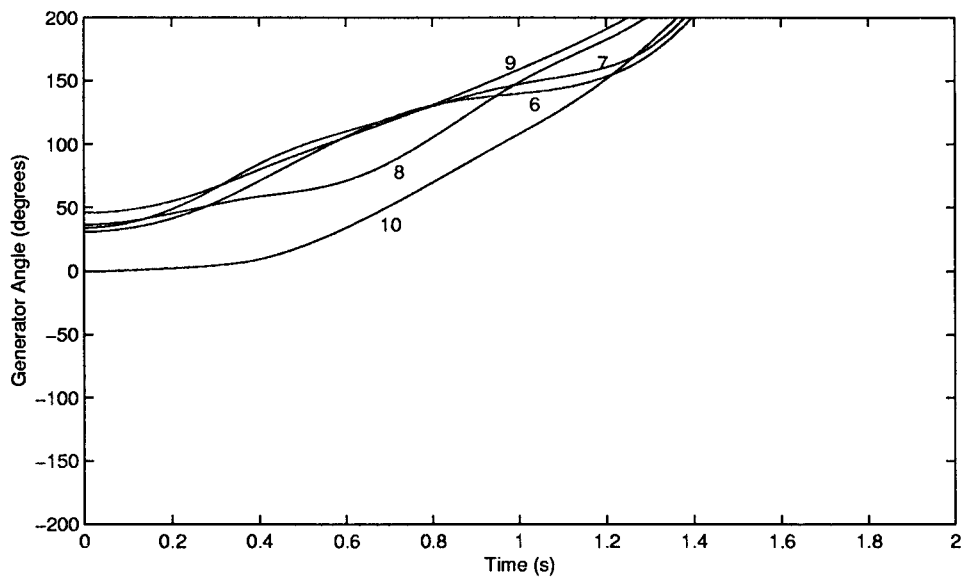
(a) Stable (t_{cl} = 0.34 s)

(b) Unstable (t_{cl} = 0.35 s)

Figure 12.13: Swing Curves - 10 Generator system (Detailed Model)
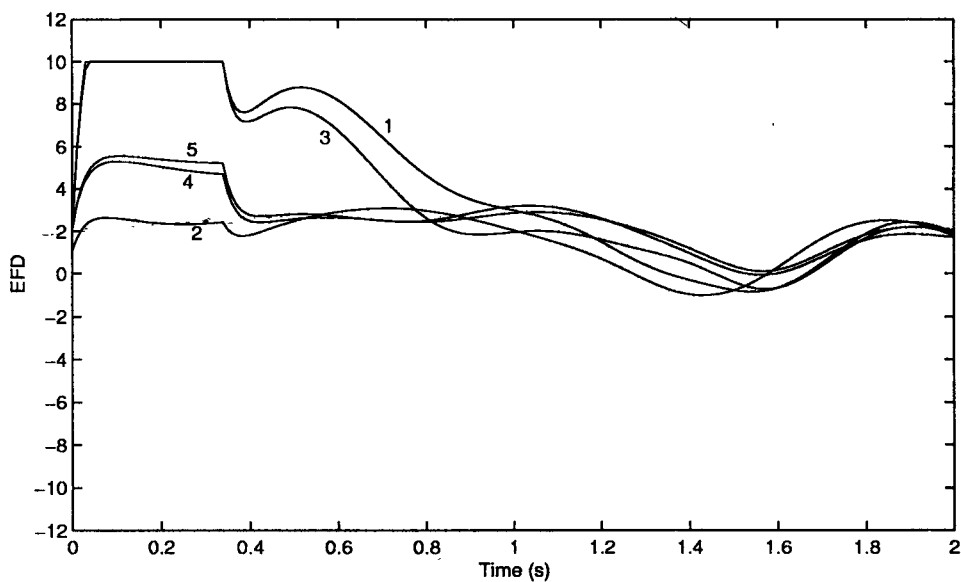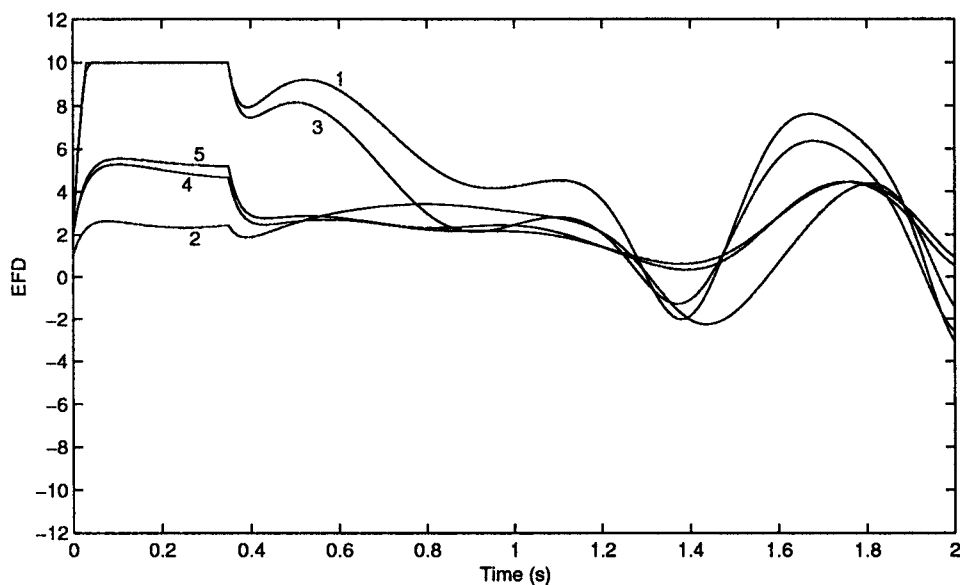
Figure 12.14: Variation of E_{FD} - 10 Generator system (Detailed Model)
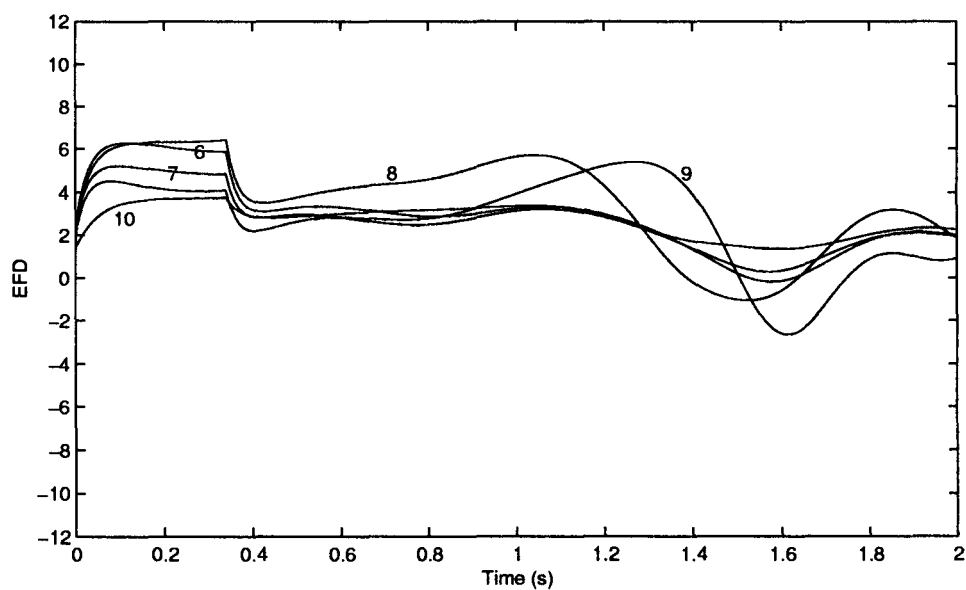
(a) Stable (t_{cl} = 0.34 s)
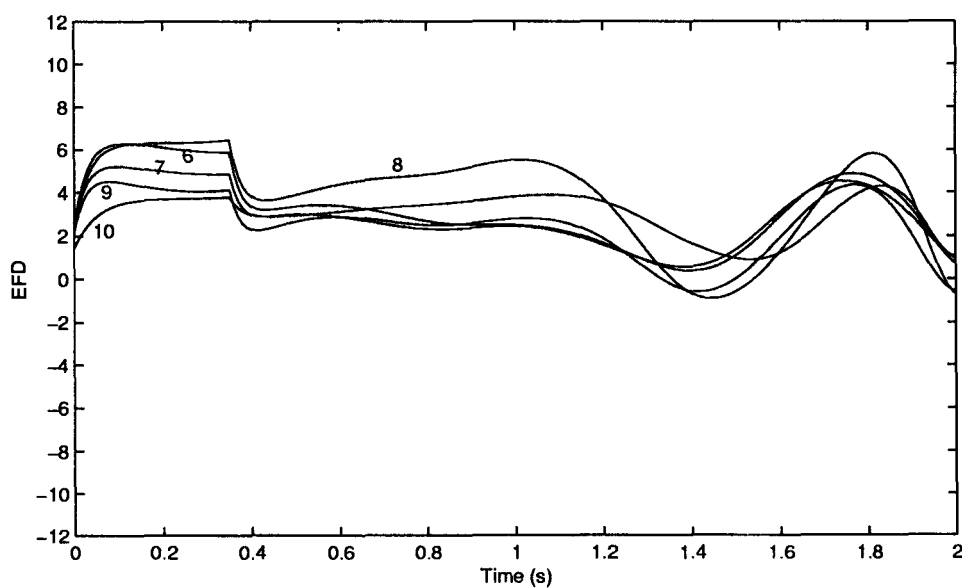
(b) Unstable (t_{cl} = 0.35 s)

Figure 12.15: Variation of E_{FD} - 10 Generator system

The dynamic equivalents based on modal analysis involve a two stage procedure of

(a) construction of matrices which represent equivalents of the external system

(b) Interfacing these matrices with the transient stability simulation of the study system to simulate the complete system

The construction of the modal equivalent produces linear equations of the form

$$\dot{x} = [A]x + [B]\Delta V_T \tag{12.76}$$
$$\Delta I_T = [C]x + [D]\Delta V_T \tag{12.77}$$

where V_T and I_T are terminal bus voltage and current injection at terminal bus respectively (expressed in rectangular coordinates).

In general, these equations cannot be interpreted as representing models of physical devices. Furthermore, model reduction based on modal analysis requires computation of eigenvalues and eigenvectors which can be time consuming.

Coherency based equivalents involve a two stage procedure of

(a) Identification of coherent groups in the external system

(b) Dynamic aggregation of a coherent group of generating units into an equivalent generating unit that exhibits the same speed, voltage and total mechanical and eletrical power as the group during any disturbance where the units in the group remain coherent.

A coherent group of generating units is defined as a group of generators oscillating with the same angular speed and terminal voltages in a constant complex ratio for a set of disturbances. Thus, all the units in a coherent group can be attached to a common bus, if necessary through a complex ratio (involving phase shift) transformer.

Identification of coherency can be based on heuristics such as the concept of electrical distance [14] or utilizing a simplified and linearized power system model [15]. The coherent groups are identified in the latter approach using linear simulation for specific disturbances. The justification for the use of simplified models are based on the following assumptions.

1. The coherent groups of generators are independent of the size of the disturbance. Therefore, coherency can be determined by considering a linearized system model.

2. The coherent groups are independent of the amount of detail in the generator model. Therefore a classical synchronous machine can be considered for the identification of the coherent groups.

References and Bibliography

1. B. Stott, "Power system dynamic response calculations", Proc. IEEE, Vol. 67, No. 2, Feb. 1979, pp. 219-241.

2. H.W. Dommel and N. Sato, "Fast transient stability solutions", IEEE Trans. Vol. PAS-91, July/Aug. 1972, pp. 1643-1650.

3. G.T. Vuong and A. Valette, "A complex Y-matrix algorithm for transient stability studies", IEEE Trans. Vol. PAS-105, No. 12, Dec. 1985, pp. 3388-3394.

4. EPRI Report, "Extended transient-midterm stability package", Report EL-4610, Electric Power Research Institute, Palo Alto, CA, Jan. 1987.

5. W.F. Tinney and J.W. Walker, "Direct solutions of sparse network equations by optimally ordered triangular factorization", Proc. IEEE, Vol. 55, Nov. 1969, pp. 1801-1809.

6. J.M Undrill, "Structure in the computation of power-system nonlinear dynamical response", IEEE Trans. Vol. PAS-88, No. 1, 1969, pp. 1-6.

7. T.S. Parker and L.O. Chua, **Practical numerical algorithms for chaotic systems**, Springer-Verlag, New York, 1989.

8. IEEE Committee Report, "Transient stability test systems for direct stability methods", IEEE Trans. on Power Systems, Vol. 7, Feb. 1992, pp. 37-43.

9. M.A. Pai, **Energy function analysis for power system stability**, Kluwer Academic Publishers, Boston 1989.

10. Vijayan Immanuel, **Application of structure preserving energy functions for stability evaluation of power systems with static var compensators**, Ph.D. Thesis submitted to Indian Institute of Science, Bangalore, August 1993.

11. H.E. Brown, R.B. Shipley, D. Coleman and R.E. Neid Jr., "A study of stability equivalents", IEEE Trans. Vol. PAS-88, No. 3, 1969, pp. 200-207.

12. J.M. Undrill and A.E. Turner, "Construction of power system electromechanical equivalents by modal analysis", IEEE Trans. Vol. PAS-90, Sept/Oct. 1971, pp. 2049-2059.

13. J.M. Undrill, J.A. Casazza, E.M. Gulachenski and L.K. Kirchmayer, "Electromechanical equivalents for use in power system studies", IEEE Trans. Vol. PAS-90, Sept./Oct. 1971, pp. 2060-2071.

14. S.T.Y. Lee and F.C. Schweppe, "Distance measures and coherency recognition transient stability equivalents", IEEE Trans. Vol. PAS-82, Sept./Oct. 1973, pp. 1550-1557.

15. R. Podmore, "Identification of coherent generators for dynamic equivalents", IEEE Trans. Vol. PAS-97, No. 4, 1978, pp. 1344-1354.

16. A.J. Germond and R. Podmore, "Dynamic aggregation of generating unit models", IEEE Trans. Vol. PAS-97, No. 4, 1978, pp. 1060-1069.

17. W.W. Price et al., "Testing of the modal dynamic equivalents technique", IEEE Trans. Vol. PAS-97, No. 4, 1978, pp. 1366-1372.

18. A. Bose, "Parallel processing in dynamic simulation of power sytems", Sadhana, Indian Academy of Sciences, Vol. 18, part 5, 1993, pp. 815-828.

Chapter 13

Application of Energy Functions for Direct Stability Evaluation

13.1   Introduction

Transient stability evaluation using digital simulation requires solution of nonlinear differential algebraic equations over a time interval (following the initiation of a large disturbance such as a three phase fault) extending to several seconds. This is computationally burdensome particularly in view of the fact that, even for a given system configuration and loading conditions with a specified generation pattern (an operating point), the transient stability is also a function of the disturbance (or contingency). Thus, several credible contingencies need to be considered to evaluate transient stability of a system.

Thus, there is a need for a fast (or direct) method for stability evaluation which does not require extensive solution of differential-algebraic equations. For a two machine system (or a SMIB system), the equal area criterion is a direct method which can determine stability based only on the knowledge of the system state (angle and velocity) at the time of clearing. An extension of this approach to multimachine systems is formulated using energy functions.

The application of energy functions to power system has a long history. The earliest work was reported by Magnusson in 1947 [1]. An energy integral criterion was proposed by Aylett in 1958 [2]. As Lyapunov's function is a generalization of energy functions, the works by Gless [3], El-Abiad and Nagappan [4] were the first application of Liapunov's method for power system stability. There were several developments since then, which are summarized in the monographs by Pai [5,6]. There are also state of the art papers [7-9] which survey the current research efforts in the area.

Liapunov's method, although general in nature, suffered from conservativeness of results when applied to practical systems. There were also barriers in extending the method to more complex systems with detailed models. For. example, even with classical generator models and constant impedance type .

loads (which enabled reduction of the network to generator internal buses) the presence of transfer conductances prevents the use of Liapunov functions unless gross approximations are used. (It is to be noted that even if transmission system is assumed to be lossless, the network reduction results in large transfer conductances).

Recent developments in this field have been aimed at solving the problems of

1. Accurate determination of critical clearing time for a given fault

2. Application to detailed generator and load models

3. The inclusion of controllers such as excitation, HVDC and SVC

4. Applications to on-line dynamic security assessment

The inclusion of load models and network based controller models (such as HVDC and SVC) has been made feasible due to the development of Structure Preserving Energy Functions (SPEF) defined on structure preserving system models [12-19]. Previously the loads were represented as constant impedances and the network was reduced to retain only the internal buses of generators (represented by classical models). This procedure is not desirable even if loads can be modelled as constant impedances as the reduced network admittance matrix has transfer conductances and energy functions cannot be strictly defined for such systems.

13.2 Mathematical Formulation

Consider that a power system is described by nonlinear differential equations

$$\dot{x} = f_I(x), \qquad t_o < t < t_F \tag{13.1}$$

It is assumed that a fault occurs at time t_F. There is no loss of generality in assuming $t_F = 0$. Also, it is assumed that the system is in equilibrium prior to the instant of fault. During the fault, the system is described by

$$\dot{x} = f_F(x), \qquad t_F \leq t < t_c \tag{13.2}$$

where t_c is the instant of clearing of fault. The postfault system is described by the equation

$$\dot{x} = f(x) \qquad t_c \leq t < \infty \tag{13.3}$$

The postfault dynamics is generally different than the prefault dynamics since the clearing of the fault is usually accompanied by disconnection of line(s).
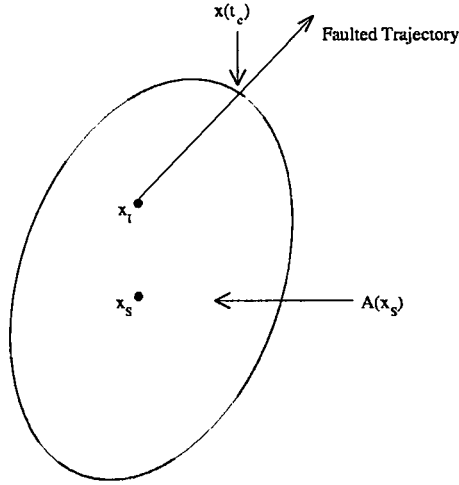
Figure 13.1: Definition of critical clearing time

Assuming that a stable equilibrium point (SEP) exists for the postfault system, the problem of transient stability evaluation is to determine whether the initial state (for the post fault system) lies in the region of attraction (stability) around the SEP. If $x(t_c) \in A(x_s)$ where $A(x_s)$ is the region of stability around the SEP (x_s) the system is stable.

There are two steps in this evaluation

i) characterization of the boundary of stability region, $\partial A(s)$

ii) computation of post-fault initial state $x(t_c)$ and comparison with $\partial A(s)$.

The fault-on trajectory normally traverses the boundary of stability (see Fig. 13.1) at a time $t = t_{cr}$. If the clearing time $t_c < t_{cr}$, the system is transiently stable. Thus, t_{cr} is termed as critical clearing time for a given fault. This is a function of $x(t_F)$, the initial condition for the faulted trajectory, (also identical to SEP of the pre-fault system assuming equilibrium prior to the fault) and the faulted system.

The boundary of the region of attraction is expressed in terms of stable manifolds $M^s(x_i)$ of the unstable equilibrium points (of type 1) lying on the boundary. A type 1 UEP has only one dimensional unstable manifold $M^u(x_i)$. It can be shown that [10], under some conditions,

$$\partial A(x_s) = \bigcup_{x_i \in E_1 \bigcap \partial A} M^s(x_i)$$

(13.4)

where E_1 is the set of type 1 equilibrium points.

Stable and unstable manifolds of a hyperbolic equilibrium point, x_i, (the system Jacobian evaluated at the hyperbolic EP has the property that its eigenvalues lie either in RHP or LHP) are defined as

$$M^s(x_i) = \{x \mid \phi(x,t) \to x_i \text{ as } t \to \infty\}$$
$$M^u(x_i) = \{x \mid \phi(x,t) \to x_i \text{ as } t \to -\infty\}$$

where $\phi(x,t)$ is a solution curve (trajectory) starting from x at $t = 0$. Thus,

$$\phi(x,0) = x$$

The stability region is defined by

$$A(x_s) = \{x \mid \lim_{t \to \infty} \phi(x,t) = x_s\} \tag{13.5}$$

The sufficient conditions that guarantee the result of Eq. (13.4) are [10]

1. All the equilibrium points on the stability boundary are hyperbolic.

2. The intersection of $M^s(x_i)$ and $M^u(x_j)$ satisfies the transversality condition for all the equilibrium points x_i, x_j on the stability boundary.

3. There exists a C^1 function (continuous with continuous derivatives) $W : R^n \to R$ such that

   (i) $\dot{W}(\phi(x,t)) \leq 0$ at $x \notin E$ where E is the set of equilibrium points. The equality is satisfied only at some points on the trajectory and not over a finite time interval.

   (ii) $W(\phi(x,t))$ is bounded implies $\phi(x,t)$ is bounded. W is termed as the energy function.

The assumptions 1 and 2 are generic properties of dynamical systems (true for almost all dynamic systems). The transversality condition means that at every point of intersection between the two manifolds, the tangent spaces of the two manifolds span the tangent space R^n.

Condition (i) in assumption (3) implies that every trajectory must either go to infinity or converge to one of the equilibrium points. It guarantees that bounded oscillatory trajectories such as limit cycles or chaotic motions do not exist. Because of condition 3(i), the energy function on the stable manifold of a UEP x_i, reaches its minimum value at x_i.

The region of attraction is unbounded if the system does not have a source (EP with all the eigenvalues of the Jacobian lying in the RHP). If the

stability region is bounded, the energy function achieves a local maximum at a source on the stability boundary $\partial A(x_s)$.

The transversality condition is not satisfied in case of a saddle to saddle connection (or heteroclinic orbit). An example of this is shown in Fig. 13.2 where a trajectory connects two UEPs. There can also be a homoclinic orbit which is a trajectory connecting a UEP with itself.

(a) Heteroclinic orbit   (b) Homoclinic orbit
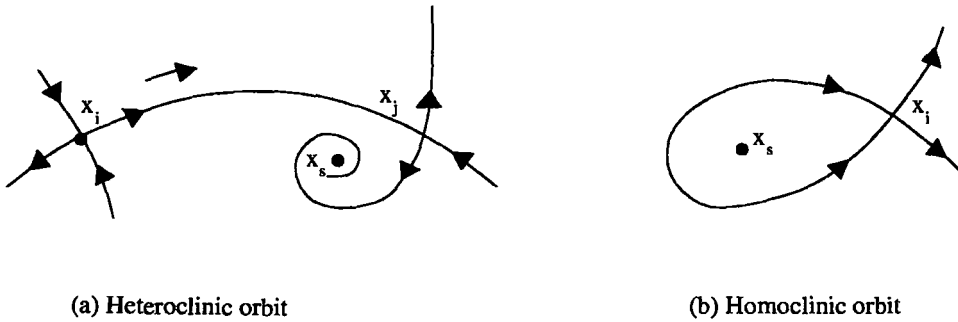
Figure 13.2: An example where transversality condition is not satisfied

The energy function can be used to approximate the stability region. The bounded region

$$W(x) \leq W_{cr} \tag{13.6}$$

is an estimate of the stability region if W_{cr} (termed as critical energy) is suitably chosen. There are two ways in which W_{cr} can be selected. These are

$$(A) \quad W_{cr} = \min\{W(x_i)\}, \quad x_i \in E_1 \bigcap \partial A \tag{13.7}$$

W_{cr} is chosen as the minimum value of W evaluated at all UEPs on the stability boundary. The UEP at which this minimum occurs is termed as the critical (closest) UEP. This gives an underestimate of the stability region (see Fig. 13.3). This is because, in most cases, we need to predict the exit point p of the faulted system trajectory at the stability boundary. The exit point lies on the stable manifold of a UEP that is termed as the controlling UEP, x_c, which is close to the faulted system trajectory. Thus an accurate estimate of stability boundary is given by

$$(B) \quad W_{cr} = W(x_c), \quad x_c \text{ is the controlling UEP} \tag{13.8}$$

Stability Criterion
This is a two step procedure given below

Step 1 Compute the controlling UEP lying on the boundary $\partial A(x_s)$. Calculate W_{cr}.
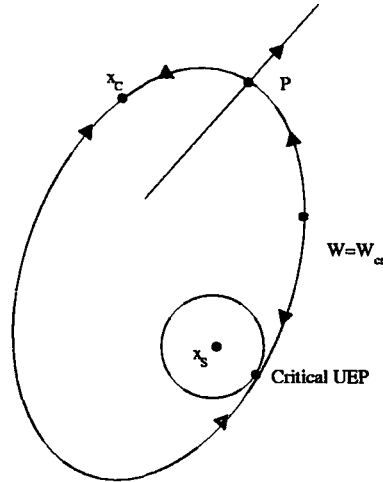
Figure 13.3: Critical and controlling UEP

Step 2 At the instant of clearing of the fault, compute $W(t_c)$. If $W(t_c) \leq W_{cr}$, the system is transiently stable. When $W(t_c) = W_{cr}$, the clearing time is said to be critical.

The issues that are important in the application of energy functions for direct stability evaluation are

  (i) Formulation of an appropriate energy function

 (ii) Determination of W_{cr}

(iii) Approximate determination of $W(t_c)$ without having to integrate the faulted system equations.

These issues are discussed in the following sections. The equivalence of equal area criterion to the criterion in terms of energy function is shown in the next section.

13.3   Energy Function Analysis of a Single Machine System

Consider a single machine connected to an infinite bus as shown in Fig. 13.4. The synchronous machine is represented by the classical model of a voltage source E_g behind a reactance x_g. The equivalent circuit is shown in Fig. 13.5.

The swing equation for the machine is given by

$$M\frac{d^2\delta}{dt^2} = P_m - P_e \tag{13.9}$$
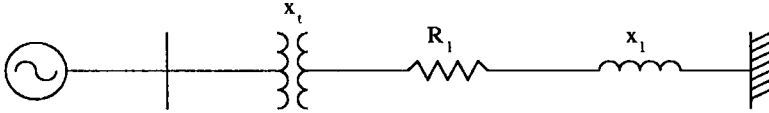
Figure 13.4: A single machine system
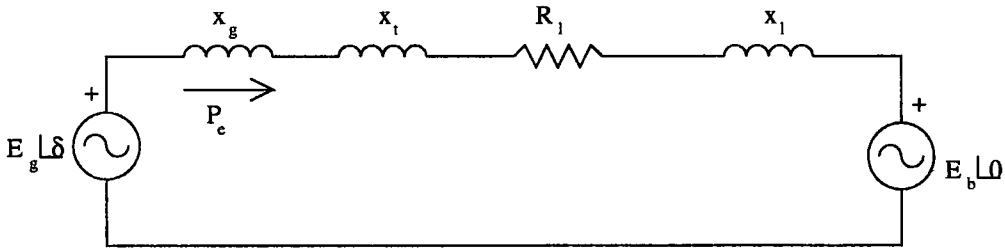
Figure 13.5: Equivalent circuit for system in Fig. 13.4

The electric power output of the machine can be derived from the equivalent circuit of Fig. 13.5 as

$$P_e = GE_g^2 - GE_gE_b\cos\delta - BE_gE_b\sin\delta \tag{13.10}$$

where

$$G + jB = \frac{1}{R_l + j(x_g + x_t + x_l)}$$

Substituting Eq. (13.10) in (13.9), we have

$$M\frac{d^2\delta}{dt^2} = P'_m - P'_e(\delta) \tag{13.11}$$

where

$$\begin{aligned}
P'_m &= P_m - GE_g^2 \\
P'_e &= -GE_gE_b\cos\delta - BE_gE_b\sin\delta
\end{aligned}$$

It is to be noted that B is negative (due to inductive susceptance).

Multiplying both sides of Eq. (13.11) by $\left(\frac{d\delta}{dt}\right)$ and integrating, we have

$$\frac{1}{2}M\left(\frac{d\delta}{dt}\right)^2 + \int [P_e'(\delta) - P_m']d\delta = \text{constant} = k_1$$

$$\frac{1}{2}M\left(\frac{d\delta}{dt}\right)^2 + BE_gE_b\cos\delta - GE_gE_b\sin\delta - P_m'\delta = k_1 \qquad (13.12)$$

The L.H.S. of (13.12) can be expressed as the sum of kinetic energy W_k and potential energy W_p given by

$$W_k\left(\frac{d\delta}{dt}\right) = \frac{1}{2}M\left(\frac{d\delta}{dt}\right)^2 \qquad (13.13)$$

$$W_p(\delta) = BE_gE_b\cos\delta - GE_bE_g\sin\delta - P_m'\delta \qquad (13.14)$$

$$W_k + W_p = W(x) = \text{constant} = k_1 \qquad (13.15)$$

where $x^t = \begin{bmatrix} \delta & \frac{d\delta}{dt} \end{bmatrix}$

There is no loss of generality in expressing energies with reference to a SEP x_s, such that

$$W(x_s) = 0 \qquad (13.16)$$

Thus Eq. (13.15) can be revised to

$$\frac{1}{2}M\left(\frac{d\delta}{dt}\right)^2 + BE_gE_b[\cos\delta - \cos\delta_s] - GE_gE_b[\sin\delta - \sin\delta_s] \qquad (13.17)$$
$$-P_m'(\delta - \delta_s) = \text{constant} = k_2$$

The constant k_2 is determined from the initial condition $W(t = t_c)$.

Remarks

1. The energy function, $W(x)$ is defined for the postfault system. The initial condition for this corresponds to $t = t_c$ where t_c is the fault clearing time.

2. The initial energy (k_2) at $t = t_c$, is determined from the integration of the faulted system equation.

Equivalence with Equal Area Criterion

The criterion for stability using an energy function is given by

$$W(t = t_c) \leq W_{cr}$$

where $W_{cr} = W(x_u) = W_p(\delta_u)$

where x_u is an appropriate (controlling) UEP. Fig. 13.6 shows the power angle curves for (i) the prefault (ii) faulted and (iii) post fault systems. For convenience, $G = 0$ is assumed in drawing these curves.

From Fig. 13.6 it is easy to see that the area $(A_2 + A_3)$ is given by

$$(A_2 + A_3) = \int_{\delta_s}^{\delta_u} (P'_e - P'_m)d\delta = W_p(\delta_u) = W_{cr} \tag{13.18}$$

At the time of fault clearing, the kinetic energy is given by

$$W_k(t = t_c) = \int_{\delta_I}^{\delta_c} (P'_m - P'_{ef})d\delta = A_1 \tag{13.19}$$

where δ_I is the initial (prefault) angle.
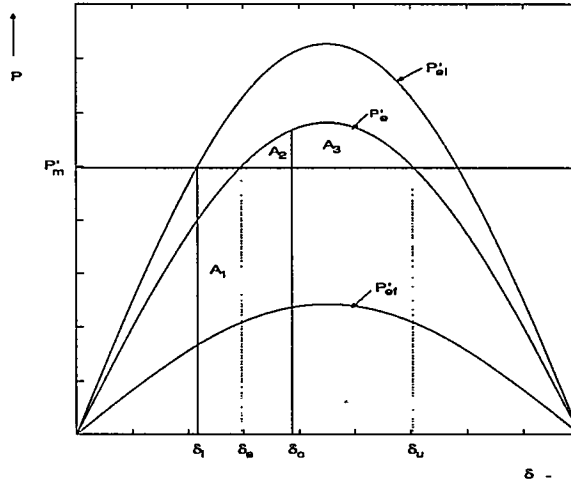
Figure 13.6: Power angle curves

The potential energy at the time of clearing is given by

$$W_p(t = t_c) = \int_{\delta_s}^{\delta_c} (P'_e - P'_m)d\delta = A_2 \tag{13.20}$$

Using Eq. (13.18) to (13.20) in the stability criterion gives

$$A_1 + A_2 \leq A_2 + A_3$$
$$A_1 \leq A_3 \tag{13.21}$$

Thus, the stability criterion using energy function is equivalent to the equal area criterion for stability.

Remarks

1. The damping was neglected in the above analysis. Thus, the energy function remains constant along the post fault trajectory (at a value equal to the energy gained during the fault).

2. If damping were to be considered then

$$W(t) = W(t_c) - \int_{t_c}^{t} D\left(\frac{d\delta}{dt}\right)^2 dt$$

which implies

$$\frac{dW}{dt} = -D\left(\frac{d\delta}{dt}\right)^2 \qquad (13.22)$$

As $\frac{d\delta}{dt}$ is not identically zero along the post fault trajectory, Eq. (13.22) satisfies the condition 3(i) defined in the previous section.

3. There is only one UEP on the stability boundary for a single machine system in most of the cases. For a lossless system $(G = 0)$ this is given by $\delta_u = \pi - \delta_s$ and normally lies along the faulted system trajectory. The potential energy along fault-on trajectory reaches a local maximum when $\delta = \delta_u$. This shows that even without the knowledge of δ_u, it is possible to compute W_{cr} by tracking the potential energy during fault-on conditions and capturing its maximum value. (However, this is not generally true for multimachine systems as fault-on trajectory is not expected to exactly pass through controlling UEP).

For a single machine system, the kinetic energy goes to zero along the postfault trajectory at the instants when the potential energy is maximum. Also, for a system with no damping, the oscillations don't decay and the exchange between the potential and kinetic energies is continually taking place.

4. The controlling UEP need not always lie along the faulted trajectory. For example, in a single machine system if fault resistance is present, it is possible (though improbable) that the machine decelerates during the fault and comes closer to the UEP, $\delta'_u = -(\pi + \delta_s)$. See Fig. 13.7 (a). However for small damping $(D \simeq 0)$, this UEP is not the controlling UEP. It can be shown that the system although stable in the first swing, will be unstable in the back (reverse) swing. See Fig. 13.8 for a typical swing curve. This follows from the fact that $W_p(\delta'_u) > W_p(\delta_u)$ (see Fig. 13.7 (b)). This example shows the need for correct identification of the controlling UEP for the determination of accurate value of W_{cr}.
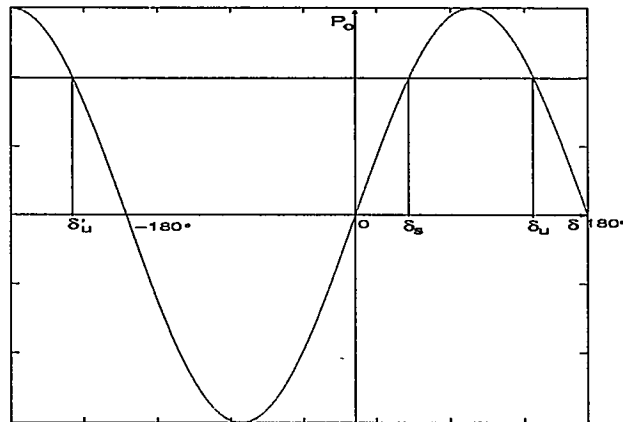
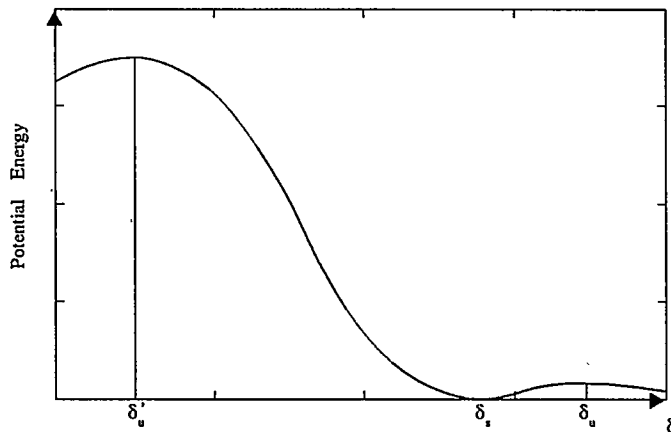Figure 13.7: (a) Equilibrium points in a single machine system

Figure 13.7: (b) Potential energy variation

13.4 Structure Preserving Energy Function

The extension of energy function, defined for a single machine system in the previous section, to multimachine power systems is complicated by the following factors

1. The existence of global energy functions for multimachine systems with transfer conductance is doubtful [34]. This is not surprising as the presence of transfer conductance can result in the existence of unstable limit cycles around SEP, which reduce the region of attraction (stability).

   The path dependent energy component due to transfer conductances can
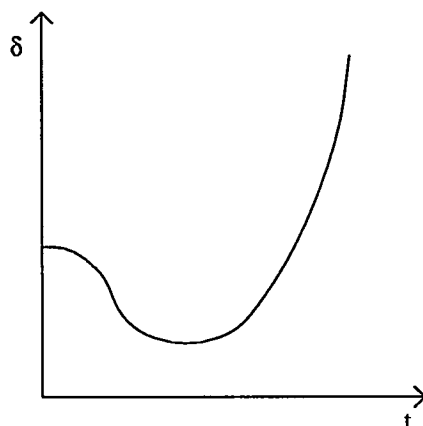
Figure 13.8: A swing curve

be utilized in the numerical computation but has no theoretical validity.

2. The number of UEPs on the stability boundary increase considerably with the system size and the computation of the controlling UEP (or critical energy) can be a problem.

3. The inclusion of voltage dependent load models and detailed generator models with AVR need to be considered to increase the scope of application of energy functions for practical systems.

The first and third factors listed above, can be accounted for if structure-preserving model of power systems is used in the formulation of energy functions [12]. This not only enables consideration of detailed load models (and inclusion of SVC and HVDC controllers), but can also overcome the problem of transfer conductances which can be significant if reduced network model is used. On the other hand, transmission losses in EHV transmission network are small and can be neglected. With the retention of load buses (and voltage dependent load models), it can be shown that energy functions exist if following assumptions are used

1. The transmission network is lossless

2. The synchronous machines are represented by classical model

3. The active power load at any bus is constant (independent of the voltage).

It will be shown later that the assumption 2 can be relaxed to consider two axis model with flux decay and a damper winding. Also the first and last assumptions can be relaxed by introducing path dependent components of energy functions

that can be numerically evaluated. The accuracy of this approach is good if the path dependent terms are small (in relation to other terms).

System Equations

Consider a n-bus system having m machines supplying nonlinear voltage dependent loads. In addition to the assumptions 1 and 2 mentioned earlier, it is also assumed that the damping is negligible. This results in a conservative system with no dissipation of energy.

The motion of ith machine with respect to the COI (Centre of Inertia) reference frame is described by the differential equations

$$M_i \dot{\omega}_i = P_{mi} - P_{ei} - \frac{M_i}{M_T} P_{COI} \tag{13.23}$$

$$\dot{\theta}_i = \omega_i \tag{13.24}$$

where

$$P_{ei} = \frac{E_i V_i \sin(\theta_i - \phi_i)}{x'_{di}},$$

$$M_T = \sum_{i=1}^{m} M_i, \quad P_{COI} = \sum_{i=1}^{m} (P_{mi} - P_{ei})$$

From the definition of the COI variables given by

$$\theta_i = \delta_i - \delta_o, \quad M_T \delta_o = \sum_{i=1}^{m} M_i \delta_i \tag{13.25}$$

We have,

$$\sum_{i=1}^{m} M_i \theta_i = 0 \text{ and } \sum_{i=1}^{m} M_i \omega_i = 0 \tag{13.26}$$

In the load model considered here, both active and reactive powers are assumed to be arbitrary functions of respective bus voltages. Thus, the equations for the system loads can be written as

$$P_{li} = f_{pi}(V_i) \tag{13.27}$$

$$Q_{li} = f_{qi}(V_i) \tag{13.28}$$

The power flow equations for the lossless system, are given below.

The active power injected into the network at bus i is

$$\left. \begin{array}{rl} \dot{P}_i &= g_{1i} + g_{2i}, \quad i = 1, 2....m \\ &= g_{2i}, \quad i = m+1, m+2, ...n \end{array} \right\} \tag{13.29}$$

The reactive power injection at bus i is

$$Q_i = g_{3i} + g_{4i}, \quad i = 1, 2....m \atop = g_{4i}, \quad i = m+1, m+2, ...n \Bigg\} \tag{13.30}$$

where

$$g_{1i} = \frac{E_i V_i \sin(\phi_i - \theta_i)}{x'_{di}}, \quad g_{2i} = \sum_{j=1}^{n} V_i V_j B_{ij} \sin \phi_{ij}$$

$$g_{3i} = \frac{V_i^2 - E_i V_i \cos(\theta_i - \phi_i)}{x'_{di}}, \quad g_{4i} = \sum_{j=1}^{n} V_i V_j B_{ij} \cos \phi_{ij}$$

$$B_{ij} = \text{Im}[Y_{BUS}(i,j)]$$

Y_{BUS} is the admittance matrix of the network (without including the machine reactances). It is assumed that the generator i is connected to bus i. ϕ_i is the angle of bus i, with respect to COI.

The power flow equations at bus i can be written as

$$P_i + P_{li} = P_i + f_{pi}(V_i) = 0 \tag{13.31}$$

$$Q_i + Q_{li} = Q_i + f_{qi}(V_i) = 0 \tag{13.32}$$

A Structure Preserving Energy Function

Consider the energy function (defined for the post-fault system)

$$W(\omega, \theta, V, \phi, t) = W_1(\omega) + W_2(\theta, V, \phi, t) \tag{13.33}$$

where

$$W_1(\omega) = \frac{1}{2} \sum_{i=1}^{m} M_i \omega_i^2$$

$$W_2(\theta, V, \phi, t) = W_{21}(\theta) + W_{22}(t) + W_{23}(V)$$
$$+ W_{24}(V, \theta, \phi) + W_{25}(V, \phi)$$

$$W_{21}(\theta) = - \sum_{i=1}^{m} P_{mi}(\theta_i - \theta_{io})$$

$$W_{22}(t) = \sum_{i=1}^{n} \int_{t_o}^{t} P_{li}(V_i) \frac{d\phi_i}{dt} dt$$

$$W_{23}(V) = \sum_{i=1}^{n} \int_{V_{io}}^{V_i} \frac{f_{qi}(x_i)}{x_i} dx_i$$

$$W_{24}(V, \theta, \phi) = \sum_{i=1}^{m} [(E_i^2 + V_i^2 - 2E_i V_i \cos(\theta_i - \phi_i))$$

$$- (E_{io}^2 + V_{io}^2 - 2E_{io}V_{io}\cos(\theta_{io} - \phi_{io}))] \frac{1}{2x'_{di}}$$

$$W_{25}(V, \phi) = -\frac{1}{2}\sum_{i=1}^{n}\sum_{j=1}^{n} B_{ij}(V_i V_j \cos\phi_{ij} - V_{io}V_{jo}\cos\phi_{ijo})$$

W_1 is termed as kinetic energy and W_2 as potential energy. It can be proved by direct verification, that the system energy is constant along the post-fault trajectory.

Proof
Taking partial derivatives of W with respect to V_i, ϕ_i, t, θ_i and ω_i respectively, one can show

$$\frac{\partial W}{\partial V_i} = \frac{1}{V_i}(Q_{li} + Q_i) = 0 \text{ from Eq. (13.32)} \tag{13.34}$$

$$\frac{\partial W}{\partial \phi_i} = -\frac{E_i V_i \sin(\theta_i - \phi_i)}{x'_{di}} + \sum_{j=1}^{n} B_{ij}V_j V_i \sin\phi_{ij}, \quad i = 1, 2, ..m$$

$$= \sum_{j=1}^{n} B_{ij}V_i V_j \sin\phi_{ij}, \quad i = (m+1), ...n$$

$$= P_i \tag{13.35}$$

$$\frac{\partial W}{\partial t} = \sum_{i=1}^{n} P_{li}\frac{d\phi_i}{dt} \tag{13.36}$$

$$\frac{\partial W}{\partial \theta_i} = -P_{mi} + P_{ei} \text{ and}$$

$$\frac{\partial W}{\partial \omega_i} = M_i \omega_i \tag{13.37}$$

Using Eq. (13.31), we have

$$\sum_{i=1}^{n} \frac{\partial W_i}{\partial \phi_i}\frac{d\phi_i}{dt} + \frac{\partial W}{\partial t} = \sum_{i=1}^{n} (P_{li} + P_i)\frac{d\phi_i}{dt} = 0 \tag{13.38}$$

and using Eq. (13.26), we get

$$\sum_{i=1}^{m} \left(\frac{\partial W}{\partial \omega_i}\frac{d\omega_i}{dt} + \frac{\partial W}{\partial \theta_i}\frac{d\theta_i}{dt} \right) = \sum_{i=1}^{m} (M_i \dot{\omega}_i - P_{mi} + P_{ei})\omega_i$$

$$= \sum_{i=1}^{m} \frac{M_i}{M_T}P_{COI}\omega_i = 0 \tag{13.39}$$

Hence, from Eqs. 13.34, 13.38 and 13.39, we get

$$\frac{dW}{dt} = \sum_{i=1}^{m} \left[\frac{\partial W}{\partial \omega_i} \frac{d\omega_i}{dt} + \frac{\partial W_i}{\partial \theta_i} \frac{d\theta_i}{dt} \right] + \sum_{i=1}^{n} \left[\frac{\partial W}{\partial V_i} \frac{dV_i}{dt} \right]$$
$$+ \left[\sum_{i=1}^{n} \left(\frac{\partial W}{\partial \phi_i} \frac{d\phi_i}{dt} \right) + \frac{\partial W}{\partial t} \right] = 0 \qquad (13.40)$$

This shows that the total energy of the system is conserved.

Remarks

1. It is assumed that the system models are well defined in the sense that the voltages at the load buses can be solved in a continuous manner at any given time during the transient. This implies that the system trajectories are smooth and there are no jumps in the energy function.

2. Consider the term W_{22}. For constant P_{li}, the integral can be expressed as a path independent term given by

$$W_{22} = \int_{t_o}^{t} P_{li} \frac{d\phi_i}{dt} dt = P_{li}(\phi_i - \phi_{io}) \qquad (13.41)$$

   If P_{li} is not a constant, then W_{22} has to be integrated numerically. Using trapezoidal rule of integration

$$W_{22}(t + h) = W_{22}(t) + \frac{1}{2}[P_{li}(t) + P_{li}(t + h)][\phi_i(t + h) - \phi_i(t)] \qquad (13.42)$$

3. The terms W_{24} and W_{25} represent the energy in the machine reactances and transmission line reactances. It can be shown that this energy can be expressed as half the sum of reactive power loss in each element of the network (including machine reactances). Thus,

$$W_{24} + W_{25} = \sum_{k=1}^{n_l} \frac{1}{2} Q_k = \frac{1}{2} [\sum_{i=1}^{m} Q_{gi} - \sum_{j=1}^{n} Q_{lj}] \qquad (13.43)$$

   where Q_{gi} is the reactive power output (at the internal bus) of generator i, n_l is the total number of elements in the network (including machine reactances).

   The R.H.S. of Eq. (13.43) is easily calculated at the end of power flow solution at each step, during the transient. Also, the overall energy function computations are simplified.

Note that the energy component W_{23} is path independent as the integral can be obtained as function of bus voltage V_i. For example, if

$$Q_{li} = b_o + b_1 V + b_2 V^2$$

then,

$$\int_{V_{io}}^{V_i} \frac{Q_{li}}{V_i} dV_i = b_o \ln \frac{V_i}{V_{io}} + b_1 (V_i - V_{io}) + \frac{b_2}{2} (V_i^2 - V_{io}^2)$$

where ln indicates natural logarithm.

13.5 Structure-Preserving Energy Function with Detailed Generator Models

In the previous section, a SPEF was formulated for systems with classical models for generators. Simplified (classical) generator models are acceptable only if the transient stability could be determined within the time frame of less than a second (before AVR can respond). However, for large systems with low frequency interarea modes of oscillations, this premise is not correct. Hence, it becomes necessary to look for the formulation of energy function with more detailed generator models. In what follows, an energy function is presented and derived for machine model (1.1) including AVR. The presence of AVR contributes a component of energy which is path dependent.

A Structure-Preserving Energy Function

Consider the following function defined for the post fault system

$$W(\theta, \omega, E_q', E_d', V, \phi, t) = W_1(\omega) + \sum_{i=1}^{11} W_{2i} \qquad (13.44)$$

where

$$W_1(\omega) = \frac{1}{2} \sum_{i=1}^{m} M_i \omega_i^2$$

$$W_{21}(\theta) = - \sum_{i=1}^{m} T_{mi} (\theta_i - \theta_{io})$$

$$W_{22}(t) = \sum_{i=1}^{n} \int_{t_o}^{t} f_{pi}(V_i) \frac{d\phi_i}{dt} dt$$

$$W_{23}(V) = \sum_{i=1}^{n} \int_{V_{io}}^{V_i} \frac{f_{qi}(x_i)}{x_i} dx_i$$

$$W_{24}(\theta, E_q', V, \phi) = \sum_{i=1}^{m}[E_{qi}'^2 + V_i^2 - 2E_{qi}'V_i\cos(\theta_i - \phi_i)$$

$$-(E_{qio}'^2 + V_{io}^2 - 2E_{qio}'V_{io}\cos(\theta_{io} - \phi_{io}))](\frac{1}{2x_{di}'})$$

$$W_{25}(V, \phi) = -\frac{1}{2}\sum_{i=1}^{n}\sum_{j=1}^{n}B_{ij}(V_iV_j\cos\phi_{ij} - V_{io}V_{jo}\cos\phi_{ijo})$$

$$W_{26}(\theta, V, \phi) = -\sum_{i=1}^{m}[V_i^2(\cos 2(\theta_i - \phi_i) - 1) - V_{io}^2(\cos 2(\theta_{io} - \phi_{io}) - 1)] \times$$

$$\frac{(x_{di}' - x_{qi}')}{4x_{di}'x_{qi}'}$$

$$W_{27}(\theta, E_d', V, \phi) = \sum_{i=1}^{m}[E_{di}'^2 + V_i^2 + 2E_{di}'V_i\sin(\theta_i - \phi_i) -$$

$$(E_{dio}'^2 + V_{io}^2 + 2E_{dio}'V_{io}\sin(\theta_{io} - \phi_{io}))]\left(\frac{1}{2x_{qi}'}\right)$$

$$W_{28}(V) = -\sum_{i=1}^{m}\frac{(V_i^2 - V_{io}^2)}{2x_{qi}'}$$

$$W_{29}(t) = -\sum_{i=1}^{m}\int_{t_o}^{t}\left[\frac{E_{fdi}}{(x_{di} - x_{di}')}\right]\frac{dE_{qi}'}{dt}dt$$

$$W_{210}(E_q') = \sum_{i=1}^{m}\left[\frac{(E_{qi}'^2 - E_{qio}'^2)}{2(x_{di} - x_{di}')}\right]$$

$$W_{211}(E_d') = \sum_{i=1}^{m}\left[\frac{(E_{di}'^2 - E_{dio}'^2)}{2(x_{qi} - x_{qi}')}\right]$$

The subscript '*o*' in the above expressions indicates quantities at initial equilibrium (operating point).

It can be proved that the time derivative of W is non-positive along the post-fault trajectory. That is

$$\frac{dW}{dt} = -\sum_{i=1}^{m}\left[\frac{T_{doi}'}{(x_{di} - x_{di}')}\left(\frac{dE_{qi}'}{dt}\right)^2 + \frac{T_{qoi}'}{(x_{qi} - x_{qi}')}\left(\frac{dE_{di}'}{dt}\right)^2\right] \qquad (13.45)$$

Proof
Partial differentiation of W_2 with respect to $E_{qi}', E_{di}', V_i, \phi_i, \theta_i$ and t yields the

following expressions after some algebraic manipulations.

$$\frac{\partial W_2}{\partial E'_{qi}} = -\frac{T'_{doi} \cdot \frac{dE'_{qi}}{dt}}{(x_{di} - x'_{di})} + \frac{E_{fdi}}{(x_{di} - x'_{di})} \tag{13.46}$$

$$\frac{\partial W_2}{\partial E'_{di}} = -\frac{T'_{qoi} \cdot \frac{dE'_{di}}{dt}}{(x_{qi} - x'_{qi})} \tag{13.47}$$

$$\frac{\partial W_2}{\partial V_i} = 0 \tag{13.48}$$

$$\frac{\partial W_2}{\partial \phi_i} = P_i \tag{13.49}$$

$$\frac{\partial W_2}{\partial \theta_i} = -P_{mi} + P_{ei} \tag{13.50}$$

$$\frac{\partial W_2}{\partial t} = \sum_{i=1}^{n} f_{pi}(V_i) \frac{d\phi_i}{dt} - \sum_{i=1}^{m} \frac{E_{fdi}}{(x_{di} - x'_{di})} \frac{dE'_{qi}}{dt} \tag{13.51}$$

Since

$$\frac{\partial W_1}{\partial \omega_i} = M_i \omega_i,$$

$$\frac{\partial W_1}{\partial \omega_i} \frac{d\omega_i}{dt} + \frac{\partial W_2}{\partial \theta_i} \frac{d\theta_i}{dt} = (M_i \dot{\omega}_i - P_{mi} + P_{ei})\omega_i$$

$$= -\frac{M_i \omega_i}{M_T} P_{COI} \tag{13.52}$$

Thus,

$$\sum_{i=1}^{m} \left(\frac{\partial W_1}{\partial \omega_i} \frac{d\omega_i}{dt} + \frac{\partial W_2}{\partial \theta_i} \frac{d\theta_i}{dt} \right) = -\sum_{i=1}^{m} \frac{M_i \omega_i}{M_T} P_{COI} = 0 \tag{13.53}$$

It can be shown using Eqs. (13.45) to (13.50) that

$$\frac{dW}{dt} = \sum_{i=1}^{m} \left(\frac{\partial W_1}{\partial \omega_i} \frac{d\omega_i}{dt} + \frac{\partial W_2}{\partial \theta_i} \frac{d\theta_i}{dt} \right) +$$

$$\sum_{i=1}^{n} \left[\left(\frac{\partial W_2}{\partial V_i} \frac{dV_i}{dt} \right) + \frac{\partial W_2}{\partial \phi_i} \frac{d\phi_i}{dt} \right] + \frac{\partial W}{\partial t} +$$

$$\sum_{i=1}^{m} \left[\frac{\partial W_2}{\partial E'_{qi}} \frac{dE'_q}{dt} + \frac{\partial W_2}{\partial E'_{di}} \frac{dE'_{di}}{dt} \right] = -\sum_{i=1}^{m} \left[\frac{T'_{doi}(\frac{dE'_{qi}}{dt})^2}{(x_{di} - x'_{di})} + \frac{T'_{qoi}(\frac{dE'_{di}}{dt})^2}{(x_{qi} - x'_{qi})} \right]$$

$$\tag{13.54}$$

Remarks

1. The first five terms in the potential energy (W_{21} to W_{25}) are the same as those defined in the previous section, except that in term W_{24}, E'_{qi} is replaced by E_i (for the classical model)

2. The term W_{26} accounts for transient saliency and is identically zero if $x'_d = x'_q$

3. The terms W_{27}, W_{28} and W_{211} arise due to the presence of the damper windings in the the quadrature axis. If this winding is neglected, then $E'_d = 0$ and

$$W_{27} + W_{28} = 0 = W_{211}$$

4. If $E_{fd} = $ constant (AVR is neglected), then

$$W_{29} = -\sum_{i=1}^{m} E_{fdi} \frac{(E'_{qi} - E'_{qio})}{(x_{di} - x'_{di})} \tag{13.55}$$

becomes a path-independent function of E'_q. If AVR is considered, then E_{fd} is variable and the terms W_{29} has to be computed by numerical integration. Using trapezoidal rule, we have

$$W_{29}(t + h) = W_{29}(t) - \frac{1}{2} \sum_{i=1}^{m} [E_{fdi}(t + h) + E_{fdi}(t)] \cdot \frac{[E'_{qi}(t + h) - E'_{qi}(t)]}{(x_{di} - x'_{di})}$$

Note that any type of excitation system can be considered as E_{fdi} is treated as a variable parameter in the energy function.

5. If E_{fd} and the active load P_l are constants then the energy function defined is a general (global) Liapunov function having the properties stated in section 13.2

6. The governor and prime mover dynamics have generally minor effects on the first swing stability. However if these effects are included, the mechanical power (torque) will be time-varying and the term W_{21} is modified to

$$W'_{21} = -\sum_{i=1}^{m} \int_{t_o}^{t} T_{mi}(t) \left(\frac{d\theta_i}{dt} \right) dt \tag{13.56}$$

A Simpler Expression for SPEF

For the analysis of first swing stability, it is convenient to introduce two extra (path-dependent) terms in the potential energy such that the total energy

W remains constant along the post-fault trajectory. Thus a modified energy function, defined below, is introduced

$$W' = W_1 + W'_2 = W_1(\omega) + \sum_{i=1}^{13} W_{2i} \qquad (13.57)$$

where

$$W_{212} = \sum_{i=1}^{m} \int_{t_o}^{t} [T'_{doi}/(x_{di} - x'_{di})] \left(\frac{dE'_{qi}}{dt} \right)^2 dt$$

$$W_{213} = \sum_{i=1}^{m} \int_{t_o}^{t} [T'_{qoi}/(x_{qi} - x'_{qi})] \left(\frac{dE'_{di}}{dt} \right)^2 dt$$

Although the number of terms are increased by two, some simplifications are possible by grouping the terms. It can be shown that

$$(1) \quad W_{24} + W_{25} + W_{26} + W_{27} + W_{28} = \tfrac{1}{2} \sum_{k=1}^{n_l} (Q_k - Q_{ko}) = W'_{24} \qquad (13.58)$$

$$(2) \quad W_{29} + W_{210} + W_{212} = \sum_{i=1}^{m} \int_{t_o}^{t} i_{di} \left(\frac{dE'_{qi}}{dt} \right) dt = W'_{25} \qquad (13.59)$$

$$(3) \quad W_{211} + W_{213} = -\sum_{i=1}^{m} \int_{t_o}^{t} i_{qi} \left(\frac{dE'_{di}}{dt} \right) dt = W'_{26} \qquad (13.60)$$

Thus, a simpler expression for the energy function is obtained as

$$W' = W_1(\omega) + W_{21} + W_{22} + W_{23} + W'_{24} + W'_{25} + W'_{26} \qquad (13.61)$$

where W'_{24}, W'_{25} and W'_{26} are defined above. Note that for the classical model, both W'_{25} and W'_{26} are zero. For one-axis model, $W'_{26} = 0$.

It is to be noted that W'_{25} accounts for both the field coil and effects of AVR, while W'_{26} accounts for the damper winding on the q-axis. The term W'_{24} accounts for the energy stored in all the reactances including the transient reactances of the machine. With transient saliency considered, the energy stored in the machine reactances is given by

$$\frac{1}{2}(x'_d i_d^2 + x'_q i_q^2)$$

If $x'_d = x'_q = x'$, then this component reduces to $\frac{1}{2} x' I_a^2$ where $I_a^2 = i_d^2 + i_q^2$

The expression for SPEF given in this and the previous section have considered the datum (reference) at the value corresponding to the initial (pre-fault) operating point. There is no loss of generality in doing so as the critical

value of W will also change appropriately. To explain this, consider the stability criterion

$$W(t = t_c) \le W_{cr} \qquad (13.62)$$

where W is defined as

$$W(x) = W^*(x) - W^*(x_s) \qquad (13.63)$$

such that, $W(x_s) = 0$ and W_{cr} is the value of W computed at the controlling UEP.

Let

$$\begin{aligned} W'(x) &= W^*(x) - W^*(x_I) \quad \text{and} \\ W'_{cr} &= W_{cr} + W^*(x_s) - W^*(x_I) \end{aligned}$$

then the stability criterion of (13.6) is transformed to

$$W'(t = t_c) \le W'_{cr} \qquad (13.64)$$

(Note that W^* denotes the energy expression involving only x). W'_{cr} is the value of W' evaluated at the controlling UEP.

If there are no path-dependent terms in the energy expressions, there is no difference between the use of stability criterion (13.62) or (13.64). However, whenever path-dependent terms are present, it is convenient (and accurate) to use (13.64) rather than (13.62), particularly when W_{cr} is determined from the PEBS (Potential Energy Boundary Surface) method described in the next section.

13.6   Determination of Stability Boundary

For all practical purposes, the determination of stability boundary for a particular fault is equivalent to determining W_{cr} (the critical energy) for that fault. The critical energy can be determined from computing

  a) Controlling UEP

  b) Potential Energy Boundary Surface

It will be assumed, for simplicity, that the generators are represented by classical models. However, the analysis can be extended for more complex models.

13.6.1   Controlling UEP

In this method, the critical energy is determined as

$$W_{cr} = W(x_u^*) = W_2(\delta_u^*) \tag{13.65}$$

where x_u^* is the type 1 UEP lying on the stability boundary and whose stable manifold is intersected by the fault-on trajectory. As the rotor velocity deviation, ω, is zero at any equilibrium point, the critical energy is the same as potential energy W_2 evaluated at the value δ_u^* corresponding to the controlling UEP.

The determination of controlling UEP can be complex. There are several approaches to the determination of controlling UEP. Two prominent approaches which have been applied for large systems are

1. Mode of Disturbance (MOD) or Instability (MOI) [9]

2. BCU (Boundary Controlling UEP) method. (Also termed as exit point method) [27]

The second approach is related to PEBS method.

Mode of Disturbance Method

This method relies on the approximate determination of candidate UEPs first. For a given mode of instability (determined by machines having advanced angles) the approximate UEP is given by

$$\left. \begin{array}{rl} \theta_i^u & = \; \theta_i^s \text{ if } i \notin I \\ & = \; \pi - \theta_i^s \text{ if } i \in I \end{array} \right\} \tag{13.66}$$

where I is the set of generators with advanced rotor angles. θ_i^s is the angle of ith generator at SEP.

It is necessary to correct the approximate UEP given in (13.65) to account for the constraint

$$\sum M_i \theta_i^u = 0$$

Hence the determination of approximate θ^u is modified as follows

(i) Indentify two groups according to the chosen mode of instability
    Group I: Advanced generators
    Group II: Rest of the generators

(ii) Compute

$$\theta_I^s = \frac{1}{M_I} \sum_{i \in I} M_i \theta_i^s, \quad M_I = \sum_{i \in I} M_i$$

$$\theta_{II}^s = \frac{1}{M_{II}} \sum_{i \in II} M_i \theta_i^s, \quad M_{II} = \sum_{i \in II} M_i$$

$$\theta_{I-II}^s = \theta_I^s - \theta_{II}^s$$

(iii) Compute

$$\Delta\theta_I = (\pi - 2\theta_{I-II}^s)\frac{M_{II}}{M_I + M_{II}}$$

$$\Delta\theta_{II} = (\pi - 2\theta_{I-II}^s)\frac{M_I}{M_I + M_{II}}$$

(vi) Calculate

$$\theta_i^u = \theta_i^s + \Delta\theta_I \text{ for } i \in I$$

$$\theta_i^u = \theta_i^s + \Delta\theta_{II} \text{ for } i \in II$$

Selection Among Approximate UEPs

This is based on the assumption that the controlling UEP is closest to the trajectory at the time of fault clearing. The distance to UEP is measured in terms of the normalized potential energy margin defined by

$$\Delta V_{PEm} = \frac{\Delta W_{PE}}{W_{KE}\,|_{corr}} = \frac{W_{PE}^u - W_{PE}^c}{W_{KE}\,|_{corr}} \tag{13.67}$$

where W_{PE}^u is the potential energy evaluated at a candidate UEP and W_{PE}^c is the potential energy evaluated at the instant of clearing of the fault. The kinetic energy W_{KE} is corrected to account for only that component of kinetic energy that leads to system seperation. Thus

$$W_{KE}\,|_{corr} = \frac{1}{2}M_{eq}(\omega_{eq}^c)^2 \tag{13.68}$$

where

$$M_{eq} = \frac{M_I M_{II}}{M_I + M_{II}}, \quad \omega_{eq}^c = \omega_I - \omega_{II}$$

$$\omega_I = \frac{1}{M_I} \sum_{i \in I} M_i \omega_i^c, \quad \omega_{II} = \frac{1}{M_{II}} \sum_{i \in II} M_i \omega_i^c$$

The superscript c indicates the value computed at the clearing time.

Computation of UEP

The selection of the approximate UEP (among the candidates) is used to determine the starting point for the determination of the exact UEP which is found from the solution of the nonlinear equations given by

$$f_i(\theta_i) = P_{mi} - P_{ei} - \frac{M_i}{M_T} P_{COI} = 0 \qquad (13.69)$$

These equations can be solved directly using Newton-Raphson method. The starting point is determined as a point along the ray connecting the SEP θ^s, to the approximate UEP $\hat{\theta}^u$ at which the potential energy is maximum (the point lying on PEBS). Note that $\hat{\theta}^u$ is selected from among the candidate UEPs and has the minimum normalised potential energy margin.

Instead of solving Eq. (13.69) directly, the exact UEP can also be determined by formulating a nonlinear least squares minimization problem with the objective function defined as

$$F(\theta) = \sum_{i=1}^{m} f_i^2(\theta) \qquad (13.70)$$

where m is the number of generators.

The minimization can be carried out using

a) Davidon-Fletcher-Powell (DFP) algorithm or

b) Gauss-Newton technique

BCU Method

BCU stands for Boundary of stability region based Controlling Unstable equilibrium point. This method is based on the relationship between the stability boundary of the (post-fault) classical power system model and the stability boundary of the following (post-fault) reduced system model defined as

$$\dot{\theta}_i = f_i(\theta) = P_{mi} - P_{ei} - \frac{M_i}{M_T} P_{COI} \qquad (13.71)$$

The state variables of this reduced system are rotor angles only with dimension of $(m-1)$ while the dimensions of the original system is $2(m-1)$. It is easy to see that if $\hat{\theta}$ is an equilibrium point of (13.71) then $(\hat{\theta}, 0)$ is an equilibrium point of the original system. Under the condition of small transfer conductances, it can be shown that

(i) $(\hat{\theta}_s)$ is a SEP of the reduced system if and only if $(\hat{\theta}_s, 0)$ is a SEP of the original system.

(ii) $(\hat{\theta}_u)$ is a type-k equilibrium point of the reduced system if and only if $(\hat{\theta}_u, 0)$ is a type-k equilibrium point of the original system.

(iii) If the one-parameter transversality condition is satisfied, then $(\hat{\theta})$ is on the stability boundary $\partial A(\hat{\theta}_s)$ of the reduced system if and only if $(\hat{\theta}, 0)$ is on the stability boundary $\partial A(\hat{\theta}_s, 0)$ of the original system.

The above results establish a relationship between the stability boundary $\partial A(\hat{\theta}_s)$ and the stability boundary $\partial A(\hat{\theta}_s, 0)$ and suggest a method of finding the controlling UEP of the original system via the location of controlling UEP of the reduced system.

One version of the BCU method involves the following steps for the determination of the controlling UEP

STEP 1: From the fault-on trajectory, detect the exit point θ^* which is the point where the projected trajectory $\theta(t)$ exits the stability boundary of the reduced system. This exit point corresponds to the point at which the first local maximum of the potential energy W_{PE} is reached.

STEP 2: Use the point θ^* as the initial condition and integrate the post-fault reduced system of (13.71) to find the first local minimum of

$$\sum_{i=1}^{m} \| f_i(\theta) \|, \text{ say at } \theta_o^*$$

STEP 3: Use the point θ_o^* as the initial guess to solve

$$\sum_{i=1}^{n} \| f_i(\theta) \| = 0, \text{ say at } \theta_{co}^*$$

The controlling UEP of the original system is given by $x_u^* = (\theta_{co}^*, 0)$.

The reduced system equations may be stiff and suitable integration method has to be used in Step 2.

Recent tests on realistic systems indicate that MOD method is not always reliable. In comparison, the BCU method, when properly tuned to the system, provides a good compromise in reliability and computational speed.

13.6.2 PEBS (Potential Energy Boundary Surface)

It is possible to express the differential equations for the conservative system as

$$\left. \begin{array}{rcl} \dot{\theta} & = & \omega \\ M_i \dot{\omega}_i & = & -\dfrac{\partial W_{PE}}{\partial \delta_i} \end{array} \right\} \tag{13.72}$$

For a single machine system, the variation of potential energy with the rotor angle δ is shown in Fig. 13.7 (b). It is assumed that the stability region extends from $\delta'_u < \delta < \delta_u$ (not always true !) and the potential energy reaches local maximum at the boundary (δ'_u and δ_u).

(Note: δ_u is the controlling UEP most of the time and always lies on the stability boundary. δ'_u does not always lie on the stability boundary).

It is conjectured that even for multimachine systems, the stability region is inside a potential bowl. In other words, at the stability boundary, W_{PE} reaches a local maximum.

The Potential Energy Boundary Surface (PEBS) is made up of surfaces in the angle space which contain UEPs that lie on the stability boundary. It is characterized by the fact that at any point on the PEBS, the directional derivative of W_{PE} is zero along the direction of the normal (perpendicular) to PEBS. This implies that if the projected trajectory intersects PEBS orthogonally, then the potential energy reaches a local maximum at the intersection point. An example of a PEBS for a 3 machine system in the two dimensional space of θ_1 and θ_2 is shown in Fig. 13.9 [21].

PEBS is also viewed as the rim of the potential bowl at the bottom of which lies the SEP (of the post-fault system). A point on PEBS satisfies the following equation

$$\sum_{i=1}^{m} g_i(\theta) f_i(\theta) = 0 \tag{13.73}$$

where $g_i(\theta)$ is the ith component of the normal to PEBS at the point θ on it.

There is some ambiguity in the way PEBS is defined by different authors. Athay *et al* [20] use the following equation to characterize PEBS

$$\sum_{i=1}^{m} f_i(\theta)(\theta_i - \theta_i^s) = 0 \tag{13.74}$$

This is a particular case of the Eq. (13.73).
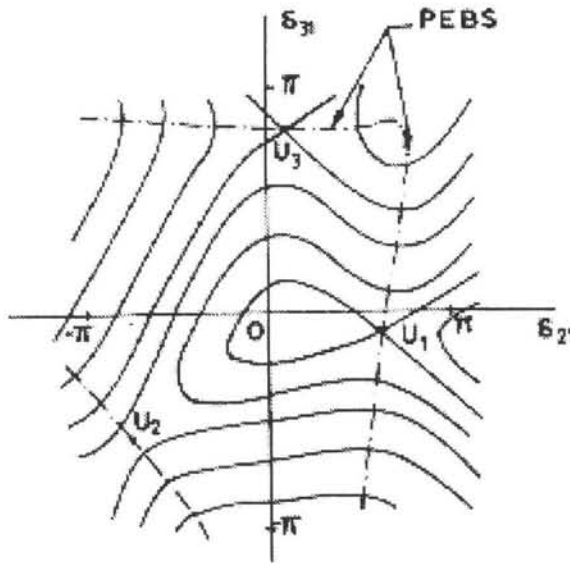
Figure 13.9: Equipotential curves for a 3-machine system and PEBS[21]

The advantage of PEBS as originally defined by Kakimoto *et al* [21] is that a simple procedure for the computation of stability boundary can be given. The computation of the critical clearing time is given below

Step 1 Integrate the fault-on trajectory until W_{PE} reaches a local maximum. This value is an estimate of the true W_{cr}.

Step 2 From the fault-on trajectory, determine the instant when $W = W_{cr}$. This is the CCT (Critical Clearing Time, t_{cr}). Fig. 13.10 shows this graphically.

It is meaningful to view PEBS as the stability boundary of a reduced gradient system (in the angle space only) given by

$$\dot{\theta}_i = f_i(\theta) = -\frac{\partial W_{PE}}{\partial \theta_i} \tag{13.75}$$

Chiang *et al* [25] show that the PEBS defined as the stability boundary of the reduced dynamical system is consistent with the geometric construction procedure suggested in the paper by Kakimoto *et al* [21]. This is in view of the fact that the stability boundary for (13.75) is given by

$$\partial A(\theta^s) = \bigcup_i M^s(\theta^i) \tag{13.76}$$
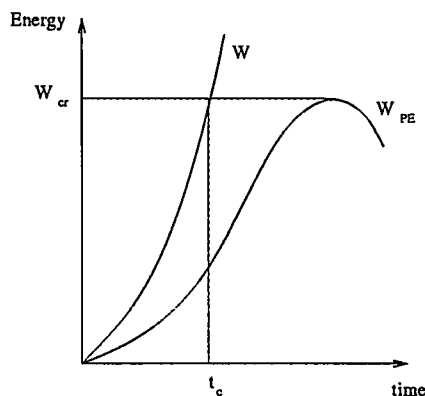
Figure 13.10: Determination of t_{cr} using PEBS
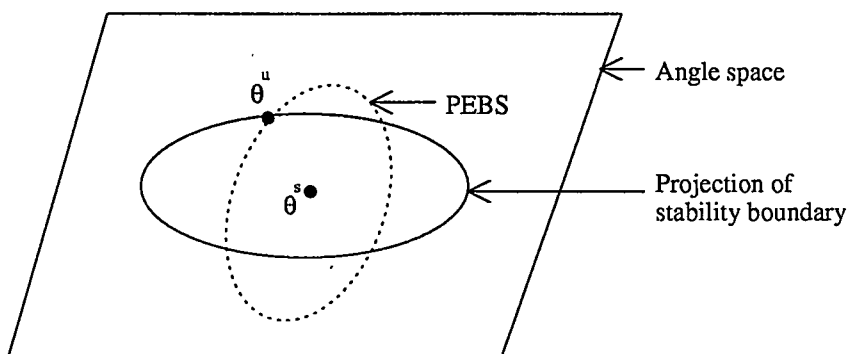
Figure 13.11: Relationship between PEBS and projection of the stability boundary

where θ^i is the type 1 UEP lying on the stability boundary and M^s indicates the stable manifold of θ^i. It is easy to see that PEBS defined above intersects the level surface $W_{PE}(\theta) = C$, orthogonally as the vector field is orthogonal to the level surface.

However, PEBS is not identical to the projection of the stability boundary of the original system in the subspace characterized by $\omega = 0$. The PEBS intersects the projection of the stability boundary of the original system at the UEPs that lie on the stability boundary (see Fig. 13.11).

An important result given in [25] is stated below.

Theorem: Let $(\theta^u, 0)$ be a UEP on the stability boundary $\partial A(\theta_s, 0)$ of the original system. Then the connected constant energy surface $\partial W(\theta^u, 0)$ intersects

the stable manifold $M^s(\theta^u, 0)$ only at the point $(\theta^u, 0)$; moreover the connected component of the set $W(\theta, \omega) < W(\theta^u, 0)$ does not contain any point which belongs to the stable manifold $M^s(\theta^u, 0)$.

The graphical illustration of this theorem is shown in Fig. 13.12 .
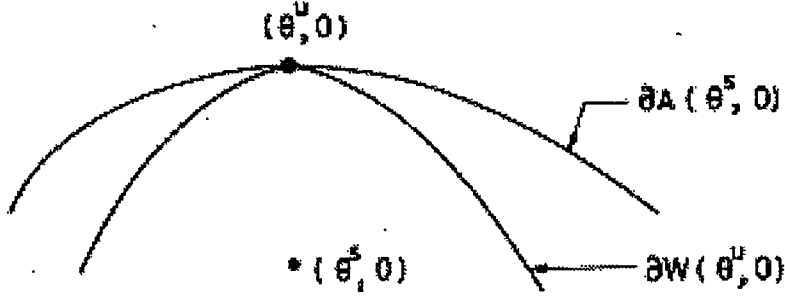
Figure 13.12: Illustration of the theorem

Chiang *et al* [25] also show the PEBS method can give either optimistic or slightly pessimistic results depending upon the point of intersection of the fault-on trajectory with the PEBS. They propose a modified PEBS method as follows:

Step 1: From the fault-on trajectory, detect the point θ^* at which the projected trajectory $\theta(t)$ crosses the PEBS.

Step 2: Find the equilibrium point of the system whose stable manifold contains the point θ^*, say θ^u. The value of $W_{PE}(\theta^u)$ is the critical energy W_{cr}.

Note that in the original PEBS method, $W_{cr} = W_{PE}(\theta^*)$. This modification is the basis of the BCU method described earlier. The calculation of θ^u is implemented using the procedure given below

(i) Use the point θ^* as the initial condition and integrate the post-fault gradient system (13.74) until the local minimum of $\frac{\partial W_{PE}}{\partial \theta}$ is achieved, say at θ^o.

(ii) Find the equilibrium point of the post-fault gradient system using θ^o as the initial guess. The solution is the required θ^u. This procedure is illustrated in Fig. 13.13. The computed exit point (PEBS crossing) is θ^* while the correct PEBS crossing is θ^e. If $\theta^* \simeq \theta^e$ then $\theta^o \simeq \theta^u$.
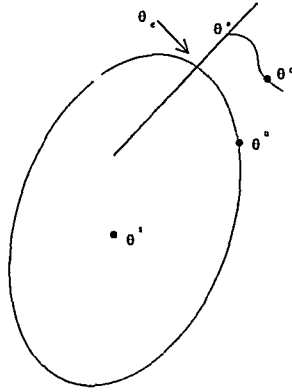
Figure 13.13: Illustration of BCU method

13.7 Extended Equal Area Criterion (EEAC)

A simple, yet reasonably reliable approach for direct stability evaluation is suggested in [43,44]. This is based on the conjecture that "the loss of synchronism of a multimachine system, whenever it occurs, is triggered off by the machine's irrevocable separation into two groups; hence, the idea of subdividing the system machines into the 'critical group', generally comprising a few machines, and the remaining group, comprising the majority of machines". This conjecture is supported by theoretical analysis of Chiang *et al* [10] where it is shown that the controlling UEP lying on the stability boundary is usually of type 1.

Based on the conjecture, it is further assumed that the system stability can be assessed by replacing of the machines of each group by an equivalent and finally the two equivalent machines replaced by a SMIB system. The equal area criterion is then applied to this SMIB system for stability assessment.

The formulation of EEAC method is given below. The generators are represented by classical models and loads by constant impedances. There is no need for the use of COI reference frame.

13.7.1 Formulation

The machine equations are given by

$$M_i \frac{d^2 \delta_i}{dt^2} = P_{mi} - P_{ei} \qquad (13.77)$$

where

$$P_{ei} = E_i^2 Y_{ii} \cos \beta_{ii} + \sum_{j=1, j \neq i}^{m} E_i E_j Y_{ij} \cos(\delta_i - \delta_j - \beta_{ij}) \tag{13.78}$$

$Y_{ij} \angle \beta_{ij}$ is the ij^{th} element of the reduced admittance matrix $[Y]$. The other symbols are as defined earlier.

Denoting S to be the set of critical machines and A, the set of remaining machines, we assume that

$$\delta_k = \delta_s \quad \forall \ k \in S, \qquad \delta_l = \delta_a \quad \forall \ l \in A \tag{13.79}$$

Based on (13.78), we can derive two swing equations for the two equivalent machines representing the two groups S and A. These are,

$$M_s \ddot{\delta}_s = \sum_{k \in S}(P_{mk} - P_{ek}), \quad M_a \ddot{\delta}_a = \sum_{l \in A}(P_{ml} - P_{el}) \tag{13.80}$$

where

$$M_s = \sum_{k \in S} M_k, \qquad M_a = \sum_{l \in A} M_l$$

Finally, setting

$$\delta = \delta_s - \delta_a \tag{13.81}$$

and using Eq. (13.80), we can derive

$$M \ddot{\delta} = P_m - [P_c + P_{max} \sin(\delta - \alpha)] = P_m - P_e \tag{13.82}$$

13.7.2   Approximation of Faulted Trajectory

The use of Taylor series helps to compute critical time based on critical clearing angle, without having to integrate faulted system equations.

Taylor series contains only even derivatives of δ. Truncating the series after t^4 term, yields

$$\delta = \delta_o + \frac{1}{2}\gamma t^2 + \frac{1}{24}\ddot{\gamma} t^4 \tag{13.83}$$

where γ denotes the second order derivative of δ at $t = 0^+$ (immediately after the fault) and $\ddot{\gamma}$ its fourth derivative also at $t = 0^+$.

Athay *et al* [20] have proposed an alternative approximation of faulted trajectory (although not in the context of EEAC). They assume that during the fault, the swing equation can be approximated as

$$M \ddot{\delta} = f \doteq a + b \cos \eta t \tag{13.84}$$

where the constants a, b and η can be determined from initial conditions.

13.7.3   Identification of Critical Cluster

The procedure for the identification of the critical cluster is given below

1. Draw up a list of candidate critical machines.
   This can be done using initial acceleration criterion which consists of
   a)classification of machines in a decreasing order of their initial accelera-
   tions and b) selection of machines which have accelerations close to that
   of the top machine.

2. Consider candidate critical clusters composed of one, two ... machines and
   obtained by successively combining the candidate critical machines.

3. Compute the corresponding candidate CCT: The smallest one is the actual
   CCT; the actual critical cluster is precisely that which furnishes the CCT.

The reliable identification of critical clusters is not a simple task and improve-
ments in the above procedure have been suggested [45].

13.8   Case Studies

Two case studies, one each on the 17 generator IEEE transient stability test
system and the 10 generator New England system are presented in this section.
Structure preserving energy function (SPEF) is used and the critical energy
determined from PEBS method. Several disturbances are considered, in some
of which, the prefault and postfault network configurations are same. Both
classical and detailed machine representations are included.

13.8.1   17 Generator System

All the machines are represented by classical models and loads are modelled
as constant impedances. The disturbances considered are three phase faults at
different buses followed by line clearing. The critical energy is computed by
PEBS method which is obtained as the peak of the potential energy during
fault-on trajectory. (The energy is calculated for the postfault system).

The comparison of critical clearing times obtained by prediction and simulation
are given in Table 13.1 for 15 different disturbances. For faults at bus #15
and bus #131, the postfault network is assumed to be same as the prefault
network. It is interesting to observe that for all the disturbances considered, the
predicted critical clearing times are in very good agreement with those obtained
from simulation. Thus, the use of PEBS method with SPEF gives accurate
results.

Table 13.1   17 Generator System: t_{cr} and W_{cr}

| Sl. No. | Fault bus # | Line Cleared (from bus # to bus #) | Critical clearing time | | W_{cr} |
			Prediction t_{cr}	Simulation t_{cr}	
1.	75	75–9	0.34–0.35	0.35–0.36	25.43
2.	95	95–97	0.30–0.31	0.30–0.31	7.11
3.	52	52–79	0.34–0.35	0.35–0.36	8.46
4.	93	93–91	0.24–0.25	0.24–0.25	9.66
5.	110	110–141	0.27–0.28	0.26–0.27	14.02
6.	15	15–11	0.25–0.26	0.25–0.26	17.72
7.	1	1–2	0.21–0.22	0.21–0.22	18.39
8.	124	124–109	0.34–0.35	0.36–0.37	40.98
9.	112	112–120	0.19–0.20	0.20–0.21	14.52
10.	70	70–149	0.23–0.24	0.23–0.24	13.61
11.	126	126–127	0.25–0.26	0.26–0.27	68.72
12.	130	75–130	0.30–0.31	0.30–0.31	11.29
13.	27	27–25	0.35–0.36	0.35–0.36	72.58
14.	15	—	0.21–0.22	0.22–0.23	12.69
15.	131	—	0.25–0.26	0.25–0.26	20.80

For the fault at bus #75, the variations of total (W), kinetic (W_1) and potential (W_2) energies with time are shown in Fig. 13.14. Both stable and unstable cases are considered. It is interesting to observe that while W is approximately constant (as expected) after the fault is cleared, the kinetic energy W_1 continues to increase when the system is unstable. The increase in W_1 is not monotonic but superimposed with oscillatory component. The variation in potential energy, W_2 are of similar nature except that W_2 continues to decrease. If transmission line resistances (which are included in this example) are neglected, W would be exactly constant after the fault is cleared.

The variations of the components of the potential energy are shown in Fig. 13.15. These components are defined as

$$W_{21} = -\sum_{i=1}^{m} T_{mi}(\theta_i - \theta_{io})$$

$$W_{22} = \sum_{i=1}^{n} \int_{t_o}^{t} P_{li}(V_i)\frac{d\phi_i}{dt}dt$$
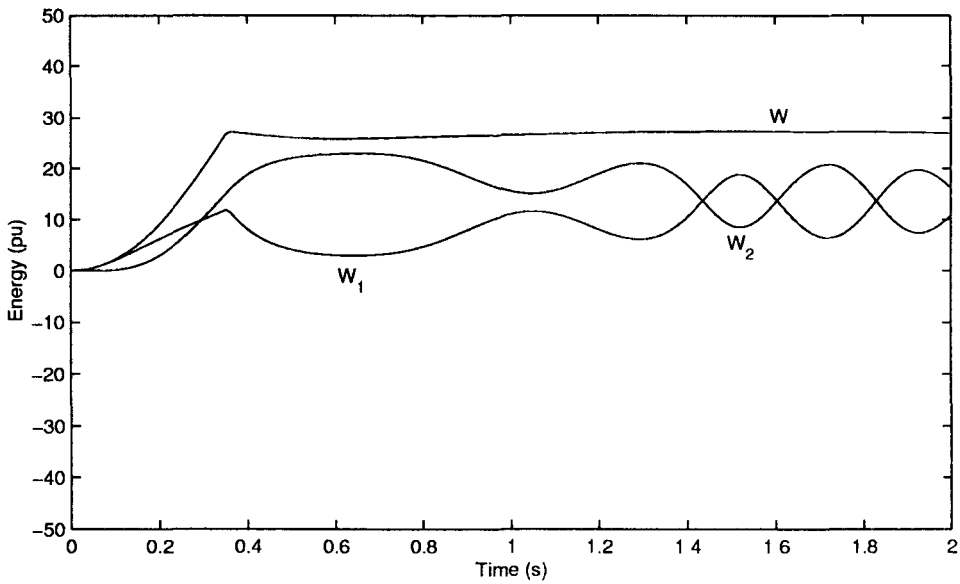
(a) Stable (t_{cl} = 0 354 s)
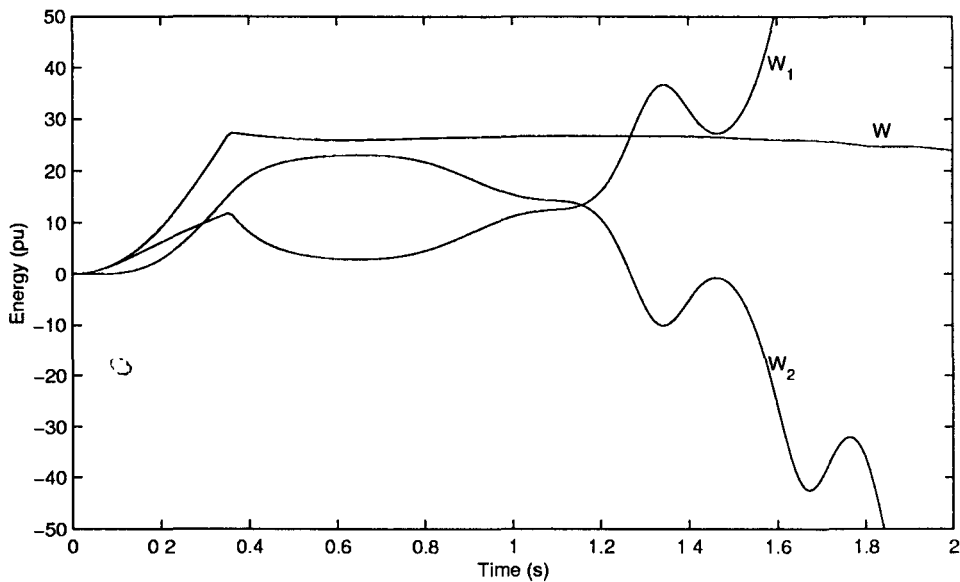
(b) Unstable (t_{cl} = 0.355 s)

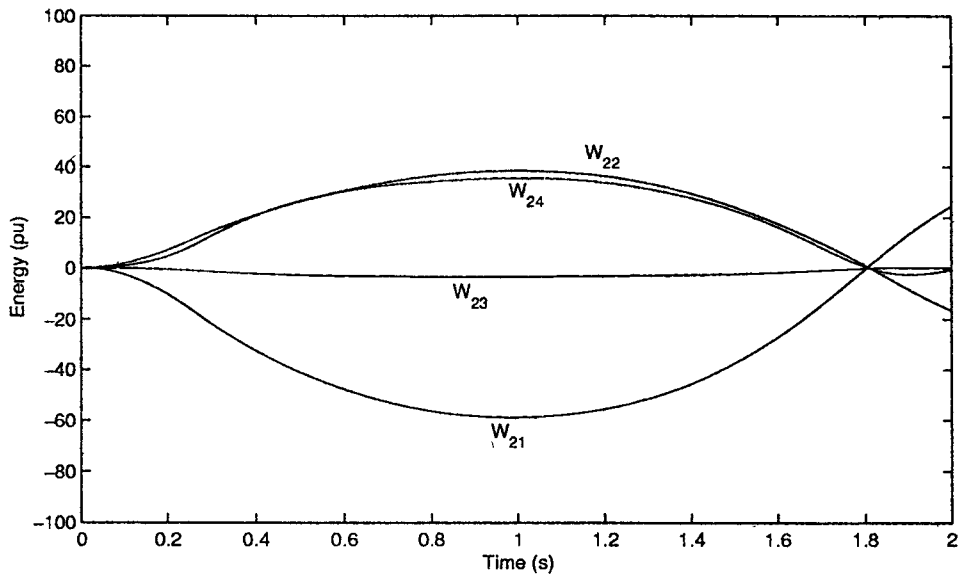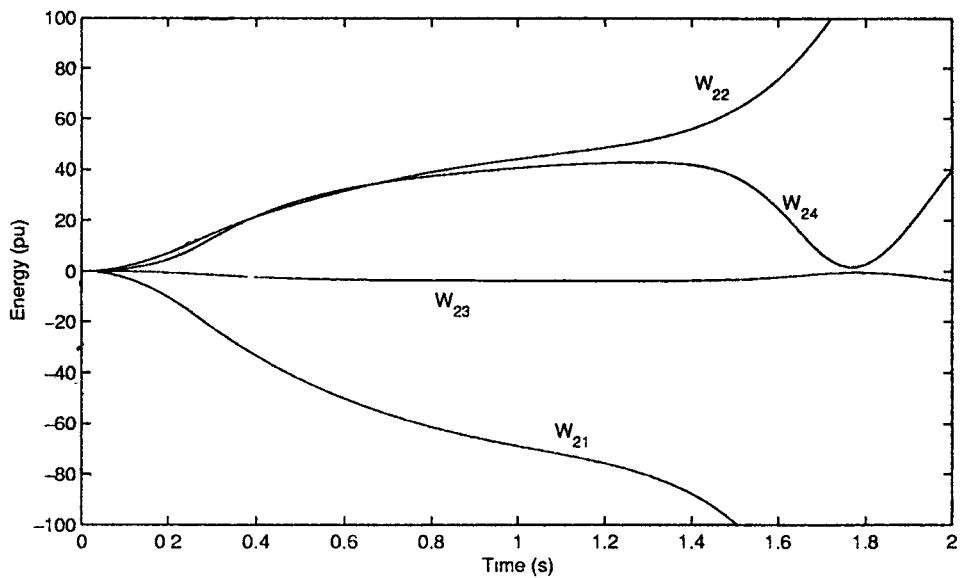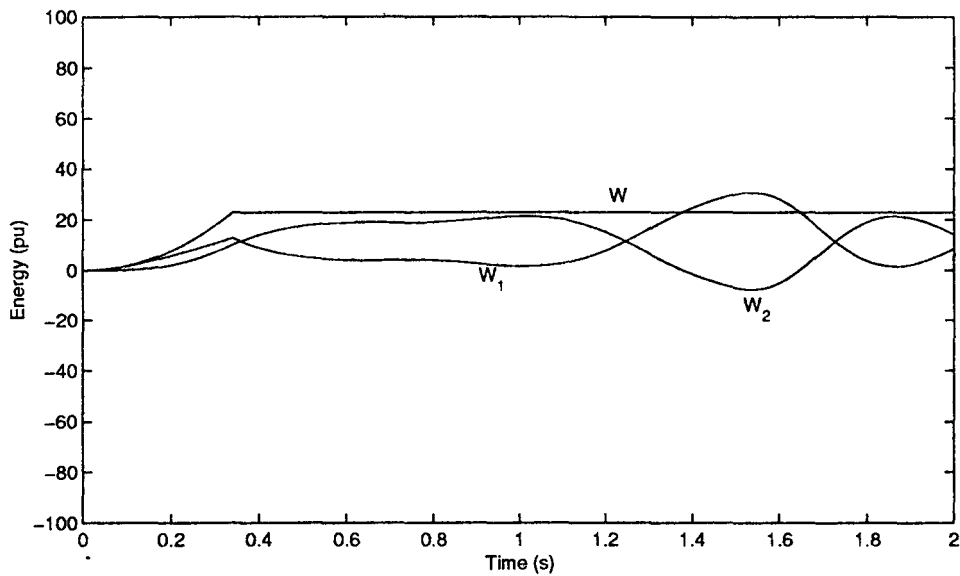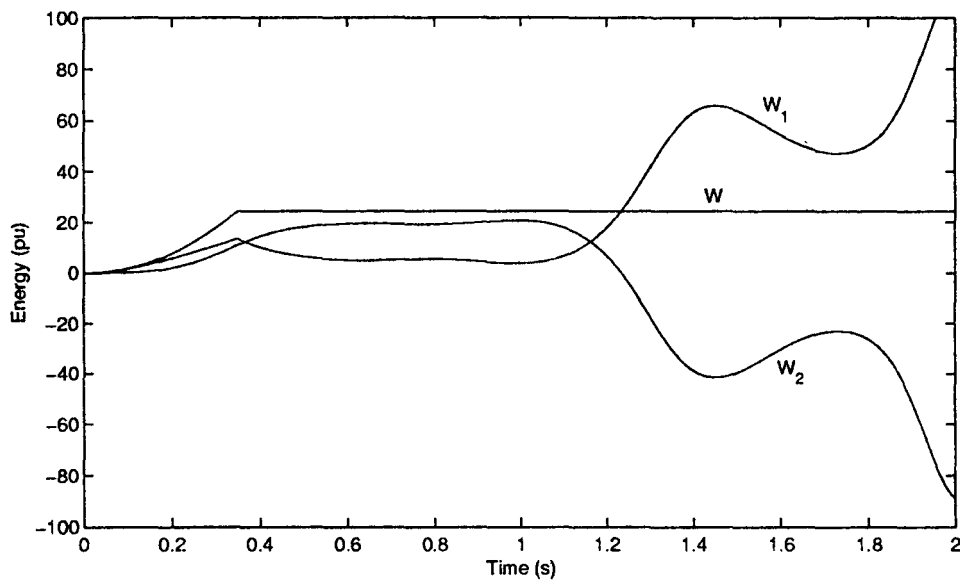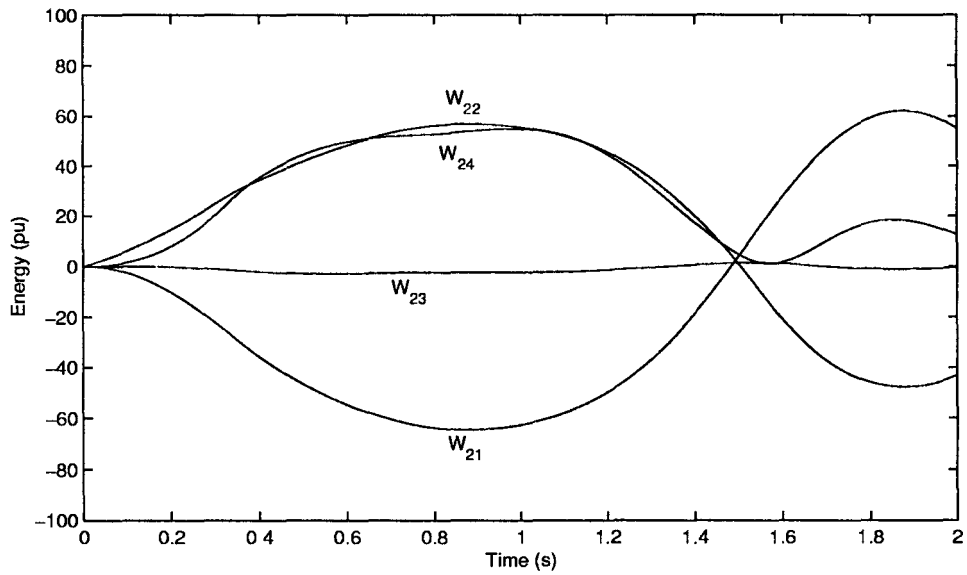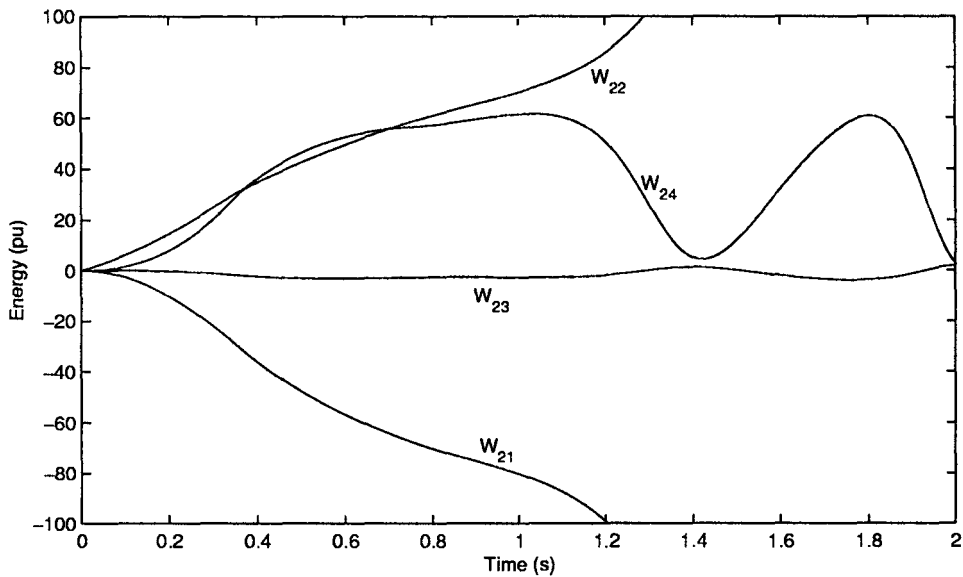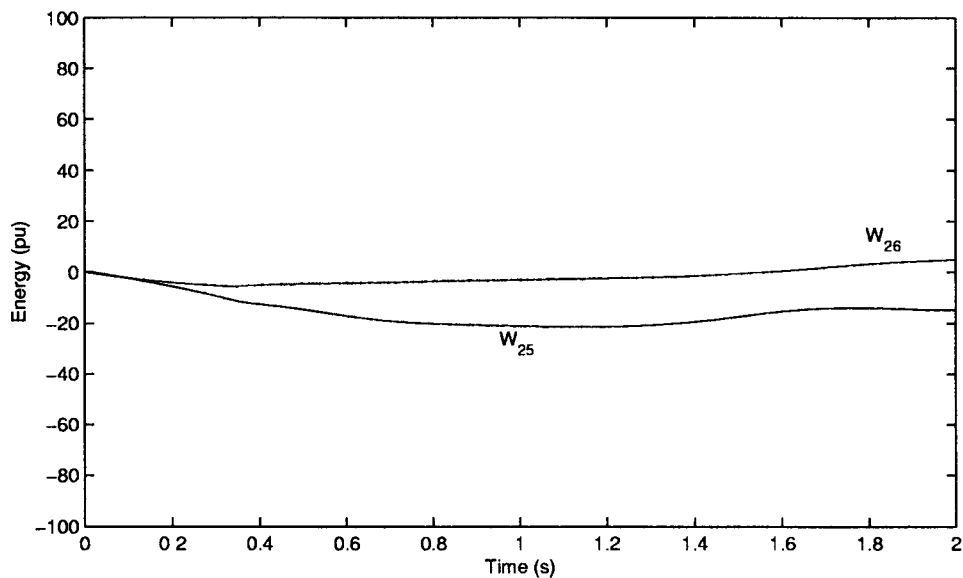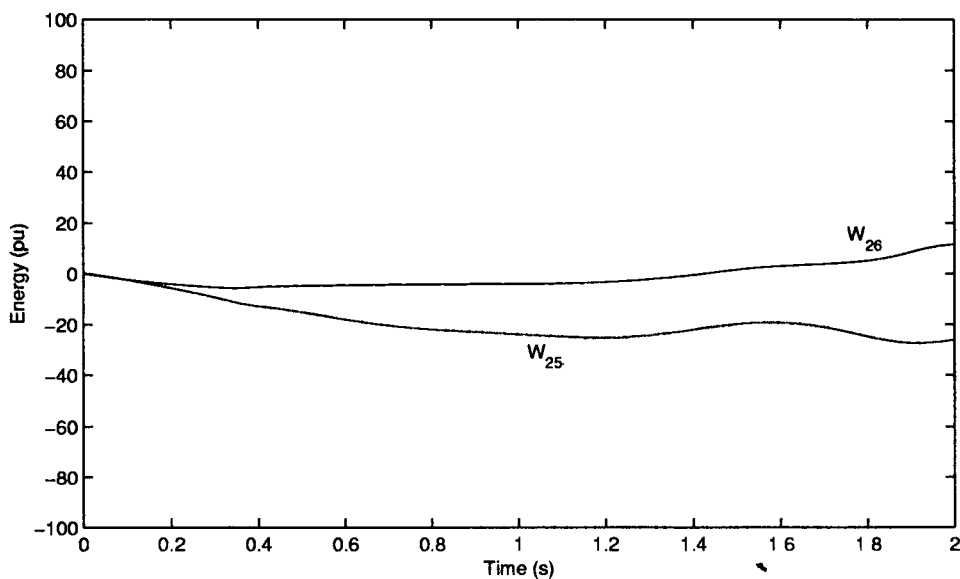Figure 13.14: Plots of W, W_1, W_2 (17 Generator system)
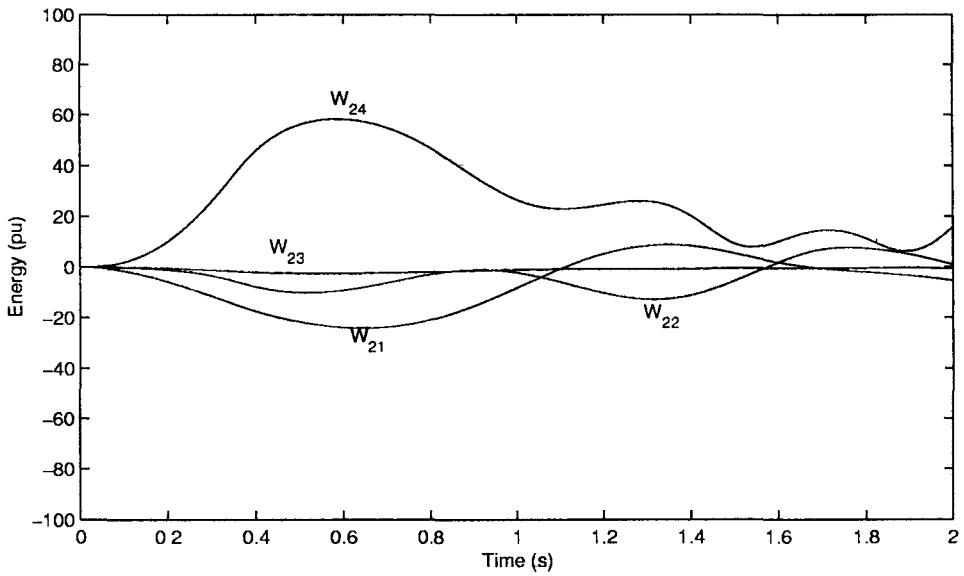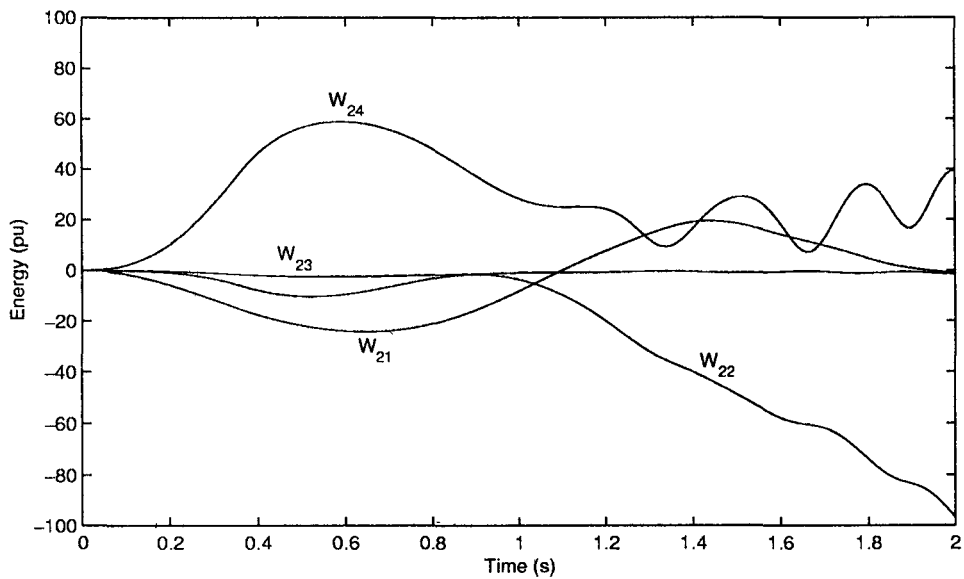
(a) Stable (t_{cl} = 0.354 s)

(b) Unstable (t_{cl} = 0.355 s)

Figure 13.15: Plots of W_{21}, W_{22}, W_{23} and W_{24} (17 generator system)

$$W_{23} = \sum_{i=1}^{n} \int_{V_{io}}^{V_i} \frac{f_{qi}(x_i)}{x_i} dx_i$$

$$W_{24} = \frac{1}{2}[\sum_{i=1}^{m} Q_{gi} - \sum_{j=1}^{n} Q_{lj}], \quad \text{where}$$

$$Q_{gi} = E'_{di} i_{qi} - E'_{qi} i_{di}$$

For classical model of the machine, T_{mi} (mechanical torque of ith machine) is approximated by P_{mi} and $E'_{di} = 0$. Also, E'_{qi} remains constant during a transient.

From Fig. 13.15, it is observed that the components W_{23} and W_{24} are bounded. In this example W_{21} also appears to be bounded while W_{22} is unbounded for the unstable case. The oscillations in W_{24} are due to intermachine oscillations during the transient. The component W_{23} is small compared to others.

13.8.2   10 Generator System

The disturbance considered is a three phase fault at bus #14 followed by clearing line between bus #14 and bus #34. The effect of generator modelling on critical clearing time is investigated. The results are shown in Table 13.2.

Table 13.2. 10 Generator System Fault at Bus # 14

Machine Model		Prediction		Simulation
		t_{cr}	W_{cr}	t_{cr}
I.	**Classical**	0.25–0.26	11.27	0.26–0.27
II.	**One-Axis**			
	Saliency Neglected:			
	(i) Without AVR	0.18–0.19	6.07	0.19–0.20
	(ii) With AVR	0.36–0.37	26.54	0.37–0.38
	Saliency Included:			
	(i) Without AVR	0.16–0.17	5.10	0.16–0.17
	(ii) With AVR	0.35–0.36	27.59	0.36–0.37
III.	**Detailed**			
	(i) Without AVR	0.16–0.17	4.06	0.17–0.18
	(ii) With AVR	0.34–0.35	18.75	0.34–0.35

The results show that the PEBS method predicts accurately the critical clearing time in practically all the cases considered. The effect of AVR on improving

transient stability is significant. The machine model (1.0) (one axis model) is accurate compared to model (1.1) (two axis model). This is not surprising as the damper winding mainly helps in damping rotor oscillations. The classical model gives higher critical clearing time than the model (1.1) neglecting AVR. This is due to the fact that flux decay is neglected in the classical model. The performance of static exciter with gain $K_A = 25$, ($T_A = 0.025$ s, $E_{fdmax} = 10$, $E_{fdmin} = -10$) is better than just maintaining constant field flux.

It is interesting to note that the effect of including transient saliency ($x_q \neq x'_d$) with model (1.0) is to slightly reduce the critical clearing time.

The variations of W_1, W_2 and W with time for the case, when machines are represented by classical models, are shown in Fig. 13.16. The components of the potential energy - W_{21}, W_{22}, W_{23} and W_{24} are shown in Fig. 13.17. In this case, both W_{21} and W_{22} are unbounded when the system is unstable. It is interesting to observe that the oscillations in W_{21} and W_{24} are in antiphase. It is to be noted that for this system, the transmission losses are neglected.

The variations of W_1, W_2 and W when the generators are represented by detailed models (including AVR) are shown in Fig. 13.18. The components of the potential energy W_{21}, W_{22}, W_{23} and W_{24} are shown in Fig. 13.19. The remaining components W_{25} and W_{26} are shown in Fig. 13.20. W_{25} and W_{26} are defined as

$$W_{25} = \sum_{i=1}^{m} \int_{t_o}^{t} i_{di} \left(\frac{dE'_{qi}}{dt} \right) dt$$

$$W_{26} = -\sum_{i=1}^{m} \int_{t_o}^{t} i_{qi} \left(\frac{dE'_{di}}{dt} \right) dt$$

These components are identically zero when classical model is considered. W_{26} is small when the system is stable, but continues to increase with time when the system is unstable.

The variations in the remaining energy components are not qualitatively different when compared to those for the case with classical machine models. It is observed from the examples presented, that energy function based methods are useful in predicting transient stability. However, it is to be noted that direct methods are incapable of predicting oscillatory instability (or dynamic instability) caused by fast acting excitation systems and lack of inherent system damping. Thus, it is stated that direct methods predict only 'first swing' stability (although the concept of first swing is somewhat vague in multimachine systems). Actually with classical machine models, constant active power loads and lossless transmission network, energy function method can predict system

(a) Stable (t_{cl} = 0.26 s)

Time (s)
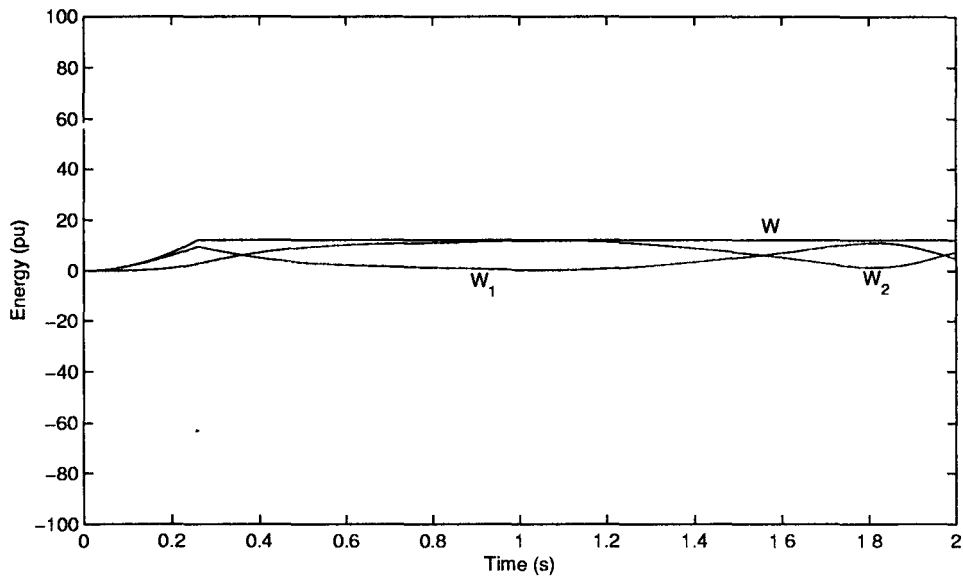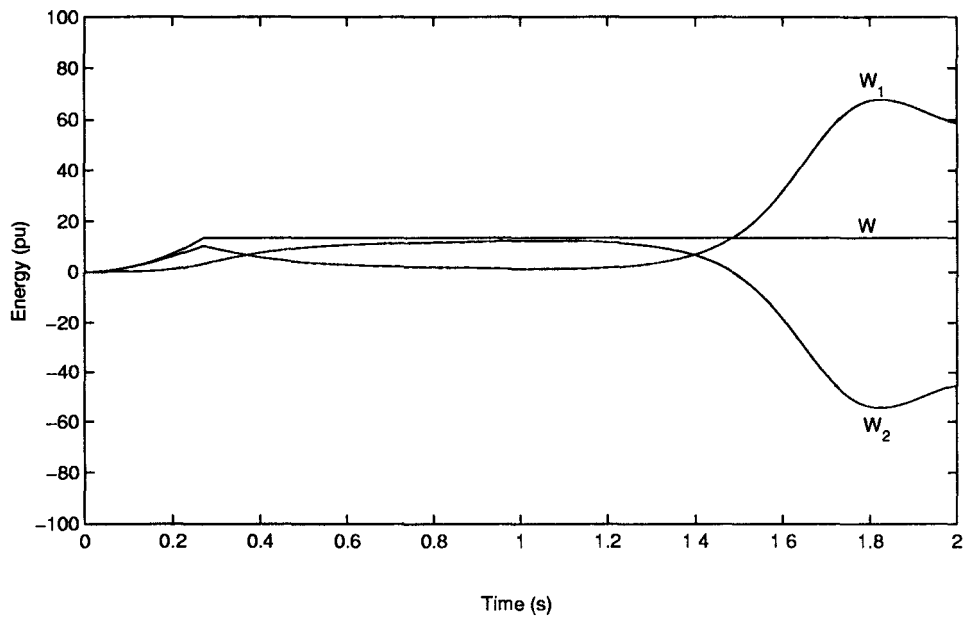
(b) Unstable (t_{cl} = 0.27 s)

Figure 13.16: Plots of W, W_1, W_2 (10 generator system - classical model)

(a) Stable (t_{cl} = 0.26 s)

(b) Unstable (t_{cl}= 0.27 s)

Figure 13.17: Plots of W_{21}, W_{22}, W_{23} and W_{24} (10 generator system - classical model)

(a) Stable (t_{cl} = 0.34 s)

(b) Unstable (t_{cl} = 0.35 s)

Figure 13.18: Plots of W, W_1, W_2 (10 generator system - detailed model)

(a) Stable (t_{cl} = 0.34 s)

(b) Unstable (t_{cl} = 0.35 s)

Figure 13.19: Plots of W_{21}, W_{22}, W_{23} and W_{24} (10 generator system - detailed model)

(a) Stable (t_{cl} = 0.34 s)

(b) Unstable (t_{cl} = 0.35 s)

Figure 13.20: Plots of W_{25} and W_{26} (10 generator system - detailed model)

stability accurately and there is no need to qualify that only first swing stability is predicted. Although, the application of energy function is not mathematically justified for power systems with excitation system models, the results from the examples show that direct methods based on SPEF give accurate prediction of critical clearing time. Thus, the application of structure preserving energy functions offer promise as effective tools for on-line dynamic security assessment and devising emergency control strategies.

The use of SPEF is desirable even when the loads are modelled as constant impedances. Firstly the problem of path dependent component of energy function is minimized with structure preserving model. Secondly, in large systems, the retention of the structure of the system results in sparse bus admittance matrix and there could be computational advantages using sparsity.

References and Bibliography

1. P.C. Magnusson, "Transient energy method of calculating stability", AIEE Trans. Vol. 66, 1947, pp. 747-755.

2. P.D. Aylett, "The energy integral-criterion of transient stability limits of power systems", Proc. IEE (London), Vol. 105C, No.8, 1958, pp. 527-536.

3. G.E. Gless, "Direct method of Lyapunov applied to transient power system stability", IEEE Trans. Vol. PAS-85, No. 2, 1966, pp. 159-168.

4. A.H. El-Abiad and K. Nagappan, "Transient stability regions of multi-machine power systems", IEEE Trans. Vol. PAS-85, No. 2, 1966, pp. 169-178.

5. M.A. Pai, **Power system stability - analysis by the direct method of Lyapunov**, New York, N.Y:North Holland, 1981.

6. M.A. Pai, **Energy function analysis for power system stability**, Kluwer Academic Publishers, 1989.

7. M. Ribbens-Pavella and F.J. Evans, "Direct methods for studying dynamics of large-scale electric power systems - a survey", Automatica, Vol. 32, January 1985, pp. 1-21.

8. P.P. Varaiya, F.F. Wu and R.L. Chen, "Direct methods for transient stability analysis of power systems: recent results", Proc. of IEEE, Vol. 73, 1985, pp. 1703-1715.

9. A.A. Fouad and V. Vittal, "The transient energy function method", Int. J. of Elec. Power and Energy Syst., Vol. 10, No. 4, 1988, pp. 233-246.

10. H.D. Chiang, F.F. Wu and P.P. Varaiya, "Foundations of direct methods for power system transient stability analysis", IEEE Trans. on Circuits and Systems, Vol. CAS-34, No. 2, 1987, pp. 160-173.

11. IEEE Committee Report, "Application of direct methods to transient stability analysis of power systems", IEEE Trans. Vol. PAS-104, May 1985, pp. 1629-1636.

12. A.R. Bergen and D.J. Hill, "A structure preserving model for power system stability analysis", IEEE Trans. Vol. PAS-100, No. 1, 1981, pp. 25-35.

13. N. Narasimhamurthi and M.R. Musavi, "A general energy function for transient stability analysis of power systems", IEEE Trans. on Circuits and Systems, Vol. CAS-31, No. 7, 1984, pp. 637-645.

14. N.A. Tsolas, A. Arapostathis and P.P. Varaiya, "A structure preserving energy function for power system transient stability analysis", IEEE Trans. on Circuits and Systems, Vol. CAS-32, No. 10, 1985, pp. 1041-1049.

15. K.R. Padiyar and H.S.Y. Sastry, "Application of topological energy function for the direct stability evaluation of power systems with voltage dependent loads", Conf. Proc. 83 CH 1962-0, IEEE Systems Man and Cybernatics Society, 1983.

16. T.V. Cutsem and M. Ribbens-Pavella, "Structure preserving direct methods for transient stability analysis of power systems", Proc. 29th Conf. on Decision and Control, Fort Lauderdale, FL., December 1985

17. A.R. Bergen, D.J. Hill and C.L. de Marcot, "Lyapunov functions for multimachine power systems with generator flux decay and voltage dependent loads", Int. J. of Elec. Power & Energy Syst. Vol. 8, No. 1, 1986, pp. 2-10.

18. K.R. Padiyar and H.S.Y. Sastry, "Topological energy function analysis of stability of power systems", Int. J. of Elec. Power & Energy Syst., Vol. 9, No. 1, 1987, pp. 9-16.

19. K.R. Padiyar and K.K. Ghosh, "Direct stability evaluation of power systems with detailed generator models using structure-preserving energy functions", Int. J. of Elec. Power & Energy Syst., Vol. 11, No. 1, 1989, pp. 47-56.

20. T. Athay, P. Podmore and S. Virmani, "A practical method for direct analysis of transient stability", IEEE Trans. Vol. PAS-98, pp. 573-584.

21. N. Kakimoto, Y. Ohsawa and M. Hayashi, "Transient stability analysis of electric power systems via Lure type Lyapunov function, Part I: New critical value for transient stability; Part II: Modification of Lure type

Lyapunov function with effect of transfer conductances", Tran., IEE of Japan, Vol. 98, No. 5/6, 1978, pp. 62-71; 72-79.

22. M. Ribbens-Pavella, P.G. Murthy and J.L. Horward, "The acceleration approach to practical transient stability domain estimation in power systems", Proc. of the 20th IEEE Conf. on Decision and Control, San Diego, CA, 1981, pp. 471-477.

23. B. Toumi, R. Dhifaorei, Th van Cutsem and M. Ribbens-Pavella, "Fast transient stability assessment revisited", IEEE Trans. on Power Systems, Vol. PWRS-1, No. 2, 1986, pp. 211-220.

24. A.A. Fouad and S.E. Stanton, "Transient stability of multimachine power systems, Part I:Investigation of system trajectories", IEEE Trans. Vol. PAS-100, 1981, pp. 3408-3414.

25. H.D. Chiang, F.F. Wu and P. Varaiya, "Foundations of PEBS method for power system transient stability analysis", IEEE Trans. on Circuits and Systems, Vol. CAS-35, June 1988, pp. 712-728.

26. P.W. Sauer, A.K. Behera, M.A. Pai, J.R. Winkelman and J.H. Chow, "Trajectory approximations for direct energy methods that use sustained faults with detailed power system models", IEEE Trans. on Power Systems, Vol. 4, No. 2, 1989, pp. 499-506.

27. H.D. Chiang, F.F. Wu and P. Varaiya, "A BCU method for direct analysis of system transient stability", IEEE PES Summer Meeting, 91 SM 423-4,PWRS, 1991, IEEE Trans. on Power Systems, Vol. 9, No. 3, 1994, pp. 1194-1208.

28. P.W. Sauer, K.D. Demaree and M.A. Pai, "Stability limits load supply and interchange capability", IEEE Trans. Vol. PAS-102, Nov. 1983, pp. 3637-3643.

29. M.A. El-Kady, C.K. Tang, V.F. Carvalho, A.A. Fouad and V. Vittal, "Dynamic security assessement utilizing the transient energy function method", IEEE Trans. on Power Systems, Vol. PWRS-1, 1986, pp. 284-291.

30. J. Tong, H.D. Chiang and T.P. Conneen, "A sensitivity-based BCU method for fast derivation of stability limits in electric power systems", IEEE Trans. on Power Systems, Vol. 8, No. 4, 1993, pp. 1418-1428.

31. F.A. Rahimi, M.G. Lauby, J.N. Wrubel and K.L. Lee, "Evaluation of the transient energy function method for on-line dynamic security analysis", IEEE Trans. on Power Systems, Vol. 8, No. 2, 1993, pp. 497-507.

32. G.A. Maria, C. Tang and J. Kim, "HYBRID transient stability analysis", IEEE Trans. on Power Systems, Vol. 5, No. 2, 1990, pp. 384-391.

33. K.R. Padiyar and K.K. Ghosh, "Dynamic security assessment of power systems using structure-preserving energy functions", Int. J. of Elec. Power & Energy Syst., Vol. 11, No. 1, 1989, pp. 39-46.

34. H.D. Chiang, "Study of the existence of energy functions for power systems with losses", IEEE Trans. on Circuits and Systems, Vol. CAS-36, Nov. 1989, pp. 1423-1429.

35. C.J. Tavora and O.J.M. Smith, "Characterization of equilibrium and stability in power systems", IEEE Trans. Vol. PAS-91, No. 3, 1971, pp. 1127-1130.

36. K.R. Padiyar and H.S.Y. Sastry, "Fast evaluation of transient stability of power systems using a structure preserving energy function", Electric Machines and Power Systems, Vol. 11, 1986, pp. 421-441.

37. K.R. Padiyar and K.K. Ghosh, "Integrating direct methods in power system dynamic simulation ɪ rogram", J. of Institution of Engineers (India), Electrical Engg. Division, (Pt EL6), Vol. 69, 1988, pp. 7-13.

38. K.R. Padiyar and K.K. Ghosh, "A novel structure preserving energy function for direct stability evaluation of power systems with known modes of instability", Elec. Machines and Power Systems, Vol. 13, 1987, pp. 135-148.

39. K.R. Padiyar and K.K. Ghosh, "A new structure preserving energy function incorporating transmission line resistance", Elec. Machines and Power Systems, Vol. 14, No. 4, 1988, pp. 324-340.

40. K.R. Padiyar and H.S.Y. Sastry, "A structure preserving energy function for stability analysis of AC/DC systems", Sadhana (Proc. in Engg. Sciences, Indian Academy of Science) Vol. 18, part 5, 1993, pp. 787-799.

41. K.R. Padiyar and P.P. Varaiya, "A network analogy for power system stability analysis", preprint, Dec. 1983.

42. K.R. Padiyar and Vijayan Immanuel, "Modelling of SVC for stability evaluation using structure preserving energy function", Int. J. of Elec. Power and Energy Syst., Vol. 16, No. 5, 1994, pp. 339-348.

43. Y. Xue, Th.Van Cutsem and M.Ribbens-Pavella, "Extended equal area criterion: justifications, generalizations, applications", IEEE Trans. on Power Systems, Vol.4, No.1, 1989, pp. 44-52.

44. Y. Xue, L. Wehenkel, R. Belhomme, P. Rousseaux, M. Pavella, E. Euxibie, B. Heilbronn and J.F. ᒍasigne, "Extended equal area criterion revisited", IEEE Trans. on Power Systems, Vol.7, No. 3, 1992, pp. 1012-1022.

45. Y. Xue and M. Pavella, "Critical-cluster identification in transient stability studies", IEE Proc. (London) Part C, Vol.140, No.6, 1993, pp. 481-489.

46. IEEE Committee Report, "Transient stability test systems for direct stability methods", IEEE Trans. on Power Systems, Vol. 7, Feb. 1992, pp. 37-43.

47. Vijayan Immanuel, **Application of structure preserving energy functions for stability evaluation of power systems with static var compensators**, Ph.D. Thesis submitted to Indian Institute of Science, Bangalore, August 1993.

Chapter 14

Transient Stability Controllers

Transient stability is important from the viewpoint of maintaining system security - that is, the incidence of a fault should not lead to tripping of generating unit(s) due to loss of synchronism and the possibility of a cascaded outage leading to system black out. Unlike steady state or small signal stability which has to be continuously maintained at all times, the transient stability is a function of the disturbance. The improvement of transient stability can be achieved not only by adequate system design but also from the use of control action which is not continuous, but is initiated following a disturbance and is temporary in nature. An example is the operation of dynamic braking using shunt or series connected resistors. Such controllers are termed as discrete supplementary controllers [1] as opposed to primary controllers which are speed governor and excitation systems in addition to protective relaying. In this chapter, the factors that affect transient stability of power systems are discussed and the application of discrete supplementary controls is reviewed.

14.1   System Design for Transient Stability

Transient Stability Criteria

The transient stability criteria chosen by different utilities can vary to some extent. However, in most cases the criteria include the ability of the system to withstand a three phase bus fault at critical locations such as terminals of heavily loaded generators and lines carrying large amounts of power. Although three phase bus faults are convenient to specify, the statistical data indicate single line to ground (S-L-G) faults are most prevalent on HV and EHV lines [2]. On 500 kV lines the incidence single phase to ground faults is more than 90% of the total number of faults compared to three phase faults which occur about 1 % of the total number. The misoperation of relay can result in double contingency faults which are more common than three phase faults. However, three phase faults are more severe and transient stability criteria usually include ability to withstand

(a) Three phase faults cleared by primary protection

(b) Single line to ground faults cleared by back up protection (due to stuck primary breaker)

Effects of System Parameters

The dominant system parameters that affect transient stability are

1. Generator reactances and inertia

2. Transmission system reactance under normal and contingency (postfault) conditions

3. Switching devices, their number, arrangement and speed of operation

The critical clearing time (T_c) for a three phase fault at the generator high voltage bus varies approximately as [3]

$$T_c = k \sqrt{\frac{H}{(x_d' + x_t)(x_d + x_t)}} \tag{14.1}$$

where k is a proportionality constant, H is the inertia constant, x_t is transformer reactance, x_d and x_d' are direct-axis synchronous and transient reactances.

Eq. (14.1) shows that transient stability is improved by increasing H and reducing the reactances. Unfortunately with modern generators of large ratings with improved cooling and increased power output per unit weight, the inertia is lower while reactances are higher. For a 2-pole machine, the inertia H may be lower than 2.0 and x_d larger than 2.0 pu (all expressed on generator base). Generators with superconducting field windings (yet to be commercially introduced) are expected to have lower reactances.

The reactances of the external network (viewed from the generator terminals) also affect transient stability limits. The reactance under normal operating condition can be reduced by introducing additional circuits (an expensive solution), series or shunt capacitors and higher voltage of transmission. The reactance under contingency condition (following fault clearing by line tripping) can be reduced by introducing high tension bussing with switching stations at intermediate locations along the line and insertion of series capacitors. Diverting of power flow to a parallel HVDC link also helps to relieve a contingency. As most faults are of transient nature, it is desirable to have circuit breakers with high speed reclosing feature. As most of the faults are of single phase to ground type, single phase tripping and auto-reclosing is quite attractive.
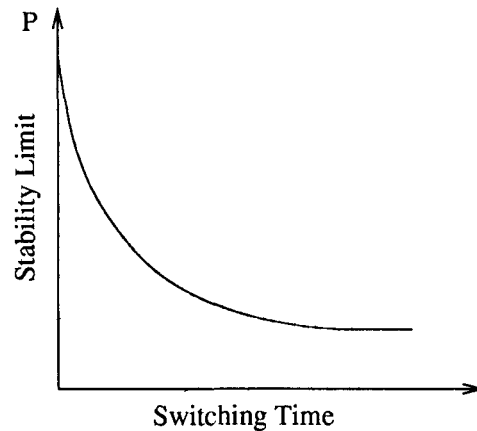
Figure 14.1: Variation of stability limit with switching time

The introduction of quick opening circuit breakers of high interrupting capacities has resulted in major improvements in transient stability limits. The typical variation of stability limit with switching time is shown in Fig. 14.1 which clearly shows the importance of fast clearing of faults. Modern circuit breakers open within 3 cycles (inclusive of relaying time). This has eliminated the need to introduce neutral resistors (effective in limiting generator acceleration during unbalanced faults involving ground).

Effects of Excitation and Prime-Mover Control

The excitation control helps to overcome the armature reaction following a fault and acceleration of the generator rotor. The demagnetizing current increases during the fault and is high even after the fault is cleared, due to increase in the rotor angle. High initial response excitation systems with large ceilings (for field forcing) contribute to first swing stability. However they also affect the damping of subsequent swings.

For steam turbines, the governor action has small but beneficial influence on the first swing stability. This is due to the fact that rotor speed change is not appreciable in the first half second or so which is critical for first swing stability. (The governor is provided with deadband so that it does not respond to minor fluctuations in speed). On the other hand, the governor action for hydroturbines is not beneficial due to water inertia effects, but is small as in the case of steam turbine governors.

Modern steam turbine speed control systems have the capability of fast

actuation of control valve and intercept valve closure (within a fraction of a second). These features were primarily meant to control turbine overspeed under load rejection conditions and they can also be triggered by special logic upon detection of abrupt loss of power output during faults. The valves are reset at slower opening speeds following a finite delay of about a second.

With moderate speeds of response, excitation systems are not as effective as fast turbine valving in enhancing first swing stability. However this applies to steam turbines. For hydro turbines, other arrangements such as dynamic braking (use of braking resistors) may be required.

14.2 Discrete Supplementary Controls

As mentioned earlier, discrete controls refer to initiation of control action only after the detection of a fault or contingency condition. It does not include continuous control action due to excitation and turbine-governor systems.

In an IEEE committee report published in 1978 [1], the following controls are listed

1. Dynamic braking

2. High speed circuit breaker reclosing

3. Independent pole tripping

4. Discrete control of excitation systems

5. Controlled system separation and load shedding

6. Series Capacitor insertion

7. Power modulation of HVDC lines

8. Turbine bypass valving

9. Momentary and sustained fast valving

10. Generator tripping

With the introduction of SVCs and FACTS devices such as Controllable Series Compensation (CSC), Thyristor Controlled Phase-angle Regulators (TCPR), fast control to maintain system security is feasible. Along similar lines as HVDC converter controls, FACTS controllers based on high power semiconductor devices such as Thyristors can be programmed to provide discrete control action in the event of a major disturbance which may threaten transient stability of the system.
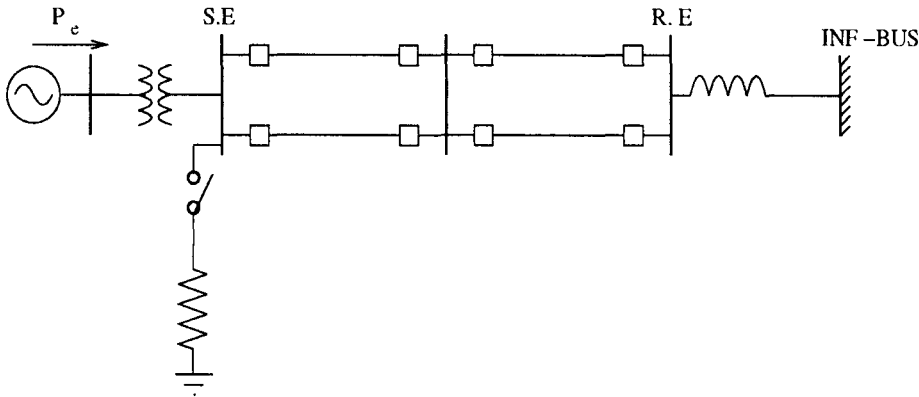
Figure 14.2: Application of shunt braking resistor

In the following sections, some of the discrete controls, which have been in use or have the potential for future applications, are reviewed.

14.3   Dynamic Braking [5-9]

This concept involves the use of braking resistors, mostly connected in shunt, which are switched in, following a fault clearing, to correct the temporary imbalance between the mechanical power input and electrical power output of generators. In principle, the use of braking resistors of suitable size and appropriate logic to implement controllable duration of resistor insertion can overcome the problem of transient stability. However, the cost of resistor capable of dissipating the required amount of energy and associated switching equipment is a deterrent as there have been very few applications so far. Peace River in British Columbia, Canada and Chief Joseph Substation of Bonneville Power Administration in Western U.S.A. are few of the modern applications of the concept.

Fig. 14.2 shows typical location of shunt connected resistors at the sending end of a long double circuit transmission line.

When the inertia of the sending end generator is small compared to that of the receiving end, series braking resistors are also effective in controlling the relative angle. Consider a two machine system shown in Fig. 14.3. The equation governing the relative angle $\delta_{12} = \delta_1 - \delta_2$, is given by

$$\frac{d^2\delta_{12}}{dt^2} = \left(\frac{P_{m1}}{M_1} - \frac{P_{m2}}{M_2}\right) - \left(\frac{P_{e1}}{M_1} - \frac{P_{e2}}{M_2}\right) \qquad (14.2)$$
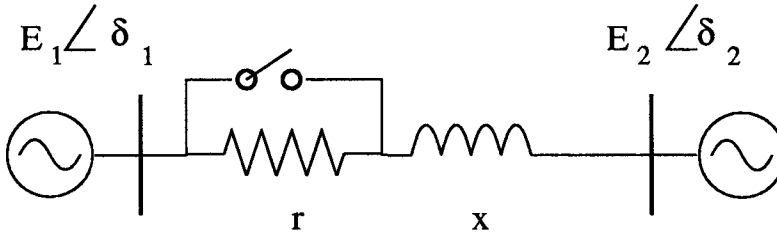
Figure 14.3: Application of series connected brake

where M_1 and M_2 are inertias of machines 1 and 2 defined by

$$M_1 = \frac{2H_1}{\omega_B}, \quad M_2 = \frac{2H_2}{\omega_B}$$

Multiplying Eq. (14.2) by M_{eq} where

$$M_{eq} = \frac{M_1 M_2}{M_1 + M_2} \tag{14.3}$$

We get

$$M_{eq}\frac{d^2\delta_{12}}{dt^2} = P_m^{eq} - P_e^{eq} \tag{14.4}$$

where

$$P_m^{eq} = \frac{P_{m1}M_2}{M_1 + M_2} - \frac{P_{m2}M_1}{M_1 + M_2}$$

$$P_e^{eq} = \frac{P_{e1}M_2}{M_1 + M_2} - \frac{P_{e2}M_1}{M_1 + M_2}$$

Neglecting generator impedances, the expressions for P_{e1} and P_{e2} can be obtained as

$$P_{e1} = E_1^2\frac{r}{Z^2} + \frac{E_1 E_2}{Z}\sin(\delta_{12} - \alpha) \tag{14.5}$$

$$P_{e2} = E_2^2\frac{r}{Z^2} - \frac{E_1 E_2}{Z}\sin(\delta_{12} + \alpha) \tag{14.6}$$

where $Z = \sqrt{r^2 + x^2}$, $\alpha = \sin^{-1}\frac{r}{Z}$, E_1 and E_2 are generator voltages.

For $E_1 = E_2 = 1.0, x = 1.0, \frac{M_1}{M_2} = 10$, the power angle curve (of P_e^{eq} vs δ_{12}) is plotted in Fig. 14.4 for different values of $\frac{r}{x}$. For nonzero r, the peaks of the curves occur at $\delta > 90^o$. (This is to be compared with shunt resistor, where peak occurs at $\delta < 90^o$).
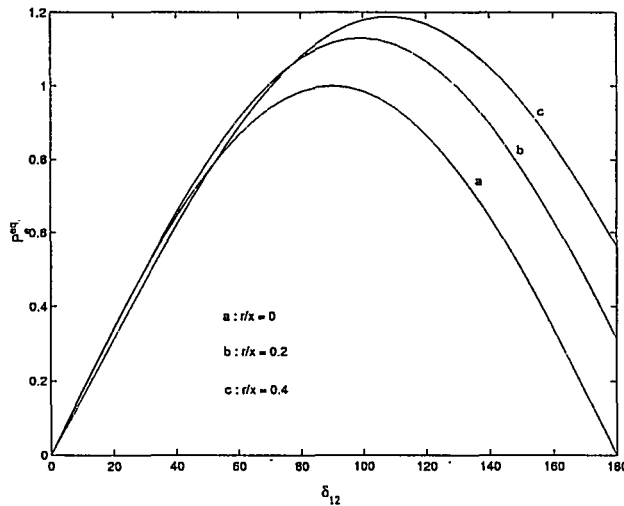
Figure 14.4: Power angle curve with series connected brake

Series braking resistors can be inserted by connecting them between the neutral and ground on the high voltage (line) side of the step-up transformers. This simplifies the design of the resistors from the insulation point of view. The other advantages of series connected dynamic brake are

1. Speed of insertion is related to opening of a circuit breaker across the resistor as opposed to the closing of a breaker as in the case of the shunt resistor. This permits faster action of the brake and is effective in reducing the severity of the fault in case of prolonged faults by stuck breakers. It is to be noted that series braking resistors are inserted as soon as the fault is detected while shunt braking resistors are switched on as soon as the fault is cleared.

2. The displacement of the peak value of P_e^{eq} beyond $\delta_{12} > 90^o$ is beneficial as it allows more time for the synchronizing torques to act.

3. The size and cost of series braking resistor tend to be smaller than that of the shunt resistor because of factors listed above.

The effectiveness of the series braking resistors is considerably reduced if M_1 and M_2 are comparable. This is due to the fact that both machines are decelerated equally when $M_1 = M_2$ and the relative deceleration is zero.

The application of 1400 MW shunt dynamic brake at BPA's Chief Joseph substation resulted in the increase in the transient stability limit of power flow on Pacific Northwest - Southwest (PNW-SW) intertie [6]. The influence of the
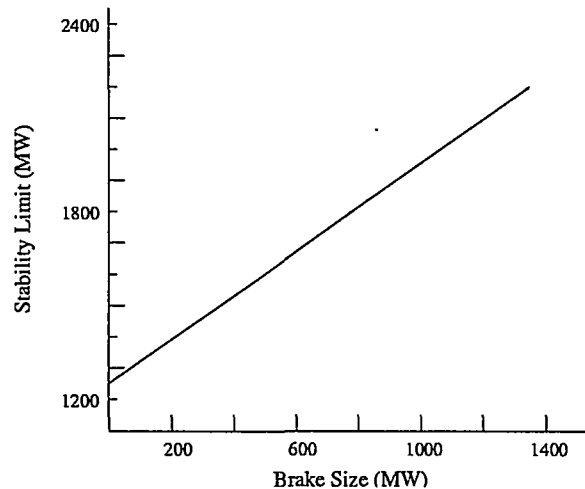
Figure 14.5: Influence of brake size on stability limit

brake size on the stability limit is shown in Fig. 14.5. (This is shown for a particular disturbance of a three phase fault on a 500 kV line). This shows an increase of 900 MW in stability limit for a brake size of 1400 MW.

Brake Control Scheme

The control logic for switching of the brake can be explained with reference to the stability boundaries drawn in the phase plane (rotor relative speed $\frac{d\delta}{dt}$ versus rotor angle δ) shown in Fig. 14.6. This is applicable to a single machine system connected to an infinite bus. The closed curve 'A' represents the stability boundary of the postfault system. If the system state at the instant of fault clearing lies within the region of stability bounded by A, there is no need for a brake. The outer curve 'B' corresponds to the region in which the application of the brake can result in the trajectory entering the stability region A. The region bounded by 'B' (excluding that bounded by 'A') can be subdivided into three regions

  I. the region predominantly in the fourth quadrant where the brake is switched off

 II. the shaded region in which the brake is switched on once until the postfault trajectory enters the stability region (crosses A). However to reduce the oscillations in the rotor angle, the brake may be kept on until the speed $\left(\dfrac{d\delta}{dt}\right)$ goes to zero.

III. the rest of the region where the brake is switched on until it enters region I when it is switched off. The post fault trajectory then enters region II
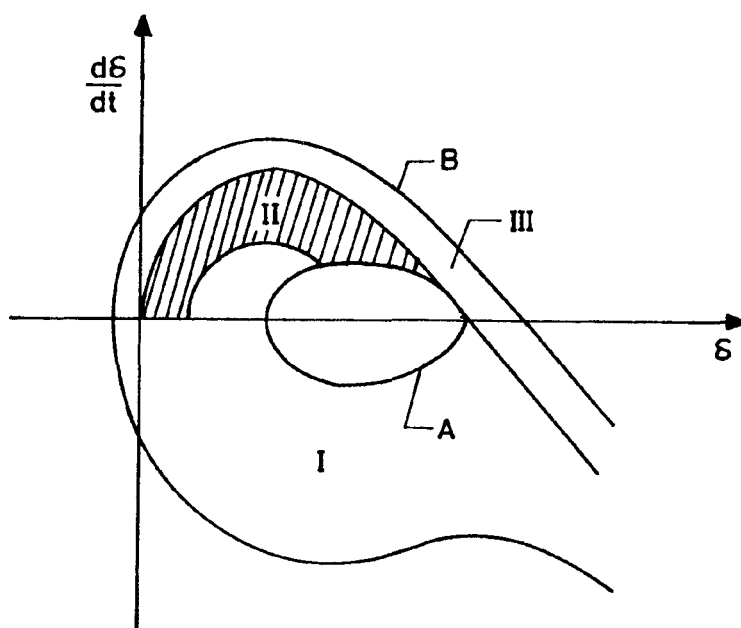
Figure 14.6: Stability boundaries in phase plane

when the brake is switched on second time until it is switched off after the speed goes to zero.

At Chief Joseph substation in BPA system, the braking resistor is. connected to the 230 kV bus through a normally closed 230 kV oil circuit breaker and normally open 230 kV vacuum switch. The controllers located at Chief Joseph and John Day substations detect a sudden decrease of power in the plant output with a simultaneous decrease in bus voltage. When either of the controllers detects sudden drop of more than 300 MW and a simultaneous decrease in the bus voltage greater than 10% of the normal bus voltage, an output is produced which closes the 230 kV vacuum switch to apply the brake. The brake is applied for the duration of about 0.5 second. Since the required duration of the brake application was relatively constant, there was no need to make any speed related measurements to switch off the brake.

14.4   Discrete control of Excitation Systems [18-22]

Fast acting static exciters with high ceiling voltages coupled with high gain AVRs can improve transient stability. However they can also result in oscillatory instability by negative damping of low frequency rotor oscillations. Power System Stabilizers (PSS) with control inputs derived from rotor speed, power or terminal frequency are used to modulate the generator voltage and damp oscillations. The application of PSS does not result in improvement of transient stability.

The improvement in transient stability can be achieved by the provision of discrete signals to control excitation during a transient disturbance. Ontario Hydro has developed a scheme [20] where a signal proportional to the rotor angle is used (during the transient period) in addition to the terminal voltage and rotor speed signals. The rotor angle signal cannot be used continuously as it results in dynamic instability.

Fig. 14.7 shows the block diagram representation of the excitation control scheme. The angle signal is derived by integrating the speed signal (used as input signal for PSS). The angle signal is generated during a transient disturbance by closing the switch S when there is a sudden drop in terminal voltage followed by the rise in rotor speed above a preset value. The relay contact S is opened when the speed drops below the preset level or the exciter comes out of saturation. The output of the integrator will then decay exponentially with time constant T. The value of this constant is chosen such that the output is proportional to the rotor angle for the relevant oscillation frequencies.

The effect of the discrete control is to maintain the field voltage and consequently the terminal voltage at a high level during the positive swing in the rotor angle. However, the terminal voltage is limited to 1.15 pu. From studies carried out, the discrete control of excitation was found to be as effective as fast valving scheme in a particular application where the interarea mode dominates over local modes.

The rise in the terminal voltage to 1.15 pu during the transient disturbance (with the application of discrete control) which may last for about 1 second, also affects the transformers (step-up transformer and those feeding the auxiliaries). The differential protection applied to transformer windings may have to be modified to account for increased magnetizing current during the operation of the discrete control.

The major motivation for the discrete control of excitation was to over-
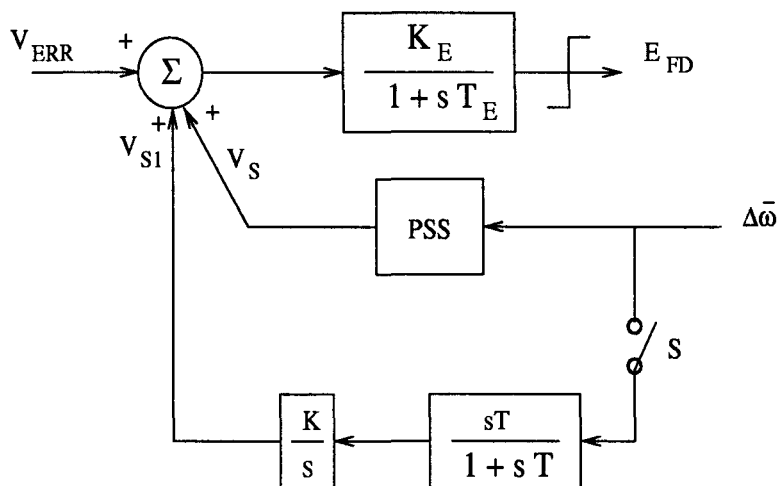
Figure 14.7: Discontinuous excitation control

come the limitations imposed by the PSS action which reduces excitation when the rotor speed deviation is negative. Alternative schemes are possible which give priority to improving the first swing transient stability immediately following a large disturbance. Bang-bang control of excitation not only provides maximum field voltage when desired, but also helps to damp postfault trajectories [18-19].

14.5 Momentary and Sustained Fast Valving [22-25]

Modern steam turbine driven generators are available with ratings up to 1300 MW. These have low inertia constants and high reactances which complicate the problem of transient stability. Fast valving is a means of decreasing turbine mechanical power when a unit is being accelerated due to a transmission system fault. It can be initiated by load unbalance relays, acceleration transducers or by relays that recognize only severe transmission faults. The fast valving is not designed to operate for remote faults.

Fast valving is a natural extension of the inherent capabilities of the modern electro-hydraulic (EH) turbine control system. Normal speed control and valve operation are not fast enough to limit overspeed to a desirable level following a major load rejection (greater than 20 % of full load). The EH overspeed control anticipates rotor acceleration by monitoring the mismatch between turbine driving power and generator load and initiates fast closure of control and intercept valves (within 0.1 to 0.2 sec) when mismatch exceeds the

limit (approximately 40 %). The fast closure is achieved by means of special solenoid operated disc dump valves which (when actuated) release the hydraulic fluid from the bottom of the pistons causing the valves to close rapidly.

The EH overspeed control systems have been modified to incorporate the fast valving function. Upon detection of a fault condition of sufficient severity, fast closure of intercept valves is initiated followed by immediate reopening thereby momentarily reducing unit accelerating power and improving stability. This is termed as momentary fast valving. It is to be noted that normal speed governor action also acts to limit rotor acceleration but has little effect within the time span of (about 1 second) first swing stability.

The steam flow path through a modern fossil-fired, tandem-compound, single-reheat turbine generator unit is shown in Fig. 14.8 [24]. High pressure steam enters the high-pressure (HP) turbine through main inlet stop valves, control valves and connecting piping. Reheat steam flows into the intermediate-pressure (IP) turbine through reheat stop valves, intercept valves and connecting piping.

The simplest way to reduce turbine power rapidly is to "fast valve" only the intercept valves which control approximately 70 % of the total unit power. During the closing and reopening of the intercept valves, the large reheater volume acts as a cushion, absorbing steam flow ahead of the intercept valves for several seconds with negligible effect on the throttle flow. Reheater safety valves may operate limiting reheater pressure to approximately 10 % above full load pressure. Reopening after a fast closure is inherently delayed for approximately one second (to allow for restoration of the oil to the hydraulic cylinder) and then takes up to 10 seconds for full reopening. This results in the power output being restored to its prior value.

The momentary fast valving may not be adequate if the postfault system is not strong. In this case, it is also desirable to reduce the power output in steady state. Sustained fast valving is the rapid closure of intercept valves with simultaneous repositioning of control valves and immediate partial reopening followed by full reopening of intercept valves at a predetermined rate. Thus the unit output can be reduced to a desired level without a tripout and full output can be restored within minutes after the disturbance. When a large unit is tripped off line, it can take hours or days before the unit can be put back on line.

The fast closing of control valves (in addition to intercept valves) resulting in the sudden stoppage of main stream flow would impose a severe transient on the boiler and control systems. Potential problems include the lifting of boiler safety valves, combustion and feedwater control problems, turbine ther-
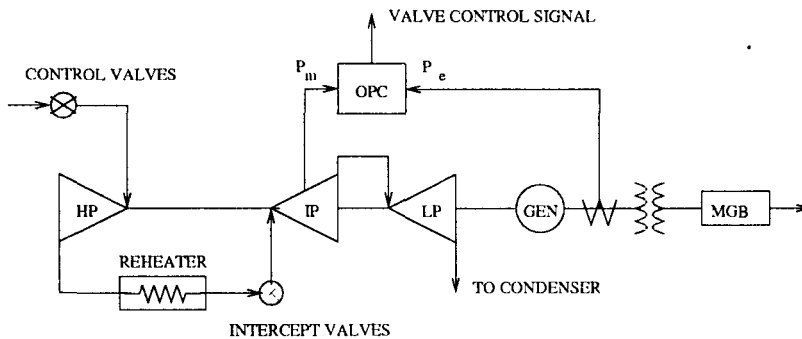
Figure 14.8: Steam flow path

mal stresses, transient thrust unbalance and overloading of the last few HP stages. Closing only of the control valves would have all the previous drawbacks and the disadvantage of slow intermediate (IP) and low pressure (LP) power decay due to uncontrolled expansion of the steam stored in the reheater.

Fast Valving Logic

The logic is incorporated in the overspeed protection controller (OPC) shown in Fig. 14.8. Mechanical power input is measured with a reheater pressure transducer and compared to electric power output of the generator (measured by a Hall effect transducer). If the electrical power is suddenly lost, a power unbalance exists. If the unbalance exceeds A % and reheater pressure exceeds preset level then two possibilities arise

(i) If the main generator breaker (MGB) is closed indicating a system fault condition and partial load loss, fast valving of intercept valves is initiated. At the same time, the closing signal initiates intercept valve reopening with an adjustable time delay, provided the MGB has remained closed.

(ii) If the MGB is open, a signal is sent to the overspeed control logic to close turbine control and intercept valves. A typical power response to fast valving is shown in Fig. 14.9.

14.6 Discrete Control of HVDC Links [26-28]

Modern HVDC converter stations use thyristor valves for conversion and are controlled to maintain power flow in the line at a preset value determined from load dispatch. As fast control of power flow is achievable due to thyristor controllers, modulation of power is feasible and is implemented at several HVDC

T $_1$ – Time delay to sense

T $_2$ – Time delay of solenoid and valve
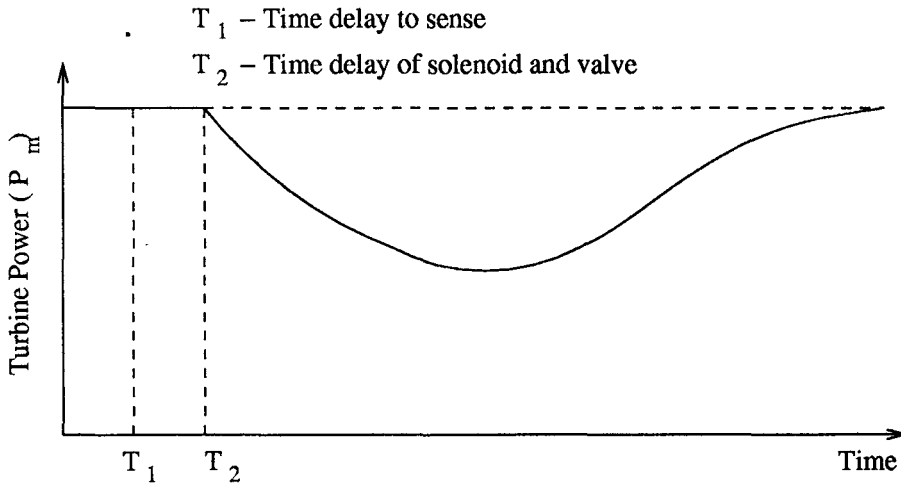
Figure 14.9: Power response to fast valving

links. While continuous, small-signal power modulation is beneficial in improving steady-state stability, discrete control of power can result in improving transient stability. The power flow can even be reversed under the influence of the control signal that is generated on the detection of the disturbance. The power can be ramped up (or down) within 0.1 to 0.2 sec. The control signal can be generated from (a) power flow in parallel AC ties or (b) rate of change of power in AC line or (c) frequency deviation at either end of the HVDC interconnection.

14.7 Series Capacitor Insertion [29-34]

Consider a two machine system shown in Fig. 14.10. Each machine represents an equivalent generator for an area and the two areas are interconnected by a double circuit AC intertie. Suppose that a short circuit occurs at point X in one of the circuits (as shown in the figure) and is cleared without reclosure. The power angle curves for the case with the switch closed are shown in Fig. 14.11. The curve N applies when all the lines are in service. Curve F is applicable during short circuit and curve PF refers to the postfault system condition when the faulted line section is disconnected. The initial operation is at $\delta = \delta_o$. The transient stability limit (L_1) is found by adjusting the height of L_1 for equality of areas A_1 and A_2, while simultaneously adjusting the clearing angle δ_{c1} to satisfy a fixed clearing time.

Fig. 14.12 shows the effect of inserting a series capacitor dimensioned to
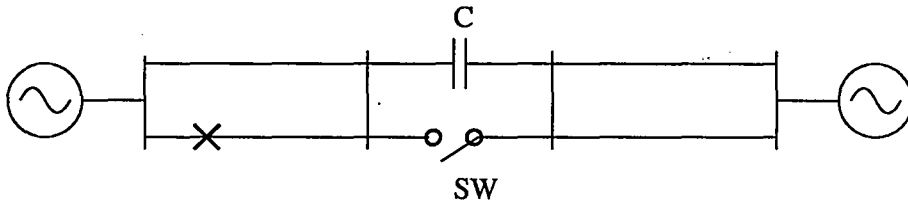
Figure 14.10: A two area system
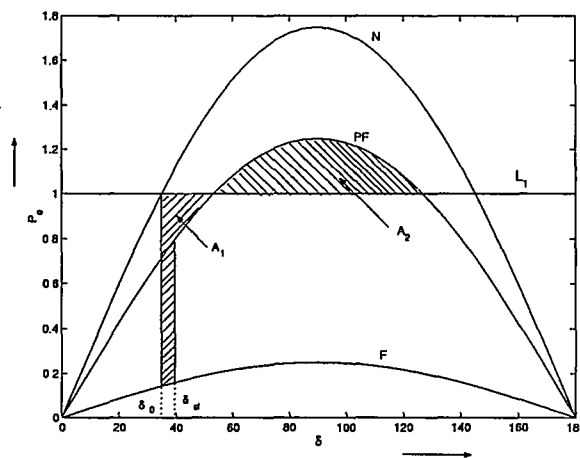
Figure 14.11: Power angle curves with switch closed

give the same transfer reactance between the two areas when all line sections are in service. The capacitor is inserted by opening the switch at the instant when the fault is cleared. The transient stability limit is now L_2 (found by equating areas A_3 and A_4) which is much higher than L_1. If it is assumed that $\delta_{c1} \simeq \delta_o$ then the transient stability limit is identical to the steady state stability limit of the normal system.

Switched capacitors have been applied to the 500 kV, double circuit AC intertie between Pacific Northwest and Southwest which is paralleled by ±400 kV (now upgraded to ±500 kV) HVDC intertie. The AC intertie is compensated by fixed series compensation in addition to switched series capacitors. In case of loss of the parallel HVDC link, the rapid insertion of switched series capacitors enable the AC line to temporarily carry without instability the additional load initially carried by the DC link.

For a specified transient stability limit, a judicious combination of switched

and fixed series capacitors result in smaller rating of the capacitors when compared to the case when all are fixed (or unswitched). The insertion of series capacitors also reduces angular swing and the voltage fluctuations at the load especially those near the electrical centre of the system.
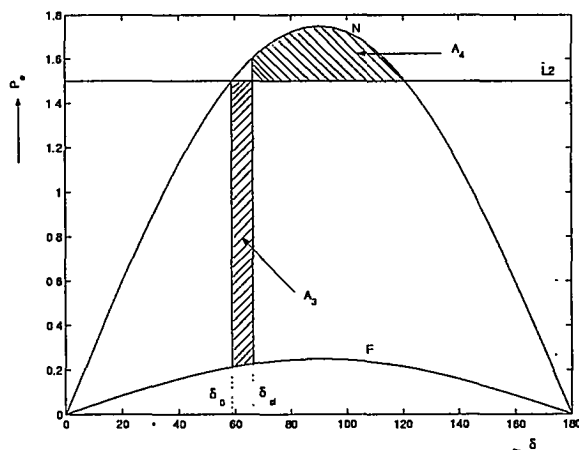
Figure 14.12: Power angle curves with switch open

Transient stability is also improved by either switching in shunt capacitors or switching off shunt reactors. But the rating of the shunt devices required will be in the range of 3-6 times the rating of the switched series capacitors for the same increase of stability limit.

The application of thyristor controllers with shunt capacitors and reactors constitute Static Var Compensators (SVC) which are first generation FACTS devices. The voltage and auxiliary controllers of SVC help in improving stability [35-38].

An important new FACTS device is Controlled Series Compensation (CSC) using thyristor switched capacitors (TSC) and thyristor controlled reactors (TCR) (see Fig. 14.13). In addition to discrete control of capacitors (switching in or out), continuous control is also possible using phase control of TCR connected across a capacitor [43,44]. With appropriate control strategies, the transient stability of the system can be improved.

Another important FACTS controller is Static Phase Shifter (SPS) or Thyristor Controlled Phase angle Regulator (TCPR). This device with appropriate control can improve transient stability by temporarily modifying the power angle curve. Although, unlike CSC, the maximum power flow is unaffected by phase shifter, the phase angle control results in a significant improvement of
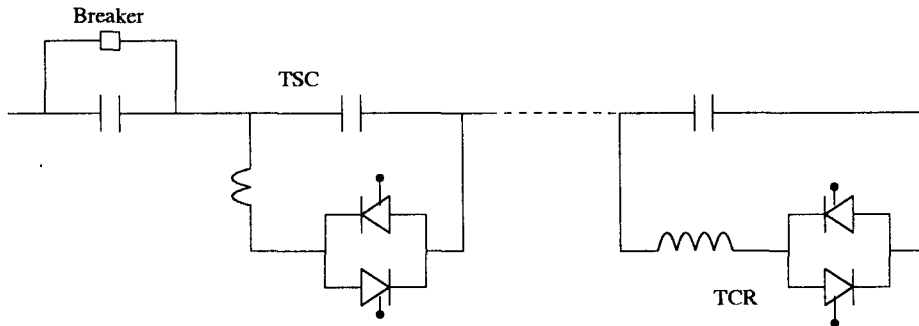
Figure 14.13: Components of controlled series compensation

transient stability [45-47]. As a matter of fact, a generator connected to a AC transmission line through a static phase shifter with a range of 360° phase shift can operate in asynchronous mode just as if it were connected to a HVDC line.

Another simple approach of providing phase shift when there is imminent loss of synchronism, is to disconnect two groups of generators and then reclose with 120° phase rotation [39]. Transient stability is improved because fast valving or excitation control is allowed more time to become effective.

14.8 Emergency Control Measures

There are occasions when the discrete controllers discussed in the previous sections are unable to prevent instability of the system. If no further action is taken, then the system may break apart due to uncontrolled tripping of generators (from out of step protection) and formation of islands which are unstable.

There are two emergency control measures (to be used as last resort) to prevent catastrophic failure of power systems leading to blackouts. These are

1. Controlled system separation and load shedding

2. Generator tripping

14.8.1 Controlled System Separation and Load Shedding

The objective here is to achieve a near balance between load and generation within each island formed by tripping the transmission line connecting the areas. Controlled system separation is applied in the following situations

(a) to prevent transmission line overloading following disturbances and loss of other lines

(b) when oscillatory instability occurs between load/generation areas during certain system conditions. Interties between areas can be programmed to open if rate and magnitude of power oscillations over the tie exceed permissible values.

However interties should not be opened until the benefits of maintaining power interchange among areas are exhausted and the need of the hour is to retain as much of the system intact as possible. Thus, controlled system separation goes together with load shedding when there is deficit of generation and generator tripping when there is excess.

The controlled system separation may often be done manually since the response time for the operator intervention is adequate to prevent collapse in many systems. When automatic separation is applied, voltage, current, power or frequency transducers are used to detect limit violations. Controlled separation is not widely used to improve system stability. This is because the boundaries for system separation are not well defined for all possible system conditions. It has been applied in the Western System in U.S.A. to reduce the effects of severe disturbances in one area, on the rest of the areas which are connected as a ring (or doughnut).

Load shedding programs have been used by many utilities, in distribution systems or major industrial loads. The objective is to prevent frequency decay and maintain equilibrium between generation and load when there is loss of generation. Load shedding can help in preventing interties from opening due to transmission overloads. Load shedding is initiated by underfrequency relays based on discrete underfrequency values or rates of frequency decay. Load shedding is generally done in three to six steps to prevent excessive load dropping after frequency levels off at an acceptable value. The underfrequency relay settings are based on the limitations on the underfrequency operation of turbine-generators and power plant auxiliaries.

14.8.2　Generator Tripping

The selective tripping of generators for transmission line outages has been used extensively to improve stability. Generating tripping is one form of power control and can be compared to fast valving and dynamic braking. If 'N' number of identical generating units in parallel are connected to an infinite bus through an external reactance of x_e, the tripping of one unit is equivalent to decreasing x_e by the ratio $\dfrac{N-1}{N}$. This improves both steady state and transient stability.

Generator tripping has been mainly employed to improve stability of remote generation. It can also be used to improve interconnected system operation where tripping of an intertie can lead to instability. In western U.S.A., the tripping of Pacific HVDC intertie can lead to instability, under certain conditions. The automatic tripping of certain hydrogenerators in the Northwest helps in controlling the power flow on the parallel 500 kV AC ties, thereby averting transient instability.

Generator tripping is initiated from a transfer trip scheme or by arranging the protection scheme at the power plant such that, when a transmission line is tripped following a line fault, one or more generators are also automatically tripped.

The impact of tripping and consequent full load rejection on a thermal unit needs to be studied because of the response of the prime mover and the action of over speed controller can vary. When a thermal unit is tripped, the unit will normally go through its standard shutdown and start-up cycle and full power may not be available for some hours. To overcome this problem, one method is to connect the station load to the unit tripped. The unit can then be rapidly reloaded after the disturbance is cleared. This requires that the unit and its controls be specifically designed for this mode of operation in which case, the unit can be resynchronized to the system and full load restored within about 15-30 minutes. However, it is essential that frequent tripping of thermal generators be avoided.

References and Bibliography

1. IEEE Committee Report, "A description of discrete supplementary controls for stability", IEEE Trans., Vol. PAS-97, No. 1, 1978, pp. 149-165

2. IEEE Committee Report, "Single phase tripping and reclosing of transmission lines", IEEE Trans. on Power Delivery, Vol. 7, No. 1, 1992, pp. 182-192

3. C. Concordia and P.G. Brown, "Effects of trends in large system steam turbine driven generator parameters on power system stability", IEEE Trans., Vol. PAS-90, Sept/Oct 1971, pp. 2211-2218

4. H.E. Lokay and P.O. Thoits, "Effects of future turbine-generator characteristics on transient stability", IEEE Trans., Vol. PAS-90, Nov/Dec. 1971

5. H.M. Ellis, J.E. Hardy, A.K. Blythe and J.W. Skoogland, "Dynamic stability of Peace River Transmission system", IEEE Trans., Vol. PAS-85, June 1966, pp. 586-600

6. M.L. Shelton, W.A. Mittelstadt, P.F. Winkleman and W.L. Bellerby, "Bonneville Power Administration 1400 MW braking resistor", IEEE Trans., Vol. PAS-94, March 1975, pp. 602-611

7. W.H. Croft and R.H. Hartley, "Improving transient stability by the use of dynamic braking", AIEE Trans., Power Apparatus and Systems, Vol. 59, April 1962, pp.17-26

8. W.A. Mittelstadt and J.L. Saugen, "A method for improving power system transient stability using controllable parameters", IEEE Trans., Vol. PAS-89, No. 1, 1970, pp. 23-27

9. F.P. DeMello, "The effects of control", **Modern Concepts of Power System Dynamics**, IEEE Tutorial Course, 70 M62-PWR,1970

10. J. Meisel, P.D. Barnard and R.S. Elliott, "Dynamic control of multimachine power systems based on two-step optimization over admissible trajectories", IEEE Trans. Vol. PAS-91, No. 3, 1972, pp. 920-927

11. R.J. Thomas, J.S. Thorp and C. Pottle, "A model referenced controller for stabilization of large transient swings in power systems", IEEE Trans. on Automatic Control, Vol. AC-21, No. 5, 1976, pp. 746-750

12. J. Zaborszky, A.K. Subramanian, T.J. Tarn and K.M. Lu, "A new state space for emergency control in interconnected power systems", IEEE Trans. on Automatic Control, Vol. AC-22, No. 4, 1977, pp. 505-517

13. J. Zaborszky, K. Whang and Krishna Prasad, "Stabilizing control in Emergencies, Part I: Equilibrium point and state determination, Part II: Control by local feedback", IEEE Trans. Vol. PAS-100, No. 5, 1981, pp. 2374-2389

14. J. Zaborszky, M. Ilic-spong, G. Huang and F. Dobraca, "Computer control of large power system during faults for inherently adaptive selective protection", IEEE Trans. on Power Systems, Vol. PWRS-2, No. 2, 1987, pp. 494-504

15. U.Di Caprio, "Emergency control", Int. J. of Elec. Power & Energy Syst., Vol. 4, No. 1, 1982, pp. 19-28

16. IEEE Committee Report, "Emergency control practices", IEEE Trans., Vol. PAS-104, No. 9, 1985, pp. 2336-2341

17. U.O. Aliyu and A.H. El-Abiad, "A local control strategy for power systems in transient emergency state, Part I: Functional analysis, Part II: Implementation and test results by simulation", IEEE Trans., Vol. PAS-101, No. 11, 1982, pp. 4245-4262

18. G.A. Jones, "Transient stability of a synchronous generator under conditions of bang-bang excitation scheduling", IEEE Trans., Vol. PAS-84, No. 2, 1965, pp. 114-120

19. O.J.M. Smith, "Optimal transient removal in a power system", IEEE Trans., Vol. PAS-84, No. 5, 1965, pp. 361-374

20. J.P. Bayne, P. Kundur and W. Watson, "Static exciter control to improve transient stability", IEEE Trans., Vol. PAS-94, No. 4, 1975, pp. 1141-1146

21. R.G. Harley, T.A. DeMeillon and W. Janischewskyj, "The transient stabilization of synchronous machine by discontinuous supplementary excitation control", IEEE Trans., Vol. PAS-104, 1985, pp. 1394-1399

22. F. Ishiguro, S. Tanaka, M. Shimomura, T. Maeda, K.Matsushita and H.Sugimoto, "Coordinated stabilizing control of exciter, turbine and braking resistor", IEEE Trans. on Power Systems, Vol. PWRS-1, No. 3, 1986, pp. 76-80

23. R.H. Park, "Fast turbine valving", IEEE Trans., Vol. PAS-92, May/June 1973, pp. 1065-1073

24. E.W. Cushing, G.E. Drechsler, W.P. Killgoar, H.G. Marshall and H.R. Stewart, "Fast valving as an aid to power system transient stability and prompt resynchronization and rapid reload after full load rejection", IEEE Trans., Vol. PAS-91, July/Aug 1972, pp. 1624-1636

25. W.A. Morgan, H.B. Peck, D.R. Holland, F.A. Cullen and J.B. Ruzek, "Modern stability aids for Calver Cliffs units", IEEE Trans., Vol. PAS-90, No. 1, 1971, pp. 1-10

26. IEEE Committee Report, "Dynamic performance characteristics of North American HVDC systems for transient and dynamic stability evaluations", IEEE Trans., Vol. PAS-100, No. 7, 1981, pp. 3356-3364

27. T. Berntsen and I. Glende, "Emergency power control of Skagerrak HVDC link as a part of a coordinated network protection scheme", CIGRE Study Committee 01, 1979, Paper 32-79

28. K.S. Turner, J. Arrillaga, M.D. Heffernam and C.P. ARnold, "HVDC control strategies to improve transient stability in the interconnected power systems", IEEE Trans., Vol. PAS-102, No. 7, 1983, pp. 2323-2330

29. E.W. Kimbark, "Improvement of system stability by switched series capacitors", IEEE Trans., Vol. PAS-85, No. 2, 1966, pp. 180-186

30. O.J.M. Smith, "Power system transient control by capacitor switching", IEEE Trans., Vol. PAS-88, No. 1, 1969, pp. 28-35

31. E.W. Kimbark, "Improvement of power system stability by changes in the network", IEEE Trans., Vol. PAS-88, No. 5, 1969, pp. 773-781

32. N. Rama Rao and D.K. Reitan, "Improvement of power system transient stability using optimal control: bang-bang control of reactance", IEEE Trans., Vol. PAS-89, May/June 1970, pp. 975-984

33. D.K. Reitan and N. Rama Rao, "A method of improving transient stability by bang-bang control of tie-line reactance", IEEE Trans., Vol. PAS-93, Jan/Feb 1974, pp. 303-311

34. R.H. Webster and O.J.M. Smith, "Series capacitor switching to quench eletromechanical transients in power systems", IEEE Trans., Vol. PAS-90, No. 2, 1971, pp. 427-433

35. A.Olwegard, K. Walve, G. Waglund, H. Frank and S. Torseng, "Improvement of transmission capacity by thyristor controlled reactive power", IEEE Trans., Vol. PAS-100, No. 8, 1981, pp. 3930-3939

36. A. Hammad, "Analysis of power system stability enhancement by static VAR compensators", PICA 1985 Conference Proceedings, pp. 438-443

37. K.R. Padiyar, "Improvement of system stability with SVC control", in **Recent Advances in Control and Management of Energy Systems**, Interline Publishing, Bangalore, 1993, pp. 136-156

38. K.R. Padiyar and Vijayan Immanuel, "Direct evaluation of transient stability improvement with static var compensators using a structure preserving energy function", Electric Machines and Power Systems, Vol. 23, No. 3, 1995

39. R.L. Cresap, C.W. Taylor and M.J. Kreipe, "Transient stability enhancement by 120-degree phase rotation", IEEE Trans., Vol. PAS-100, Feb. 1981, pp. 745-753

40. S. Nishida and S. Takeda, "A method to construct a control strategy in emergency control of power systems on the basis of energy function", Electrical Engineering in Japan, Vol. 102, No. 5, 1982, pp. 77-84

41. C.W. Taylor, F.R. Nassief and R.L. Cresap, "Northwest Power Pool transient stability and load shedding controls for generation-load imbalances", IEEE Trans., Vol. PAS-100, July 1981, pp. 3486-3495

42. IEEE Committee Report, "Bibliography on the application of discrete supplementary controls to improve power system stability", IEEE Trans. on Power Systems, Vol. PWRS-2, May 1987, pp. 474-485

43. E. Larsen, C. Bowler, B. Damsky and S. Nilsson, "Benefits of thyristor controlled series compensation", CIGRE conf. Proceedings, 1992, Paper 14/37/38-04

44. N. Christl et al., "Advanced series compensation (ASC) with thyristor controlled impedance", CIGRE Proceedings, 1992, Paper 14/37/38-05

45. C.P. Arnold, R.M. Duke and J. Arrillaga, "Transient stability improvement using thyristor controlled quadrature Vol. age injection", IEEE Trans., Vol. PAS-100, No. 3, 1981, pp. 1382-1388

46. R. Baker, G. Guth, W. Egli and P. Eglin, "Control algorithm for a static phase shifting transformer to enhance transient and dynamic stability of large power systems", IEEE Trans., Vol. PAS-101, No. 9, 1982, pp. 3532-3542

47. A. Edris, "Enhancement of first-swing stability using a high-speed phase shifter", IEEE Trans. on Power Systems, Vol. PWRS-6, No. 3, 1991, pp. 1113-1118

"This page is Intentionally Left Blank"

Chapter 15

Introduction to Voltage Stability

Voltage has always been considered as an integral part of the power system response and is an important aspect of system stability and security. Thus, voltage instability and collapse cannot be separated from the general problem of system stability. However, in the recent years, the analysis of voltage stability has assumed importance, mainly due to several documented incidents of voltage collapse in France, Japan, Belgium and Florida [1]. There are several factors which contribute to voltage collapse such as increased loading on transmission lines, reactive power constraints, on-load tap changer (OLTC) dynamics and load characteristics.

In contrast to voltage stability, the problem of loss of synchronism due to uncontrolled generator rotor swings is termed as angle stability. Loss of synchronism may also be accompanied by voltage instability. However in the present context, voltage instability implies an uncontrolled decrease in voltage triggered by a disturbance, leading to voltage collapse and is primarily caused by dynamics connected with the load. Although the frequency may increase on voltage collapse, the generators normally remain in synchronism.

The problem of voltage stability has received considerable attention in the recent years. There are several aspects of the problems related to voltage profile in a system and it is important to distinguish them to avoid confusion. What is presented here is an attempt to define the problem of voltage instability and to outline the methods of analysis.

15.1   What is Voltage Stability ?

It is to be clearly understood that the problem of low voltages in steady state conditions, should not be confused with voltage instability. As a matter of fact, it is possible that the voltage collapse may be precipitated even if the initial operating voltages may be at acceptable levels.

Voltage collapse may be fast (due to induction motor loads or HVDC converter stations) or slow (due to on-load tap changers and generator excitation

limiters). Voltage stability is sometimes also termed as load stability. The terms voltage instability and voltage collapse are often used interchangeably. It is to be understood that the voltage stability is a subset of overall power system stability and is a dynamic problem. The voltage instability generally results in monotonically (or aperiodically) decreasing voltages. Sometimes the voltage instability may manifest as undamped (or negatively damped) voltage oscillations prior to voltage collapse.

A CIGRE Task Force [2] has proposed the following definitions for voltage stability.

Small-disturbance Voltage Stability

A power system at a given operating state is **small-disturbance voltage stable** if, following any small disturbance, voltages near loads are identical or close to the pre-disturbance values. The concept of small-disturbance voltage stability is related to steady-state stability and can be analyzed using small-signal (linearized) model of the system.

Voltage Stability

A power system at a given operating state and subjected to a given disturbance is **voltage stable** if voltages near loads approach post-disturbance equilibrium values. The disturbed state is within the region of attraction of the stable post-disturbance equilibrium.

The concept of voltage stability is related to transient stability of a power system. The analysis of voltage stability usually requires simulation of the system modelled by nonlinear differential-algebraic equations.

Voltage Collapse

Following voltage instability, a power system undergoes **voltage collapse** if the post-disturbance equilibrium voltages near loads are below acceptable limits. Voltage collapse may be total (blackout) or partial.

The absence of voltage stability leads to voltage instability and results in progressive decrease of voltages. When destabilizing controls (such as OLTC) reach limits or due to other control actions (undervoltage load shedding), the voltages are stabilized (at acceptable or unacceptable levels). Thus abnormal voltage levels in steady state may be the result of voltage instability which is a dynamic phenomenon.

There are other concepts such as power controllability and maximum

. loadability which are related to the voltage problem but should not be confused with voltage stability.

The **power uncontrollability** is a steady state problem accompanied by low voltages, when switching in more load results in reduced load power. A related concept is **maximum power transfer capability or maximum loadability** which is connected to power system static properties - such as transmission network impedances viewed from the load bus and load impedance. Maximum loadability is not necessarily a stability limit. In this context it is necessary to make a distinction between **nominal load power** (at nominal frequency and voltage) and **consumed load power** actually consumed at the operating voltage and frequency.

The voltage instability and collapse may occur in a time frame of fraction of a second. In this case the term **'transient voltage stability'** is used. Sometimes, it may take up to tens of minutes in which case the term **'long-term voltage stability'** is used.

15.2 Factors affecting voltage instability and collapse

The voltage collapse occurs invariably following a large disturbance or large load increase in a heavily stressed power system. This results in an increased reactive power consumption and voltage drop. The voltage drop causes initial load reduction triggering control mechanisms for load restoration. It is the dynamics of these controls that often lead to voltage instability and collapse.

Transient Voltage Instability

Induction motors supplying loads with constant torques draw constant power independent of applied voltage. However, during faults or periods of low voltage, they decelerate as the electrical torque is not adequate to meet the required mechanical torque. Following the clearing of the fault, the motor may not regain the original speed and continue to decelerate leading to stalling of motors which in turn aggravates the low voltage problem.

This phenomenon can be explained with reference to the torque-slip characteristics of an induction motor shown in Fig. 15.1. Under normal operating conditions, the peak torque is T_{p1} and the motor operates stably at slip S_1. During a fault the peak torque T_{p2} is less than the load torque T_m and the motor decelerates. If the fault is cleared before the slip increases to S_2, the motor regains its original speed. On the other hand if the motor slip goes beyond S_2,
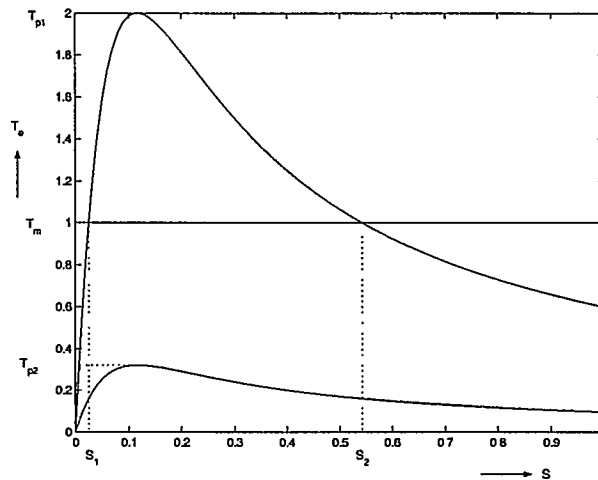
Figure 15.1: Torque-slip characteristics

the motor fails to recover even after the fault is cleared and the motor continues to decelerate and will stall eventually. Stalled motors draw large currents which can depress the voltages and lead to stalling of other motors in the vicinity.

There is a critical clearing time for a given fault to avoid stalling of motors. This can be obtained from solving the equation for the slip given by

$$2H_m \frac{dS}{dt} = T_m - T_e \tag{15.1}$$

where H_m is the motor inertia.

Transient voltage stability is also associated with HVDC links, particularly inverter terminals connected to AC systems with low short circuit capacity. The characteristics of reactive power consumption at the inverter and the shunt capacitor compensation are factors affecting voltage instability. Constant voltage control instead of constant extinction angle (CEA) control at the inverter can result in improved voltage stability [3,4].

Long Term Voltage Instability

On-load tap-changing (OLTC) transformers and distribution voltage regulators act within a time frame of tens of seconds to tens of minutes to regulate the load voltages. This results in the restoration of voltage sensitive loads. Another form of load restoration is due to the thermostatic control of heating or cooling loads.

An important factor in long term voltage stability is the current limiting at generators. Generator field and armature windings have overload capabilities

of duration up to few minutes. Field current is limited by overexcitation limiters which can be modelled as shown in Fig. 15.2 [5]. If the field current exceeds the high setting (I_{fmax2}) the current is ramped down without a time delay to its continuous limit. (see Fig. 15.3). If the field current exceeds the continuous limit (I_{fmax1}) but is below the high setting, the current is ramped down to its continuous limit after a time delay dependent on the level of the field current and the excitation limiter settings.
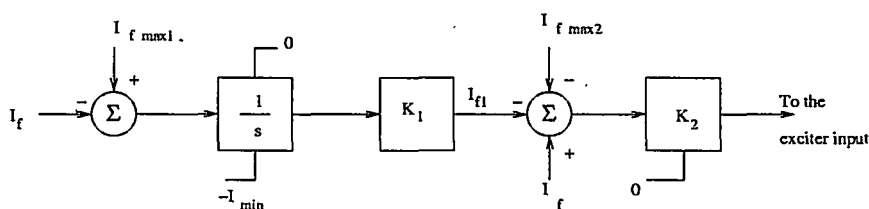
Figure 15.2: Model of over excitation limiter
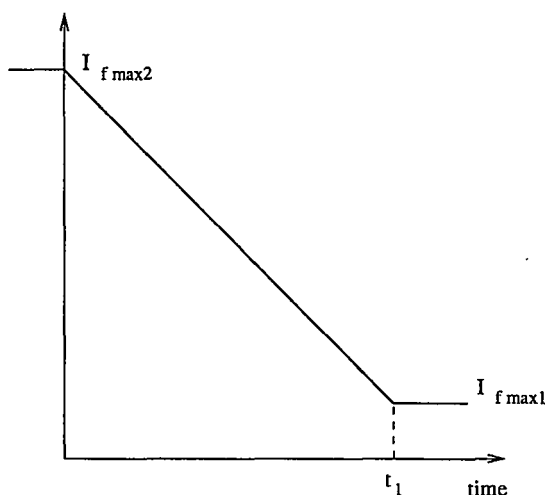
Figure 15.3: Over excitation limiter characteristics

Once the current is limited at one generator, the required reactive power has to be supplied by the remaining generators farther away (from the load centre) leading to cascading of current limiting. Field current limiting and loss of terminal voltage control can result in armature overcurrent that must be relieved by the operation of protection. A typical generator Q-V diagram is shown in Fig. 15.4 [2].
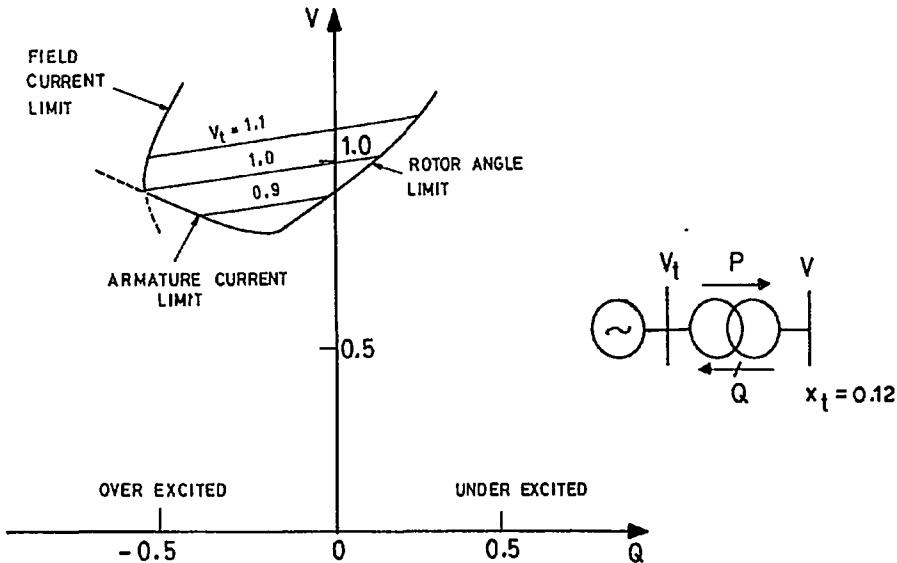
Figure 15.4: Q-V diagram of a generator

15.3   Comparison of Angle and Voltage Stability

As mentioned earlier, the analysis of power system stability in the past pertained to the power angle dynamics expressed in terms of swing equations of synchronous generators. In the context of voltage or load stability and dynamics related to it, the stability of the system based on power angle dynamics can be termed as angle stability where the major concern is the loss of synchronism. On the other hand, in the analysis of voltage stability, the major concern is the voltage collapse, although the generators may remain in synchronism. Both situations - loss of synchronism and voltage collapse can affect system security and lead to stability crisis, thereby threatening the integrity of the system.

The simplest system for the analysis of angle stability is the Single Machine Infinite Bus (SMIB) System. This has been discussed in detail. It is to be noted that in this system, the power received at the infinite bus in steady state is determined from the power output of the generator. As there is no load bus in the simple two bus SMIB system, there is no load dynamics to be considered.

Only the generator dynamics affect (angle) stability. However it is to be noted that loss of synchronism in a SMIB system is accompanied by voltage instability at the generator terminal bus. (see Figs. 15.5 and 15.6) The disturbance considered is increase in T_m by 0.01 at $t = 1$s. If AVR is not considered, there is aperiodic or monotonic decrease in terminal voltage. On the other hand,
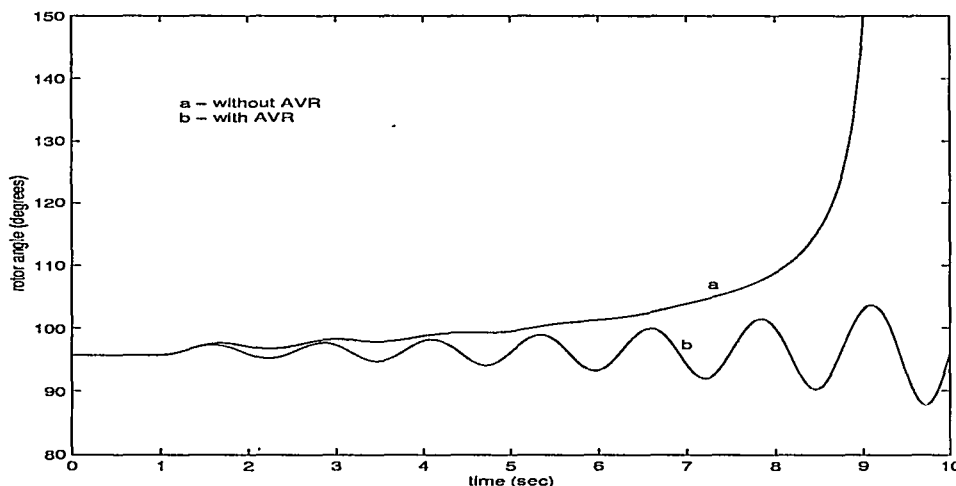
Figure 15.5: Swing curves

with fast acting excitation system and high gain AVR, there is oscillatory instability which can lead to subsequent loss of synchronism. It is to be noted that negatively damped oscillations in the rotor angle are also accompanied by voltage oscillations which increase in amplitude. When the generator loses synchronism, the terminal voltage has large oscillations with increasing frequency. However, voltage stability is normally associated with load buses. Thus, the simplest system that can be considered for the study of voltage stability is the Single Machine Load Bus (SMLB) system shown in Fig. 15.7.

Analysis of SMLB System

The system shown in Fig. 15.7 contains an equivalent machine of several coherent generators (swinging together). The load is initially considered to be of static type - with voltage dependent active and reactive power characteristic. A shunt capacitor is connected across the load for reactive power compensation.

The synchronous machine can be modelled with only field flux decay considered (neglecting damper windings). The excitation system is assumed to
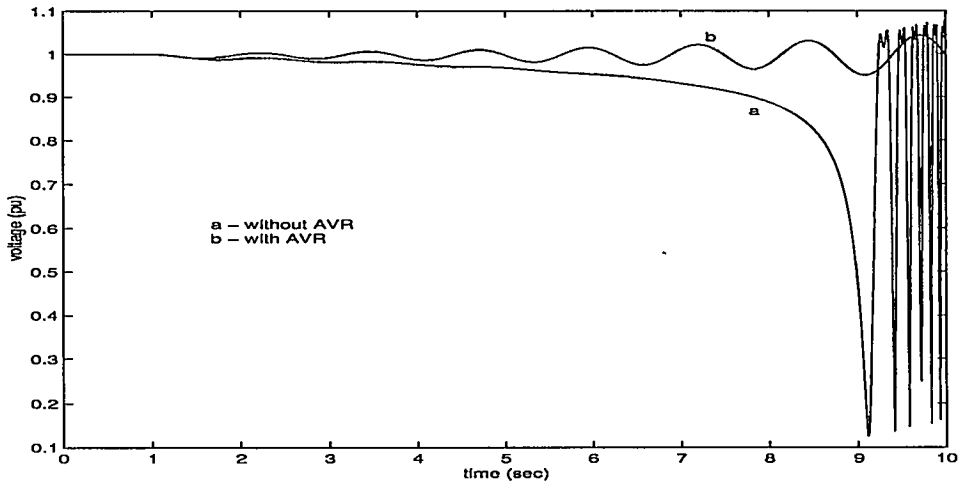
Figure 15.6: Variation of terminal voltage
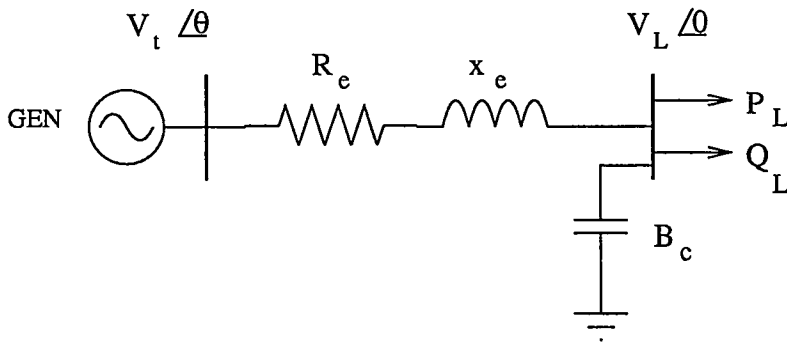
Figure 15.7: An SMLB System

be represented by a simple transfer function given by

$$E_{fd} = \frac{K_E}{1 + sT_E}(V_{ref} - V_t) \tag{15.2}$$

The limiters are ignored as only small signal analysis is carried out. The electrical torque T_e is given by

$$T_e = E_q' i_q - (x_q - x_d') i_d i_q \tag{15.3}$$

The stator equations (neglecting armature resistance) are

$$E_q' + x_d' i_d = v_q \tag{15.4}$$

$$-x_q i_q = v_d \tag{15.5}$$

The network and load equations are

$$v_q = -x_e i_d + R_e i_q + v_{qL} \tag{15.6}$$

$$v_d = R_e i_d + x_e i_q + v_{dL} \tag{15.7}$$

$$v_{qL} + j v_{dL} = \frac{P_L + j(Q_L - V_L B_c^2)}{(i_q - j i_d)}, \quad V_L = \sqrt{v_{dL}^2 + v_{qL}^2} \tag{15.8}$$

$$P_L = P_{Lo} \left(\frac{V_L}{V_{Lo}} \right)^{m_p} \tag{15.9}$$

$$Q_L = Q_{Lo} \left(\frac{V_L}{V_{Lo}} \right)^{m_q} \tag{15.10}$$

Linearizing Eqs. (15.3) to (15.10) and simplifying, it can be shown that

$$\Delta i_d = Y_d \Delta E_q' \tag{15.11}$$

$$\Delta i_q = Y_q \Delta E_q' \tag{15.12}$$

and

$$\Delta T_e = K_2 \Delta E_q' \tag{15.13}$$

It is interesting to note that the torque deviation ΔT_e depends only on $\Delta E_q'$ in this case in contrast to a SMIB system where

$$\Delta T_e = K_1 \Delta \delta + K_2 \Delta E_q' \tag{15.14}$$

Thus, a SMLB system cannot exhibit angle instability. The power output of the generator (as well as electrical torque in per unit) is determined by the load power. In the absence of angle dynamics, the only relevant dynamics is that corresponding to the field flux decay and excitation system (see block diagram of Fig. 15.8). Here K_3 and K_6 are analogous to Heffron-Phillips constants.

The characteristic equation for the system shown in Fig. 15.8 is given by

$$s^2 + \left(\frac{1}{T_{do}' K_3} + \frac{1}{T_E} \right) s + \frac{1 + K_3 K_6 K_E}{T_{do}' K_3 T_E} = 0$$

If $K_E K_6 K_3 \gg 1$, then the criteria for stability are

$$\frac{1}{T_{do}' K_3} + \frac{1}{T_E} > 0, \quad K_6 > 0$$

If the generator is represented by the classical model of a constant voltage source E_g behind a constant reactance x_g, there is no possibility of voltage
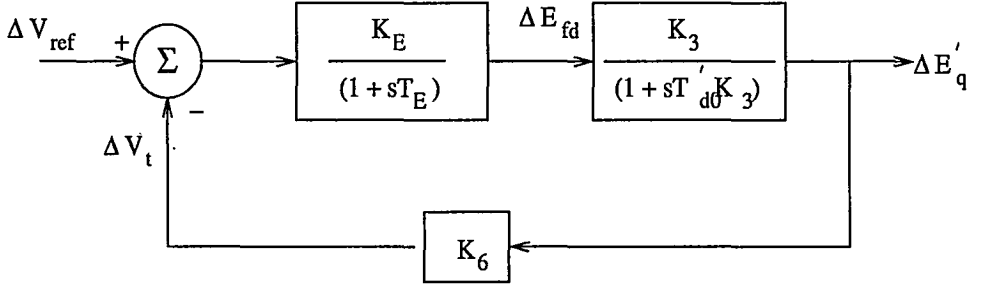
Figure 15.8: Block diagram of voltage control loop
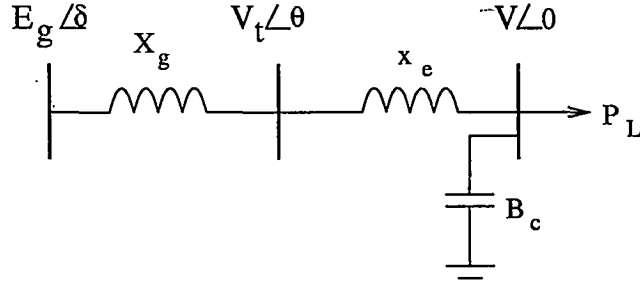
Figure 15.9: A simplified SMLB system

instability and collapse as there is no voltage dynamics that can lead to instability. The system with the generator internal bus is shown in Fig. 15.9. If the network is assumed to be lossless for simplicity, and the load is considered to be of unity power factor, the received active power and load voltage are given by the following expressions

$$P = \frac{E_g^2 \sin 2\delta}{2X(1 - B_c X)} = P_L \tag{15.15}$$

$$V = \frac{E_g \cos \delta}{(1 - B_c X} \tag{15.16}$$

where $X = x_g + x_e$.

The plot of voltage V as a function of P is shown in Fig. 15.10, for the following parameters

$$E_g = 1.0, \quad X = 0.5, \quad B_c = 0.0 \quad \text{and} \quad 0.1$$

This is termed as the 'nose' curve. Similar curve can be obtained even if the load has reactive power component. It is observed that for a constant power
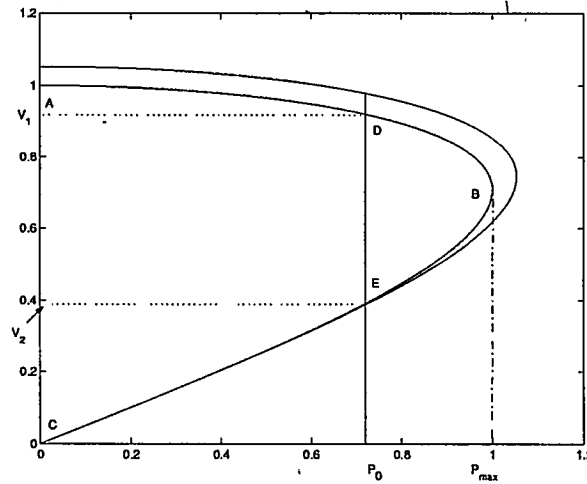
Figure 15.10: PV diagram at the load bus

load of $P = P_o$, there are two voltage solutions V_1 and V_2. In the literature, it is often mentioned that the high voltage solution V_1 is stable while the low voltage solution V_2 is unstable. This statement requires an explanation based on system dynamics which is often ignored. It is also mentioned that the operation in the lower portion of the nose curve (BC) is unstable.

As mentioned earlier, if the generator is represented by the classical model, it is incorrect to say that the region BC is unstable unless load dynamics is considered. Even if detailed generator dynamics is considered, it is unlikely that the voltage instability can arise. The only statement that can be made is that in the region BC, there is power uncontrollability and the maximum loadability is determined by point B.

Dynamics of Load Restoration

It is assumed that the load is voltage sensitive and there is a control mechanism (using OLTC or voltage regulator) to restore the load, which can be modelled by the equation

$$\frac{dV}{dt} = \frac{1}{T_p}[P - P_o] \tag{15.17}$$

where P_o is the nominal load power that is to be maintained at all voltages. Since P is a function of V, the stability of the equilibrium point is determined from the criterion

$$\frac{dP}{dV} < 0 \tag{15.18}$$

The system is stable at operating point D $(V = V_1)$ and unstable at operating point $E(V = V_2)$. The region of attraction for the equilibrium point D is ADBE. The voltage instability and collapse can result following a distrubance if the transient voltage falls below V_2. The probability of this increases as the operating power P_o is close to the maximum power P_{max}. Alternately, if $(V - V^*)$ is below a specified margin, it can be said that the system is prone to voltage instability and collapse.

At the load bus, the following equations apply, using the Jacobian

$$\begin{bmatrix} J_1 & J_2 \\ J_3 & J_4 \end{bmatrix} \begin{bmatrix} \Delta\delta \\ \Delta V \end{bmatrix} = \begin{bmatrix} \Delta P \\ 0 \end{bmatrix} \tag{15.19}$$

where

$$J_1 = \frac{\partial P}{\partial \delta}, \quad J_2 = \frac{\partial P}{\partial V}, \quad J_3 = \frac{\partial Q}{\partial \delta}, \quad J_4 = \frac{\partial Q}{\partial V}$$

If $J_3 \neq 0$, it can be shown that

$$\frac{dP}{dV} = J_2 - J_1 J_3^{-1} J_4 \tag{15.20}$$

The RHS of Eq. (15.20) is zero if the determinant of the Jacobian is zero (the Jacobian is singular). Thus, determinant of the Jacobian can also indicate proximity to voltage collapse.

A better index for the evaluation of voltage stability margin is obtained if it is recognized that Eq. (15.17) can be expressed as

$$T_p \frac{dV}{dt} = -\frac{\partial W}{\partial V} \tag{15.21}$$

where $W = \int_{V_1}^{V} (P_o - P) dV$ is termed as potential energy. The energy margin defined by

$$\Delta W = \int_{V_1}^{V_2} (P_o - P) dV \tag{15.22}$$

can be used as an index for voltage security. A little reflection shows that when active power is treated as constant, the reactive power versus voltage $(Q - V)$ curve can be used for evaluating the margin. In this case, Eq. (15.17) is replaced by

$$\frac{dV}{dt} = \frac{1}{T_q} [Q(V) - Q_o] \tag{15.23}$$

and Eq. (15.22) is replaced by

$$\Delta W' = \int_{V_1}^{V_2} (Q_o - Q) dV \tag{15.24}$$

It is to be noted, in general, that the following equation applies at the load bus

$$Q = Q_L - Q_C \tag{15.25}$$

where Q is the received reactive power and Q_C is the reactive power supplied by the reactive compensator at the load bus. It is assumed that

$$Q_o = Q_{Lo} - Q_{Co} \tag{15.26}$$

Instead of Eq. (15.23), the reactive power compensator may be described by the equation

$$\frac{1}{T_c}\frac{dQ_C}{dt} = V_o - V \tag{15.27}$$

In this case the criterion for stability is

$$\frac{dV}{dQ_c} > 0 \tag{15.28}$$

Remarks

Based on the discussion given above the following points are worth noting

1. In contrast to SMIB system, in SMLB system, the swing equation has no role to play in stability analysis.

2. While the voltage dynamics in the generator can contribute to voltage instability, the primary factor is the dynamics of load restoration at the load bus. The voltage collapse may take several seconds or minutes based on the time constants T_p or T_q.

3. If load dynamics is ignored, the underside of the nose curve does not indicate voltage instability. It only indicates power uncontrollability.

4. The modelling of load (restoration) dynamics can vary depending upon the physical characteristics of the controller.

5. It has been observed during incidents of voltage collapse, the disabling of OLTC helps to overcome voltage instability. This fact is easily explained from the analysis given above.

6. The proximity to voltage collapse can be measured by several indices. Many of them utilize the fact that the load flow Jacobian is close to being singular (the determinant of the Jacobian is close to zero).

7. Although static analysis (neglecting system dynamics) can be used as an approximation in the study of voltage stability, particularly in long term voltage stability, dynamic analysis is essential for accurate prediction of the phenomenon.

The analysis of voltage stability will be taken up in the next section.

15.4   Analysis of Voltage Instability and Collapse

Simulation [6,7]

As mentioned earlier, voltage instability is a dynamic phenomenon and the system is described by nonlinear differential algebraic equations. For the study of voltage stability under large disturbances, it is necessary to simulate the system. Midterm stability programs that can simulate the system upto a few minutes can be utilized for this purpose provided that they can model the load characteristics accurately and also include the dynamics of OLTC and overexcitation limiters. The representation of OLTCs can significantly increase the simulation time frame as they have an intrinsic time delay of the order of 30 s and an additional 1-5 s is taken for each subsequent tap movement [6]. It is also necessary to model correctly step size, initial tap position and tap range. If AVR line drop compensation is used to control voltages remote from the generator terminals, they have a major effect on the reactive power outputs of a set of generating units and this needs to be represented as well in addition to overexcitation limiters.

Load representation should include not only static loads which are voltage dependent but also dynamic loads such as induction motors and thermostatic loads.

All the reactive compensation devices - switched shunt reactors, capacitors, SVC (with limiting action) need to be represented adequately. In addition, special protection schemes such as under voltage load shedding, OLTC blocking, reactor tripping and generator runback should be modelled [6].

Small Signal (Linear) Analysis

There are two approaches here - static analysis (considering only algebraic equations) and dynamic analysis (considering system dynamics). It is to be understood that static analysis is an approximation which may give reasonably accurate results in identifying critical situations. By defining Voltage Collapse Proximity Indicators (VCPI) it is possible to implement security assessment. The sensitivity information can be used to devise corrective measures to overcome the problem of voltage collapse.

The system equations are

$$\dot{x} = f(x, y) \tag{15.29}$$

$$0 = g(x, y) \tag{15.30}$$

The load flow equations are included in (15.30). Linearizing Eqs. (15.30) and

(15.30) we get

$$\Delta \dot{x} = [J_{SYS}]\Delta x \qquad (15.31)$$

where

$$[J_{SYS}] = \left[\frac{\partial f}{\partial x}\right] - \left[\frac{\partial f}{\partial y}\right]\left[\frac{\partial g}{\partial y}\right]^{-1}\left[\frac{\partial g}{\partial x}\right] \qquad (15.32)$$

$[J_{SYS}]$ is termed as the system Jacobian matrix and is distinct from the load flow Jacobian matrix $[J_{FL}]$. All the eigenvalues of the system Jacobian matrix should lie in the LHP $(Re(\lambda_i) < 0)$ for the equilibrium (operating) point to be stable.

It is assumed that the system Jacobian matrix is dependent on a parameter μ (say load at a specified bus) which is varied. For $\mu < \mu_c$, the equilibrium point is stable. At $\mu = \mu_c$, the critical value of the parameter, a bifurcation is said to occur [8] and the equilibrium point becomes unstable for $\mu = \mu_c$. At $\mu = \mu_c$, the system Jacobian matrix can have either

(a) a real eigenvalue which is zero or

(b) a complex pair on imaginary axis

The loci of the critical eigenvalues for the two cases are shown in Fig. 15.11. In the first case, instability is due to the crossing of a real eigenvalue into the RHP and the bifurcation is said to be of saddle-node type. In the second type, the instability is due to the crossing of a complex pair into the RHP and it is termed as Hopf bifurcation.

If it is assumed that the voltage instability and collapse is due to saddle-node bifurcation, then the system Jacobian matrix is singular at the critical value of the parameter $\mu = \mu_c$ as one of its eigenvalues is zero. In this case, static analysis based on the rank properties of the system Jacobian matrix can give accurate results.

Another implicit assumption used in the static analysis is that the rank properties of the system Jacobian matrix are related to that of the load flow Jacobian matrix. Venikov et al [9] showed that the rank of load flow Jacobian matrix is equal to the rank of system Jacobian provided that

1. The active power and voltage magnitude are specified at each generator bus

2. Loads are of constant power (P and Q) type

3. The slack node is an infinite bus

(a) Saddle Node bifurcation   (b) Hopf bifurcation
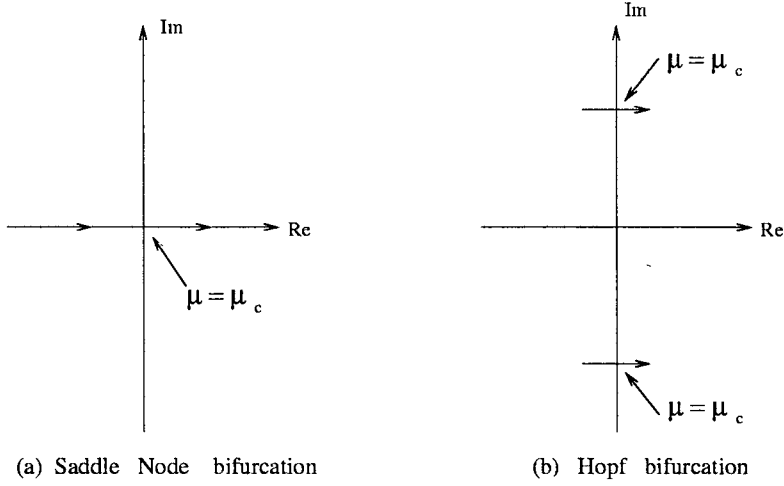
Figure 15.11: Loci of critical eigenvalues

With these conditions, the determinant of the load flow Jacobian matrix is identical to the product of all the eigenvalues of the system Jacobian matrix. It is shown in [10] that in general, the system Jacobian matrix can have a zero eigenvalue even when the load flow Jacobian matrix is nonsingular. The load level which produces a singular load flow Jacobian matrix should be considered as an optimistic upper bound on maximum loadability.

Using the load flow Jacobian matrix, $[J_{LF}]$ defined by

$$[J_{LF}] \cdot \begin{bmatrix} \Delta \theta \\ \Delta V \end{bmatrix} = \begin{bmatrix} J_{P\theta} & J_{PV} \\ J_{Q\theta} & J_{QV} \end{bmatrix} \begin{bmatrix} \Delta \theta \\ \Delta V \end{bmatrix} = \begin{bmatrix} \Delta P \\ \Delta Q \end{bmatrix} \qquad (15.33)$$

The rank of $[J_{LF}]$ is identical to that of the reduced Jacobian matrix $[J_R]$ defined by

$$[J_R] = [J_{QV} - J_{Q\theta} J_{P\theta}^{-1} J_{PV}] \qquad (15.34)$$

provided that $J_{P\theta}$ is nonsingular. This follows from Schur's formula

$$\det[J_{FL}] = \det[J_{P\theta}] \cdot \det[J_R] \qquad (15.35)$$

Reference [11] suggests a singular value decomposition of the reduced Jacobian matrix $[J_R]$ and the use of the smallest singular value, σ_n as a measure of the proximity of voltage stability limit.

A $n \times n$ matrix $[A]$ can be expressed by its singular value decomposition

$$[A] = [U][D][V]^t = \sum_{i=1}^{n} \sigma_i u_i v_i^t \qquad (15.36)$$

where $[U]$ and $[V]$ are $n \times n$ orthogonal matrices with columns u_i and v_i, $(i = 1, 2 \ldots, n)$ respectively. $[D]$ is a diagonal matrix of singular values σ_i, $i = 1, 2 \ldots, n$. Also $\sigma_i \geq 0$ for all i. Without loss of generality, it can be assumed that

$$\sigma_1 \geq \sigma_2 \geq \sigma_3 \geq \ldots \geq \sigma_n \geq 0 \qquad (15.37)$$

For a real symmetric matrix, the absolute values of eigenvalues are the singular values. In general, σ_i is the square root of the eigenvalue of the matrix $[AA^t]$ or $[A^t A]$.

The singular value decomposition is well conditioned and the singular values are insensitive to perturbation in the matrix elements. Given the system of linear equations

$$[A]x = b \qquad (15.38)$$

the solution can be expressed as

$$x = [A]^{-1}b = [UDV^t]^{-1}b = \sum_{i=1}^{n} \frac{u_i^t b}{\sigma_i} v_i \qquad (15.39)$$

If $\Delta P = 0$, Eq. (15.33) can be expressed as

$$[J_R]\Delta V = \Delta Q \qquad (15.40)$$

Applying (15.39) to the solution of (15.40) it is seen that

1. The smallest value σ_n is an indicator of proximity to the voltage stability limit

2. The right singular vector v_n, corresponding to σ_n is an indicator of affected (sensitive) bus voltages

3. The left singular vector u_n corresponding to σ_n is an indicator of the most sensitive direction for changes in the reactive power injections

Reference [5] uses eigenvalue analysis based on the reduced Jacobian matrix for the study of voltage stability.

In reference [12] it is shown that voltage instability can occur due to Hopf bifurcation which cannot be predicted from static analysis. The instablity is caused by the exciter mode which can be damped by suitable design of a stabilizer.

The results given in [4] show that the voltage instability at the inverter bus is due to Hopf bifurcation while the instability at the rectifier bus is normally due to saddle-node bifurcation. While the results obtained from static analysis are in agreement with the results obtained from dynamic analysis if the bifurcation is of saddle-node type, the static analysis can give very optimistic and hence misleading results if the bifurcation is Hopf.

15.5 Integrated Analysis of Voltage and Angle Stability

The use of fast acting excitation systems with high gain voltage regulators gives rise to the problem of undamped low frequency oscillations. This problem has been viewed as a part of the angle stability problem (see chapter 7) and the small signal stability analysis of a SMIB system based on Heffron - Phillips constants was presented by De Mello and Concordia [14].

As discussed earlier, a SMIB system cannot exhibit voltage instability and a SMLB system cannot exhibit angle instability. A three bus system consisting of a generator bus, load bus and an infinite bus is the smallest system that can exhibit both voltage and angle instabilities. The work of [14] can be extended to such a system and the results based on a detailed study are reported in [15].
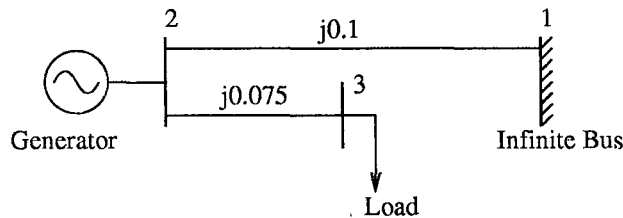
Figure 15.12: 3 bus system for study.

Consider the system shown in Fig 15.12. The load is assumed to be constant power type with constant power factor. The active power received by the infinite bus is kept constant at 1.0 pu. Using Heffron - Phillips constants, it is possible to obtain the region of stability (ROS) for a given load in the $K_E - T_E$ (regulator gain and time constant) plane. The ROS for $P_l = 3.43$ is shown in Fig. 15.13. The ROS is bounded by ABC and a straight line (corresponding to constant K_E) DC. This is typical and it was observed that ROS shrinks as the load is increased.

It can be shown that instability for operating points above the line ABC is due to undamped oscillations (HB) and the instability below line DC is monotonic due to saddle node bifurcation (SNB). For a constant regulator gain (below the maximum), low values of T_E resulted in instability of the swing mode. At high values of T_E, instability is due to the exciter mode. There is a range of T_E for which the system was stable. The loci of both swing and exciter modes for $K_E = 350$ as T_E varied, are shown in Fig. 15.14. This shows that the system is stable for $1.215 < T_E < 5.050$.
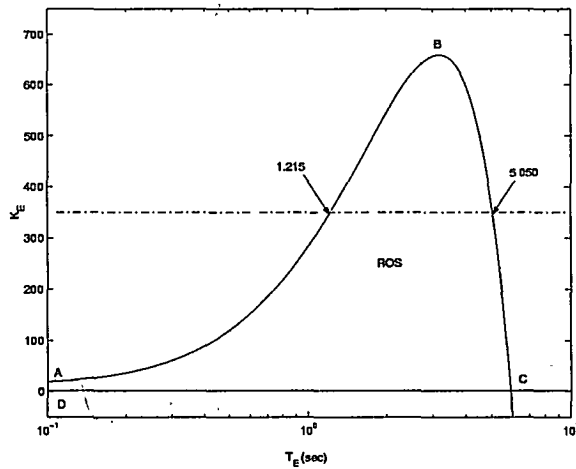
Figure 15.13: ROS at $P_l = 3.43$
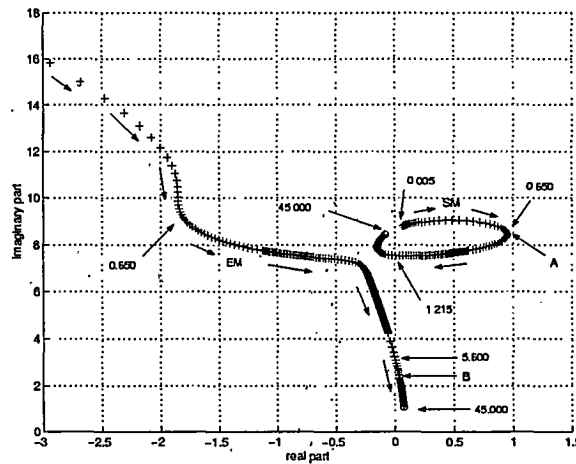
Figure 15.14: Root Loci of 3 bus 2 line system at $K_E = 350.0, P_l = 3.430$ pu. T_E is changing.

The simulation results for a small disturbance for $K_E =, 350, T_E = 7.0$ are shown in Fig 15.15. This shows the exciter mode instability affects on the load bus voltage and not the power swing in the line connecting the infinite bus to the generator. The voltage oscillations increase in magnitude while the power swings are damped. The simulation results for $K_E = 0.5$, $T_E = 1.0$ are shown in Fig. 15.16. This shows similar results with exciter mode instability not affecting power swings. There is monotonic collapse in the load bus voltage due to SNB.

(a) Oscillations in power P_{21} tend to stabilize. $K_E = 350.0, T_E = 7.0$ sec.

(b) Growing oscillations in load bus voltage for $K_E = 350.0$ and $T_E = 7.0$ sec.
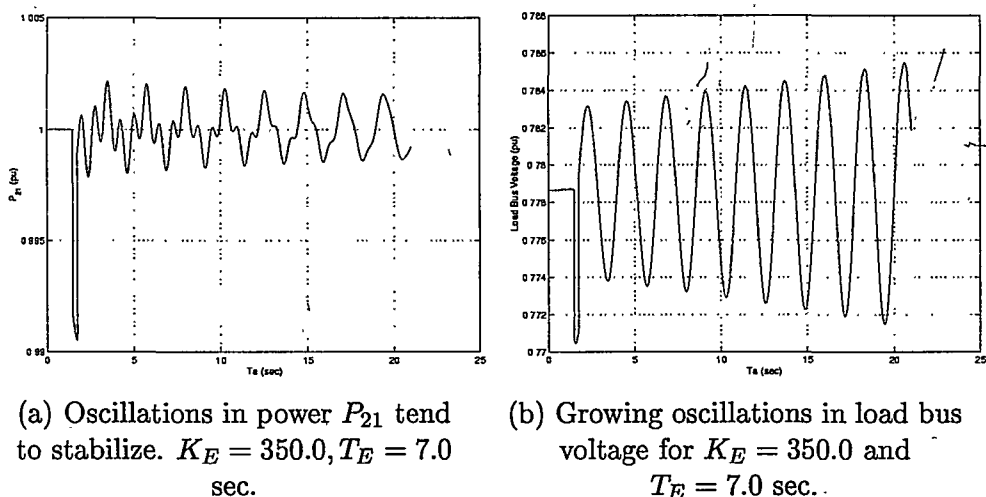
Figure 15.15: System response at high gain and high time constant of the exciter : at $P_l = 3.43$ pu

(a) Monotonic fall in load bus voltage for $K_E = 0.5$ and $T_E = 1.0$ sec.

(b) Oscillations in P_{21} stabilise.
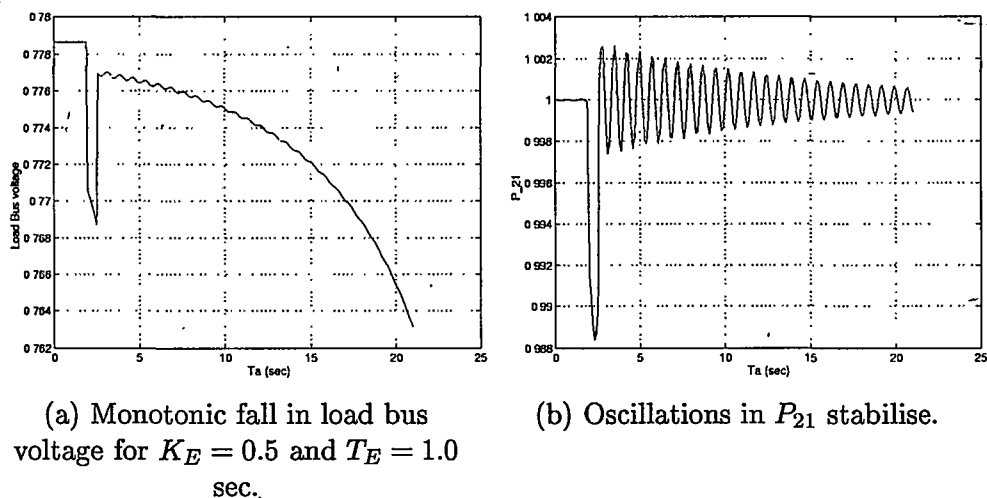
Figure 15.16: System response at low gain and high time constant of the exciter : at $P_l = 3.43$ pu

　　　　The results for the 3 bus system can be extended to multimachine system also. Following conclusions can be reached on the nature of instability.

1. As the system loading is increased, with normal operation of AVRs; the

initial instability is due to the swing mode which can be stabilised by damping controllers.

2. The voltage instability appears to be the result of unstable exciter mode at higher loadings which is affected by the regulator gain and time constant.

    Low gains and high time constants can result in the instability of the exciter mode, the nature of the instability dependent on the gain. Below a critical gain, the instability is due to SNB while at higher gains, the instability occurs at higher time constants.

    If it is assumed that an equivalent generator can represent all the generators (which remain in synchronism) in a multimachine system, the equivalent K_E and T_E are affected by the overexcitation limiters. Under abnormal conditions, increase in T_E (slowing down of the exciter response) or decrease in the effective K_E can cause voltage instability.

3. The increase in the load results in shrinking of the region of stability (ROS).

Interestingly, these conclusions are not much affected even with dynamic modelling of loads.

Attempts have been made recently [16, 17] to decouple voltage and angle stability analysis if it is assumed that the generators remain in synchronism following a disturbance. Ignoring the rotor swing dynamics has little effect on the prediction of instability of modes leading to voltage instability.

15.6   Control of Voltage Instability

Voltage instability along with angle instability pose a threat to the system security. Uncontrolled load rejection due to voltage collapse can cause system separation and blackouts. Hence the system must be planned in such a way as to reduce the possibility of voltage instability. Also the system must be operated with adequate margin for voltage stability. In the event of voltage instability due to unforeseen contingencies, the system control must prevent widespread voltage collapse and restore the loads as quickly as possible.

The incidence of voltage instability increases as the system is operated close to its maximum loadability limit. Environmental and economic constraints have limited the transmission network expansion, while forcing the generators to be sited far away from the load centres. This has resulted in stressing the existing transmission network.

The present trend is to operate the existing transmission facilities optimally to utilize the inherent margins available. The concept of Flexible AC Transmission System (FACTS) is an important step in this direction. The availability of FACTS controllers such as SVC, Controlled Series Compensation (CSC), Static Condenser (STATCON) permit operation close to the thermal limit of the lines without jeopardizing security.

The reactive power compensation close to the load centres as well as at the critical buses in the network is essential for overcoming voltage instability. The location, size and speed of control have to be selected properly to have maximum benefits. The SVC and STATCON provide fast control and help improve system stability.

The design of suitable protective measures in the event of voltage instability is also necessary. The application of under voltage load shedding [13], controlled system separation and adaptive or intelligent control are steps in this direction.

References

1. M.A. Pai and V. Ajjarapu, "Voltage stability in power systems - An overview" published in **Recent Advances in Control and Management of Energy Systems**, Interline Publishing, Bangalore 1993, pp. 189-218

2. CIGRE Task Force 38.02.10, "Cigre technical brochure:Modelling of voltage collapse including dynamic phenomena", ELECTRA, No. 147, April 1993, pp. 71-77

3. K.R. Padiyar and V. Kalyana Raman, "Study of voltage collapse at converter bus in asynchronous MTDC-AC systems", Int. J. of Elec. Power and Energy Syst., Vol. 15, No. 1, Feb. 1993, pp. 45-53

4. K.R. Padiyar and S. Suresh Rao, "Dynamic analysis of voltage instability in AC-DC systems", To appear in Int. J. of Elec. Power & Energy Syst.

5. G.K. Morrison, B. Gao and P.Kundur, "Voltage stability analysis using static and dynamic approaches", IEEE Trans. on Power Systems, Vol. 8, No. 3, August 1993, pp. 1159-1171

6. P. Kundur, K. Morrison and B. Gao, "Practical considerations in voltage stability assessment", Int. J. of Elec. Power & Energy Syst., Vol. 15, No. 4, 1993, pp. 205-215

7. M. Stubbe,A. Bihain and J. Deuse, "Simulation of voltage collapse", Int. J. of Elec. Power & Energy Syst. Vol. 15, No. 4, 1993, pp. 239-243

8. J. Guckenheimer and P. Holmes,**Nonlinear Oscillation,Dynamical Systems and Bifurcations of Vector Fields**, Springer-Verlag, New York, 1983

9. V.A. Venikov,V.A. Stroev,V.I. Idelehick and V.I. Tarasov, "Estimation of electrical power system steady-state stability in load flow calculations", IEEE Trans. Vol. PAS - 94, No. 3, May/June 1975, pp. 1034 - 1041

10. P.W. Sauer and M.A. Pai, "Power system steady-state stability and load flow Jacobian", IEEE Trans. on Power Systems, Vol. 5, No. 4, Nov. 1990, pp. 1374 - 1383

11. P.A.Lof,G. Anderson and D.J. Hill, "Voltage stability indices for stressed power systems", IEEE Trans. on Power Systems, Vol. 8, No. 1, Feb. 1993, pp. 326-385

12. C. Rajagopalan,B. Lesieutre,P.W. Sauer and M.A. Pai, "Dynamic aspects of voltage/power characteristics", IEEE Trans. on Power Systems, Vol. 7, No. 3, Aug. 1992, pp. 990-1000

13. C.W. Taylor, "Concepts of undervoltage load shedding for voltage stability", IEEE Trans on Power Delivery, Vol. 7, No. 2, April 1992, pp. 480-488

14 F.P. de Mello and C. Concordia, "Concepts of Synchronous Machine Stability as Affected by Excitation Control", IEEE Transactions on Power Apparatus and Systems, Vol. PAS-88, No. 4, 1969, pp. 316-329

15 K.R. Padiyar and Kalyani Bhaskar, "An Integrated Analysis of Voltage and Angle Stability of a Three Node Power System", to appear in the International Journal of Electrical Power & Energy Systems.

16 K.R. Padiyar and S.S. Rao, "Dynamic Analysis of Small Signal Voltage Instability Decoupled from Angle Instability", International Journal on Electric Power and Energy Systems, Vol. 18, No. 7, 1996, pp. 445-452

17 C.D. Vournas, P.W. Sauer and M.A. Pai, " Relationship Between Voltage and Angle Stability of Power Systems", International Journal on Electric Power and Energy Systems, Vol. 18, No. 8, 1996, pp. 493-500

18 C.W. Taylor, "Power System Voltage Stability", NY, McGraw-Hill, 1994

19 Thierry Van Cutsem and Costas Vournas, "Voltage Stability of Electric Power Systems", Kluwer Academic Publications, Boston, 1998.

"This page is Intentionally Left Blank"

Appendix A

Numerical Integration

The computer simulation of power system dynamics involves primarily the numerical integration of the set of ordinary differential equations describing the system. These equations can be expressed as

$$\frac{dx}{dt} = f(x, u) \tag{A.1}$$

where u is a vector of input variables which are either constants or specified functions of time. For example, u may consist of voltage and speed references at every generator.

The initial value of x, is specified at the initial time t_o (which may be chosen as zero) and the problem is to determine the values of x at future times. This problem is termed as initial value problem as opposed to boundary value problem in which some of the dependent variables may be specified at different times. It will be assumed that the equation (A.1) has a unique solution in the range, $t_o < t < t_{max}$ where $t_{max} \to \infty$. Actually, if the function f satisfies Lipschitz condition given by

$$\mid f(x, u) - f(x^*, u) \mid \leq L \mid x - x^* \mid \tag{A.2}$$

where L is a constant (called Lipschitz constant) the existence of a unique solution with the initial condition $x(t_o) = x_o$ is guaranteed.

A.1 Numerical Approximation of the Solution

There are two basic approaches to the numerical approximation of solution of differential equations. One is to represent an approximate solution by the sum of a finite number of independent functions, for example a truncated power series or expansion in terms of orthogonal functions. The second and more important approach is the difference method. The solution is approximated by its value at a sequence of discrete points called the mesh points. We will assume that these

points are equally spaced, i.e. $t_k = kh \quad (t_o = 0)$, where h is the spacing between adjacent points. However, spacing or step size h, will affect the error (in the numerical approximation) and this may differ from one region of the interval $(0 - t_{max})$ to the other. Consequently, we may use a variable step size in which case

$$t_{k+1} = t_k + h_k, \quad t_o = 0 \tag{A.3}$$

A difference method is also called a step by step method and provides an algorithm for computing the approximation at step k to $x(t_k)$ in terms of values of x at t_{k-1} and preceding points. There are two types of errors in this approximation

1. **Truncation Error** resulting from the difference in the exact solution and the solution given by the algorithm

2. **Round-off Error** due to the fact that numbers cannot be represented exactly in the numerical processes involved (due to the finite precision of numbers represented on digital computers).

A major concern about numerical approximation is accuracy-how well the numerical solution approaches the exact solution. The concept of convergence of a numerical method implies that any desired degree of accuracy can be achieved for any problem satisfying Lipschitz condition by selecting a small enough step size. It is assumed here that the round-off errors can be kept under control by selecting higher precision as the step size is reduced.

Another basic concept is **stability** of a numerical method, which guarantees that small changes in the initial values only produce bounded changes in the numerical approximation provided by the method. If there exists an $h_o > 0$ for each differential equation such that a change in the starting values by a fixed amount produces a bounded change in the numerical solution for all $0 \le h \le h_o$, then the method is stable. Stability does not require convergence, although the converse is true. For example, the "method" $x_k = x_{k-1}, k = 1, 2...N$ is stable but not convergent for any but the trivial problem $\dot{x} = 0$.

The concepts of convergence and stability are associated with the limiting process as $h \to 0$. In practice, the number of steps are finite and we are interested in knowing whether the errors introduced at each step (truncation and round-off) have small or large effects on the solution. In this context, **absolute stability (A-stability)** is defined as follows. A method is absolutely stable for a given step size and a given differential equation, if the change due to a perturbation of size δ in one of the mesh (discrete) values x_k is not larger than δ in all subsequent values $x_n, n > k$. This definition is dependent on the problem, hence a test equation

$$\dot{x} = \lambda x \tag{A.4}$$

is considered where λ is a complex constant. The region of absolute stability is the set of values of h (real non-negative) and λ for which a perturbation in a single value x_k will produce a change in subsequent values which does not increase from step to step.

A.2 Types of Methods

The numerical methods for integration of differential equations can be classified as

1. Single-step algorithms

2. Multi-step algorithms

In the first class of methods, the computation of x_k requires only the information on x_{k-1} (in addition to the evaluation of derivatives in the time interval t_{k-1} to t_k). In multi-step algorithms, past information about the trajectory is also used. A m-step algorithm uses the m previous points $x_{k-1}, x_{k-2}, x_{k-m}$ and the values of derivatives at these points to estimate x_k.

The order of an algorithm (single step or multi-step) refers to the accuracy of the algorithm when the solution of the equation can be expressed as a polynomial (Note that any analytic funtion can be approximated arbitrarily closely by a high-order polynomial). An algorithm of pth order is free of truncation error for systems whose solution is a polynomial of order p or less.

Higher order single-step algorithms tend to be computationally inefficient, particularly if the computations per evaluation of derivative function f is high. In general, there are p evaluations of f for each step in a pth order single-step algorithm. In contrast, multi-step algorithms require only one new function evaluation per step and therefore more efficient per step than a comparable single-step algorithm. However, single-step algorithms can allow a larger step size due to extra function evaluations per step and are self-starting.

There is another classification of numerical methods for integration, namely

A. Explicit

B. Implicit

In explicit methods, the algorithm gives an explicit solution of x_k at the end of kth step. Implicit methods in general require solution of algebraic equations for

the calculation of x_k. Although this requires more computations per step, in general, implicit algorithms are more stable and can tolerate larger step-size. In stiff systems where both slow and fast dynamics are present, the considerations of numerical stability require very small step sizes (even when one is interested in capturing only slow dynamics) if explicit algorithms are used. Thus, if only slow transients are of interest, implicit algorithms are computationally efficient as larger sizes of steps can be used.

A.3   Integration Algorithms

In this section only some representative algorithms both explicit and implicit, single-step and multi-step are described. For an exhaustive coverage of various algorithms reader is referred to books [1,2] on numerical solution of ordinary differential equations. In what follows, the differential equations are assumed to be of the form

$$\dot{x} = f(x, t) \tag{A.5}$$

The numerical algorithm is to compute x_k in terms of previous value(s) and derivatives evaluated at discrete points.

Single Step Algorithms (Runge-Kutta Methods)

First Order: Forward Euler
The algorithm is given by

$$x_k = x_{k-1} + hf(x_{k-1}, t_{k-1}) \tag{A.6}$$

Backward Euler

$$x_k = x_{k-1} + hf(x_k, t_k) \tag{A.7}$$

Note that while forward Euler method is explicit, the backward Euler method is implicit.

Second Order:
Trapezoidal

$$x_k = x_{k-1} + \frac{h}{2}[f(x_k, t_k) + f(x_{k-1}, t_{k-1})] \tag{A.8}$$

This is an implicit method and used extensively in power system studies.

Modified Euler-Cauchy Algorithm

$$x_k = x_{k-1} + hf\left(x_{k-1} + \frac{h}{2}f(x_{k-1}, t_{k-1}), t_{k-1} + \frac{h}{2}\right) \tag{A.9}$$

This is an explicit method.

Modified Euler-Heun Algorithm

$$x_k = x_{k-1} + \frac{h}{2}[f(x_{k-1}, t_{k-1}) + f(x_{k-1} + hf(x_{k-1}, t_{k-1}), t_k)] \qquad (A.10)$$

This is also an explicit method.

Fourth order Runge-Kutta

This is an explicit algorithm that uses intermediate points in the interval (t_{k-1}, t_k) to calculate state at time t_k.

Defining

$$
\begin{aligned}
k_1 &= f(x_{k-1}, t_{k-1}) \\
k_2 &= f\left(x_{k-1} + \frac{h}{2}k_1, t_{k-1} + \frac{h}{2}\right) \\
k_3 &= f\left(x_{k-1} + \frac{h}{2}k_2, t_{k-1} + \frac{h}{2}\right) \\
k_4 &= f(x_{k-1} + hk_3, t_k)
\end{aligned}
$$

the final state is calculated from

$$x_k = x_{k-1} + \frac{h}{6}[k_1 + 2k_2 + 2k_3 + k_4] \qquad (A.11)$$

Multi-Step Algorithms

A general form for an m step algorithm is given by

$$
\begin{aligned}
x_k =\ & a_1 x_{k-1} + a_2 x_{k-2} + \dots a_m x_{k-m} \\
& + h[b_o f(x_k, t_k) + b_1 f(x_{k-1}, t_{k-1}) + b_2 f(x_{k-2}, t_{k-2}) \\
& + \dots b_m f(x_{k-m}, t_{k-m})] \qquad (A.12)
\end{aligned}
$$

where t_{k-i} are evenly spaced with time step h. Different choices of the coefficients a_i and b_i lead to different integration algorithms. If $b_o = 0$, the algorithm is explicit; otherwise, it is implicit.

Adams-Bashforth

The pth order Adams-Bashforth algorithm is generated by setting $m = p$, $b_o = 0$ and $a_i = 0$ for $i = 1, 2 \dots p$. The remaining coefficients are chosen such that the algorithm is exact for polynomials of order p. Since $b_o = 0$, this is an explicit algorithm.

The first, second, third and fourth order algorithms are given below
First order

$$x_k = x_{k-1} + f(x_{k-1}, t_{k-1}) \qquad (A.13)$$

Second order

$$x_k = x_{k-1} + \frac{h}{2}[3f(x_{k-1}, t_{k-1}) - f(x_{k-2}, t_{k-2})] \qquad \text{(A.14)}$$

Third order

$$x_k = x_{k-1} + \frac{h}{12}[23f(x_{k-1}, t_{k-1}) - 16f(x_{k-2}, t_{k-2}) + 5f(x_{k-3}, t_{k-3})] \quad \text{(A.15)}$$

Fourth order

$$\begin{aligned} x_k &= x_{k-1} + \frac{h}{24}[55f(x_{k-1}, t_{k-1}) - 59f(x_{k-2}, t_{k-2}) \\ &\quad + 37f(x_{k-3}, t_{k-3}) - 9f(x_{k-4}, t_{k-4})] \end{aligned} \qquad \text{(A.16)}$$

It is to be noted that the first order algorithm is identical to forward Euler's method.

Adams-Moulton

The pth order Adams-Moulton algorithm is generated by setting $m = p - 1$ and $a_i = 0$ for $i = 1, 2...(p - 1)$. The remaining coefficients are chosen such that the algorithm is exact for polynomials of order p. The pth order Adams-Moulton algorithm is a $(p - 1)$ step algorithm. Since $b_o \neq 0$, this is an implicit algorithm.

The first to fourth order Adams-Moulton algorithm are given below
First order
$$x_k = x_{k-1} + hf(x_k, t_k) \qquad \text{(A.17)}$$

Second order

$$x_k = x_{k-1} + \frac{h}{2}[f(x_k, t_k) - f(x_{k-1}, t_{k-1})] \qquad \text{(A.18)}$$

Third order

$$x_k = x_{k-1} + \frac{h}{12}[5f(x_k, t_k) + 8f(x_{k-1}, t_{k-1}) - f(x_{k-2}, t_{k-2})] \qquad \text{(A.19)}$$

Fourth order

$$x_k = x_{k-1} + \frac{h}{24}[9f(x_k, t_k) + 19f(x_{k-1}, t_{k-1}) - 5f(x_{k-2}, t_{k-2}) + f(x_{k-3}, t_{k-3})]$$
$$\text{(A.20)}$$

It is to be noted that the first and second order algorithms are identical to backward Euler and trapezoidal algorithms respectively.

Predictor-Corrector methods involve the sequential application of Adams-Bashforth and Adams-Moulton algorithms. The former is used to predict the value of x_k and the latter is used to correct it.

Gear's Algorithm

The pth order Gear's algorithm is obtained by setting $m = p$ and $b_i = 0$ for $i = 1, 2....p$. The remaining coefficients are chosen such that the algorithm is exact for polynomials of order p. Since $b_o \neq 0$, it is implicit in nature.

First order Gear's algorithm is identical to backward Euler algorithm. The second to fourth order algorithms are given below

Second Order

$$x_k = \frac{1}{3}[4x_{k-1} - x_{k-2} + 2hf(x_k, t_k)] \tag{A.21}$$

Third Order

$$x_k = \frac{1}{11}[18x_{k-1} - 9x_{k-2} + 2x_{k-3} + 6hf(x_k, t_k)] \tag{A.22}$$

Fourth Order

$$x_k = \frac{1}{25}[48x_{k-1} - 36x_{k-2} + 16x_{k-3} - 3x_{k-4} + 12hf(x_k, t_k)] \tag{A.23}$$

A.4   Error Analysis

The local error ϵ is defined as the error at each step of the algorithm. Assuming the exact solution of the equation (A.5) at time $t = t_k$ as $\phi_{t_k}(x_{k-1}, t_{k-1})$ where the initial condition is $x = x_{k-1}$ at $t = t_{k-1}$, the local error is given by

$$\epsilon = \| x_k - \phi_{t_k}(x_{k-1}, t_{k-1}) \| \tag{A.24}$$

where x_k is generated by the numerical integration algorithm. The local error includes both truncation and round-off errors. For a pth order algorithm, the local truncation error is given by

$$\epsilon_t = \alpha_k h^{p+1} \tag{A.25}$$

where α_k is a real constant dependent on both f and x_k, but independent of h.

The local round-off error ϵ_r depends on the number and type of arithmetic operations per step and is independent of the step size. The magnitude of the round-off error depends on the hardware (of the digital computer) used. The local round-off error can be reduced by increasing the precision of the floating-point representation. Typically, single-precision representations use 32 bits and are accurate to about 7 decimal places; double-precision representations use 64 bits and are accurate to about 15 decimal places.
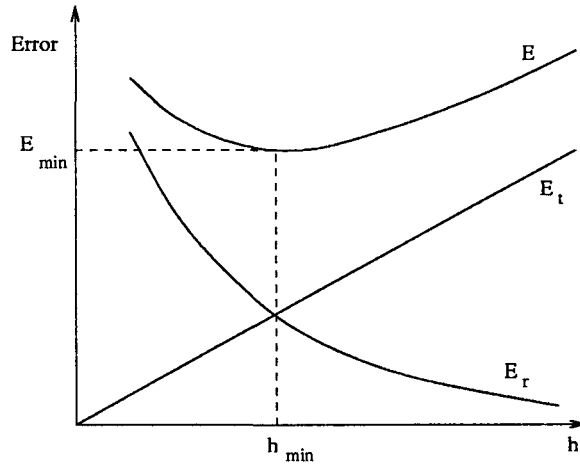
Figure A.1: Error as function of step size (Euler's method)

Global Errors

The global errors are accumulations of local errors per unit time. If $h \ll 1$, the total number of integration steps are

$$N = \frac{1}{h} \tag{A.26}$$

The global round-off error is given by

$$E_r = N\epsilon_r = \frac{N}{h} \tag{A.27}$$

The global truncation error, neglecting the dependence of α_k on x_k is given by

$$E_t = N\epsilon_t = \alpha h^p \tag{A.28}$$

for a pth order algorithm.

The total error $E = E_r + E_t$, as a function of step size h, where $p = 1$, is shown in Fig. A.1. This shows that the error decreases at first as h is reduced; but there is an optimum value of $h(h_{min})$ at which the total error is minimum. Most of the times, the requirements on accuracy permit values of h much above h_{min}. If better accuracy is required, which dictates that E_{min} be reduced, the precision of numbers used in the computer has to be increased. For every ten-fold decrease in h, more than one decimal digit of precision must be added if it is assumed that the round-off error is constant per step.

Variable step size

A practical integration routine should automatically adjust the step-size h such that it satisfies the user supplied error tolerance. This way, the total computations can be minimized and also the accumulated round-off error. This is achieved by estimating the error at each step and reducing or increasing the step size as required. Variable step-size is easily implemented in single step algorithms. Sometimes, integration routines also incorporate variable order of the algorithm.

References

1. L. Lapidus and J.H. Seinfeld, **Numerical Solution of Ordinary Differential Equations**, Academic Press, New York, 1971

2. C.W. Gear, **Numerical Initial Value Problems in Ordinary Differential Equations**, Prentice-Hall, Englewood Cliffs, 1971

"This page is Intentionally Left Blank"

Appendix B

Data for 10 Generator System

The data for the 39 bus, 10 generator system is given here. This is adapted from [1]. The single line diagram of the system is shown in Fig. B.1. The machine data, line data, load flow and transformer data are given in tables B.1 to B.4 respectively. The AVR data is given below.

Table B.1 Machine Data

Gen #	R_a	X_d	X'_d	X_q	X'_q	H	T'_{do}	T'_{qo}	T_c	D
1	0.0	0.2950	0.0647	0.2820	0.0647	30.3	6.56	1.5	0.01	0.0
2	0.0	0.0200	0.0060	0.0190	0.0060	500.0	6.0	0.7	0.01	0.0
3	0.0	0.2495	0.0531	0.2370	0.0531	35.8	5.7	1.5	0.01	0.0
4	0.0	0.3300	0.0660	0.3100	0.0660	26.0	5.4	0.44	0.01	0.0
5	0.0	0.2620	0.0436	0.2580	0.0436	28.6	5.69	1.5	0.01	0.0
6	0.0	0.2540	0.0500	0.2410	0.0500	34.8	7.3	0.4	0.01	0.0
7	0.0	0.2950	0.0490	0.2920	0.0490	26.4	5.66	1.5	0.01	0.0
8	0.0	0.2900	0.0570	0.2800	0.0570	24.3	6.7	0.41	0.01	0.0
9	0.0	0.2106	0.0570	0.2050	0.0570	34.5	4.79	1.96	0.01	0.0
10	0.0	0.2000	0.0040	0.1900	0.0040	42.0	5.7	0.50	0.01	0.0

Note: T_c is the time constant of the dummy coil considered to represent transient saliency.

AVR Data: $K_A = 25$, $T_A = 0.025$, $V_{rmax} = 10$, $V_{rmin} = -10$

Table B.2 Line Data

Bus No.		R_L	X_L	B_c
From	To			
37	27	0.0013	0.0173	0.3216
37	38	0.0007	0.0082	0.1319
36	24	0.0003	0.0059	0.0680
36	21	0.0008	0.0135	0.2548
36	39	0.0016	0.0195	0.3040
36	37	0.0007	0.0089	0.1342
35	36	0.0009	0.0094	0.1710
34	35	0.0018	0.0217	0.3660
33	34	0.0009	0.0101	0.1723
28	29	0.0014	0.0151	0.2490
26	29	0.0057	0.0625	1.0290
26	28	0.0043	0.0474	0.7802
26	27	0.0014	0.0147	0.2396
25	26	0.0032	0.0323	0.5130
23	24	0.0022	0.0350	0.3610
22	23	0.0006	0.0096	0.1846
21	22	0.0008	0.0135	0.2548
20	33	0.0004	0.0043	0.0729
20	31	0.0004	0.0043	0.0729
19	2	0.0010	0.0250	1.2000
18	19	0.0023	0.0363	0.3804
17	18	0.0004	0.0046	0.0780
16	31	0.0007	0.0082	0.1389
16	17	0.0006	0.0092	0.1130
15	18	0.0008	0.0112	0.1476
15	16	0.0002	0.0026	0.0434
14	34	0.0008	0.0129	0.1382
14	15	0.0008	0.0128	0.1342
13	38	0.0011	0.0133	0.2138
13	14	0.0013	0.0213	0.2214
12	25	0.0070	0.0086	0.1460
12	13	0.0013	0.0151	0.2572
11	12	0.0035	0.0411	0.6987
11	2	0.0010	0.0250	0.7500

Table B.3 Load Flow Data

Bus No.	V	ϕ	P_G	Q_G	P_L	Q_L
1	.98200	.00000	5.04509	1.36036	.09200	.04600
2	1.03000	-9.55016	10.00000	1.95746	11.04000	2.5000
3	.98310	3.20174	6.50000	1.59104	.00000	.00000
4	1.01230	4.61664	5.08000	1.58151	.00000	.00000
5	.99720	5.57217	6.32000	.95582	.00000	.00000
6	1.04930	6.62654	6.50000	2.76414	.00000	.00000
7	1.06350	9.46958	5.60000	2.35485	.00000	.00000
8	1.02780	3.16537	5.40000	.63019	.00000	.00000
9	1.02650	9.04654	8.30000	.84790	.00000	.00000
10	1.04750	-2.47597	2.50000	1.46483	.00000	.00000
11	1.03829	-7.79710	.00000	.00000	.00000	.00000
12	1.02310	-4.89487	.00000	.00000	.00000	.00000
13	.99576	-8.07759	.00000	.00000	3.22000	.02400
14	.95894	-9.35310	.00000	.00000	5.00000	1.84000
15	.95660	-8.29471	.00000	.00000	.00000	.00000
16	.95688	-7.56925	.00000	.00000	.00000	.00000
17	.95140	-9.97400	.00000	.00000	2.33800	.84000
18	.95276	-10.5017	.00000	.00000	5.22000	1.76000
19	1.01028	-9.92054	.00000	.00000	.00000	.00000
20	.95988	-4.71314	.00000	.00000	.00000	.00000
21	.99046	-2.98024	.00000	.00000	2.74000	1.1500
22	1.01550	1.62430	.00000	.00000	.00000	.00000
23	1.01344	1.34841	.00000	.00000	2.74500	.84660
24	.98179	-5.45955	.00000	.00000	3.08600	.92200
25	1.02088	-3.68918	.00000	.00000	2.24000	.47200
26	1.01822	-4.76321	.00000	.00000	1.39000	.17000
27	1.00150	-6.92554	.00000	.00000	2.81000	.75500
28	1.02204	-.95906	.00000	.00000	2.06000	.27600
29	1.02143	1.95588	.00000	.00000	2.83500	.26900
30	.98832	-.62515	.00000	.00000	6.28000	1.03000
31	.95760	-5.69316	.00000	.00000	.00000	.00000
32	.93795	-5.68713	.00000	.00000	.07500	.88000
33	.95912	-5.47342	.00000	.00000	.00000	.00000
34	.96168	-7.20767	.00000	.00000	.00000	.00000
35	.96683	-7.32475	.00000	.00000	3.20000	1.5300
36	.98196	-5.55956	.00000	.00000	3.29400	.32300
37	.99086	-6.73437	.00000	.00000	.00000	.00000
38	.99197	-7.71437	.00000	.00000	1.58000	.30000
39	.98770	.34648	.00000	.00000	.00000	.00000

Table B.4 Transformer Data

Bus No.		R_T	X_T	Tap
From	To			
39	30	0.0007	0.0138	1.0
39	5	0.0007	0.0142	1.0
32	33	0.0016	0.0435	1.0
32	31	0.0016	0.0435	1.0
30	4	0.0009	0.0180	1.0
29	9	0.0008	0.0156	1.0
25	8	0.0006	0.0232	1.0
23	7	0.0005	0.0272	1.0
22	6	0.0000	0.0143	1.0
20	3	0.0000	0.0200	1.0
16	1	0.0000	0.0250	1.0
12	10	0.0000	0.0181	1.0
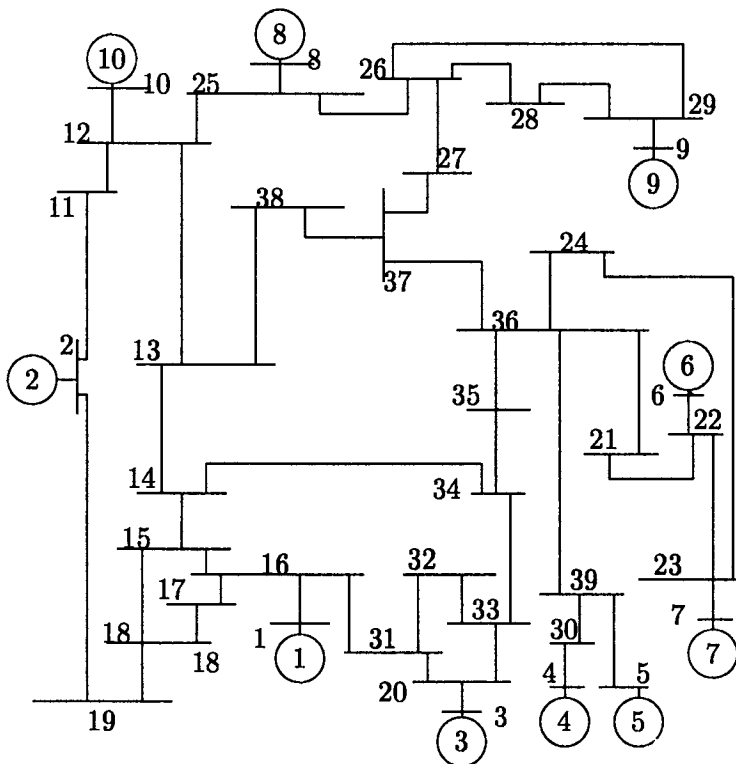
Figure B.1: 39 Bus, 10 generator test system

The load flow results are given for the case when transmission losses are neglected. This is assumed in the examples given in chapters 12 and 13. The network losses are included in the example given in Chapter 9.

Reference

1. A.K. Behera, **Transient stability analysis of multimachine power systems using detailed machine models**, Ph.D Thesis, University of Illinois at Urbana-Champaign, 1988

"This page is Intentionally Left Blank"

Appendix C

List of Problems

1. A generator is supplying power to an infinite bus through an external reactance of 0.8 pu. The terminal voltage is maintained at 1.0 pu through field control. If $E_b = 1.0, x_g = 0.2$ pu,

   (a) find the equilibrium points when supplying power of 1.0 pu. Test their stability.
   (b) find the maximum power supplied if the voltage regulation is manual.
   (c) Repeat (b) if the voltage regulation is achieved using an ideal AVR.

2. Consider the system shown in C.1.

   The generator is represented by a voltage source $E_g \angle \delta$ in series with reactance x_g.
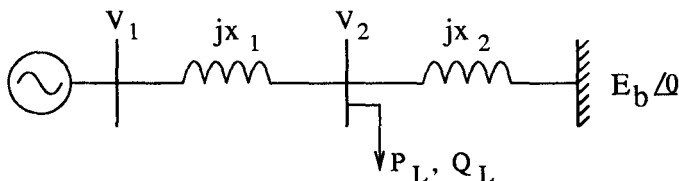
Figure C.1:

   (a) If $|V_1| = |V_2| = 1.0$ pu and $P_g = P_b = 1.0$ pu, $(P_L = 0.0, Q_L = 0.0)$, find the value of δ corresponding to equilibrium. Test the stability of all the equilibrium points. Assume $x_g = 0.3, x_1 = 0.5$ and $x_2 = 0.2$.
   (b) Find the steady state stability limit of power. Assume V_1 and V_2 are maintained at 1.0 pu by slow control as the power is increased. Assume $P_L = Q_L = 0.0$.

3. In figure C.1, the load at the intermediate bus is assumed to be of constant impedance type with $Z_L = 1.0 + j0.0$ pu.

If $x_1 = x_2 = 0.25$ and $x_g = 0$ $(V_1 = E_g \angle \delta)$ obtain expression for P_g and P_b as functions of δ. Assume $E_b = E_g = 1.0$ pu.

Find the received power at the staibility limit. Can the received power be higher than this limit? Explain.

4. In figure C.1,   the load is assumed to be of constant power type with $P_L = 1.0$ and $Q_L = 0.5$. Find the equilibrium points if $P_g = 2.0$ and test their stability. Assume $E_g = E_b = 1.0$ pu, $x_1 = x_2 = 0.25, x_g = 0.0$.

What is the maximum power output of the generator and the critical \angle?

5. For the system shown in figure C.1, a controllable reactive source is connected at the intermediate bus instead of the load and can be modelled as a voltage source E_s in series with the reactance x_s. Assume $x_1 = x_2 = 0.25, x_g = 0.0, E_b = E_g = 1.0$ pu. Obtain the expression for P_g as a fucntion of δ. What is the maximum power output of the generator and the critical angle? Assume $E_s = 1.0, x_s = 0.1$.

6. If in problem 5, a fixed capacitor $(B_c = 0.5)$ is connected at the intermediate bus instead of controllable reactive source, obtain expression for P_g as a function of δ.

7. A salient pole generator is connected to an infinite bus through an external reactance (x_e) of 0.5 pu. The field voltage is adjusted such that the terminal voltage is 1.0 pu when the power output is 1.0 pu.

   (a) What is the expression for power (P_g) as a function of δ in steady state?

   (b) Repeat (a) in transient state.

   (c) What is the maximum power supplied in steady state? Assume $x_d = 1.0, x_q = 0.6, x'_d = 0.35, E_b = 1.0$.

8. Consider a two area system shown in figure C.2. Each area is represented by an equivalent generator and load at unity power factor. The generator reactances can be neglected.

   (a) Write the equation for $\delta_{12} = \delta_1 - \delta_2$.

   (b) If P_{m1} is reduced to 10 at $t = 0$, find the expression for δ_{12} assuming linearity.

   Data : $X = 0.5, P_{L1} = 10, P_{L2} = 20, P_{m1} = 11, P_{m2} = 19, H_1 = 25,$
   $H_2 = 60, f_B = 50$ Hz, $E = 1.0$.
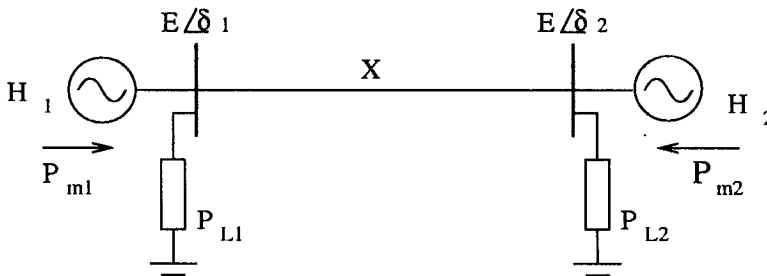
Figure C.2:

9. A synchronous generator is delivering 1.0 pu power at 0.9 pf (lagging) through a circuit breaker to an infinite bus having a voltage of 1.0 pu. If the circuit breaker is opened, how long may it be kept open before being closed without loss of synchronism? Assume $x_g = 0.4, H = 3.0, f_B = 50$ Hz.

10. Consider the system shown in figure C.3. The generator is initially supplying power of 1.0 pu with the terminal voltage at 1.0 pu.

    If a three phase fault occurs at the sending end of one of the lines followed by tripping, find the critical angle.
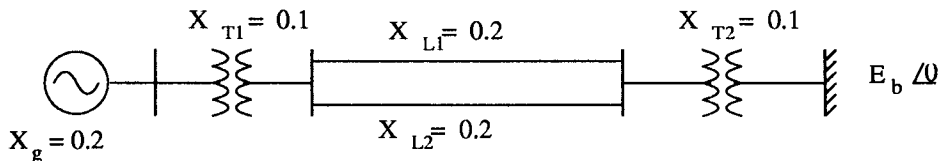
Figure C.3:

11. For the system shown in figure C.2, the load P_{L1} is decreased suddenly and P_{L2} is increased simultaneously by the same amount at $t = 0$. What is the maximum step change in the loads that can be permitted without loss of synchronism? Assume the data given in problem 8.

12. Consider the system shown in figure C.4. The reactance of each line section is 0.8 and is compensated 50 % by using series capacitors. Following a fault in one of the sections, it is tripped. Neglecting the effect of the fault, compute the transient stability limit

    (a) if the switch S remains closed.

    (b) if the switch S is opened as soon as the line is tripped.
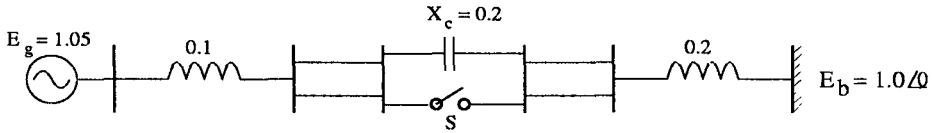
Figure C.4:

13. A synchronous generator rated at 10 MVA, 11KV, 50 Hz is running at rated speed on no load. The field current is initially zero and the field voltage ($E_{fd} = 1.0$) is suddenly applied at $t = 0$. Neglecting damper windings, obtain expression for $v_a(t)$.

    Data : $x_d = 1.0, x_q = 0.6, R_f = 0.001, R_a = 0.0, x_{df} = 0.9, x_f = 1.05$.

14. The generator described in problem 13 is connected to a positive sequence voltage source of 11 KV. The mechanical input power is 0.8 pu and $E_{fd} = 1.2$ pu. Compute steady state values of i_d, i_q, Ψ_d, Ψ_q, P and Q (at terminals). What is RMS line current in amperes?

    Is the answer affected by the presence of damper windings?

15. Repeat problem 14 if the voltage at the generator terminals has a negative sequence component which is 10 % of the positive sequence component. Assume field flux to be constant. Does   ressure of damper windings affect the answers?

16. The generator described in problem 13 is connected to a positive sequence current source of 1.0 pu. If $T_m = 0.8, E_{fd} = 1.2$, find the steady state values of i_d, i_q, v_d, v_q, P and Q.

17. A generator has positive sequence currents flowing in the armature with $i_a = 0.8156 \sin \omega_B t$. If $E_{fd} = 1.2$ and shaft power is zero, obtain the expression for v_a in steady state.

    Data : $x_d = 1.75, x_{df} = 1.55, x_f = 1.80, x_q = 1.75, R_f = 0.001, R_a = 0.0,$
           $f_B = 50$ Hz.

18. A synchronous generator is initially running at rated speed on no load with open circuit voltage of 1.0 pu. A sudden three phase short circuit occurs at the terminals at $t = 0$. Neglecting armature transients and effect of damper windings, obtain expressions for $i_d(t)$, $i_q(t)$ and $i_f(t)$. Assume the generator data same as that given in probelm 17.

19. A synchronous generator has positive sequence currents flowing in the armature with $i_d(t) = 0.8156 \sin 100\pi t$. The rotor angle with respect to a stationary axis is $\theta = 98\pi t$. Neglecting damper windings and assuming

constant field flux linkages, obtain expressions for $v_a(t)$ and $T_e(t)$. Neglect $p\Psi_d$ and $p\Psi_q$ terms.

Data : $x_d = 1.75, x_q = 1.65, x'_d = 0.25, R_a = 0.0, E_{fd} = 1.0$.

20. Obtain the expression for $G(s)$ and compute the time constants T'_{do}, T'_d, T''_{do} and T''_d. The d-axis equivalent circuit has the following parameters
$x_c = 0.3, \ x_d = 1.8, \ x'_{fc} = 0.25, \ R'_f = 0.001, \ R'_h = 0.025, \ x_{hc} = 0.0,$
$f_B = 50$ Hz.

21. Obtain the expression for $X_d(s)$ and compute the reactances x'_d, x''_d from the d-axis equivalent circuit parameters :- $x_c = 0.3, \ x_d = 1.8,$
$x'_{hc} = 0.18, x'_{fc} = 0.25, R'_f = 0.0008, R'_h = 0.022, f_B = 50$ Hz. What are the time constants T'_d and T''_d?

22. Obtain the expression for $X_q(s)$ and compute the time constants T'_{qo}, T'_q, T''_{qo} and T''_q and reactances x'_q and x''_q. The q-axis equivalent circuit parameters are $x_{a\sigma} = 0.2, \ x_q = 1.7, \ x_{g\sigma} = 0.33, \ x_{k\sigma} = 0.11, \ R_g = 0.008,$
$R_k = 0.010, \ f_B = 50$ Hz.
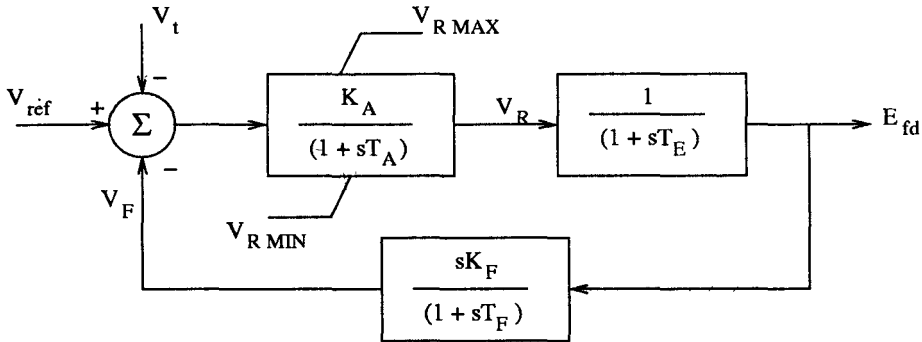
Figure C.5:

23. Consider an excitation system whose block diagram is shown in figure C.5.

    (a) Write the state equations for this excitation system.

    (b) In steady state, $E_{fd} = 2.5, V_t = 1.0$. Find the equilibrium values of the state variables and V_{ref}.

    (c) If there is a step decrease in V_t by 0.1, obtain the response of E_{fd} as a function of time. Assume the following data.
    $T_A = 0.02, \ T_E = 0.8, \ T_F = 1.0, \ K_A = 400, \ K_F = 0.03,$
    $V_{RMAX} = 4.0, \ V_{RMIN} = -4.0$.

24. When the generator is on no load the transfer function between V_t and E_{fd} is given by

$$V_t(s) = \frac{1}{1 + sT'_{do}} E_{fd}(s)$$

   For the excitation system shown in figure C.5

   (a) Obtain the root locus as K_A is varied if $T'_{do} = 5.0$, $K_F = 0$. Assume other data as given in problem 23.

   (b) At what value of K_A is the system just on verge of instability?

   (c) Obtain the root locus with variation in K_F if $K_A = 400$.

25. Consider the excitation system shown in figure C.6.
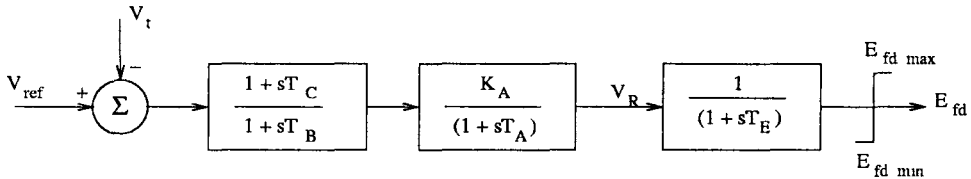
Figure C.6:

   (a) Neglecting TGR, obtain the root locus as K_A is varied. Assume generator on no load and $T_E = 0.8$ s, $T_A = 0.02$ s, $T'_{do} = 5.0$ s.

   (b) Obtain the root locus as K_A is varied with TGR considered. Assume $T_B = 10$ s, $T_C = 1.0$ s.

26. For the excitation system shown in figure C.6

   (a) Write the state equations.

   (b) In steady state, $E_{fd} = 2.5$, $V_t = 1.0$. Find the equilibrium values of state variables and V_{ref}. Assume $T_B = 10$ s, $T_C = 1.0$ s, $T_A = 0.02$ s, $T_E = 0.8$ s, $K_A = 400$.

   (c) If there is a step decrease in V_t by 0.1, obtain the response of E_{fd} as a function of time. Assume $E_{fdmax} = 4.0$, $E_{fdmin} = -4.0$.

27. Write the state equations for PSS whose block diagram is shown in figure C.7.

28. The speed governing system for a hydrogenerator can be approximately reperesented as shown in figure C.8. If $H = 4.0$, $T_W = 1.0$ s, $T_R = 5.0$ s
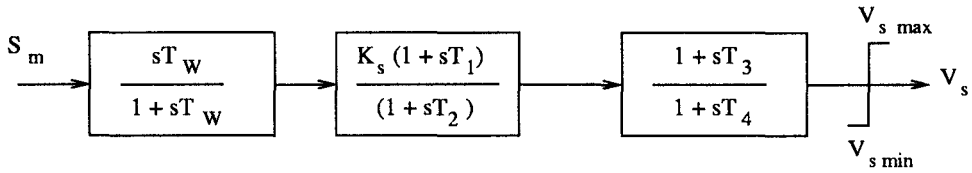
Figure C.7:
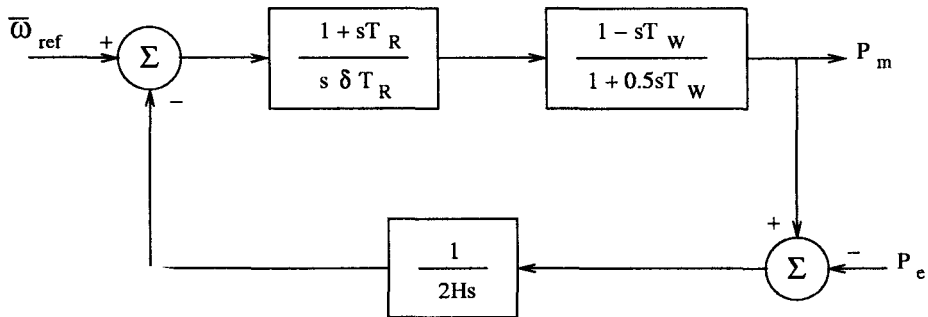
Figure C.8:

(a) Obtain the root locus as δ is varied.

(b) What is the value of δ if the damping ratio is 0.7.

29. Consider the system shown in figure C.9.

   (a) With $X = 0.5$, $E = 1.0$, plot V as a function of P for (i) $B_c = 0.0$ and (ii) $B_c = 0.5$. What is the maximum power supplied in both cases?

   (b) If the load (P) is of constant current type given by $P = V$, what is the power drawn for (i) $B_c = 0.0$ and (ii) $B_c = 0.5$.

30. An induction motor load has the following data.
   $R_s = R_r = 0.02$, $X_s = X_r = 0.5$, $X_m = 28.5$, $H_m = 0.44$.

   (a) With the applied voltage at 1.0 pu, obtain the torque slip character-istic. Assume $f_B = 50$ Hz.

   (b) The motor is initially operating at a slip $= 0.012$. The terminal voltage is suddenly reduced to zero at $t = 0$ due to a fault. What is the maximum duration of the fault for which the motor does not stall? Assume the load torque (T_m) as constant and the voltage is restored to its prefault value of 1.0 pu when the fault is cleared.
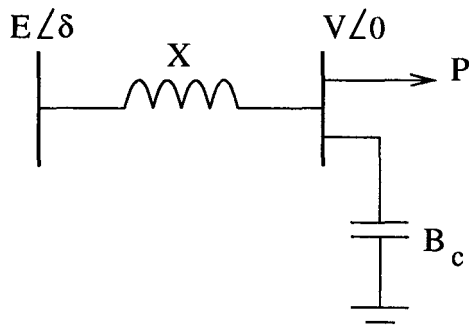
Figure C.9:
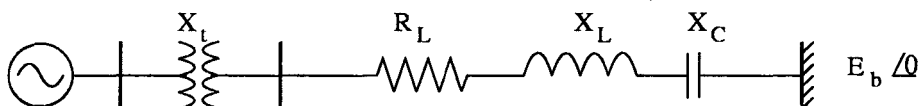
Figure C.10:

31. Consider the system shown in figure C.10. The generator is represented by a voltage source $E_g \angle \delta$ in series with the reactance X_g. Obtain the differential equations for the network in D-Q variables.

32. A synchronous generator is connected to an infinite bus through an external impedance of $j0.5$ pu. The generator is supplying power of 1.0 pu with terminal voltage V_t at 1.0 pu. Compute the operating values of δ, E'_q, E'_d, E_{fd}, v_d, v_q.

    Data : $x_d = 1.7$, $x_q = 1.7$, $x'_d = 0.25$, $x'_q = 0.45$, $T'_{do} = 6.5$ sec, $T'_{qo} = 0.7$ sec, $H = 4.0$, $D = 0.0$, $R_a = 0.0$, $f_B = 50$ Hz, $E_b = 1.0$.

33. In probelm 32, the system is initially in equilibrium and at $t = 0$, the external impedance is suddenly changed to $j0.3$ pu

    (a) Compute the values of i_d, i_q, V_t and T_e at $t = 0^+$.

    (b) What is the value of δ in steady state if
        i. there is no AVR and
        ii. there is high gain AVR

34. A synchronous generator is connected to an infinite bus through an external impedance of $j0.35$ pu. In equilibrium state, $i_d = -0.8$, $E_{fd} = 2.2$, and $E_b = 1.0$. Compute E'_q, E'_d, δ, v_d and v_q.

Data : $x_d = 1.75$, $x_q = 1.65$, $x'_d = 0.25$, $x'_q = 0.45$, $T'_{do} = 6.0$ sec,
$T'_{qo} = 0.8$ sec, $H = 4.0$, $D = 0.0$, $R_a = 0.0$, $f_B = 50$ Hz.

35. For the system described in problem 34 the infinite bus voltage is suddenly increased to 1.1 pu at $t = 0$

    (a) Compute i_d, i_q, V_t and $\frac{d^2\delta}{dt^2}$ at $t = 0^+$.

    (b) Assuming high gain AVR, compute E_{fd} in steady state.

36. (a) Compute the Heffron-Phillips constants for the system described in problem 32. Assume machine model (1.0).

    (b) Compute the upper limit on AVR gain, if any, beyond which there is instability. Assume fast acting exciter and neglect the effect of damper winding.

    (c) What is the frequency of the rotor oscillations on the verge of instability?

37. A synchronous generator is connected to an infinite bus through an external impedance of $j0.4$ pu. The generator is initially operating with $P_g = 1.0$, $V_t = 1.0$ and $E_b = 1.0$. The generator data : $x_d = 1.6$, $x_q = 1.55$, $x'_d = 0.32$, $T'_{do} = 6.0$ sec, $x'_q = 0.32$, $T'_{qo} = 0.8$ sec, $H = 5.0$, $D = 0.0$, $R_a = 0.0$, $f_B = 60$ Hz.

    (a) Compute the initial conditions.

    (b) Simulate the system and obtain responses of E'_q, E'_d, S_m, δ, V_t and T_e if there is a step increase in E_{fd} of 0.2 pu.

    (c) Repeat (b) if $x'_q = 1.55$.

38. Repeat problem 37 if the operating data is changed to $P_g = 0.5$, $V_t = 1.0$, $E_b = 1.0$.

39. For the operating data given in problem 38 (and generator data given in problem 37)

    (a) Simulate the system if there is a step increase in T_m by 0.2 pu.

    (b) What is the maximum step increase in T_m possible without losing synchronism?

40. The generator in problem 37 is equipped with a static exciter having data : $T_B = T_C = 10$ s, $K_A = 200$, $T_A = 0.025$ s, $E_{fdmax} = 6.0$, $E_{fdmin} = -6.0$. With the same operating conditions as in problem 37 simulate the system for

    (a) Step increase in V_{ref} by 0.2 pu

(b) Step increase in T_m by 0.1 pu

(c) Repeat (a) and (b) if $x'_q = 1.55$.

41. Repeat problem 40 if the operating data is changed to $P_g = 0.5$, $V_t = 1.0$, $E_b = 1.0$.

42. For the system of problem 37, there is a sudden increase in E_b of 0.1 pu. Simulate the system

    (a) Without AVR (constant E_{fd})

    (b) With AVR (data given in problem 40)

43. There is a sudden three phase fault at the terminals of the generator of problem 37. The fault is cleared in three cycles and the post fault configuration is same as the prefault one. Simulate the system

    (a) Without AVR

    (b) With AVR of data given in problem 40.

    What is the critical clearing time in both cases.

44. Consider the system shown in figure C.11. The generator data (on its own base) : $x_d = 1.0$, $x_q = 0.6$, $x'_d = 0.3$, $x'_q = 0.2$, $T'_{do} = 5.0$ sec, $T'_{qo} = 0.12$ sec, $H = 4.0$, $D = 0.0$, $R_a = 0.0$, $f_B = 50$ Hz. The generator has a static exciter whose data is given in problem 40. The transformer leakage reactance (on its own base) is 0.15 pu. Each circuit of the transmission line has $R = 0.0216$, $x = 0.408$, $b = 0.184$ (R is the series resistance, x is the series reactance, b is the shunt susceptance) on 1000 MVA base. $x_2 = 0.18$ pu (on 1000 MVA base). The generator and transformer are each rated at 5200 MVA. The system is initially operating with $V_t = 1.03$, $P_b = 2.0$, $Q_b = 0.0$.
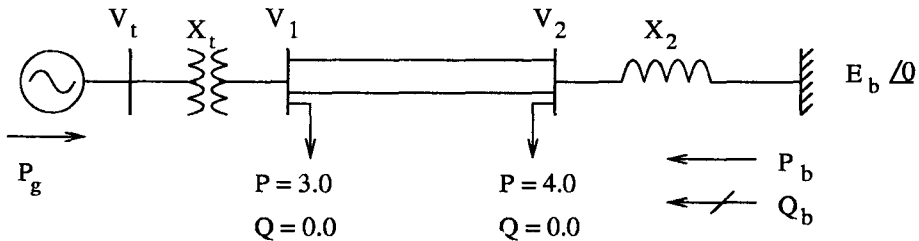
Figure C.11:

    (a) Compute initial conditions

    (b) Simulate the system for a step increase in V_{ref} of 0.2 pu

    (c) Simulate the system for a step increase in E_b of 0.1 pu.

45. For the system shown in figure C.11, there is a three phase fault at the receiving end of one of the lines which is cleared by tripping the line at the end of 3 cycles. Assuming the system data given in problem 44,

    (a) Simulate the system

    (b) What is the critical clearing time?

46. Consider the system shown in figure C.12. The generator is represented by model (1.0) with the data : $x_d = 1.6$, $x_q = 1.55$, $x'_d = 0.32$, $T'_{do} = 6.0$ sec, $H = 5.0$, $D = 0.0$, $R_a = 0.0$, $f_B = 50$ Hz. Exciter data : $T_E = 0.025$ s, $0 < K_E < 400$.
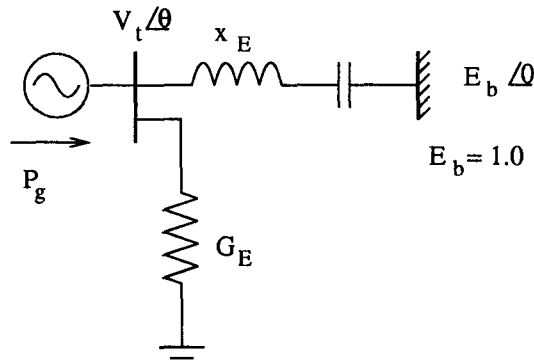
Figure C.12:

    (a) Compute the constants K_1 to K_6 if $P_g = 1.0$, $V_t = 1.0$, $x_E = 0.3$, $G_E = 0.0$.

    (b) Plot the loci of eigenvalues if K_E is varied from 0 to 400.

47. Repeat problem 46 if $P_g = 1.0$, $V_t = 1.0$, $G_E = 0.5$ and $x_E = 0.6$, other data remaining the same.

48. Repeat problem 46 if $P_g = 0.5$, $V_t = 0.9$, other data remaining the same.

49. Design PSS for the system of problem 46. Assume PSS transfer function

$$PSS(s) = \frac{K_s \, s \, T_W \, (1 + s \, T_1)}{(1 + s \, T_W) \, (1 + s \, T_2)}$$

Assume $K_E = 200$, $T_W = 2.0$.

50. Repeat problem 49, if the operating data is that given in problem 47.

51. Repeat problem 49, if the operating data is that given in problem 48.

52. Test the performance of PSS designed in problem 49, if there is a three phase fault at the generator terminals followed by clearing after 0.05 s. Assume post fault system same as the prefault system. The limits on V_s are ±0.05 pu.

53. Repeat problem 52 if the PSS is designed in problem 50 is used along with the system given in problem 47.

54. A turbogenerator shaft has six masses with the following data :
    Inertias : $H_1 = 0.021$, $H_2 = 0.727$, $H_3 = 1.54$, $H_4 = 1.558$,
    $H_5 = 0.284$, $H_6 = 0.104$ (all in seconds).
    Shaft spring constants (in pu) : $K_{12} = 32.1$, $K_{23} = 86.2$, $K_{34} = 113.16$,
    $K_{45} = 105.7$, $K_{56} = 39.5$.

    (a) Compute modal inertias and frequencies.
    (b) Compute mode shapes (columns of [Q] matrix).

55. A generator is connected to an infinite bus through a series compensated line. The generator data : $x_d = 1.0$, $x_q = 0.66$, $x'_d = 0.35$,
    $x'_q = 0.32$, $T'_{do} = 7.5$ sec, $T'_{qo} = 0.06$ sec, $R_a = 0.005$ (includes generator step-up transformer), $f_B = 50$ Hz. The reactances of the step-up transformer and receiving end reactances are $x_t = 0.17$, $x_r = 0.20$. The transmission line has the parameters $x = 0.75$, $b_c = 0.50$ and $R = 0.329$ (where x, b_c and R are the series reactance, shunt susceptance and resistance respectively). Series capacitive reactance (x_c) is variable (0 - 0.7).

    (a) Write system state equations including network transients. Assume constant (rated) rotor speed.
    (b) Obtain the locus of the critical network mode that is affected by induction generator effect as x_c is varied from 0 to 0.7 pu.

56. In problem 55, consider the speed of the generator variable with total inertia $(H_T) = 3.3$ s. Assuming generator output as $P_t = 0.0$,
    $Q_t = -0.25$ obtain linearized state space equations. Assuming transmission line resistance as variable, with $x_c = 0.65$, obtain the limits (minimum and maximum) on the transmission line resistance such that the system is stable.

57. The system corresponding to IEEE Second Benchmark Model (SBM) is shown in figure C.13. The system data is (on a 100 MVA base) are given below.

Transformer : $R_T = 0.0002, \; X_T = 0.02.$

Transmission line : $R_1 = 0.0074, \; X_{L1} = 0.08.$
: $R_2 = 0.0067, \; X_{L2} = 0.0739.$
: $R_{SYS} = 0.0014, \; X_{SYS} = 0.03, \; f_B = 60$ Hz.

The generator subtransient reactances are $x_d'' = x_q'' = 0.0333.$

(a) Write the network equations. Assume that the generator is modelled by a constant voltage source behind subtransient reactance.

(b) With X_C varied from 10% to 90% of X_{L1}, plot the variation of the frequencies of the network modes.
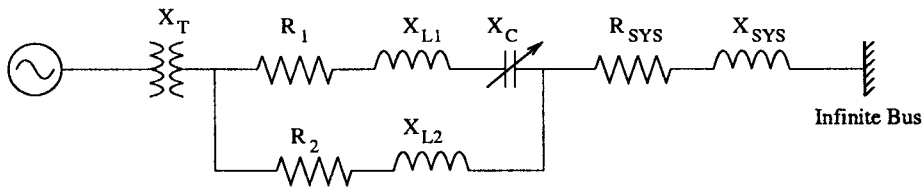
Figure C.13:

58. For the generator in IEEE SBM, there are four rotor intertias corresponding to exciter, generator, LP and HP turbines. The modal quantities are given below.

Mode	f_n (Hz)	H_n (sec)	σ_n (rad/sec)
1	24.65	1.55	0.05
2	32.39	9.39	0.05
3	51.10	74.80	0.05

The mode shapes are given below.

Rotor	Mode 1	Mode 2	Mode 3
EXC	1.307	1.683	-102.6
GEN	1.000	1.000	1.000
LP	-0.0354	-1.345	-0.118
HP	-1.365	4.813	0.0544

Compute the inertias (H), spring constants (K) and damping (D) for the mechanical system.

59. The unit # 2 in IEEE SBM (system # 2) has the 3 rotor inertias and the following modal data

Rotor mode shapes

Rotor	Mode 1	Mode 2
GEN	1.000	1.000
LP	-0.601	-4.33
HP	- 1.023	11.56

The modal parameters are

Mode 1 : $H_n = 2.495$ s, $f_n = 24.65$ Hz, $\sigma_n = 0.025$.

Mode 2 : $H_n = 93.960$ s, $f_n = 44.99$ Hz, $\sigma_n = 0.025$.

Compute inertias, spring constants and damping for the mechanical system.

Index